AN EXPERIMENTAL AND THEORETICAL INVESTIGATION INTO THE PERFORATED ZONES FOR NUCLEAR REACTOR PRESSURE VESSELS

A thesis submitted for the Degree of
Doctor of Philosophy
in the Faculty of Engineering
of the University of London

by

G.D. STEFANOU, BSc(Eng),Dipl.Ing,DIC,AMICE.

Imperial College of Science and Technology
London

May, 1970.

A B S T R A C T

The cylindrical prestressed concrete pressure vessels now being constructed in Great Britain to contain the gas pressures in nuclear reactor systems, are highly redundant structures, because of, inter alia, the asymmetries, discontinuities and restraints in their arrangements, and temperature gradients.

Their design, and the design of their elements, such as the end slabs to the cylinders, increasingly call for more experimental data and better analytical techniques.

Moreover, the vessel concrete is subjected to varying temperature gradients and long-term mechanical loadings. There is consequently, a need for a proper understanding of not only the behaviour of the vessel under these circumstances, but also the effects of the resultant time-dependent phenomena. These phenomena include creep and shrinkage. In addition, a study of the behaviour of the perforated end slabs against these effects is particularly required.

Accordingly, the object of the present investigation is to analyse the mode of action of the end slabs under the particular conditions of constant elevated temperature and radial load. These simplified conditions have been chosen in order to limit the study, in this first instant, to the more readily achieved objectives.

For this purpose, a series of experiments have been carried out on representative models of flat circular concrete plates, some perforated and reinforced with steel liners, and some unperforated.

Consequent upon these experiments, a method of analysis has been developed which predicts the stresses and strains within these plates taking into account elastic, thermoelastic and time-dependent effects. Creep data are used in the form of specific creep curves obtained from the plots of experimental observations. Shrinkage data has also been utilized from experimental results.

A full solution is accomplished in a step-by-step manner using small-time intervals during which the stresses are assumed to remain constant. The incompatibility caused by the creep and shrinkage strains at the end of the interval under consideration is corrected by an elastic solution based on a finite element formulation.

A comparison of analytical results with observed data, shows acceptably close agreement.

The applicability of the proposed method to actual design is discussed in detail.

It is concluded that the full analytical procedure proposed in this thesis, concerning itself with both elastic and time-dependent effects, adequately predicts the stress resultants operating in models of the configuration adopted in these tests. Furthermore, the procedure is capable of being extended to permit a comprehensive analysis of a full-scale pressure vessel end cap under any loading and any geometry.

A C K N O W L E D G E M E N T S

The author wishes to express his gratitude to Professor A.L.L. Baker, D.Sc., F.I.C.E., M.I. Struct.E., under whose guidance the investigation reported herein was conducted.

He is also grateful to Dr. C.W. Yu, Ph.D., D.I.C., M.A.S.C.E., for his valuable help and assistance at every stage of this work.

The author wishes to express his indebtness to Dr. Dr. G.L. England, B.Sc. (Eng.), Ph.D., M.I.C.E., of King's College, London, for his valuable advice and suggestions throughout this research.

Sincere thanks are also due to Mr. S. Gill, B.Sc.(Tech), M.I.C.E., A.M.I. Mech. E., of The City University, London, for his help and great interest at every stage of this work.

Appreciation is due to the following Organizations and Institutions, without whose co-operation, the research in this thesis would not have been possible.

The United Kingdom Atomic Energy Authority, for financing the project.

The Ministry of Co-Ordination, Athens, and the NATO Authorities, for the award of the grant.

The National Technical University, Athens, for their sponsorship.

The author wishes to express his thanks to the Laboratory Staff of the Imperial College, London, for their assistance in the preparation of the experiments.

.....

C O N T E N T S.

PAGE:

PAGE:

PAGE:

CHAPTER I

INTRODUCTION

1.1. Historical Note.

1.1.1. The Nuclear Reactor as a Heat Source.

The atomic reactor when used for power generation can be considered to be a nuclear furnace fuelled by uranium. (Fig.1.1).

The reactor core is contained in a pressure vessel and is associated with heat exchangers, cooling and fuelling systems. (Fig.1.2).

The heat, generated inside the reactor, and subsequently removed from the core by gaseous carbon dioxide coolant circulated under pressure, is transferred to the heat exchangers where the hot gas, flowing over a sealed water system, produces steam. (Fig.1.3).

The steam is conveyed to the turbine house where it is expanded through the turbo-generators to produce electrical power.

The energy released in fission, particularly the neutrons and gamma rays, are harmful to human tissue necessitating the provision of biological shielding to protect both the operating personnel and the general public.

The early designs incorporated a spherical steel pressure vessel (Fig.1.1) and a separate concrete biological shield. Recent proposals have adopted the prestressed concrete vessel to enclose the reactor core, and the concrete in this case, acts in the dual capacity of gas pressure container and biological shield.

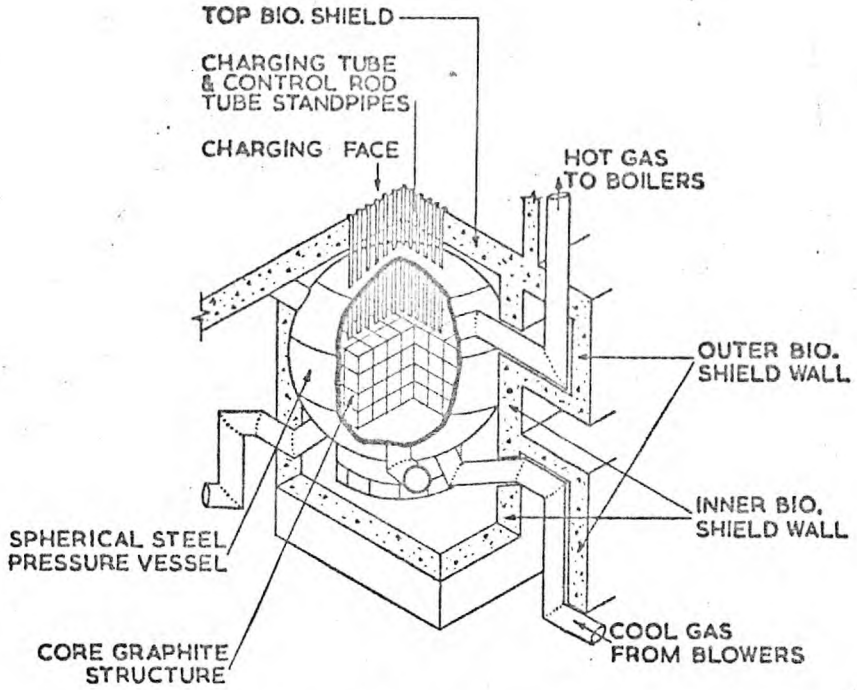

FIG.1.1.

REF.112.

Diagram of Simple Reactor Arrangement.

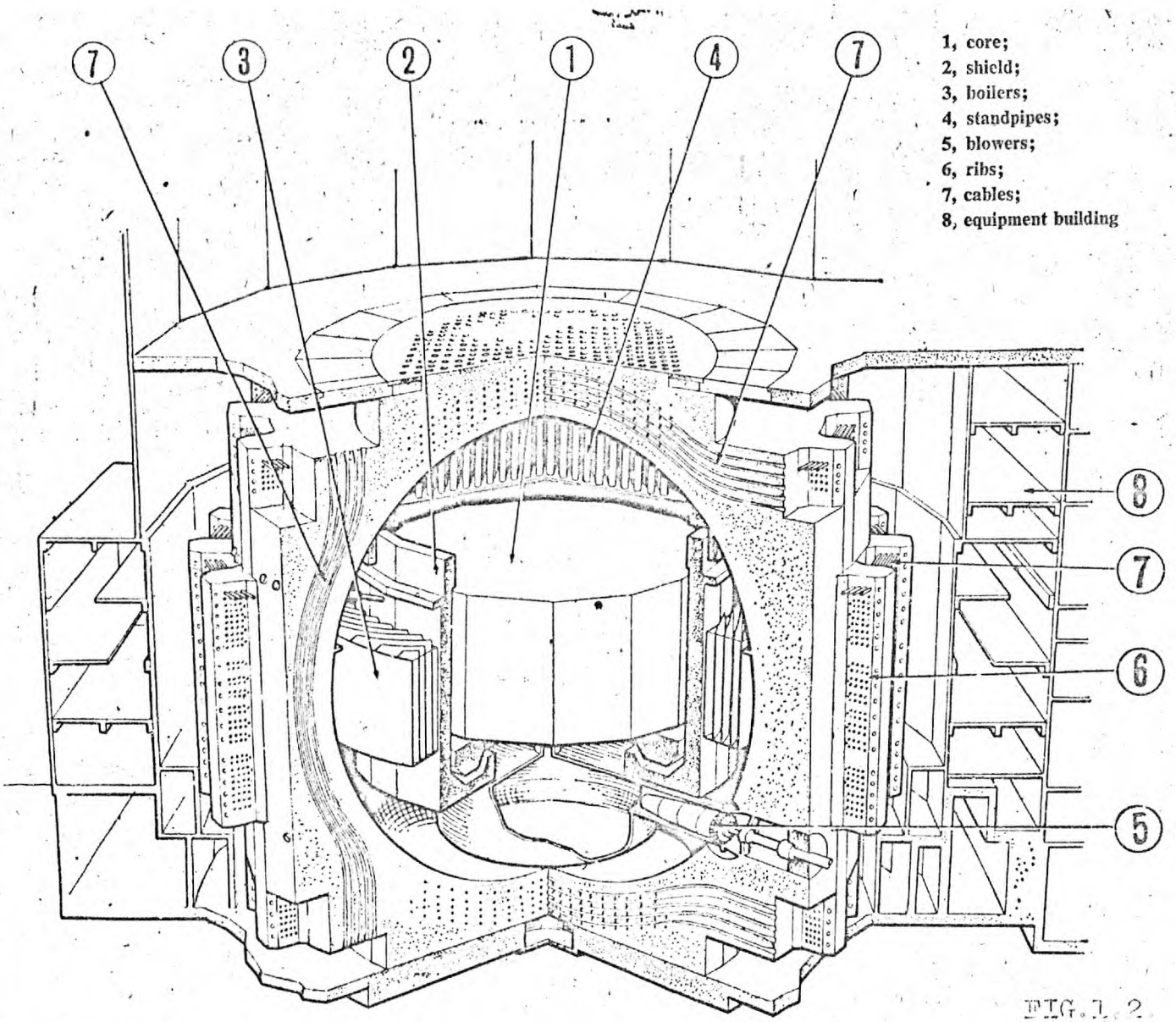

FIG.1.2.

General arrangement of reactor and pressure vessel

REF.113.

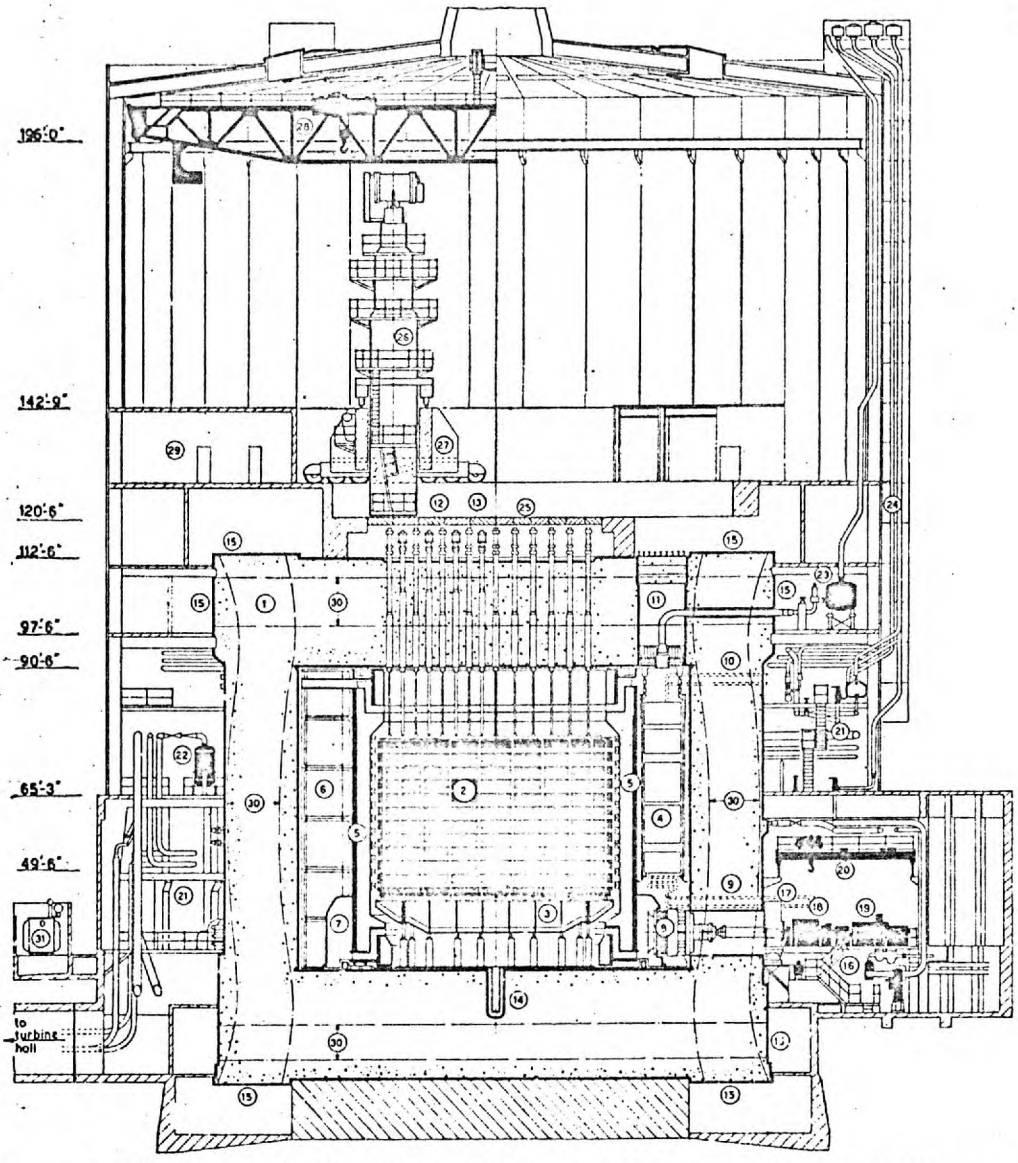

1. Transverse elevation showing the general arrangement of the compact system reactor unit for Oldbury.

1 pre-stressed concrete pressure vessel; **2** graphite core; **3** core support grid; **4** boiler; **5** boiler shield wall; **6** boiler end piece; **7** gas circulator outlet duct; **8** gas circulator; **9** boiler feed penetrations; **10** HP and LP steam penetrations; **11** boiler loading slot; **12** charge standpipe; **13** control standpipe; **14** debris mortuary tube; **15** pressure vessel stressing galleries; **16** gas circulator pony motor; **17** gas circulator turbine; **18** gas circulator auxiliaries; **19** gas circulator shield doors; **20** gas circulator crane (20 tons); **21** steam and feed pipework; **22** boiler start-up vessels; **23** reactor safety valves and filters; **24** relief valve pipes to atmosphere; **25** charge floor; **26** charge/discharge machine; **27** charge/discharge machine gantry; **28** charge hall crane (25 tons); **29** B.C.D. room; **30** stressing cables; **31** transformers.

FIG.1.3.
REF. 112.

The concrete of the vessel walls and roof is heated by normal conduction, convection and radiation processes from the hot core. In addition, in attenuating the neutron and gamma fluxes incident on the concrete, the pressure vessel walls become further sources of heat as the particles are absorbed. This leads to varying temperature gradients throughout the structure.

1.1.2. Development of the Prestressed Concrete Pressure Vessel.

The original nuclear reactor designs as explained above, following the Calder Hall pattern, (Fig.1.4) incorporated a cylindrical biological shield whose only function was to protect operating, technical and scientific personnel from the harmful effects of radiation. The wall thickness was of the order of 8'-0" to 10'-0", and the roof about 12'-0" to 14'-0" thick.

The replacement of the steel vessel (Fig.1.1) and its surrounding biological shield by thick prestressed concrete (Fig.1.5) serving as pressure vessel and shield was an obvious and advantageous concept.

In the United Kingdom, the original concept of the concrete pressure vessel was developed by the United Kingdom Atomic Energy Authority, who in the middle fifties examined its feasibility and cost, and decided at that time that it held so significant advantage. It was left to private industry to resurrect the scheme, develop it on somewhat different lines and to establish its practicability, increased safety and economic promise during the four succeeding years. The model which was designed, constructed and successfully tested by Simon-Carves Limited, during the years 1958 and 1959, marked the end of the first phase of development. (Fig.1.6).

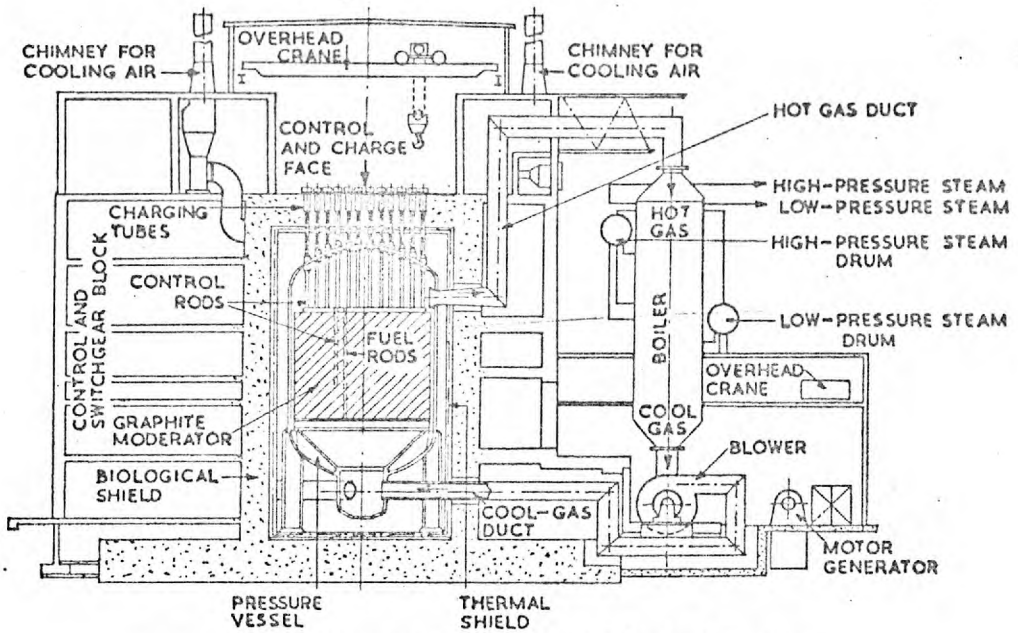

Cross-section through a Calder Hall Reactor.

FIG.1.4. (a)

REF.112.

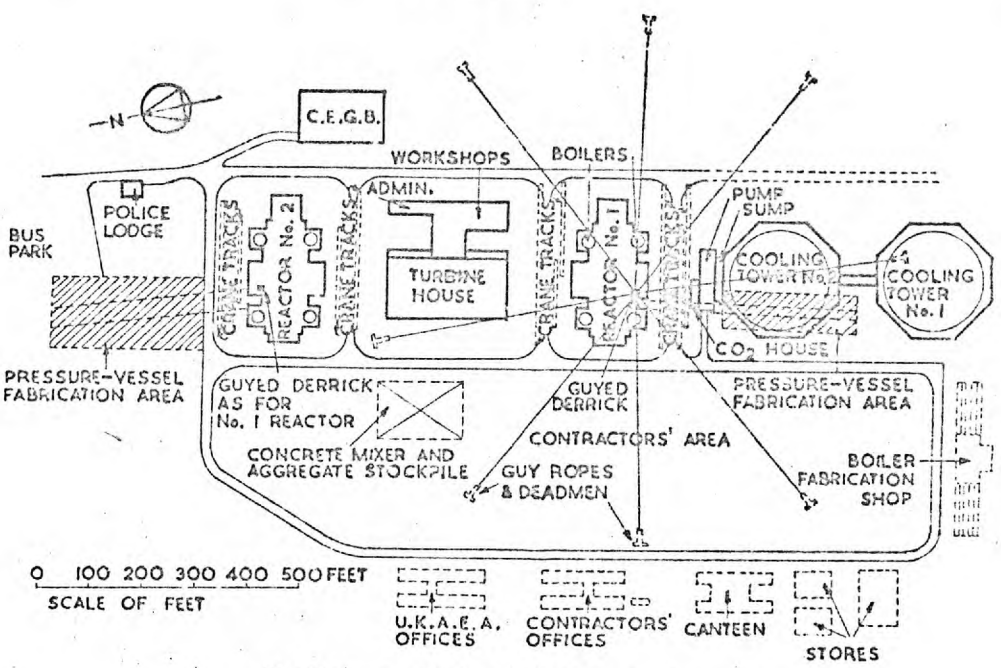

Site Layout. Calder Hall Power Station. Stage 1.

FIG.1.4. (b)

REF.112.

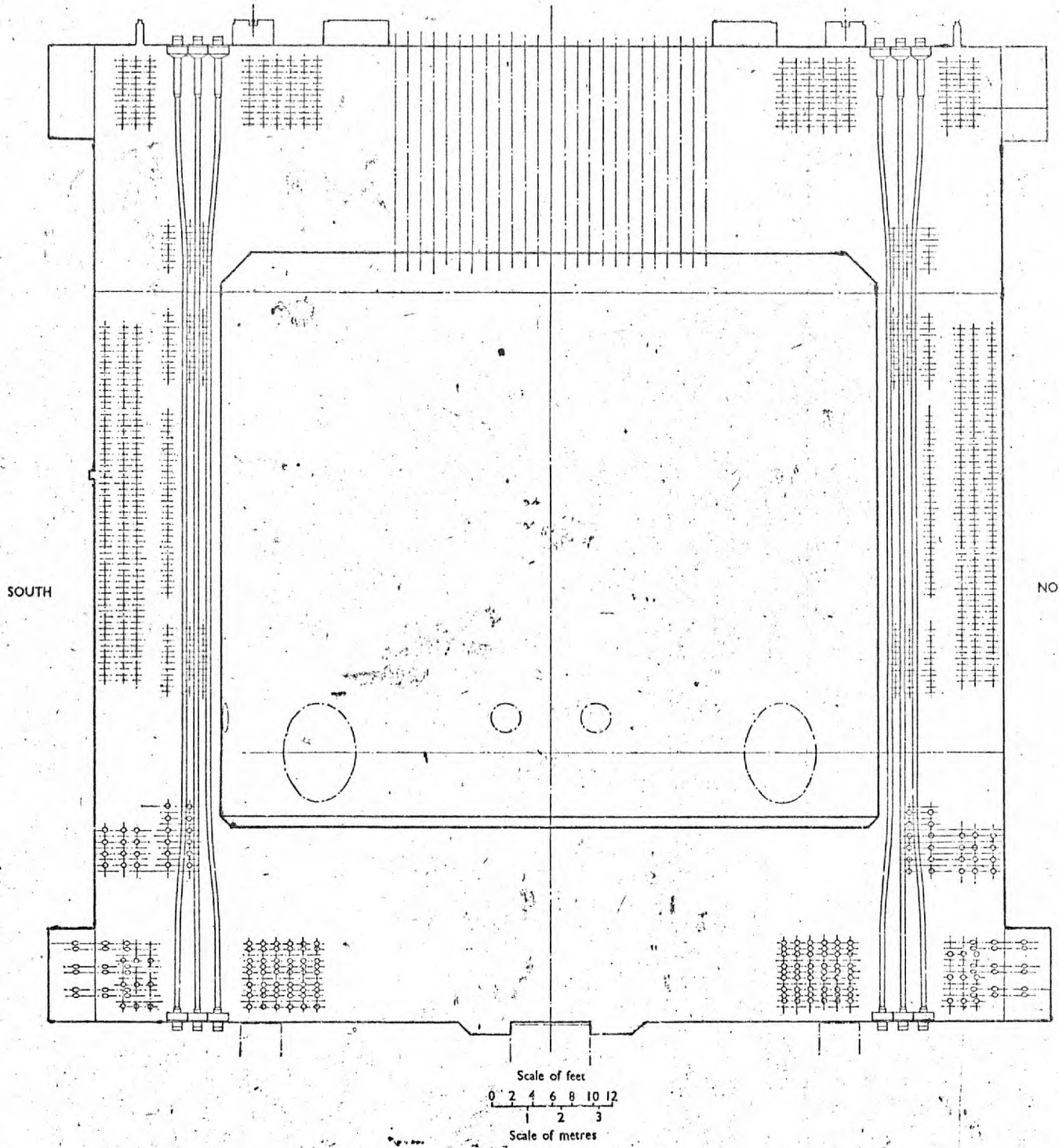

FIG.1.5.

REF. 114.

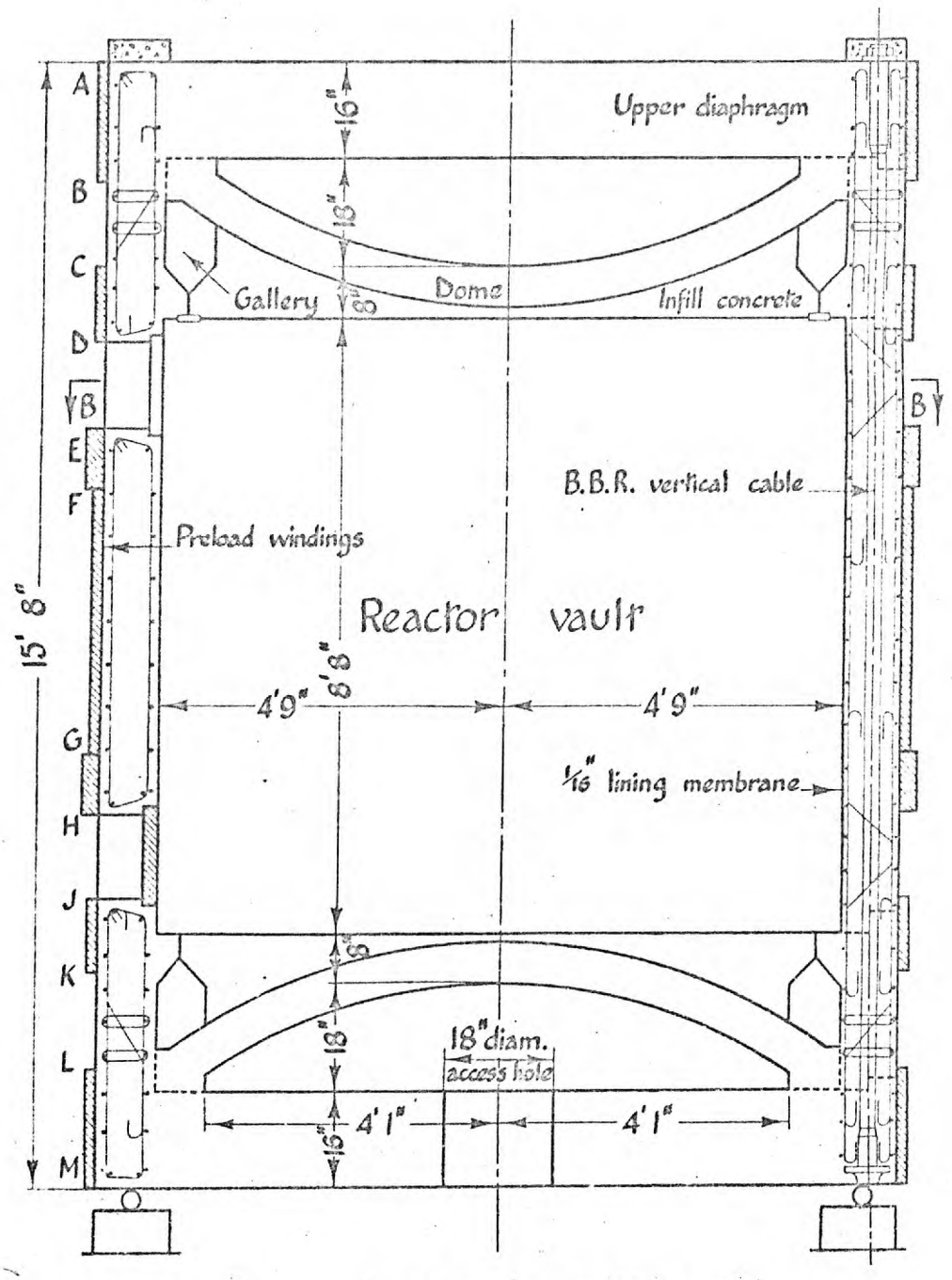

General Arrangement of Model.

FIG.1.6.

REF.112.

By contrast with the bio-shield, the walls and roof caps of these recently-constructed prestressed concrete pressure vessels are of the order, respectively, of 15'-0" and 25'-0" thick (in places). However, these thicknesses in the case of the P.C.P.V., are now governed by prestressing requirements rather than, as for the original bio-shield, by radiation protection considerations.

There is an undoubted trend towards greater pressures and temperatures, in order to improve the thermal efficiency of the heat transfer cycle. As a result, the duty of the concrete in respect of mechanical loading and heat loading has been made considerably more severe. Simple thickening of concrete sections provides no answer to this increased problem.

What is required is a better understanding of the properties of the concrete, and of the way in which it will behave under the more onerous conditions, and in particular, a knowledge of ways in which the technique of analysis can be refined, so that the need for model testing is removed.

1.1.3. The Cylindrical Prestressed Concrete Pressure Vessel.

The original prototype of the concrete pressure vessel was cylindrical, but later, spherical designs were investigated. However, now the trend appears to be back to the cylindrical form.

The present preference for a cylindrical shape for the vessel is mainly based on the fact that the vessel is required to contain a reactor core, itself essentially cylindrical. Moreover, an orthogonal arrangement of prestressing cables in the longitudinal and circumferential directions is most conveniently provided about a cylinder.

1.2 The End Slabs of the Cylindrical Vessel.

The closing top end caps of such cylinders take the form of flat circular perforated plates subjected to temperature loading, in-plane radial loading, the transverse gas pressure and peripheral bending moments. (Fig.1.7).

The perforations are reinforced with steel liners and such reinforced holes contribute to the overall rigidity of the plate, and in particular, to the stiffness of the perforated zone of the plate.

The variables which affect the degree of rigidity bestowed on the plate, are the liner thickness, the ligament dimension between holes, the hole diameter, the pattern of the stand-pipes, and the modular ratio between the materials concerned.

In the operating reactor vessel, as previously explained, the radiant and convected heat from the core, together with the heat generated in the concrete after absorption of nuclear radiation, cause temperature gradients to be set up across the thickness of the circular end slab. These gradients vary in magnitude along the diameter.

The causes of the various force components acting on the slab are well known and can be summarized thus:-

a) In-plate radial compression from the prestressing.

b) Transverse loading from the internal gas pressure normal to the slab.

c) Peripheral restraining moments from the cylindrical walls.

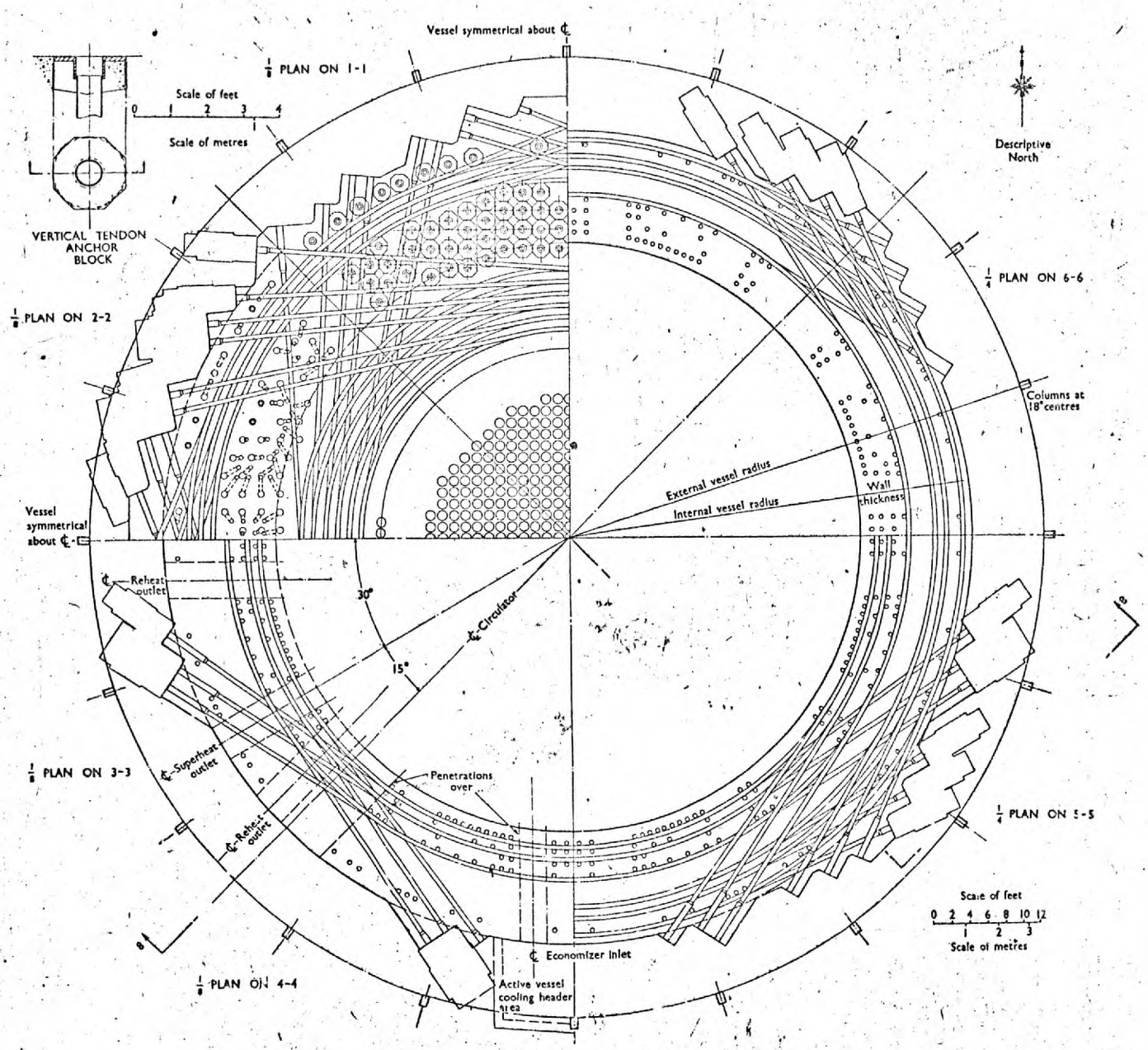

Layout of prestressing tendons

FIG.1.7.

REF. 114.

d) Varying temperature gradients across the slab.

e) Differences in average temperatures between the end slab and the wall.

In a general analysis of a whole prestressed concrete pressure vessel, all these effects can be included and the resulting stress components assessed.

In such analyses, however, it has hitherto been considered satisfactory to assess the overall rigidity of the perforated zone by postulating a modified elasticity for the zone as if its behaviour was that of a homogeneous (but hypothetical) material.
Part of the work described herein, has concerned itself with the establishing experimentally of an equivalent modulus value for the perforated zone.

However, a more rigorous analysis of the perforated zone would demand a more detailed knowledge of the way in which load is distributed around and within the area of the reinforced holes and ligaments, a distribution governed essentially by the geometry of the penetration lattice, the compatibility of the concrete and liner strains, and the elastic constants of the materials involved.

Accordingly, another section of the present work involves the measurement of strains within the ligaments and the change in diameters of the stand-pipe penetrations under loading, with the aim in view of investigating the stress distribution within the perforated zone.

For reasons stated earlier in this investigation only item a) of the previous list and a uniform temperature have been dealt with in the experimental and theoretical assessment of the end slab behaviour.

1.3. Statement of the Problem.

In the P.C.P.V., the design temperatures of the hotter face of the concrete may be as much as 90°C or even higher and the temperature gradients may range from 2°C per foot to a considerably greater figure.

Operating temperatures are limited to conservative values by an expensive cooling system in the vessel walls and roof. If the concrete can be shown to be capable of tolerating higher temperatures over the long term, significant savings may be achieved in the insulation and cooling systems.

Such a step forward would, however, require a much improved understanding of the thermal effects on the highly-stressed concrete. It would also demand an intimate knowledge of the way in which creep and shrinkage characteristics change in the hot concrete. Moreover, the increasing use of P.C.P.Vs., subjected to sustained elevated temperatures and temperature gradients, have usually called for detailed experimental studies of concrete model structures under similar conditions.

Thermal stress problems have been tackled by a great many investigators, but mostly these have concerned themselves with the behaviour from short-term point of view.

Creep is a major non-elastic strain phenomenon of concrete, and it has received considerable attention. Under sustained stresses, the strains continue to increase with time but at a decreasing rate. Shrinkage, another time-dependent phenomenon of concrete, occurs when the concrete dries out, even in the absence of loads.

In addition to the effect of thermal creep and other phenomena in modifying the properties of the concrete, certain structural problems arise from the geometry of the end caps.

For example, the stability and security of the perforated end slabs to P.C.P.Vs., have always constituted a major pre-occupation of designers.

The top of this slab represents the charging face for the uranium fuelling machine and the perforations in the slab provide means of access for the charging probes which penetrate below the slab to register on any one of a group of core channels. Thus, the standpipe penetrations are numerically fewer than the graphite core channels.

Nevertheless, the number of standpipe penetrations is very large and they are arranged in a rectangular lattice which leaves little room in the concrete ligaments between standpipes, for the arrangement of either cold worked reinforcement or prestressing tendons. The annular cooling lobes fitted outside the inner standpipe liner occupy some of this space. Thus, most end slabs receive their prestress through calbes which operate only around the slab perimeter. Indeed, some slabs contain neither internal reinforcement nor prestressing elements.

The transverse gas pressure imposes large bending stresses and shear forces in the slab which have engaged the concern of designers since the earliest arrangements. The possibility of the entire perforated zone being pushed out as a "plug" under the large vertical shear forces has always been feared. This mode of failure warrants more detailed study against the possibility of prestress loss within the perforated zone as a result of redistribution of stress due to long-term thermal creep of the concrete.

For the purposes of the present investigation, it has been considered appropriate to approach the problem by considering a simplified model wherein the elevated temperature applied has been kept uniform along and across the slab and the transverse gas pressure has been ignored.

The separate effects of mechanically-applied radial compression, creep, shrinkage and thermal expansion have been evaluated at different ages and temperatures of the concrete with the object of assessing the results of the redistribution of stress in the slab.

The test specimens used in the experiment have been subjected to a selected radial prestress and temperature test programme which approximately represents operating conditions.

A comparison between corresponding perforated and unperforated specimens can be expected to reveal a means of allowing for the effect the liner tubes have on the shrinkage and creep histories of the plain concrete.

In the present work, it has been possible by comparing all the specimens to evaluate the shrinkage and creep effects separately. These results can be used to prepare calculations predicting the behaviour of a large composite specimen having a central perforated zone and an outer solid annulus. These predictions can then be compared with the measured behaviour.

Thus, the test specimens have not been used to predict the stresses and behaviour of a prototype. They have been used only to verify the proposed method of analysis. It is anticipated that this will give an indication of whether it will apply to an actual full-scale vessel.

This would represent a considerable step forward towards a more comprehensive fundamental interpretative approach which would provide a method of predicting the long-term behaviour of a perforated zone in a full-scale vessel where age and dimensions could differ materially, and the stress history and temperature history could differ almost randomly from any model test programme.

The comparative solution to the end slab problem proposed as a result of this investigation is appropriate to the geometry of the models tested.

Although the geometry of the models and the loading conditions are only approximately representative of a true prototype end slab, the tests carried out and the analysis proposed can form the basis for a later more comprehensive investigation.

1.4. Creep and Shrinkage at Ordinary and Elevated Temperatures.

The phenomena of creep and shrinkage have been widely observed in experimental investigations over the last two decades and have attracted an extensive literature.

The mechanisms of both effects are associated with the water movement within the concrete mass. Shrinkage may be defined as the volume change due to water loss from the concrete (from capillaries and gel pores). Creep is usually defined as the time-dependent strain in excess of the initial elastic strain mostly for a state of constant stress.

The rates of both creep and shrinkage increase with temperature and decrease with time.

a) At Ambient Temperatures.

In the case of prestressed concrete pressure vessels, creep can be advantageous in assisting the concrete mass to flow under localized stress to take up its least stressed condition. It can be dis-advantageous in causing loss of prestress as the concrete deforms under the prestressing steel force, thus reducing the precompression. Furthermore, creep effects may cause redistribution of stresses.

b) At Elevated Temperatures.

At elevated temperatures, the long-term effects of creep and shrinkage are more significant than those apparent at ambient temperatures.

Shrinkage, which is caused by drying out of the concrete, also takes place at a more rapid rate at elevated temperatures.

In structures, such as concrete pressure vessels, where the temperatures vary three-dimensionally, the temperature gradients would induce different rates of creep strains in the various planes and the net result leads to an indeterminate state of stress in the structure.

1.5. Brief Explanation of the Experimental Work and Test Programmes.

The experimental work described in this investigation is an extension of the Research Project for a spherical ribed vessel (Fig.1.8), which was constructed and tested in the Concrete Structures Laboratory of the Imperial College, for the United Kingdom Atomic Energy Authority.

A graphical representation of the chronology of the test programmes are shown in (Figs. 1.9, 1.10, 1.11). The configuration of the model specimens are shown in (Fig.1.12).

It was necessary to take observations in the first instance on one specimen referred to subsequently as the large composite specimen, which would represent, at least approximately, the end slab of a P.C.P.V. This composite specimen had a central circular zone perforated with holes on a rectangular lattice and an outer solid annulus.

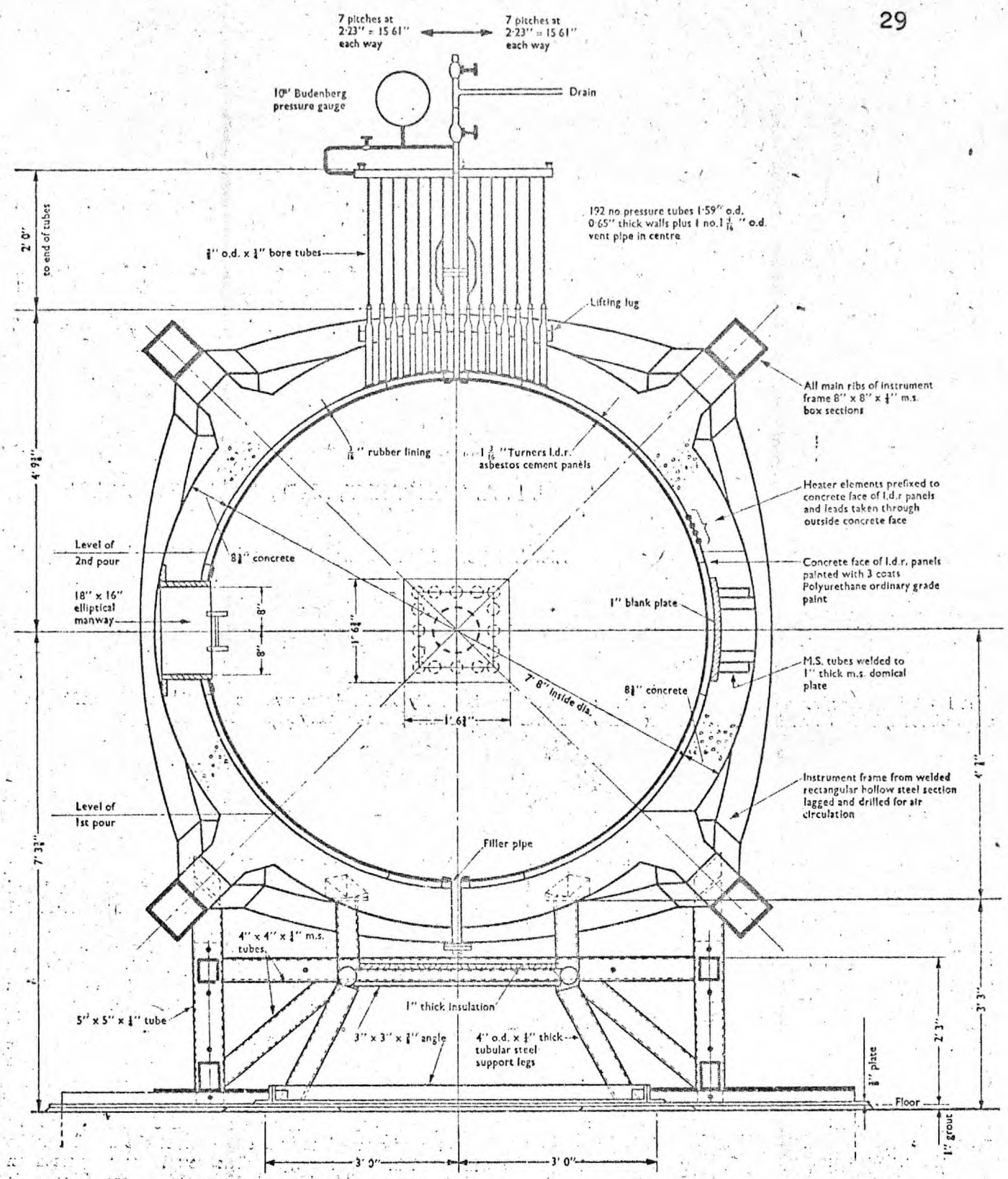
7 pitches at 2·23" = 15 61" each way
7 pitches at 2·23" = 15 61" each way
10" Budenberg pressure gauge
Drain
192 no pressure tubes 1·59" o.d. 0·65" thick walls plus 1 no. 1 1/16" o.d. vent pipe in centre
3/4" o.d. x 1/2" bore tubes
2' 0" to end of tubes
Lifting lug
All main ribs of instrument frame 8" x 8" x 1/4" m.s. box sections
1/16" rubber lining
1 1/16" Turners l.d.r. asbestos cement panels
Heater elements prefixed to concrete face of l.d.r panels and leads taken through outside concrete face
Level of 2nd pour
8 1/2" concrete
Concrete face of l.d.r. panels painted with 3 coats Polyurethane ordinary grade paint
18" x 16" elliptical manway
8"
8"
1' 6 1/2"
1" blank plate
M.S. tubes welded to 1" thick m.s. domical plate
7' 8" inside dia.
8 1/2" concrete
1' 6 1/2"
4' 1"
Instrument frame from welded rectangular hollow steel section lagged and drilled for air circulation
Level of 1st pour
7' 3 1/2"
Filler pipe
4" x 4" x 1/4" m.s. tubes
1" thick insulation
5" x 5" x 1/4" tube
3" x 3" x 1/4" angle
4" o.d. x 1/4" thick tubular steel support legs
3' 3"
2' 3"
1/2" plate
Floor
1" grout
3' 0"
3' 0"

FIG.1.8.

REF.60.

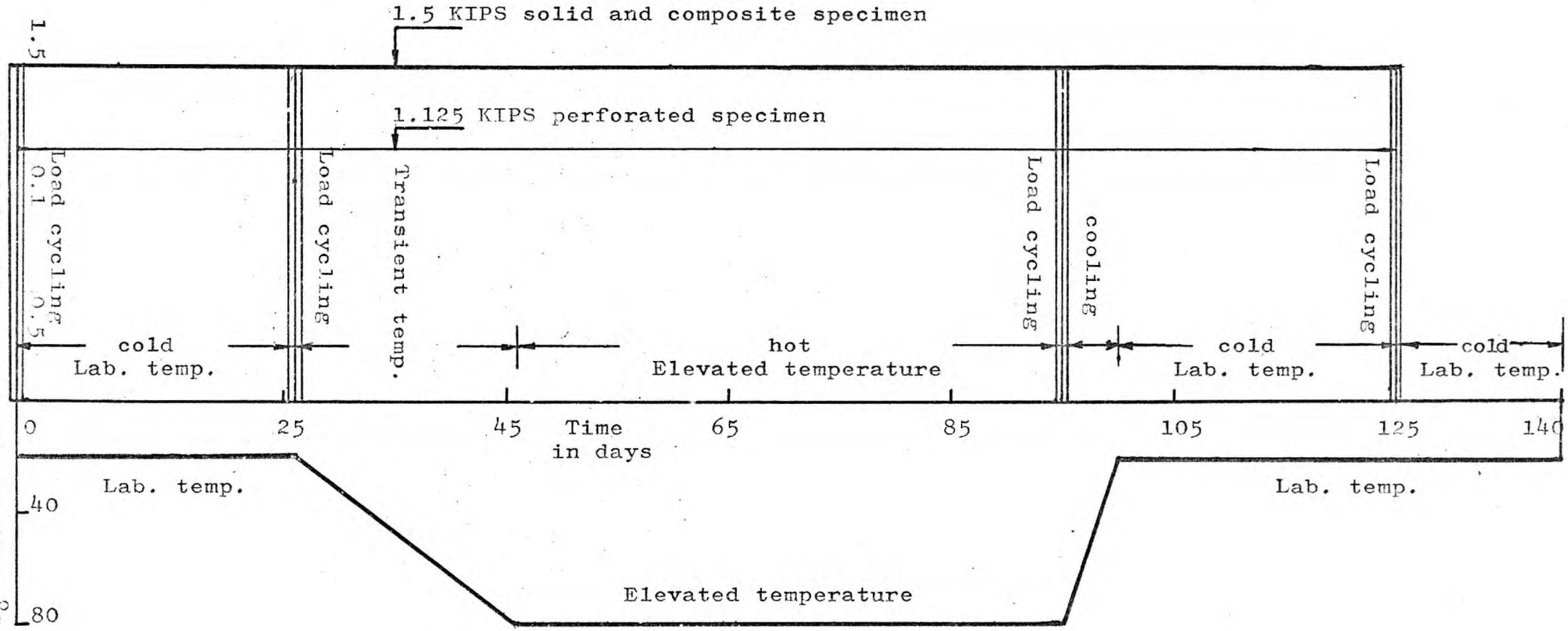

FIG. 1.9 SERIES 1 TEST PROGRAMME

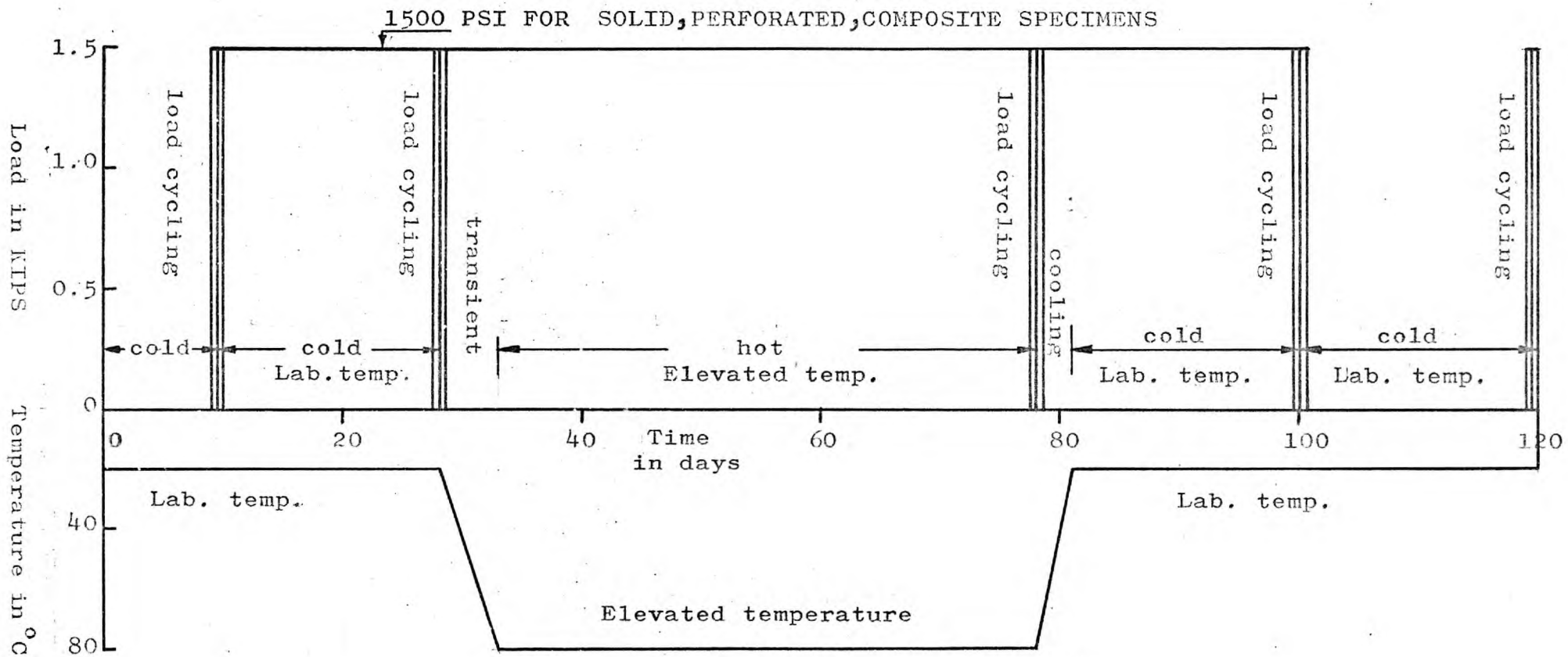

FIG. 1.10 SERIES 2 TEST PROGRAMME

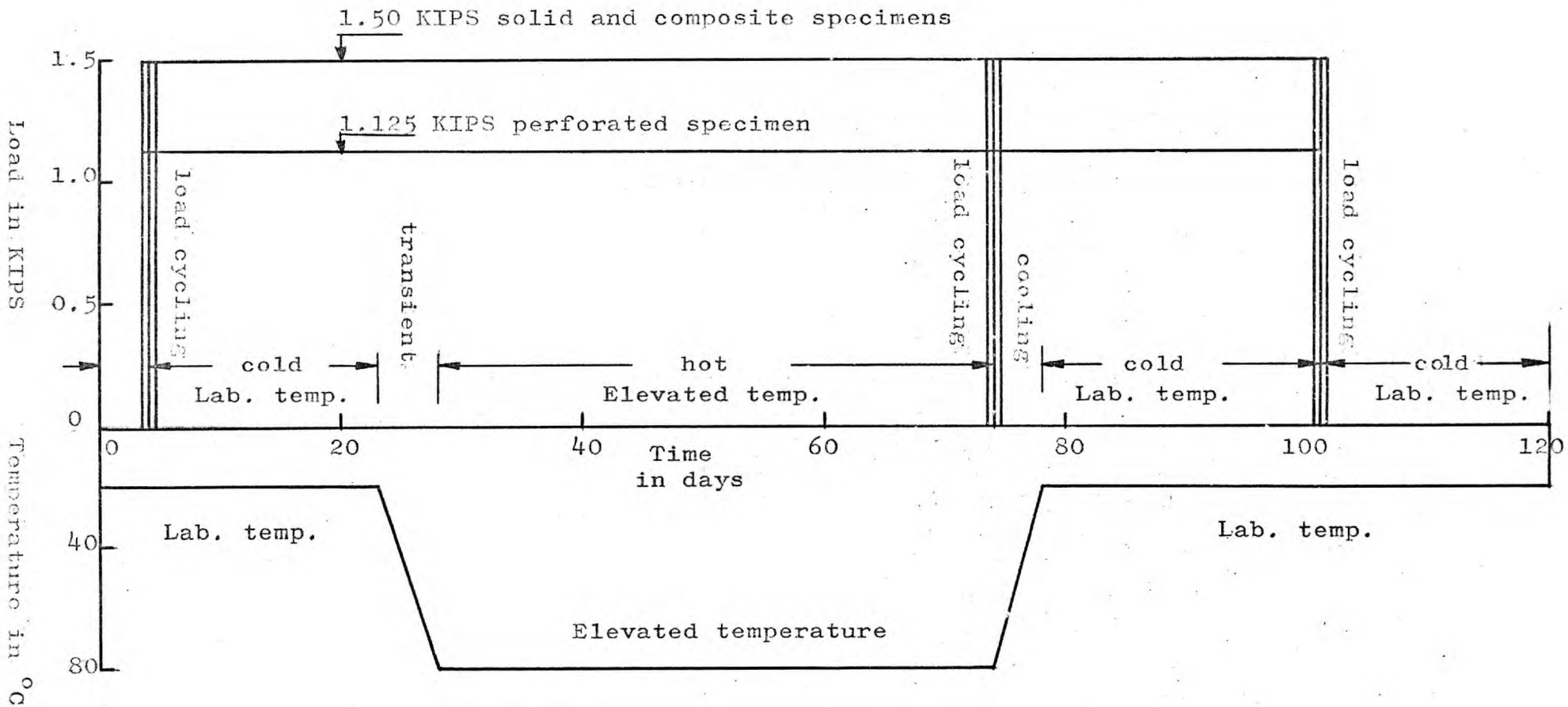

FIG. 1.11 SERIES 3 TEST PROGRAMME

THE FIVE CONCRETE TEST SPECIMENS

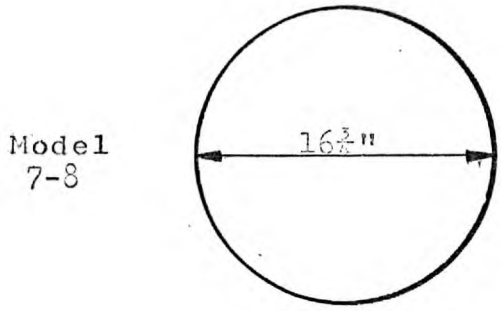

Fig. (a)

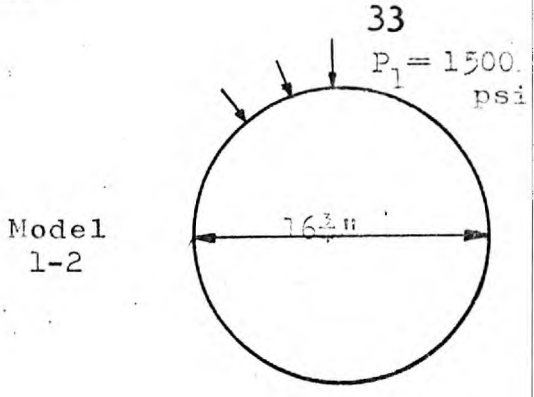

Fig. (b)

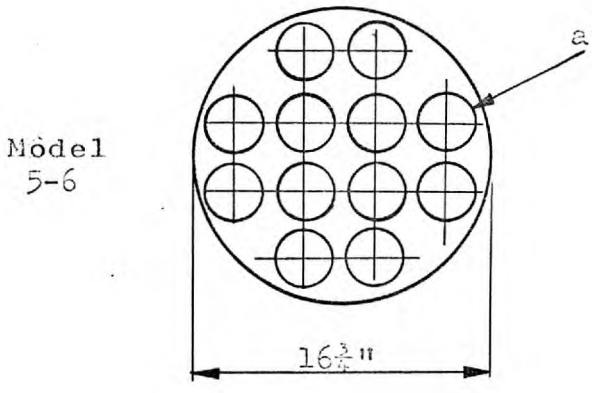

Fig. (c)

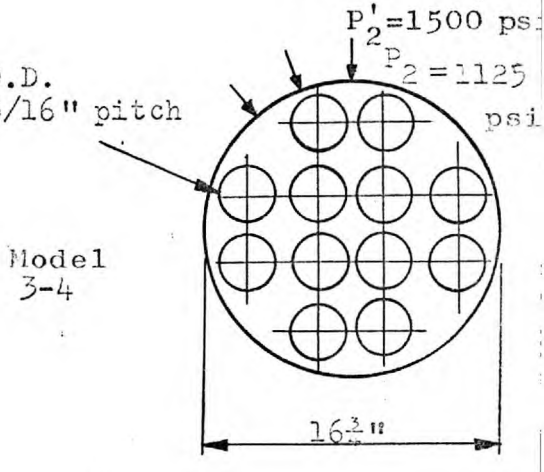

Fig. (d)

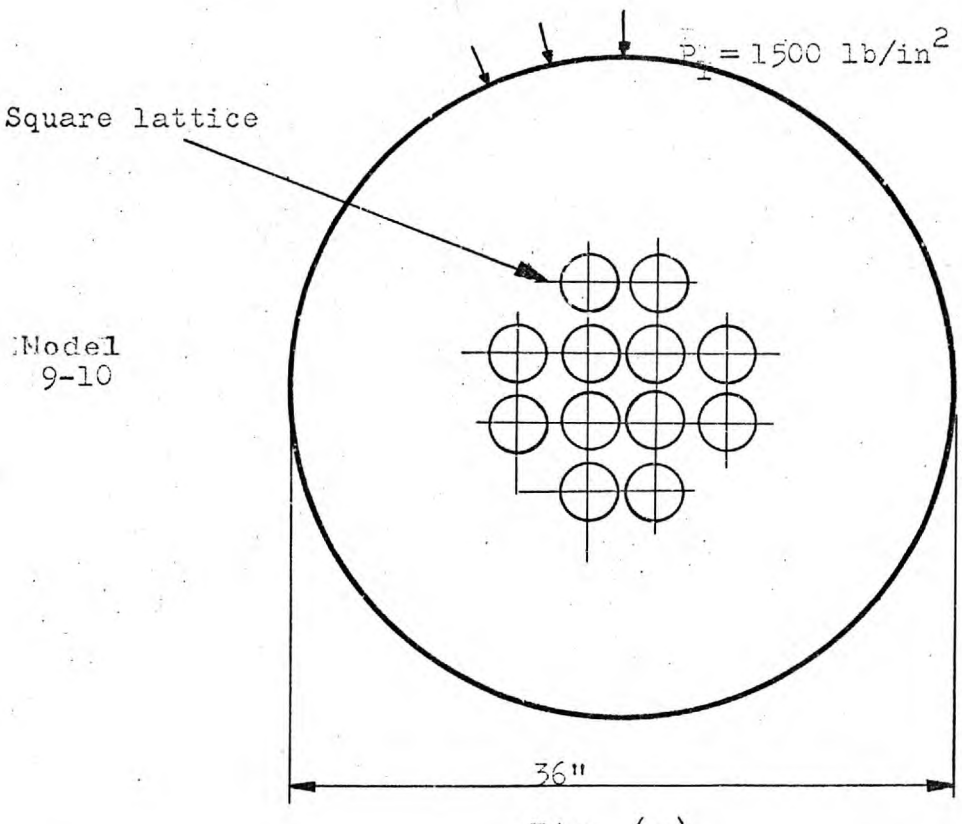

Fig. (e)

FIG. 1.12

However, since it is not possible to identify the effects of creep and shrinkage separately in a single specimen, it was also necessary to test other control specimens in which creep and shrinkage could be separately quantified.

To achieve this, four smaller control specimens were cast, two of them solid, and two perforated with a pattern of holes identical to that in the center of the large composite specimen.

The holes in the small perforated control specimen covered the whole of its surface and the diameter of this small specimen was identical to the diameter of an imaginary circle drawn around the perimeter of the perforated zone of the large composite specimen. The small solid specimens were also of this diameter.

Accordingly, since the testing programme allowed for simultaneous rim loading of the large composite specimen, and one solid, and one perforated small specimen, and also allowed for the unloaded shrinkage of the other small solid and perforated specimens, it became possible to obtain the values of all the separate strain-causing effects, i.e., the elastic, the creep and the shrinkage effects of all the specimens.

In addition, at the heating stage of the programme, the thermal expansions caused by the uniform temperature of 80°C which was applied to all five specimens could be experimentally measured.

In the theoretical analysis which has been proposed in order to take into account the time-dependent strains, it was essential to be able to incorporate creep and shrinkage data from experimental observations on the actual concrete in the models. Thus, strains were obtained after subtracting the shrinkage strains measured in the small unloaded shrinkage specimen, from the combined creep and shrinkage strains measured in the identical small loaded specimen.

The creep data thus evaluated were in fact, plotted in the form of specific creep curves.

By similar simple arithmetical subtraction, each of the effects of elastic loading, creep, shrinkage and temperature were made available for use in the subsequent calculations. These data, in fact, became available, for both solid and perforated concrete areas, for ambient and elevated temperature regimes, and at any age of the concrete.

In fact, this data could have been obtained either by calculation or graphically, since all strains - total and net, have been plotted separately for all specimens. Similarly, since load cycling was carried out on all the loaded specimens at each change of test regime, the various concrete constants required, also became available for insertion in the calculation. To obtain some of these constants, control tests described elsewhere in this thesis, were necessary, e.g., tensile tests, coefficient of thermal expansion tests, and crushing strength tests on separate specimens cast at the same time as the main five specimens and of the identical concrete mix.

As for the phasing of loading and heating in the test programme, these were arranged to be representative, approximately, of the commissioning procedures, of an actual roof cap of a full-scale reactor vessel. For example, the early period of cold loading represents the initial period of applied prestress before the reactor becomes critical and the heating phase in the experiment simulates the period either during commissioning or operation when the end cap is both hot and prestressed.

Subsequently, a typical shut down of the reactor involving cooling of the slab whilst the peripheral prestress is still operative is represented by the cold loaded phase of the experiment.

The periods under each loading or heating phase were chosen to permit the concrete adequately to display the effects consequent upon each condition.

The readings during each phase were taken over a period sufficiently long to allow meaningful curves to be plotted even where the strains were of a low order, and thus to be able clearly to identify trends. This procedure allowed for the situation where the readings might be subject to some experimental or observational variation.

CHAPTER II

A REVIEW OF LITERATURE RELATING TO MATERIAL PROPERTIES AT ORDINARY AND ELEVATED TEMPERATURES WITH SPECIAL REFERENCE TO THE PRESENT INVESTIGATION

2.1 Introductory Note on Creep and Shrinkage.

The mechanical properties of a material in general, whether at the atomic, molecular, microscopic, macroscopic or phenomenological dimensional levels, are expressed in terms of relations between the forces acting on it, the deformations that result, and their variation with time.

The ever-increasing demands of economy require the design of plain and reinforced concrete to be based on more reliable knowledge of its mechanical properties.

Since creep and shrinkage are mechanical properties of structural concrete, an understanding of these two phenomena is of great importance not only from a structural point of view, but also in the domain of properties of concrete.

Creep and shrinkage which are both expressed in terms of strain, have important effects on the stresses and deflections of concrete structures.

Most available information relating to creep and shrinkage of concrete have been obtained either from laboratory or field tests.

Although the two properties are intimately related since both involve a change in strain due to

moisture movement, they are determined separately in the laboratory.

2.2. Mechanisms of Creep and Shrinkage.

Creep is a time-dependent strain (shortening or lengthening) resulting from mechanical loading, the total amount of which increases at a decreasing rate from the time of loading. Creep is also proportional to the applied stresses (for low stress levels).

Shrinkage is also a time-dependent strain which increases at a decreasing rate and occurs, with or without the application of mechanical loads, from water evaporation.

Various theories of the mechanism of creep have been proposed to explain this behaviour. (1)*. The most widely supported of all is the one combining of the following two:-

a) The Seepage Theory:

Creep and shrinkage are due to the movement or expulsion of gel water from within the gel pores. Creep results from water migration from small spaces or pores in the gel under the action of the external load, and shrinkage from water evaporation.

b) The Viscous Theory:

On loading a specimen, viscous flow of the cement paste occurs, and as a result load is transferred from cement to aggregate. Creep is therefore,

---

* Numbers in parenthesis refer to those given in the list of references at the end of this thesis.

considered to be a shear process of multi-plate crystal surfaces sliding one over the other, lubricated by water.

The Seepage Theory implies that when all the water is squeezed out from the appropriate places in the gel, there can be no further creep. Furthermore, if a dry specimen under compression is wetted, the total expansion must exceed the creep contruction.

The Viscous Theory implies that moisture movement is not essential, but it may facilitate creep.

The assumption that shrinkage in a given concrete, depends on its moisture content and age, is a rather elusive quantity.

Shrinkage is now generally assumed to be made up of two parts:-

a) Due to the free moisture (drying or ecological shrinkage).

b) Due to the chemical changes occuring in the hydration of the cement (intrinsic shrinkage).

The former appears to be a predominant effect.

2.3. Separation of Creep from Shrinkage, Elastic and Thermal Strains.

When a specimen is subjected to sustained loading and elevated temperatures, the total strain observed experimentally will be a combination of four different effects:-

$$e_T = e_e + e_c + e_s + e_t \qquad \ldots\ldots \quad 2.1.$$

To obtain the creep strain e_c, the elastic e_e, thermal e_t, and shrinkage e_s, strains must be deducted. The elastic strain can be measured directly. The thermal strain may be obtained if we know the

coefficient of linear expansion of the concrete, and the shrinkage strain may be obtained from unloaded control specimens kept under the same conditions as the loaded specimens.

Creep strains are isolated on the principle that creep and shrinkage strains are additive.
Strictly speaking, creep strains may be measured if creep is independent of shrinkage. However, there is an inter-dependence between these two phenomena, and the above principle is not absolutely true.

The assumptions here are:-

i) that loading does not inhibit shrinkage.
ii) that non-uniform shrinkage does not increase the stresses.

A large number of investigators deduct a constant instantaneous strain from the overall measured strains assuming that the value of the Young's modulus of concrete does not change. This is again not strictly true.

2.4. Characteristic Creep Curve.

Fig. 2.1 shows the longitudinal deformations of a typical concrete specimen subjected to a constant uniaxial compression for a considerable time before unloading.

On loading there is an instantaneous strain e_o, followed by a gradually increasing strain called the inelastic or creep e_c strain.

On unloading there is an instantaneous or elastic recovery e_{el}, followed by a delayed inelastic or

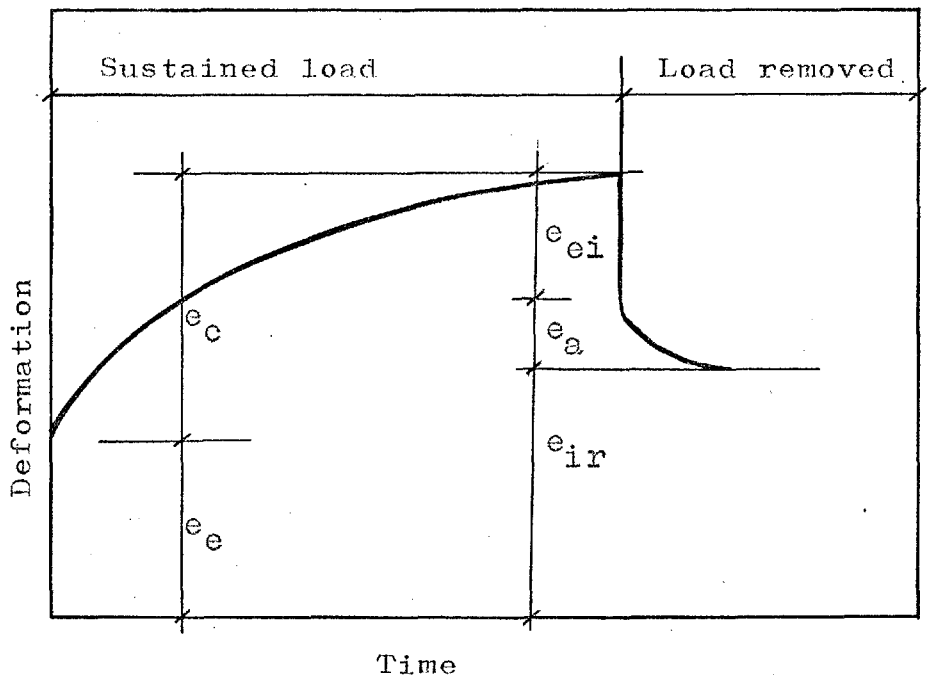

FIG. 2.1. CHARACTERISTIC CREEP CURVE

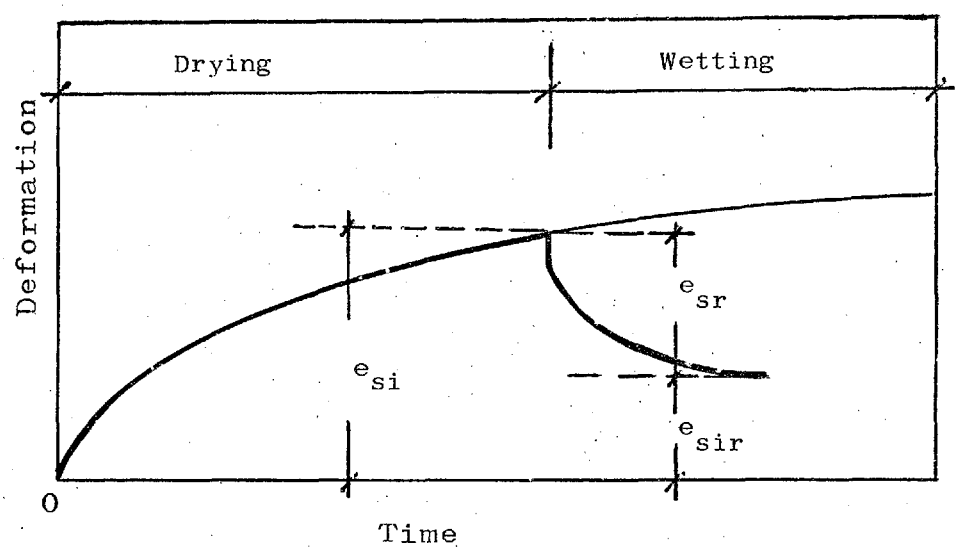

FIG. 2.2. CHARACTERISTIC SHRINKAGE CURVE

e_{si} = Initial shrinkage

e_{sr} = Reversible shrinkage

e_{sir} = Irreversible shrinkage.

creep recovery e_a, but eventually, a residual or irrecoverable deformation e_{ir} remains.

Such creep behaviour has long been recognised and despite the vast amount of literature available, the actual mechanisms of creep are still the subject of much controversy.

2.5. Characteristic Shrinkage Curve.

The shrinkage-time curve has the same shape as the creep-time curve differing only in magnitude. (Fig. 2.2). The magnitude of shrinkage could be of the same order as creep if the specimens are loaded to their working stress.

2.6. Variables Influencing Creep and Shrinkage.

Creep and shrinkage in concrete could be affected in various ways. According to Troxtel, Raphael and Davies, (2), some of these factors are:-

a) the aggregate - cement ratio.
b) the water - cement ratio.
c) the composition and fineness of the cement.
d) the nature of the aggregate and its texture.
e) the maximum size of aggregate.
f) the magnitude of the applied stresses.
g) the conditions of curing.
h) the size of test specimen.
i) the age of specimen at time of loading.
j) the duration of loading.
k) the presence of strain induced by the reinforcement.
l) the ambient relative humidity.
m) the temperature.

2.6.1. Effects of Cement, Cement Content and Cement Paste.

The effect of cement type upon creep is related to the rate at which hydration occurs. The lower the rate of hydration, the higher the creep rate (3).

Fineness of the cement does not appear to have any significant effect on the creep properties of mortars and concretes (4).
Davis et al (3), confirms that creep is proportional to the cement content and to the water/cement ratio.

Shrinkage is affected by both type and fineness of cement. Ordinary Portland cement shows least shrinkage, whereas, Low Heat and Portland pozzolana (5) cements exhibit an increasing shrinkage.
Davis et al, investigating the cement effects for the Hover Dam reported that fine cements exhibit a slight increase in shrinkage (6).

The water/cement ratio is one of the major factors influencing shrinkage in concrete (5).
Experiments on concrete with varying water/cement ratio show that shrinkage is proportional to this ratio.

Cement paste is the basic component responsible for creep in concrete, the presence of aggregate simply modifying the creep magnitude. Neville (7), has shown that mixes having the same paste content develop the same proportion of their long-term creep after any given time, independently of all other variables.

2.6.2. Effects of Magnitude and Type of Stress on Creep and the Age of Specimen when First Loaded.

Creep is proportional to the applied stress (7), (8), (9), for stress less than 75% of the ultimate.

Above this level the proportionality no longer holds and thus, creep produces "time failure." At low stress levels the effects of shrinkage over-ride the effect of creep (10).

The above conclusions have been drawn from uniaxial, compressive and bending tests on concrete. However, creep tests carried out under tension (11), torsion (12), two (13), or three (12) dimensional stress, do not indicate otherwise. Identical specimens (14), were found to creep more in tension than in compression. Ishai (15), reported that torsional creep exhibits the same components of flow as under uniaxial stress.

The rate of creep and the ultimate magnitude of creep are reduced when the age at which the loading is applied increases (16), (17),under normal temperature. This is possibly due to the development of strength with age of concrete (18), (19), (20).

It is well established that the strength of concrete is a function of the degree of hydration, and the ultimate magnitude of creep decreases for an increase in hydration. It may also be said that creep varies inversely as the strength of concrete. At later ages, however, the creep rate becomes independent of age at loading.

2.6.3. Effect of Type and Grading of Aggregate.

It has been shown that the type of aggregate affects the creep. Stiffness and porosity of aggregate influence the creep of concrete considerably.

Concretes with sandstone aggregates exhibit more creep whereas, limestone aggregates creep less, (1300.10^{-6}in/in, 550.10^{-6}in/in), for a stress of 800psi., over five years.

eep also decreases as the maximum size of aggregate ncreases.

The aggregate if well compacted, with the particles interlocked, forms a firm structural framework which resists creep deformation.
The type of aggregate also influences the amount of shrinkage of the concrete (21).
Shrinkage also decreases as the maximum size of aggregate increases.

2.6.4. Effect of Curing and Storage Conditions.

The effect of curing influences creep in two ways:-

1) by affecting the rate of hydration of cement. The hydration is more rapid for moist-cured concretes than for air-cured, and hence, creep is reduced.

2) by producing either pre-swollen specimens from moist-curing, or pre-shrunk specimens from dry-curing. Pre-swollen specimens would exhibit more creep than the dry-cured specimens.

Low-humidity storage produces higher creep strains (16) possibly due to the easy escape of the expelled gel water.

Water-stored specimens exhibit less creep than air-stored specimens while creeping. Changing the humidity or alternate wetting and drying increases the creep.

The effect of the duration of curing on the magnitude of shrinkage is small if allowance is made for swelling during moist-curing. At low ambient relative humidity, the shrinkage is much greater.

The shrinkage rate is proportional to the ambient temperature.

2.6.5. Shape and Size of Specimen as Affecting Creep.

Creep values tend to decrease as the size of the specimen increases. This is possibly due to a lower rate of drying shrinkage (9), (22).

Basic creep is probably unaffected by changes in size and shape of member; but drying creep is. Hansen and Mattock (12), found that the rate and the final values of creep and shrinkage decrease as the member becomes larger. For very large members the creep approached the value of basic creep as determined from a sealed specimen.

Ross (23), found that creep is a function of volume/surface ratio. However, for later ages shrinkage and creep is independent of the size of the specimen (22), (24).

2.7. Creep Related to Strength at Ordinary Temperatures.

As previously discussed, limestone-concretes creep less than half of that of sandstone-concretes. Increase of cement paste content in concrete increases its creep considerably (2). Concrete specimens loaded at later ages exhibit less creep than those loaded at earlier ages. Concretes of higher water/cement ratio, creep more than those made with lower values of water/cement (25). In general, a reasonably good correlation can be obtained, under constant storage conditions, between creep of concrete and its strength (10), (26). The stronger the concrete, the less its creep.

2.8. Delayed Elasticity and Viscous Deformation.

It is well known that creep recovery takes place when a specimen in unloaded. This has led a number of investigators (27), (15), (28), to postulate that creep consists of two parts:-

i) a reversible creep - also known as delayed elasticity.

ii) a non-reversible creep, analogous to a viscous deformation.

This has further led to a number of rheological models being postulated for explaining creep behaviour and also to serve as a basis for incorporating creep in the structural analysis. A simple model was suggested by Ross(29).

2.9. Basic Creep and Drying Creep.

Many investigators have proved that drying concrete creeps more than a concrete which is not drying. Also, alternate drying and wetting increases creep considerably. In order to explain these phenomena, creep is said (27), (30), to consist of two parts:-

i) Basic creep, occurring in the absence of moisture migration.

ii) Drying creep, occurring in excess of basic creep under conditions of moisture change.

2.10. Specific Creep and Creep Coefficient.

As creep has been found to be proportional to the applied stress, within limits of 30 to 50% of ultimate strength, the term specific creep or unit creep is used to denote creep strain per unit stress.
The term creep coefficient is used to denote the ratio of the ultimate (long-term) creep strain to the instantaneous elastic strain under a load.

2.11. Effects of Reinforcement on Creep and Shrinkage.

Apart from the stresses developed in the concrete and steel due to the action of the applied load, it is possible for substantial stresses to be developed as a result of creep and shrinkage of the concrete.

Creep is useful in that it permits a redistribution of the state of stress with time.

Hence, highly-stressed zones of a concrete structure will tend to shed some of the load to less highly-stressed parts which permits a better use of the load-carrying capacity of all parts of the structure. This is true in special cases only.

However, in prestressed concrete construction the creep of concrete has its disadvantages in that the inelastic displacements lead to significant reduction in the initial prestressing force provided by the stretched high tensile steel wires or tendons.

In reinforced concrete beams subjected to transverse loads, the concrete below the neutral axis creeps in tension, and that above creeps in compression.

The tensile creep of concrete transfers the tension to the steel in the tensile zone, and the concrete stress will decrease with time. The same will apply to the reinforcement in the compression zone (31).

Shrinkage in the tensile zone is restrained by the steel causing additional compressive stress in the steel and tensile stress in the concrete.

In reinforced columns, creep and shrinkage of the concrete will transfer the load from the concrete to the steel (3).

2.12. Creep at Elevated Temperatures.

When concrete is subjected to constant elevated temperatures or temperature gradients its creep and shrinkage characteristics are affected considerably.

In general, temperature affects drastically most of the elastic properties of concrete. Creep and shrinkage are increased with temperature, whereas, the elastic modulus, and the compressive and tensile strengths decrease.

The influence of temperature on the various properties of concrete has been taken into account by Murashev (32), and Kurenkov (33), concerning design methods for plain and reinforced concrete structures in Russia.

The first experiments on concrete at elevated temperatures were carried out with the aim of studying the creep effects, crack-formation and crack-propagation effects in mass concrete.

During the hydration period, heat is generated causing a rise in temperature. The temperature rise is very high for massive structures such as Dams. It may be of the order of 40°C to 60°C, (34).
If the concrete is restrained, compressive stresses are set up which in turn are reduced due to creep relaxation. Subsequent cooling results in tensile contraction stress causing cracks.

Lee (35), confirmed that rapid cooling causes cracking, but gradual cooling minimises the tensile stress, and cracking may be avoided.

From tests which he carried out at constant temperatures on sealed specimens, he confirmed that creep magnitude and creep rate increase with temperature at early ages.

Theuer (36), tested small concrete cylinders at temperatures ranging from 26°F to 123°F for saturated, dry and semi-dry concrete. Two types of concrete were tested, namely "strong" and "weak" concretes. He found for both types of concrete, when in a saturated or semi-dry condition, the time-deformations (creep) as well as the residual deformations (after unloading) were greater, the higher the temperature of the concrete. For oven-dry specimens, he found that creep-deformations to be relatively small and practically the same for all test temperatures.

England and Ross (37), found that the creep of concrete increases as with temperature for both sealed and unsealed specimens. The test temperatures ranged from 20°C to 140°C. The increase was not linear; but within a range of 20°C to 80°C the increase was practically linear. (Figs. 2.3, 2.4).

Nasser and Neville (38), found that creep increased with temperature upto about 70°C at high stress-strength ratios (above 0.6), and thereafter decreased. The specimens which they tested were sealed and water-stored.

At lower stress-strength ratio (0.35), creep continuously increased upto 90°C. Beyond this temperature the pattern was irregular. Creep was found proportional to stress at these elevated temperatures as well, even for stress-strength ratios as high as 70%. Creep recovery seemed to be independent for both temperature and of the magnitude of the stress that had been removed and such a recovery was much smaller than the preceding creep.

Arthanari and Yu (39), also found that the specific creep after any specified time showed more or less linear variation with temperature, under both

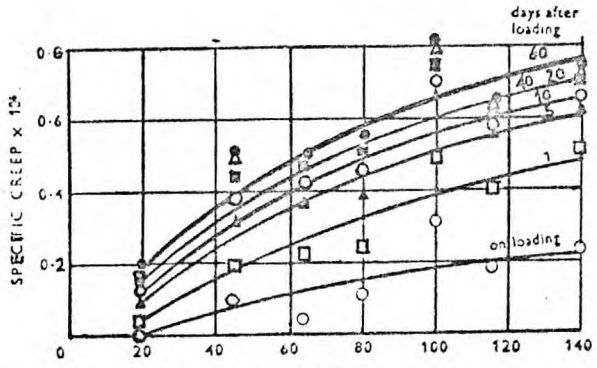

FIG.2.3.

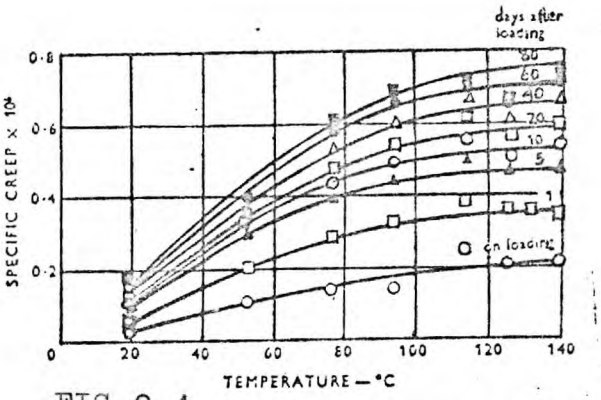

FIG.2.4.

Variation of specific creep with temperature and time for unsealed and sealed specimens.

From England and Ross

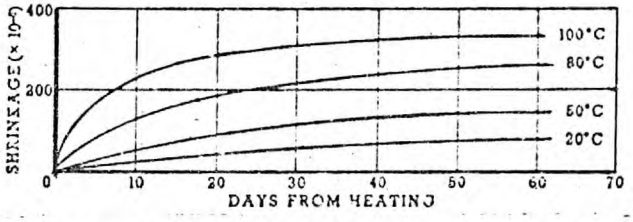

Variation of shrinkage with time for unsealed specimens maintained at various constant temperatures.

FIG.2.5. From England and Ross

uniaxial and biaxial systems of loading. The temperature range in their tests was between 20°C to 80°C.

Tensile creep, too, was found to increase with temperature by Hannant (40). He also stated (41), that the increase in creep is linear between 27°C and 77°C.

From the extensive load-deforation measurements made on sealed concrete specimens cast from the Wylfa Prestressed Concrete Pressure Vessel mix, Browne (42), reported that creep increased rapidly as the sustained temperature level was raised from 20°C to 94°C, and thereafter creep levelled off.

2.13. Discussion.

All available data show an increase in creep for concrete specimens at elevated temperatures. Most of the tests were conducted in the range of 20°C to 60°C, and show that creep is approximately proportional to temperature in that range. England and Ross (37), found the proportionality to exist upto 70°C.

Concrete at elevated temperatures will crack if cooled rapidly. This effect may be explained by the large creep rate which reduces the compressive stress in the initial period of rising temperature. When the temperature begins to fall, these compressive stresses are reduced to zero, and with further cooling tensile stresses develope. Concrete of course, creeps in tension, but at this stage the concrete is more mature and creeps very little, so cracking may finally occur.

2.14. Shrinkage at Elevated Temperatures.

Shrinkage also increases with temperature and tends to stabilize more quickly at higher temperatures.

A heated specimen looses more water in reaching moisture equilibrium with the surrounding atmosphere, than a non-heated specimen.

Although shrinkage is not proportional to water loss, an increased water loss generally causes increased shrinkage.

The shrinkage rate under high temperature falls off later more rapidly when the water to be drawn out becomes small.

England and Ross (37), working on reinforced concrete under thermal gradients plotted curves for shrinkage at different times for concrete heated to various constant temperatures. The concrete was a 1; 2; 4; mix, with a water/cement ratio of 0.45 and tested at 14 days.

It can be seen that higher temperatures cause a large increase in the rate of shrinkage and after 60 days at 100°C, it may be 4 to 5 times the value at ordinary temperatures. Fig.2.5 , (page 51).

Saemann, Warren and Washa (43), working on the effects of curing on shrinkage observed an increase in the water loss and also in the rate of water loss in the first day of drying.

Stress appears to increase the shrinkage effect (44), (7), but such inter-relationships appear to be secondary, and have indeed, been ignored by most investigators.

C H A P T E R III

ELASTIC CONSTANTS OF THE MATERIALS - EFFECTS OF AGE AND ELEVATED TEMPERATURES

3.1. Introduction.

Before an analysis of a structure can be made with confidence, it is clearly important to know the elastic constants of the materials involved and their variation with time and temperature.

Some of these constants, such as the compressive and tensile strengths of concrete are needed in order to assess the safe limits of stress while a few others, such as Young's modulus and the elastic Poisson's ratio are required actually to evaluate the stress.

Age and elevated temperatures affect the values of these parameters. In this chapter a review is made of the literature regarding such effects.

3.2. Compressive Strength of Concrete.

The compressive strength of concrete changes considerably with age and temperature. For moist-cured concrete the strength increases with age, but a sudden withdrawal of moisture especially at an early age, arrests the process of hydration (10), causing a small "spurt" in the strength. Thereafter, the strength decreases with age, though slowly.

Glucklich (45), considering the test results of Rusch and others, concludes that the strength of concrete under sustained loading, is considerably lower than its "short-term" strength. Roll (46), however, found that there was an increase in strength due to sustained loads.

Fulton (47), states, "from an extensive search of the literature, it would appear that the consensus of expert opinion is that under long-term loading, failure occurs at stresses well below the ultimate as determined by normal test procedure."

The strength of concrete is affected in two ways when the concrete is subjected to elevated temperature.

If the elevated temperature is applied at an early age the concrete gains strength rapidly due to the higher maturity; on the other hand, the strength stabilises very quickly due to high water losses (48), and over a period, a reduction in the strength may take place (47). Also, a specimen of mature concrete when subjected to a uniform temperature rise exhibits a compressive strength lower than that of a similar specimen maintained at ambient temperatures.

Malhotra (49), found that the "residual" strength of concrete, after heating was removed, was approximately a fifth less than the "hot strength." Saemann and Washa (50), concluded that the compressive strength of concrete showed a decrease of about 10% when the temperature reached a range of $90^{\circ}C$ - $100^{\circ}C$.

3.3. Tensile Strength of Concrete.

The tensile strength of concrete is closely related to the compressive strength of concrete. Neville (10), states that the ratio of tensile strength to compressive strength is affected to some extent by the properties of fine aggregate, grading of the aggregate, age and curing conditions. In general, this ratio diminishes as the compressive strength increases.

It is possible that at elevated temperatures, the tensile strength of concrete decreases at a more rapid rate than the compressive strength. The strength in flexure of concrete (50), decreases somewhat more than the corresponding decrease in compressive strength. Hannah (51), found that such a loss in compressive strength could reach 40% of the ambient strength even at 90°C.

3.4. Poisson's Ratio for Concrete.

For concrete under long-term tests three types of Poisson's ratios may be recognised.

1) the conventional Poisson's ratio; it is obtained by measuring the immediate deformations on loading.

2) the creep Poisson's ratio; which is obtained from longitudinal and lateral deformations that occur in addition to the "immediate" deformations.

3) the effective Poisson's ratio; which is obtained from the total deformations, that is, from the sum of immediate and creep deformations.

If the first two have the same magnitude (at a given time), the third will also have the same value.

Kordina (52), found the effective Poisson's ratio to increase between 25% and 33% over a long period of time under sustained uniaxial loads. Davis and Troxell (53), found that the creep Poisson's ratio increased with age, but became constant after 500 days of sustained loading.

Ross (13), however, surmised that the creep Poisson's ratio approximates to zero. Duke and Davis (54), who conducted uniaxial and triaxial compressive creep tests, concluded that Poisson's ratio remains constant during the creep process of concrete.

Tests carried out by Hermite (55), showed that the lateral to axial time-dependent deformation was similar to the elastic Poisson's ratio upto 200 days. Hannant (41), who investigated the strain behaviour of concrete upto 95°C for different types of stresses and sustained loading, concluded that the creep Poisson's ratio is similar in magnitude to the elastic Poisson's ratio.

Results carried out by the United States Bureau of Reclamation (56), showed that there was no significant change in Poisson's ratio with time.

3.5. Modulus of Elasticity of Concrete.

At ordinary temperatures there is a considerable degree of correlation between the modulus of elasticity and the strength of concrete (27). A wet specimen has a higher modulus than a dry one (53), but strength decreases with increase in moisture content. The properties of the aggregate influence the modulus much more than they do to the compressive strength; at later ages the modulus increases more rapidly than the strength (10). Davis and Troxell (53), found the modulus to decrease under sustained stress, while Washa and Fluck (31), found it to increase.

At elevated temperatures, the strains obtained from a loaded specimen are greater than those obtained at ambient temperatures. There are two main explanations for this:-

i) part of the increase is caused by the increased creep at elevated temperatures.

ii) part of it is caused by a reduction in the elastic modulus.

Philleo (57), found the dynamic modulus of elasticity to decrease with an increase in the test temperature. At about 90°C, the dynamic modulus was about 0.86 - 0.89 of the dynamic modulus at room temperature. Saemann and Washa (50), found the static modulus to decrease between 10% and 25% as test temperatures were raised to about 100°C.

Hanson (27), has proposed that the value of the elastic modulus at a given temperature can be found from the following relation:-

$$E = A - BT \qquad \ldots\ldots \quad 3.1.$$

Where: E = is the elastic modulus
T = is the temperature in degrees absolute and,
A, B are empirical constants.

Serafim and Guerriro(58), observed a reduction of 10% in the elastic modulus at 45°C from that at room temperature for young concretes.

England (59), loaded some specimens sealed against moisture loss and also some unsealed specimens to 100 psi., at various temperatures in the range of 20°C to 140°C. After 80 days, of sustained loading, the loads were removed and the modulus of elasticity obtained on unloading showed a general reduction of 20% - 25% from 20°C to 100°C, for sealed and unsealed specimens.(Fig.3.1). Glucklich and Ishai (28), also found that the modulus of elasticity reduces with temperature.

It appears that the decrease in the modulus occurs immediately after heating (or, immediately after first loading if heating has been applied earlier on).

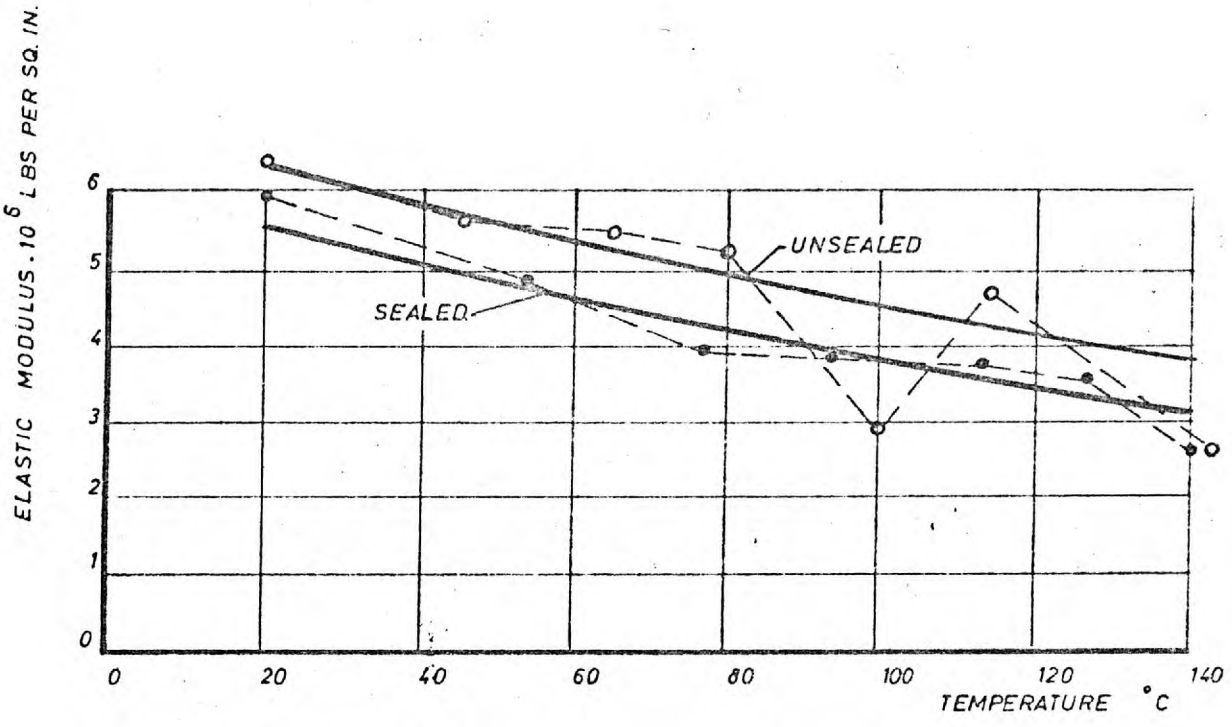

VALUES OF E_c CALCULATED FROM STRAINS ON UNLOADING, FOR SEALED AND UNSEALED SPECIMENS LOADED TO 1000 LBS PER SQ IN.

FIG. 3.1. (a)

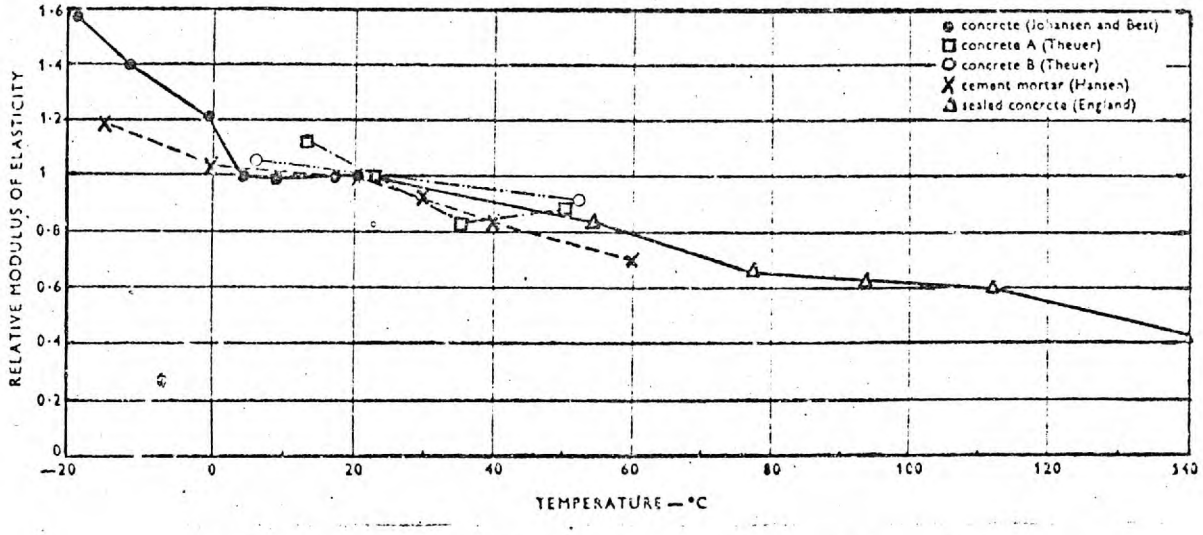

Effect of temperature on modulus of elasticity of concrete

From Ross, Illston and England

FIG. 3.1. (b)

Sustained heating does not seem to cause much further reduction of the modulus either for sealed or unsealed specimens (41).

3.6. Coefficient of Thermal Expansion of Concrete.

When the concrete is heated, its volume increases. The coefficient of expansion is the linear coefficient and is given as a strain increase per unit increase in temperature. An accepted value for the coefficient of concrete in this country and in U.S.A., is 5.5 x $10^{-6/°F}$, or 9.9 x $10^{-6/°C}$. For concrete made of different aggregates (28), this value may vary from 6.1 to 13. 1 x $10^{-6/°C}$, depending on:-

a) the range of temperature of test.

b) the age of concrete.

c) the ambient relative humidity.

Phillco (57), found that below 500°F the coefficient of linear expansion of concrete was the same (57) as that at room temperature, but above 800°F, the coefficient was higher. It decreased by an increase in age and decreased also by an increase in Relative Humidity (57).

The value of the coefficient of thermal expansion of concrete depends both on the composition of the mix and its hygral state at the time of the temperature change (10).

Browne (42), has demonstrated using the results of Meyers, that as concrete dries from saturation level, the coefficient increases to a maximum when the relative humidity is about 70%, and further drying causes a slow decrease in the value of the coefficient.

Sealed specimens tested by Browne indicated only slight changes in the value of the coefficient for various ages of concrete at test.
This is confirmed by Arthanari (60).

Browne (42), has suggested that the coefficient for concrete during the first heating may be greater than for cooling and subsequent thermal cycling. Philleo (57), found that the concrete cools with a lower coefficient while Hannant (40), concludes from his tests that the coefficient would decrease with time under heating.

Salmanov (61), gives the following empirical expression governing the coefficient of expansion $\alpha_{\delta t}$ of concrete at any temperature.

$$\alpha_{\delta t} = \alpha_{\delta} + \frac{K(T - 50)}{650} 10^{-6/^{o}C} \qquad \ldots\ldots \quad 3.2.$$

Where: α_{δ} = coefficient of linear expansion at normal temperature (normal temperature has not been defined).

K = coefficient depending on the kind of aggregate (may be 4, for ordinary concrete).

T = temperature of concrete at which the coefficient is required in ^{o}C.

This formula indicates that temperature has an extremely small effect on the coefficient of linear expansion of concrete.

3.7. Heat Flow Factors.

To determine the temperature distribution in a concrete mass, at any time after placing the heat generation characteristic of cement, the thermal properties of concrete, the initial and boundary conditions and details of the procedure of construction are needed (62).

Ross and Bray (62), have indicated step-by-step methods for the purpose among others.

The heat generation characteristic of the cement can be obtained from numerous publications available, for exapple, the one published by Davey and Fox (63).

The thermal properties of concrete that are required are termed the heat flow factors of concrete. They are:-

Thermal conductivity, specific heat, density and thermal diffusivity.

Brewer (64), finds that the conductivity of concrete varies directly with unit weight and free water content of the concrete. He gives curves and tables from which the conductivity can be estimated as the unit weight and moisture content change.

Klein, et al. (65), discusses the effects of adiabatic curing on these factors and finds them to be significantly different from those obtained from ordinary laboratory specimens cured in the normal manner. Diffusivity which in general, is calculated from conductivity and heat capacity per unit volume, is found by them to decrease by about 20% as the temperature increased through 55°C. The type of coarse aggregage used, also affects diffusivity significantly. For ordinary Portland cement concrete, the suggested (63) range of the values of diffusivity is 0.008 - 0.010, in C.G.S., units, the higher values applying for younger concretes.

C H A P T E R IV

METHODS OF TIME-DEPENDENT ANALYSIS

4.1. General Considerations.

The time-dependent structural analysis may be classified into two main types:-

a) the direct or one-step methods.

b) the time-step or iterative methods.

The most accurate ones are considered to be the iterative methods which provide accurate solutions for any time and loading conditions, with a disadvantage that they require long running times on large computers. On the other hand, the direct methods require less time for the solution, but their applicability is limited to a certain type of problems.

A number of existing methods relating to time-dependent analyses, applicable to two-dimensional concrete structures subject to long-time loading, are discussed briefly in this chapter. In addition, a few of them which appear promising are developed in detail for purposes of carrying out the analyses. Though the basic principles of the adopted procedures may be suitable for any two-dimensional problems, the equations have been derived with reference to the radially-loaded and uniformly-heated slab.

It is intended, furthermore, to quote certain creep strain expressions which have been used in the past. These are listed in a subsequent section of this chapter.

4.2. Assumptions made in the analysis.

It has been assumed that the behaviour of the material will be such that creep strains occuring at any point of the structure can be considered as proportional to the stress and are affected by the temperatures in a manner as prescribed by a specific thermal creep law.

A further tacit assumption is that the nature of creep of the material is similar in both tension and compression.

4.3. How creep of concrete at ordinary temperatures has been considered.

Since, at working loads, creep strain of concrete can be considered as proportional to the stress at any given time, a reduced value for the modulus of concrete can be adopted such, that the new modulus would indicate the sum of elastic and creep strains. The modular ratio can be estimated using this reduced modulus for concrete.

In conventional reinforced concrete design, such a modular ratio, is utilized, and the analysis of structures is further carried out as if the whole structure is elastic, and is under short-term only.

In a linear or two-dimensional structural analysis of a load -induced problem as distinct from a displacement-induced problem, it is seen that the distribution of stress resultants over a structure is not affected by the actual value of the modulus of elasticity of the material as long as the stress proportionality with strain is assured, and the relative values of the modulus do not change at the various parts of the structure.

In effect, no redistribution of stresses can occur, due to creep of concrete, in structures that are subject to ordinary working loads, provided the creep is uniform at all parts of the structure. For such problems, the conventional approach of disregarding creep except to adopt a reduced modulus, seems to be justified.

In the analysis of prestressed concrete structures, the modulus of elasticity of concrete is not reduced, but allowance is made for the losses of prestressing forces that occur due to the creep of concrete. The methods used to estimate such losses of prestressing forces are not discussed here. Leonhardt (66), discusses a number of cases of prestressed concrete sections in the methods which he has given.

Ross (67), has used an affective modulus (which is obtained as the reciprocal of the sum of initial-elastic and creep strains for a unit stress), in his method for determining the loss of prestress.

4.4. How creep is estimated at elevated temperatures.

Even where a certain amount of experimental data from a laboratory is available, it is difficult to estimate the creep of various structural members made of a particular concrete, subject as they are to changing conditions of temperature and humidity. Where no experimental data is available for the concrete mix to be used, the task is harder still.

Ross (68), using the formula that goes under his name, evaluated the constant, b, from the test results of many investigators, and produced a chart from which a designer can read off the value of b,

knowing the water/cement ratio, the stress level, the relative humidity, the age of the concrete at loading, and the size of member. He further suggested that a value of 100 x b, be assigned to the constant a. The chart, generally, governs the range of handrodded concretes of low strengths. In a subsequent paper (67), he published a table from which the creep of high strength concretes can be estimated.

Leonhardt (66), suggests that the creep strain e_k of a concrete be estimated as:-

$$e_k = e_e \cdot \emptyset \cdot k_1 \cdot k_2 \qquad \ldots \quad 4.1.$$

Where e_e = is the instantaneous strain on loading,

$\emptyset$ = is a coefficient dependent upon the humidity surrounding the structure,

k_1 = a coefficient dealing with the degree of hydration at the age of loading,

k_2 = a coefficient taking account of a characteristic value, k_w, the value of which is arrived at from the water/cement ratio, mortar content, cement content and the thickness of the member.

Hansen and Mattock (12), arrived at a formula very similar to that of Lorman, stating that:-

$$c = \frac{K \times t}{N + t} \qquad \ldots 4.1.(a)$$

Where c = is the specific creep,

K = is the ultimate specific creep and,

N = a constant. They gave the value for N as:-

$$N = 26.0\ e^{0.36(v/s)} \qquad \ldots 4.1.(b)$$

Where e = is the Naperian base and,

v/s = is the volume/surface of the structural member. They stated that, apparently, for a variety of concretes, the value

of N is the same, though the value given above was found from two types of concretes loaded at the age of 8 days and exposed to one value of relative humidity. The value of K has still to be estimated by other means.

Hansen (27), from a "theoretical" consideration of the delayed elasticity and viscous behaviour of concrete, derived a specific creep equation in terms of the water/cement ratio, the volume concentration of cement paste, the type of cement, the age at loading, and the time under sustained loading. With suitable assumptions, the basic creep of a concrete can be predicted from the expression given by him.

4.5. Creep - Temperature - Time Relationship Specific thermal creep.

At elevated temperatures upto a certain temperature limit, creep has been found to vary very nearly linearly with temperature by a majority of the investigators. This limit varies from 70°C to 94°C. Also, at these temperatures, creep is still seen to be proportional to the applied stress, in a manner similar to creep occuring at atmospheric temperatures. Accordingly, it should be possible to represent the creep-temperature-time relationship by expressions similar to those indicated earlier, making a suitable modification for the temperature level.

Browne (42), has used the expression:-

$$e = f(K\theta) + f'(K\theta) \log_{10} (t + 1), \quad \ldots 4.2.$$

Where

e = specific strain, i.e., the sum of elastic, and creep strains per unit stress

K = age at loading (and heating)

t = time after commencement of loading

θ = temperature of the concrete under load

$f(K\theta)$, $f'(K\theta)$ = (experimentally determined factors,)which depend on K and θ

This expression is very similar to the U.S.B.R., expression for creep of concrete at ordinary temperatures. From the extensive experimental data he had at his disposal, it was possible for him to arrive at the values of $f(K\theta)$, and $f'(K\theta)$, at various temperatures and for ages of loading varying from 7 to 400 days. He was able to accommodate the variations in the instantaneous elastic strains in his expression.

However, where such extensive data is unavailable, it is reasonable to use the following expression:-

$$c = \phi(T) \times c' \qquad \ldots 4.3.$$

Where c = is the specific or unit creep

$\phi(T)$= a temperature function, and

c' = a term denoted as specific thermal creep. (Fig. 4.1).

In most cases the creep strain data for concrete are normalized with respect to stress and temperature, and a single curve of specific thermal creep against time is obtained. This curve is a single-valued function varying with time and may be interpreted, when $\phi(T) = T$ as creep strain per unit stress per degree centigrade.

Specific thermal creep, thus, by definition is a function of time only, in which temperature is not another variable.

If $\phi(T)$ is known or can be deduced, it should be possible to evalue c' from experimental data.

Within the range of 20°C - 80°C, the near linearity in the increase of creep with temperature suggests that $\phi(T)$ is a simple liner frunction of T, such as $T + K$ where K is a constant. A further approximation which would not be far wrong, is to assume K to be zero, since an examination of the experimental results of the authors (earlier cited), shows that K would be small compared to T. For example, Hannant's data (41), indicates that K is near zero for creep values measured from 10 days to about a year. An examination of the experimental data of Arthanari (60) (sealed and unsealed specimens, subjectto uniaxial and biaxial stress), indicates that a maximum divergence of K from zero would be about 15°C and in many cases, K has values near zero. England (69), has made suggestions similar to this, and has stated that the rate of creep can be represented as being directly proportional to temperature in degrees centigrade.

4.6. Thermal stresses without creep.

Thermal stresses in concrete structures of homogeneous properties depend upon the type of end restrains and, in certain cases, upon the internal restraints (70).

Analyses of structural members subject to a thermalgradient or uniform temperature rise, are made with the usual assumptions of elastic design. In addition, any effect due to the difference in the coefficients of thermal expansion of concrete and steel is usually neglected.

In the present work, this difference has been taken into account. Thermal-expansive of contractive deformations are considered to be additive (algebraically) to the usual deformations, with a precaution that the strain diagrams that are needed to convert strains to stresses are separated for the purpose. Essentially, thermal stress analysis of a structure is a displacement-induced problem. It is seen readily that even if creep is uniform in all parts of the structure, creep of concrete should cause a redistribution of stresses with time in a statically indeterminate structure subject to thermal stresses.

4.7. The effective modulus method.

The principle of this method is well known. "The Young's modulus at each point of the structure is replaced by an effective modulus E'." Equation 4.4. defines the effective modulus E' in terms of the specific or unit creep c, that has occured after some elapsed time, t, from loading.

$$E' = \frac{1}{E^{-1} + c} \qquad \ldots 4.4.$$

Equation 4.5. defines E' in terms of the specific thermal creep.

$$E' = \frac{1}{E^{-1} + \phi\,(T)\, c'} \qquad \ldots 4.5.$$

In this expression, c' represents the specific thermal creep at the time considered.

ϕ (T), is a function of temperature.

In this investigation, ϕ (T), has been assumed to be equal to the applied temperature T

For problems concerned with creep at ambient temperatures, the effective modulus is the same at all parts of the structure. However, in dealing with problems at elevated temperatures, the value of the effective modulus may not always be the same, and will depend on the temperature at the various parts of the structure.

In this work the applied temperature is assumed to be uniform and therefore, the effective modulus will be the same for all parts of the structure.

The solution at a given time is obtained by calculating the mechanical and thermal stresses using the effective moduli. The values of the specific thermal creep ϕ (T) c', used in the calculation of E', are obtained from experimental creep curves corresponding to the temperatures in the structure.

4.8. Discussion.

This method of analysis recognises the influence of time and non-uniform temperature on the creep of concrete by modifying the instantaneous elastic modulus to take into account time-dependent effects. It reflects the general pattern of redistribution of strain which is known to take place in non-uniformly heated structures. (Fig.4.2).

The effective modulus principle pre-supposes complete recovery of strain on removal of an applied stress and that there is no permanent set occurring in the material. This is not true of structural concrete.

The whole principle is based on the assumption that the creep strain in an element depends upon

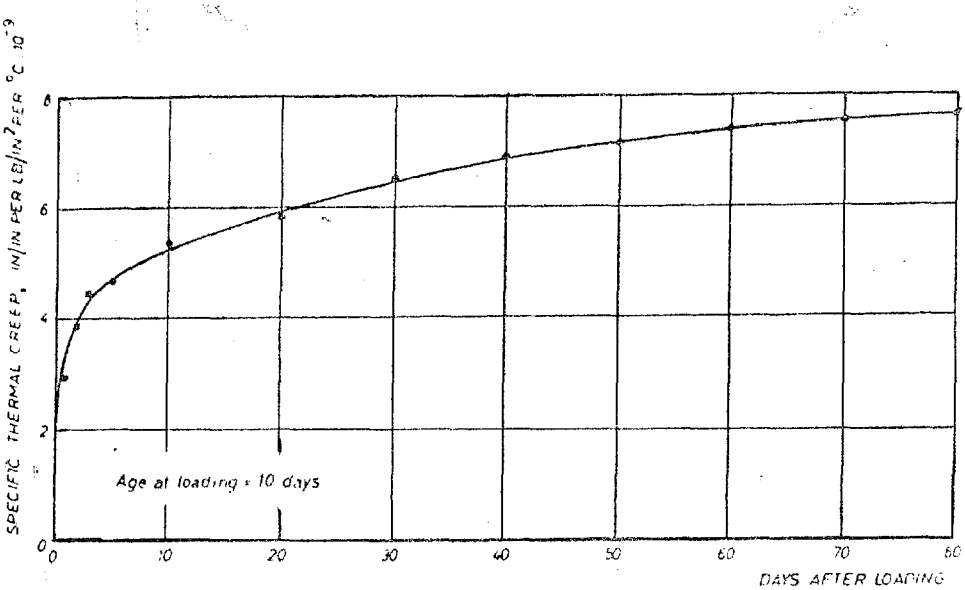

Specific thermal creep curve for a sealed concrete loaded and heated at age of 10 days

FIG. 4. 1. (Ref. 69).

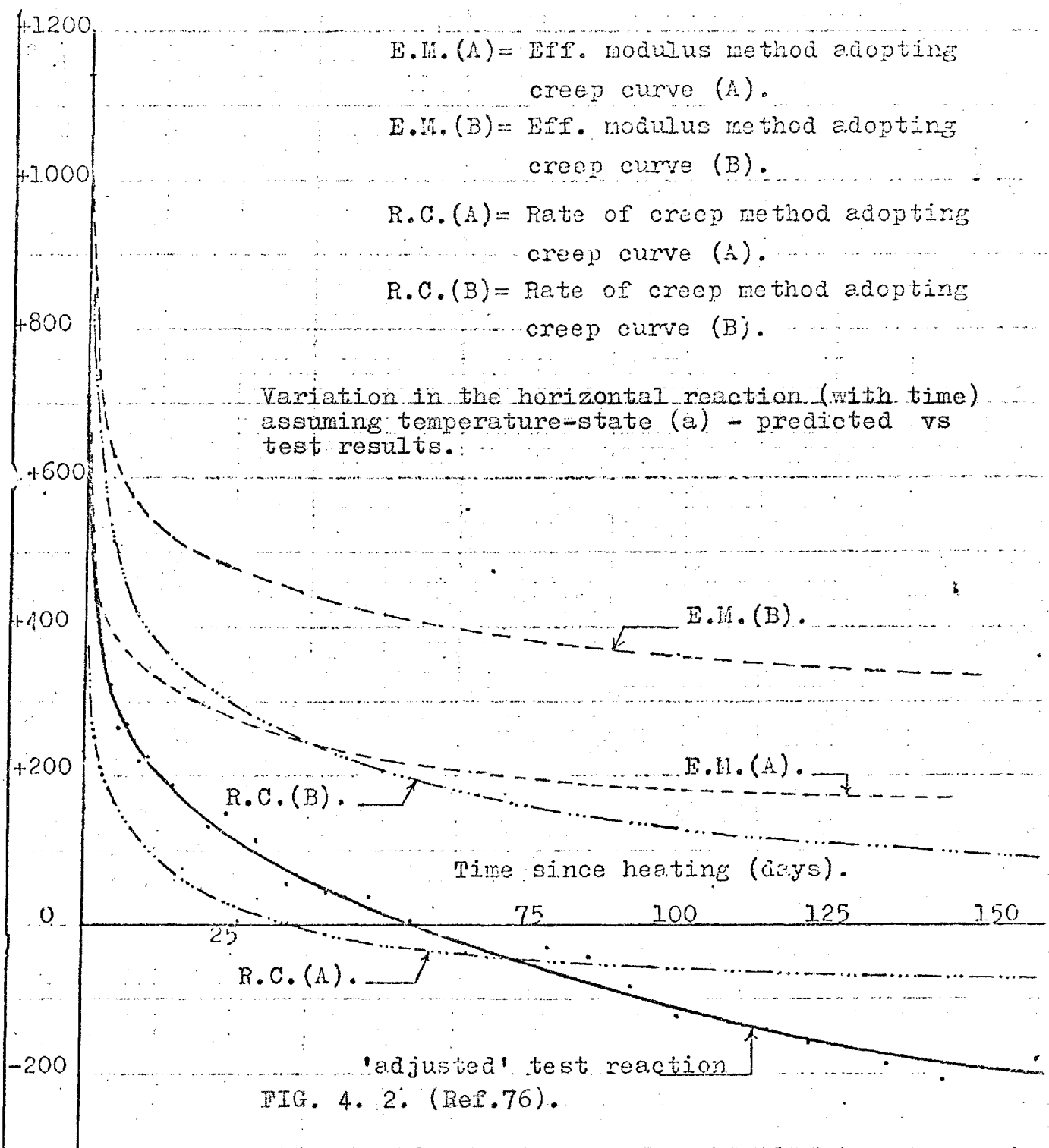

FIG. 4. 2. (Ref.76).

the current stress only (i.e., the stress in it at the time considered), and a specific creep or specific thermal creep law. It, therefore, does not take into consideration any incremental creep strains that will have occurred in the element due to past incremental stresses over and above the current stress. It is only a one-step method as far as the time variable is concerned, requiring only the current stress acting on the structure at the time considered to be taken into account, together with the corresponding specific creep value. It should not be used if the variation of stress is severe and particularly if strains after unloading completely are required.

One of the advantages of this method is that it may yield a solution from only one set of calculations, as opposed to iterative methods where a series of calculations have to be performed, to compute the stresses in a structure.

For uniform temperatures, the effective moudlus method provides a suitable method of analysis for structures under sustained loads, where strains continue to change with time, but stresses are constant. Such conditions apply to statically determinnate and indeterminate planar structures, as well as to two-dimensional problems.

4.9. The reduced modulus method.

This is one of the simplest but most inaccurate methods of estimating long-term stresses in concrete structures at ambient temperatures. The elastic Young's modulus of the whole structure is reduced by a factor of 0.40 to 0.50, such that the new modulus would indicate the sum of elastic and creep strains. The modular ratio can then be estimated using this reduced modulus for concrete and the analysis further carried out as if the whole structure is elastic and is under short-term only.

Both, applied mechanical and thermal stresses, are computed using this constant reduced modulus.

4.10. Discussion.

The method predicts a proportional reduction in thermal stresses, but does not affect applied load stresses.
When strains are caused by restraining effects, the reduced modulus analysis yields a proportional reduction everywhere with time. When strains are due to mechanically applied loads, strains do not change.

At uniform elevated temperatures, this method is practically the same as the effective modulus method, and may be employed with some reservations as to its validity, but it differs, and is in error when the temperatures are not uniform, because considerable redistribution of stress then results, even when applied loads and temperatures do not vary with time.

4.11. The rate of creep method.

In this method, the analysis is based on the property of the material of the structure, be it a one, two or three dimensional which is governed by a law that takes the following general form:-

$$-\frac{de_c}{dt} = f(\sigma, T, t) \qquad \ldots 4.6.$$

In which the rate of creep strain

$$\frac{de_c}{dt}$$

is a function of the current stress σ, the temperature T of the structure, and the time t, that has elapsed since loading. The term e_c represents the creep strain. This law is characteristic of the material property of the concrete for time-dependent behaviour.

It is an analysisthat usually requires a step-by-step approach, and a history solution.

Ross (17), used the rate of creep method to take into account a variable stress history of an element.

The increment of rate of creep during a time interval δ_t is calculated as:-

$$\frac{dc}{dt}\ \delta_t,$$

Where $\frac{dc}{dt}$ = the rate of change of specific creep strain with respect to time. After a period of time τ , the total creep strain of an element is:-

$$C = \int_{t=o}^{\tau} \sigma \left(\frac{dc}{dt}\right) d\tau \qquad \ldots 4.7.$$

In summation form, and for a small interval of time, the creep strain C is given by:-

$$C = \sum_{t=o}^{\tau} \sigma_t\ \delta c_t \qquad \ldots 4.8.$$

and in terms of the specific thermal creep

$$C = \sum_{t=o}^{\tau} \sigma_t\ \phi\ (T)\ \delta c'_t \qquad \ldots 4.9.$$

Using these equations in a step-by-step analysis, we assume that the stress remains constant during a short-time interval. During the interval creep strains are set up. These additional creep strains destroy strain compatibility.

The compatibility is then restored instantaneously by adjusting the strains. An elastic solution is then carried out at the end of the interval, and the new set of stresses computed. With the new set of stresses, known at the end of the first interval, we may proceed to the next time interval in the same way as the first interval.

The method requires as data only, a single unit creep curve, and a knowledge of the variation of the elastic modulus with time.

This principle was used by Ross to estimate the creep strains of uniaxially stressed concrete members, which were subjected to (discrete) changes of stresses under laboratory temperature conditions. When the stresses increased, strains so estimated were less than those observed in the test members, while under diminishing stresses they were greater. The latter behaviour is to be expected of this principle, since it presumes no recovery of creep for a stress-decrement. He found, that despite these deficiencies, the calculated values using this principle showed a good agreement with experimental results. For purposes of analysis, the modulus of elasticity is assumed to be unchanged during the creep period, but cases with changing modulus of elasticity may be considered, when the appropriate method of analysis is used.

Successful use of the rate of creep principle in the analysis of reinforced and prestressed concrete beams with thermal loads has been reported by Ross, England, Arthanari and others (71), (37), (39).

The principls is utilized here in the analysis of circular solid slabs, for fully-perforated ones and for slabs perforated in the central region. The equations developed have particular reference to a two-dimensional stress analysis.

4.12. Discussion.

The creep rate is one of the most straight forward methods of analysis for predicting inelastic time-dependent effects in concrete structures. It requires the least experimental data for its application, i.e., the specific thermal creep curve of the material. The curve may be either drawn from direct strain measurements on the specimens during the course of the experiment, as in the present investigation, or from control specimens subject to same enviromental, age and loading conditions as the test specimens.

The latter is to be considered a very important advantage of the method.

If the shrinkage is to be included in the analysis, then the shrinkage laws are also required.

The computational time required for a rate of creep analysis is also an advantage credited to the method since the solution at each time considered is a total one and no further record of the creep strain is necessary for subsequent time interval calculations.

When the analysis is programmed in a digital computer, this will cut computer storage to its minimum.

However, the method is liable to be inaccurate, especially if large changes of stress occur after the initial loading. On the other hand, the inaccuracies in cases may be improved by the simplification of ignoring the effects of the change in the modulus of elasticity with time.

The method attempts to take into account the stress history, but the rate of creep is assumed to be constant at the time considered, neglecting whether the concrete was previously stressed severely or negligible, (Fig. 4.3).

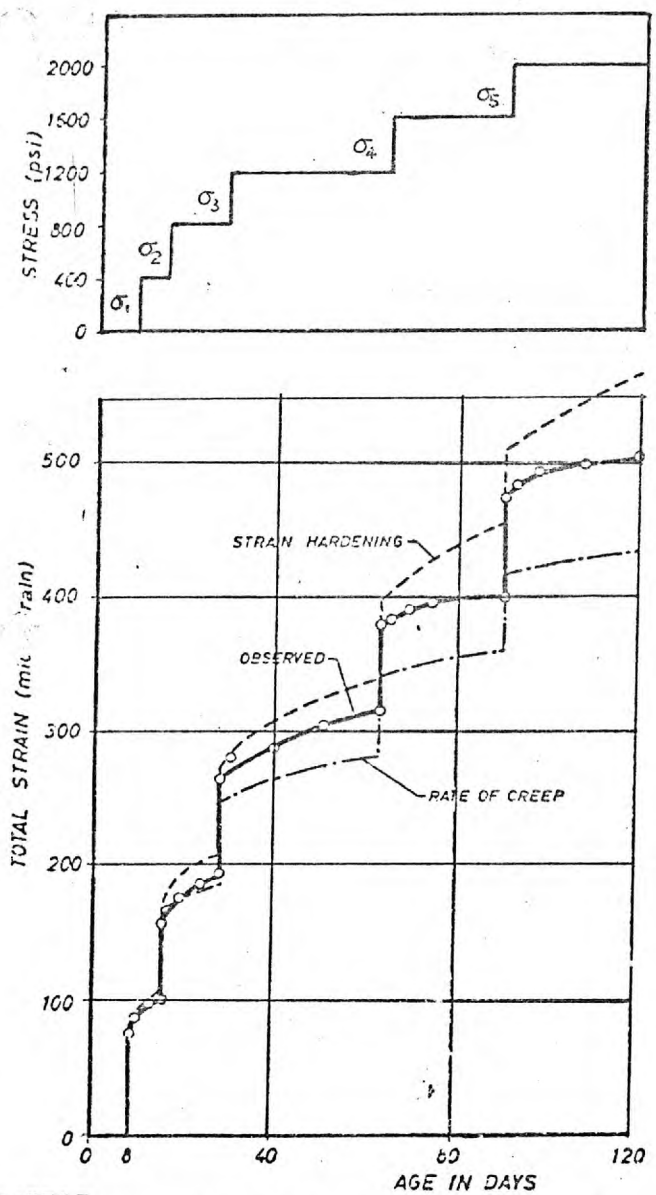

(a) —Comparison of recorded strains (from Refer- 73) with predictions by rate of creep and strain hardening methods of analysis

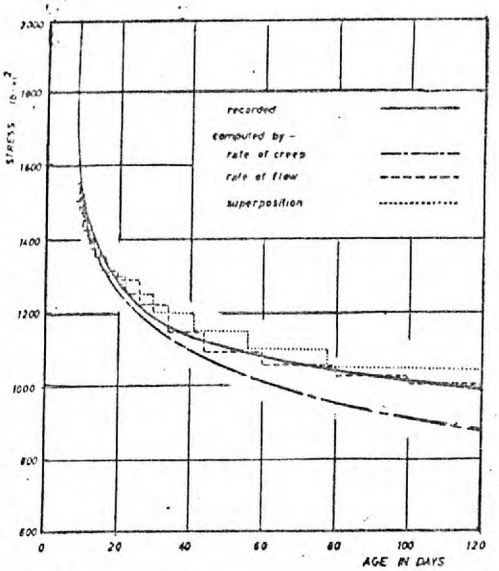

(b)- Computations for the relaxation of stress under a constant strain of 360×10^{-6} in/in.

(Ref. 73).

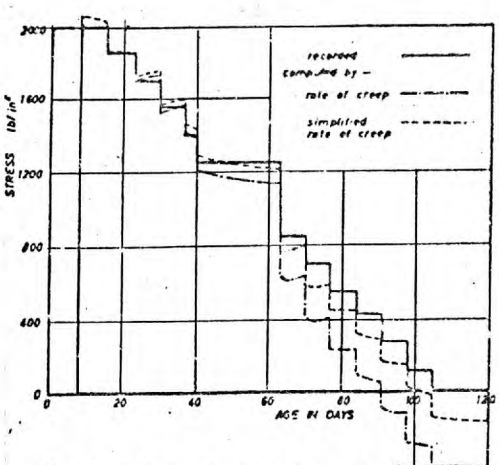

(c)-Comparison of computed stresses by the rate of creep and simplified rate of creep methods.(Ref.73).

FIG. 4. 3.

On removal of the applied stress no recovery of creep is predicted and this is regarded to be a deficiency of the method. It also assumes that the creep rate is governed by the current values of temperature and stress, and that no additional effects result from changes of these quantities with time.

The fact that the method fails to recognise these transient effects will introduce some errors. The rate of creep analysis does not take into account fully the delayed elastic response of concrete under increasing stress.

4.13. The method of superposition.

If the deformation due to several loads applied simultaneously or in succession is considered, then within a good degree of approximation, the resulting deformation at any time is given by the sum of the individual deformations corresponding to that time.

This "linearity" or "superposition" principle appears to have been first stated by Boltzmann, and was modified by McHenry (72), to apply to creep strains of concrete and in general to materials which undergo changes in properties with increasing age. The modified principle states:-

"The strain produced in concrete at any time $t = t_1$ by a stress increment applied at time $t = to$ is independent of stress applied either earlier or later than time $t = to$. The stress increment can be either positive or negative. The superposition principle is illustrated graphically in (Fig.4.4).

Using this principle, it is possible to obtain a strain history for any desired variation of stress. Decrements of stress are treated in accordance with the principle assuming of course, that creep in tension is the same as creep in compression for equal stresses.

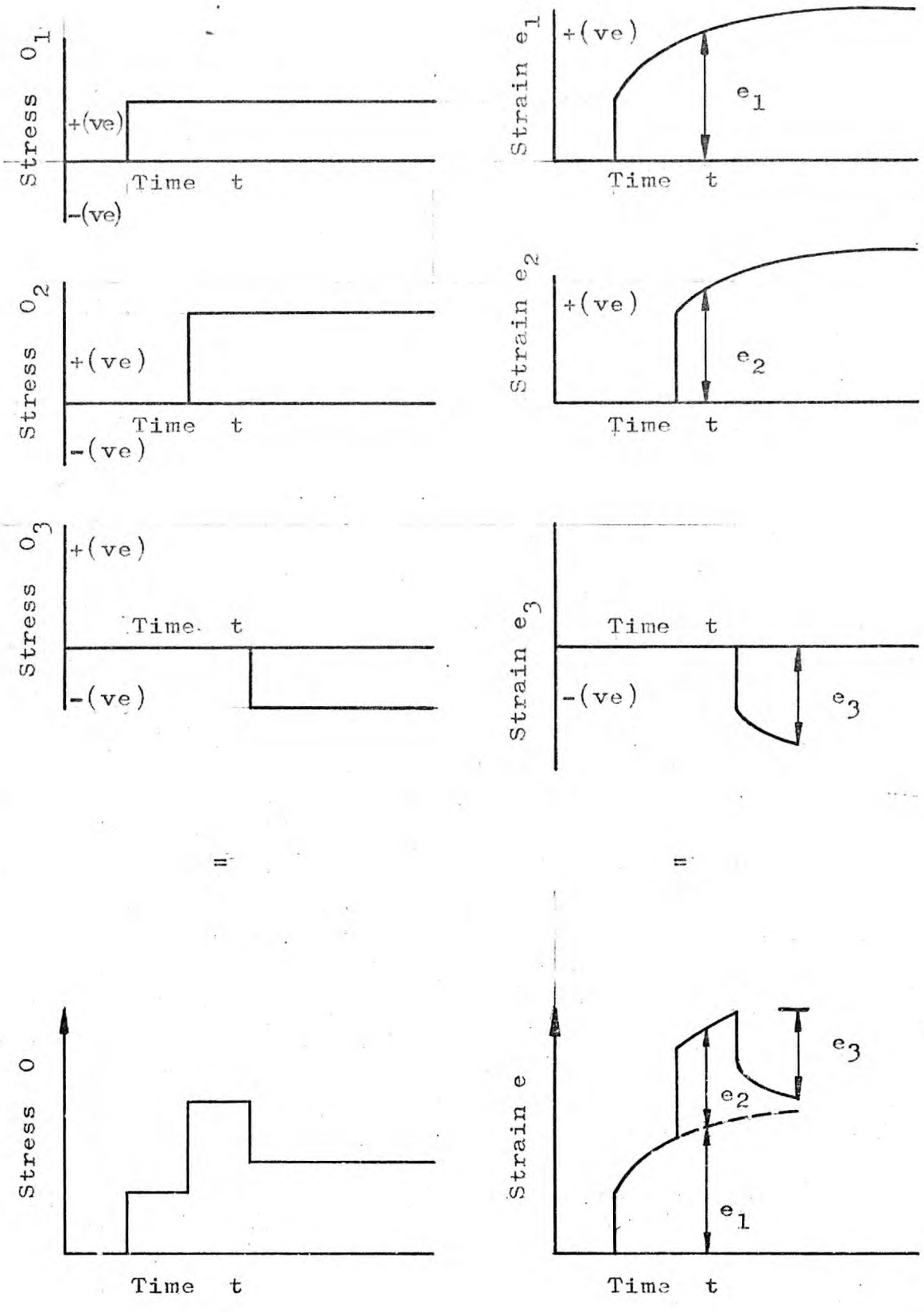

FIG. 4.4. ILLUSTRATION OF THE PRINCIPLE OF SUPERPOSITION

4.14. Discussion.

The method takes into account the entire stress history and also the changes in the properties of concrete due to aging effects. McHenry, found this to hold for sealed specimens loaded at 28 days and unloaded at 90 days.

However, the principle overlooks the experimental evidence that concrete does not exhibit the same creep strain recovery due to a decrement of stress, as it does due to creep on loading (i.e., increment of stress), both being considered at the same time.

Ross (17), tested this method by subjecting concrete specimens to severe increases and reductions of stresses in steps. He also tested the relaxation of stress in a specimen subjected to constant strain. Furthermore, he compared the method with the effective modulus and the rate of creep method. The experimental strains were compared with predicted values and found that this principle over-estimated creep under increasing stresses and vice-versa. The method gave better results than the effective modulus method, but not much better than the rate of creep method.

From the relaxation tests, he found that if the variation of stress is gradual and not too large, the method should give acceptable predictions of creep strains.

England and Illston (73), used the principle to compute stresses in concrete from a history of measured strain. They also found that the method of superposition gave better results than the rate of creep method, but required more data. If the computation is performed with the help of a general equation for the creep surface, extra work is needed to determine the appropriate values of the equation's parameters, (Fig.4.6).

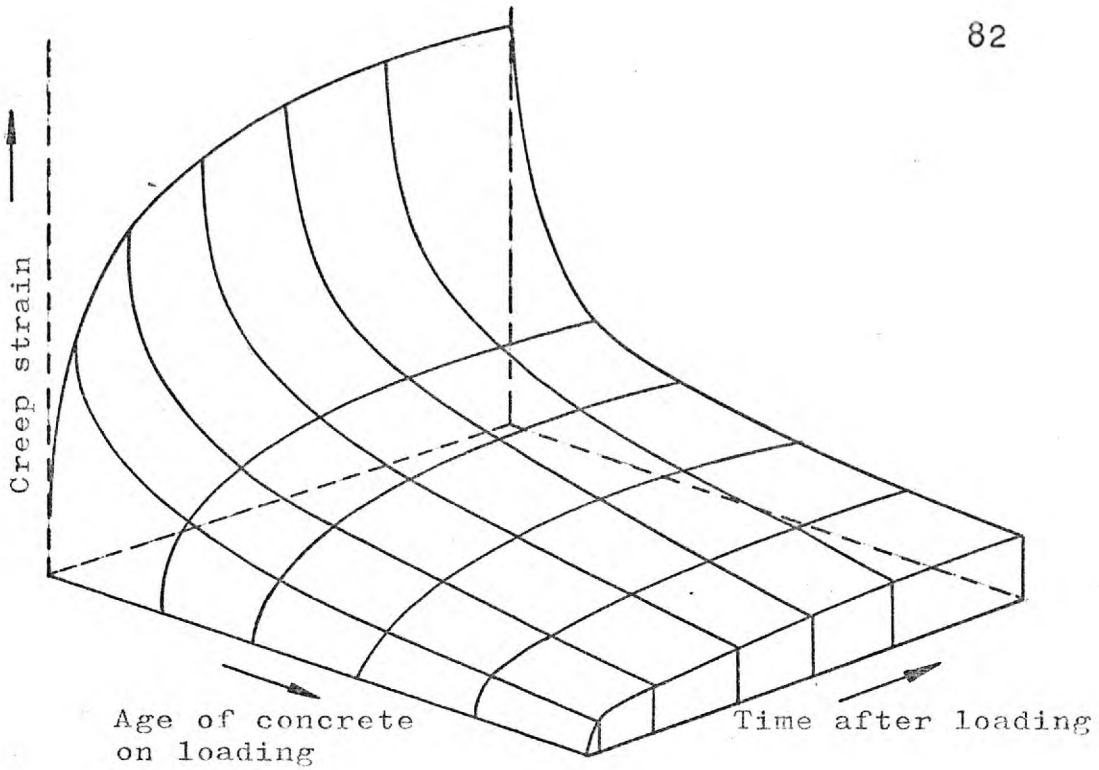

FIG. 4.5. TYPICAL CREEP SURFACE FOR CONCRETE

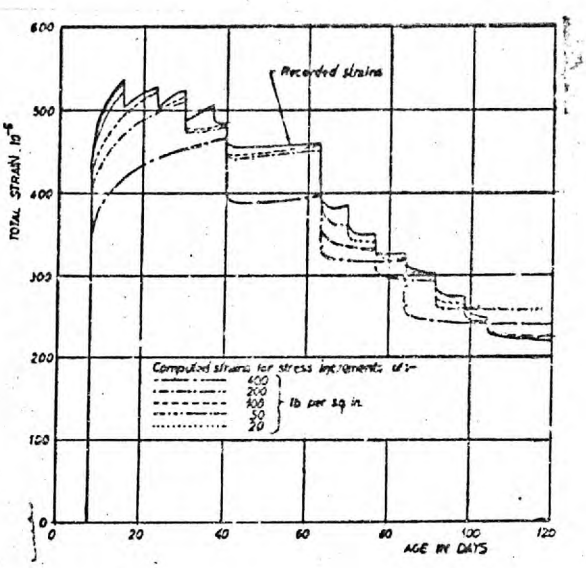

FIG. 4.6. A COMPARISON OF RECORDED AND COMPUTED STRAINS FOR VARIOUS INCREMENTS OF STRESS BY THE METHOD OF SUPER POSITION (Ref.73.)

However, from the theoretical point of view, the superposition method should be exact considering that it takes into account the entire stress history.

For the purposes of structural analysis the method requires a new creep curve whenever there is a change in stress. In fact, a family of creep curves defining the creep behaviour of concrete for various ages of loading, spanning the entire loading history of the structure is required.

These data can normally take the form of a creep surface (Fig.4.5), which is a three-dimensional figure with a surface representing the variation of creep strain with age, at loading and time after loading.

Producing such data is difficult and one obtained, their use involves very tedious calculations.

Moreover, under elevated temperatures though the creep of concrete is high, creep recovery seems to be small while the permanent set is fairly large. In such cases, the principle of superposition will be in error.

The principle is well-suited to processing by electronic computer. Like most of the numerical methods, it results in a fairly simple programme which is rapid in execution by considering small intervals of time during which the stress is assumed constant.

For computer analyses, however, it is convenient to supply the machine with a unit surface in the form of a mathematical expression.

This expression was found to give close agreement to experimental results over the range of ages at loading from 8 to 120 days, but may be inadequate for very young concretes.

$$C = e^{(a+bA)d\sqrt{T}} \qquad \ldots 4.10.$$

Where C = unit creep strain
A = age at loading in days
T = time after loading in days
e = Naperian base and,
a,b,d = constants determined experimentally.

Of course, the choice of the method depends on the accuracy required and the amount of data available. Nevertheless, the principle of superposition was not used in the analysis of this work, because the creep data available from tests, were considered to be inadequate.

4.15. The relaxation method.

This method is based on the principle that the stresses are relaxed in accordance with a known relaxation "law", while the strains remain constant. England (74), in his work on numerical creep analyses for concrete structures, suggested that this relaxation "law" for uniaxial state of stress may take the form of:-

$$\sigma_r = \sigma_i \, e^{-E \phi (T) c'} \qquad \ldots \quad 4.11.$$

Where σ_r = relaxed stress

σ_i = initial stress

E = modulus of elasticity

$\phi(T)$ = function of temperature

c' = specific thermal creep and,

e = the Naperian base.

This equation is the relaxation function of Maxwell's rheological model, with the specific thermal creep as the independent function.

for uniaxial compression the rate of creep is given by:-

$$\frac{de_c}{dt} = \sigma \phi (T) \frac{dc}{dt} \qquad \ldots 4.12.$$

The equation of total strain in an element under stress is the sum of elastic and creep strain, i.e.,

$$\frac{de}{dt} = E^{-1} \frac{d\sigma}{dt} + \sigma \phi (T) \frac{dc}{dt} \qquad \ldots 4.13.$$

which gives the strain with time t as the independent variable. If this equation is modified with the specific thermal creep as the independent variable, it becomes:-

$$\frac{de}{dc} = E^{-1} \frac{d\sigma}{dc} + \sigma \phi (T) \qquad \ldots 4.14.$$

This modification is possible bearing in mind that the specific thermal creep curve is a single valued function.

In the relaxation method for a time interval the strain is assumed constant. Therefore, in equation 4.14., $\frac{d\sigma}{dc} = 0$, and the solution of this equation gives the relaxation "law."

The relaxation method is the alternative of the rate of creep method.

In the rate of creep method, when we consider the equilibrium and compatibility of an element in a structure, we assume that the stresses in the element during a time interval remain constant while the strains increase or decrease (depending on the nature of the applied mechanical load), according to a specific thermal creep function.

In the relaxation method, we assume that the strains remain constant during the considered interval and the stresses change or "relax" according to a known relaxation function

In this approach, the conditions of compatibility are satisfied during the interval, whereas, the equilibrium is destroyed. To restore equilibrium at the end of the interval, a new set of stress distribution is needed. These new stresses are superimposed on the existing relaxed stresses, and the new system balances the actions on the section.

Corresponding to those additional stresses will be elastic strains, which must also conform to the compatibility conditions.

The sum of the relaxed stresses plus those imposed to restore compatibility, gives the final stresses in the element at the end of the interval. The strains of the element are composed of the initial constant values and those due to the equilibirum restoring stresses,

With these strains and stresses as initial values, we may proceed to the next time interval. The calculations are based on the elastic theory.

4.16. Discussion.

This method, like all the previously described ones, does not take into account creep recovery on removal of stress. To obtain good results from the method, the step-lengths in the analysis must be as small as possible, (Fig. 4.7), (a), (b).

The method is best suited to strain or displacement-induced problems, rather than to load or stress-induced ones, (Fig. 4.7), (c).

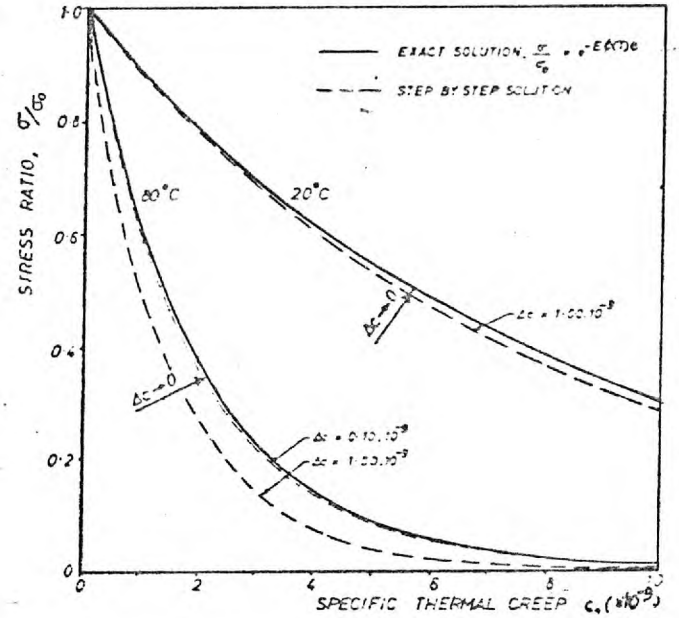

(a) -Relaxation curves by step-by-step analyses showing the significance of Δc; $\phi(T) = T$ assumed here

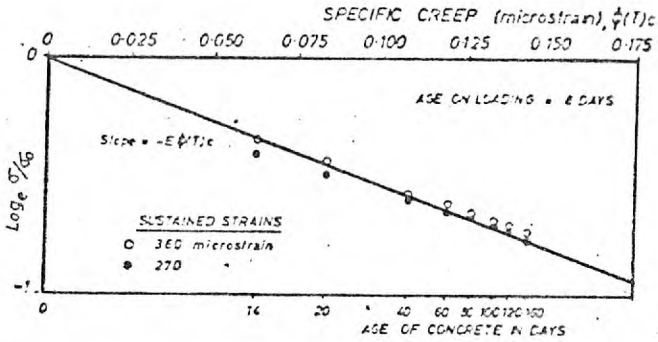

(b) -Comparison of predicted and experimentally recorded relaxation values; from Ref.

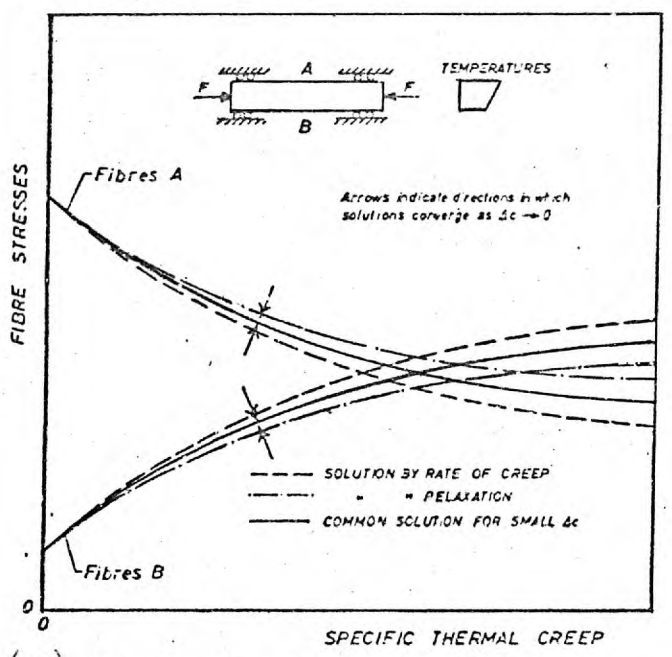

(c) Influence of magnitude of specific thermal creep increment Δc, on the computed results for fiber stresses of flexurally restrained beam; $\phi(T) = T$

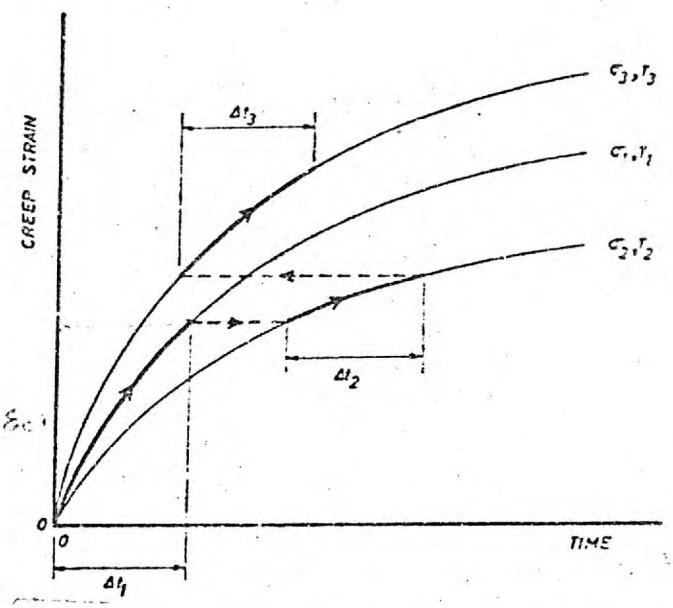

(d) Cumulative creep strains as derived by the strain hardening method of analysis

FIG. 4. 7. (Ref. 74).

Although, it is rather difficult to assess in which category a problem falls as most of the practical problems seem to be intermediate between the two types. The problem in this investigation is considered to be a stress-induced one and therefore, the method is not well suited for the analysis.

4.17. The strain hardening method.

This method is mentioned here as another possible technique by which time dependent effects in concrete may be investigated. The method is most suitable for metallic creep rather than creep in concrete.

The governing law for the strain hardening method of analysis is given by the following expression:-

$$\frac{de_c}{dt} = f(\sigma \quad T \quad e_c) \qquad \ldots 4.15.$$

in which $\frac{de_c}{dt}$ the rate of creep strain is a function of the applied stress, the temperature and the creep strain since loading. It is, therefore, evident that the strain hardening approach takes into account strain history.

The method is dependent on the value of the creep strain accumulating at any stage, and if it is used with creep data obtained from uniaxial state of stress, then the uniaxial stress-strain rate relationship

$$\frac{de_c}{dt} = \emptyset\ (T)\ \sigma\ \frac{dc}{dt} \qquad \ldots 4.16.$$

may be applied for a particular time interval temperature and stress.

The method is suitable to a step-by-step analysis, similar to that described in the rate of creep

and superposition methods with a difference only in the diferentiation of the specific thermal creep increment. The increment of an element in the specific thermal creep in the strain hardening technique depends on the cumulative creep strain already developed in the element.

4.18. Discussion.

The strain hardening method is most suited for application to problems in which the stresses increase with time, but the increase is not so rapid.

Experimental evidence shows that the predicted strains are over-estimated for positive steep gradients of stress change, but in case where the stresses do not change significantly, the predictions of strains should be in good agreement with the observed strains. However, for problems where the stresses decrease with time, the method is not well suited for application. (Fig.4.3), (a).

The strain hardening method was considered to be unsuitable for application in the present investigation.

4.19. The steady state method.

This method of analysis is based on the principle that the stresses in a concrete structure which is subjected to sustained loads and elevated temperatures and redistribution, reach after some time a "steady-state" although, the strains continue to change.

After the "steady-state"has been reached, there are no further changes in the values of moments, axial forces, shearing forces, or the stresses occuring, even though the material of the structure may exhibit further time dependent deformations. England (69), working on uniaxially concrete structures subjected to sustained temperatures and loads, proposed a "steady-state" theory, by which the "steady-state" values of

moments, shearing forces, and stress, can be calculated without any reference to either the elastic or thermal properties of the material.

From the basic creep laws that creep within the working range is proportional to the applied stress and temperature for the range between $20^{o}C$ to $100^{o}C$, the term specific thermal creep c' may be defined by the equation

$$\frac{dC}{dt} = \frac{dc'}{dt} \phi (T) \sigma \qquad \ldots 4.17.$$

Where C = creep strain
$\phi(T)$ = temperature function
σ = stress and
t = time

Considering uniaxial state of stress, the total strain in an element is:-

$$e_T = C + e \qquad \ldots 4.18.$$

Where C = creep strain and
e = elastic strain

Assuming now that plane sections remain plane, a linear law in the distribution of strain of the following form must exist:-

$$e_T = a + bx \qquad \ldots 4.19.$$

Therefore, $C + e = a + bx$

Considering further the equilibrium and compatibility of an element for the "steady-state" conditions, the displacements, stresses and strain of the element may be calculated.

For biaxial or triaxial state of stress, the "steady-state" stress may also be obtained.

In the two-dimensional case equation will be of the form:-

$$(\sigma_x+v\sigma y)\ T\ \frac{dc}{dt} = \left(\frac{dC}{dt}\right)_x \qquad \ldots\ 4.20.$$

$$(\sigma_y-v\sigma x)\ T\ \frac{dc}{dt} = \left(\frac{dC}{dt}\right)_y \qquad \ldots\ 4.21.$$

and for the three-dimensional one equation becomes:-

$$\left[\sigma_x-v(\sigma_y+\sigma_z)\right]\ T\ \frac{dc}{dt} = \left(\frac{dC}{dt}\right)_x \qquad \ldots\ 4.22.$$

$$\left[\sigma_y-v(\sigma_z+\sigma_x)\right]\ T\ \frac{dc}{dt} = \left(\frac{dC}{dt}\right)_y \qquad \ldots\ 4.23.$$

$$\left[\sigma_z-v(\sigma_x+\sigma_y)\right]\ T\ \frac{dc}{dt} = \left(\frac{dC}{dt}\right)_z \qquad \ldots\ 4.24.$$

Where the creep Poisson's ratio v and the temperature T are function of x, y, z.

The assumptions for the "steady-state" solution are:-

i) sufficient creep capacity exists in the material of the structure in order that a "steady-state" may be reached.

ii) temperatures in every element is non-time varying.

iii) compatibility is maintained at all times, including that at the "steady-state."

As time elapses creep occurs, and redistribution takes place. For further treatment of the theory, it is proposed that instead of adopting time as the independent variable, the parameter c' be adopted as the independent variable. The relationship between c' and t can be defined by the specific thermal creep "law" which is of an empirical nature.

4.20. Discussion.

The method is a good tool for providing limiting stress values in a structure, under uniaxial state of stress, lie between the initial state stress values, caused by the applied mechanical loads and temperatures, and the limiting "steady-state" stress values. It gives, therefore, upper and lower bound solutions which are of great importance from a designer's point of view, (Fig. 4.8), (a), (b).

For biaxial and triaxial state of stress, solutions may also be obtained by direct calculations though it is difficult in some cases to represent the temperature distribution by mathematical expressions in which case a numerical method may be advantageous. For structures with complicated geometry, the application of the "steady-state" method becomes extremely complex, but no more so than obtaining a conventional elastic solution.

Furthermore, it is difficult to define when a "steady-state" has been reached in the structure, and adopting a simple creep law (creep curve) for the problem does not necessary mean that we may determine directly whether the stresses have reached limiting values.

In general, there are no defined strains corresponding to the "steady-state" stresses. For these reasons no attempt has been made to use the method in the present investigation.

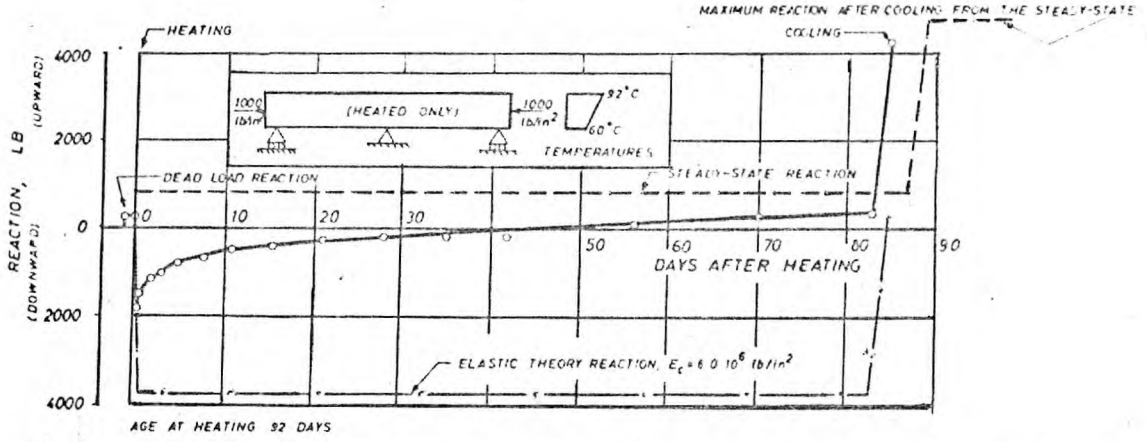

(a) Plot of central reaction against time for prestressed beam subjected to temperature-crossfall only.

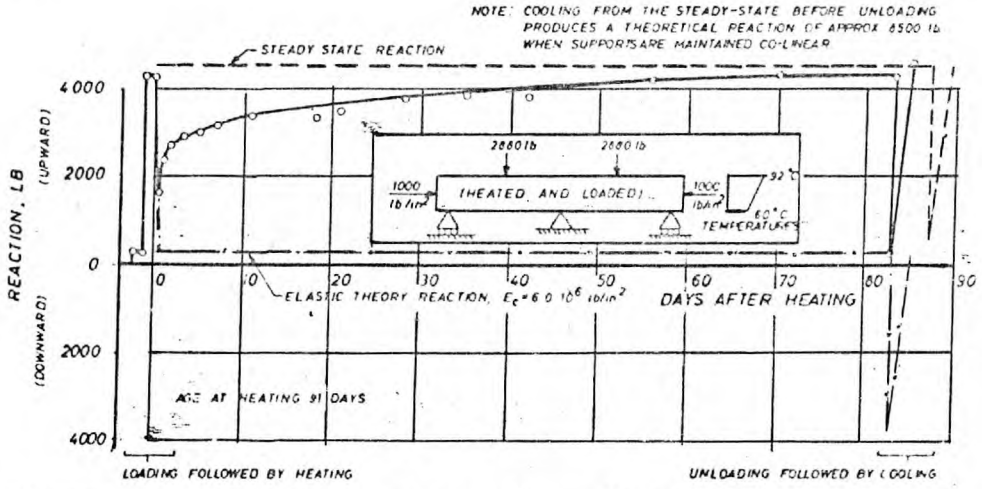

(b) Plot of central reaction against time for prestressed beam subjected to temperature-crossfall and mechanical loading.

FIG. 4. 8. (Ref. 69).

4.21. Visco-elastic approach.

In a visco-elastic analysis use of rheological models is made. As long as creep is proportional to stress, a linear visco-elastic model, can be used. Further, if all parts of a member exhibit the same creep behaviour, one model would suffice. Ross (29), proposed one such model. The model included a "thresh-hold value" of a retarding force such that the irrecoverable part of creep can be represented on unloading. Rheological models basically yield a differential equation of the type:-

$$\sum a_m \frac{d^m}{dt^m} (e) = \sum b_m \frac{d^m}{dt^m} (\sigma)$$

Where the subscript m can take values from o to any number depending on the number of springs and dashpots, arranged in a suitable combination. The solution of this equation is possible, once the combination has been decided upon, and the coefficients, a and b, are evalued for cases where the stress or strain is kept constant. But the evaluation of these constants from experimental data is a complex procedure. Again, as has been stated earlier, in a linear visco-elastic analysis of load-induced problems, the distribution of moments over a linear structure shall not change from what they were at time t = o (after load application), and this implies that the stresses do not change. Only the strains, and consequently, the curvatures and deflections change, but their evaluation is an analysis of a structure is usually secondary.

Thus, their utility seems restricted to problems that are displacement-induced. In the later type of problems, however, the stress and strains change

with time and the incorporation of the stress-strain relationship of equation 4.25, even in the simple cases, gets extremely complex.
Zienkiewicz (75), has adopted a procedure in which the above differential equation is solved for a constant stress applied at a time $t = \tau$

This solution represents the "creep compliance" of the rheological model. If this be $c(\ , t)$, Zienkiewicz shows that the total strain in an element at some time, t, due to an application of a time-varying stress, can be represented by a Duhamel type integral.

$$e(t) = \int_0^t c(\tau, t) \frac{d}{d\tau} \left[\qquad \right] d\tau \quad \ldots 4.26.$$

He considers that this integral can be written as:-

$e(t) = C\ \sigma(t)$ if C is an operator of the form:-

$$C = \int_0^t c(\tau, t) \frac{d}{d\tau} \left[\ (\ ) \ \right] d\tau \quad \ldots 4.27.$$

This leads to a visco-elastic/elastic analogy, as C is analogous to $\frac{1}{E}$

Where E = is the modulus of elasticity.

Further, Zienkiewicz, shows that the operator C can be applied to the load functions on the structure, and these "modified" loads would indicate the time-dependent deformations of a loaded structure.

Zienkiewicz, has also used the visco-elastic/elastic analogy in a thermal stress problem. Instead of obtaining the "creep compliance," it is also possible to apply a relaxation test, that is, the stress is to be kept constant. This leads to the time-varying stress expressed as:-

$$\sigma(t) = Re(t)$$

Where R = becomes analogous to E.

In the elastic solution for stresses or reactions, if operator R is used instead of E, the corresponding visco-elastic solution is obtained. Further, the temperature-induced displacements can be modified using the operator R such that the modified temperature displacements and the original elastic modulus leads to the solution.

In addition to the tedious procedure involved in evaluating the coefficients of a rheological model, the integration of the load functions with the operator C, or that of the displacement functions with the operator R, has to be performed in most of the cases numerically.

More important, and not considered by Zienkiewicz (75), in his example is that the specific creep curve of concrete is different for different temperatures. This means, that one rheological model cannot define the material of an entire member or structure, but a number of such models, will have to be postulated to refer to structural elements of different temperatures.

4.22. Creep-time relationship at ordinary temperature.

A number of expressions have been proposed to predict creep strains at ambient temperatures. The majority of these formulae are expressed in terms of specific or unit creep, but none of them can be easily adapted to meet situations where both temperature and stress are changing. Ali and Kesler (76), have reviewed a number of these expressions:-

Straub:

$$C = K\sigma^{p} t^{q}$$

Where C = creep strain
σ = applied stress and,
t = time after application of stress.
K, p, q = are empirical coefficients. A typical value suggested for p was 1.15.

Shank:

$$c = K \sqrt[a]{t}$$

Where c = creep strain
t = time after application of stress.
K, a = are empirical constants. It is seen here that K is the creep per unit stress, at the end of one day.

Ross:

$$c = \frac{t}{a + bt}$$

Where c = creep strain
t = time after application of stress.
a, b = are empirical constants.

Hence $\frac{t}{c} = a + bt$

Plotting $\frac{t}{c}$ against t we get a straight line, and the constants can be evaluated from the slope and the intercept on the y-axis.
For time t_∞, $c_\infty = \frac{1}{b}$.

Lorman:

$$c = \frac{mt}{n+t}\sigma$$

Where c = creep strain
t = time after application of stress
σ = applied stress
n,m = empirical constants.

The above equation can be rearranged in the form:-

$$t = \frac{m\sigma t}{c} - n$$

Plotting $\frac{t\sigma}{c}$ against t, m and n, can be obtained from the slope and intercept respectively.

For $t=\infty$ $c_\infty = m\sigma$
If $t=n$ $c=\frac{1}{2} m \sigma$
i.e., one-half of the ultimate creep is reached at time $t=n$

The constant m is the creep coefficient, and is equal to the ultimate creep strain per unit stress, and n is the time at which half the value of the ultimate creep is attained.

Thomas:

$$c = K\sigma\left[1 - e^{-A\{(t+a)^b - a^b\}}\right]$$

Where K = ultimate specific creep
t = time after application of stress
e = the Naperian base
A,a,b = are empirical constants.

Salliger:

$$c = a_t \sigma$$

Where $a_t = A \quad t$

a_t = creep coefficient

Hence $c = A \quad t \quad \sigma$

McHenry:

$$c = A(1-e^{-rt}) + Be^{-pk}(1-e^{-qt})$$

Where k = age at time of loading
A,B,p,q,r = are empirical constants.
This can be simplified if r and q are assumed equal to:-

$$c = (A+Be^{-pk})\ (1-e^{-rt})$$

Glanville and Thomas:

$$c = K\left[1-e^{f(t)}\right]$$

Where f(t) = is an empirical time function
K = ultimate specific creep.

Dischinger:

$$c = K\left[1-e^{-at}\right] \quad , \quad K \text{ as above.}$$

Koerner:

$$e_c + e_e = \sigma \; e^{t/\tau}$$

Where e_e = instantaneous (elastic) strain

τ = relaxation time at the end of which the stress has relaxed to $\frac{1}{e}$ times its initial value at a constant deformation.

Friedrich:

$$c = C \sqrt[4]{\frac{t}{1400}}$$

Where t = is time in days.

After 1400 days,

$c = C$, a constant value.

Aroutiounian:

$$c(T,k) = \beta(T)\left[1 - e^{-a(T-k)}\right]$$

Where $c(T,k)$= specific creep at time T after casting and loading at age k.

$\beta(T)$= are empirical time function

a= empirical exponent.

Lyse:

$$c = S(1 - e^{-st})\; p\; \frac{\sigma a}{\sigma sh}$$

Where σa = applied sustained stress

σsh = magnitude of an equivalent sustained stress, which would give creep equal to the shrinkage of the concrete at the givenrelative humidity.

p = percentage of cement paste in concrete.

s = rate of shrinkage
S = limiting shrinkage per one percent of paste in the concrete at the given relative humidity.

United States Bureau of Reclamation:

$$c = f(k)\log_e(t + 1)$$

Where $f(k)$ = a function represting the rate of creep deformation with time.

L'Hermite:

$$c = C_\infty\left[1-e^{-(a_1 \log \frac{k+t}{k} + bt)}\right]$$

k = age at loading
a_1, b = are empirical constants.

Erzen:

$$c = Ae^{\{a\left[1-(k/t)^{b}\right]\}}$$

k = age at loading
A,a,b = are empirical constants.

4.23. Discussion on creep expressions.

The creep strain-time relationships for concrete are of an hyperbolic or exponential type. However, in modifying some of the factors for a particular mix, it is feasible to express creep by a standard curve.

Straub's and Shank's exponential expressions would indicate that creep goes on increasing (though at a decreased rate), and that there will not be a limiting value of creep at a finite time. The expressions that use the Naperian base are rather cumbersome when used to fit experimental data. Unless, the experimental observations are quite closely spaced in time, the determined value of ultimate creep may be erroneous.

Saliger's expression assumes that maximum creep is reached at time $t = 30$ months. This is not exactly true, as it would mean that concrete loaded after 30 months will show no creep.

The U.S.B.R., formula which uses a logarithmic type of equation though easy to apply, indicates that creep does not reach a limiting value in finite time, and at very great age, would indicate higher values of creep than occur.

The hyperbolic expressions of Ross and Lorman, have the merit of being simple to use and indicate limiting values of creep, but on the other hand, they may under-estimate creep at very long periods.

Since the nature and mechanisms of creep have not been established without doubt, it is sufficient for a designer to use a simple expression than can reasonably fit the experimental data he has.

4.24. General discussion on the time-dependent analyses.

As stated in Chapter I, the intention was for the test programme to simulate approximately the commissioning operational and shut-down procedures of the reactor.

The aim is to develop a suitable method of analysis which will be able to predict the behaviour of the perforated end cap zone of a reactor pressure vessel, for the conditions of loading described.

The data available from the tests were the radial and tangential displacements or strains resulting from the loading and temperature conditions.

In addition, shrinkage strains could also be made available from identical control specimens.

It has also been possible to record the elastic response of the models at various stages of the test programme from measured strains and hence, to assess the Young's modulus of the concrete and the Effective elastic modulus of the perforated zone.

Moreover, the creep and shrinkage laws for the concrete have also been obtained from direct strain measurements on the specimens during the course of the tests.

This information was considered to be most useful and valuable as it eliminated the need for additional control tests to collect the data required.

Because of the limited time available and the information obtained from these tests, it was considered that the most suitable method for incorporating the time-dependent properties of the concrete in the analysis would be the Rate of creep method. This method requires only the knowledge of the elastic constants of the materials and their variation with time as well as the specific creep and shrinkage laws. All these parameters were obtained from the tests.

For these considerations and because of the nature of the problem, the Rate of creep method was chosen.

The merits and demerits of the method have been discussed earlier. Possibly, the method of superposition would give better results, but was disregarded because it requires data which could not be made available from these tests.

The Effective modulus method should give similar results to the Rate of creep, at least for cases of uniform temperature. Whereas, the relaxation and strain hardening methods were considered to be unsuitable.

In conclusion, the Rate of creep method requires less data, less computational time, and is more accurate for the application envisaged.

C H A P T E R V

EXPERIMENTAL INVESTIGATION

5.1. Object.

The experimental work performed in this investigation was intended mainly to establish the following:-

a) Methods of assesing the overall elastic creep shrinkage and thermal, strains for circular perforated zones reinforced with steel liners and subjected to radial compression at ambient and at elevated temperatures.

b) Methods of assesing the internal distribution of load, between the perforated and unperforated zone, the stress distribution around and within the area of the standpipes and ligaments, and the notional material properties for an equivalent homogeneous material which can replace the perforated zone.

In order to collect the information needed, the experimental work performed, was carried out under two different sections:-

i Short-term control tests at ambient and elevated temperatures to establish the elastic constants of the material.

ii Long-term tests at ambient and elevated temperatures to obtain creep and shrinkage data.

5.2. Description of model specimens.

Three series of tests were carried out. Each series required the casting of five model specimens. The specimens in each series were identical with their corresponding opposite numbers in the other series, except for different wall thickness in the standpipes, and the differences in the test programmes.
Series 1 - standpipe liners were 16 swg thick.
Series 2 - the liners were $\frac{1}{4}$" thick.
Series 3 - the liners were 16 swg thick.

5.2.1. Dimensions.

The five specimens comprising a series were as follows:-

1 solid $16\frac{3}{4}$" diameter, 6" thick concrete shrinkage specimen. Fig. 1.12 (a).

1 solid $16\frac{3}{4}$" diameter, 6" thick concrete bi-axial creep and shrinkage specimen. Fig. 1.12 (b).

1 perforated $16\frac{3}{4}$" diameter, 6" thick concrete shrinkage specimen. Fig. 1.12 (c).

1 perforated $16\frac{3}{4}$" diameter, 6" thick concrete bi-axial creep and shrinkage specimen. Fig. 1.12 (d).

1 composite 36" diameter, 6" thick concrete bi-axial creep and shrinkage specimen, having combined perforated and unperforated zones. Fig. 1.12(e).

For all perforated specimens, the following geometrical data applied:-

Standpipe O.D.	-	3"
Standpipe pitch	-	$3\frac{13}{16}$"
Standpipe thickness	-	16 swg (1st series)
		$\frac{1}{4}$" (2nd series)
		16 swg (3rd series)

5.2.2. Penetrations.

The perforated specimens had the standpipe penetrations arranged in a square central lattice, symmetrical about two orthogonal axes. In each of the three specimens there were 12 standpipes.

A typical arrangement of the standpipes, demec gauge points, and the geometrical data of the penetrations, is shown in figures 5.1, 5.2, and 5.3.

5.2.3. Concrete mix design.

The concrete mix design was identical to the one adopted for the spherical pressure vessel model previously tested at Imperial College. Ref. 39.

1) Specification of concrete.

The preliminary specification drawn up for the concrete mix for the models was:-

Minimum cube crushing strength:

5000 lb/in^2 at 28 days.

Maximum cube crushing strength:

6000 lb/in^2 at 28 days.

Shrinkage, creep and thermal expansion properties:

As low as possible, but representative of normal concretes.

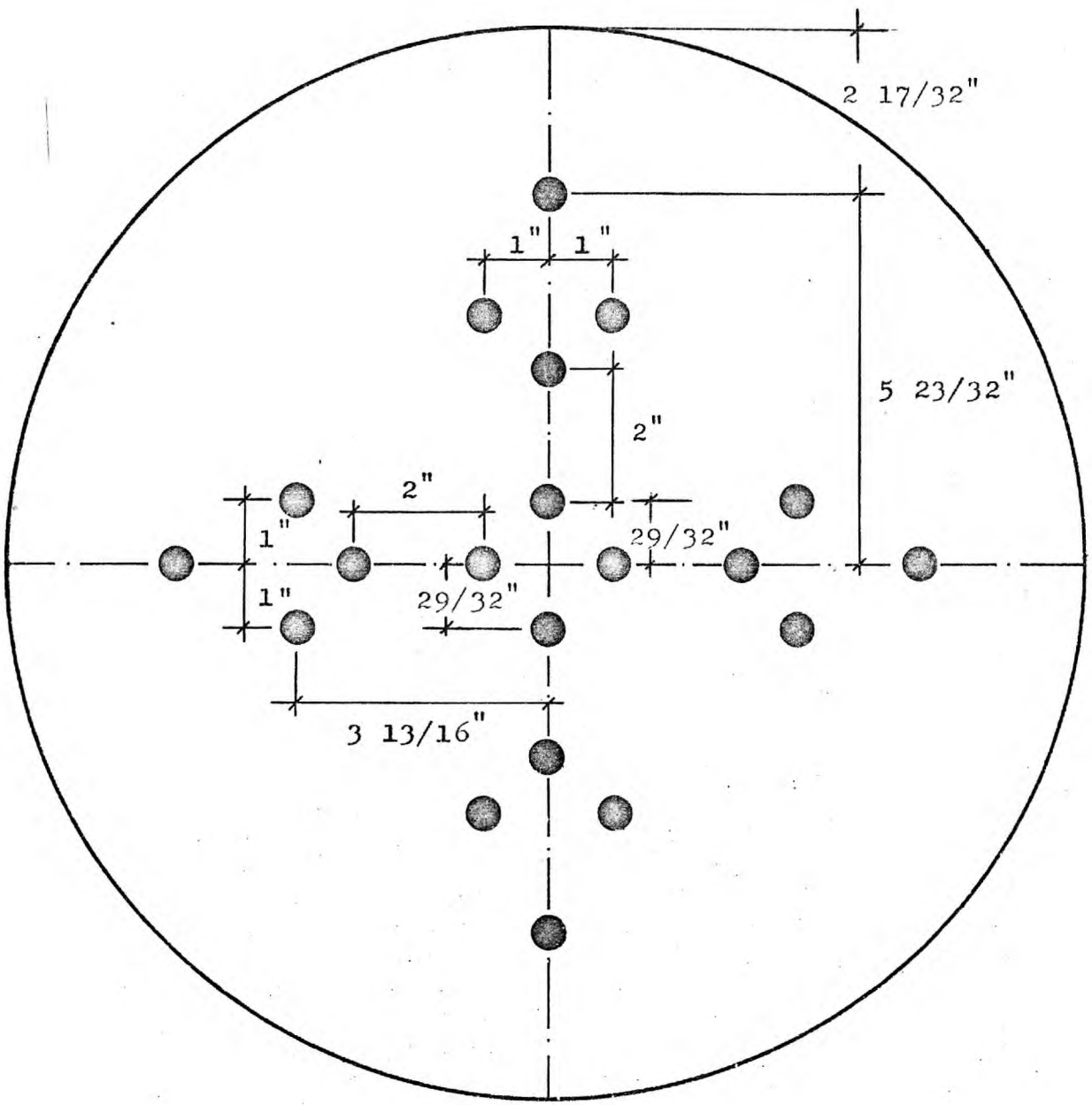

FIG. 5.1. MODELS 1/2 AND 7/8(SOLID)
TYPICAL ARRANGEMENT OF DEMEC GAUGE POINTS

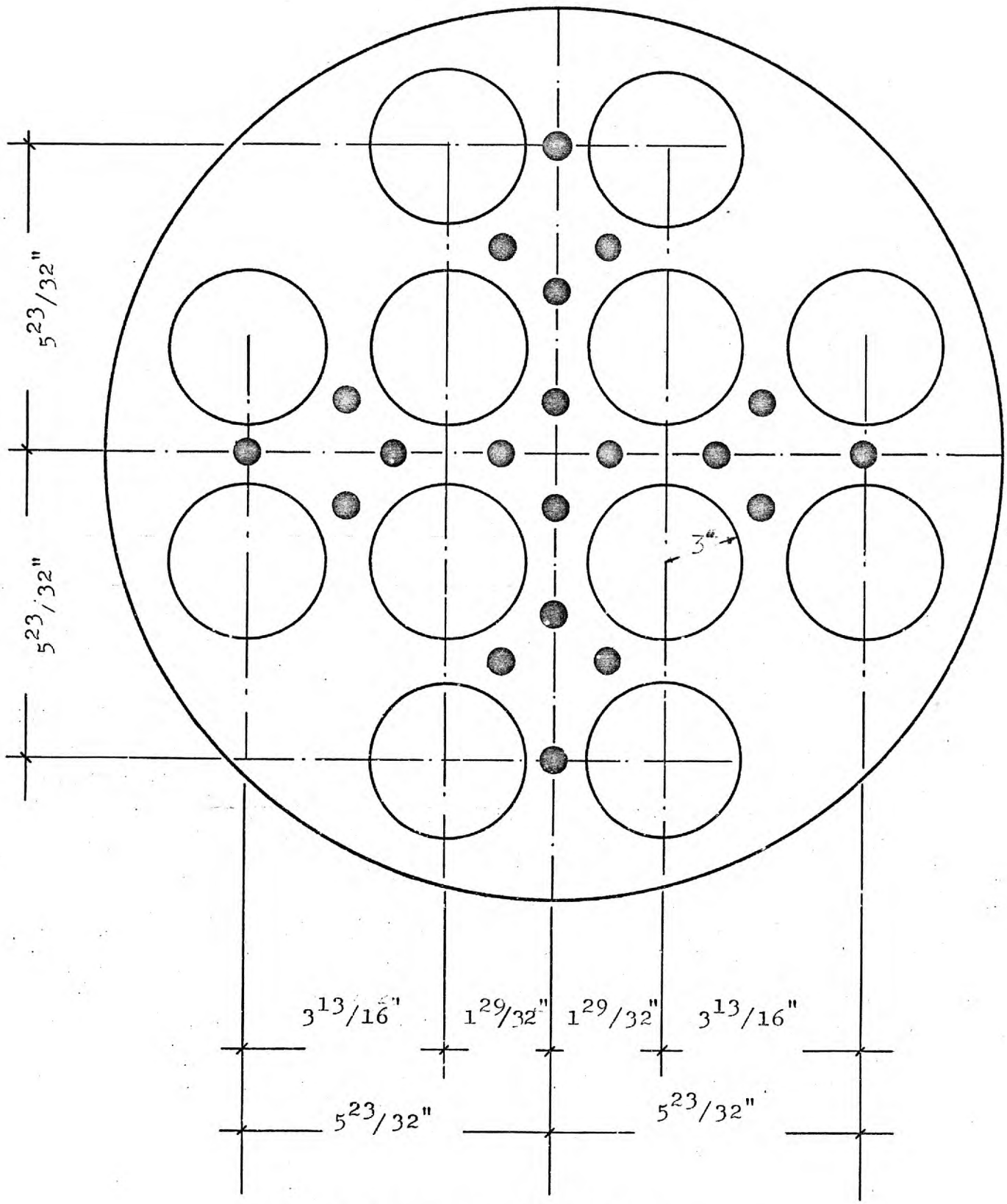

FIG. 5.2. MODELS 3/4 AND 5/6
TYPICAL ARRANGEMENT OF STANDPIPES
(MODEL 9/10 ARRANGEMENT IDENTICAL)

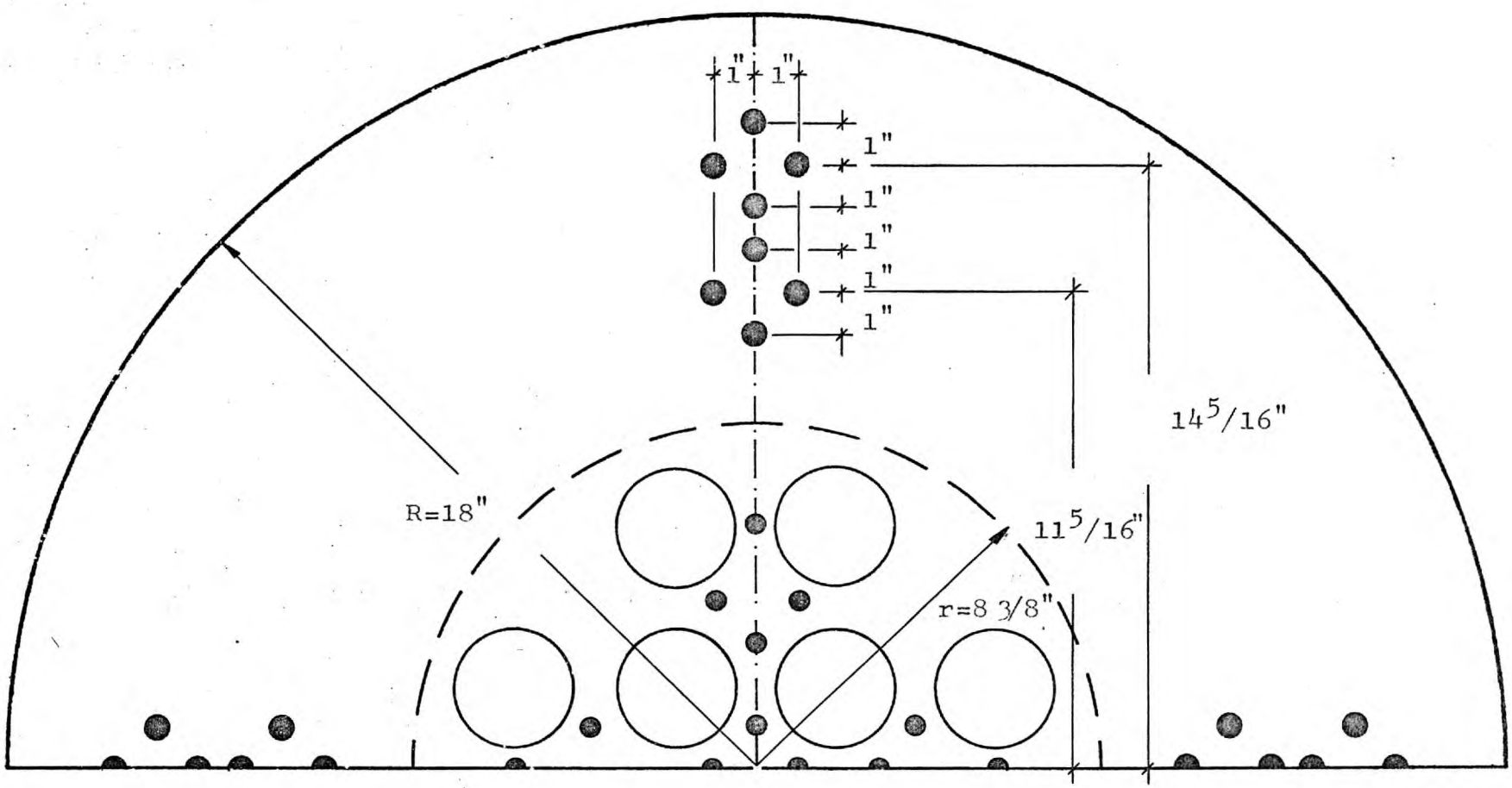

FIG. 5.3 MODEL 9/10 COMPOSITE
TYPICAL ARRANGEMENT OF DEMEC GAUGE POINTS IN THE ANNULUS

Workability:

2ins., slump approximately, but concrete should have a high degree of mobility. Vibrational methods of compaction to be used.

Aggregate type, size and grading:

Thames Valley River gravel was chosen as representative of typical aggregate economically available. The maximum size to be as large as possible for workability reasons, but small enough to enable concrete to be placed in congested sections. The grading to be consistent with strength and workability requirements.

2) Mix design approach and properties of materials.

To prevent excessively high shrinkage, creep and thermal expansion, the cement content of the mix was limited by ensuring that the aggregate/cement ratio was not less than 3.0 (by weight). To obtain suitable mobility, the sand content of the mix was restricted to not more than 30% by weight of the total aggregage.

Subsequently, first choice of the most suitable mix proportions for workability and strength was made on the basis of data presented in Road Note 4, Research Report No. 2, and the paper by Erntroy and Shacklock, (77).

3) Aggregates.

The Thames Valley River gravel coarse aggregate and sand were supplied by T.W. Howard Ltd., from their Thorney Mill Road Pit, Iver, Bucks. The coarse aggregate, norminal grading 3/8 - 3/16 in.,

comprised uncrushed gravel material which can be classified as irregular in shape. The gradings of the separate corase aggregate and natural river sand are given in Table 5.1.

Table 5.1.

Grading of Aggregates:

	% passing						
	3/8 in.	3/16 in.	7	14	25	52	100
			B.S.Sieve.				
3/8 - 3/16in., river gravel.	99	2	0	0	0	0	0
Sand* 3/16in., 100 B.S.S.	100	100	91	75	54	13	2

* Zone 2 sand, B.S. 822:1954:

The coarse aggregates and sand were batched in an air-dry condition in three separate sizes:- 3/8 - 3/16in., 3/16in., - 25 100 B.S. Sieve. The dry sand was separated into two sizes to avoid segregation in the storage hoppers, and was always recombined to give the grading shown in Table 5.1.

4) Cement.

Ordinary Portland cement was supplied in bulk by the Cement Marketing Company Ltd., from their Kent works.

5) Trial mixes.

To ascertain the most suitable mix proportions, a series of trials was undertaken with trial mixes to establish the water/cement ratio required to give a concrete with a 28-day strength of 600 lb/in^2. maximum.

The casting was undertaken of models to establish the most suitable method of placing and compacting the concrete, and the optimum amounts of sand and cement.

6) Concrete trial mixes.

Two trial mixes were manufactured. The coarse aggregate, sand and water were first mixed together for a period of 2 minutes, and then the cement was added and mixing continued for 3 minutes.

Slump and compacting factor tests were made 10 minutes after discharging the concrete from the mixer. Six 6-in., cubes were then cast from each mix, and cured under water before testing two cubes at each age of 7, 14 and 28 days. All tests were performed generally in accordance with B.S. 1881:1952 (Methods of testing concrete). The trial mix proportions are given in Table 5.2., and the test results in Table 5.3.

Table 5.2.

Mix proportions of concrete trial mixes.

Trial Mix	Aggregate/ cement ratio by wt.	Sand wt-%	Volume fraction coarse aggregate,%	Water/cement ratio	
				Total	Effective
C1	4.0	25	49	0.55	0.48
C2	3.75	30	44	0.564	0.50

Table 5.3.

Workability and strength of concrete trial mixes.

Trial Mix	Slump in	Compacting factor	Cube strength, lb/in^2 (average of 2 specimens).		
			7 days	14 days	28 days
C 1	3"	0.980	5480) 5400(5440	6130) 6500(6315	7250) 7300(7275
C 2	3"-4"	0.955	4760) 4560(4660	5550) 5580(5565	6650) 6720(6685

7) Trial casting of dummy specimens.

As already mentioned earlier, in order to facilitate the choice of trial mix, dummy specimens both 36in., and 16^3/4 in., in diameter were cast in the steel moulds.

These dummies were subsequently, broken to permit examination of the internal nature of the concrete particularly in the ligament region.

As a result of the casting, workability and compressive strength trials, mix C2, was chosen as the most appropriate for our purpose.

8) Concrete mixing for test specimens.

The actual concrete mixes for the models were manufactured in a 150-litre Eirich counter-flow pan mixer in batches of 3ft. cube approximately. The coarse aggregate, sand and cement were added to the mixer simultaneously, followed immediately by the metered water; mixing continued for 10 minutes before discharging.

The quantities of materials used by weight for each batch were as follows:-

TABLE 5.4.

Material	Quantity
Sand 3/16" to N°25 Sieve	31.5 kgs.
25 - 100	13.5 kgs.
Aggregate 3/8in. - 3/16in.	105.0 kgs.
Cement	40.0 kgs.
Water	49.7 kgs.

5.2.4. Steel moulds.

The moulds for the models consisted of machined steel baseplates and semi-circular vertical steel side walls. The walls were bolted together and then bolted down to the baseplate. Three sets of five specimens were cast in these moulds. Each series consisted of:-

Two $16\frac{3}{4}$" diameter, 6" thick slabs with 12/3" O.D., standpipe perforation on a square lattice.

Two solid $16\frac{3}{4}$" diameter 6" thick slabs, and one 36" diameter 6" thick slab with a perforated zone in the centre identical to that of the small perforated specimens.

The moulds were assembled, carefully cleaned and lightly greased before placement of concrete commenced. Plates P1, P2 and P3.

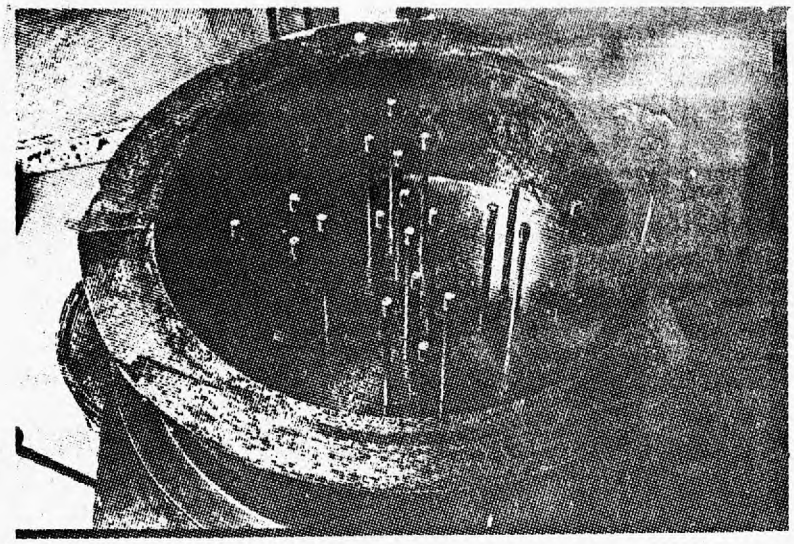

PLATE P1.
Steel mould for solid specimens.

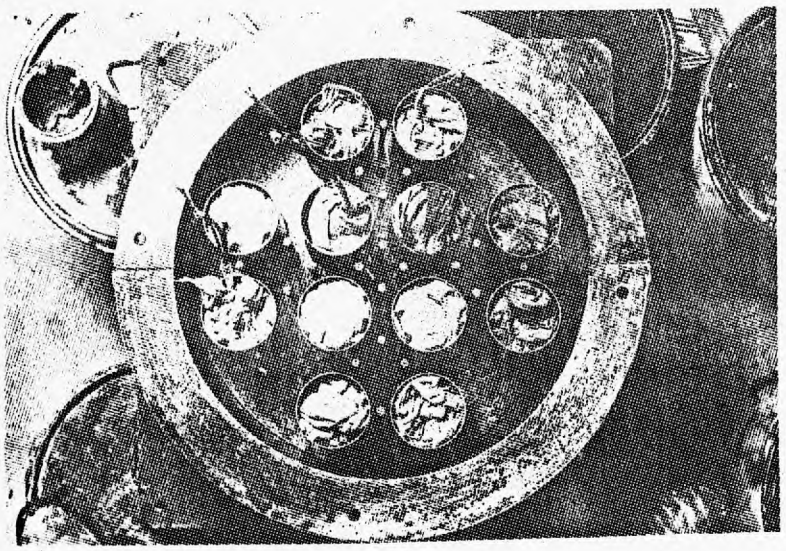

PLATE P2.
Steel mould for perforated specimens.

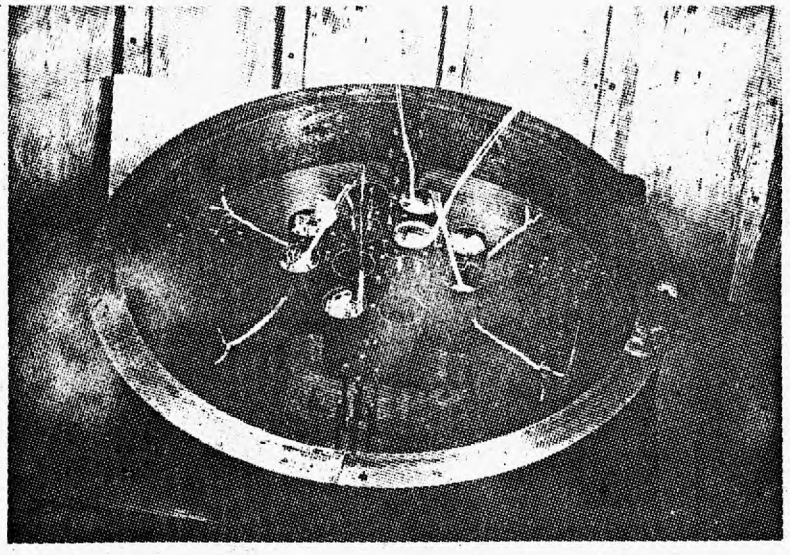

PLATE P3.
Steel mould for composite specimen.

1) Standpipe fixing.

For the first series of five specimens, the 6" long and 3" O.D. standpipe liners for the perforated models, had a wall thickness of 16 swg., and were commercial steel tubes. They were located and rigidly fixed to the baseplate at the bottom only by a tight push-fit-over male steel plugs recessed and secured to the baseplate by countersunk bolts. Fig. 5.4.(a). The wall thickness of the standpipes for the perforated models in the second series of five specimens was $\frac{1}{4}$", and in the third series was 16 swg. Plate P4.

2) End-threaded cubes.

In addition to the standpipes, end-threaded tubes $\frac{1}{4}$" in diameter and 6" long were bolted on the baseplate for all specimens. Fig. 5.4.(e). Plate P5.

For the 3rd series and end-threaded tubes were hexagonal in section to ensure good bonding with the concrete.

These tubes were threaded to take 1" long hexagonal brass studs subsequently screwed into the tube ends, after the slabs had been removed from the moulds. The brass studs were indented in their ends with Demec centering holes. Fig. 5.4. (c).

The patterns of the standpipe tubes and the Demec gauge points with their numbering are shown in Figs. 5.5. to 5.14.

3) Cruciform jig.

To ensure accuracy of positioning of the $\frac{1}{4}$" tubes and subsequently of the Demec points, in the ends of the brass studs, a cruciform jig was made up in the form of a steel template, through which were positioned by screwing a series of conical steel spigots. When the cruciform jig was bolted into position, over the moulds,

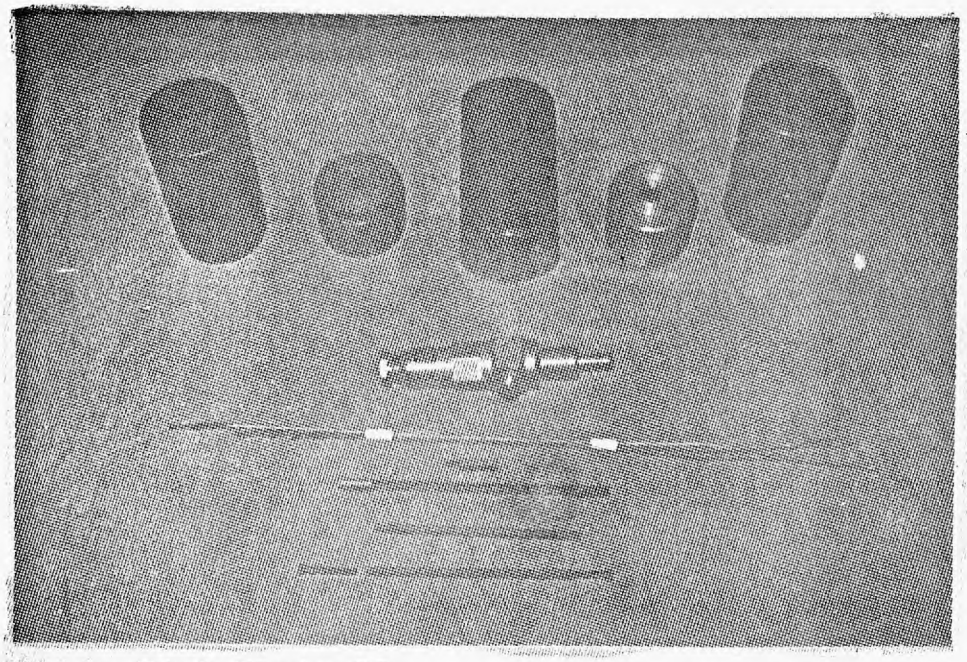

Plate P4 & Plate P5.

Standpipes and plugs, pressure releasing valve thermocouples, Demec gauge brass bar, and hexagonal tubes:

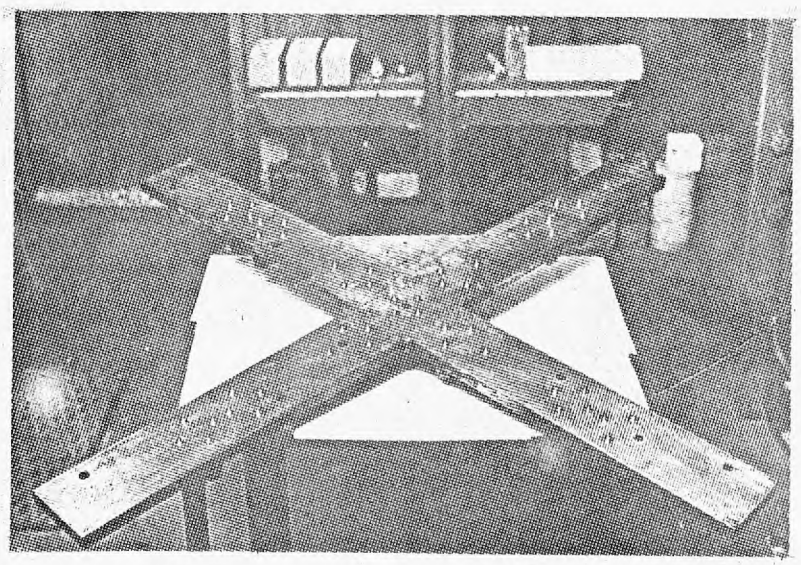

Plate P6.

The Cruciform jig.

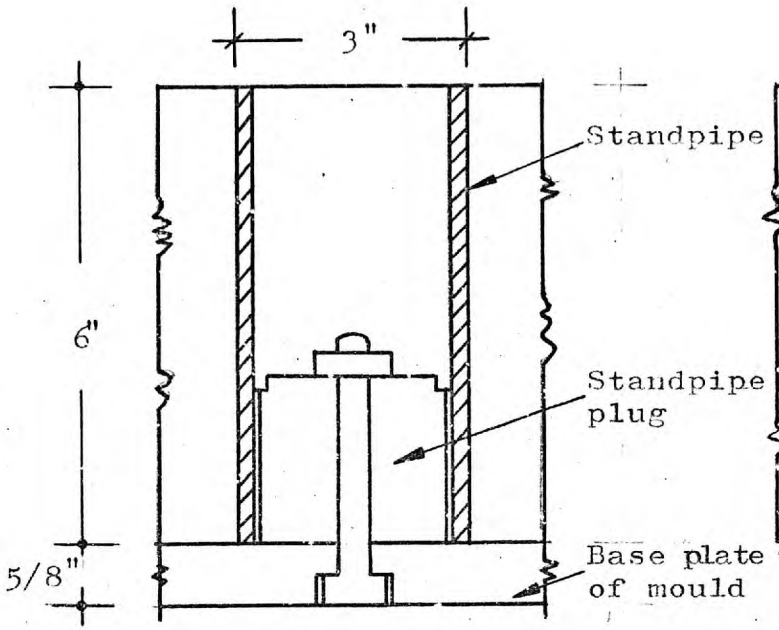

(a) Section through specimen showing standpipe in position.

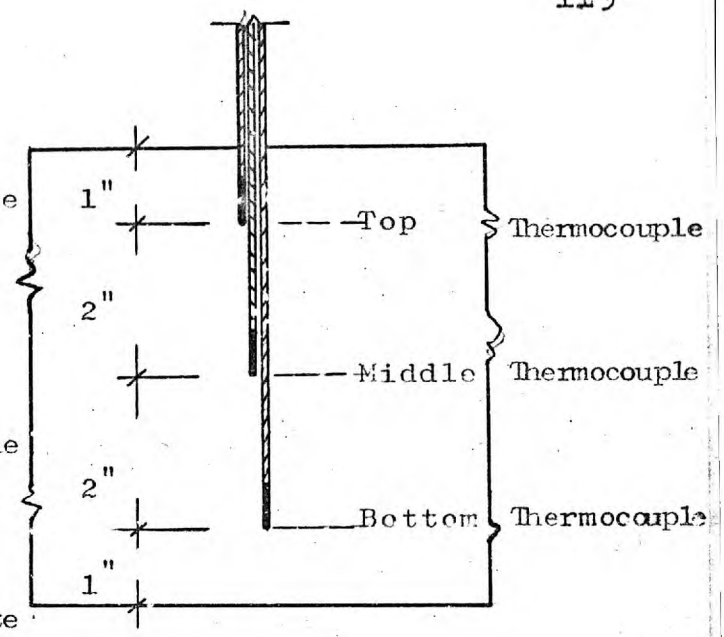

(b) Section through specimen showing positions of thermocouples.

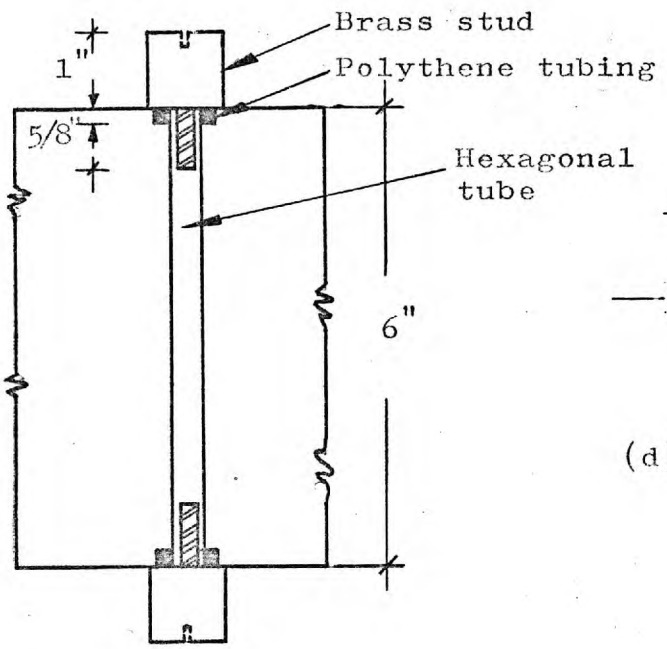

(c) Section through specimen showing arrangement of brass stud and hexogonal bar

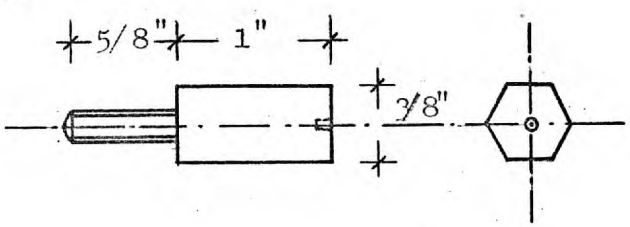

(d) Demec gauge brass stud

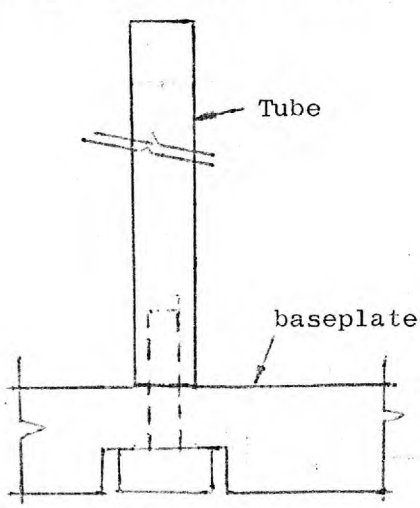

(e) End threaded tube bolted on the base plate.

FIG. 5.4.

DEMEC POINT POSITIONS FOR SIDES 1 & 2

SPECIMEN
1 - 2

Sides 1-Nos.1-20
Sides 2-Nos.21-40

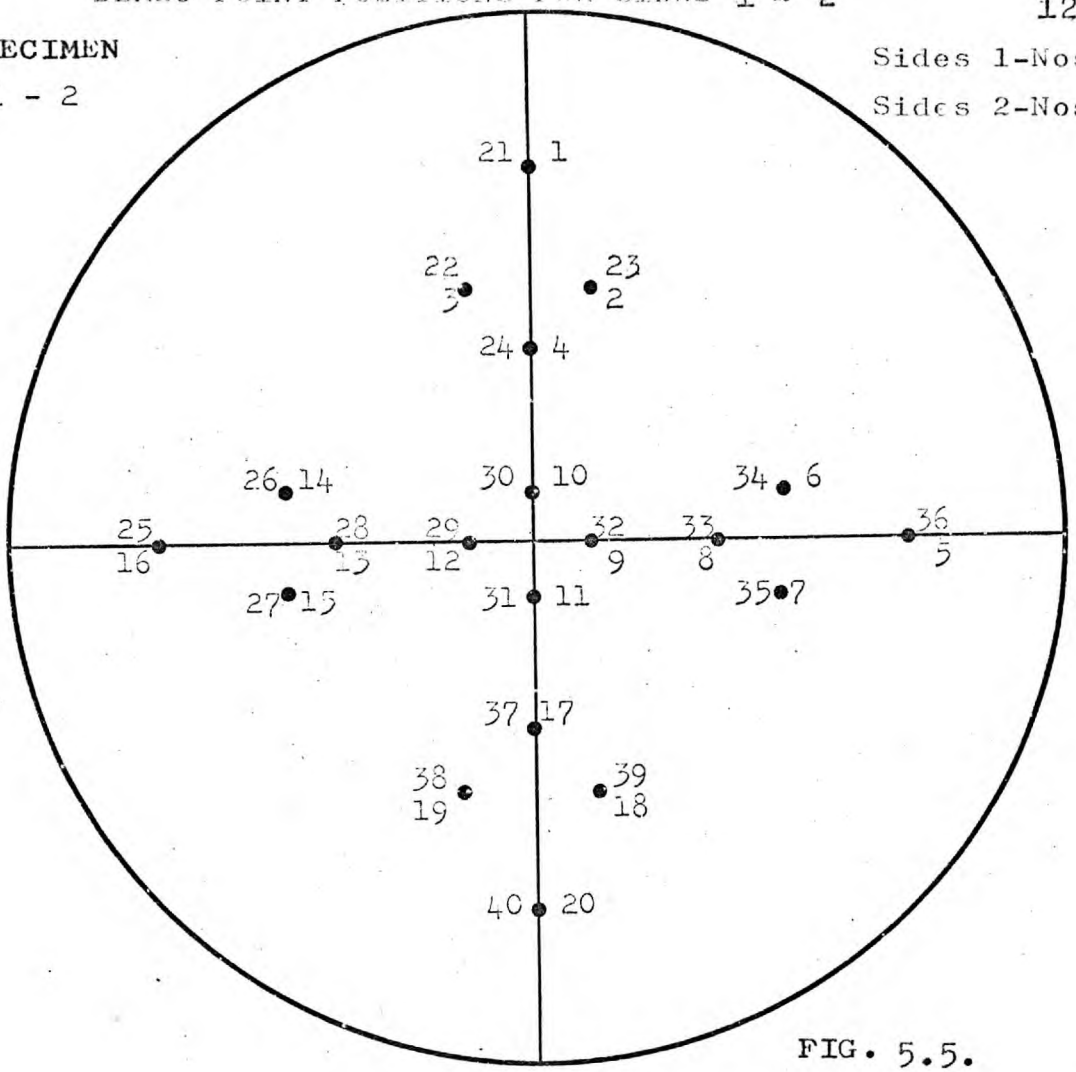

FIG. 5.5.

THERMOCOUPLE POSITIONS VIEWED FROM SIDE 2(TOP)

SPECIMEN
1-2

t - top
m - middle
b - bottom

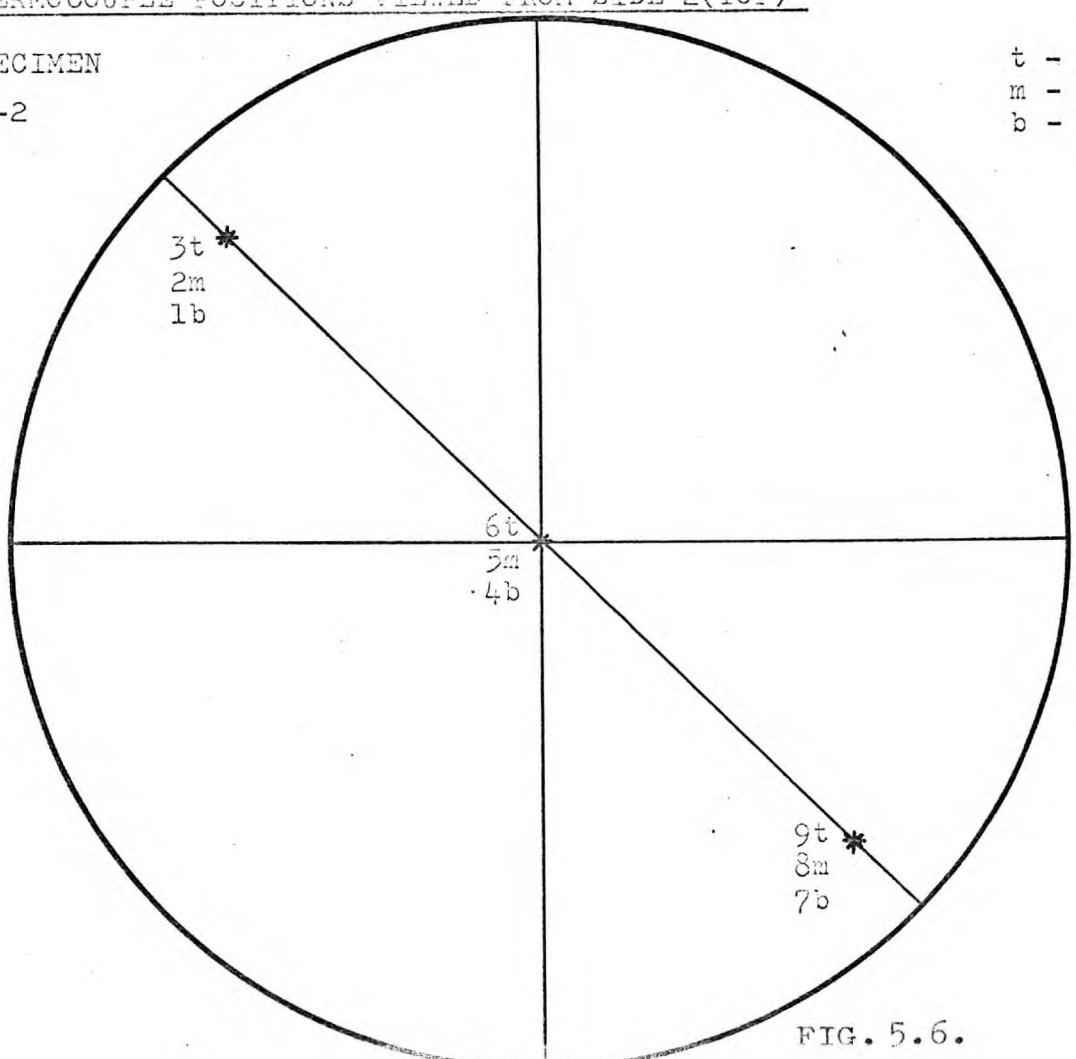

FIG. 5.6.

DEMEC POINTSPOSITIONS SIDES 3 AND 4

SPECIMEN
3-4

Side 3-Nos. 41-60
Side 4-Nos. 61-80

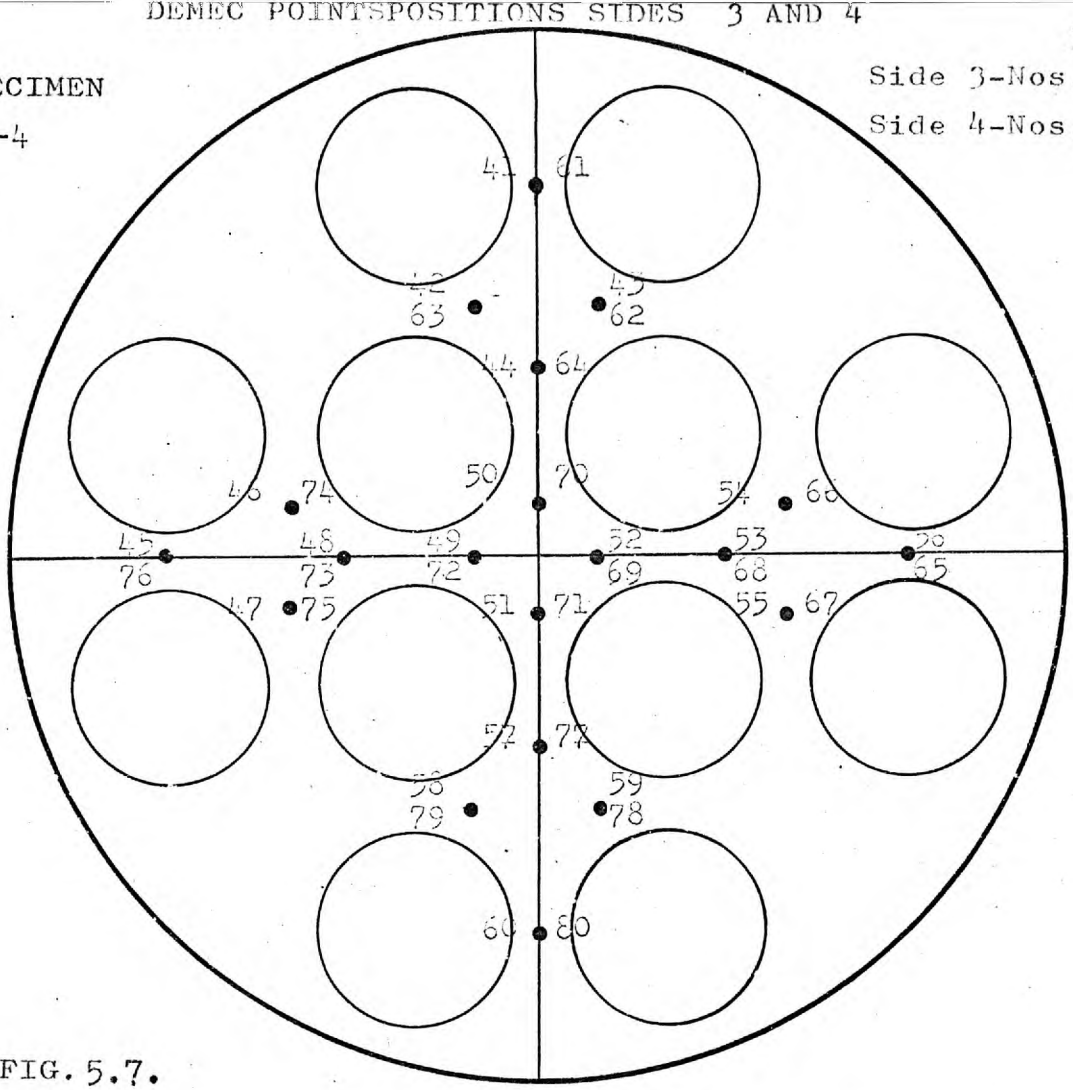

FIG. 5.7.

THERMOCOUPLE POSITIONS VIEWED FROM SIDE 3(TOP) & STANDPIPE POINTS

SPECIMEN
3-4

t - top
m - middle
b - bottom

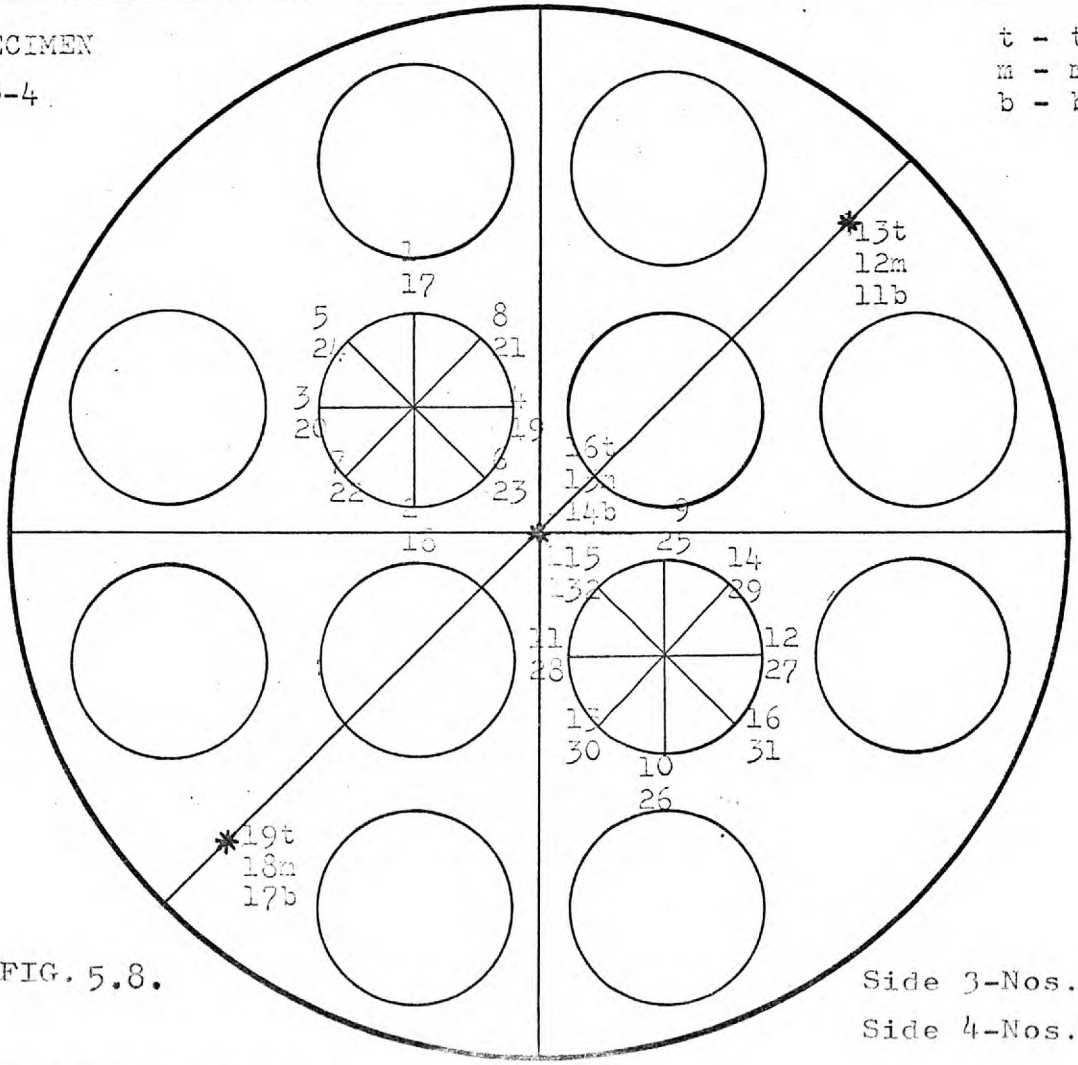

FIG. 5.8.

Side 3-Nos. 1-16
Side 4-Nos.17-32

DEMEC POINT POSITION SITES 5 AND 6

SPECIMEN

5-6

Side 5-Nos.81-100

Side 6-Nos.101-120

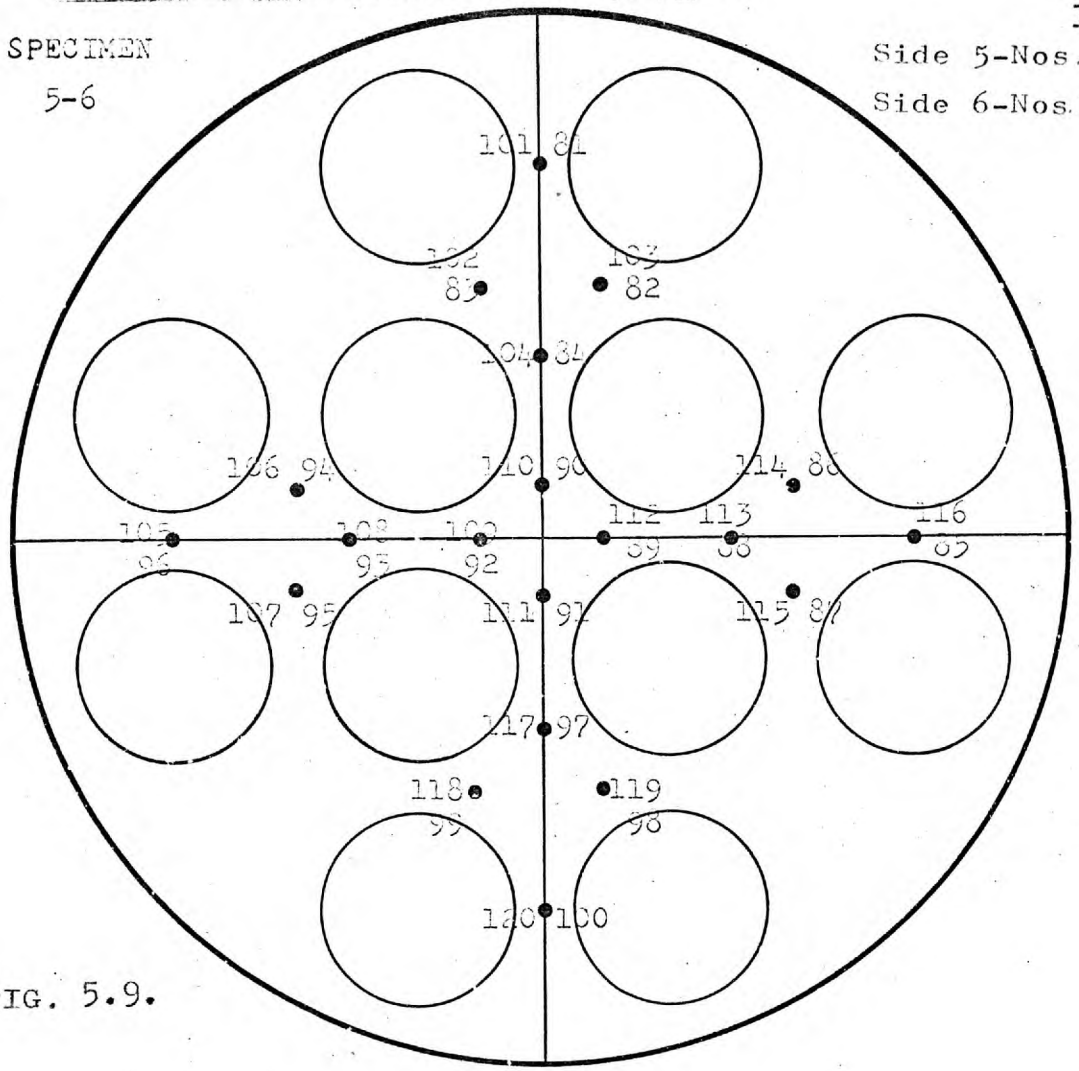

FIG. 5.9.

THERMOCOUPLE POSITIONS VIEWED FROM SIDE 6(TOP) & STANDPIPE POINTS

SPECIMEN

5-6

t - top
m - middle
b - bottom

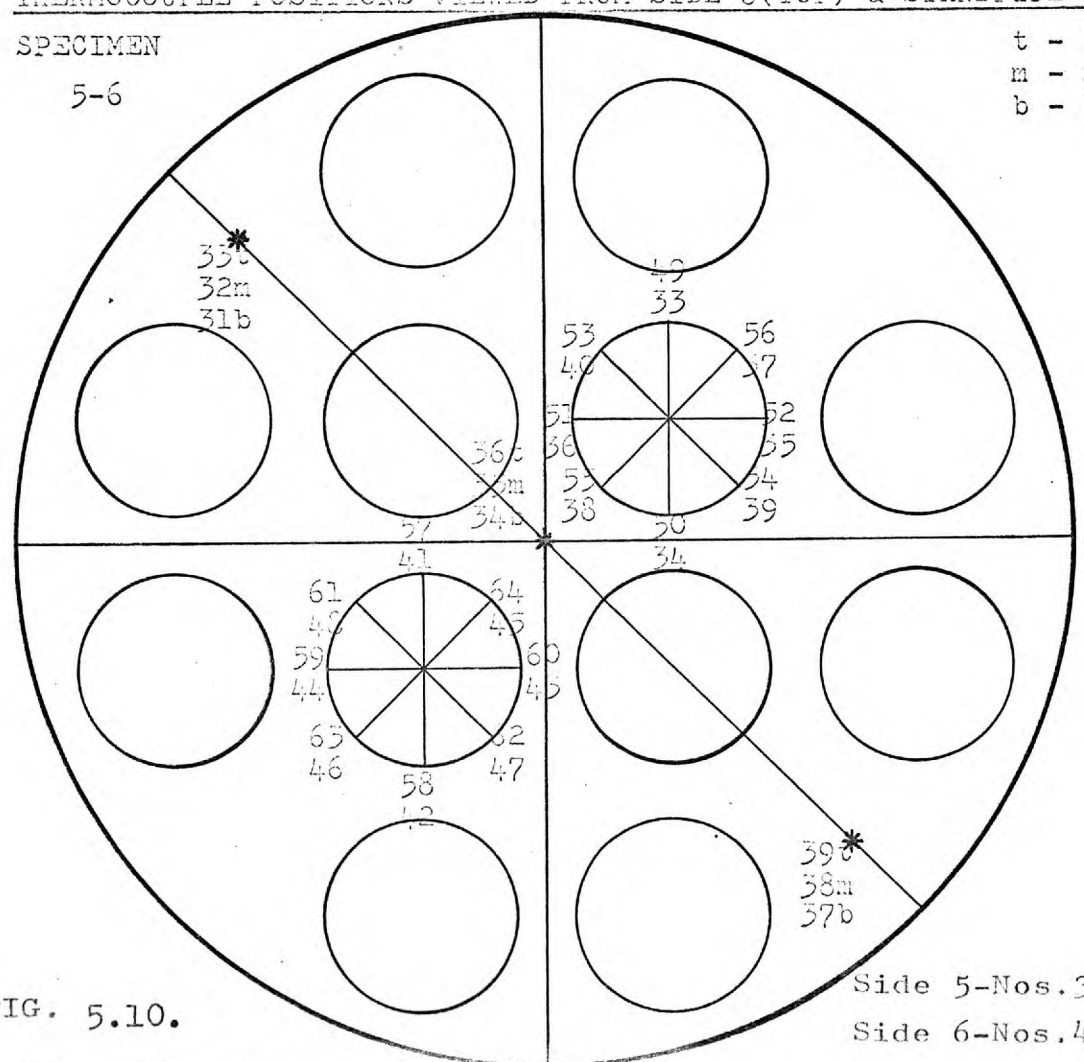

FIG. 5.10.

Side 5-Nos.33-48

Side 6-Nos.49-64

DEMEC POINT POSITION SITES 7 AND 8

SPECIMEN

7-8

Side 7-Nos. 121-140

Side 8-Nos. 141-160

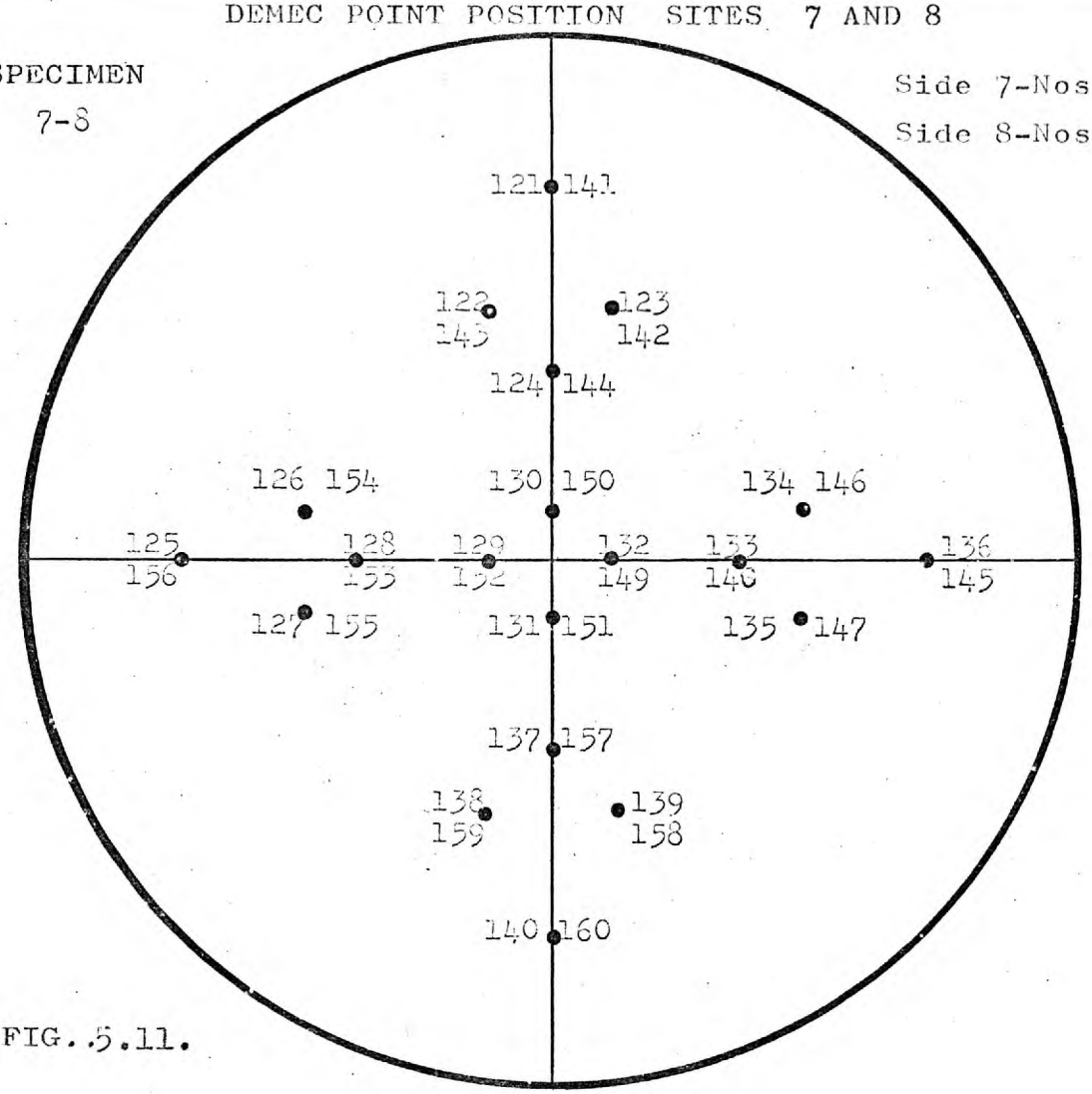

FIG. 5.11.

THERMOCOUPLE POSITIONS VIEWED FROM SIDE 7(TOP)

SPECIMEN

7-8

t - top
m - middle
b - bottom

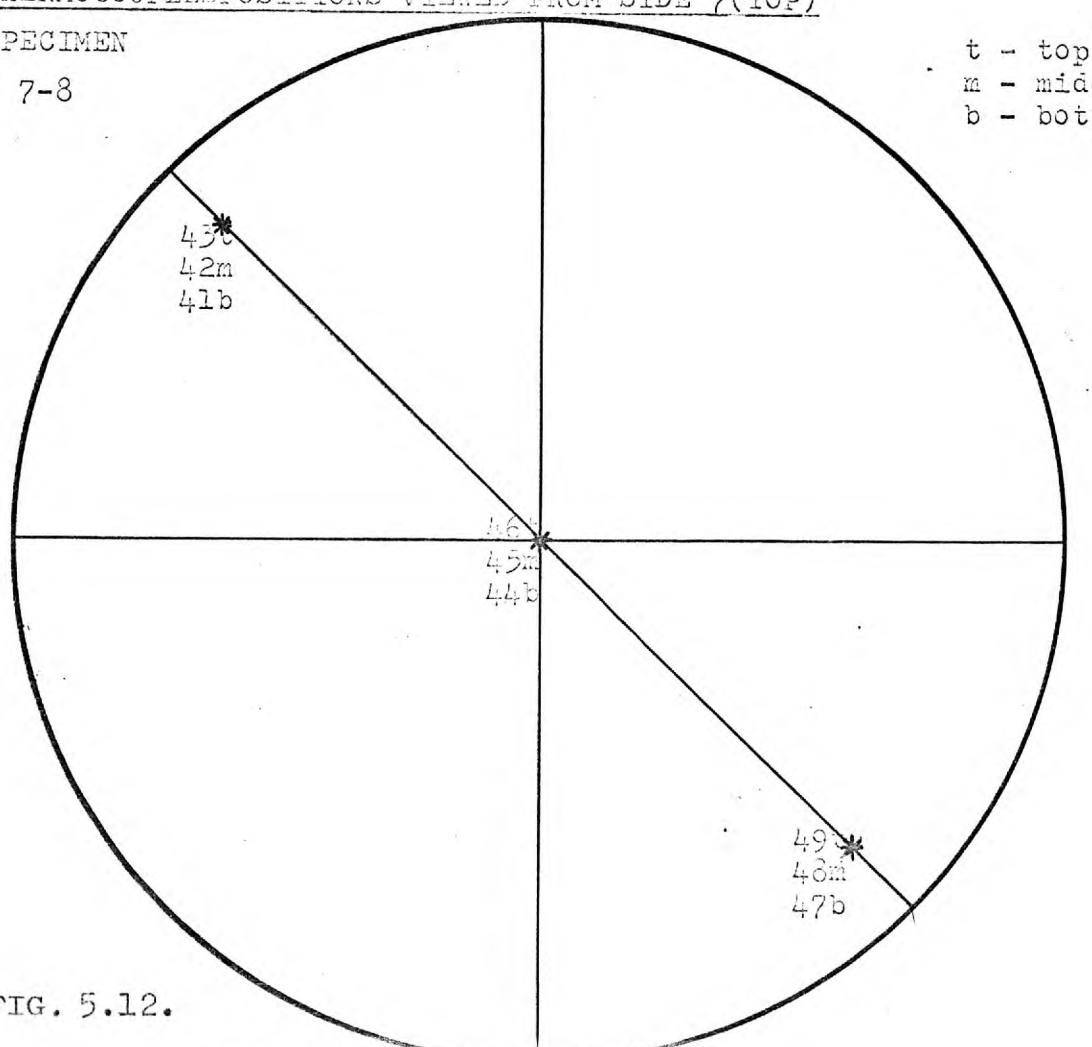

FIG. 5.12.

DEMEC POINT POSITIONS FOR SIDES 9 & 10

SPECIMEN

9-10

Side 9-Nos. 161-212

Side 10-Nos. 213-264

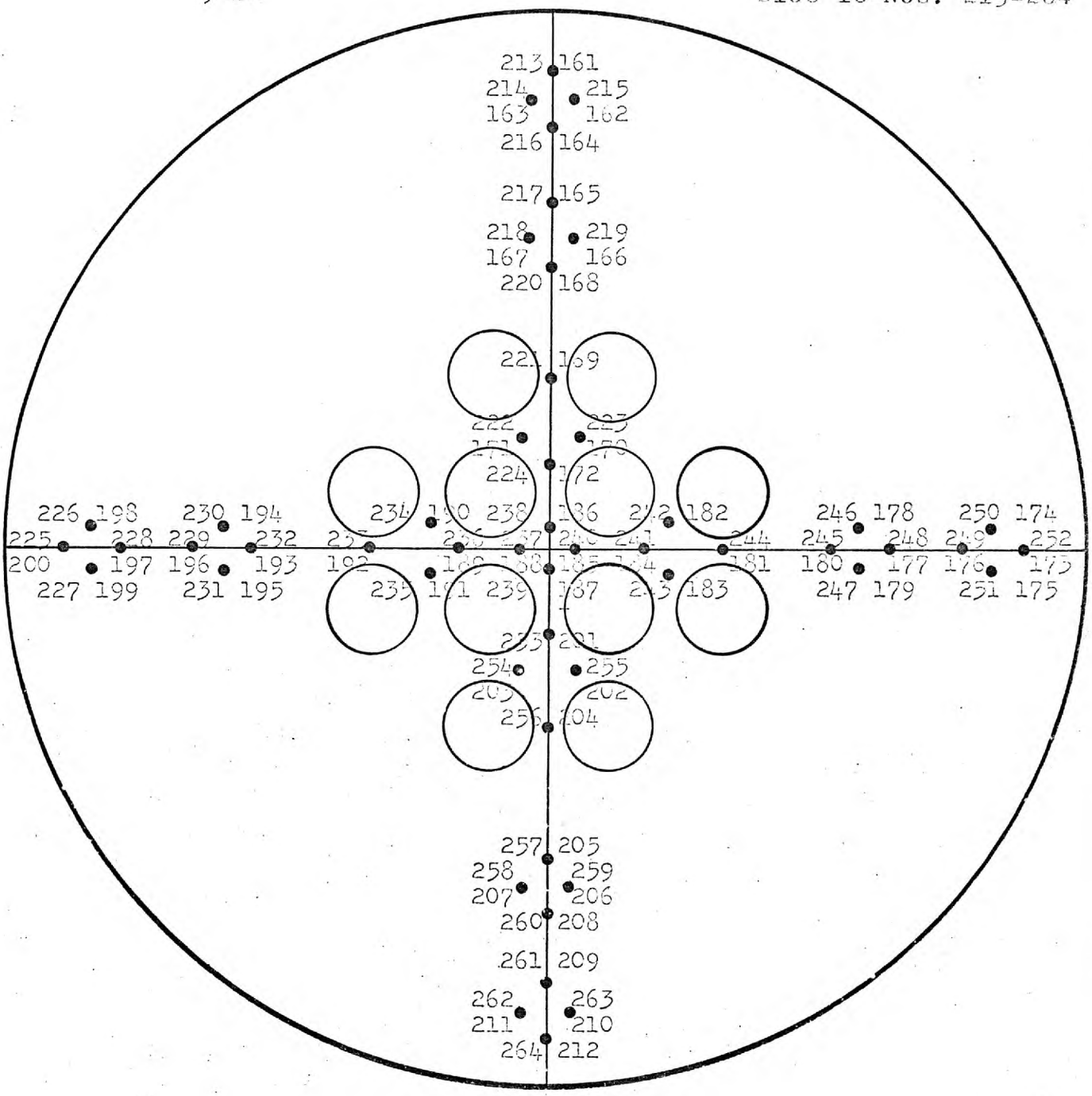

FIG.5.13.

THERMOCOUPLE POSITIONS VIEWED FROM SIDE 9 & STANDPIPE POINTS

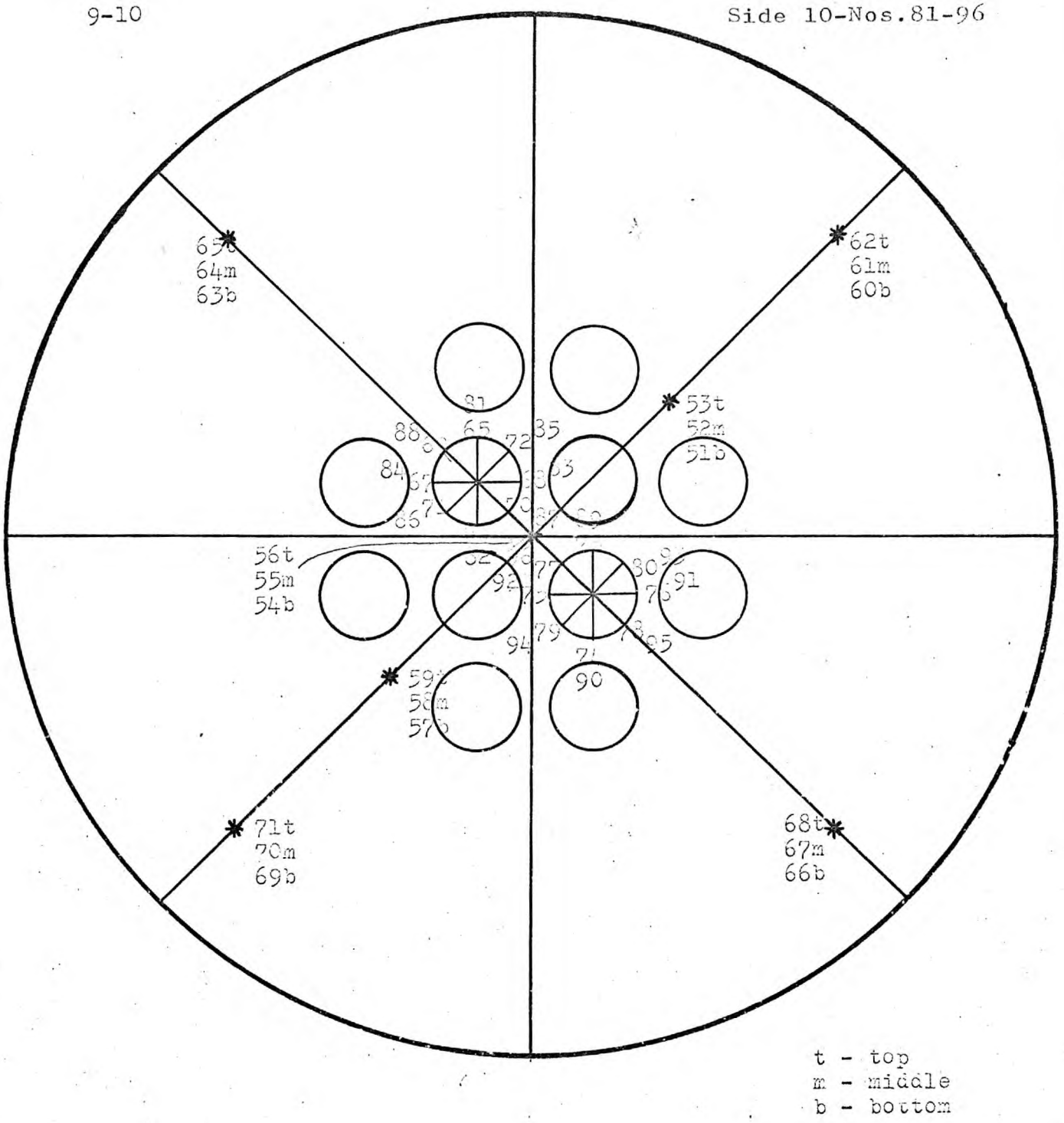

FIG. 5.14.

the conical spigots registered and located in precise positions over ¼" tubes. The jig was used for drilling the baseplate, registering and positioning the Demec positions accurately. It was removable during concrete placing. Plate P6.

5.2.5. Casting procedure - preliminaries.

1) Thermocouple positioning.

Before concreting, a series of thermocouples were positioned in the ligaments and elsewhere according to the arrangements shown in Figs. 5.15, and 5.16. In the case of the specimens containing standpipes, the thermocouples were introduced down the standpipe tubes and entered the concrete ligaments via mid-depth holes in the tube walls. In the solid specimens, the thermocouples were merely cast directly into the concrete at the required positions. Figs. 5.4. (b), and 5.15. Nine thermocouples were cast into each of the $16^3/4$" specimens in an arrangement of three sets of three, spaced across the diameter. For the position and numbering of the thermocouples, see Figs., 5.6, 5.8, 5.10 and 5.12. Of each set of three, one was at mid-slab, and the other two were 1" from opposing concrete faces.

Twenty-one thermocouples were placed in the 36" diameter specimen in an arrangement of seven sets of three. Fig. 5.14. Plate P3, (P2, perf. spec.). Three of these sets of three, were in positions corresponding to those in the $16^3/4$" slabs. The other four sets, were positioned, one set in each quadrant in the outer region.

2) Thermostat tubes.

In addition, two steel thermostat tubes were cast into each specimen near the ends of a diametral

LAYOUT OF THERMOCOUPLES IN THE SOLID SPECIMENS

(MODELS 1/2 AND 7/8)

Nine thermocouples in three sets of three

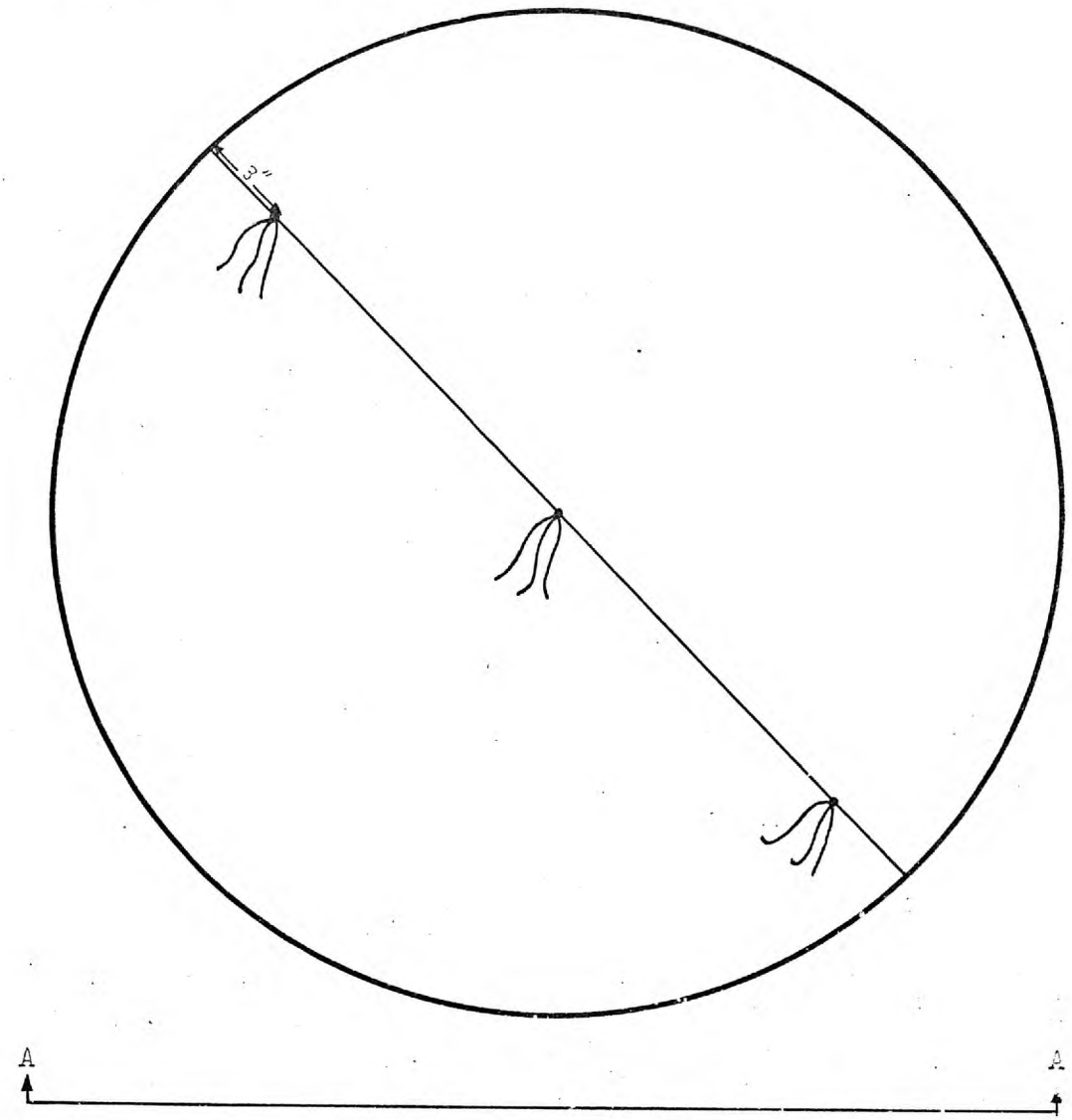

PLAN

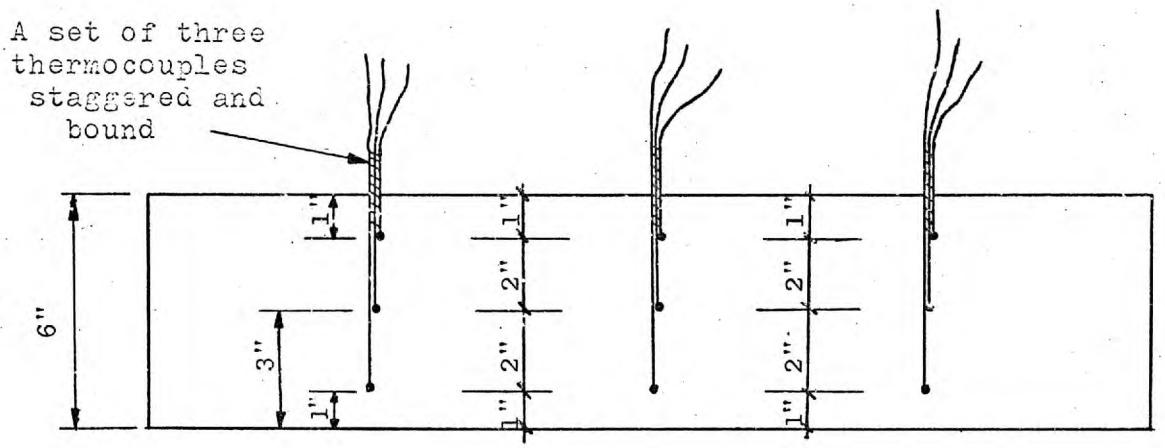

VIEW ON A-A

FIG. 5.15.

LAYOUT OF THE THERMOCOUPLES IN THE 36" DIAMETER COMPOSITE SPEC

(The layout of the thermocouples in the perforated zone is typical of the layout in the 16½" diameter perforated specimens)

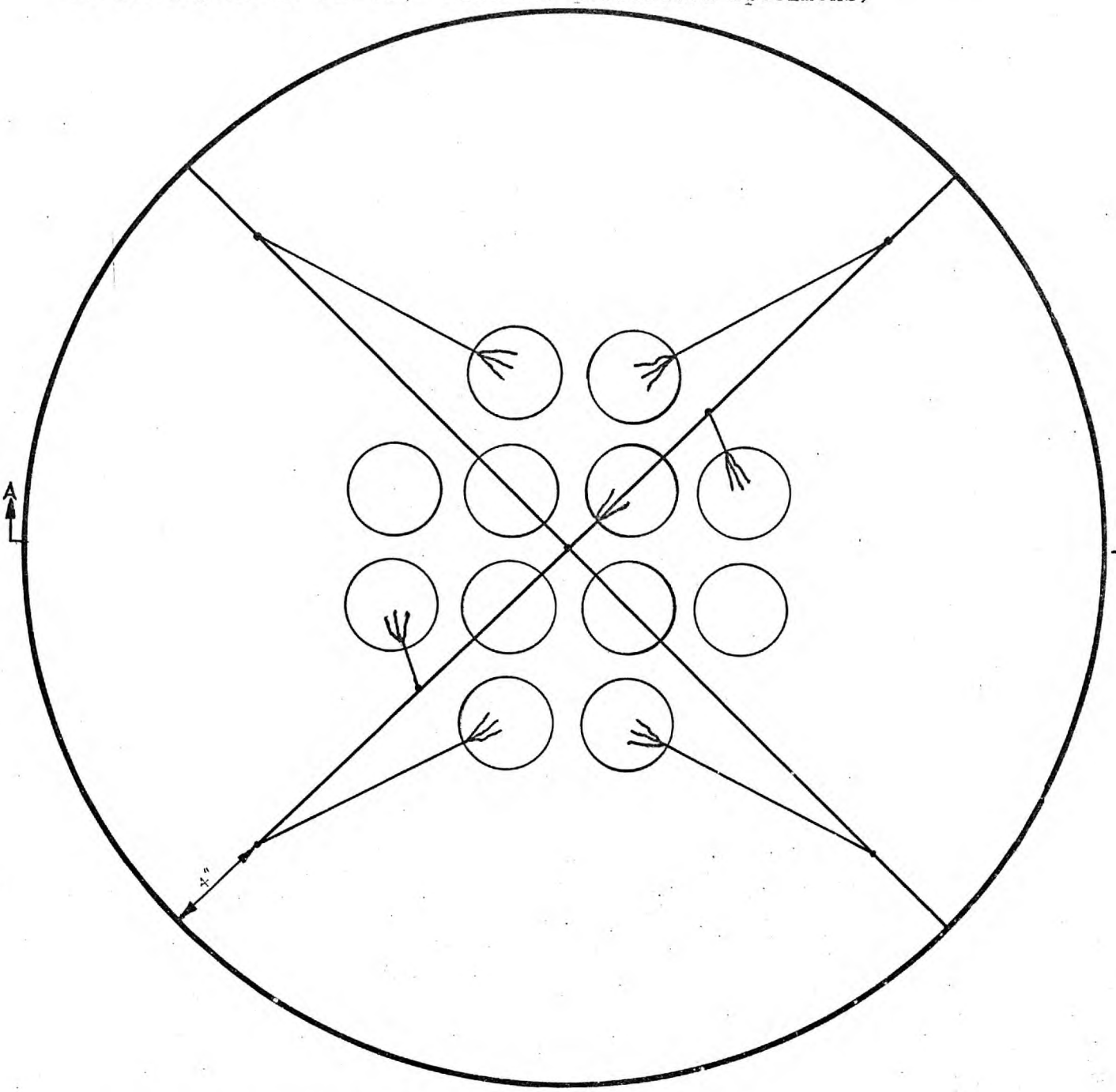

Twenty-one thermocouples in seven sets of three

PLAN

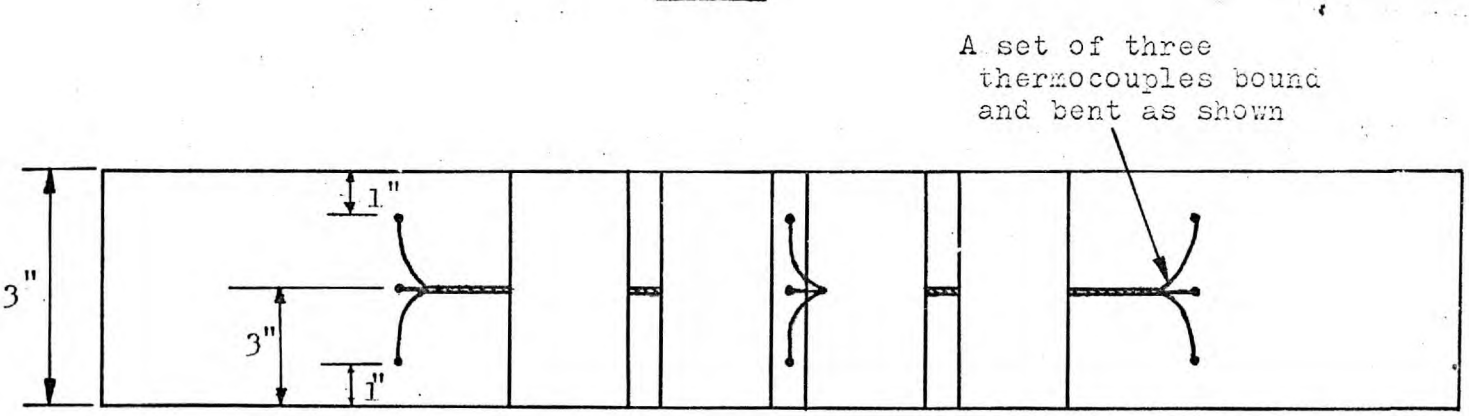

FIG.5.16. VIEW ON A-A

line, to take the thermostat probes. In the 3rd series the thermostat tubes were omitted. Each probe governed the temperature of each heating circuit. There were two separate heating circuits, one for each face of each specimen.

When these arrangements had been made, and the standpipes, Demec tubes, thermocouples and thermostat tubes firmly fixed, the open ends of all tubes were temporarily plugged to prevent ingress of concrete, and placement could begin. Plates P2, P3.

3) Casting.

All the specimens were cast with the moulds on a vibrating table, and the five specimens in each series plus the additional control specimens, required three batches from the pan mixer. The concrete was placed in position with small hand tools and carefully and evenly introduced into the ligament sections in several layers before vibration started. Care was taken to ensure even distribution of aggregate throughout each specimen both in the congested and uncongested sections.

During casting the positions of Demec tubes were checked by means of the cruciform jig, and finally the top surfaces of the specimens were floated off evenly by hand trowel.

4) Control Specimens.

The following control specimens were cast from the same mix for testing, during the succeeding period:-

Batch 1:

4/4"x4"x4" cube specimens for crushing strength.

2/4"x12" prisms for E value tests.

2/4"x12" prisms for coefficient of linear expansion tests.

2/6"x9" cylinders for the Brazilian tensile test.

Batch 2:
As for Batch 1:

Batch 3:
As for Batch 1, except for the cylinders.

In addition, compacting factors and slump tests were made for each batch.

5.2.6. Curing prior to testing.

The large specimens and the control specimens were cured under wet hessian in a temperature and humidity-controlled atmosphere for periods upto 28 days, or until required for testing.

5.2.7. Coating.

After the specimens had been removed from curing, three coats of Peridite thixotropic paint were applied around the edge of the specimens. This paint was applied to seal the edge, and so prevent moisture loss in that direction.

5.3. Test equipment. TABLE 5.6.

Loading Rigs. Fig. 5.17. Plate P7.
Pressure Circuit. Fig. 5.18.
Heating Circuit. Fig. 5.19*.
Temperature Measurement Circuit. Fig.5.20*.
Insulation Shield. Fig. 5.21.
Sealing
Crack Detection Circuit. Fig. 5.22.
ERSG Circuit. Fig. 5.23.

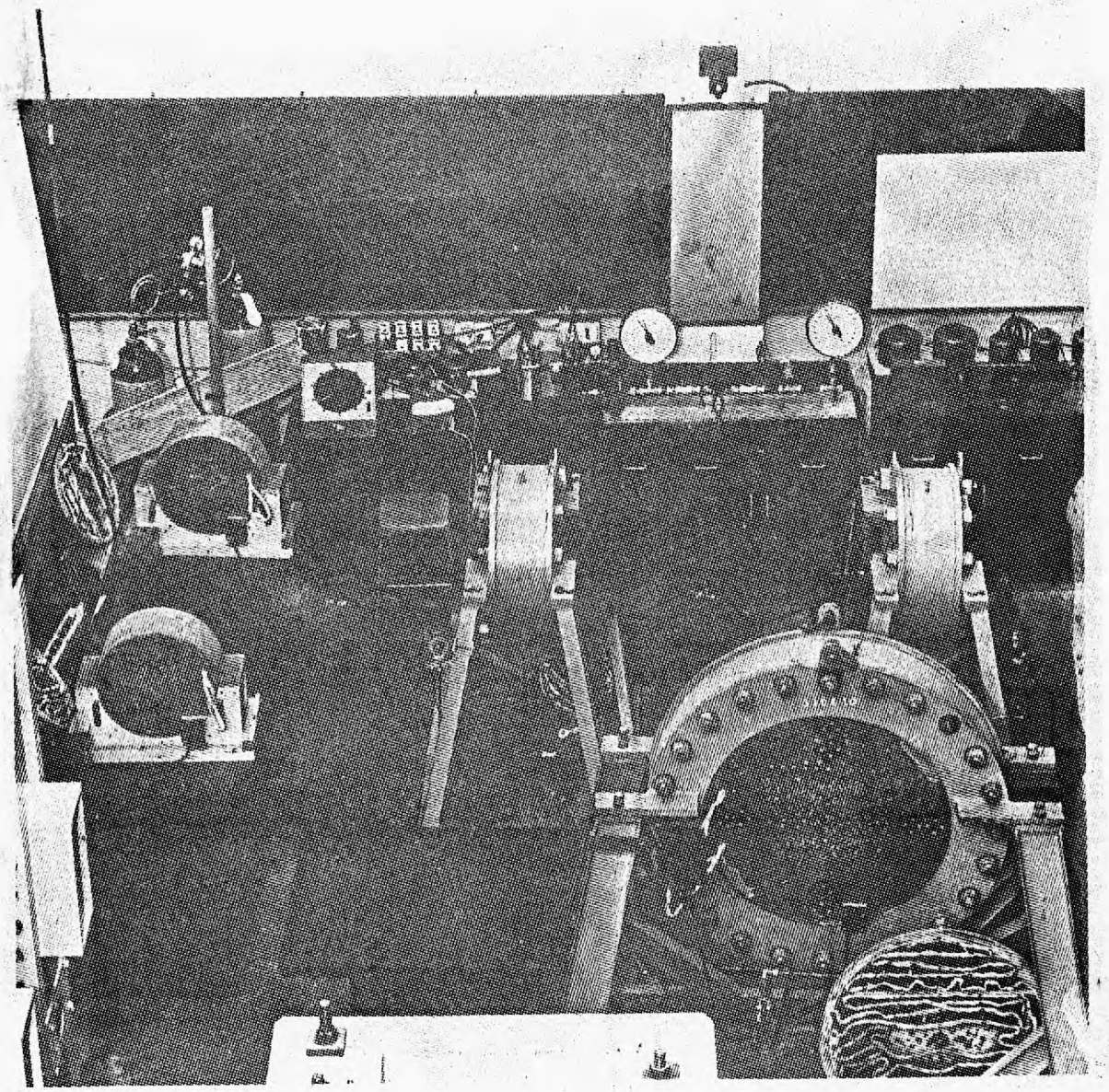

PLATE P7.

General view of test specimens.

Table 5.6

MODEL	PLAIN STANDPIPES	ST.P. WITH MEAS. HOLES	ST.P. WITH TH'C. HOLES	THERMO-PROBE TUBES FOR THERMOSTATS	ROUND OIL HEXAGONAL STEEL TUBES	DEMEC GAUGE BRASS STUDS	THERMO-COUPLES
16 3/4 DIA Solid Plate (Shrinkage Spec.)	-	-	-	2	20	20	9
16 3/4 DIA Solid Plate (Shr. & Creep Spec.)	-	-	-	2	20	20	9
16 3/4 DIA Perf. Plate (Shrinkage Spec.)	7	2	3	-	20	20	9
16 3/4 DIA Perf. Plate (Shr. & Creep Spec)	7	2	3	-	20	20	9
36" DIA Composite Plate (Shr. & Creep Spec.)	3	2	7	-	52	52	21
TOTAL	17	6	13	4	132	132	57

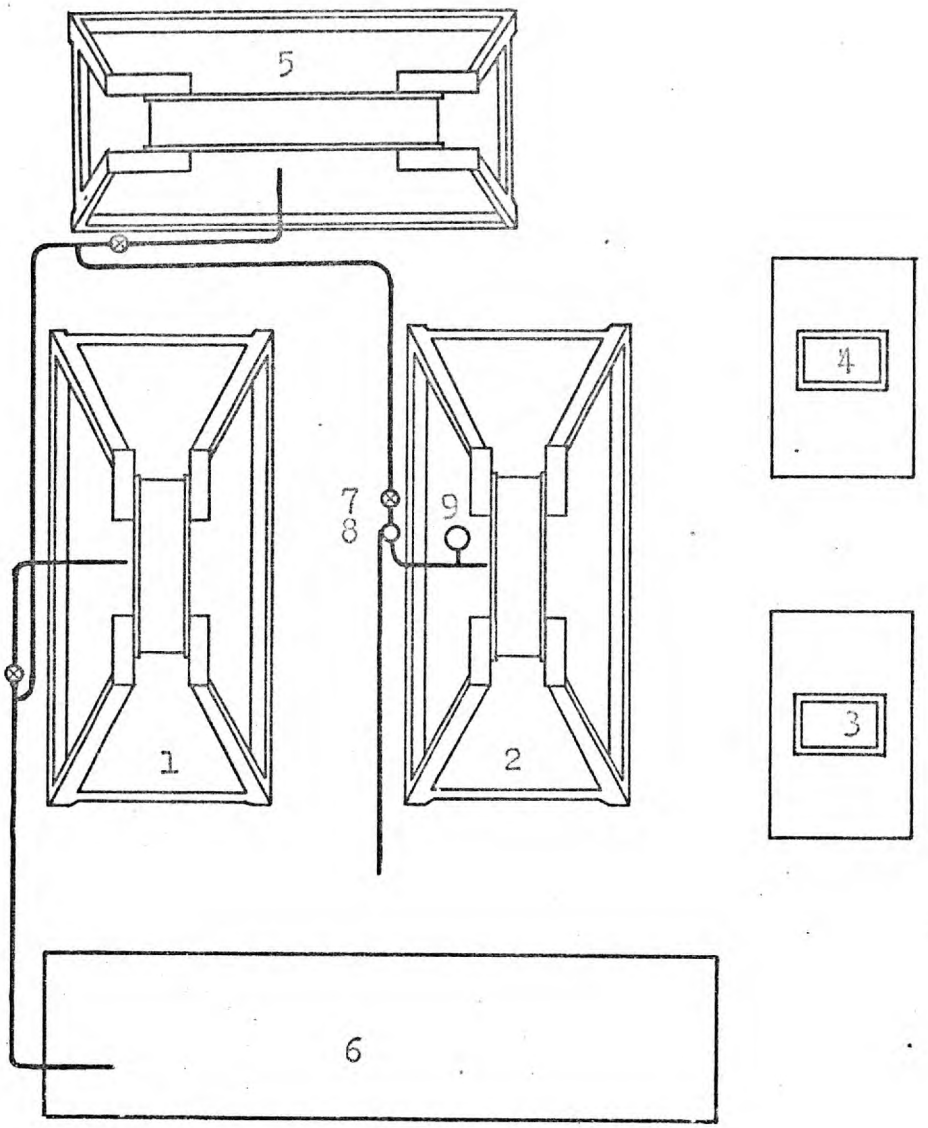

FIG. 5.17 LAYOUT OF RIGS AND FRAMES

1. Rig for 16 3/4" diameter solid specimen
2. Rig for 16 3/4" diameter perforated specimen
3. Sadle for 16 3/4" diameter perforated specimen
4. Sadle for 16 3/4" diameter solid specimen
5. Rig for 36" diameter composite specimen
6. Table assembly (See Plate P16.)
7. Pressure relief valve
8. Pressure reducing valve
9. Pressure gauge

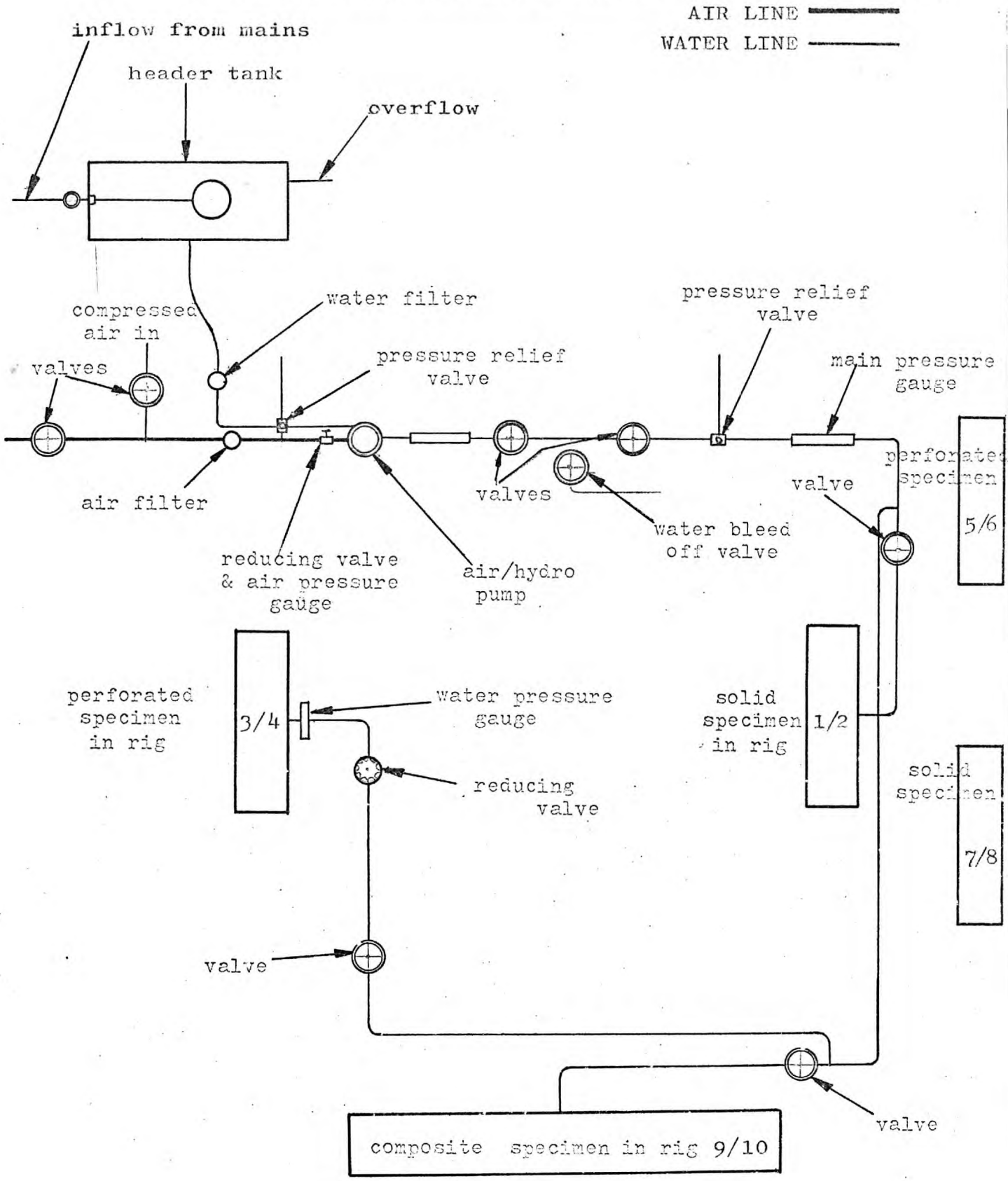
AIR LINE
WATER LINE
inflow from mains
header tank
overflow
compressed air in
valves
water filter
pressure relief valve
pressure relief valve
main pressure gauge
air filter
reducing valve & air pressure gauge
air/hydro pump
valves
water bleed off valve
valve
perforated specimen 5/6
perforated specimen in rig
3/4
water pressure gauge
reducing valve
solid specimen in rig
1/2
solid specimen 7/8
valve
valve
composite specimen in rig 9/10

FIG. 5.18.

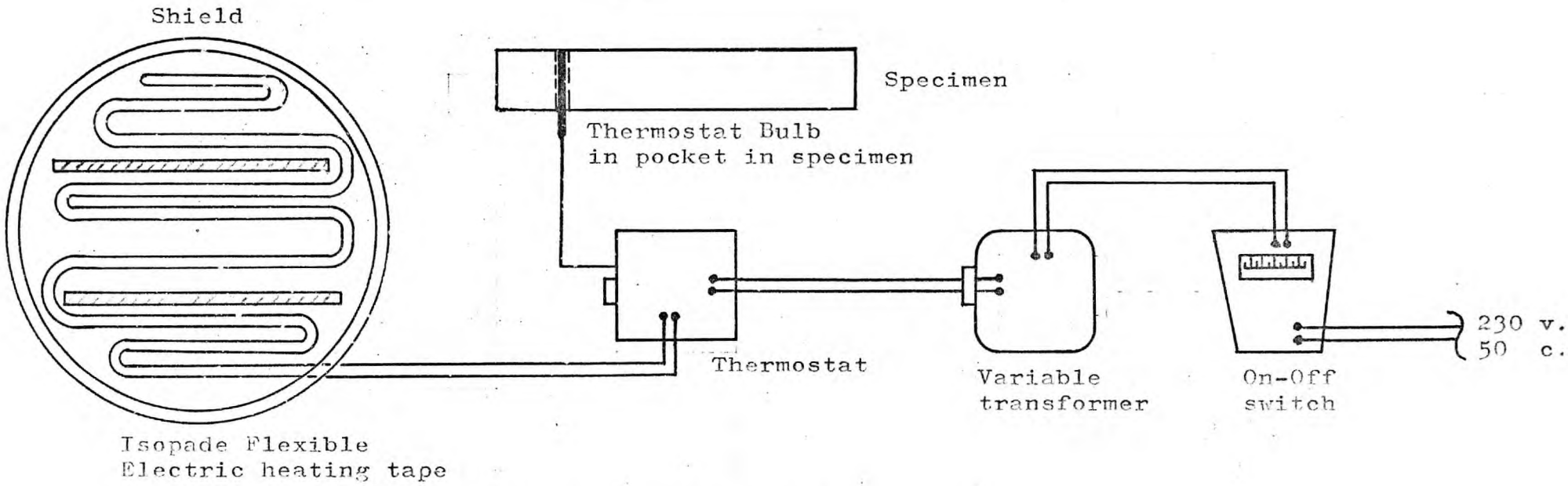

FIG. 19 HEATING CIRCUIT

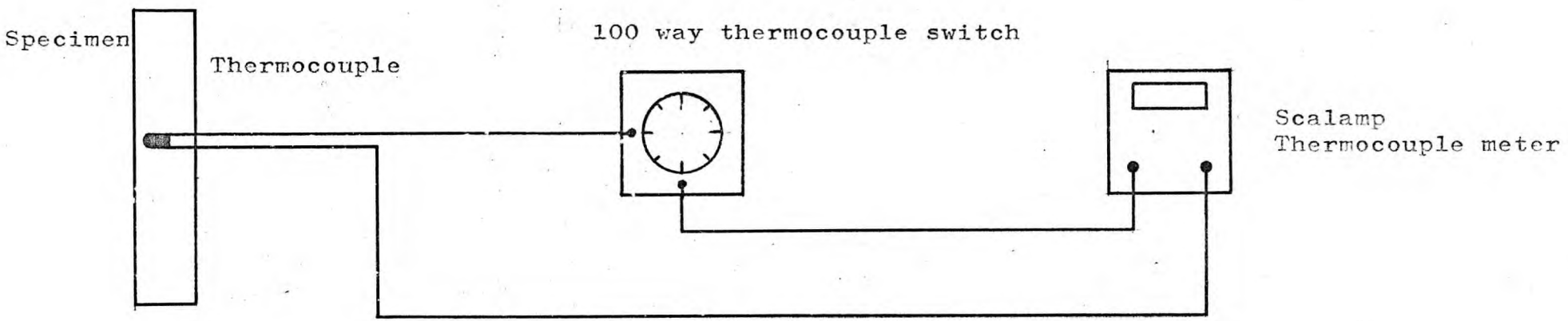

FIG. 20 THERMOCOUPLE CIRCUIT (temperature measurement circuit)

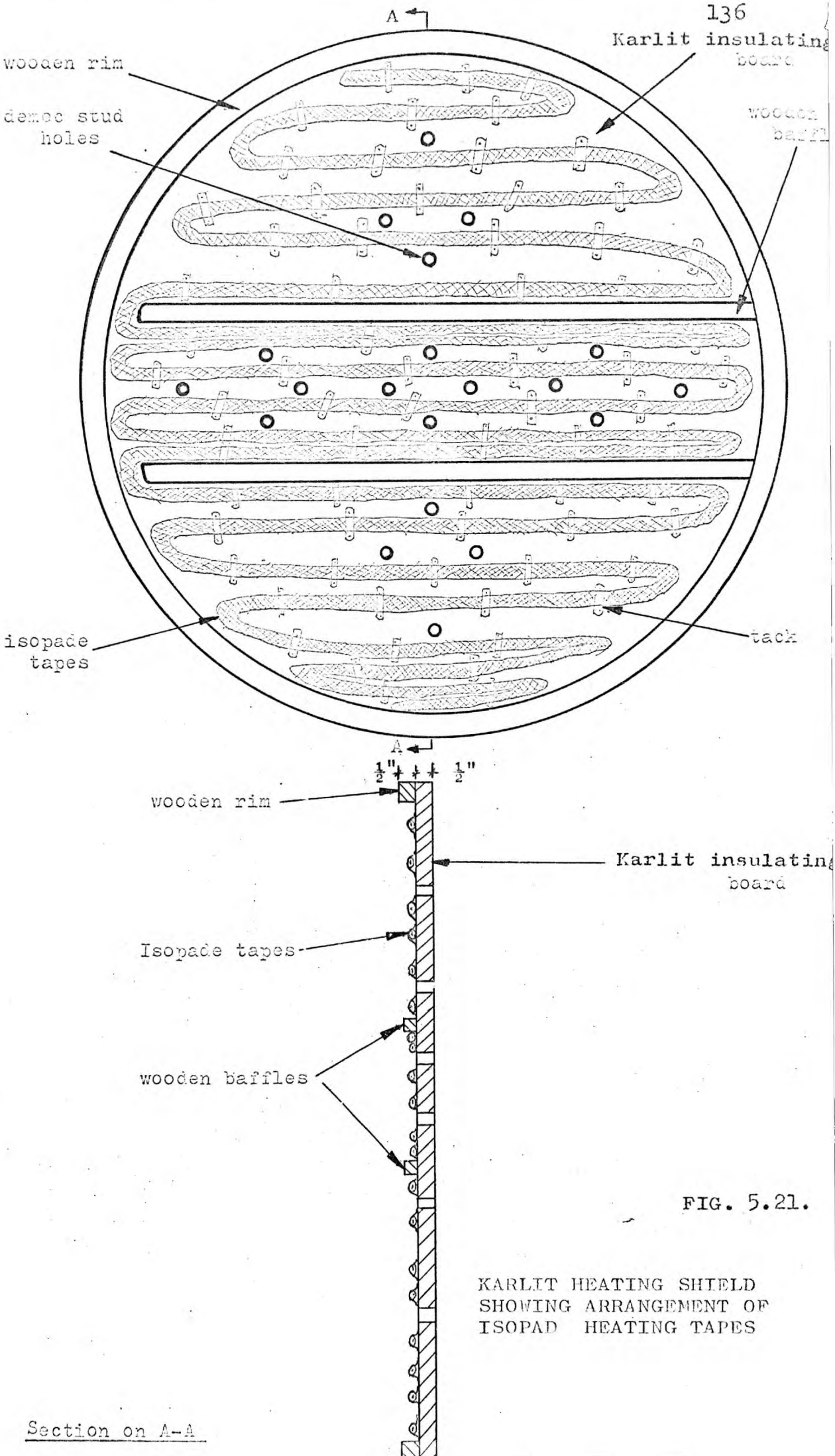

FIG. 5.21.

KARLIT HEATING SHIELD SHOWING ARRANGEMENT OF ISOPAD HEATING TAPES

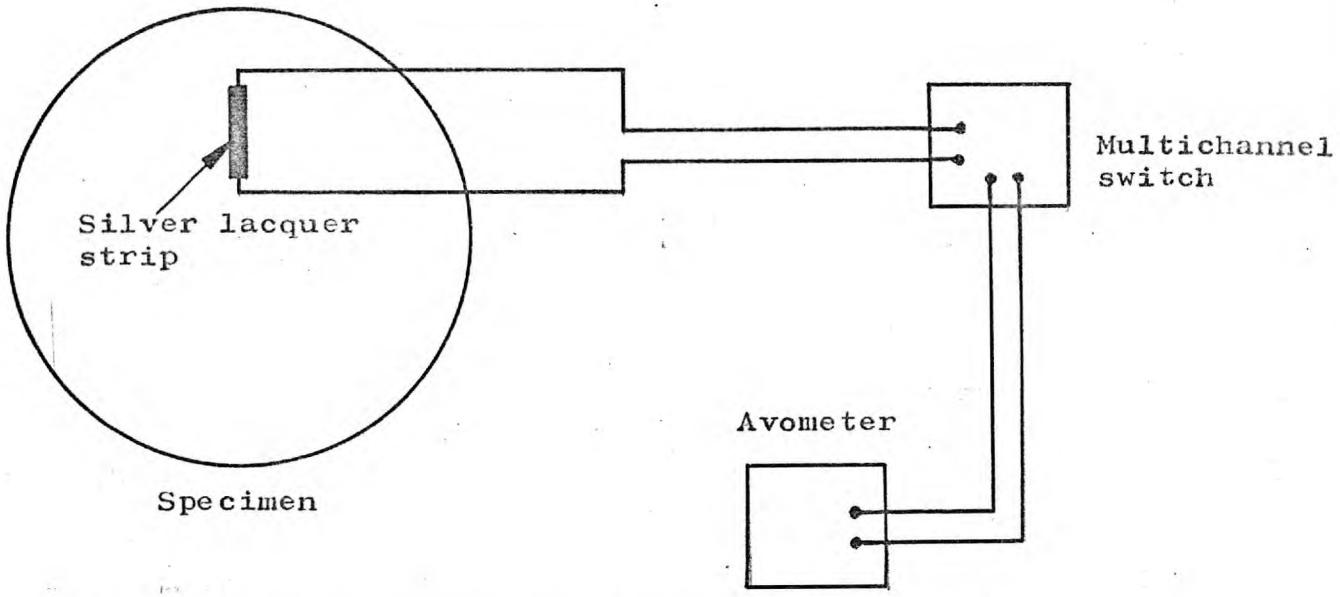

FIG.5.22. CRACK DETECTION CIRCUIT

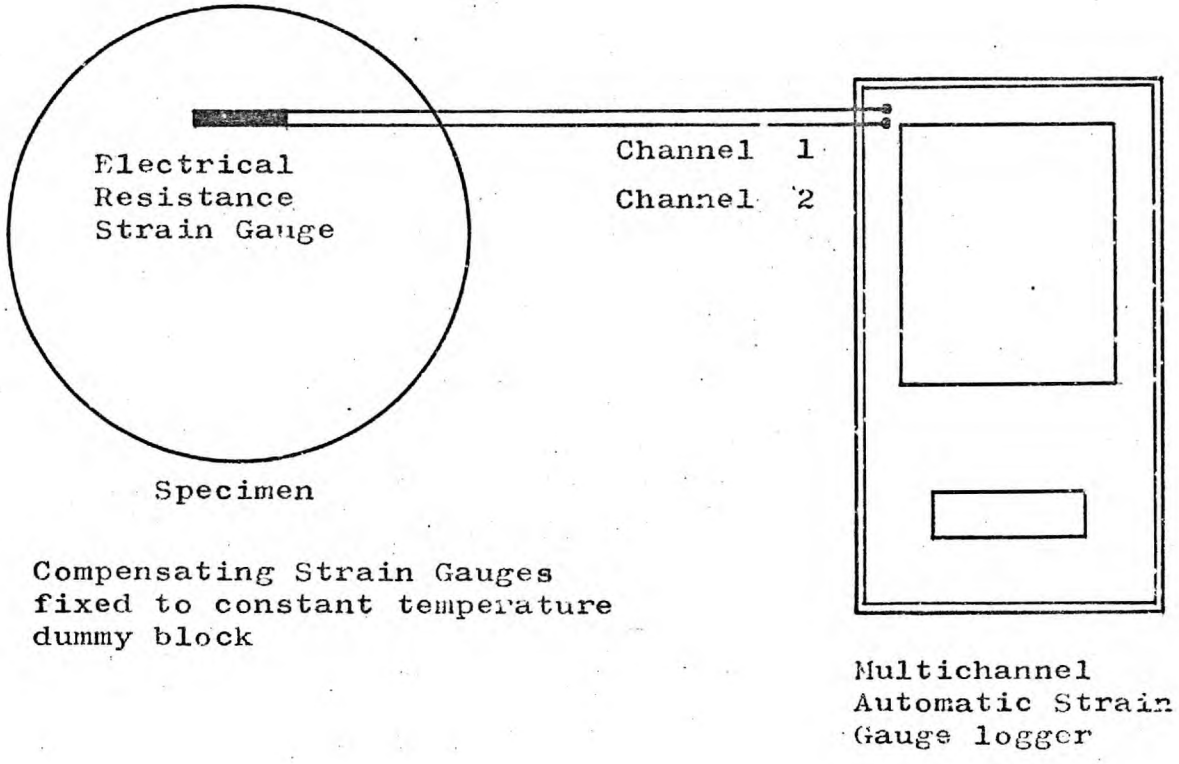

FIG. 5.23. ELECTRICAL RESISTANCE STRAIN GAUGE CIRCUIT

5.3.1. Loading rigs.

The layout of a section of the radial loading rig is shown in Figs. 5.24, 5.25, and 5.26. The upper part of the rig consisted of a vertical circular loading arrangement, which was removable from its supporting stand. Plate P8.

This upper section consisted essentially of a vertical steel retaining hoop between which, and the installed circular concrete specimen within, was confined a stiff neoprene rubber water bag. The bag had an air vent connection at its top, and a water inlet at the bottom, both accessible through the hoop thickness. Plate P9.

As the water bag was pressurized from the pressure circuit, it was constrained between the hoop and the specimen, thus applying a radial compression to the concrete.

The hoop, which was $38\frac{1}{2}$" I.D. x $42\frac{3}{4}$" O.D. x $7\frac{1}{2}$" wide x $2\frac{1}{8}$" thick, was forged from a single steel piece and had machined edges and other surfaces.

Between the concrete specimens and the rubber bag was positioned a $7\frac{1}{2}$" wide $\frac{1}{2}$" thickness of tough conveyor belting designed to protect the rubber bag from the effects of the 80°C temperature to which the specimens were subjected. Plate P10.

Steel shim inserts were used to mask the joining edges of the belting and a heavy terylene cloth was also inserted to prevent damage to unprotected surfaces. French chalk was applied to the various surfaces to reduce friction during installation and operation.

The side reaction from the edge of the rubber bag was taken by two machined mild steel flanges

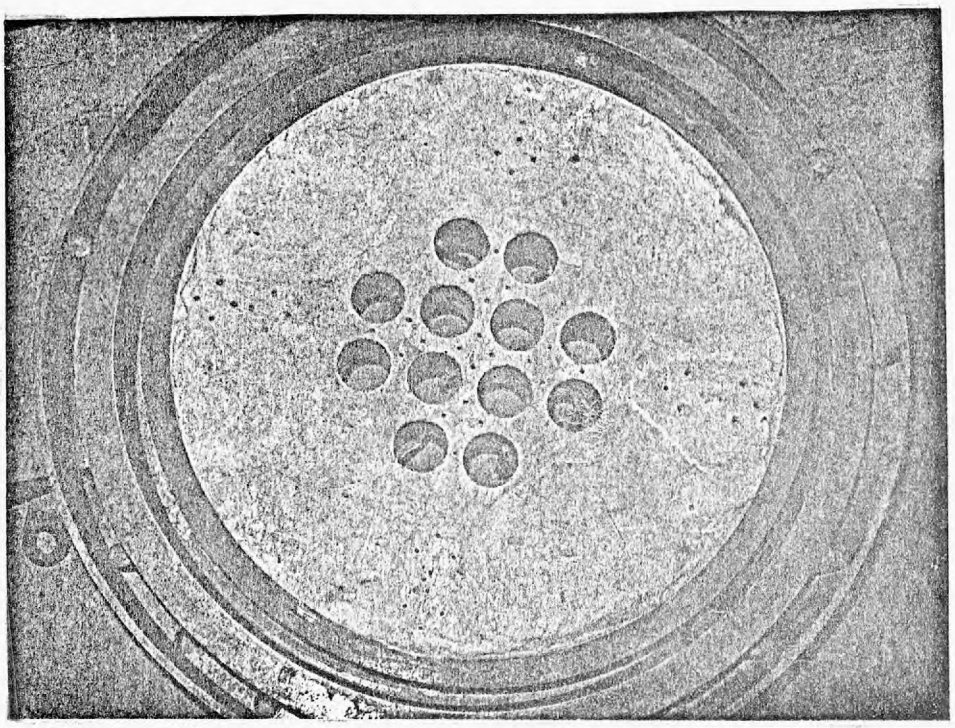

Plate P8.

View of test with flange plate removed and the specimen in position.

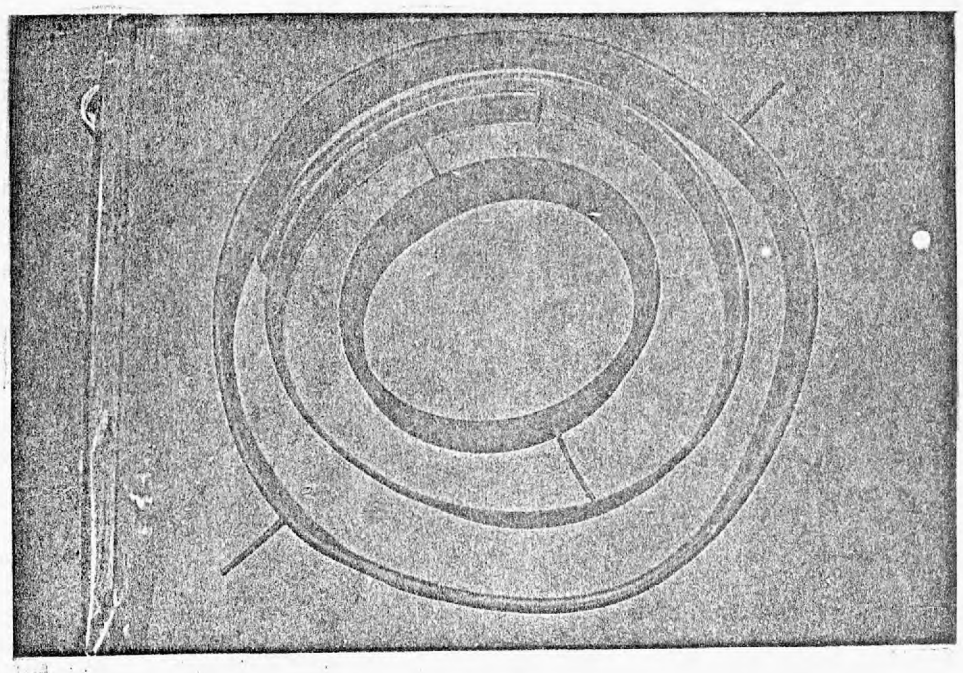

Plate P9. and Plate P10.

View of rubber bags and conveyor belting.

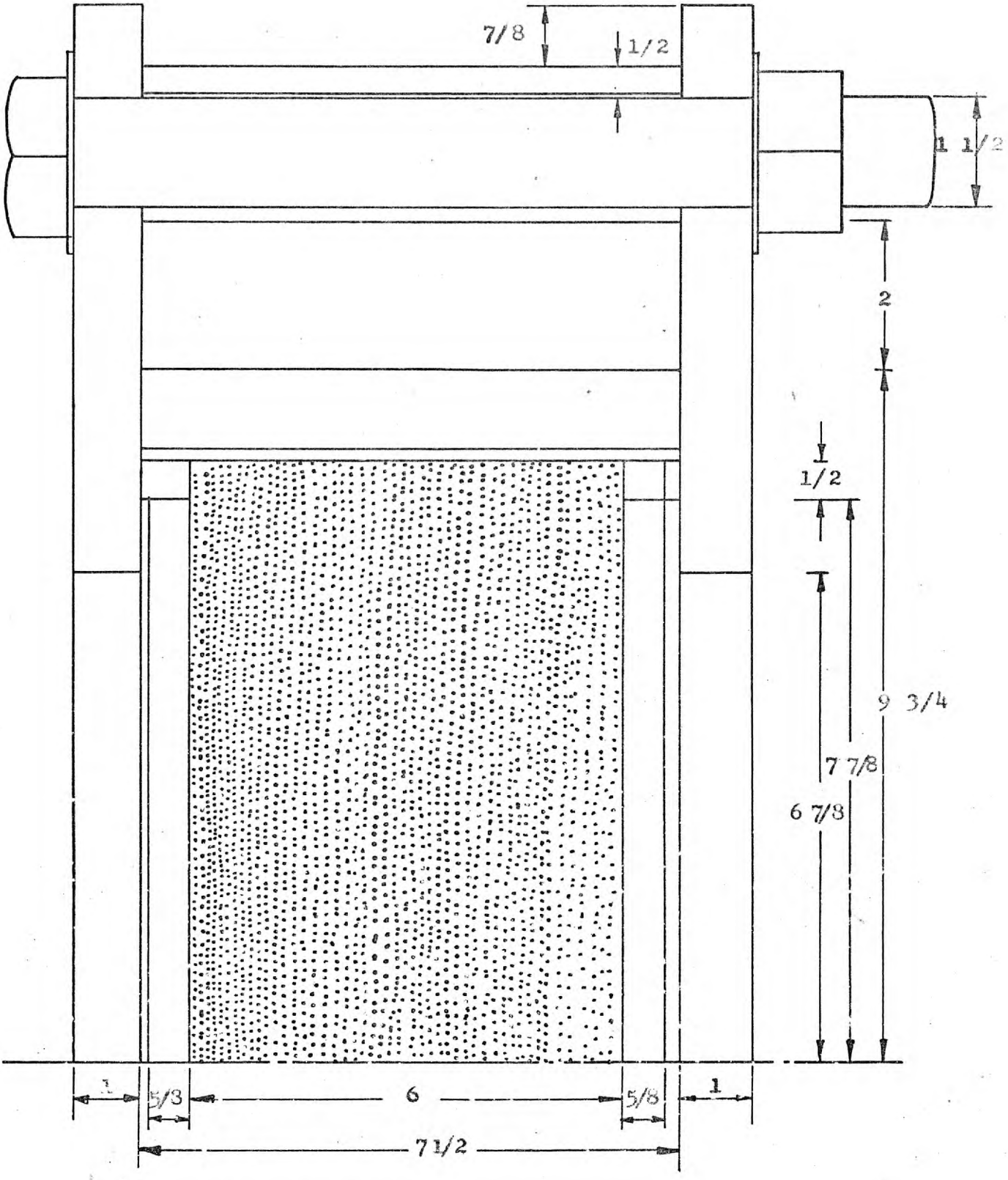

FIG.5.24. VERTICAL SECTION
THROUGH 16 3/4 DIAMETER SPECIMEN LOADING RIG

A VERTICAL SECTION THROUGH 36" DIAMETER SPECIMEN LOADING RIG

(Model 9/10)

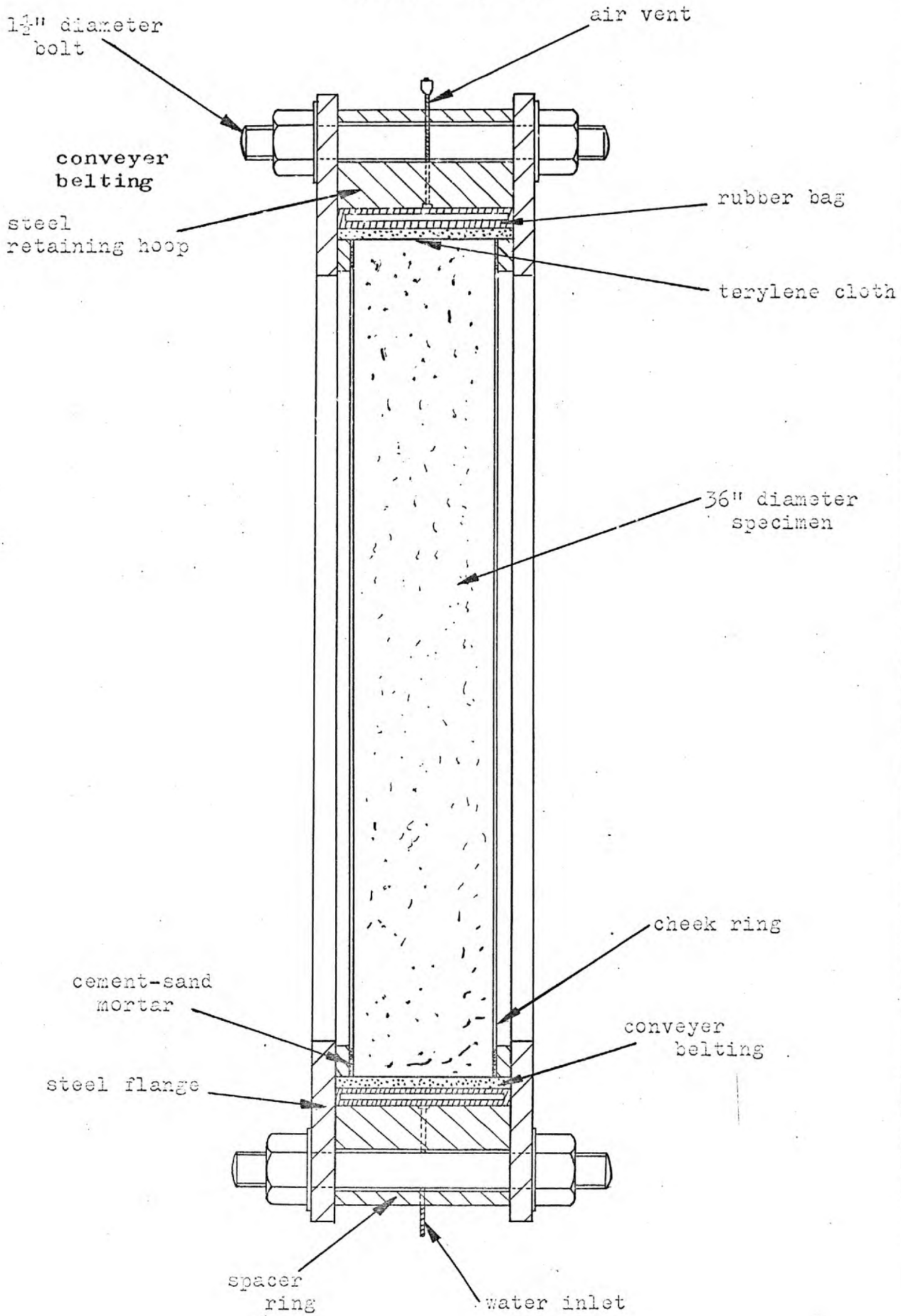

FIG. 5.25.

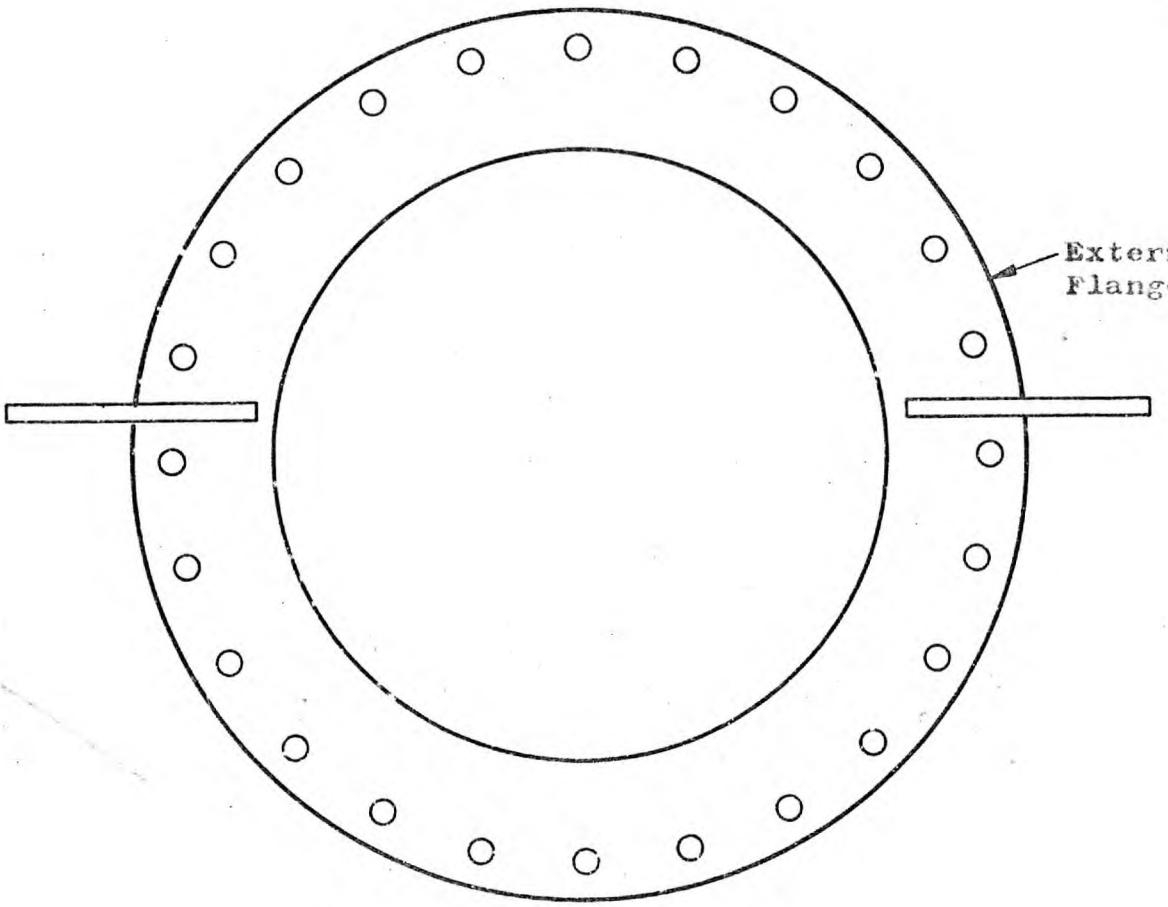

(a) VIEW WITH FLANGE PLATE IN POSITION

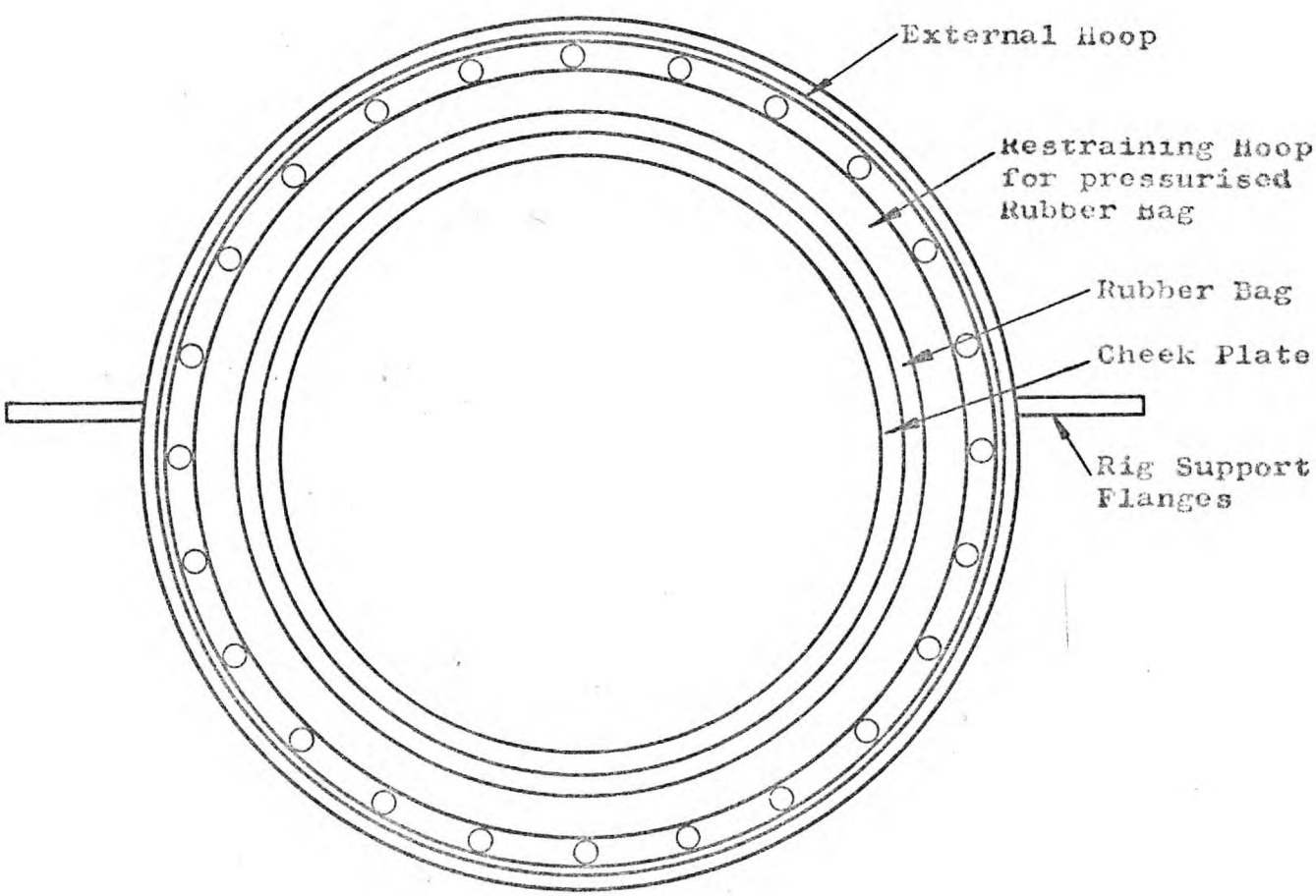

(b) VIEW WITH FLANGE PLATE REMOVED

FIG. 5.26. DETAIL OF 36" DIAMETER RIG

one on each side of the bag. The flanges took the form of rings33" I.D. x 48½" O.D. x 15/16" thick, arranged in a vertical plane. The two flanges on each side of a rig were held 7½" apart, and the side trust taken by 24/1½" H.T. bolts tightened with a torque spanner. These bolts were spaced on a pitch circle immediately outside the position of the hoop.

To keep the flanges in equilibrium by balancing the bolt thrust, a machined steel spacer ring was arranged outside the bolt pitch circle. The spacer ring was46½" I.D. x 47½" O.D. x 7½" wide.

Since the space between the inner faces of the two mild steel flanges was 7½" and the concrete specimen width was only 6", two machined steel checkrings were required, one on either side to help restrin the specimen in a vertical position. However, a 1/8" gap was still left on each side between the specimen and the inner face of the cheek rings. This was intended to provide a certain tolerance for manufacture and installation.
During installation of the specimen in the rig - an operation which was performed with the rig lying on its side on the laboratory floor - the 1/8" on each side of the concrete slab was filled with a cement and sand mortar thus, bedding the cheek rings firmly.

The whole of the rig described was arranged with the specimen supported in a vertical plane. Welded to the sides of the steel flanges were brackets arranged at positions which permitted a four-point support onto a robust mild steel angle framework. The circular section of the rig, could thus, be bolted to the framework, and was manoeuvred on and off by overhead electric crane for installation or removal of the specimens. Plates P11 to P15, illustrate the five specimens in position ready for testing.

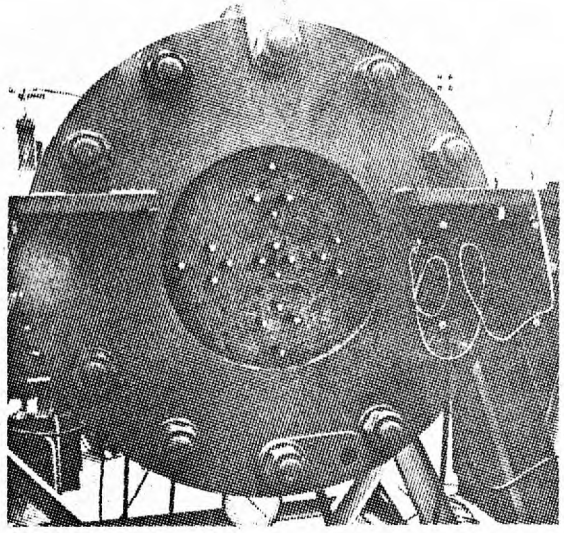

PLATE P11.

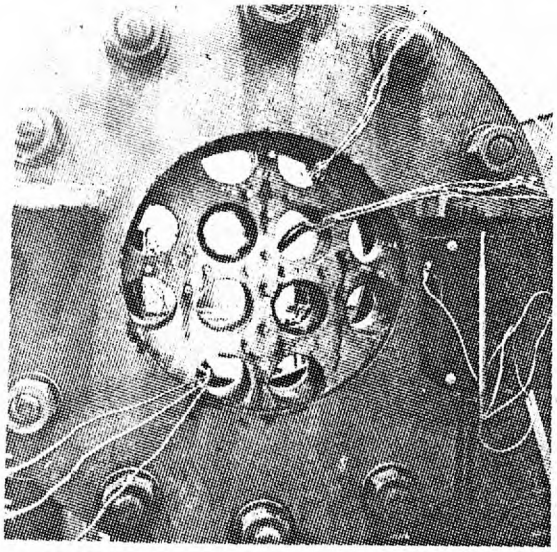

PLATE P12.

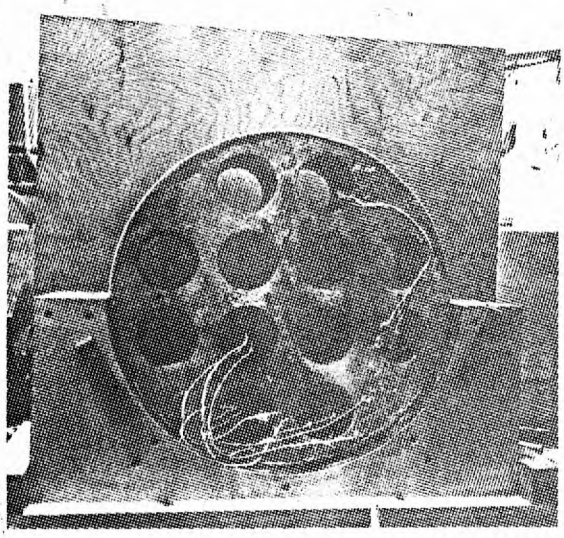

PLATE P13.

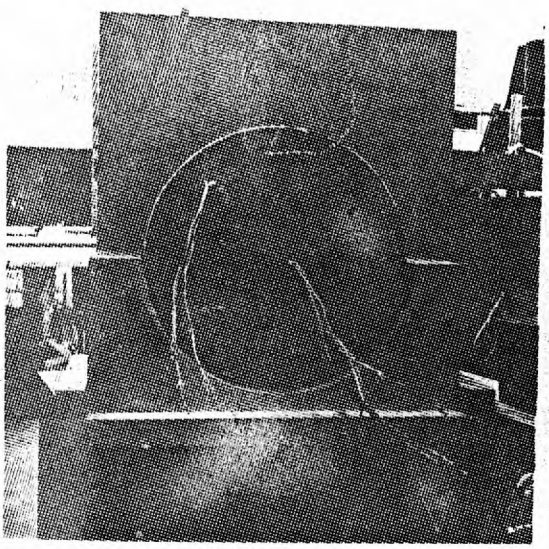

PLATE P14.

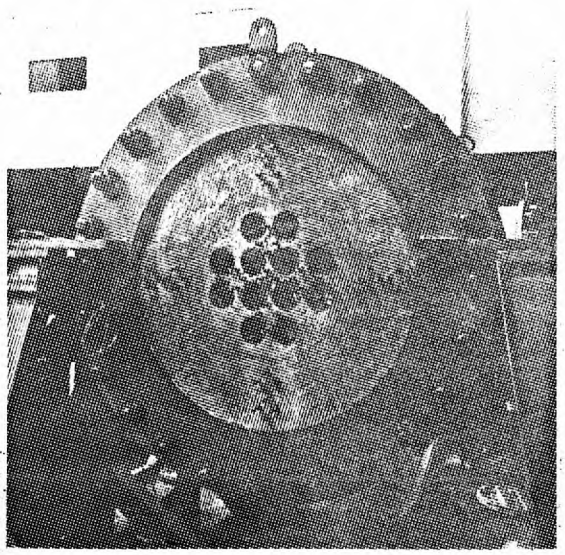

PLATE P15.

Specimens before commencement of test.

5.3.2. Pressure circuit.

This circuit is shown diagrammatically in the illustration Fig.5.18. The pressure was developed by an air-hydro pump which was driven by compressed air or alternatively, from a nitrogen cylinder, and which transferred the pressure at the outlet side to a water line. A pressure relief valve was provided on the air inlet side of the pump set to a pressure such that the test pressure of the loading rigs could not exceed the determined value. Plate P16.

It will be seen from Plate P17,that nitrogen cylinders were provided on the inlet side of the pump in such a manner, that either the laboratory compressed air line, or the cylinders could be used to provide the inlet pressure to activate the pump. Either source of pressure could be mobilized by valves.

It was expected that under service conditions, the pump could cut into the circuit very infrequently, and that the capacity of the two nitrogen cylinders would suffice to maintain the required pressures, except when the pump, the circuit and the pipeline to the rigs were being commissioned. The air supply was provided originally, in fact, to permit a large supply of air during the set-up of the apparatus and commissioning.

In practice, however, it was discovered that, the air-hydro pump was frequently called upon to maintain pressure, due to various unimportant but persistant small leakages in the circuit at valves etc. As a consequence, the pressure circuit was virtually continously connected to the air supply throughout the tests.

A reducing valve and an air pressure gauge were installed on the air line immediately before the

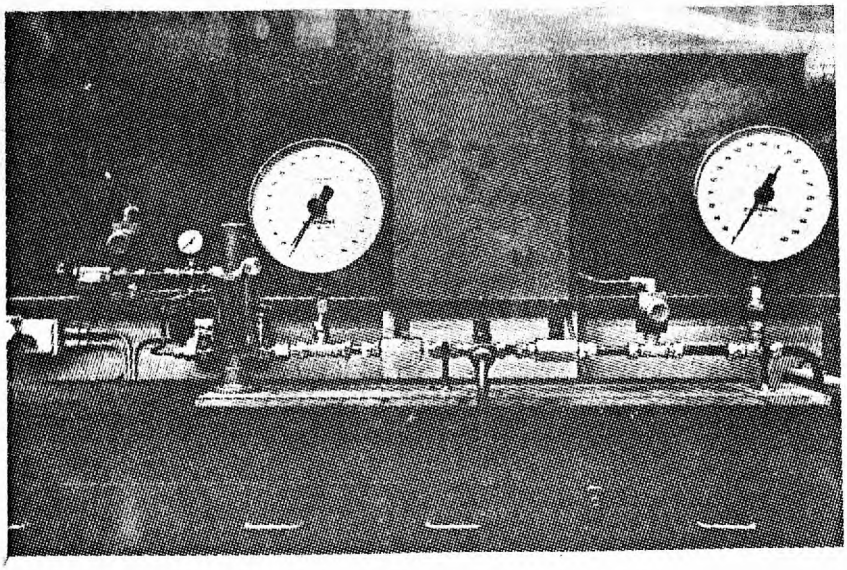

PLATE P16.

Air-hydro pump.

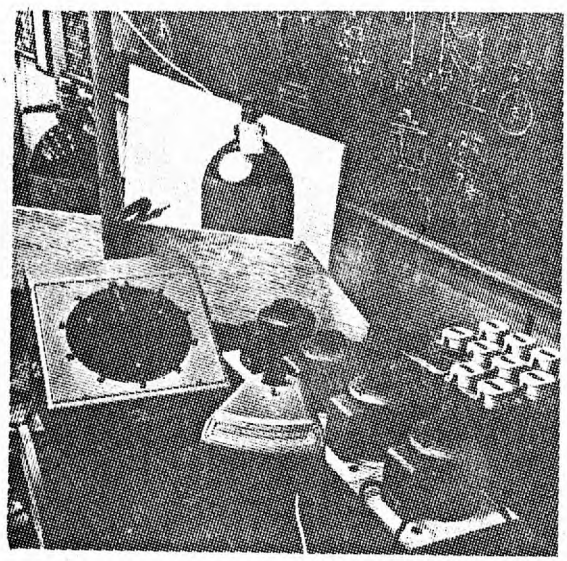

PLATE P17.

Nitrogen cylinders, scalamp galvanometer, variac transformer, 100-way switch-box.

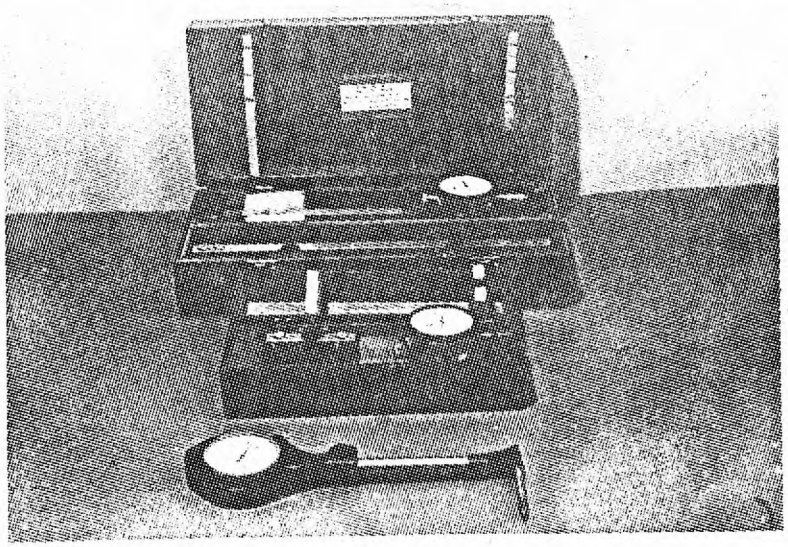

PLATE P18.

Demec gauges, mercer cylinder bore gauges.

pump to control the pressure applied to the pump and specimens. A Norgram air filter and a Norgram water filter governed the quality of the flow of the inlets to the pump.

A water bleed-off point incorporating a needle valve provided means of reducing the pressure in the circuit.

A further pressure relief valve was provided in the water circuit just before the main service pressure gauge, and was set at a controlling pressure limit.

Thereafter, the water line led to the three water bags in the pressure-loading rigs via pipe-lines each of which was separately valved to permit loading of any one or all of the rigs.

5.3.3. Heating circuit.

Heat was applied to the ten faces of the five specimens in a series, by means of glass cloth protected Isopad heating tapes. Each face was heated by an entirely independent circuit. Fig. 5.19.

The tapes were fixed to the inner faces of circular Karlit insulation shields $\frac{1}{2}$" thick. The diameter of the shields permitted them to be fitted closely inside the inner periphery of the cheek rings where appropriate. For the unpressured slabs, the shields were clamped to the concrete faces. A wooden rim at the outside edge of the insulation shields around the circumference, held off the central part of the shield from contact with the concrete surface. Plates P19, and P20.

The isopad tapes on the inside of the shields, were thus, prevented from closely contacting the concrete and causing hot spots. The tapes were fixed

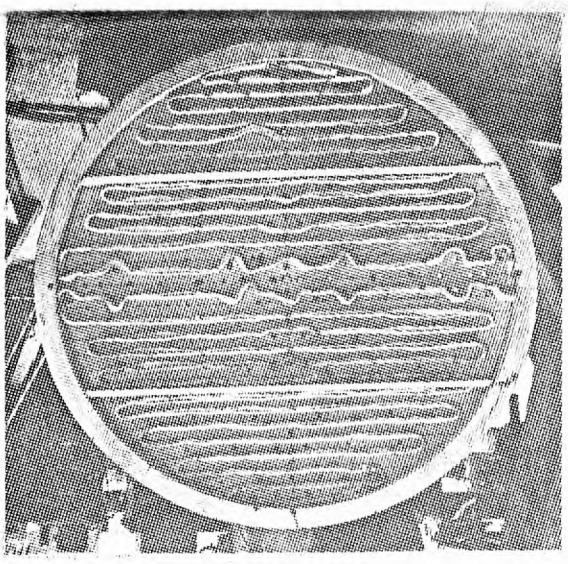

Plate P19.

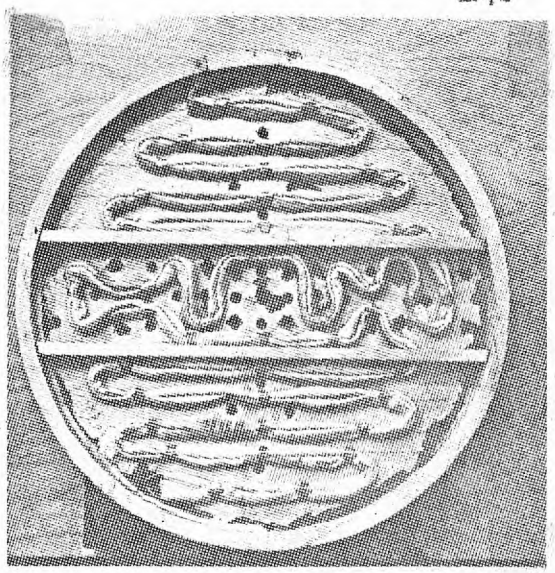

Plate P20.

Karlit heating shieldings showing arrangement of Isopad heating tapes.

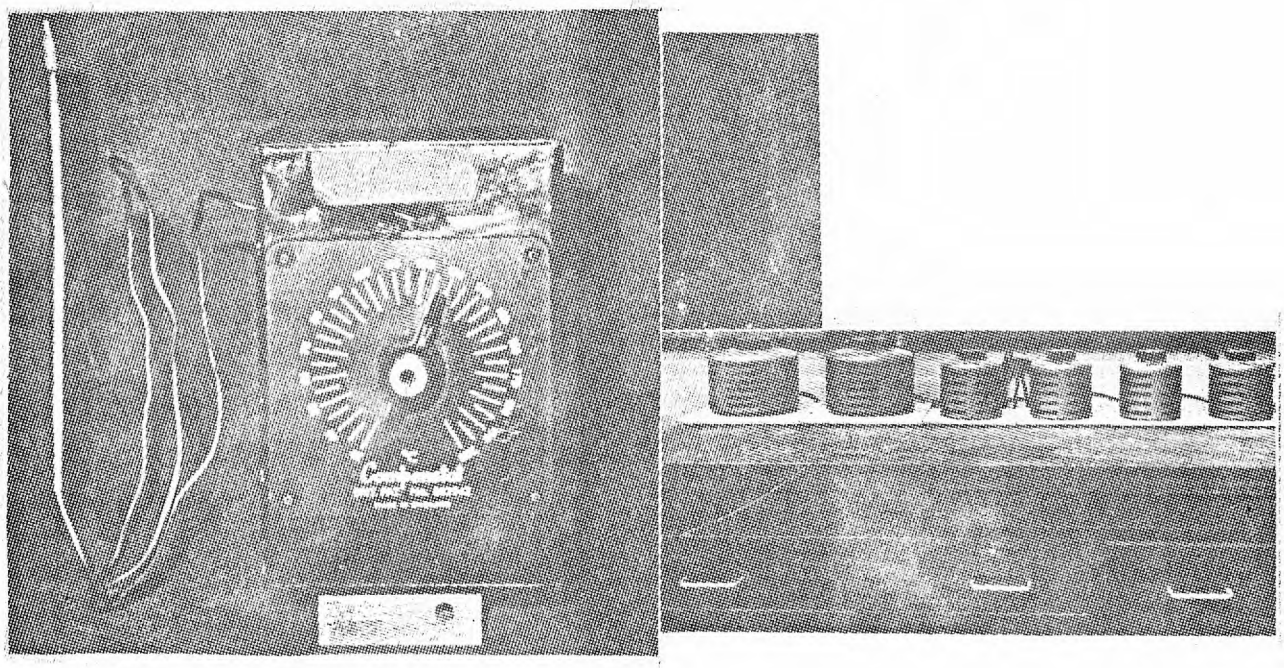

Plate P21.

View of variacs and thermoregulator.

horizontally in rows on the shield at centres which increased from the bottom to the top of the shield. This arrangement led to less heat being applied at the top of the specimen, to offset the increased heat there, due to the convection of hot air to the upper parts.

In addition, two wooden baffles were provided across the shield horizontally, again with the object of evening out the heating effects, by restricting air convection to local sections of the inner shield face.

The heating tapes were of the I.T.A. type, those for the large 36" specimen being of 750 watts capacity, and those for the smaller specimen of 260 watts capacity.

These tapes led from the insulation shields to TM 500 thermo-regulators, of a range 30° - 200°C, one regulator being provided for each face circuit. These regulators were each supplied from a Variac variable transformer of upto 270 volt capacity. Plates P17 and P21.

The control probe of each thermo-regulator was initially inserted into the specimens through the cast in thermostat tube. The thermostat monitored the specimen temperature, and cut out the heater if excessive temperatures were developing.

The intention was in fact, to use the thermostat as a safety control to prevent a temperature surge in the concrete due to malfunction of the transformer.

However, it became apparent that the on-off temperature range of the equipment was good insensitive to maintain a controlled temperature satisfactorily close to 80°C, and the probes were eventually left out of the specimens. It proved possible to maintain the required steady temperature by fine adjustment of the Variacs alone.

Holes were bored in the insulation shields at positions corresponding to the projecting brass Demec studs to permit access to the studs for Demec measurements, with the heating on and the shields in position. In addition, a pattern of ventilating holes was drilled to permit a differential cooling of various hot spots in the concrete specimens, as these revealed themselves during testing when the thermocouples were scanned by means of the switch-box. Plats P17, P22 and P23.

5.3.4. Temperature measurement.

The thermocouples installed in all the specimens were made from chromel/alumel wire 19 swg. type 1C Insuglas for the first and second series and for the third series. Plate P4.
The insulation of this wire could not be used above 150°C.

The wires were spot welded at their junction and were then dipped in PS adhesive. This formed a quick-setting, water-proof and heat-resistant coating over the junction, 19" long sections of thermo-couples were installed at temperature measurement positions in all the slabs. This dimension permitted sufficient free wire outside the concrete, however remotely any thermocouple was positioned, to make satisfactory connections to the compensating cables.

The thermocouple wires were off the single strand twinned type, each wire being insulated and the two insulated wires being themselves enclosed by further insulation.

The flexible lead compensating cables which were joined to the thermocouples, were multi-strand wires paired in an insulating cover.

To make the connection between the thermocouple and the compensating cable, each of the four

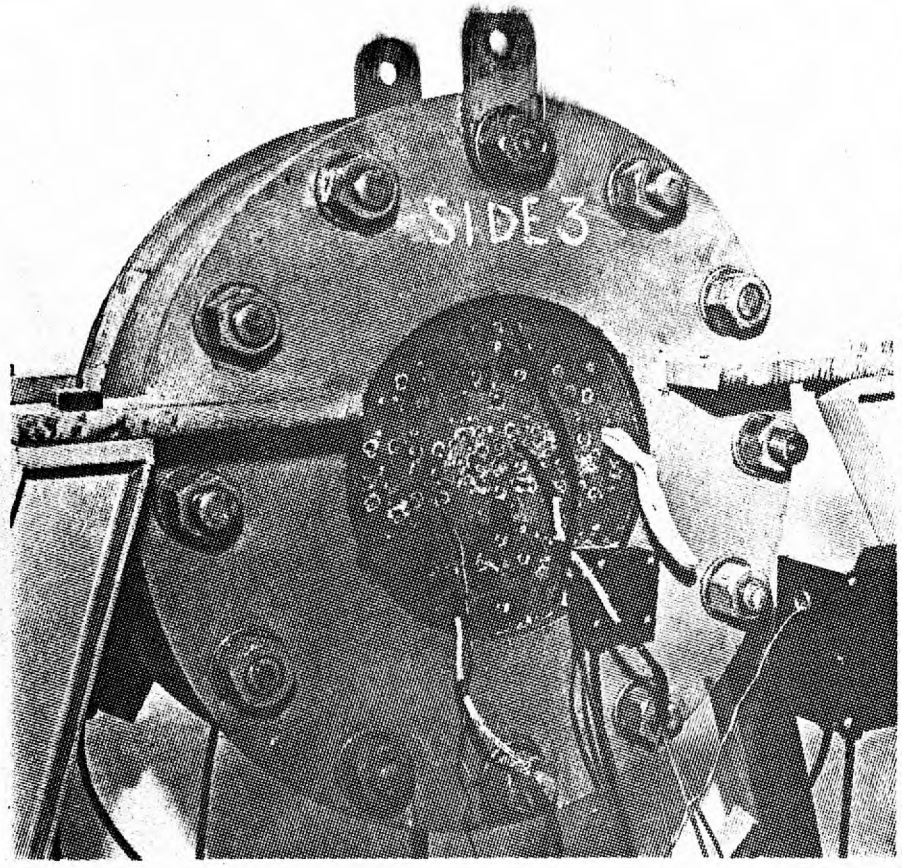

PLATE P22.
Specimen 3/4

Insulation shielding and thermocouple leads during heating and loading phase.

PLATE P23.
Specimen 9/10

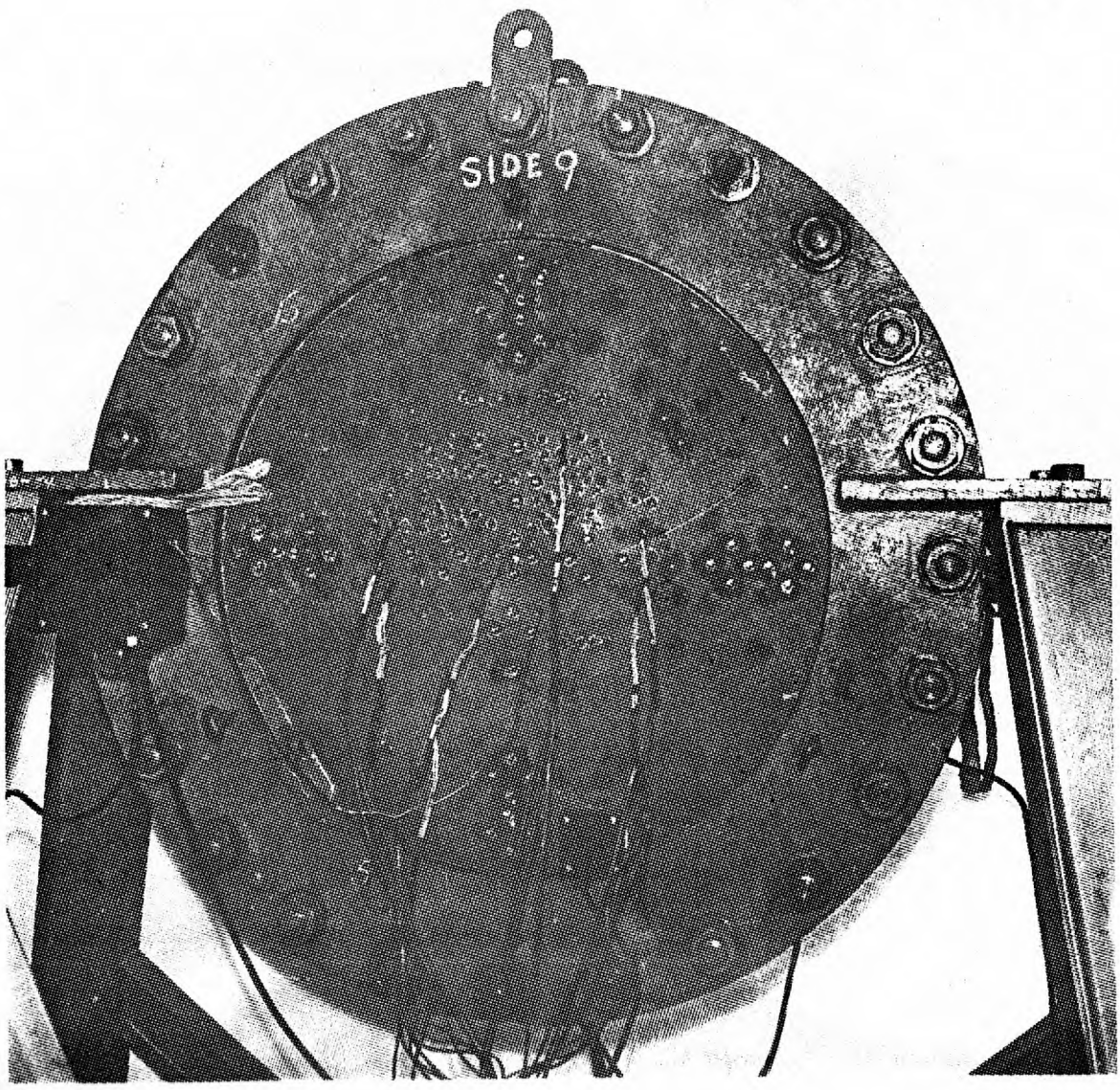

wire ends were bared, and the two appropriate pairs of ends tightly twisted together and soldered. Each connection was then wrapped in insulating tape. The two joints thus formed, were arranged in close proximity along the wires so that the temperature of the two connections would not differ.

The lengths of all cable leads were identical. The cables were connected to a 25-way Amphenol plugs. The 57 thermocouples involved were distributed between four such Amphenol plugs. The plugs were connected to a 100-way switch-box.

The switch-box was itself connected to a Pye Scalamp thermocouple meter reading directly in degree centigrade. The Scalamp and thermocouple circuit required colibration against fixed temperatures, i.e., the boiling point of pure water. The Scalamp reading scale was adjusted accordingly.

5.3.5. Demec gauges.

This is a mechanical gauge which was developed by the Cement and Concrete Association. Plate P18.

Two types of Demec gauge were used throughout the experiments. The most frequently used was the standard 2" gauge.
This instrument was read by means of a dial gauge, one division on the dial of which was equivalent to 25.3 micro-strain. Thus, the gauge factor used for converting reading differences into strain was 2.53×10^{-5}, for the first and second series and 2.47×10^{-5} for the third series.

The other Demec gauge used, incorporated a gauge length of 11.438"
This dimension was specially required to take readings over

three standpipe pitches.

Demec points were provided on the ends of 11" long hexagonal brass studs positioned in two pairs at right angles to each other across each slab, each demec point in a pair being three standpipe pitches from its neighbour.

A standard 12" Demec gauge was specially drilled and provided with a registering point to suit this special dimension of 11.438". One division on the dial gauge of this instrument was equivalent to 6.99 and 4.85 microstrains. Thus the gauge factor used in converting reading differences to strains was:- 6.99×10^{-6} for series one and two, and 4.85×10^{-6} for series three.

The types of gauges were manufactured under licence by W. H. Mayes & Son.

1) Method of taking readings.

The Demec gauge readings were read to 0.1 of a division.

The reading from a standard Invar bar was taken before and after each set of readings, so that readings could be corrected from the effects of temperature on the gauge.

The standpipe readings were also read to 0.1 of a division, by a Mercer cylinder bore gauge.

2) Elimination of operator effects.

All the Demec gauge readings in every test were taken by the same operator. It was though that more consistent readings would be obtained in this way, and that

more accurate readings would be obtained as the operator became more experienced. The same applied for the standpipe readings for similar reasons.

5.3.6. Mercer cylinder bore gauge

To measure the standpipe diameters, a standard cylinder bore gauge was shortened in length and the standard ends were replaced by conical spigots in such a way that the leverage ratios, and thus the gauge factor were unchanged. Plate P18.

The standpipe bores were measured over four diameters each 45° apart round the circumference. Holes were bored to take the conical spigots of the instrument in a circle 1" in from the end of the standpipe.

An identical set of holes were bored at the other end of each chosen standpipe to permit average readings to be calculated. In each perforated specimen in the first and third series, two standpipes were measured. For the second series, three standpipes were chosen for each perforated specimen.
The positions and numbering of the bores are shown in Figs. 5.8, 5.10, and 5.14.

5.3.7. Crack-detection circuits.

These circuits were used towards the end of the tests on the two series of model specimens, at the final unloading stage. Fig. 5.22.

The object was to provide a means of instantly locating and observing cracks as they occurred in the ligaments, during unloading by scanning each crack detection strip at each load decrement, and identifying electrically any break in the circuit.

The strips were painted on the ligaments in such a way that the cable ends were fixed and connected. Conducting paint containing silver in alcohol was applied. Dag dispersion 962 was the particular specification selected. This had satisfactory properties of conduction, adhesion and brittleness.

The connecting cables from the strips led to a switchbox which could scan each conducting strip. Two methods of identifying circuit failure due to cracking were tried. First a bulb was used with a 9 volt battery, to give a quick visual indication of an incipient cracking when the bulb faded or went out. The resistances of the various circuits varied so widely, however, that the bulb light intensity for each circuit varied in proportion, and this method proved too insensitive.

Subsequently, an Avometer with a battery was employed in conjunction with the switchbox. The resistance scale on the meter registered infinite resistance by flicking over the scale suddenly when a crack was encountered.

The method did not give very positive results, possibly doe to the paint being applied in too great a thickness.

5.3.8. Electrical resistance strain gauge circuits.

The strain gauges were used only during the short-term elastic unloading tests at the end of each of the two test series. Fig. 5.23. Plates P24 - P29.

Because of the generally recognised long-term problems of drift and instability with electrical resistance strain gauges, it was not considered practicable

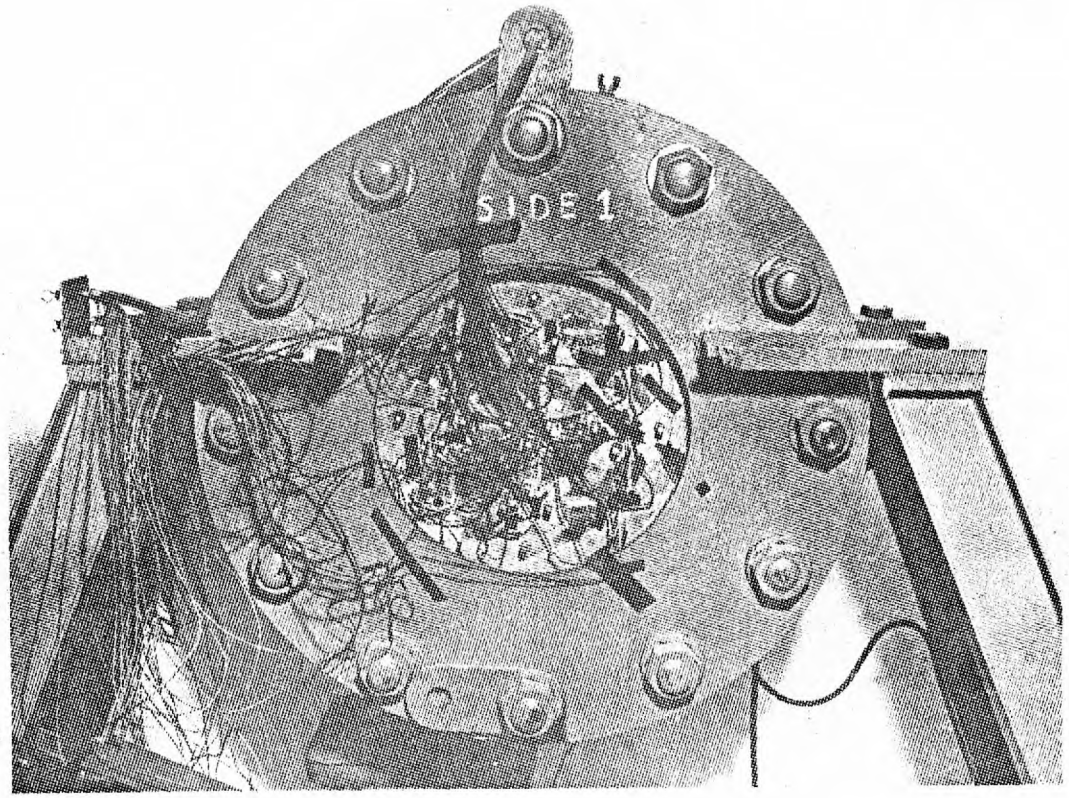

PLATE P24.

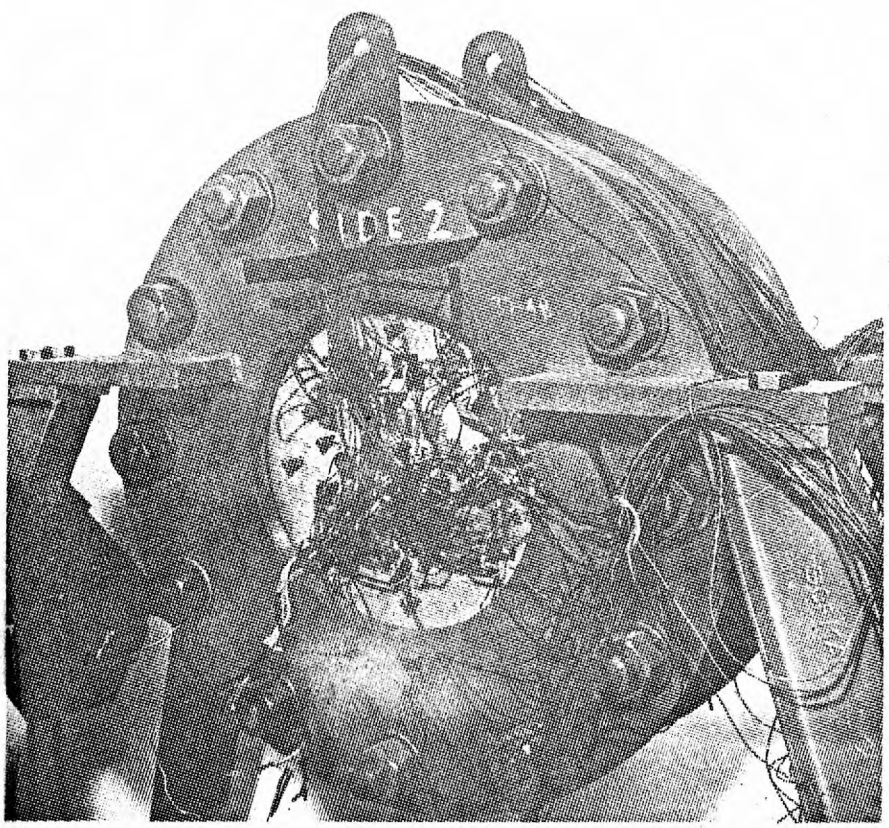

Specimen 1/2 ERSG. Wiring during final unloading phase.

PLATE P25.

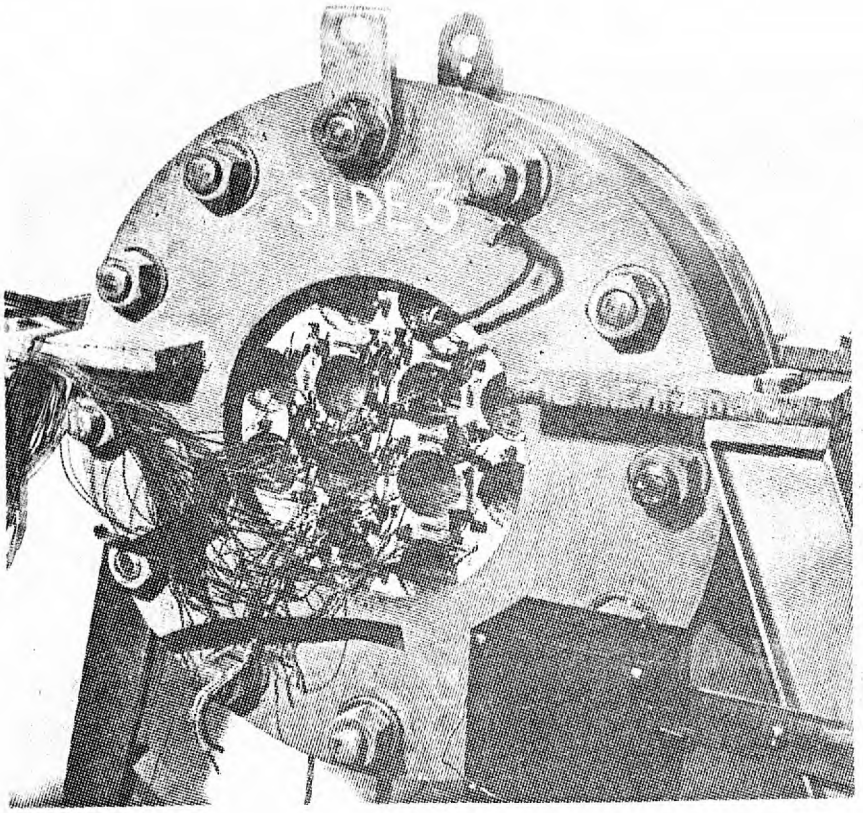

PLATE [illegible].

Specimen 3/4
Etch: Warning
during final
[illegible]

PLATE 227.

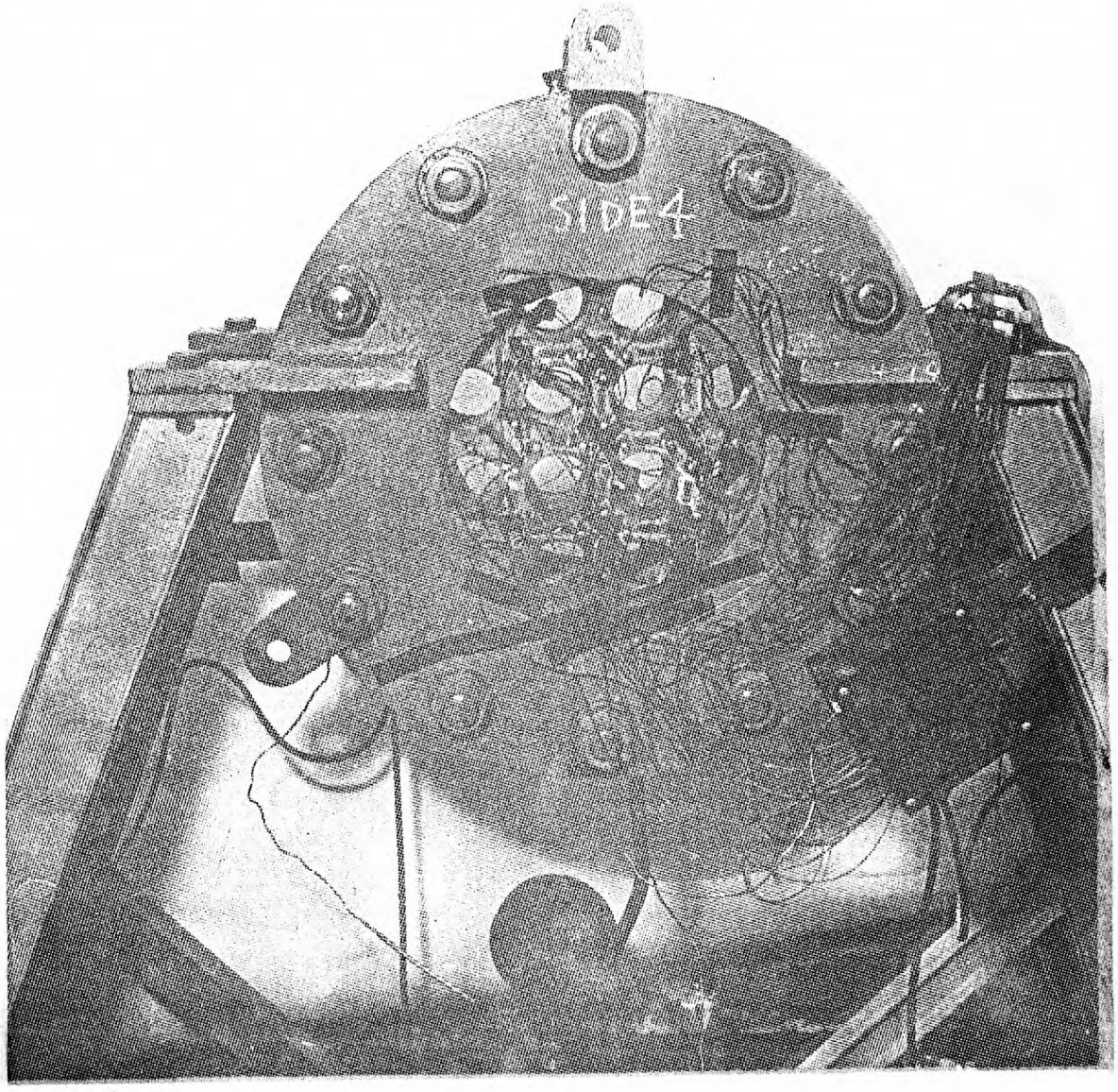

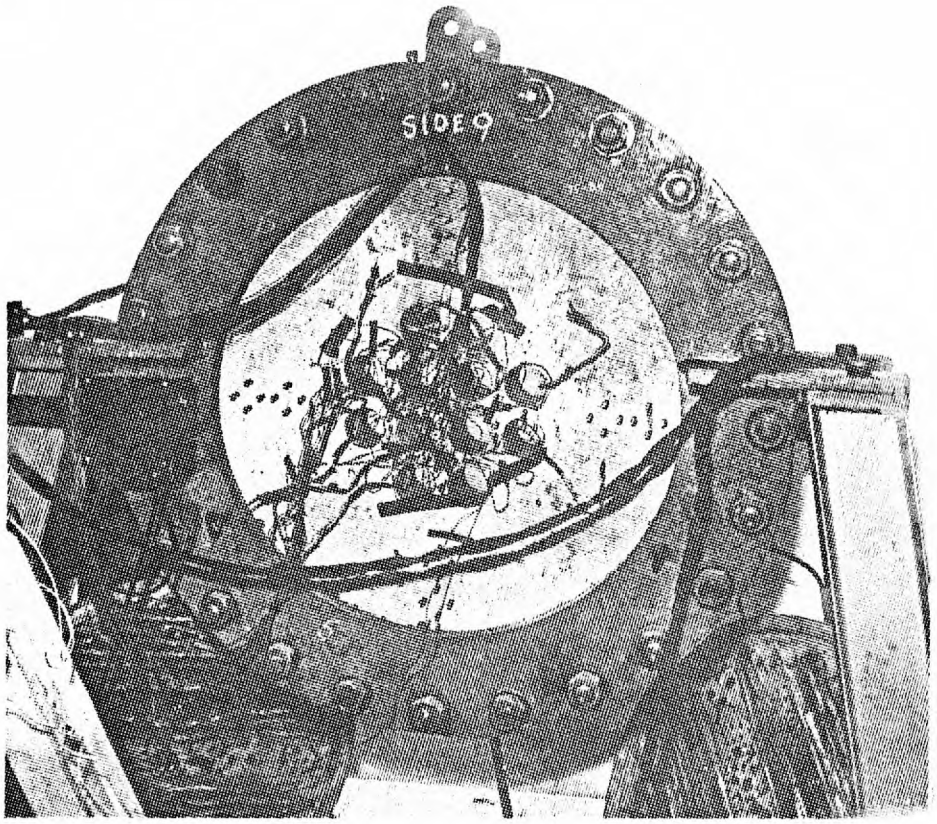

PLATE P28.

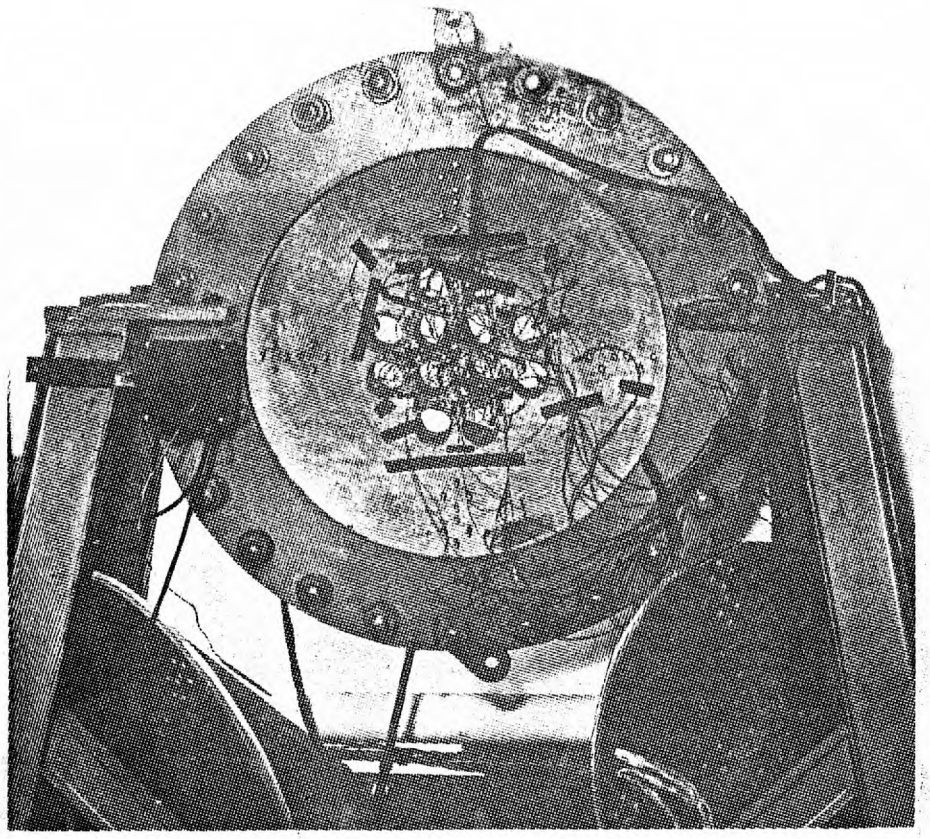

PLATE P29.

Specimen 9/10
ERSG. Wiring during final unloading phase.

to attempt to record creep and shrinkage strains by this means, over the several months that each test lasted.

The gauges used were ½" Budd E.R.S.Gs., of the foil type specified by the Budd numbers. C6-181B. They had a gauge factor of 2.08 ± ½%, and a resistance of 120 ± 0.2 ohms.

There were 12 E.R.S.Gs., on each face of each pressurized specimen, making 72 in all. For the perforated $16\frac{3}{4}$" specimen, and the 36" specimen, the gauges were fixed along the ligament lengths. For the other pressurized solid $16\frac{3}{4}$" specimen, the gauges were fixed in exactly identical positions. Figs. 5.27 and 5.28, illustrate the positioning of the gaugos.

Before fixing the gauges on the specimens, the concrete surface was first smoothed and cleaned with acetone. The adhesive used was a Japanese polyester resin containing a filler and known by the letters PS. The filler assisted in making an intimate contact with the concrete by penetrating the surface. The PS adhesive is quick-setting, temperature and moisture-proof, although the necessity for the two latter properties was absent during unloading.

The concrete was primed by smearing with a thin layer of PS adhesive. This was wiped off while wet, so that the concrete was again exposed, but the pores filled. After drying and smoothing, a second layer of PS was applied and the gauge pressed on to the concrete surface, so that it was firmly in conctact. At the time of pressing on, the gauge was covered and screwed with a pressure-senstive tape to permit final drying and hardening of the adhesive without the danger of the gauge peeling off.

The lead connections to each E.R.S.G., were made by soldering. The leads, which led from the

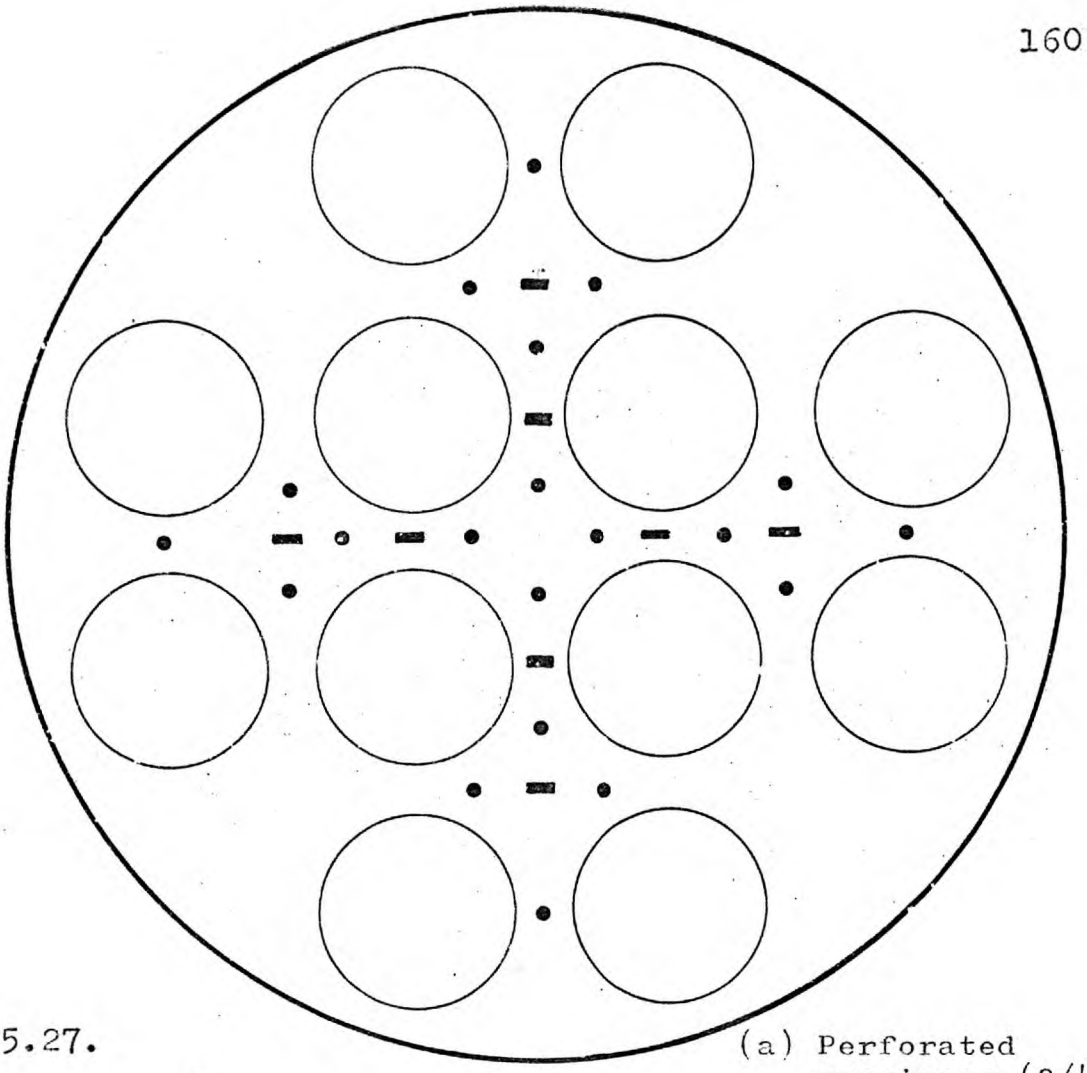

FIG. 5.27.

(a) Perforated specimens (3/4) and (9/10)

— ERSG

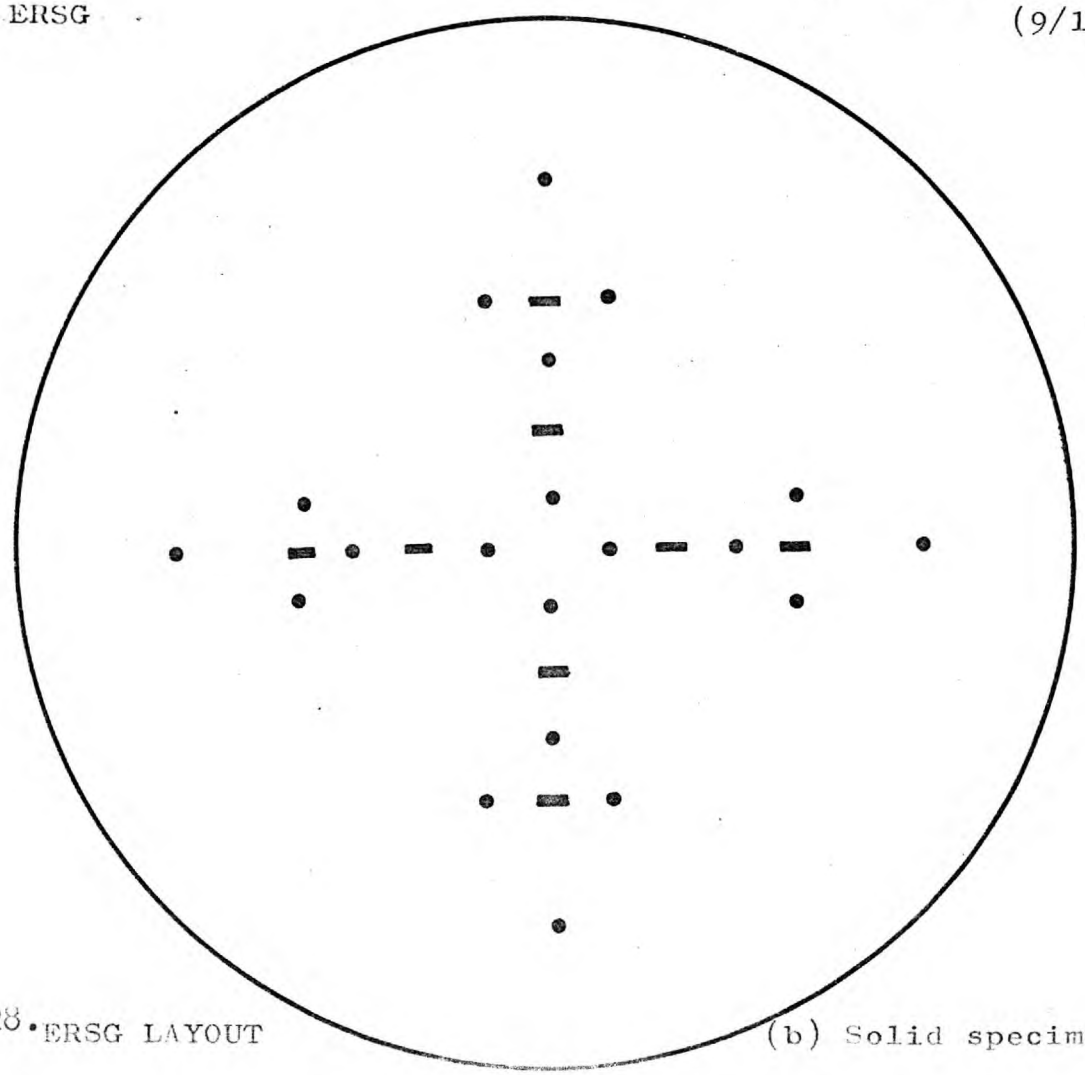

FIG. 5.28. ERSG LAYOUT

(b) Solid specimen ($\frac{1}{2}$)

gauges to the Solartron Data Logger, were 14/.0076" multi-strand wires, and were PVC - covered. The connections to the Solartron were made through standard Amphenol plugs.

The Solartron had separate sockets for the active gauges and for the dummy gauges. The resistances of all leads for the active and dummy gauges were arranged to be the same. The Solartron layout incorporated half the Wheatstone bridge, the power supply, an amplifier, and the gauge channels were scanned through a commutator switch-box. The amplifier output led to a digital voltmeter, all channels being automatically scanned and the output reading given directly in microstrain as explained hereafter. The data were, in fact, presented in the form of in-line printed figures on continuous output paper.

To obtain direct microstrain readings from the Solartron, it was necessary to calibrate it, assuming a gauge factor k, of 2, by means of a standard microstrain calibration box. Thus, the output readings gave the value of $\frac{1}{K} \frac{R}{R}$ directly. This is the strain required from the relationship $\frac{L}{L} = \frac{1}{K} \frac{R}{R}$. To correct the readings to allow for the fact that the gauge factor was, in practice, 2.08, the Solartron microstrain reading was multiplied by $\frac{2.0}{2.08}$

5.3.9. The rubber bags.

These bags were manufactured from neoprene rubber $\frac{1}{4}$" thick. Two bags were made for use in the $16\frac{3}{4}$" pressurized rigs with one spare, and one was made for use in the 36" rig also with one spare. Plate P9.

The dimensions of the small bags were $17\frac{3}{4}$" ID x $19\frac{1}{4}$" OD x $7\frac{1}{2}$" wide, and those of the larger bags were 37" ID x $38\frac{1}{2}$" OD x $7\frac{1}{2}$" wide.

The cross-section of each bag was that of a hollow rectangle formed of four $\frac{1}{4}$" thick flat rubber sections vulcanized and glued together at the corners.

Openings in each bag, one a water pressure inlet at the bottom, and one an air vent at the top, were formed with 175A type Schrader valves each opening being positioned on the centre of the $7\frac{1}{2}$" dimension. The stems of these valves passed through the steel hoop thickness. The corners of the hole through the hoop were radiused to prevent damage to the rubber bag at the valve root. The $\frac{1}{2}$" diameter hoope hole was also stepped up to $3/4$" diameter for the inner $\frac{1}{4}$" length, to take the locking nut on the valve stem.

The neoprene was required to remain stable over several weeks under a temperature of $80^{o}C$, and to be capable of sustaining both this temperature, and transmitting a maximum pressure of 1500 psi., over an extended period.

It was specified that the pressure inside the bag should not be raised or lowered in steps greater than 100 psi., and that at least 400 changes in pressure could be anticipated. In practice, these figures were exceeded without any noticeable effect on the performance of the bags.

5.4. Testing Programme.

A diagrammatic representation of the testing procedure is shown in detail in Figs.1.9, 1.10, and 1.11, for each series, and the chronology of events in Tables 5.7, 5.8, and 5.9.

TABLE 5.7.

SERIES 1 - CHRONOLOGY OF EVENTS

Days from start of test	Date	Operation
	20. 6.1967	Casting of Specimens
0	24.11.1967	Load cycling
1	25.11.1967	Loaded at lab. temp.
4	28.11.1967	
6	30.11.1967	
11	5.12.1967	
19	13.12.1967	
25	19.12.1967	
26	20.12.1967	Heat applied-transient period
46	9. 1.1968	
47	10. 1.1968	Loaded elevated temp.
49	12. 1.1968	
54	17. 1.1968	
55	18. 1.1968	
59	22. 1.1968	
60	23. 1.1968	
61	24. 1.1968	
62	25. 1.1968	
66	29. 1.1968	
67	30. 1.1968	
68	31. 1.1968	
69	1. 2.1968	
73	5. 2.1968	
74	6. 2.1968	
76	8. 2.1968	
80	12. 2.1968	
82	14. 2.1968	
83	15. 2.1968	
88	20. 2.1968	
90	22. 2.1968	
94	26. 2.1968	
97	29. 2.1968	Load cycling - H O T
98	1. 3.1968	Heat switched off-cooling period
101	4. 3.1968	
101	4. 3.1968	
102	5. 3.1968	Loaded lab. temp.
108	11. 3.1968	
109	12. 3.1968	
110	13. 3.1968	
111	14. 3.1968	
116	19. 3.1968	
117	20. 3.1968	
118	21. 3.1968	
122	25. 3.1968	
123	26. 3.1968	

(continued page 60)

(Continued - SERIES 1)

TABLE 5.7.

Day from start of test	Date	Operation
129	1. 4.1968	Unloaded lab. temp.
130	2. 4.1968	
136	8. 4.1968	
137	9. 4.1968	
139	11. 4.1968	
144	16. 4.1968	
145	17. 4.1968	
146	18. 4.1968	
150	22. 4.1968	
151	23. 4.1968	
153	25. 4.1968	
154	26. 4.1968	E N D

TABLE 5.8.

SERIES 2 - CHRONOLOGY OF EVENTS

Days from start of test	Date	Operation
	6.3.1968	Casting of Specimens
1	1.5.1968	Unloaded lab. temp.
2	2.5.1968	
3	3.5.1968	
6	6.5.1968	
8	8.5.1968	
9	9.5.1968	Load cycling
10	10.5.1968	Loaded lab. temp.
13	13.5.1968	
15	15.5.1968	
17	17.5.1968	
20	20.5.1968	
22	22.5.1968	
24	24.5.1968	
27	27.5.1968	
28	28.5.1968	
29	29.5.1968	Heat applied - transient period
31	31.5.1968	
32	1.5.1968	
36	5.6.1968	Loaded elevated temp.
38	7.6.1968	
41	10.6.1968	
44	13.6.1968	
48	17.6.1968	
51	20.6.1968	
56	25.6.1968	
58	27.6.1968	
62	1.7.1968	
65	4.7.1968	
70	9.7.1968	
73	12.7.1968	
76	15.7.1968	
78	17.7.1968	Load cycling - H O T
79	18.7.1968	Heat switched off-cooling period
81	20.7.1968	
84	23.7.1968	Loaded lab. temp.
86	25.7.1968	
90	29.7.1968	
92	31.7.1968	
94	2.8.1968	
96	4.8.1968	
98	6.8.1968	
100	8.8.1968	Load cycling - unloading stage
104	12.8.1968	Unloaded lab. temp.
108	16.8.1968	
111	19.8.1968	
114	22.8.1968	
118	26.8.1968	
119	27.8.1968	
120	28.8.1968	E N D

TABLE 5.9.

SERIES 3 - CHRONOLOGY OF EVENTS

Days from start of test	Date	Operation
	7.1.1969	Casting of Specimens
1	4.3.1969	Unloaded lab. temp
2	5.3.1969	
3	6.3.1969	
4	7.3.1969	Load cycling
7	10.3.1969	Loaded lab. temp.
9	12.3.1969	
11	14.3.1969	
14	17.3.1969	
18	21.3.1969	
21	24.3.1969	
23	26.3.1969	
24	27.3.1969	Heat applied-transient period
28	31.3.1969	
31	3.4.1969	Loaded elevated temp.
37	9.4.1969	
39	11.4.1969	
42	14.4.1969	
46	18.4.1969	
49	21.4.1969	
53	25.4.1969	
56	28.4.1969	
60	2.5.1969	
63	5.5.1969	
67	9.5.1969	
70	12.5.1969	
72	14.5.1969	
74	16.5.1969	
75	17.5.1969	Load cycling - H O T
77	19.5.1969	Heat switched off-cooling period
81	23.5.1969	Loaded lab. temp.
87	29.5.1969	
94	5.6.1969	
101	12.6.1969	
101	12.6.1969	Load cycling - unloading stage
107	18.6.1969	Unloaded lab. temp.
114	25.6.1969	
120	1.7.1969	
121	2.7.1969	E N D

1) Specimens unloaded at ambient temperature.

The test programme was started at ambient temperature. Laboratory temperature and relative humidity were recorded. Datum strain measurements were then established on all Demec gauge lengths, and on the standpipe diameters.

2) Load cycling at ambient temperature.

The two $16^3/4$" shrinkage specimenswere positioned on wooden saddles. The two $16^3/4$" and the 36" diameter creep and shrinkage specimens were installed in the pressure rigs and load-cycled with radial compressions. 1500 psi., (p^1) maximum compression was applied to the 36" specimen, and to the solid $16^3/4$" creep specimen. The perforated $16^3/4$" creep slab was subjected to a maximum of 1125 psi., for the 1st and 3rd series.

The object of the initial load-cycling of the creep specimens was to obtain at ambient temperature, the elastic modulus of the solid concrete, the effective modulus of the perforated zone, and the elastic response of the composite 36" slab. The loading and unloading were carried out in 3 cycles.

3) Loaded at ambient temperature.

Thereafter, the three creep specimens were subjected to a constant radial compression - 1500 psi., for the 36", and for the solid $16^3/4$" specimen, and 1125 psi., for the perforated $16^3/4$" specimen. For the second series all specimens were subjected to 1500 psi., radial compression. The Demec strains and standpipe diameters were continued to be measured for the loaded specimens, and for the unloaded shrinkage specimens for a period of three weeks, generally on alternate days.

4) Loaded at elevated temperature.

Heat was then applied, and the average temperature of all specimens was taken upto 80°C, over a period of three days approximately. The transient temperature history was recorded.

The creep and shrinkage strains for all the specimens were then recorded at approximately 48 hour intervals, over a further period of six to eight weeks, for the three series, the temperature being kept constant at 80°C.

5) Load-cycling at elevated temperature.

Before allowing the specimens to cool, the pressure loading was again cycled over a relatively narrow range three times, in order to obtain the elastic responses (at 80°C), comparable to those obtained at the start of testing. The value of the loads was not reduced below 800 psi., in order to avoid the possibility of cracking.

6) Loaded at ambient temperature.

At this point, the temperature was reduced to the ambient value in the Laboratory, and the insulated heating shields were removed. The transient temperature history was recorded during cooling. The cooling took place whilst the loaded specimens remained under their maximum loads, and lasted for two days.

7) Load-cycling at ambient temperature.

A restricted load-cycling was carried out under this condition, the pressure never being allowed to fall below 750 psi., again, to avoid possible cracking.

Creep and shrinkage strains and standpipe diametral strains were continued to be measured for a further period of three weeks.

8) Unloading stage.

Electrical resistance strain gauges were then installed on the ligaments of all loaded specimens, and the loads were gradually reduced whilst the onset of cracking was sought in the ligaments. The E.R.S.G., readings were recorded on the Solartron Data Logger.

Crack-detection equipment was used to assist in this process. In fact, four methods were employed to detect cracks.

a) Visual examination with magnifying glass.
b) Crack-detection circuits.
c) Examination for sudden large differences in Solartron readings.
d) Examination for large Demec reading differences.

Each of the crack-detection paint strips, was investigated at each load decrement by means of a switchbox scanner. The positions of E.R.S.Gs., and crack-detection strips were arranged to coincide as near as was practicable. The layout of the crack-detection circuit is shown in Fig. 5.22.

9) Load-cycling.

After completly unloading, the cracked and uncracked specimens were again subjected to three loading cycles to obtain the elastic responses.

10) Creep recovery.

Finally, with the specimens unloaded, strains were measured on all specimens until full creep recovery had occurred.

At this ultimate stage, a further load-cycling was applied.

5.5. Discussion of testing techniques.

The reliability of the testing techniques and the consequent validity of the resulting readings, can be analysed under three main headings relating to the specimens.

a) Specimen details.
b) Pressure system.
c) Heating and temperature measurement systems.

5.5.1. Specimens.

First, it is worth emphasizing, that all specimens in each series were treated from concrete mixing to final preparation for testing in an identical manner.

All specimens were cast and vibrated on the same vibrating table. They were cured under wet hessian and wrapped in polythene sheeting, each specimen under similar conditions for equal periods of time.

1) Sealing of specimens.

The sealing of the rims of all specimens with thixotropic paint was carried out to simulate the condition in an actual reactor vessel, where the wall inhibits radial loss of moisture.

However, to apply three coats of paint, allowing time for drying of the concrete surface after curing, and drying periods, between each coat of paint, meant that several days of shrinkage had occurred before datum readings could be established. However, shrinkage readings which included the effects of radial moisture movements, would not have been directly comparable with shrinkage readings subsequent to rim sealing, so the delay was not significant.

2) Threaded tubes - hexagonal tubes.

With regard to the ½" tubes 6" long across the thickness of the specimens, two points are of interest, Firstly, the external shape was made hexagonal in the second and third series to prevent rotation relative to the concrete; secondly, 3/8" long plastic sleeves were introduced over each end of the ¼" tubes. The object of the latter arrangement was to ensure that only concrete strains were measured which originated in a median zone of the slab thickness. Plate P4.

3) Standpipe measurements.

Difficulty was at first experienced in measuring the bores of the standpipe tubes for two main reasons. The Mercer bore gauge, fitted with a spring-loaded steel bar conically-pointed at the end, was too long in the shank to manipulate accurately in this application. Secondly, the registering points for measurement were intended to be steel walls on opposite ends of four diameters. The balls were glued into seatings within a stiff plastic ring fixed inside the standpipe bore.

It proved impracticable, however, to measure the diameters of the standpipes, between two spherical surfaces, and finally, the bore gauge shortened in length to facilitate manipulation, was operated with the conical-points registered in paired bored holes on four diameters of each chosen standpipe.

4) Sealing of shrinkage specimens.

During the heating phase of the experiments, attempts were made to ensure that the rims of all the specimens were under the same conditions of insulation. Fabric of various kinds was intoduced round, and secured to the rims of the shrinkage specimens to eliminate uncontrolled heat loss.

Identical sealing by painting had already been achieved, as described, but the fact that the pressurized specimens were fairly closely in contact with the water in the rubber bags, whereas, the shrinkage-only specimens were not, made a difference to the heat loss conditions of the two kinds of slabs. Perfect temperature control, i.e., the attainment of static, identical temperatures at all points of all specimens, proved virtually impossible.

5) Surface cracking of perforated shrinkage specimens.

Another factor which may have affected some readings in both series of tests was the sligh surface cracking which was observed on side 5 of specimen 5/6, (the $16\frac{3}{4}$" perforated shrinkage specimen) after mould stripping. Plate P30.
This was due to the tightness of the fit of one of the fixing and locating plugs in the steel mould, within the bore of one of the standpipes. In knocking out the plug from side 6 after stripping the moulds, slight spolling and cracking was noticed on side 5 for the second series.

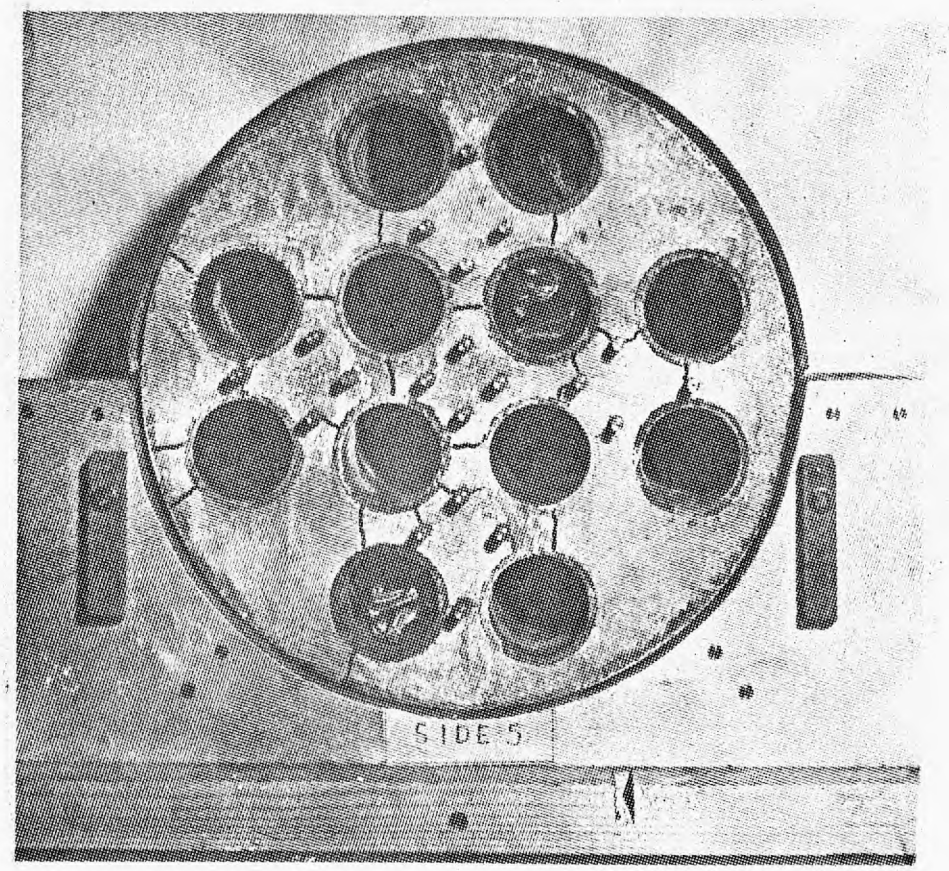

Plate P30.

Surface cracking on side 5 (Model 5/6) on removal of heat.

6) Checks on the uniformity of radial pressure.

To check that the radial compression from the $7\frac{1}{2}$" rubber water bag was uniformly distributed over the 6" thick rim of the concrete specimen, electrical resistance strain gauge readings were taken on the side steel cheek rings during a short-load cycling test.

The fear was felt that due to the embedment of the cheek rings onto each face of the concrete slabs at the rim edge by cement-mortar grout, the friction involved, might lead to uneven loading on the concrete rim. The strain readings resulting from this test indicated that this fear was groundless.Table 5.10.

5.5.2. Pressure system.

Leaks from valves, and at certain gauges in the system, periodically affected the accuracy and control of steady pressure conditions. This led to the air-hydro pump cutting into the system at fairly regular intervals and inevitable variations in pressure. Infrequently, the pump stuck and failed to cut in early enough. The maximum range of variation, however, did not represent at any time, more than 7% of the required 1500 lbs/sq.in.

Another difficulty in experimental technique was due to the insensitivity of the pressure control valve used to limit the pressure on specimen 3/4 (the $16\frac{3}{4}$" perforated pressurized specimen) to 1125 lbs/sq.in., for the first series. This problem did not arise for the third series, and was not necessary for the second series.

T A B L E 5.10.

CHECK ON THE UNIFORMITY OF RADIAL PRESSURE:

SIDE NO:	ERSG. NO:	READING:	PRESSURE IN psi:	STRAINS:
10	1	1432.0)	zero.	
	2	1607.0 (		
	3	1518.6)		
9	4	1587.0 (		
	5	1585.0)		
	6	1506.2 (		
10	1	1366.0)	1500.	660
	2	1551.0 (		560
	3	1462.0)		566
9	4	1505.0 (		820
	5	1527.0)		580
	6	1459.0 (		472

Strain = Difference of reading x $\frac{2.00}{2.08}$ (in microstrains).

Note: The ERSG., paired on opposite sides:-
1 & 5, 2 & 6, 3 & 4.

.....

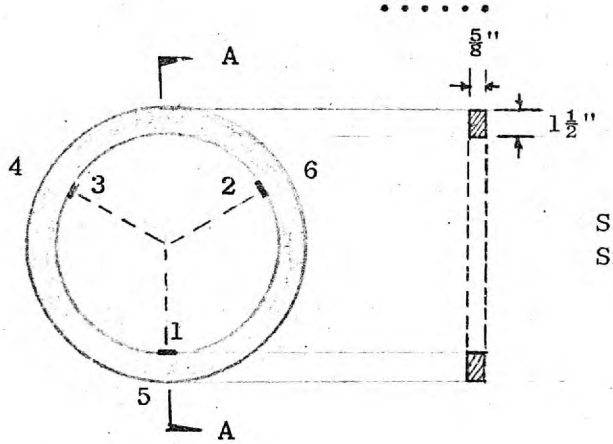

Side 10: ERSG Nos 1, 2, 3.
Side 9: ERSG Nos 4, 5, 6.

Ring Elevation and Section

5.5.3. Heating system.

In earlier heating runs carried out, the on-off temperature range of the thermostats was found to be too great, and the thermostats, in general, therefore, too insensitive to maintain a constant temperature of 80°C. In later work, the heating load was maintained constant by means of adjustment of the variac alone.

Other points of interest illustrating the work involved on heating control, were the method developed for ensuring relatively even temperature distribution. Four measures were taken:-

(1) The heating tapes were affixed at centres which increased towards the top.

(2) Wooden separators babbled the convection of hot air.

(3) Aluminium sheets were used inside the insulation shields over the face of the concrete, and threaded over the brass hexagons in order to even out the heat flow by conduction.

(4) Holes were bored through the shields to help even temperature distribution by ventilation.

The shields with their tapes on the inside, were only pushed home over the brass hexagonal studs into contact with the concrete, at the times of taking Demec readings. At all other times, the shields were held back slightly to marked positions, to ensure that there existed a small gap to prevent contact and hot-spots.

1) Dummy heating runs.

Dummy heating runs were made on the previously cast dummy specimens, in order to check on the methods proposed for achieving a constant 80°C. These dummy runs proved successful, but, in practice, three out of the five specimens had heat loss conditions different from that of the dummy specimens. This was in the case of the three specimens pressurized by means of water bags.

The coolant effect of the water would appear to have made a considerable difference to the heat loss conditions. At any rate, the problem of temperature control for the shrinkage specimens proved to be more simple than that for the pressurized specimens.

It was necessary to remove each shield whenever the diameters of the standpipe bores were to be measured. This had to be done progressively, face by face, for the three perforated specimens.

For each set of measurements a period of 3 or 4 minutes for each face, therefore, elapsed every 48 hours, approximately, when heat loss occurred from only one side or the other of a specimen. These uninsulated measurement periods, led to a fall of 2°C - 4°C, in the appropriate outer thermocouple readings. The central thermocouple was unaffected in each case.

2) Thermocouple calibration.

To ensure that the thermocouples were recording the correct temperatures, a calibration test was carried out.

For this purpose, one thermocouple and compensating cable was made equal in length to the thermocouples installed in the specimens.

This thermocouple was placed in melting ice, and the output connected to a Pye Scalamp galvanometer, which was adjusted to zero.

A mercury in glass thermometer was also placed in the melting ice.

The thermocouple and thermometer were then placed in boiling water and the readings on the Scalamp and thermometer noted.

The water was allowed to cool, and corresponding readings in the Scalamp and thermometer were recorded at intervals, particularly, over the working range of the tests.

A graph was drawn of the thermocouple readings against thermometer readings, enabling the Scalamp galvanometer to be calibrated. Fig. 5.29.

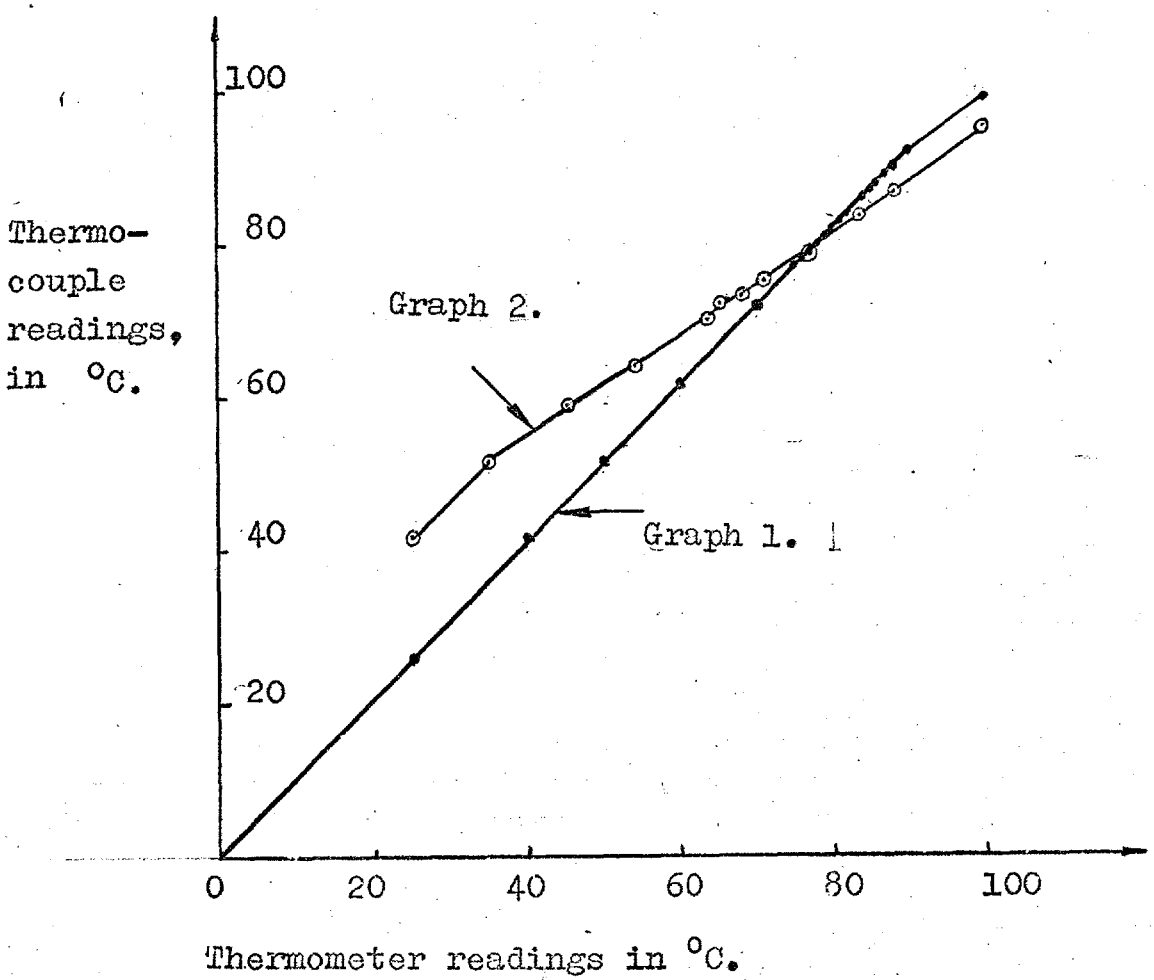

FIG. 5.29. Thermocouple calibration graph.

For the three test series.

Note: Graph 1 - Thermocouple calibration for series 1 & 2.

Graph 2 - Thermocouple calibration for series 3.

C H A P T E R VI

THEORETICAL INVESTIGATION

6.1. Introduction.

1) Nature of the problem.

Many of the recent technological advances have required the refined analysis and design of complex structural systems. An important class of structural systems, which the analyst must be prepared to cope with is the two-dimensional structure subjected to in-plate loading.

From the description of tested models, in the preceding Chapter V, it was seen that three out of the five specimens in each series were loaded.

The three specimens, of which one was a solid circular slab and the other two were perforated circular slabs with steel liners in the penetrations, were subjected to a radial in-plate prestressing load and a uniform elevated temperature.

The problem, therefore, is a two-dimensional one in practice with time-dependent effects arising from the phenomena of bi-axial thermal creep and shrinkage of the material under the sustained load and temperature. A method of analysis is, therefore, needed capable of predicting the variation of stress distribution with time at any point in a structure consisting of two different but homogeneous materials.

2) Choice of the proposed method.

Two basic requirements are needed for the adopted method of analysis to be successful.

The first is that we must have a method of stress analysis yielding a homogeneous elastic solution of the structure capable of being repeated at every stage at which the stress distribution is required for the mechanical or thermal loads.

The second requirement is that the method should provide for the time-dependent thermal creep and shrinkage strains to be incorporated in the analysis.

The method of analysis adopted in this work is the finite element method for two dimensional stress analysis.

Using an appropriate matrix formulation for linear solutions, the method will supply an answer to the first requirement.

The second requirement may also be satisfied by extending the finite element technique into the non-linear range, using a step-by-step procedure. The rate of creep is used to incorporate the laws governing the stress-strain-time relation of concrete in the analysis.
The effective modulus is also utilized, first to calculate the load distribution in the periphery between the perforated zone, and the annulus, and second, to calculate the stress in the structure.

3) Purpose and scope.

The purpose of the theoretical investigation is to develop a method of analysis, using the finite element technique for two-dimensional stress analysis for plane stress elastic problems, taking into account . problems which exhibit time-dependent material properties.

It has been assumed that the material has an instantaneous initial elastic response on loading which is then followed by an enelastic deformation which is dependent upon stress level and time.

The creep strains occuring at any point of the structure, may be considered proportional to the stress, and are affected by the temperatures in such a manner as prescribed by a specific thermal creep law.

6.2. Difficulties in the analysis of the perforated end cap zone.

The problem of circular or tectangular perforated plates has been treated by a number of analysts in the past, purely from a theoretical point of view.

Most of the early work concerns itself with the analysis of simple cases where the elastic stress patterns were investigated for various simple boundary and loading conditions.

In recent years, however, the problem of perforated plates has received a considerable amount of attention because of its practical application in highly specialised engineering structures, such as the perforated end caps of the prestressed concrete pressure vessel for nuclear reactors.

In studying the stress patterns set up in a concrete pressure vessel, we require the solutions of structural systems loaded by a uniform axial load, and having a large number of circular penetrations which are reinforced with steel liners. A full description of the perforated end cap zone, its function, structural form, and the force components acting on it, is given in Chapter 1 , paragraph 1.2 , of this thesis.

The problem would, of course, be made more complex by the additional application of temperature load. In fact, the problem of perforated plates or slabs with reinforced holes subjected to sustained in-plate loading and uniform temperature with special reference to the perforated zone of the end cap of the reactor vessel, has received little attention.

In the past years, experimental methods, such as that of photo-elasticity, have been used to analyse two-dimensional structures, or verify results from theoretical analyses.

However, for complex structures subjected to sustained loading, constant or changing, and uniform temperature or temperature gradients, where long-term effects are dominating, this approach becomes extremely difficult if not impossible. Scale factors, material properties, real boundary and loading condition representations, are some of the disadvantages of the method. Moreover, structures with irregular configurations and boundary conditions complicate further the analysis.

Recent thechnological advances in the development of electronic computers have made it possible to handle and solve large problems by numerical or mathematical approximate methods.

Mathematical approaches to the solution have been attempted in the past by many investigators, using the long established principles of linear elasticity and structural mechanics. When the problem is restricted to the linear elastic case for a relatively simple structure, solutions in the form of differential or integral equations may be acceptable. For complex structures, the formulation and solution of the partial differential equations is an extremely difficult task.

Although the governing differential equation have been known for over a century, closed form solutions are available only for a limited number of practical structures.

The majority of general problems with arbitrary boundary and loading conditions remain unsolved by exact methods.

Examples of exact mathematical approaches are the Colocation, Least Squares, Galerking and Ritz methods. The general procedure in these methods involves the selection of the best solution from some assumed family of trial solutions.

Considering the mathematical approximate methods, the well known Finite Difference approach is considered to be one of the most powerful of the methods. It involves the replacement of derivatives in the differential equation and boundary conditions with difference equations.
It has been used on several linear problems by many investigators.

Even this method has several inherent problems. The matrix relating the external forces and displacements is not always symmetric and does not have any guarantee of being positive definite. When central differences are used, the bi-harmonic equation requires points outside the boundary, and other difference methods give unreliable answers. Real boundary conditions are very hard to satisfy if a rectangular net is used, and indeed, very complex if any other net is assumed.

The Gauss-Seidel iterative procedure does not always guarantee convergence, and direct solutions are more likely to be sensitive.

Finally, it is extremely difficult for problems involving non-linear media to specify the linking equations, especially when the sections are cracked.

Dynamic Relaxation which is an iterative method based on the equations of stress-strain compatibility and those of equilibrium, which are converted into equations of motion by the addition of inertia and viscous damping terms, is virtually impossible to apply in the problem of this investigation with such a complex geometry.

The limitations of th "classical" plane stress theory are well known.

The loads must be idealized as distributed or point loads. The boundaries must be of regular geometry. Support conditions are highly restrictive.

The body must be usually homogeneous.

These conditions are not always met in practical concrete structures, and even less so, in the prestressed concrete pressure vessel. The geometry of its section is irregular. The continuity in most sections, such as the end cap,is disturbed by the stand-pipes and in the walls by large penetrations, and the prestressing cable ducts. These factors greatly influence the internal stress distribution in the vessel section, and disturbe the homogenity of its material. Further, there is a relative displacement between steel and concrete, and when cracks develop, the topology of the section is constantly changing.

The Finite Element method permits a realistic evaluation of internal stresses and displacements for such conditions, and gives satisfactory answers to most of the forementioned difficulties which are encountered in the analysis of this particular problem. This method will be used throughout this investigation.

In this procedure, the continuum is idealized by an equivalent system of discrete elements inter-connected only at discrete points.

Compatibility is explicitly satisfied at these discrete points by making certain assumptions about the displacements. The structural system which results from this formulation, is a highly indeterminate one, and may be solved either by the displacement or force method. The displacement method was used in this work.

The greatest advantage of the method is that the resulting system of equations is a system of linear simultaneous equations which is more suitable for solution by the electronic computer than a system of partial differential or integral equations resulting from an exact mathematical formulation.

6.3. Existing elastic solutions of the perforated plate.

From a general study of the existing solutions, it was understood that most of the investigators treat the problem elastically using assumed elastic constants for the materials.

In most of these cases the analysis is based on the principles of the well-established classical theory of elasticity, assuming complex stress functions to arrive at a solution given in the form of differential or integral equations.

For reasons already mentioned in the previous section, these approaches do not always give adequate solutions. Since concrete is assumed to behave as a viscous material with age-dependent properties, an elastic solution will not suffice.

In the following paragraphs, a review of literature on perforated plates is given:-

TIMOSHENKO (77) and KIRSCH (78), treat the case of an infinite plate with a circular hole remote from the edges of the plate. It was found that a solution for the infinite plate was correct for a plate with finite size and the stress concentrations were independent of the hole diameter. This is not so in practice for a hole near the boundary of the plate, as the solution then becomes more difficult and usually cannot be obtained for a given type of loading.

JEFFREY (79), considered one hole near a single straight boundary and HOWLAND (80), and KNIGHT (81), for one hole between two straight boundaries. HOWLAND (82), also considered a plate with an infinite

row of holes, while ATSUMI (83), obtained a solution for an end-loaded strip, containing two equal circular holes placed close together.

HORVAY (84), gave an approximate solution for an infinite plate completely perforated.

As the ligaments were so narrow, he assumed that the perforated plate could be replaced by a hexagonal honeycomb structure with parallel-sided load-carrying members. He made use of this approximation to obtain curves for the Effective Young's Modulus, and Poisson's Ratio, and the corresponding concentration factors. Because of the nature of the method, his results have to be extrapolated to obtain equivalent elastic properties for plates and ligaments which are more than 20% of the diameter of the holes.

DUNCAN (85), considered the bending of completely perforated plates when used as structural elements in the heat exchangers of the reactor. He concluded that the pattern of penetrations (rectangular or triangular), has a significant effect on the ligament and deflection properties of the plate.

BAILEY and HICKS (86), investigated the behaviour of end-loaded rectangular plates with circular reinforced holes, forming a square or diagonal pattern. Their work makes special reference to the plate girder grillage structure with a perforated top flange, which supports the reactor core.

Two loading systems were considered:-

1) unequal uniform extensions were applied in the x and y axis.

2) uniformly applied shear.

The plate was assumed to be infinitely extended in its own plane. The above conditions do not occur always in practice. They obtained solutions for a pitch to diameter ratio ranging between 1.2 to 3.0, which were used to draw design curves for the Effective Young's Modulus, Shear Modulus, and Poisson's Ratio, and for variation of ligament stress, applied load and stress concentration factors. Fig. 6.1 (a), (b), (c), (d).

The elastic properties of the perforated plates are given for the two systems of load:-

a) plate with square system of holes:

Case 1 - $\sigma_x = \sigma_y$

$$\sigma_x = A_1 \frac{E(Ux)_c}{C} \qquad 6.3.1.$$

Where C = for the appropriate value of pitch
a = to diameter
C:a. = ratio
A_1 = the area under the appropriate curve
E = Young's Modulus
$(Ux)_c$ = uniform symmetrical applied displacement at the boundary (x=c), in the direction of x-axis
σ_x = average applied stress in the x-axis

From Hooke's Law:-

$$\frac{(Ux)_c}{C} = \frac{\sigma_x}{EA_1} = \frac{1}{E_e} (\sigma_x - V_e \sigma_y) \qquad 6.3.2.$$

Where E_e = Effective Young's Modulus of the plate
V_e = Effective Poisson's Ratio of the plate
σ_y = average applied stress in the y-axis
σ_x = average applied stress in the x-axis.

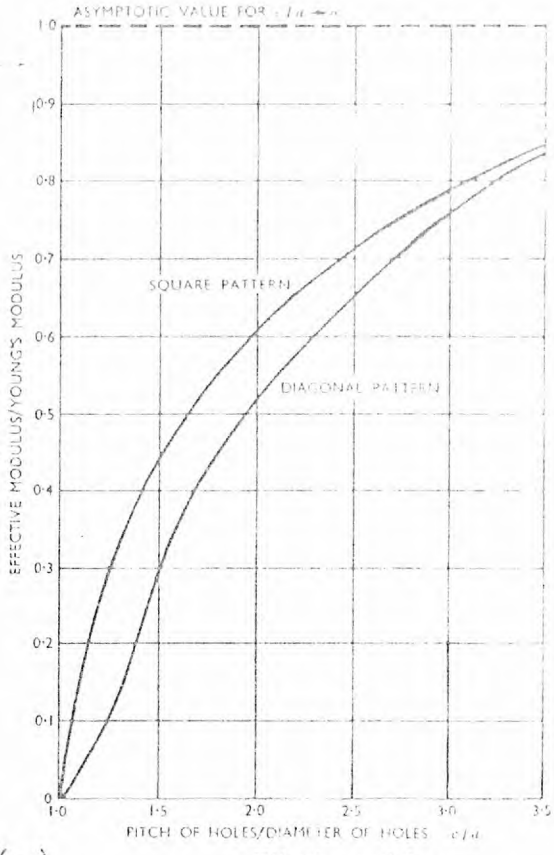

(a) *Effective modulus*

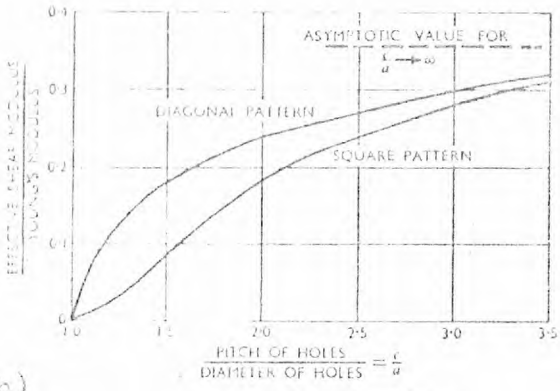

(b) *Effective shear modulus*

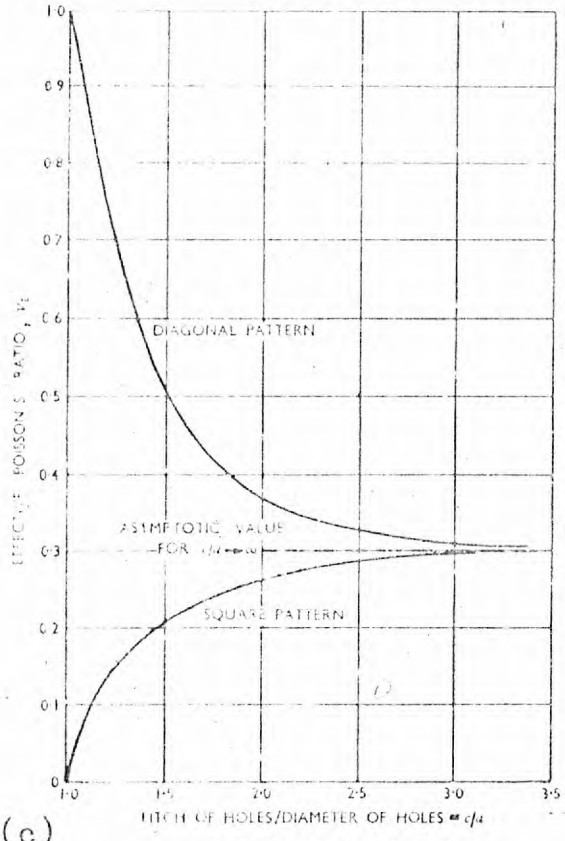

(c) *Effective Poisson's ratio*

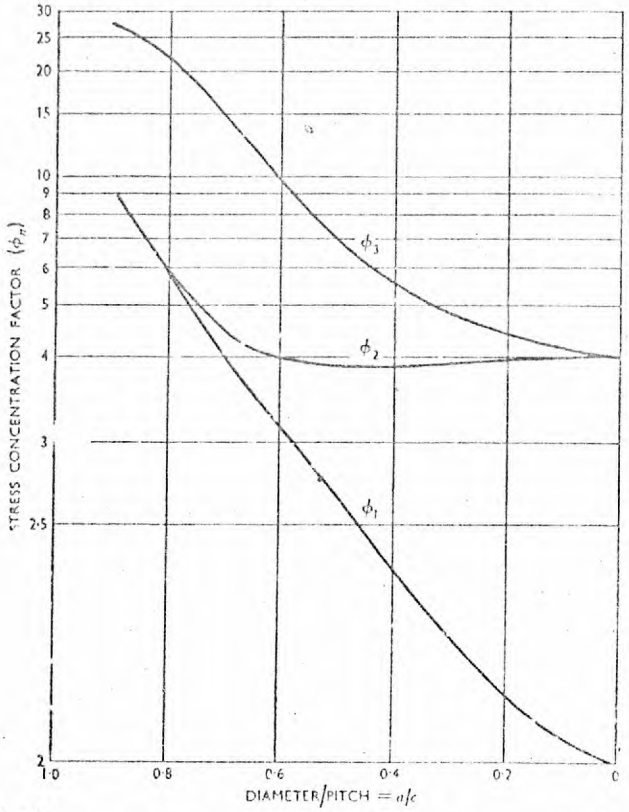

(d) *Stress concentrations and maximum stresses in plate*

Average stresses f_x and f_y ($f_x > f_y$) giving uniform displacements:

Square pattern $f_{max} = \frac{1}{2}\{\phi_1(f_x+f_y)+\phi_2(f_x-f_y)\}$

Diagonal pattern $f_{max} = \frac{1}{2}\{\phi_1(f_x+f_y)+\phi_3(f_x-f_y)\}$

Average shear stress, f_{xy}, giving uniform shear:

Square pattern $f_{max} = \phi_3 f_{xy}$

Diagonal pattern $f_{max} = \phi_2 f_{xy}$

FIG. 6.1. (Ref.86).

Case 2 - $\sigma_x = \sigma_y$

Again $\sigma_x = A_2 \frac{E(Ux)_c}{C}$ 6.3.3.

and - $\frac{(Ux)_c}{C} = \frac{\sigma_x}{EA_2} = \frac{1}{E_e}(\sigma_x + V_e \sigma_y)$ 6.3.4.

Where A_2 = area under the appropriate curve, since -

σ_x and σ_y are numerically equal, then equations 6.3.2. and 6.3.4. give:-

$$\frac{Ee}{E} = \frac{2A_1 \cdot A_2}{A_1 + A_2} \quad 6.3.5.$$

and - $$V_e = \frac{A_1 - A_2}{A_1 + A_2} \quad 6.3.6.$$

Case 3 - $\sigma_{xy} = \sigma_{yx}$

$$\sigma_{xy} = A_3 \frac{E(Uy)_c}{C} \quad 6.3.7.$$

Where A_3 = area under the appropriate curve

$(Uy)_c$ = uniform applied displacement at the boundary (y=c), in the direction of y-axis.

σ_{xy} = average applied shear.

So that - $\frac{2(Ux)_c}{C} = \frac{2\sigma_{xy}}{EA_3} = \frac{\sigma_{xy}}{Ge}$ 6.3.8.

and - $$Ge = \frac{EA_3}{2} \qquad 6.3.9.$$

Where Ge = Equivalent Shear Modulus.

b) plate with diagonal system of holes.

The elastic constants of the perforated plate may be determined in a similar manner:-

$$\frac{Ee}{E} = \frac{2A_4 A_5}{A_4 + A_5}\left(1 - \frac{a}{\sqrt{2.c}}\right) \qquad 6.3.10.$$

$$Ge = \frac{EA_6}{2}\left(1 - \frac{a}{\sqrt{2.c}}\right) \qquad 6.3.11.$$

$$V_e = \frac{A_4 - A_5}{A_4 + A_5} \qquad 6.3.12.$$

The integrations $A_1 \ldots\ldots\ldots A_6$ were carried out numerically for a complete range of pitch to hole diameter.

The maximum stresses around the holes and the stress concentration factors, are also given for the two systems of load:-

a) plates with square system of holes.

Case 1 - $\sigma_x = \sigma_y$

$$\sigma_x = \sigma_y = \frac{(f_x + f_y)}{2} \quad \text{stress} \qquad 6.3.13.$$

$$\phi_1 = \frac{\text{Max. Stress.}}{\frac{1}{2}(f_x + f_y)} \quad \text{concentration factor} \qquad 6.3.14.$$

Case 2 - $\sigma_x = \sigma_y$

$$\sigma_x = \sigma_y \frac{(f_x - f_y)}{2} \quad \text{stress} \qquad 6.3.15.$$

$$\phi_2 = \frac{\text{Max. Stress.}}{\frac{1}{2}(f_x - f_y)} \quad \text{concentration factor} \qquad 6.3.16.$$

Case 3 - σ_{xy}

$$\sigma_{xy} = 4 \sum_n \left[(n+1)\, D'n - (n-1)Dn \right] \qquad 6.3.17.$$

Where $n = 2,6,10$

$D =$ constant

$\sum =$ numerical integration

$$\phi_3 = \frac{\text{Max. Stress.}}{\sigma_{xy}} \qquad 6.3.18.$$

b) plates with a diagonal system of holes.

Similarly the concentration factors for this case are:-

Case 4 - $$\phi_4 = \frac{\text{Max. Stress.}}{\frac{1}{2}(f_x + f_y)} \qquad 6.3.19.$$

Case 5 - $$\phi_5 = \frac{\text{Max. Stress.}}{\frac{1}{2}(f_x - f_y)} \qquad 6.3.20.$$

Case 6 - $$\phi_6 = \frac{\text{Max. Stress.}}{\frac{1}{2}\sigma_{xy}} \qquad 6.3.21.$$

Where $f_x = \frac{\text{load applied to element in x-axis.}}{\text{full width of element}}$

f_y and σ_{xy} similarly defined.

HARROP and ABDUL-WAHAB (87), gave a simplified method of elastic analysis of perforated plates with reinforced and non-reinforced penetration, on an triagular grid pattern, under in-plane loading and radial bending.

Their analytical approach is based on a thick cylinder analogy. They assumed that for a uniformly applied stress field uniform distortion occurs and only a single hole need be considered. It is further assumed that this single hole system consists of a thick-walled cylinder subjected to uniform radial pressure.

They plotted curves of the Modular Ratio Ee/E, and Effective Poisson's Ratio, against ligament efficiency, pitch/span, and pitch/hole diameter ratios, and compared their theory with experimental results and previous theories. Fig. 6.2. (a), (b), (c), (d).

Using the equations for a thick-cylinder, the radial displacement at the inner boundary is given by:-

$$U_r = \frac{p.Po}{2E}\left[\frac{p^2 + d^2}{p^2 - d^2} - v\right] \qquad 6.3.22.$$

For a solid circular disc with an Effective Modulus Ee, and Effective Poisson's Ratio, v_e equal to the Poisson's Ratio of the material v, the radial displacement at the outer boundary is given by:-

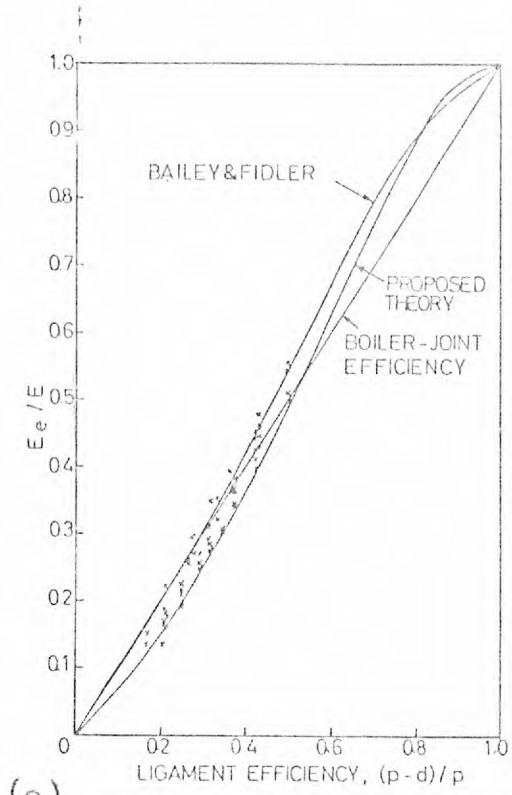

(a) Variation of E_e/E with ligament efficiency ($\nu_e/\nu = 1$).

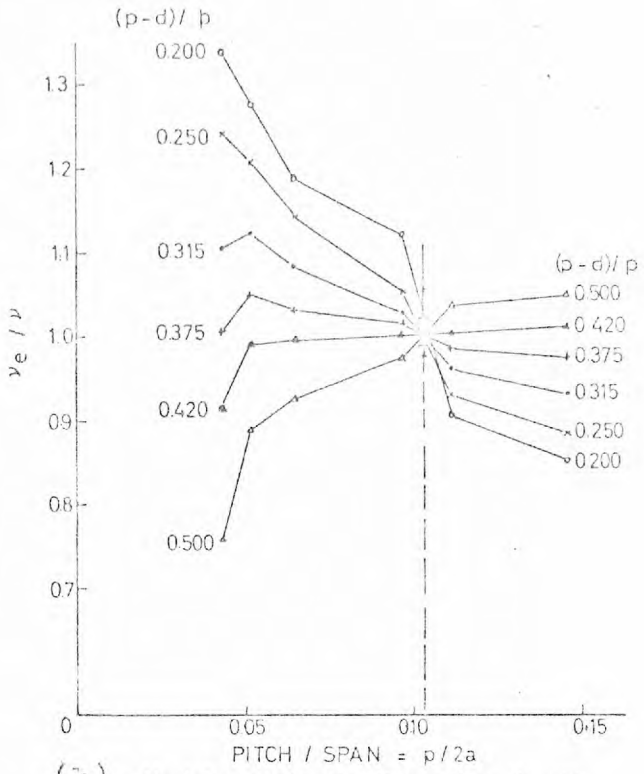

(b) Variation of effective Poisson's ratio with pitch/span ratio.

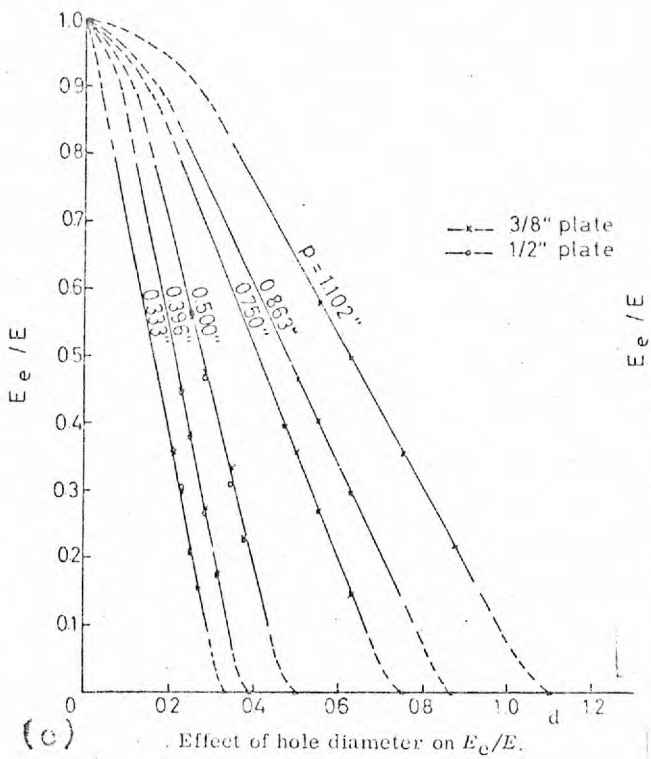

(c) Effect of hole diameter on E_e/E.

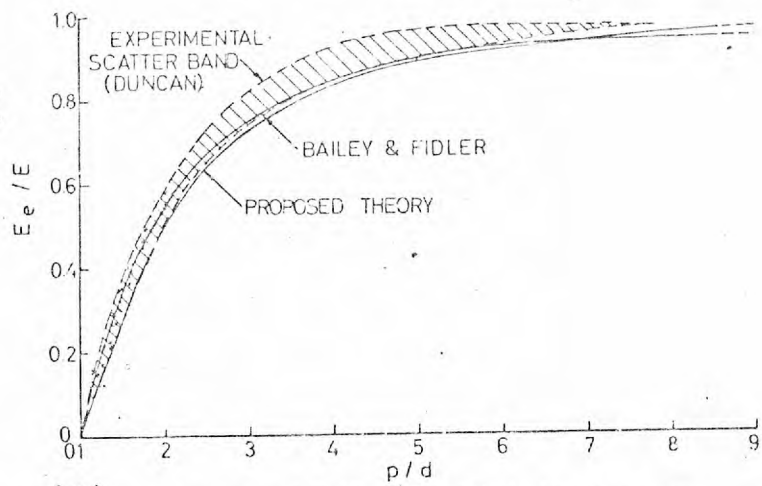

(d) Variation of E_e/E with pitch/hole diameter ratio.

FIG. 6.2. (Ref. 87).

$$U'_r = \frac{pPo}{2Ee}(1-v) \qquad 6.3.23.$$

Equating 6.3.22. and 6.3.23, we get the ratio Ee:E

$$\frac{Ee}{E} = \frac{1-(d^2p^2)}{1+(d^2/p^2)\left[(1+v)/(1-v)\right]} \qquad 6.3.24.$$

Maximum stress occurs in the tangential direction at the edge of the hole,

$$p_t = \frac{2P}{p^2-d^2}^2 - Po \qquad 6.3.25.$$

and the maximum stress concentration factor is given by:-

$$S.C.F. = \frac{2P^2}{p^2-d^2} = \frac{2}{1-(d^2/p^2)} \qquad 6.3.26.$$

Where
- p = the hole pitch which is equal to the external radius of the assumed cylinder
- d = inner radius of the cylinder
- Po = applied radial pressure acting on the outer face of the cylinder
- E = Elastic Modulus of the material
- v = Poisson's ratio of the material.

In another publication (88), the same authors give in graphical form the variation of the plate rigidity with modular ratio for varying ligament efficienty, liner thickness and liner reinforcement. Fig. 6.3. (a), (b), (c). Fig. 6. 4. (a), (b), (c).

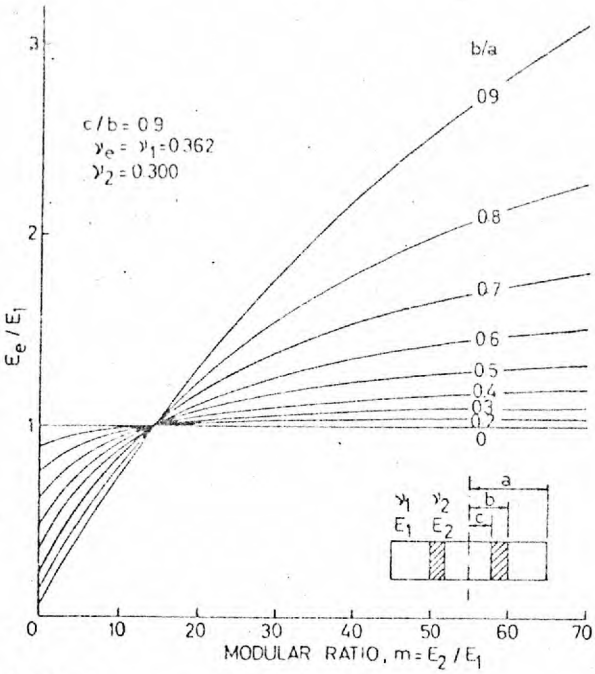

(a). Variation of rigidity with modular ratio for varying ligament efficiency.

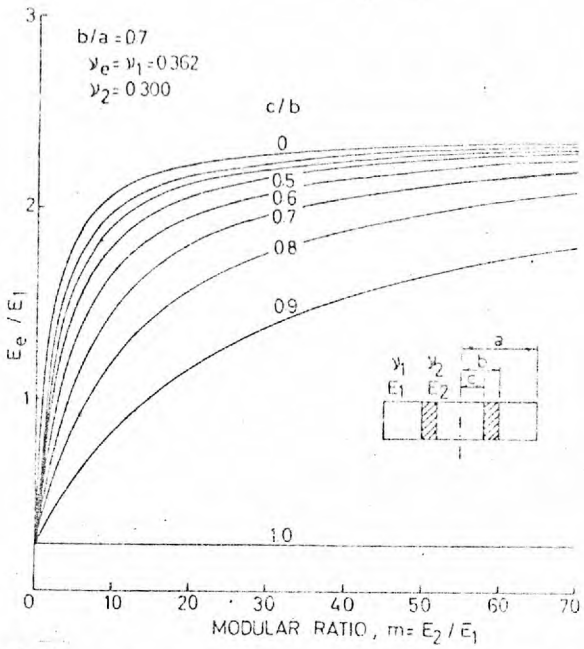

(b) Variation of rigidity with modular ratio for varying liner thickness.

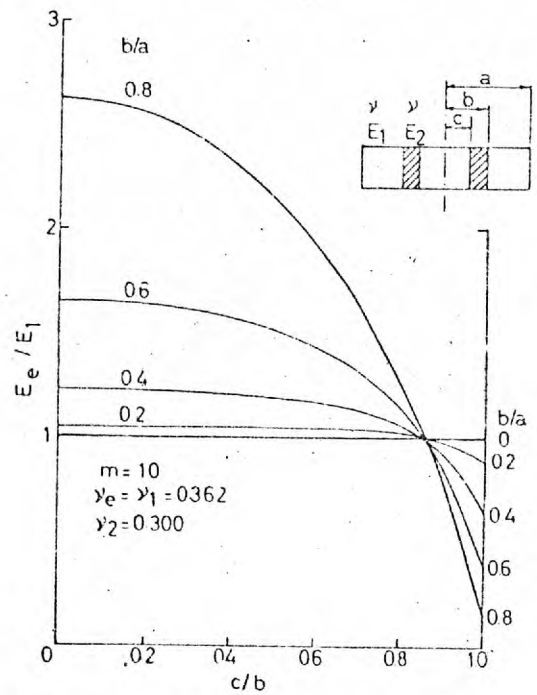

(c) Variation of rigidity with thickness of reinforcement.

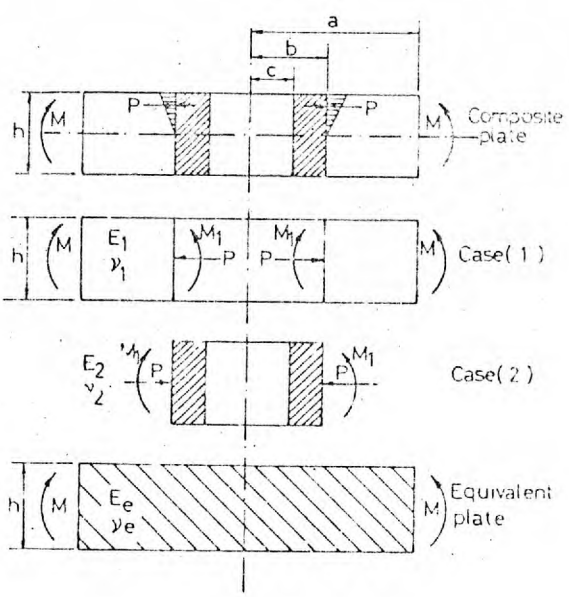

(d) Reinforced perforated plate in bending-unbonded reinforcement.

FIG. 6.3. (Ref. 88).

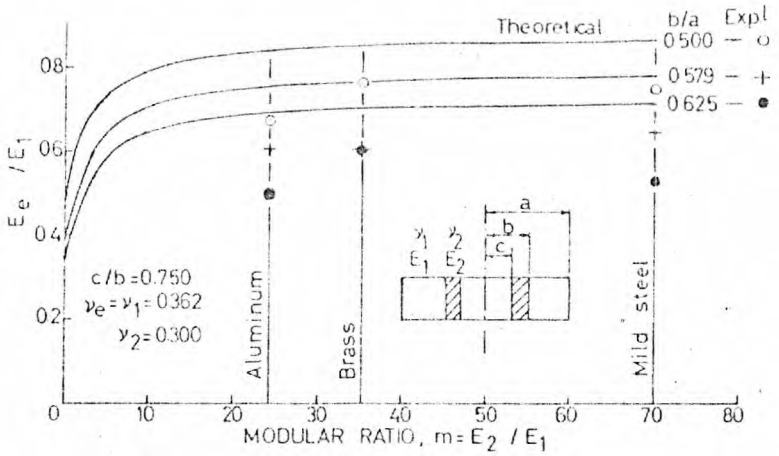

(a) Variation of rigidity with modular ratio.

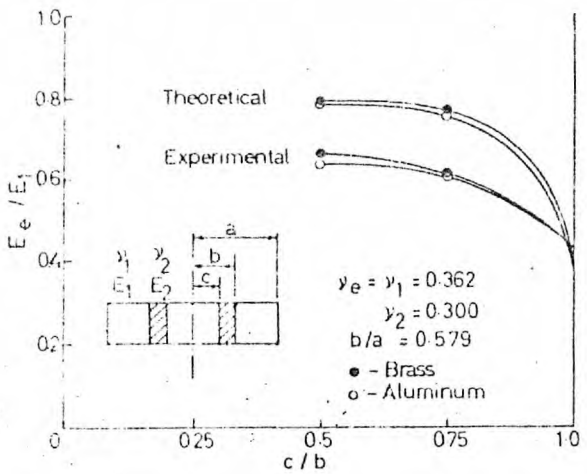

(b) Variation of rigidity with liner thickness.

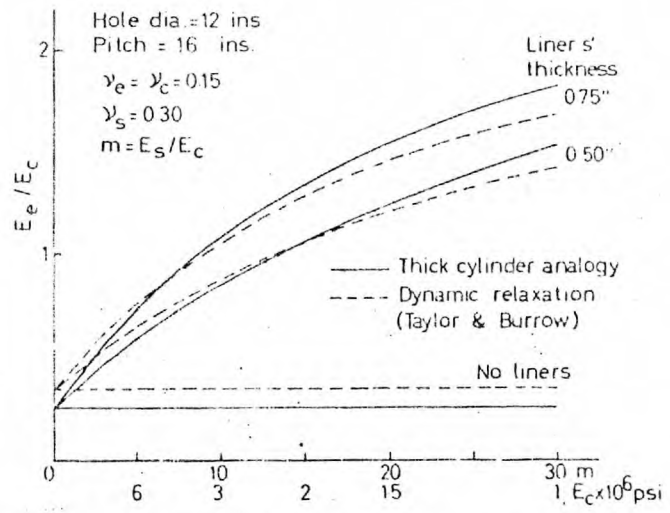

(c) Variation of rigidity of a concrete disc having steel compensated penetrations.

FIG. 6. 4. (Ref. 88).

SLOT (89), gave approximate elastic solutions for perforated square plates subjected to internal or external pressure for various hole diameter to plate width ratios of 0.5 and 0.9.

A point-matching procedure was used to generate solutions, that satisfy the internal boundary conditions exactly and the external approximately, for plate stress and plane strain conditions.

The stresses and displacements for the two cases are:-

Plane stress case.

a) Inner boundary.

$$\sigma_r / p = \sigma_\theta / p = -1 \qquad 6.3.27.$$

$$EUr / pR = -(1-v) \qquad 6.3.28.$$

$$U\theta = 0$$

b) Outer boundary.

$$\sigma_x / p = \sigma_y / p = -1 \qquad 6.3.29.$$

$$EUx / pR = -(1-v)(W/D) \qquad 6.3.30.$$

$$EUy / pR = -(1-v)(W/D)(y/y_D) \qquad 6.3.31.$$

Plane strain case.

a) Inner boundary.

$$\sigma_r / p = \sigma_\theta / p = -1 \qquad 6.3.32.$$

$\sigma_z / p = -2v$ 6.3.33.

$EUr/pR = -(1+v)(1-2v)$ 6.3.34.

$U\theta = o$

b) Outer boundary.

$\sigma_x/p = \sigma_y/p = -1$ 6.3.36.

$\sigma_z/p = -2v$ 6.3.36.

$EUx/pR = -(1+v)(1-2v)(W/D)$ 6.3.37.

$EUy/pR = -(1+v)(1-2v)(W/D)(y/y_D)$ 6.3.38.

Where R and D = radius and diameter of penetration

W = width of the plate

$\sigma_r, \sigma_\theta, t_{r\theta}$ = stress components in polar co-ordinates

$\sigma_x, \sigma_y, t_{xy}$ = stress components in cartesian co-ordinates

U_r, U_θ = displacements in polar co-ordinates

U_x, U_y = displacements in cartesian co-ordinates

E,V = Young's Modulus, Poisson's Ratio

p, p_i = pressure loading patterns.

KINKEAD (90), in his report on "round holes in prestressed concrete pressure vessels for nuclear reactors" offers an approximate solution to the problem of stress concentrations around the holes, arising under uni-directional and hydrostatic plane stress loading.

He found that the stresses increased where the openings were placed close together.

The method allows for variation in wall-thickness of the reinforcement at the penetration, and for the difference in the elastic constants of the slab and reinforcing material. No experimental or alternative theoretical results have been available to correlate with this approximate method.

BAILY and FIDLER (91), made a study of the elastic stress distribution around a pattern of reinforced holes with square and triangular patterns, under equal bi-axial stress. The Effective Elastic Modulus of the plate and the maximum stress concentration are presented in the form of curves showing variation with the pitch-to-diameter ratio and degree of reinforcement.
Fig. 6.5. (a), (b), (c), (d).

The solution is used to satisfy the boundary conditions at the reinforced hole exactly, and the boundary conditions at the axes of symmetry by point matching.

For an effective modulus of the perforated plate Ee the average strain is:-

$$\frac{1}{Ee}(\sigma_x - v\sigma_y) = \frac{Ux}{C} \qquad 6.3.39.$$

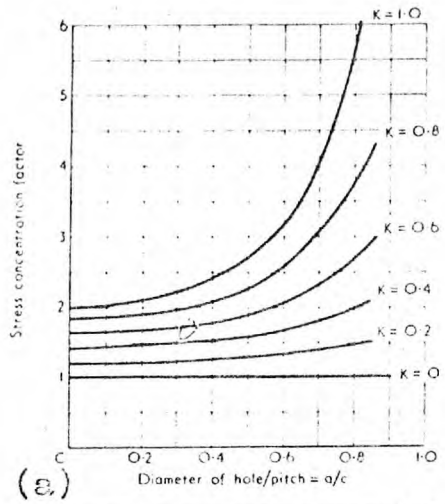

(a)

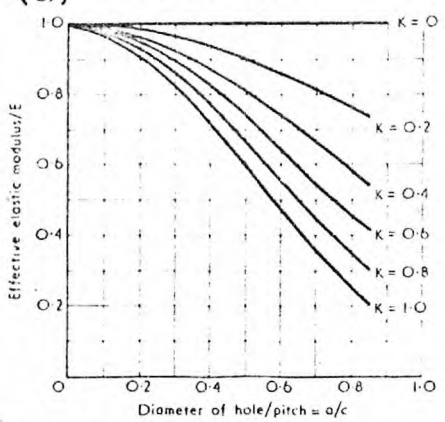

(c) Design data for a square pattern of reinforced holes.

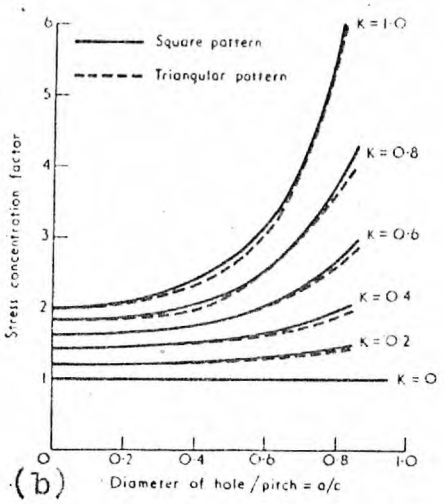

(b)

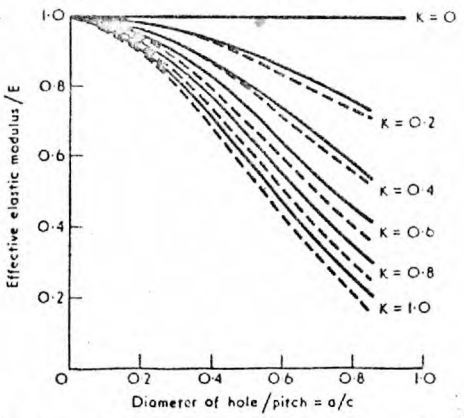

(d) Comparison between triangular and square pattern of reinforced holes.

FIG. 6. 5. (Ref. 91).

for $\sigma_x = \sigma_y$ the ratio Ee: E is:-

$$\frac{Ee}{E} = \frac{C(1-v)\sigma_y}{EUx} \qquad 6.3.40.$$

Where σ_x, σ_y= average applied stresses in x and y axis

Ux= displacement of plate in x-axis

C= pitch of holes

Ee= effective modulus of the plate

E= modulus of material

v= Poisson's ratio.

For a uniform distortion of $\frac{EUx}{a} = 1$,

the average applied stress is given from the equation below:-. (a = is the radius of the hole).

$$\sigma_x = \sigma_y = \frac{1}{C}\left[\int_a^C \sigma_{y_{\theta=o}}\, dr + \int_o^{\frac{1}{2}\pi} \sigma_{r_{r=a}}\, a \sin\theta d\theta + \int_o^{\frac{1}{2}\pi} \sigma_{r\theta_{r=a}}\, a \cos\theta d\theta\right] \qquad 6.3.41.$$

SHEFFIELD (92), studied the stress patterns in a fully perforated circular plate loaded in its plane for reinforced and unreinforced circular holes, and used his findings to determine the Effective Modulus of the plate, for both reinforced and unreinforced holes.

He has developed a general method of solution in terms of a set of linear equations for the coefficients of the general series solution.

This approach involves the inversion of large matrices to obtain a solution.

However, the author established a method of successive approximations which gives an accurate description of stress distribution for a uniform boundary pressure.

Assuming no change in the Poisson's ratio, the Effective Young's Modulus for a plate with reinforced penetrations is written as:-

$$\frac{Ee}{Ec} = \frac{1-v_c}{\frac{1+\Omega(1-2G)}{1-\Omega}} - v_c \qquad 6.3.42.$$

$$\Omega = \frac{nAh}{Ap} \qquad 6.3.43.$$

$$G = \left(\frac{2}{1-\Omega}\right) \Big/ \left[\frac{1+\Omega}{1-\Omega} + v_c + \left(\frac{2Ah-As}{As} - v_s\right)\frac{Ec}{Es}\right] \qquad 6.3.44.$$

Where
- Ee = equivalent modulus of perforated zone
- Ec = modulus of concrete
- Es = modulus of steel
- v_c = Poisson's ratio of concrete
- v_s = Poisson's ratio of steel
- Ah = area of one hole
- As = area of steel lining
- Ap = total area of plate
- n = number of holes in plate.

6.4. Proposed method of analysis.

6.4.1. Abstract.

The application of a two-dimensional Finite Element Structural Analysis to the perforated end cap zone of a Prestressed Concrete Pressure Vessel, for boundary and loading conditions, previously mentioned, is described, and the predictions are presented and compared with test results in graphical form.

Only the predicted strains at selected points on the structure are compared with experimental results, but stresses and displacements are also computed during the entire length of the test programme. The predicted stresses and strains, are given both at the nodal points and relative to the elements.

The purpose of the study was to demonstrate theadequacy and relative accuracy of two-dimensional finite element analysis for predicting long-term behaviour of the perforated end cap zone of the cylindrical reactor vessel by the Rate of Creep Method.

For purposes of comparison, the Effective Modulus approach was also used to predict the long-term behaviour. The basic principles of the two methods were outlined in Chapter IV , and a more detailed description is given in this Chapter. Both methods were programmed for solution by the electronic computer.

The programmes developed for the Finite Element solution in both methods are described in detail at the end of this Chapter.

They were written in FORTRAN language and run originally in the 7094 IBM electronic digital computer unit of the Imperial College, and finally, in the CDC 6600 unit of the Computer Centre of the University of London.

The theoretical basis for the two-dimensional finite element analysis is reviewed and the formulation presented in detail.

The equations for the inelastic time-dependent solutions are developed and introduced into the Finite Element formulation.

6.4.2. Design and development considerations.

The design and development of the Prestressed Concrete Pressure Vessel for power-generating reactors has relied heavily upon the use of large model testing, and on mathematical, approximate or numerical methods.

With the advent of the development of the electronic computers, it has become possible to use such methods for the solution of large problems. The most popular ones at present are Dynamic Relaxation, Finite Difference and the Finite Element Method.

The construction and testing of large scale models for research and development work is a costly and time-consuming operation.

As a result, increased consideration is being given to small-scale models and, in addition, increased reliance is being placed on more detailed mathematical, approximate and numerical methods of analysis.

6.5. Two-dimensional Finite Element Analysis.

6.5.1. Introduction.

The analyses of Prestressed Concrete Pressure Vessels by the Finite Element method have been mostly performed on an elastic and two-dimensional basis, with computer programmes based on either axisymmetric or plane stress assumptions.

Usually, an axisymmetric analysis is adopted for the bulk of the investigation. When an axisymmetric analysis is being used, the entire bulk of the vessel is considered as axisymmetric using postulated effective values of the elastic constants of the material in parts of the structure that do not exhibit axisymmetric features.

To study the effects of non-axisymmetric parts such as the stand-pipe penetrations, the circumferential prestressing arrangements of the non-circular parts of the vessel's section, a two-dimensional plate analysis is performed. Even in these circumstances, the general practice is again to carry out the elastic analysis by postulating the effective elastic constants of the material.

An attempt has been made in this work to investigate the actual behaviour of the perforated zone of the end caps of the vessel for the loading and boundary conditions previously described, by developing a method of analysis capable of forecasting, not only the elastic stresses, but also the thermal, creep and shrinkage effects.

For this purpose, five specimens were cast and tested in a "test programme" simulating to some extent the commissioning and operating conditions of the vessel. The casting and testing procedures are discussed in detail in Chapter V, and the test programmes in Figs. (1.9), (1.10), (1.11), of Chapter I.

The basic principles of the Finite Element Method are briefly stated in the following, to facilitate subsequent discussions on the application of this technique in this specific problem. The method is applicable to all classes of continuum problems met in engineering practice with one, two or three dimensional stress systems.

The structure is divided into an assemblage of discrete elements.

The displacement fields within the elements are assumed to vary linearly. Consequently, the strains and stresses within the element are constant.

The displacements within each element, and consequently, the strains and stresses, can be expressed as functions of the two unknown displacements at each nodal point of the element.

The fictitious forces acting at the nodes of the element, known as the nodal forces, are uniquelly defined by the displacements of these nodes.

These nodal forces must be made statically equivalent to the boundary stresses and distributed loads acting on the structure. To do this, virtual nodal displacements are imposed on the element's node, and the internal work done by the stresses and strains is adequate to the external work done by the nodal forces and corresponding displacements from the application of virtual

work. The application of this principle yields the stiffness relation, relating nodal displacements and nodal forces for the element.

Superposing the stiffness relationship of all the elements in the assemblage loads to the nodal point equilibrium equations for the entire structure.

The equilibrium equations are solved for the unknown nodal displacements, after which the element strains and stresses may be determined. The solution of the equilibirum equations is obtained by elimination. or matrix inversion, and by iteration.

6.5.2. Historical background.

SAINT VENANT, was one of the earliest investigators to introduce the concept of one-dimensional Finite Element in his work on torsion and flexure of beams.

HRENNIKOFF (93) and McHENRY (94), appear to have originated the approximation of a two-dimensional continuum by a system of one-dimensional elements to methodsof structural analysis.

They assumed that a two-dimensional continuum can be idealized as an assemblage of one-dimensional bars, capable of taking axial forces. The properties of the bars were selected to give load-deflection characteristics for the element which corresponded to the plate section represented.

This approach which is also known as "The Lattice Analogy Method," had several limitations, one of them being that Poisson's ratio had to be taken equal to 1/3. Additional difficulties were also encountered in dealing with orthotropic materials and with structures having curved boundaries.

McCORMICK (95), used more complex bars where bending was allowed, and there were no restrictions in the values of the Poisson's ratio.

The Finite Element Method of analysis was developed originally in the aircraft industry, and it is only recently that the scope and power of this method has been brought out by the formulation of general matrix equations for the solution of complex structural systems.

TURNER, CLOUGH, MARTIN and TOPP (96), were the pioneers in introducing two-dimensional elements in the analysis of aircraft structures.

LANGEFORS (97) and ARGYRIS (98), have made notable contributions in this field, while ZIENKIEWICZ (99), has been working towards a general approach on structural engineering problems.

CLOUGH (100), more recently introduced the triangular and rectangular plate element stiffness for plane stress structures.

WILSON (101), suggested that the derivation of element stiffness may be based on energy considerations, and further proposed the extension of the Finite Element Method to non-linear problems.

LANSING (102), developed the analysis of inelastic structures.

KING (103), extended the two-dimensional Finite Element Method to include time-dependent material response.

BRESLER (104), applied the method to an axisymmetric reinforced concrete member.

NGO (105) and NGO and SCORDELLIS (106), gave consideration to some of the special problems in the analysis of reinforced concrete, and finally,

MELLESH (107), GALLAGHER, PADLOG and BIJLAARD (108), and RASHID (109), made significant contributions in three-dimensional Finite Element analysis.

6.6. Theoretical considerations.

6.6.1. General procedure.

As stated previously, the matrix displacement formulation is used to apply the finite element technique.

The author is of the opinion that the displacement method has several advantages for many types of structures.

The matrix formulation for many typical problems is simpler and more compact in terms of displacements, than in terms of forces. Furthermore, the displacement method gives considerable scope for computational refinement in its formulation, and which reduces the possiblity of serious errors, virtually to zero.

Perhaps the greatest advantage of the method is its adaptability.

The necessary steps in the Finite Element technique for this particular analysis are as follows:-

(1) Structural idealization.

(2) Determination of the local and global co-ordinates.

(3) Evaluation of element stiffness k.

(4) Transformation from local to global co-ordinates.

(5) Determination of the stiffness matrix K for the complete structure.

(6) Consideration of the boundary conditions.

(7) Evaluation of the thermal creep and shrinkage load vectors, and their addition to calculate the resultant load vector.

(8) Formulation and solution of the equilibrium equations to compute displacements.

(9) Determination of the element stresses.

---

(1) Structural idealization:

a) The element.

The basic element used in place stress analysis is the two-dimensional plate element, having two degrees of freedom at each node.

The triangular two-dimensional element was adopted in this investigation because of its ability to represent structures with irregular geometries. Figs. 6.6, 6.7, and 6.8., show a typical element, with its co-ordinate axes, nodal forces and nodal displacements.

Bar elements were also used to represent the liners in the penetrations.

The structural systems were sub-divided into an assembalge of discrete elements as shown in Figs. 6.9, 6.10, and 6.11.

The analysis was performed only on a 90^{o} symmetrical quadrant for each of the three loaded specimens.

The nodal points of the mesh chosen were arranged in such a manner as to correspond with the demec gauge points previously fixed on the specimens.

The nodal points were also arranged to correspond with the diametral stand-pipe measuring positions. This arrangement made it possible to compare directly the observed experimental displacements with those resulting from the analysis.

Accordingly, the structural idealization for the three specimens was as follows:-

i) $16^{3}/4"$ diameter specimen (Model 1/2).

The mesh had a total of 60 nodal points, and 94 elements.

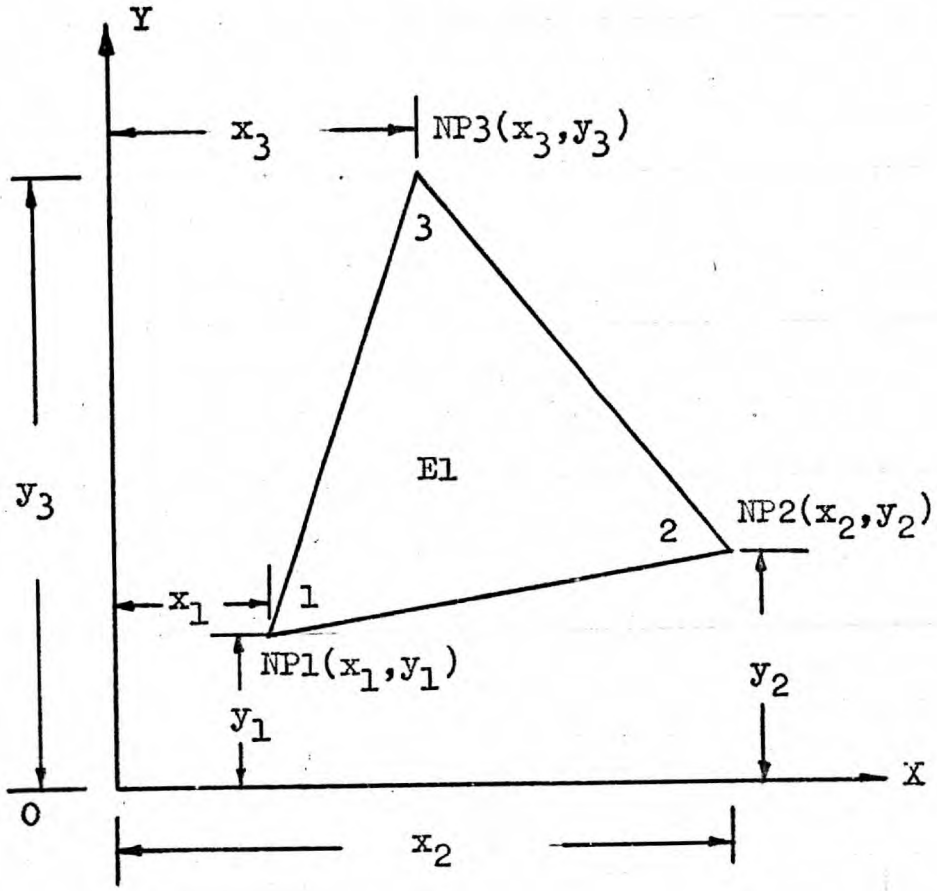

FIG. 6. 6. Triangular element

Co-ordinate axis:
(X, Y), (x, y)

Nodal points:
NP1, NP2, NP3

Nodal point co-ordinates:
NP1 = (x_1,y_1)

NP2 = (x_2,y_2)

NP3 = (x_3,y_3)

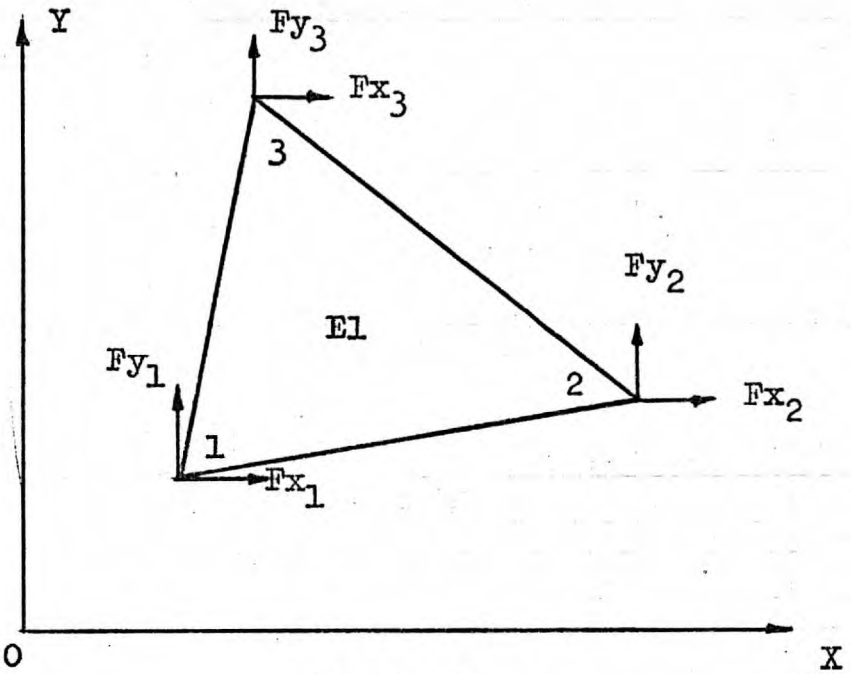

FIG. 6. 7.

Triangular elemen

Nodal forces:

$$[F] = \begin{bmatrix} F_1 \\ F_2 \\ F_3 \end{bmatrix} = \begin{bmatrix} Fx_1 \\ Fy_1 \\ Fx_2 \\ Fy_2 \\ Fx_3 \\ Fy_3 \end{bmatrix}$$

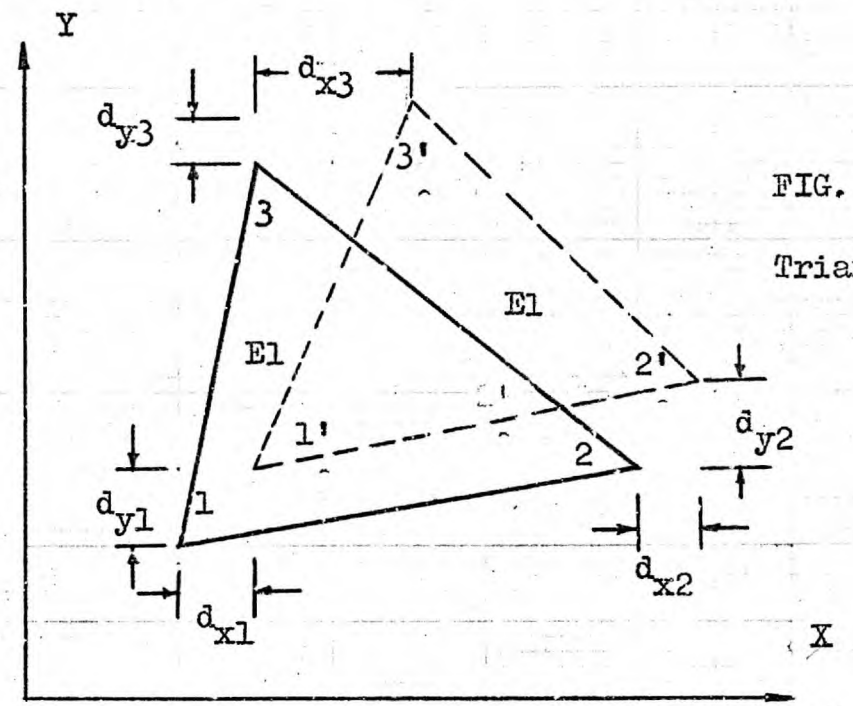

FIG. 6. 8.

Triangular element

Nodal point displacements:

$$[d] = \begin{bmatrix} d_1 \\ d_2 \\ d_3 \end{bmatrix} = \begin{bmatrix} d_{x1} \\ d_{y1} \\ d_{x2} \\ d_{y2} \\ d_{x3} \\ d_{y3} \end{bmatrix}$$

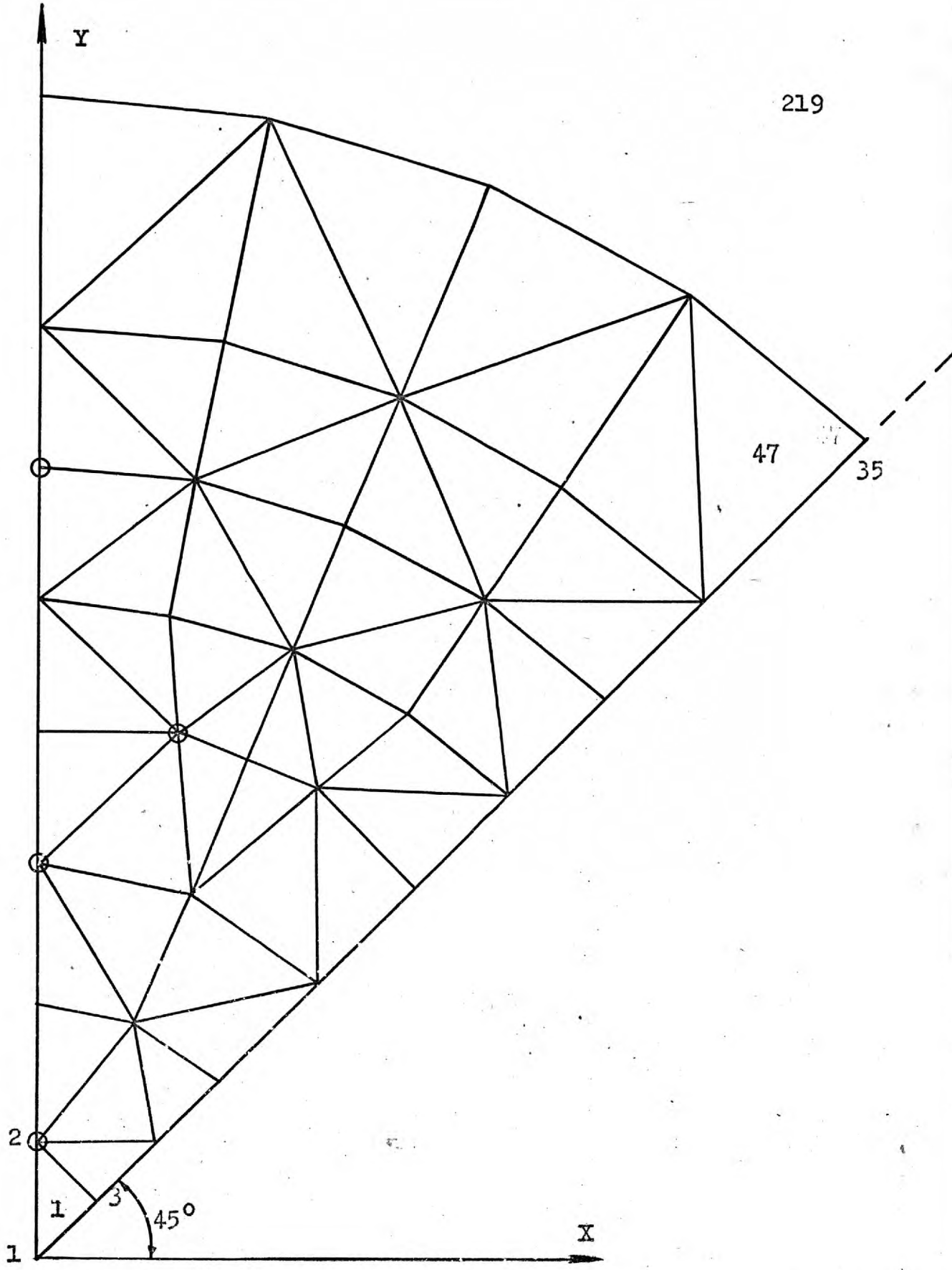

FIG. 6.9. STRUCTURAL IDEALIZATION FOR MODEL 1/2.

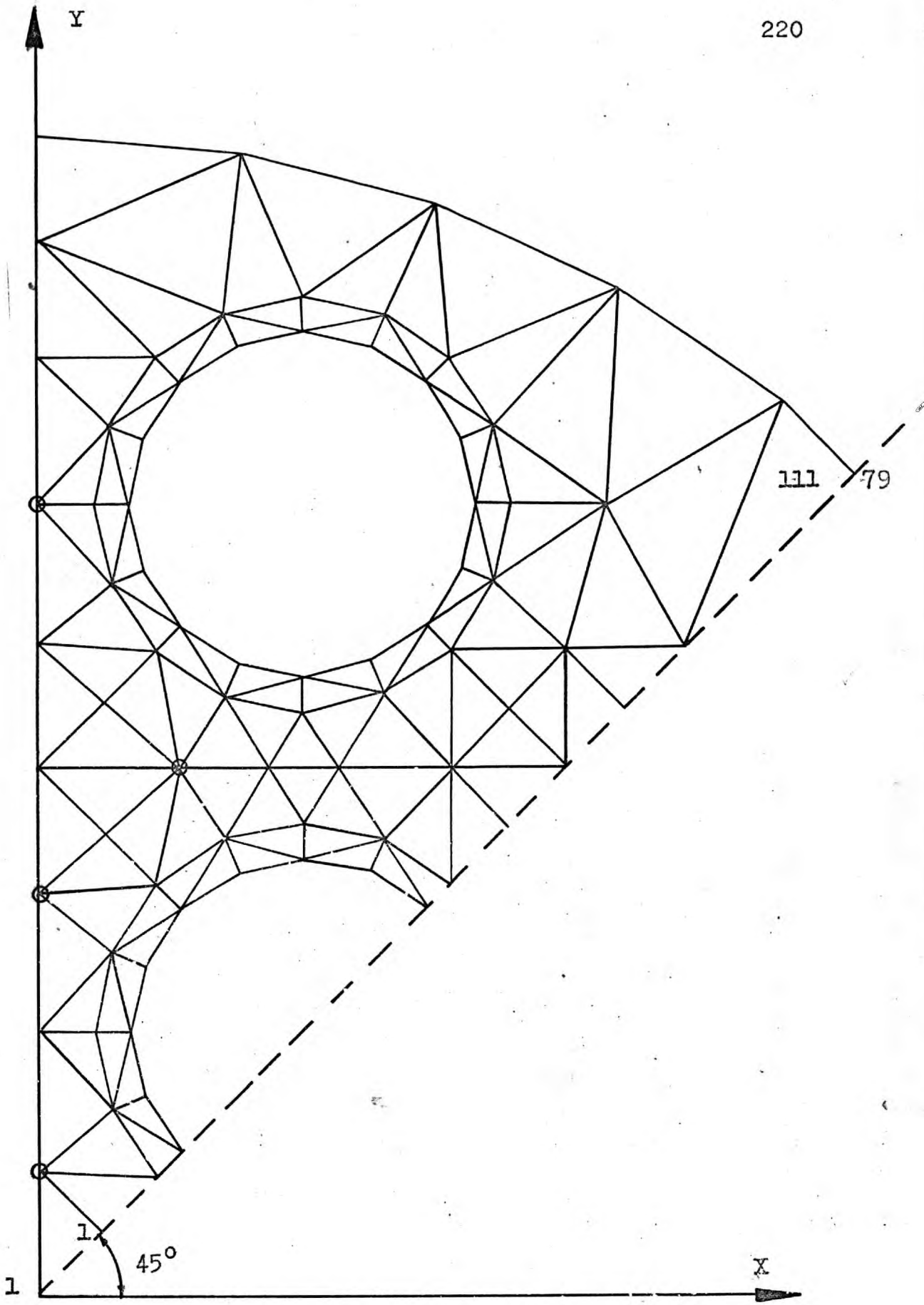

FIG.6.10. STRUCTURAL IDEALIZATION
FOR THE 16 3/4" DIAMETER SPECIMEN
'45o SECTOR

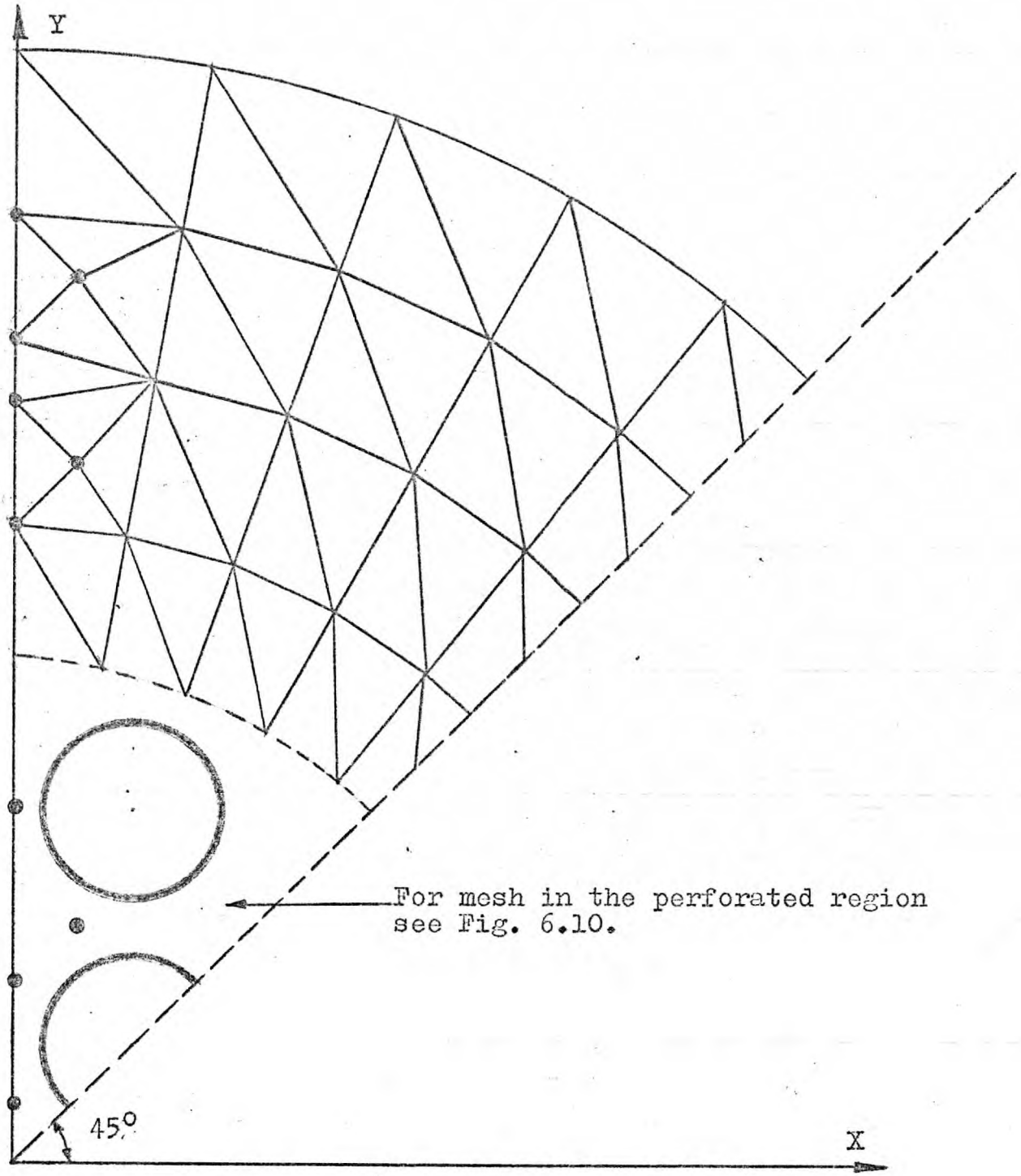

FIG. 6. 11. Structural idealization for the 36" diameter specimen 45° sector.

ii) $16\frac{3}{4}$" diameter perforated specimen (Model 3/4).

The mesh had a total of 146 nodal points and 221 elements. Ninety-six of the elements represented the stand-pipe liners.

iii) 36" diameter composite specimen (Model 9/10).

The mesh had a total of 192 nodal points and 303 elements. Ninety-six of the elements represented the stand-pipe liners.

b) Thickness of the element.

For a conventional idealization the continuum is assumed to have a uniform thickness t. In this work, all elements had the same thickness of 6" equal to the thickness of the specimens.

c) Loads.

i) Live loads.

The radial load R acting on the boundary of the loaded specimens was idealized by statically equivalent concentrated forces acting on the nodal points at the boundary of the Finite Element system.

ii) Dead loads.

The effects of the dead loads were not included in this analysis because they are negligibly small.

The self weight of the elements could have been made equivalent to statically equivalent body forces, acting on the elemental nodes, and assumed to be distributed equally at each of the three nodal points of the element.

d) Penetrations.

When the structural system has holes in the interior as in the case of the perforated and composite specimens of these tests, the situation can be dealt with in two ways:-

i) The standard triangular net can be used with the areas and thicknesses of the elements made equal to zero.

ii) The cut-outs are divided into elements, and a very small value for the elastic constants ($E = 1$, $v = 0.001$), is assumed.

For the purposes of this analysis, an alternative procedure was adopted when the idealization of perforated specimens was considered. The area of the standpipes was excluded from the mesh.

(2) Determination of local and global co-ordinates.

Local co-ordinates are taken to signify these co-ordinates relative to the element, whereas, global co-ordinates are taken as relative to the main structural quadrant.

The Cartesian co-ordinate system was used to represent the nodal points of the elements in the orthogonal system adopted both for local and global axes of reference.

This system of co-ordinates was considered to be most appropriate to the strain readings.

(3) Evaluation of element stiffness k.

The evaluation of element stiffness characteristics is the most critical step of the analysis. This can be done in several ways.

Wilson (101), employed a set of corner forces statically equivalent to the uniform internal stress distribution to establish a relationship between the nodal forces and nodal displacements.

Clough (100), used the principle of virtual work for establishing nodal force-displacement relationships without the necessity of assuming statically equivalent forces.

Gallagher (108), suggested a third approach based on strain energy and using Castigliano's theorem, while, Mallett (110), develops expressions for the element stiffness based on the application of the principle of stationary total potential energy.

In this investigation, the development of the stiffness matrix for a typical triangular element is based on the principle of virtual displacements.

To do this, it is necessary to establish the geometry of the element, and the displacement configuration which the element assumes between its nodal points when its co-ordinates one at a time undergoes a unit virtual displacement.

The state of stress which corresponds to the imposed unit displacement is also required.

This may be obtained from known stress - strain relationships.

Finally, the external work done by the virtual nodal displacement is equated to the internal work done in the element by the stress.

From these consideration, the stiffness of the element is established, resulting in a matrix equation for each element relating the nodal forces, F, to the nodal displacements, d, in terms of the stiffness coefficients k_{ij} (i, j = 1,2,2).

$$F = k.d \qquad 6.6.1.$$

Where k = is the stiffness matrix of the element, and is always a square matrix.

$$k = \begin{array}{c} \\ 1 \\ 2 \\ 3 \end{array} \begin{array}{c} \begin{array}{ccc} 1 & 2 & 3 \end{array} \\ \begin{bmatrix} k11 & k12 & k13 \\ k21 & k22 & k23 \\ k31 & k32 & k33 \end{bmatrix} \end{array} \qquad 6.6.2.$$

The elements $k11$, $k12$, etc., in the stiffness matrix above, are themselves square sub-matrices with 2 x 2 dimensions.

$$k11 = \begin{array}{c} \begin{array}{cc} 1 & 2 \end{array} \\ \begin{array}{c} 1 \\ \end{array} \begin{bmatrix} k11 & k12 \\ k21 & k22 \end{bmatrix} \end{array} \qquad 6.6.3.$$

The stiffness matrix k of the element takes the following form:-

$$k = \begin{array}{c} \begin{array}{ccc} 1 & 2 & 3 \end{array} \\ \begin{array}{cccccc} 1 & 2 & 3 & 4 & 5 & 6 \end{array} \\ \begin{bmatrix} k11 & k12 & k13 & k14 & k15 & k16 \\ k21 & . & & & & \\ k31 & . & . & & & \\ k41 & . & . & . & & \\ k51 & . & . & . & . & \\ k61 & . & . & . & . & k66 \end{bmatrix} \end{array} \qquad 6.6.4.$$

Equation6.6.1,in expanded form becomes:-

$$\begin{bmatrix} F1 \\ F2 \\ F3 \\ F4 \\ F5 \\ F6 \end{bmatrix} = \begin{bmatrix} k11 & & & & & & d1 \\ k21 & . & & & & & d2 \\ k31 & . & . & & & & d3 \\ k41 & . & . & . & & & d4 \\ k51 & . & . & . & . & & d5 \\ k61 & k62 & k63 & k64 & k65 & k66 & d6 \end{bmatrix} \quad 6.6.5.$$

(4) Transformation from local to global co-ordinates.

It was found possible to define all nodal co-ordinates in relation to the chosen orthogonal axes. There was, consequently, no need to carry out co-ordinate transformation for the elemental displacement and force component.

(5) Determination of the stiffness matrix K for the complete structure.

The stiffness matrix K of the structural system was obtained from a direct stiffness approach by superimposing the stiffness contributions of all the elements to each nodal point of the system.

From this operation an equilibrium equation results for the complete structure which relates the

externally applied nodal forces R, and the nodal displacement d, resulting therefrom.

$$R = K\,d \qquad 6.6.6.$$

(6) Considerations of the boundary conditions.

The next step was to specify the boundary conditions.

Known force and displacement boundary conditions were introduced as non-zero entries in the force and displacement vectors respetively.

(7) Evaluation of the thermal, creep and shrinkage load vectors, and addition to calculate the resultant load vector.

The specimens under test were subjected to long-term radial compression and uniform elevated temperature.

The temperature creates additional thermal strains in the structure which, under certain conditions, will cause thermal stresses to develop.

In a similar manner, the sustained loading coupled with the additional thermal load, will create additional time-dependent strains and stresses.

All these effects were incorporated in the

analysis by calculating the additional load vector which was in turn, added to the externally applied loads to form the resultant load vector.

A detailed description concerning the formulation of these vectors is given in later paragraphs of this Chapter.

(8) Formulation and solution of the equilibrium equations.

The solution of the equilibrium equations for the displacements is normally performed either by direct methods, i.e., partial inversion of the overall stiffness matrix K, and Gaussian elimination, or by iteration.

In the present development, the direct methods of matrix inversion and direct elimination were used for the solution of equation 6. 6. 6.

The advantages gained in solving the equations by matrix inversion are the reduction of the computational effort and the greater accuracy in the determination of the unknown displacements.

However, this is only possible if the elastic properties of the materials concerned, do not vary with age and temperature, and if a solution is to be obtained without any prior information available regarding nodal displacements.

The greatest disadvantage of the inversion method is the storage required by the stiffness matrix K, which for a typical finite element problem may be of the order of 300 x 300, and even larger.

The solution of the equations for the solid specimen was performed by matrix inversion. The stiffness matrix involved in this case was of the order of 120 x 120, and therefore, the problem of storing the matrix in the CDC 6600 computer unit did not exist.

With regard to the variation of the elastic properties with age and temperature, it was established experimentally that this variation was of no significance, and the analysis was carried out with the same elastic constants for all time intervals considered, and for the three phases of the test programme.

Nevertheless, solutions were also given with varying elastic constants, and the results compared.

The matrix inversion procedure is described in numerous text books, and no description will be given here.

The Gaussian elimination approach modified for the banded matrix was applied for the analysis of the perforated and composite specimens.

In this case the stiffness matrices for the two specimens of the order of 300 x 300 and 400 x 400, and the problem of storing the matrices became apparent.

The elimination procedure is briefly summarized here:-

The equation 6.6.6, may be written in expanded form as:-

$$K_{11}\, d_1 + K_{12}\, d_2 + \ldots\ldots K_{1N}\, d_N = P_1 \qquad 6.6.7.$$

$$K_{21}\, d_1 + K_{22}\, d_2 + \ldots\ldots K_{2N}\, d_N = R_2 \qquad 6.6.8.$$

$$\vdots \qquad\qquad \vdots$$

$$K_{N1}\, d_1 + K_{N2}\, d_2 + \ldots\ldots K_{NN}\, d_N = R_N \qquad 6.6.9.$$

Equations 6.6.7, and 6.6.8, may be written as:-

$$d_1 = K_{11}^{-1} (R_1 - K_{12}d_2 - K_{13}d_3 \ldots - K_{1N}d_N) \qquad 6.6.10.$$

$$d_2 = K_{22}^{-2} (R_2 - K_{21}d_1 - K_{23}d_3 \ldots - K_{2N}d_N) \qquad 6.6.11.$$

Substituting now the value of d_1 previously determined in the equation for d_2, we obtain a new equation for d_2 in terms of R_1, R_2, the known K's and d_3 ..... d_N .

In general we obtain:-

$$d_i = f(R_1 \ldots R_N, K_{mn}, d_{i+1} \ldots d_N) \qquad 6.6.12.$$

and finally,

$$d_N = f(R_1, R_2, \ldots R_N, K_{mn}) \qquad 6.6.13.$$

Then, by back substitution we obtain the values of d's.

$$d_{N-1}, d_{N-2}, \ldots d_1$$

The structure stiffness matrix is sparsely populated as only a limited number of nodal points are inter-connected directly by the elements. In most practical cases, the number of elements directly connected to a nodal point, is not more than 10 to 15.

However, for structures with irregular geometry as the perforated specimens of this test, the number of the elements may be as high as 20.

The maximum number of elements connected to a nodal point did not exceed 15. Accordingly, the non-zero entries in a row of the matrix K, did not exceed this number. This resulted in a diagonally banded matrix.

In storing the matrix K, the terms within the band-width for a given row, were shifted to the extreme left, and a rectangular matrix resulted with rows equal in number to the rows of the original matrix, but with

only as many columns as the terms in the band-width. The saving in storage capacity was substantial.

$$K = \begin{bmatrix} x & x & x & x & 0 & 0 & 0 & 0 \\ x & x & x & x & x & 0 & 0 & 0 \\ x & x & x & x & x & x & 0 & 0 \\ x & x & x & x & x & x & x & 0 \\ 0 & x & x & x & x & x & x & x \\ 0 & 0 & x & x & x & x & x & x \\ 0 & 0 & 0 & x & x & x & x & x \\ 0 & 0 & 0 & 0 & x & x & x & x \end{bmatrix}$$

Banded Matrix.

$$\underline{K} = \begin{bmatrix} x & x & x & x \\ x & x & x & x \\ x & x & x & x \\ x & x & x & x \\ x & x & x & 0 \\ x & x & 0 & 0 \\ x & 0 & 0 & 0 \end{bmatrix}$$

Shifted Matrix.

Of course, the choice of the method of solution of the equilibrium equations depends upon the characteristics of the problem.

It has been stated that for non-varying elastic properties of the materials concerned in the analysis, and when a single solution is required, the direct methods are recommended for the solution of the equations.

However, if more than one solution is

required and the elastic properties vary with time, an advantage can be gained using an iterative approach.

Small changes can be incorporated in the stiffness matrix, and a prior solution will give a good starting value for the next iteration.

An iterative solution is possible using successive over-relaxation which is a modified version of the Gauss-Seidel method. This procedure is described in detail elsewhere, and only a brief summary is given here.

In equation 6.6.6, the equation for the n^{th} displacement may be written as:-

$$R_n = \sum_{i=1,N} K_{ni} d_i = K_{n1} d_1 + K_{n2} d_2 + \ldots + K_{nN} d_n \qquad 6.6.14.$$

In which:

R_n = nodal point load externally applied at joint n.

d_i = displacement at joint i.

K_{ni} = structural force at joint n, due to unit displacement of joint i.

For an iterative solution this equation may be written:-

$$R_n = \sum_{i=1,n-1} K_{ni} d_i + K_{nn} d_n + \sum_{i=n+1,N} K_{ni} d_i \qquad 6.6.15.$$

for which:-

$$d_n^{(s+1)} = K_{nn}^{-1} \left(R_n - \sum_{i=1,n-1} K_{ni} d_i^{(s+1)} - \sum_{i=n+1,N} K_{ni} d_i^{(s)}\right) \qquad 6.6.16.$$

The superscripts indicate the number of the iteration cycle.

The rate of convergence may be increased by use of an over-relaxation factor.

The change in the displacement of a nodal point n between cycles of iteration is given from:-

$$\Delta d_n^{(s)} = d_n^{(s+1)} - d_n^{(s)} \qquad 6.6.17.$$

Substituting equation 6.6.17, into 6.6.16, yields:-

$$\Delta d_n^{(s)} = K_{nn}^{-1} \left(R_n - \sum_{i=1,n-1} K_{ni} d_i^{(s+1)} - \sum_{i=n,N} K_{ni} d_i^{(s)} \right) - d^{(s)} \qquad 6.6.18.$$

And, the new displacement n is determined from the following equation:-

$$d_n^{(s+1)} = d_n^{(s)} + \beta \Delta d_n^{(s)} \qquad 6.6.19.$$

Where β = is the selected over-relaxation factor having a value between 1.8 and 1.95.

For the present work there appeared to be no strong advantage in favour of either the direct or iterative methods. The direct methods previously discussed were adopted.

(9) Determination of the element stresses.

With the nodal displacements known , the stress and strain within each element may be obtained from relationships obtained when evaluating the element stiffness.

6.6.2. Matrix formulation.

The theoretical basis and technique for two-dimensional analysis has been described elsewhere. However, a brief description of the procedure is presented here with special reference to this work.

1) Type of stress.

The plane stress analysis for isotropic and homogeneous materials is used throughout this investigation. This type of stress was considered to be more appropriate for the analysis as compared with the plain strain solution.

The basic equations for the plane stress-strain relations for isotropic materials are stated here to facilitate subsequent discussions.

For plane stress distribution we have:-

$$\sigma_z = \sigma_{zx} = \sigma_{zy} = 0$$

Strains - $$e_x = \frac{1}{E} (\sigma_x - v \sigma_y) \qquad (a)$$

$$e_y = \frac{1}{E} (\sigma_y - v \sigma_x) \qquad (b) \qquad 6.6.20.$$

$$e_{xy} = 2 \frac{(1 + v)}{E} \sigma_{xy} \qquad (c)$$

Alternatively -

$$\begin{bmatrix} e_x \\ e_y \\ e_{xy} \end{bmatrix} = \frac{1}{E} \begin{bmatrix} 1 & -v & 0 \\ -v & 1 & 0 \\ 0 & 0 & 2(1+v) \end{bmatrix} \begin{bmatrix} \sigma_x \\ \sigma_y \\ \sigma_{xy} \end{bmatrix} \qquad 6.6.21.$$

And in matrix form:

$$\{e\} = \left[D^{-1} \right] \{\sigma\} \qquad 6.6.22.$$

Stresses -

Solving equations 6.6.20, for stress we obtain:-

$$\begin{bmatrix} \sigma_x \\ \sigma_y \\ \sigma_{xy} \end{bmatrix} = \frac{E}{1-v^2} \begin{bmatrix} 1 & v & 0 \\ v & 1 & 0 \\ 0 & 0 & \frac{1-v}{2} \end{bmatrix} \begin{bmatrix} e_x \\ e_y \\ e_{xy} \end{bmatrix} \qquad 6.6.23.$$

And in matrix form:

$$\{\sigma\} = \left[D \right] \{e\} \qquad 6.6.24.$$

Where D = the elasticity matrix.

A typical element is shown in Fig.6.12 with local co-ordinates (x, y), and corresponding displacements (u, v), for each of the three nodes of the triangle. The global co-ordinates and corresponding displacements are represented by (X, Y), and (U, V) respectively.

At the nodal point(1), of a typical element the co-ordinates are:-

$$(x_1, y_1)$$

The displacement components:-

$$d_1 = u_1, v_1$$

2) Displacement field.

A linear displacement field is assumed inside the element, and is represented by two linear polynomials of the form:-

$$U_{(x,y)} = a_1 + a_2 x + a_3 y \quad (a) \qquad 6.6.25.$$

$$V_{(x,y)} + a_4 + a_5 x + a_6 y \quad (b)$$

Where $U_{(x,y)}$ = displacement in x of any point(x,y)

$V_{(x,y)}$ = displacement in y of any point(x,y)

$a_i (i=1,6)$ = constants

And in matrix form, the above system is represented as:-

$$u = M\, a \qquad 6.6.26.$$

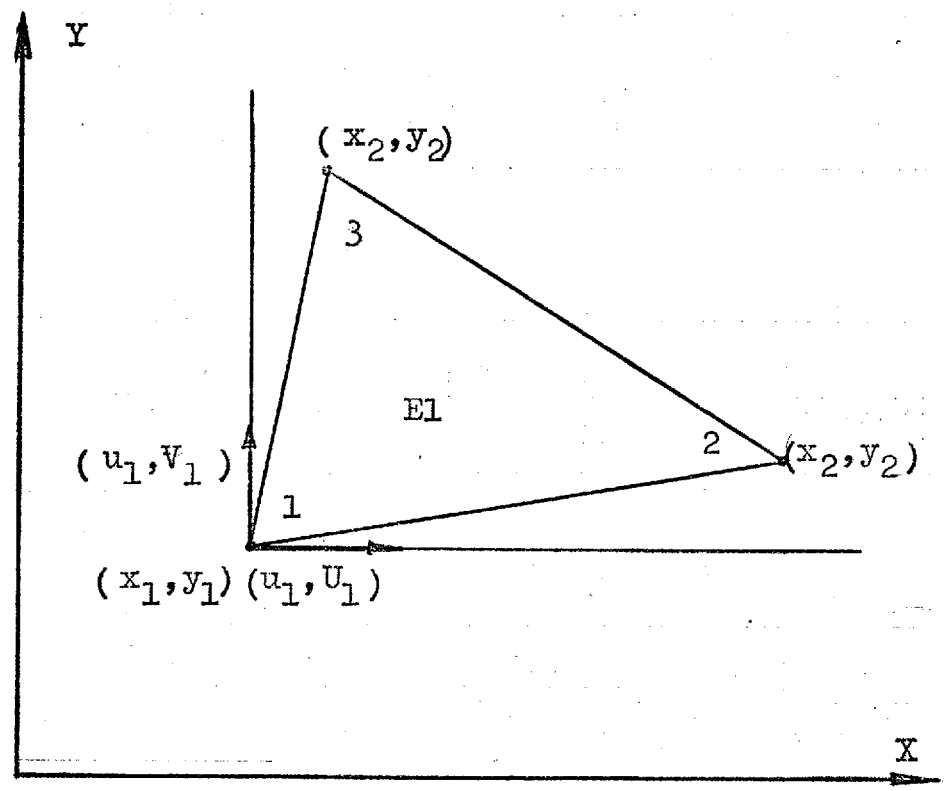

FIG. 6. 12. Typical triangular element E1

Nodal points 1, 2, 3.

Nodal point 1:

Co-ordinates (x_1,y_1)

Displacements (u_1,v_1)

Where u and a are the column vectors,

$u = u, v$

$a = a_1\ a_2\ a_3\ a_4\ a_5\ a_6$, and

M = is the displacement transformation matrix relating the two vectors, and takes the following form:-

$$M = \begin{bmatrix} 1 & x & y & 0 & 0 & 0 \\ 0 & 0 & 0 & 1 & x & y \end{bmatrix}$$

If the equation 6.6.26 is evaluated at the nodal points, the nodal displacements d or $d = d_1\ d_2\ d_3$ can be written in matrix form as:-

$$d = A \cdot a \qquad 6.6.27.$$

Where $d = \begin{bmatrix} u_1 & v_1 & u_2 & v_2 & u_3 & v_3 \end{bmatrix}$

And A = is the matrix of the nodal co-ordinates. Inverting equation 6.6.27 , gives an expression for a in terms of the nodal displacements.

$$a = A^{-1} \cdot d \qquad 6.6.28.$$

3) Displacements.

If equation 6.6.28, is substituted back into equation 6.6.26 , a relation for the element displacement in terms of nodal displacements is obtained as:-

$$u = M \cdot A^{-1} d \qquad 6.6.29.$$

Where $M \cdot A^{-1} = N$

$$\therefore \quad u = N \cdot d \qquad 6.6.30.$$

4) Strains.

The strain displacement relations can be written in matrix form as:-

$$e = L \cdot u \qquad 6.6.31.$$

Where $e = \left[e_x \; e_y \; e_{xy} \right]$

And,

$$L = \begin{bmatrix} \frac{\partial}{\partial x} & 0 & 0 \\ 0 & \frac{\partial}{\partial y} & 0 \\ 0 & 0 & \frac{\partial}{\partial y} + \frac{\partial}{\partial x} \end{bmatrix}$$

Substituting for u from equation 6.6.30 , we obtain the element strains as a function of nodal displacements in the form:-

$$e = B \cdot d \qquad 6.6.32.$$

Where $B = L \cdot N$

5) Stresses.

The stress-strain relation for an isotropic Hookean material may be written as:-

$$\sigma = D\ (e - e_o) \qquad (a)$$

6.6.33.

Or, $$\sigma = D \cdot B \cdot d - D \cdot e_o \qquad (b)$$

Where $$\sigma = \left[\sigma_x \quad \sigma_y \quad \sigma_{xy}\right]$$

e_o represents the initial strain which may be due to thermal, creep, shrinkage, crystal growth strains or strains due to lack of fit.

The matrix D is the elasticity matrix which relates the modulus of elasticity E to the Poisson's ratio v.

For the plane stress solution the elasticity matrix has the form:-

$$D = \frac{E}{(1-v^2)} \begin{bmatrix} 1 & v & 0 \\ v & 1 & 0 \\ 0 & 0 & \frac{1-v}{2} \end{bmatrix} \qquad 6.6.34.$$

6) Element and structural stiffness equations.

Applying a virtual nodal displacement and equating the external work done by the nodal forces to the internal work done by the stresses during that displacement, a general equation of the following form results:-

$$k\ d - Fo - Fg - Fp - R = 0 \qquad 6.6.35.$$

Where

$$k = \int_V B^T D\ B\ dv \qquad 6.6.36.$$

$$Fo = \int_V B^T D\ e_o\ dv \qquad 6.6.37.$$

$$Fg = \int_V N^T g\ dv \qquad 6.6.38.$$

$$Fp \int_S N^T p\ dv \qquad 6.6.39.$$

Where k = the element stiffness matrix having dimensions (6 x 6), equal to the degrees of freedom of the triangle.

Fo = the equivalent nodal forces due to initial strains.

Fg = equivalent nodal forces due to body forces

Fp = equivalent nodal forces due to surface tractions.

R_e = denotes the concentrated forces applied to the element nodes.

^e_o = the initial strains.

g = denotes the body forces per unit volume.

p = denotes the surface tractions.

Finally, with F denoting the total equivalent nodal force vector, given by:-

$$F = Fo + Fg + Fp + R_e \qquad 6.6.40.$$

The stiffness relation of the element can be written:-

$$F = k \cdot d$$

When the stiffness equations of all the elements are properly superposed, the final set of equilibrium equations for the nodes of the entire assemblage is obtained. These equations can be represented in matrix form as:-

$$R = K \cdot d$$

Where K = the structure stiffness matrix.

At this stage, displacement boundary conditions are introduced into the equations, and the unknown nodal displacements solved for, corresponding to a specific loading condition consisting of known thermal strains, body forces, surface tractions, and concentrated nodal forces.

With the nodal displacements d determined, the element strains can be found from the kinetic relationships, equation 6.6.32 , and the element stresses from the stress-strain relation, equation 6.6.33.

6.6.3. Elastic solution.

An initial calculation was carried out for the three loaded specimens in which the elastic stress and strain resulting from the instantaneous applied radial compression were obtained.

The results obtained from this solution formed the starting point for the step-by-step solution.

1) Sign convention.

a) Compression loads are assumed to be negative, and therefore, their displacements, stresses and strains are negative.

b) Tension loads are assumed to be positive, and therefore, their displacements, stresses and strains are positive.

c) Strains produced from a rise in temperature are assumed to be positive, and those produced from a fall in temperature are negative.

d) Creep strains assume the sign of the stress which produces the creep effects.

e) Shrinkage strains have opposite sign to the thermal strains.

2) Mechanical loads.

The radial load p_i applied at the boundary of the loaded specimens was replaced by concentrated forces Ri, acting at the nodal points in the boundary.

The periphery of the quadrant of the solid specimen considered in the analysis, was divided by nine nodal points to eight equal parts.

In the case of the perforated and composite specimens, ten nodal points divided the quadrant into nine equal parts.

The equivalent nodal point forces Ri, acting at the nodes of the boundary, were resolved in the x and y directions of the co-ordinate system chosen, giving components Ri $\cos\alpha_i$, and Ri $\sin\alpha_i$, respectively. Figures 6.13, 6.14, 6.15.

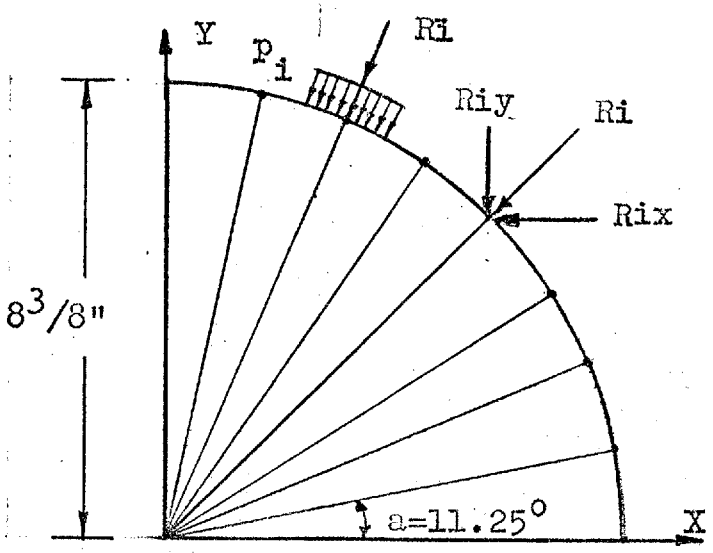

FIG.6.13. Solid specimen.

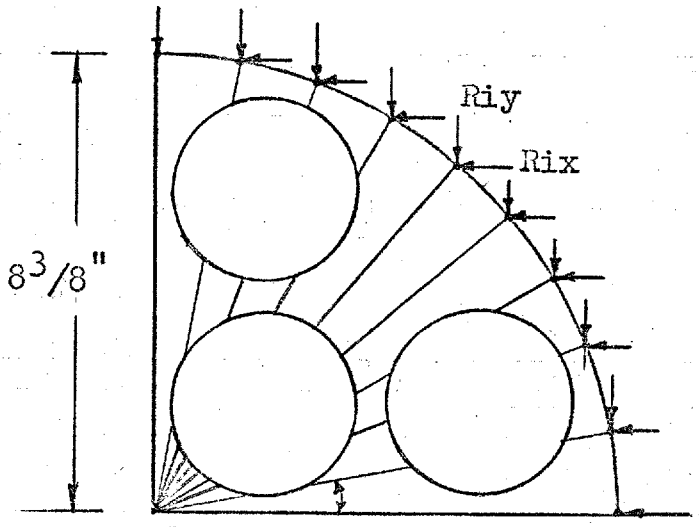

FIG.6.14. Perforated specimen.

p_i = Radial compression

Ri = Concentrated radial load at nodal points of the boundary

Rix= Ri cosa

Riy= Ri sma

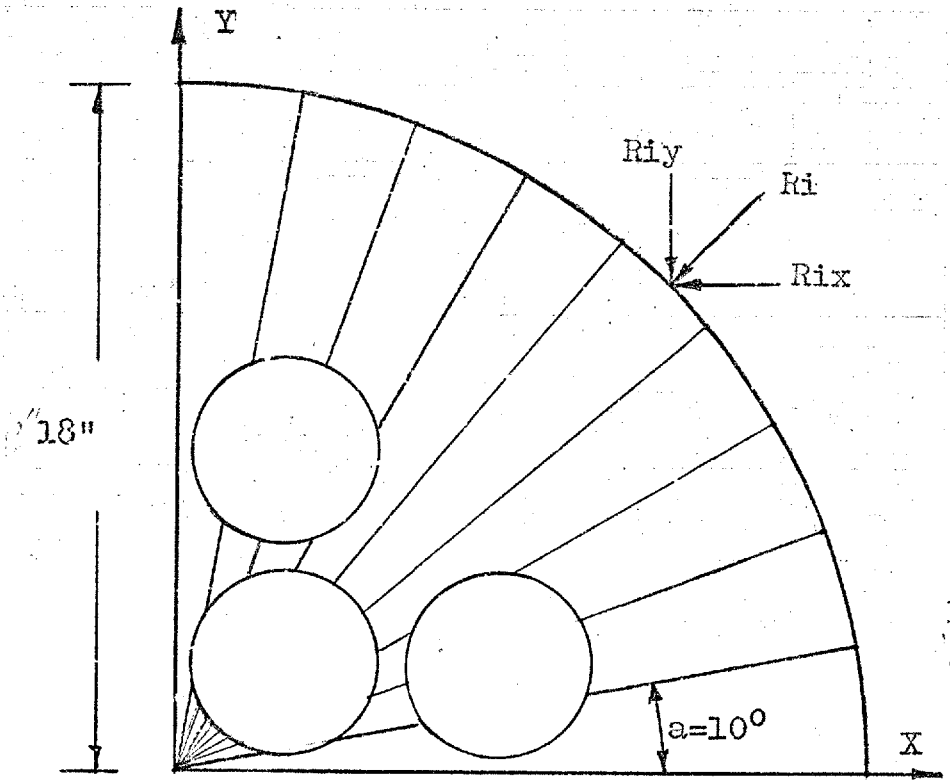

FIG. 6.15.
Composite specimen.

These components formed the external load vector for which the structures were analysed.

3) Matrix equations.

The following equations were needed for the elastic solution:-

a) Element strains in terms of nodal displacements.-

$$e = B \cdot d$$

b) Element stresses in terms of element strains.-

$$\sigma = D \left[e - e_o \right]$$

Or, $$\sigma = D \cdot B \cdot d - D \cdot e_o$$

c) The element stiffness matrix.

$$k = B^T \cdot D \cdot B \cdot t \cdot A \qquad 6.6.41.$$

Where t = thickness of the element, and,
A = area of the element.

d) The equilibrium equations for the element.

$$F = k \cdot d$$

d) The equilibrium equations for the structure.

$$R = K \cdot d$$

The matrix B in equation 6.6.41 may be determined by calculating the constants a, of equations 6.6.25, (a) and (b) , in terms of the nodal displacements.

Referring to Fig. (6.12), and inserting the nodal co-ordinates in the two polynomials, then equating the displacements to the appropriate nodal displacements, equations 6.6.25,(a) and (b) , assume the following form:-

$$u_{(x,y)} = \frac{1}{2A} (a_1+b_1 x + c_1 y)u_1+(a_2+b_2 x+c_2y) u_2 + (a_3+b_3 x+c_3y) u_3 \qquad 6.6.42.$$

And, $$v_{(x,y)} = \frac{1}{2A} (a_1+b_1 x + c_1 y)v_1+(a_2+b_2 x+c_2y) v_2 +(a_3+b_3 x + c_3y) v_3 \qquad 6.6.43.$$

Where $u_1 = a_1 + a_2x_1 + a_3 y_1$

$$u_2 = a_1 + a_2 x_2 + a_3 y_2$$

$$u_3 = a_1 + a_2 x_3 + a_3 y_3$$

And, $$a_1 = x_2 y_3 - x_3 y_2$$

$$b_1 = y_2 - y_3 = y_{23}$$

$$c_1 = x_3 - x_2 = x_{32}$$

From equations 6.6.42 and 6.6.43 -

$$B = \frac{1}{2A}\begin{bmatrix} b_1 & 0 & b_2 & 0 & b_3 & 0 \\ 0 & c_1 & 0 & c_2 & 0 & c_3 \\ c_1 & b_1 & c_2 & b_2 & c_3 & b_3 \end{bmatrix} \qquad 6.6.44.$$

The equation of the area A of the elemental triangle can be found from the above expressions, and is equal to:-

$$A = \frac{Det}{2}\begin{bmatrix} 1 & x_1 & y_1 \\ 1 & x_2 & y_2 \\ 1 & x_3 & y_3 \end{bmatrix} \qquad 6.6.45.$$

6.6.4. Thermoelastic solution for Two-dimensional Stress Analysis.

If a structure is operating at elevated temperatures, the determination of the thermal stresses plays an important part in the design, and the stress-strain equations must therefore, include the effects of temperature.

Of course, as stated in Chapter IV, paragraph 4.6, the thermal stresses in a structure, depend upon the type of end restraint, and in certain cases, upon the internal restraints.

For loaded unrestrained structures, uniform temperatures will not create additional thermal stresses, although thermal expansion will occur.

However, for a loaded unrestrained structure, non-uniform temperature will create additional thermal stresses which must be taken into account.

The specimens tested in this investigation fall into two main categories:-

a) Uniformly heated and free to expand (no external restraints), with zero temperature gradient across the thickness of the plate:
$16^3/4$" diameter solid specimens - (Model 1/2).

b) Uniformly heated with internal restraints, and zero temperature gradient across the thickness of the plate: perforated and composite specimens (Models 3/4 and 9/10 respetively).

Although the intention in this work was to carry out the tests under sustained and uniform elevated temperature, this objective was not fully achieved due to practical difficulties, in the laboratory. A difference in temperature was recorded in the perforated composite specimen, particularly in the first series of the tests.

This difference in temperature between the perforated region and the annulus, was of the order of $8^{o}C$ to $12^{o}C$. Under these circumstances, the thermoelastic problem became apparent.

However, it was possible to maintain the temperature gradient constant over the thickness of the specimens during the test, which justifies the assumption that the stresses and displacements in this direction do not vary.

The concrete was assumed to be isotropic and homogenous material, and for these assumptions the thermoelastic equations were developed and introduced in the analysis.

If an isotropic body is subjected to a temperature change, it undergoes a uniform expansion,

without any angular distorsions. Therefore, its coefficient of expansion a, is independent of direction and position.

In an unrestrained element, the thermal strains may be expressed as:-

$$e_{t_{ij}} = d_{ij}\, a\, d\, T \qquad 6.6.46.$$

Where $i, j = x, y, z$

d_{ij} = the Kronecker delta given by:-

$d_{ij} = 1$ when $i = j$

$d_{ij} = 0$ when $i \neq j$

dT = temperature rise, and

a = the coefficient of linear thermal expansion.

Equation 6.6.46 states that only normal thermal strains are produced, the shearing thermal strains being equal to zero.

The total strain at each point of a heated element consists of two parts: a) the thermal strain $e_{t_{ij}}$ due to uniform thermal expansion, and b) an elastic strain e_{ij} which is required to maintain

the displacement continuity of the element subjected to non-uniform temperature distribution.

If the element is subjected to a system of external loads, the elastic strain e_{ij} described above will also include strains arising from such loads. Therefore, the total strain, e_T, in the free element can be expressed as:-

$$e_T = e_{ij} + e_{tij} \qquad 6.6.47.$$

Substituting equation 6.6.46, in equation 6.6.47 , we obtain:-

$$e_T = e_{ij} + adT_{ij} \qquad 6.6.48.$$

Substituting now equations 6.6.20, into equation 6.6.48 , gives the total strains for the free element (elastic and thermal):-

$$e_x = \frac{1}{E}(\sigma_x - v\sigma_y) + adT \qquad (a)$$

$$e_y = \frac{1}{E}(\sigma_y - v\sigma_x) + adT \qquad (b) \qquad 6.6.49.$$

$$e_{xy} = 2\frac{(1+v)}{E}\sigma_{xy} + 0 \qquad (c)$$

And,

$$\begin{bmatrix} e_x \\ e_y \\ e_{xy} \end{bmatrix} = \frac{1}{E} \begin{bmatrix} 1 & -v & 0 \\ -v & 1 & 0 \\ 0 & 0 & e(1+v) \end{bmatrix} \begin{bmatrix} \sigma_x \\ \sigma_y \\ \sigma_{xy} \end{bmatrix} + adT \begin{bmatrix} 1 \\ 1 \\ 6.6 \\ 0 \end{bmatrix} \quad 6.6.50.$$

Or, $e_T = D^{-1} \cdot \sigma + DT$ 6.6.51.

Where $DT = adT \begin{bmatrix} 1 \\ 1 \\ 0 \end{bmatrix}$, the thermal strain matrix.

Similarly, solving equations for stress we obtain:-

$$\begin{bmatrix} \sigma_x \\ \sigma_y \\ \sigma_{xy} \end{bmatrix} = \frac{E}{1-v^2} \begin{bmatrix} 1 & v & 0 \\ v & 1 & 0 \\ 0 & 0 & \frac{1-v}{2} \end{bmatrix} \begin{bmatrix} e_x \\ e_y \\ e_{xy} \end{bmatrix} - \frac{EadT}{1-v} \begin{bmatrix} 1 \\ 1 \\ 6.6 \\ 0 \end{bmatrix} \quad 6.6.52.$$

Or,

$$\sigma_T = D \cdot e - \underline{DT} \quad 6.6.53.$$

Where $\underline{DT}$= is the thermal stress matrix.

With the thermal stress and strain matrices determined for the free element, it is now possible to proceed with the calculation of the thermal load vector for the structure.

The effects of temperature may be included in the analysis in two ways:-

1) By the method of "restraint", also known as the "freezing technique, or,

2) By the "direct formulation" of the thermal load vector.

In this investigation both methods were used.

The two methods are identical in principle, the only difference being in the steps followed:-

1) The method of restraint.

Consider a two-dimensional structure subject to a temperature increase dT. If, a, is the coefficient of linear thermal expansion, then the free strain of a typical element in the structure is equal to:-

$$e_t^f = a\ dT \begin{bmatrix} 1 \\ 1 \\ 0 \end{bmatrix} \qquad 6.6.54.$$

and it is positive for an increase in the temperature.

To solve the thermoelastic problem for the structure, the following three steps are necessary in this procedure:-

a) Assume that all points of the structure are frozen, ie., no movements of any point is permitted. It is evident that at all points, the free strain must be suppressed. This will cause a state of stress of magnitude -

$$\sigma_x = \sigma_y = -\frac{EadT}{1-v}\begin{bmatrix}1\\1\\0\end{bmatrix} \qquad 6.6.55.$$

to develop in the element.

b) To maintain the state of stress, we require:-

(i) a system of boundary loads of magnitude $\frac{EadT}{1-v}\begin{bmatrix}1\\1\\0\end{bmatrix}$, and acting in a direction normal to the boundary.

(ii) a system of body forces X and Y of suitable magnitude, acting on each element necessary to satisfy the equilibrium equations of such an element.

For the case of complete restraint, the shear stress σ_{xy} is zero, and only normal stresses

σ_x, σ_y exist. Accordingly, the equilibrium equations take the form:-

$$X = -\frac{\partial \sigma_x}{\partial x} \qquad (a)$$

$$Y = -\frac{\partial \sigma_y}{\partial y} \qquad (b) \qquad 6.6.56.$$

$$\frac{\partial \sigma_{xy}}{\partial y} = \frac{\partial \sigma_{xy}}{\partial x} = 0 \qquad (c)$$

Substituting for o_x and o_y, we obtain:-

$$X = \frac{\partial}{x} \left(\frac{EadT}{1-v}\right) \qquad (a)$$

$$Y = \frac{\partial}{y} \left(\frac{EadT}{1-v}\right) \qquad (b) \qquad 6.6.57.$$

c) To obtain now the actual displacements in the structure, and therefore, the actual thermal stresses, it is necessary to solve the elastic problem of the same structure subjected to body and boundary forces equal, and opposite to those which had to be applied to restrain the elements of the structure initially. The results of this solution could then be superposed on the original restrained condition.

The steps of the above process may be summarized as follows:-

(i) assume the structure to be restrained against temperature movements by a suitable force system, and evaluate the necessary forces.

(ii) apply to the same structure without any temperature change the reverse of the system of restraining forces found in step (i).

(iii) Superpose the displacements and stresses obtained from step (ii), on step (i).

Application of the method of restraint to the finite element technique.

In this section, the application of the method of restraint to the finite element technique will be demonstrated and the required equations developed.

Data of the problem:-

a = coefficient of thermal expansion.

dT = temperature increment.

(positive for an increase in temperature, and negative for a decrease in temperature).

Consider a triangular element subjected to a temperature rise dT. The free thermal strain in the element is equal to:-

$$e_t^f = + a\, dT \begin{bmatrix} 1 \\ 1 \\ 0 \end{bmatrix} \qquad 6.6.58.$$

Step 1: Freezing stage:
For the element.

Frozen strain in the element -

$$e_{tf} = - a\, dT \begin{bmatrix} 1 \\ 1 \\ 0 \end{bmatrix} \qquad 6.6.59.$$

Stress -

$$\sigma_{tf} = D\, e_{tf} \qquad 6.6.60.$$

Displacement -

$$d_{tf} = 0.$$

Nodal forces on the element -

$$F_{tf} = B^T D e_{tf}.t.A \qquad 6.6.61.$$

For the structure -

Thermal load vector -

$$F_{tfs} = \sum (B^T D e_{tf}.t.A.) \qquad 6.6.62.$$

Where σ_{tf} = thermal stress in the freezing stage.

e_{tf} = thermal strain in the freezing stage.

d_{tf} = thermal displacement in the freezing stage.

t = thickness of element.

A = area of element.

B^T, D, e_{tf} = as previously defined.

Step 2: Releasing stage:
For the element.

Nodal forces to balance freezing forces -

$$F_{tr} = - F_{tf}$$

$$\therefore \quad F_{tr} = - B^T D \, e_{tf}.t.A \qquad 6.6.63.$$

For the structure -

Thermal load vector -

$$F_{trs} = \sum (-B^T D \, e_{tf}.t.A) \qquad 6.6.64.$$

Equilibrium equations -

$$F_{trs} = K \quad d_{tr} \qquad 6.6.65.$$

Displacements -

$$d_{tr} = K^{-1} F_{trs} \qquad 6.6.66.$$

Strains -

$$e_{tr} = B\, d_{tr} \qquad 6.6.67.$$

Stresses -

$$\sigma_{tr} = D\, e_{tr} = D\, B\, d_{tr} \qquad 6.6.68.$$

Step 3: Releasing + freezing stage

The results of Step 1 and Step 2, are superposed to obtain the actual thermal displacements, strains and stresses in the structure.

Total displacements -

$$d_T = d_{tf} + d_{tr} \qquad 6.6.69.$$

Total strains -

$$e_T = e_{tf} + e_{tr} \qquad 6.6.70.$$

Total stresses -

$$\sigma_T = \sigma_{tf} + \sigma_{tr.} \qquad 6.6.71.$$

2) The "direct formulation."

In this approach the thermoelastic effects can be handled by introducing ficticious body and boundary forces at the nodal points of the finite element system.

The ficticious nodal point loads for the free element are calculated from the normal stresses required to give the same displacements as the known temperature gradient.

These loads constitute the thermal load vector for the element.

Having defined the elemental thermal load vector, the next step is to form the thermal load vector for the entire structure. This is done by adding the contributions of all elements to the nodes which are directly connected.

For these loads, the structure is analyzed, and the actual displacements and strains obtained. With regard to the stress distribution, the normal stresses used to simulate the thermal effects should be subtracted from the calculated stresses in the elements.

The thermoelastic equations are:-

Nodal forces for the element -

$$F_{te} = B^{T} D e_t^f t A \qquad 6.6.72.$$

Load vector for the structure -

$$F_{ts} = \sum (B^{T} D e_t^f t A) \qquad 6.6.73.$$

Equilibrium equations -

$$F_{ts} = K d_t \qquad 6.6.74.$$

Displacements -

$$d_t = K^{-1} F_{ts} \qquad 6.6.75.$$

Strains -

$$e_t = B d_t \qquad 6.6.76.$$

Stresses -

$$\sigma_t = D (e_t - e_t^f) \qquad (a)$$

Or,

$$\sigma_t = D B e_t - D e_t^f \qquad (b) \qquad 6.6.77.$$

6.6.5. Time-dependent solution.

In this section the time-dependent effects arising from the creep and shrinkage characteristics of the concrete are incorporated in the analysis.

1. Creep effects.

The basic principles of two well-known methods in concrete technology for predicting time-dependent strains in concrete structures subject to sustained loading and elevated temperatures, were applied to the problem of this investigation.

These methods are:-

a) - The Rate of Creep method.

b) - The Effective Modulus method.

.....

a) The Rate of Creep method.

i) General procedure:

The time-dependent solution is non-linear and requires either an iterative or a step-by-step approach.

The method of solution adopted by the author is a step-by-step technique, which has been

programmed for general elastic and time-dependent analyses. It is possible in this approach to extend the linear solution of an elastic problem into the non-linear time-dependent range.

The non-linearity can be introduced in one of two ways; either by introducing the governing laws which are based upon the appropriate characteristic properties of the material, or by considering the gross deformational and geometrical changes which occur in the elements of the structure.

It was decided, in this case, to adopt the first of these alternatives, in which the material properties are introduced, and in particular by utilizing the creep laws which govern the stress-strain-time behaviour of the concrete.

If the creep strains obtained from loaded and uniformly-heated specimen are made specific with respect to stress and temperature, and plotted against a time base, a single curve is obtained known as the specific thermal creep curve.

The general procedure for the step-by-step analysis will be discussed first for the uniaxial state of stress. It will then be extended to include the biaxial stress problem relating to this particular investigation.

ii) Uniaxial state of stress:

The rate of creep strain for uniaxial stress is given by equation 4.12.

$$\frac{de_c}{dt} = \sigma \phi (T) \frac{dc}{dt}$$

This equation indicates that for an increment in the rate of specific thermal creep during a time-interval t, the rate of free creep strain can be calculated provided that the stress σ at the start of the time-interval is known.

Let e_c be the increase in free creep strain during the time-interval t, σ the stress at the start of the time-interval, and c, the specific thermal creep strain increment during the same interval of time. From the foregoing, the following relation must hold:-

$$e_c = \sigma \phi (T) \quad c \qquad 6.6.78.$$

The incremental creep strain so obtained at the end of the time-interval is considered as "initial strains," and an elastic solution carried out for the interval will give the state of stress σ' at the end of this interval.

Thus, the general procedure for the step-by-step solution may be summarized as follows:-

(1) The instantaneously applied loads at time $t = to$, cause a system of elastic stresses σ_e, strains e_e, and displacements d_e to develop.

(2) Consider now a short-time-interval t_1, and assume the stresses to remain constant and the properties of the material unchanged during the interval.

At the end of the interval creep strains e_{cl} will occur as a result of the stress system σ_e at the start of the interval.

These strains may be calculated from the specific thermal creep increment c_1 obtained from the specific thermal creep curve corresponding to the time-interval t_1 and the elastic stress σ_e at the start of the interval.
Hence, equation 6.6.78 becomes:-

$$e_{cl} = \sigma_e \, \phi(T) \, c_1 \qquad 6.6.79.$$

The free creep strains so computed will cause an incompatibility in the elements of the structure at the end of time-interval t_1, which must be corrected in the following manner.

(3) At the start of the second-time-interval, t_2, if the external loads remain the same, and the material properties remain unchanged, we may consider the creep strains e_{cl} as initial strains imposed

on the structure.

Using elastic finite element analysis, the problem can be solved again for the external loads and initial strains resulting in a new stress system σ_1 and a strain system e_1.

The total state of stress at the end of the interval t_1 is:-

$$\sigma_1 = \sigma_e + \sigma_1$$

Where σ_e = is the elastic stress at the start corresponding to the external loads

σ_1 = is the incremental stress for the interval corresponding to creep effects.

The total strains are:-

$$e_1 = e_e + e_1$$

Where e_e = is the elastic strain at the start corresponding to the external loads

e_1 = is the incremental strain for the interval corresponding to the elastic strain during the interval and the creep strain.

Similarly, for the displacements:-

$$d_1 = d_e + d_1$$

(4) Consider now a second-time-interval t_2.

At the start of this interval, the stresses, strains and displacements are known from the previous time-interval.

Assume again the stresses remain constant and the material properties unchanged during the interval t_2. The creep strains at the end of this interval may be calculated as for step (2).

Hence,

$$e_{c2} = \sigma_1 \, \phi \, (T) \quad c_2 \qquad 6.6.80.$$

Step 3, is repeated forming a new stress system σ_2 at the start of time-interval t_3, and the creep strain e_{c2} at the end of this interval.

The process is repeated for any desired number of time-intervals in a similar manner.

The stresses, strains and displacements at the end of the second-time-interval t_2 are:-

$$\sigma_2 = \sigma_1 + \sigma_2 = \sigma_e + \sigma_1 + \sigma_2 \quad (a)$$

$$e_2 = e_1 + e_2 = e_e + e_1 + e_2 \quad (b) \qquad 6.6.81.$$

$$d_2 = d_1 + d_2 = d_e + d_1 + d_2 \quad (c)$$

Where σ_2, c_2 and d_2 = are the incremental stresses, strains and displacements for time-interval t_2 respectively.

In calculating the free creep strains for a particular time-interval, it is possible to improve the solution by averaging the stresses at the start of the interval with those obtained at the end of the same interval.

For time-interval t_2, therefore, the following would apply:-

Let σ_1 be the stress at the start of t_2, and σ_2 be the caluclated stress at the end of t_2.

The stress for which the free creep strain will have to be calculated is:-

$$\sigma' = \tfrac{1}{2} (\sigma_1 + \sigma_2)$$

And, the free creep strain at the end of t_2 is therefore:-

$$e'_c = \sigma' \, \phi (T) \, c_2 \qquad 6.6.82.$$

This step, however, was avoided in this work and instead the time-intervals considered were made small, which is an alternative way of improving the solution.

Of course, if both techniques are applied the solution will improve further, but the computational time required is excessive. Nevertheless, the choice of the method depends on the nature of the problem at the accuracy expected.

iii) Biaxial state of stress:

Consider a free triangular element in a specimen under test.

The instantaneously applied mechanical loads on the specimen at time $t = to$, cause a system of elastic stresses and strains to develop in the element.

For plane stress distribution, the strains in the element are given from equations 6.6.20, and the stresses from equations 6.6.23.

If the specimen is subjected to a uniform temperature, then the total strains and stresses (elastic and thermal) in the element are given from equations 6.6.49 and 6.6.52 respectively.

Consider now, the equilibrium of the element after a time-interval dt.

Under the action of the mechanical loads and temperatures, the element will creep uniformly according to the characteristic creep curve(of the material of the element).

If we assume the stresses and temperatures to remain constant during the interval as well as the material properties of the element, the free creep strains at the end of the interval may be calculated.

For biaxial state of stress the incremental free creep strains for the element are:-

$$\frac{de_{cx}}{dt} = (\sigma_x - v\sigma_y)\ \phi\ (T)\ \frac{dc}{dt} \qquad (a)$$

$$\frac{de_{cy}}{dt} = (\sigma_y - v\sigma_x)\ \phi\ (T)\ \frac{dc}{dt} \qquad (b) \qquad 6.6.83.$$

$$\frac{de_{cxy}}{dt} = 2\ (1+v)\sigma_{xy}\ \ \phi(T)\ \frac{dc}{dt} \qquad (c)$$

The resultant creep strain at the end of the interval is therefore, given by:-

$$\begin{bmatrix} e_{cx} \\ e_{cy} \\ e_{cxy} \end{bmatrix} = \phi(T)dc \begin{bmatrix} 1 & -v & 0 \\ -v & 1 & 0 \\ 0 & 0 & 2(1+v) \end{bmatrix} \begin{bmatrix} \sigma_x \\ \sigma_y \\ \sigma_{xy} \end{bmatrix} \qquad 6.6.84.$$

In matrix form this equation becomes:-

$$e_c = DC \cdot \sigma \qquad 6.6.85.$$

Where e_c = the vector for the normal and shear creep strains in the element.

σ = the stresses due to mechanical and thermal loads at the start of the time-interval, and

$$DC = \phi(T)\, dc \begin{bmatrix} 1 & -v & 0 \\ -v & 1 & 0 \\ 0 & 0 & 2(1+v) \end{bmatrix} \qquad 6.6.86.$$

= the specific thermal creep matrix.

The total strain e_T in the free element will be the sum of the elastic e_e, thermal e_t and creep e_c strains.

$$\therefore \quad e_T = e_e + e_t + e_c \qquad 6.6.87.$$

Or,

$$\begin{bmatrix} e_{Tx} \\ e_{Ty} \\ e_{Txy} \end{bmatrix} = \frac{1}{E} \begin{bmatrix} 1 & -v & 0 \\ -v & 1 & 0 \\ 0 & 0 & 2(1+v) \end{bmatrix} \begin{bmatrix} \sigma_{ex} \\ \sigma_{ey} \\ \sigma_{exy} \end{bmatrix} + a\, dT \begin{bmatrix} 1 \\ 1 \\ 0 \end{bmatrix} + DC \begin{bmatrix} \sigma_{ex} \\ \sigma_{ey} \\ \sigma_{exy} \end{bmatrix}$$

6.6.88.

Where DC= ϕ (T)dc $\begin{bmatrix} 1 & -v & 0 \\ -v & 1 & 0 \\ 0 & 0 & 2(1+v) \end{bmatrix}$

In matrix form: $e_T = D^{-1} \sigma_c + DT + DC \quad \sigma_e$

With the stress, strains and the creep matrix defined for the free element, it is now possible to proceed with the evaluation of the creep load vector for the elements and for the entire structure.

The creep effects may be incorporated in the finite element matrix equations in a similar manner as described for the thermoelastic effects.

The "Method of restraint," and the "Direct formulation" procedure were fully described when the thermoelastic effects were considered. They are equally valid for the calculation of creep effects.

iv) Matrix equations for creep effects by the "Method of Restraint."

Free creep strain e_c^f

$e_c^f = \phi (T)\, dc \cdot \sigma$

(Stress σ with proper sign).

Step 1: Freezing stage.

<u>For the element</u>.

Frozen creep strain e_{cf}.

$$e_{cf} = - DC \cdot \sigma$$

Stress σ_{cf}.

$$\sigma_{cf} = D \quad e_{cf}$$

Displacement d_{cf}.

$$d_{cf} = 0$$

Nodal forces on element F_{cf}.

$$F_{cf} = B^T \cdot D \cdot e_{cf} \cdot t \cdot A$$

<u>For the structure</u>.

Creep load vector F_{cfs}.
(total nodal force at each node).

$$F_{cfs} = \sum (B^T \cdot D \cdot e_{cf} \cdot t \cdot A)$$

Step 2: Releasing stage.

For the element.

Nodal forces to balance freezing forces.

$$F_{cr} = - F_{cf}$$

$$\therefore \quad F_{cr} = - B^T \cdot D \cdot e_{cf} \cdot t \cdot A$$

For the structure.

Creep load vector F_{crs}.

(total nodal force at each node).

$$F_{crs} = \sum (- B^T \cdot D \cdot e_{cf} \cdot t \cdot A)$$

Where B^T, D, t and A as previously defined

Equilibrium equations for the structure.

$$F_{crs} = K \cdot d_{cr}$$

Displacements for the releasing stage due to creep.

$$d_{cr} = K^{-1} \cdot F_{crs}$$

Strains for the releasing stage due to creep.

$$e_{cr} = B \cdot d_{cr}$$

Stresses for the releasing stage due to creep.

$$\sigma_{cr} = D \; e_{cr} = D \; B \; d_{cr}$$

Step 3: Releasing + freezing stage.

The results of Step 1 & 2, are superimposed, and the actual creep effects are obtained.

Total displacements d_c.

$$d_c = d_{cf} + d_{cr}$$

Total strains e_c.

$$e_c = e_{cf} + e_{cr}$$

Total stresses σ_c.

$$\sigma_c = \sigma_{cf} + \sigma_{cr}$$

iv) Matrix equations for the creep effects by the "Direct formulation" approach.

Nodal forces for the element F_{ce}.

$$F_{ce} = B^T \cdot D \cdot e_c^f \cdot t \cdot A$$

Load vector for the structure F_{cs}.

$$F_{cs} = \sum \left(B^T \cdot D \cdot e_c^f \cdot t \cdot A \right)$$

Equilibrium equations.

$$F_{cs} = K \; d_c$$

Displacements d_c.

$$d_c = K^{-1} \; F_{cs}$$

Strains e_c.

$$e_c = B \; d_c$$

Stresses σ_c.

$$\sigma_c = D \; (e_c - e_c^f)$$

Hence,

$$\sigma_c = D \cdot B \cdot e_c - D \cdot e_c^f$$

b) The Effective Modulus Method.

To incorporate the creep effects in the analysis by the Effective Modulus Method, the Modulus of Elasticity of the concrete is replaced by an equivalent modulus given in terms of the elastic modulus of the concrete and its specific creep or specific thermal creep strain curve.

The Effective Modulus is given by equations 4.4, and 4.5.

$$E' = \frac{1}{1/E + c} \quad \text{in terms of specific creep.}$$

$$E' = \frac{1}{1/E + f(T)c'} \quad \text{in terms of specific thermal creep.}$$

The Effective Modulus E' is introduced in the elasticity matrix D of equation 6.6.34,

$$D = \frac{E'}{(1-\nu^2)} \begin{bmatrix} 1 & \nu & 0 \\ \nu & 1 & 0 \\ 0 & 0 & \frac{1-\nu}{2} \end{bmatrix} \qquad 6.6.89.$$

and the elastic solution described in paragraph 6.6.3, of this Chapter is carried out again.

The solution so obtained is a total one, and may be repeated at any time-interval where the stresses are required.

A modification of this method has been used by the writer et al (111), to find the stress distribution in the periphery of the perforated zone in the composite specimen. A summary of the procedure and results obtained is given in Appendix 2.

2. Shrinkage effects.

It is well known that shrinkage effects are usually ignored for structures operating at ambient temperatures.

In certain cases, shrinkage stresses may be catered for by nominal reinforcement.

In massive concrete structures, shrinkage strains may cause stresses to develop even at ambient temperatures.

For structures operating at elevated temperatures, such as the prestressed concrete pressure vessels, shrinkage strains must be treated as an additional loading.

Shrinkage in concrete is generally considered as the moisture movement with respect to time, and is also affected by the moisture content.

Shrinkage is very difficult to assess, and an exact solution has not yet been found even for very simple types of problems.

A possible analytical approach is one using the standard diffusion equations, but its application is again restricted to idealized problems. This method was adopted for the interpretation of experimental data for the spherical (p.c.p.v., model) tested at Imperial College.

If the temperature is uniformly distributed over the structure, the problem is somewhat simpler. It is possible to assume that the shrinkage is unform in all parts of the structure, and a shrinkage-time curve can be drawn from direct strain measurements on a model structure.

The shrinkage strains at any time, may be considered as known initial strains and introduced in the analysis in exactly the same way as the creep and temperature strains.

This assumption was considered to be acceptable in this work, and the shrinkage strains were introduced in the finite element matrix equations as known strains.

For this assumption to be valid, it is necessary to consider concrete as homogeneous and isotropic material with constant elastic properties.

After the material has hardened and has obtained the above properties, known shrinkage strains are applied to the structure and the problem is solved either by the "method of restraint" or the "direct formulation approach" fully described in section 6.6.4, of this Chapter.

Since the temperature and shrinkage stresses are basically of the same type, as they are both caused by the tendency of the material to change its volume, and by the type of restraint, shrinkage strain can then be treated as a specific case of thermal strain.

Since the thermal strain in the concrete $e_t = a\,dT$ represents an increase in length of an element which results from a temperature rise dT, it should be observed that in problems where shrinkage is involved substituting the thermal strain -

$$a\,dT \text{ by } -e_s, \text{ i.e., } a\,dT = -e_s$$

(e_s, being the shrinkage strain), enables shrinkage problems to be dealt with identical lines. Accordingly, the shrinkage strains e_s in the element are:-

$$e_s = \begin{bmatrix} e_{sx} \\ e_{xy} \\ e_{sxy} \end{bmatrix} = f(T)\,ds \begin{bmatrix} 1 \\ 1 \\ 0 \end{bmatrix} \qquad 6.6.90.$$

Where $f(T)\,ds \begin{bmatrix} 1 \\ 1 \\ 0 \end{bmatrix}$ = the shrinkage strain matrix.

Only normal shrinkage strains exist, and the shear strains are zero.

For the free element the total strains due to mechanical loads, thermal, creep and shrinkage effects are:-

$$e_T = e_c + e_c + e_t + e_s$$

In expanded form, the above equation becomes:-

$$\begin{bmatrix} e_{Tx} \\ e_{Ty} \\ e_{Txy} \end{bmatrix} = \frac{1}{E}\begin{bmatrix} 1 & -v & 0 \\ -v & 1 & 0 \\ 0 & 0 & 2(1+v) \end{bmatrix}\begin{bmatrix} \sigma_{ex} \\ \sigma_{ey} \\ \sigma_{exy} \end{bmatrix} + a \cdot dT \begin{bmatrix} 1 \\ 1 \\ 0 \end{bmatrix} +$$

$$\phi(T)\ dc \begin{bmatrix} 1 & -v & 0 \\ -v & 1 & 0 \\ 0 & 0 & 2(1+v) \end{bmatrix}\begin{bmatrix} \sigma_{ex} \\ \sigma_{ey} \\ \sigma_{exy} \end{bmatrix} + \phi(T)ds \begin{bmatrix} 1 \\ 1 \\ 0 \end{bmatrix}$$

..... 6.6.91.

and in matrix form:-

$$e_T = D^{-1}, \sigma_e + DT + DC \cdot \sigma_e + DS$$

a) Matrix equations for shrinkage effects by the"Method of Restraint."

Free shrinkage strain e_s^f.

$$e_s^f = \phi(T)\ ds \begin{bmatrix} 1 \\ 1 \\ 0 \end{bmatrix}$$

Alternatively, $e_s^f = DS$

Where ds = the known incremental creep strain for the time-interval considered, and is obtained from the shrinkage strain-time graph (ds with proper sign)

DS = the shrinkage strain matrix.

Step 1: Freezing stage.

For the element.

Frozen shrinkage strain e_{sf}.

$$e_{sf} = - \phi(T)\, ds \begin{bmatrix} 1 \\ 1 \\ 0 \end{bmatrix}$$

(Shrinkage strain ds with proper sign).

Stress σ_{sf}.

$$\sigma_{sf} = D\ e_{sf}$$

Displacement d_{sf}.

$$d_{sf} = 0$$

Nodal forces on element F_{sf}.

$$F_{sf} = B^T \cdot D \cdot e_{sf} \cdot t \cdot A$$

For the structure.

Shrinkage load vector F_{sfs}.

(Sum of nodal force for each node).

$$F_{sfs} = \sum \left(B^T \cdot D \cdot e_{sf} \cdot t \cdot A \right)$$

Step 2: Releasing stage.

For the element.

Nodal forces to balance freezing forces.

$$F_{sr} = - F_{sf}$$

$$\therefore \quad F_{sr} = - B^T \cdot D \cdot e_{sf} \cdot t \cdot A$$

For the structure.

Shrinkage load vector F_{srs}.

(Sum of nodal forces at each node).

$$F_{sfs} = \sum (- B^T \cdot D \cdot e_{sf} \cdot t \cdot A)$$

Equilibrium equations for the structure.

$$F_{srs} = K \cdot d_{sr}$$

Displacements for the releasing stage due to creep.

$$d_{sr} = K^{-1} \cdot F_{srs}$$

Strains for the releasing stage due to shrinkage e_{sr}.

$$e_{sr} = B \cdot d_{sr}$$

Stresses for the releasing stage due to shrinkage σ_{sr}.

$$\sigma_{sr} = D \cdot e_{sr} = D \cdot B \cdot d_{sr}$$

Step 3: Releasing + freezing stage.

Total displacements d_s.

$$d_s = d_{sf} + d_{sr}$$

Total strains e_s.

$$e_s = e_{sf} + e_{sr}$$

Total stresses σ_s.

$$\sigma_x = \sigma_{sf} + \sigma_{sr}$$

b) Matrix equations for shrinkage effects by the "Direct formulation" approach.

Nodal forces for the element F_{se}.

$$F_{se} = B^T \quad D \quad e_s^f \cdot t \cdot A$$

Load vector for the structure F_{ss}.

$$F_{ss} = (B^T \cdot D \cdot e_s^f \cdot t \cdot A)$$

Equilibrium equations.

$$F_{ss} = K \cdot d_s$$

Displacements d_s.

$$d_s = K^{-1} \cdot F_{ss}$$

Strains e_s.

$$e_s = B \cdot d_s$$

Stresses σ_s.

$$\sigma_s = D \left[e_s - e_s^f \right]$$

Hence, $$\sigma_s = D \cdot B \cdot e_s - D \cdot e_s^f$$

6.6.6. Application of the proposed method in analysing the test specimens.

The proposed method of analysis was used to predict the behaviour of the test specimens in the following stages:-

i) At ambient temperatures:

a) Elastic solution, with the applied loads acting instantaneously.

b) Sustained loads with creep and shrinkage effects.

ii) At eleveted temperatures:

a) Sustained loads with thermal, creep and shrinkage effects.

iii) At ambient temperatures (after cooling).

a) Sustained loads with creep and shrinkage effects.

b) Loads gradually removed (unloading stage).

The step-by-step procedure, previously discussed, was adopted and total solutions were obtained at each step of the analysis.

Accordingly, the relevant equations to be set up and solved for the three stages are as follows:-

At time t = to

The external loads R were applied and an elastic solution obtained for displacements d_e , strains e_e, and stresses o_e , using equations (6.6.6.), (6.6.32) and (6.6.33). The initial strain e_o in equation(6.6.33) is zero.

At time $t = t_1$ (time-interval dt_1)

The shrinkage strains e_{osl}, and creep strains e_{ocl}, were calculated for the incremental shrinkage d_{sl}, and specific creep d_{cl}, strains occuring in the interval and using equations 6.6.90, 6.6.84 , respectively.

The stresses in equation 6.6.84, are those obtained from the elastic solution at time $t=t_o$, (see Fig.6. 16).

The specific creep and shrinkage data were obtained from experimental curves.

The creep and shrinkage strains e_{ocl} , and e_{osl}, so obtained are treated as initial strains at t_1, (end of interval dt_1, start of interval dt_2), and the

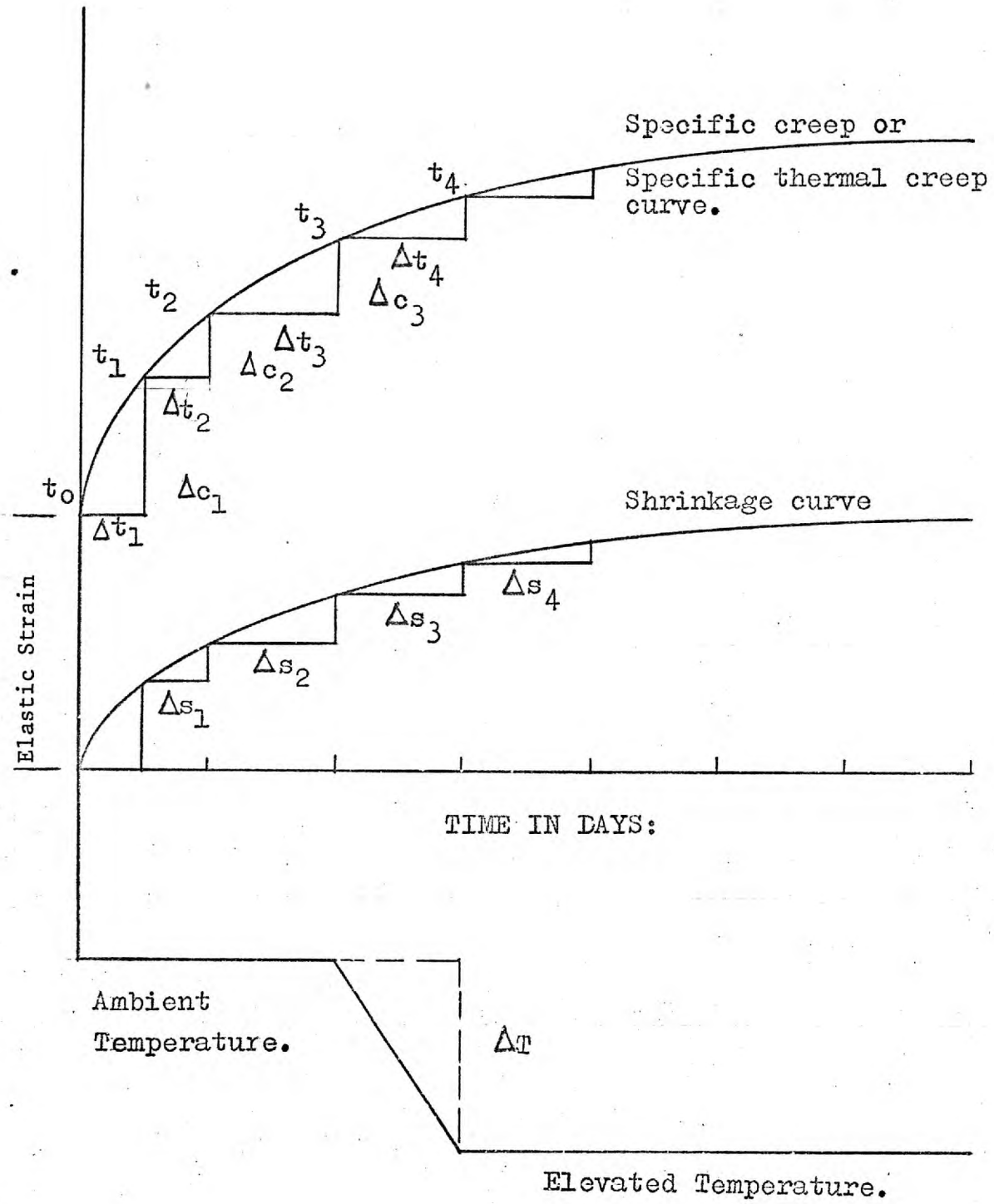
Specific creep or
Specific thermal creep
curve.
t_4
t_3
t_2
t_1
t_o
Δt_4
Δc_3
Δt_3
Δc_2
Δt_2
Δc_1
Δt_1
Shrinkage curve
Δs_4
Δs_3
Δs_2
Δs_1
Elastic Strain
TIME IN DAYS:
Ambient
Temperature.
ΔT
Elevated Temperature.

FIG. 6. 16.

ficticious nodal forces F_{oc1}, and F_{os1}, are calculated for each element from equations for creep and shrinkage.

Summing up the nodal forces of all the elements connected to a nodal point, the load vector for the structure is formed.

Denoting F_{cs}, and F_{ss}, the creep and shrinkage load vectors respectively, and adding them to the external loads R, equation 6. 6. 6. becomes:-

$$R + F_{cs1} + F_{ss1} = K \cdot d_1$$

The solution of the above equation gives the total displacements d_1, strains e_1, and stresses o_1, at time t_1. In calculating the stresses o_1, the effects of the initial strains must be included.

At time $t = t_2$ (time interval dt_2)

With the stresses known at t_1, we may now proceed to the next time interval dt_2, following the same procedure as for t_1.

When a solution is to be obtained at elevated temperatures, the thermal effects must be included in the analysis. This is accomplished by adopting the same procedure used to incorporate the shrinkage and creep effects.

The equations used for calculating the thermal strains and nodal forces are (6.6.58), and (6.6.61) respectively.

Denoting F_{ts}, the thermal load vector for the structure, the equilibrium equation 6.6.6. becomes:-

$$R+F_{cs}+F_{ss}+F_{ts} = K \quad d$$

The solution of this equation gives the total displacements strains and stresses for the external loads creep, shrinkage and temperature effects.

6.6.7. Adopted values of design parameters.

It is evident from the foregoings that the solution of equations at each stage of the test programme required the knowledge of the following design parameters.

a) The Young's modulus.

The value used for the modulus of concrete E_c, in the analysis was 5.0×10^{-6} psi.

This value was adopted for all the specimens, as it was considered that such a value was representative of the concrete.

For purposes of comparison, calculations were also carried out with different E_c values, for the three stages of the test programme.

i) At ambient temperatures 4.90×10^{-6}.

ii) At elevated temperatures 4.80×10^{-6} .

iii) At ambient temperatures (after heating) 4.70×10^{-6}.

The actual values of the Young's modulus (secant modulus), obtained from control specimens are shown in the Appendix 1.

In addition, it was possible to determine the values of the modulus of concrete by subjecting the specimens to a load cycling at times indicated in Figs. (1.9), (1.10), (1.11) of Chapter I.

The readings obtained from the solid specimen (Model 1/2), were considered for the assessment of the E_c values.

Plotting radial strains e_r against radial stresses σ_r, the value of an apparent secant modulus E_c, could be assessed.

To obtain the actual value of the Modulus of concrete E_c, the biaxial effects had to be considered.

This consideration could be made possible from the following.

For the solid specimen, it is recognized that:-

$$\sigma_r = \sigma_\theta = 1500 \text{ psi.}$$

Therefore, the apparent secant modulus of concrete E_c', is:-

$$E_c' = \frac{\sigma_r}{e_r}$$

From the equations of elasticity:-

$$e_r = \frac{1}{E_c}(\sigma_r - v\,\sigma_\theta)$$

And,

$$E_c = \frac{e_r}{\sigma_r(1-v)}$$

Hence,

$$E_c = (1-v)E_c'$$

In considering the steel liners in the perforated zones, the Young's modulus of steel E_s, was assumed unaffected by temperature, age and time-dependent effects. For the purposes of this analysis $E_s = 30.0 \times 10^{-6}$.

b) Poisson's ratio.

There were no special control tests performed to assess the value of Poisson's ratio of concrete or steel.

The value for the Poisson's ratio of concrete v_c was assumed to be 0.18, and that of steel $v_s = 0.30$. They were assumed as not changing with time and temperature during the analysis. These considerations which led to the above assumption were discussed in Chapter III. A value for $v_c = 0.2$, was also assumed.

c) Coefficient of linear thermal expansion.

The value of the coefficient of thermal expansion of concrete a_c, used in the analyses was assumed constant throughout the test, and equal to $a_c = 13.5 \times 10^{-6}$ per ^{o}C.

This is an average value obtained in the manner indicated in Appendix 1.

The value for the coefficient of thermal expansion of steel a_s, was also assumed equal to that of concrete.

d) Creep data.

It has been stated earlier that the creep data used in the analysis were obtained from direct readings on the tested specimens, and that no control tests were performed in this work to assess the creep strains which occur at ambient or elevated temperatures.

Again the solid specimen was used for the assessment of the specific creep curve.

The creep strain-time curve obtained from these observations had to be corrected in order to obtain the true specific creep values.

For this purpose equation 6. 6. 78, was considered for biaxial state of stress.

$$de_c = \sigma \, \phi(T) dc = \sigma \, dc'$$

Where $dc' = \phi(T) dc$

The radial creep strain $de_{c,r}$ is given from the relation:-

$$de_{c,r} = \phi(T) dc (\sigma_r - v_c \, \sigma_\theta)$$

Where v_c = the creep Poisson's ratio for concrete

σ_θ = the tangential stress

For the solid specimen $\sigma_r = \sigma_\theta = o$

$\therefore$ $de_{c,r} = de_{c,\theta} = de_c$

Then, $de_c = \phi(T) dc (1-v_c) \sigma$

And, $de_c = dc' (1-v_c) \sigma$

$\therefore$ $\frac{de_c}{\sigma} = dc' (1-v_c)$

Hence, $dc' = \frac{de_c}{\sigma} \left(\frac{1}{1-v_c}\right)$

Where, $\left(\frac{1}{1-v_c}\right)$ = is the multiplier.

However, it has been recognized that the specific creep curve so obtained, might have contained errors due to the following reasons:-

1) The temperatures in all specimens were not steady during the test, but exhibited small fluctuations.

These fluctuations could have introduced varying rates of creep at different times.

However, considering that their magnitude was small, it was assumed that their effect on the rate of creep could be ignored.

2) There were no control specimens to indicate strains due to temperature alone, as apart from strains due to applied stresses.

3) The temperature distribution over a gauge length could have been such, that it could not have been reasonably represented by the value of the temperature of the section.

4) The value of the coefficient of thermal expansion used might not have been representative of the entire gauge length at a particular time.

5) Swelling or shrinkage strains could have occurred dueto moisture migration from warmer layers of concrete to relatively colder.

6) The temperature function $\phi(T)$ might not have been T, as assumed, although this factor could not have affected the creep data as all specimens were assumed to have the same temperature distribution.

In fact, it was not necessary to normalise the creep strains with respect to temperature. Instead the specific creep curve was only drawn.

The uncertainties involved in obtaining the creep data were considered to be of no real significance, and the data were used in the analysis without any further corrections or modifications.

e) Shrinkage data.

The shrinkage data are those shown in Figures of Chapter VII, and were drawn from direct readings on the control shrinkage specimens (Models 5/6 and 7/8).

The assumption made here was that the perforated loaded specimen and the perforated zone of the composite specimen were considered to follow the same shrinkage as the control specimen.

6.6.8. Special assumption made for the perforated and composite specimens.

In considering creep effects in the analysis, the creep in the steel elements corresponding to the stand-pipe liners was neglected in both specimens.

This assumption seems to be justified for the temperature and stress levels considered in this work.

6.6.9. Computer programme.

1. Purpose.

The purpose of the computer programme was to determine the displacements stresses and strains in a non-homogeneous, two-dimensional structural system, composed of concrete and steel, and subjected to sustained in-plane loading and uniform elevated temperature.

The programme incorporates the general Finite element procedure, described in this Chapter, for two-dimensional elastic, thermoelastic, creep and shrinkage analyses.

2. Method of analysis.

Two-dimensional triangular plate elements were used to represent the structural system.

The programme performs three major tasks in the complete analysis of the system.

a) It generates the equilibrium equations of the structural system from a basic numerical description of the system, using the direct stiffness method for matrix structural analysis.

b) Solves these equations for the nodal point displacements by direct elimination, and uses a step-by-step procedure which permits accounting for the time-dependent material properties.

c) Calculates the stresses and strains relative to the element (centre of gravity of element), and at the nodal points.

3. Development.

The programme was developed first of all for the solid loaded specimen (Model 1/2) with triangular membrane plate elements representing the system, and for the perforated and composite specimens (Models 3/4 and 9/10 respectively) with triangular elements representing the concrete in the ligaments and the annulus, and with uniaxial bar elements for the standpipe liners.

At a later stage, triangular elements were used to represent all parts of the structure, including the standpipe reinforcement, and the results obtained were compared.

It was found that the "all triangular element" idealization gave better equilibrium conditions and therefore, more accurate results. This idealization was adopted thereafter, throughout the investigation.

The programme is coded in FORTRAN language and was originally written for the IBM 7094 computer unit of the Imperial College, having 34K (32768) word memory, and included only the elastic solution.

Later, the programme was modified for the use in the CDC 6600 computer unit of the University of London, having 134K word memory, and in its final form, it included both elastic and long-term effects.

The maximum size system that can be analysed is governed by the availability of the computer storage. However, for the CDC 6600 computer, the maximum size of a structural system that could be handled with this programme is 450 elements and 350 nodal points.

4. General procedure.

For simplicity, only the main sequence of operations of the computer programme will be described here. The details have been deliberately omitted.

a) Flow chart diagram.

b) Outline of operations.

The flow chart diagram of the main programme and an outline of the operations involved in the execution of the programme are listed in the following pages:

5 . FLOW CHART.

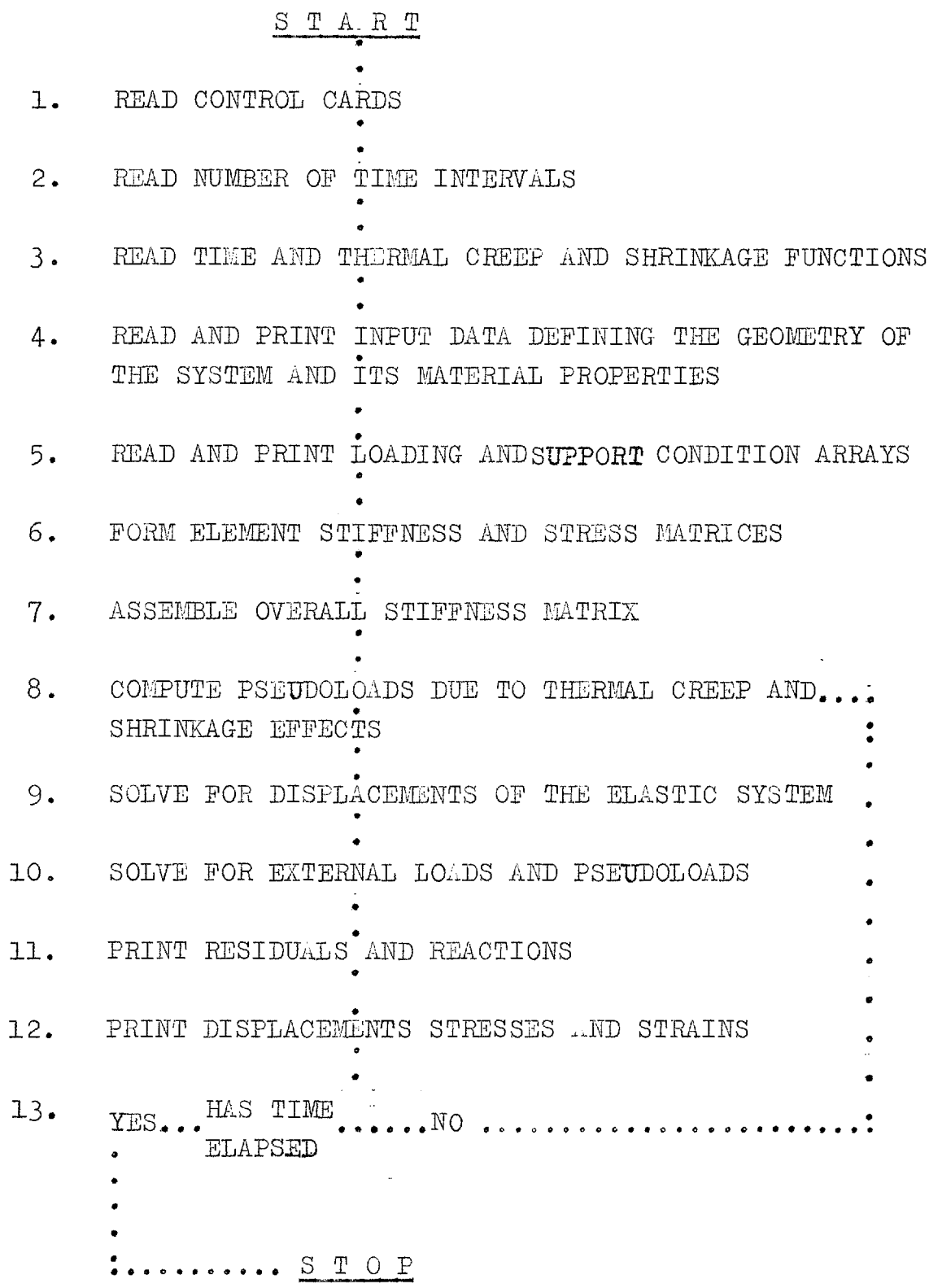
S T A R T
1. READ CONTROL CARDS
2. READ NUMBER OF TIME INTERVALS
3. READ TIME AND THERMAL CREEP AND SHRINKAGE FUNCTIONS
4. READ AND PRINT INPUT DATA DEFINING THE GEOMETRY OF THE SYSTEM AND ITS MATERIAL PROPERTIES
5. READ AND PRINT LOADING AND SUPPORT CONDITION ARRAYS
6. FORM ELEMENT STIFFNESS AND STRESS MATRICES
7. ASSEMBLE OVERALL STIFFNESS MATRIX
8. COMPUTE PSEUDOLOADS DUE TO THERMAL CREEP AND SHRINKAGE EFFECTS
9. SOLVE FOR DISPLACEMENTS OF THE ELASTIC SYSTEM
10. SOLVE FOR EXTERNAL LOADS AND PSEUDOLOADS
11. PRINT RESIDUALS AND REACTIONS
12. PRINT DISPLACEMENTS STRESSES AND STRAINS
13. HAS TIME ELAPSED
YES
NO
S T O P

6.- OUTLINE OF OPERATIONS

```
JOB(UMES006,CM64000,T250)                    STEFANOU,I.C.COURIER                    2/5
RUN(S,,,,,,23200)
LGO.
      PROGRAM MAIN (INPUT,OUTPUT,TAPE5=INPUT,TAPE6=OUTPUT)
C     G.D.STEFANOU                UMES006
C     S E R I E S  * 2 *
C     PROBLEM NO.  * 2/5 *  SOLVE  R.C.M.  C O M P O S I T E
C     METHOD  * FINITE ELEMENT ANALYSIS *
C     SOLUTION  *ELASTIC*THERMOELASTIC*CREEP*SHRINKAGE*
C     LOADING *RADIAL PRESTRESSING*
      DIMENSION
      COMMON
C     R E A D   A N D   P R I N T   D A T A
C     READ NUMBER OF INTERVALS
C     PLATE PROPERTIES ARRAY
C     TOTAL NUMBER OF ELEMENTS,NODAL POINTS,LOADED NODAL POINTS
C     SUPPORT NODAL POINTS
C     NODAL POINT ARRAY
C     TRIANGULAR ELEMENT ARRAY
C     SUPPORT CONDITION ARRAY
C     MATERIAL PROPERTY ARRAY
C     LOADING ARRAY
C     INTRODUCE NO. OF LOADED NODAL POINTS
C     W R I T E   D A T A
C     WRITE PLATE PROPERTIES
C     WRITE NODAL POINT ARRAY XY(I,J),J=1 FOR X-COORD,J=2 FOR Y-COORD
C     WRITE  TRIANGULAR ELEMENT ARRAY NEM(I,J) J=1,2,3 TAKEN ANTI-CLOCKWISE
C     WRITE SUPPORT CONDITION ARRAY
```

```
C     WRITE MATERIAL ARRAY MATAR(I) I=1 FOR CONCRETE,I=2 FOR STEEL
C     WRITE LOAD VECTOR
C     S T A R T    E X E C U T I O N
C     FORMULATE ELASTICITY MATRICES FOR PLANE STRESS
C     DC   CONCRETE  STRESS  MATRIX
C     DS STEEL STRESS  MATRIX
C     CALCULATE AREA ARRAY AREA(N)
C     CALCULATE  BT(I,J,K) MATRIX
C     COMPUTE  BAND  WIDTH  FOR  SSM  MATRIX
C     CLEAR SSM  MATRIX
C     FORMULATE ELEMENT STIFFNESS MATRIX ESM
C     TRANSFORM MATRIX
C     SELECT APPROPRIATE ELASTICITY MATRIX AND FORM PRODUCT BTD
C     FORM MATRIX B=ZT
C     TO FORM MATRIX ESM  CALL  SUBROUTINE  MPRD
C     LOCATE CONTRIBUTIONS OF ESM IN SSM AND FORM SSM
C     FORMULATE SPT TO COMPUTE REACTIONS
C     RESTRICT FREEDOM AT SUPPORTS
C     RESTRICT IN X
C     RESTRICT IN Y
C     LOCATE ELEMENTS OF SSM IN ASSM
C     CLEAR  ARRAY  OF  TOTAL  INITIAL  STRAINS
C     S T A R T   S O L U T I O N   B Y   S T E P
C     DCC CREEP MATRIX
C     EOSHR  SHRINKAGE MATRIX
C     CALCULATE INITIAL  CREEP  AND  SHRINKAGE STRAINS
C     CALCULATE  NODAL  FORCES  FOR  ELEMENT  DUE TO INITIAL STRAINS
C     ACCUMULATE STRAINS
C     FORM  PSEUDOLOAD VECTOR FOR INITIAL CREEP AND SHRINKAGE STRAINS
C     EOTC CONCRETE THERMAL STRAIN
```

```
C       EOTS STEEL THERMAL STRAIN
C       CALCULATE THERMAL NODAL FORCES FOR ELEMENT
C       FORM PSEUDOLOAD VECTOR FOR INITIAL THERMAL STRAINS
C       FORM TOTAL LOAD VECTOR
C       ADD PSEUDOLOADS TO EXTERNAL LOAD VECTOR
C       CALL  SUBROUTINE  S O L V E
C       CALCULATE DISPLACEMENTS
C       R E S U L T S
C       WRITE  RESULTS
C       WRITE DISPLACEMENTS
C       CALCULATE NORMAL AND SHEARING STRESSES AT C.G
C       CALCULATE STRESS MATRIX DB
C       SELECT ELEMENT DISPLACEMENTS
C       CALCULATE STRESSES AT ELEMENT C.G
C       INITIALIZE TOTAL INITIAL STRESSES
C       WRITE STRESSES
C       CALCULATE NODAL POINT STRESSES
C       CALCULATE STRAINS AT ELEMENT C.G
C       CALCULATE STRAINS AT NODAL POINTS
        STOP
        END
C       SUBROUTINE  MPRD
C       SUBROUTINE  LOC
C       SUBROUTINE  SOLVE
C       SUBROUTINE  SPNIST
C       SUBROUTINE  SUB1
```

7. Input information.

The programme input consists of the mesh data instruction, material properties, plate properties (thickness), loading conditions, boundary conditions and various options. The data are always printed out as soon as they are read in, which makes checking easier when wrong data have been introduced during the input.

The programme will handle problems in-plane stress analysis formulated and solved only in Cartesian co-ordinates, mechanical in-plane loads, thermal loads, as well as creep and shrinkage effects.

The mesh is hand-generated because of the irregularities in the perforated region and no attempt was made for an automatic mesh generation.

The nodal points are defined by an array giving the nodal point number and the co-ordinates of the nodes with respect to the global co-ordinate axes. The elements are defined with an array giving the element number, and the numbers of the element's nodal points, taken in an anti-clockwise direction.

The nodal point indices of the elements must be properly ordered in such a manner that the elements are correctly developed. The nodal points and elements should follow one another in consecutive order. The numbering is closely related to the band-width of the structure stiffness matrix, and is numerically equal to the product of the number of degrees of freedom per nod and the maximum difference in numbering of adjoining nodes.

When use of the band-width of the matrix is made for the solution of the equations, as in the case of this investigation, considerable time is saved in the solution of equations.

Space is also saved in storing the matrix which in turn means that larger problems can be tackled with small capacity computers.

With regard to material properties, the Modulus of Elasticity, and Poisson's ratio values for the material are assigned and fed in as data for the structure and by scanning the elements the appropriate value is selected.

The distributed loads acting at the boundary, are assumed as concentrated forces acting at the nodal points of the elements, and they are introduced in the programme by a loading array, giving the loaded point number and the components of loads along the co-ordinate axes.

Thermal properties are introduced by specifying the coefficient of the thermal expansion of the materials, and the temperature difference, as well as the current-time-interval.

The creep and shrinkage functions are also introduced in the same array.

Boundary conditions are listed as zero, or known displacements at specified nodes.

Support conditions are introduced as an array, giving the nodal point number and the restrictions in x or y directions as the case may be.

The programme also permits a variety of options that enable the user to carry out the analysis in stages.

8. Input data cards.

(1) Title card:
Columns 1-72 contain information to be printed as output title.

(2) Control card (I5):
Columns 1- 5 maximum number of time-intervals

(3) Plate properties card (5F10.2):
Columns 1-10 Young's modulus os steel
11-20 Young's modulus of concrete
21-30 Poisson's ratio of steel
31-40 Poisson's ratio of concrete
41-50 thickness

(4) Thermal properties card (2E20.8):
Columns 1-20 coefficient of thermal expansion of steel
21-40 coefficient of thermal expansion of concrete

(5) Total number of elements, nodal points, loaded nodal points, support nodal points, and nodal points with specified displacements (5I10):

Columns 1-10 number of elements in the system
11-20 number of nodal points
21-30 number of loaded points
31-40 number of support points
41-50 number of points with specified displacements

(6) Nodal point array (6X,I4,2F10.3):
Columns 1- 6 blank
7-10 nodal point number
11-20 x-co-ordinate (in.)
21-30 y-co-ordinate (in.)

(7) Triangular element array (4I10):
Columns 1-10 number of element
11-20 number of node i
21-30 number of node j
31-40 number of node k (anti-clockwise direction)

(8) Support condition array (36I2):
Columns 1- 2, 3- 4 etc.
0 = point fixed in X fixed in Y
1 = point fixed in X free in Y
2 = point free in X fixed in Y
3 = point free in X free in Y

(9) Material property array (36I2):
Columns 1- 2, 3- 4 etc.
1 = steel element
2 = concrete element

(10) Loading array (I10,2F10.3):

Columns	1-10	Nodal point number
	11-20	load in X
	21-30	load in Y

(11) Data array (2F10.1,2E10.2):

Columns	1-10	time-interval dt
	11-20	temperature increment dt
	21-30	value of creep function
	31-40	shrinkage function value

9. Output of results.

A typical output of the computed results is given in Chapter IX, Appendix 3.

The sign of the displacements stresses and strains is in accordance with the sign convension adopted (as described earlier).

The displacements are given in inches and the stresses in kips.

All the results are given with reference to the orthogonal co-ordinate axes, and in order to obtain values in polar co-ordinates, the standard transformation formulae must be applied.

Displacement components in Cartesian and polar co-ordinates.

$$U_x = U_r\cos\theta - V_\theta\sin\theta$$
$$V_y = U_r\sin\theta + V_\theta\cos\theta$$

Stress components in Cartesian and polar co-ordinates.

$$\sigma_x = \sigma_r \cos^2\theta + \sigma_\theta \sin^2\theta - \sigma_{r\theta} \sin 2\theta$$

$$\sigma_y = \sigma_r \sin^2\theta + \sigma_\theta \cos^2\theta + \sigma_{r\theta} \sin 2\theta$$

$$\sigma_{xy} = \tfrac{1}{2}(\sigma_r - \sigma_\theta)\sin 2\theta + \sigma_{r\theta} \cos 2\theta$$

10. Stresses.

(1) Element stresses.

The element stresses are calculated from equation 6.6.33, which expresses the normal and shear components of stress, in x, y and xy directions within an element (at the centre of gravity of the element) in terms of the six components of displacements of the element.

After equation 6.6.6, is solved for the displacements of the system, the stresses within each element are obtained from equation 6.6.33.

(2) Principal stresses.

With the normal and shear stresses determined at the centre of gravity of the element, the state of stress in the element is completely defined.

It is, however, important for practical applications to know the principal stresses o_1 , o_2 and their direction θ at any point in the structure. These are determined from the standard transformation equations of elementary mechanics.

$$\sigma_1 = \frac{\sigma_x+\sigma_y}{2} + \sqrt{(\frac{\sigma_x-\sigma_y}{2})^2+(\sigma_{xy})^2}$$

$$\sigma_2 = \frac{\sigma_x+\sigma_y}{2} - \sqrt{(\frac{\sigma_x+\sigma_y}{2})^2+(\sigma_{xy})^2}$$

$$\theta = - \tan^{-1}(\frac{2\sigma_{xy}}{\sigma_x-\sigma_y})$$

(3) Nodal point stresses.

It is often desirable to obtain nodal point stresses since it is at the boundaries of the element where the maximum stresses occur.

Although, in this work, the points of interest were not the boundary points of the tested specimens, but the interior points of the perforated zone, nevertheless, the nodal point stresses were calculated.

To do this, an averaging of the element stresses was necessary. Various forms of averaging have so far been used. Zienkiewicz, O.C. et al (115), has reported that an effective process is to use the average stress of two adjacent triangular elements.

The author has adopted a method in which the nodal point stresses are obtained by averaging the element stresses of all the elements connected to the nodal point.

This approach has proved to produce good results for nodal points in the interior of the structure, but breaks down when applied to nodal points at the boundary, (116).

As stated earlier, the points of interest in this investigation are the interior points in the ligaments of the perforated zone, and with this in mind, the method was considered to be acceptable.

Clough,R.W. (117), and Wilson, E.L. (101), used a"weighted average" method to calculate the nodal point stresses which seems to improve the values of the stresses. The writer used this procedure to compare his results, and found that there were no significant differences between the two methods at least for interior nodal points.

For purposes of reference, the method is briefly outlined here:

Consider figure 6.17 .

The stresses must be consistent with the nodal point displacements. Therefore, o_x approximates the horizontal stress of point A., o_y approximates the vertical stress at B., and o_{xy} approximates the shearing stress at some interior point C.

In calculating the stresses at nodal point 1, it is evident that the horizontal stress at A must be weighted more heavily than the vertical stress at B.

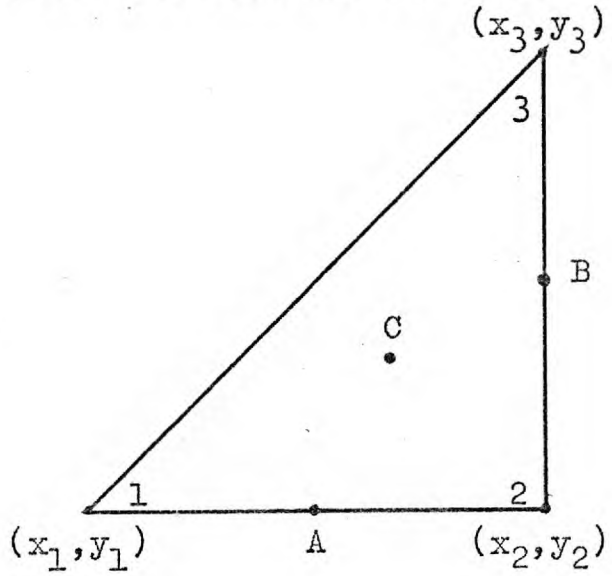

FIG. 6.17.

Hence, the "weighted average" method would reflect this behaviour.

The three components of stress at nodal point 1, of the element are:-

$$\sigma_x = \frac{1}{S_x} \sum_n \left(\frac{a^{(n)}}{a^{(n)} + b^{(n)}} \right) \sigma_x{}^{(n)}$$

$$\sigma_y = \frac{1}{S_y} \sum_n \left(\frac{b^{(n)}}{a^{(n)} + b^{(n)}} \right) \sigma_y{}^{(n)}$$

$$\sigma_{xy} = \frac{1}{N} \sum_n \sigma_{xy}{}^{(n)}$$

Where $$a^{(n)} = \left| x_3{}^{(n)} + x_2{}^{(n)} - 2x_1 \right|$$

$$b^{(n)} = y_3^{(n)} + y_2^{(n)} - 2y_1$$

$$S_x = \frac{a^{(n)}}{a^{(n)} + b^{(n)}}$$

$$S_y = \frac{b^{(n)}}{a^{(n)} + b^{(n)}}$$

The summation is performed on all N elements connected at nodal point 1.

11. Strains.

(1) Element strains.

These are calculated from equation 6.6.32, which expresses the normal and shear components of strain within an element (at the centre of gravity) in terms of the six components of displacements of the element.

(2) Nodal point strains.

The strains were also evaluated at the nodal points of the element from the element strains by the averaging procedure described earlier.

12. Timing.

The maximum time required for the solution of the problem for 31 time-intervals was as follows:-

Rate of creep method:	a)	Solid specimen	30 seconds.
	b)	Perforated "	170 "
	c)	Composite "	280 "
Effective modulus method:	a)	Solid specimen	320 "
	b)	Perforated "	470 "

C H A P T E R VII

PRESENTATION AND INTERPRETATION OF EXPERIMENTAL RESULTS COMPARISON AND DISCUSSION WITH PREDICTED VALUES

7.1. Presentation.

The results of the three test series performed, and the predicted values obtained from the adopted methods of analyses are presented and compared in this Chapter.

The test results are also discussed with reference to the expected behaviour of the material and few conclusions drawn.

The results are presented in graphical form in the following pages for each of the three series.

These graphs, indicate experimental observations of strain in comparison with theoretical forecasts of strain plotted on the same axes.

This is in respect of 2" gauge length tangential and radial strains, three pitch diametral strains, and standpipe diametral strains.

In addition, predicted stresses for a selected number of specimens and stages obtained from the two methods of analyses have also been plotted and compared.

Specimen temperatures, ambient temperatures and relative humidities are also shown on various graphs against a time base.

S E R I E S 1:

S E R I E S 2:

S E R I E S 3:

S E R I E S 1:

S E R I E S 2:

S E R I E S 3:

S E R I E S 2:

FIG. 7.69. Standpipe strains at positions 33/34, 35/36, 41/42, 43/44 - (Fig.5.10) - Model 5/6.

FIG. 7.70. Standpipe strains at positions 37/38, 45/46 - (Fig. 5.10) - Model 5/6.

FIG. 7.71. Standpipe strains at positions 39/40, 47/48 - (Fig. 5.10) - Model 5/6.

FIG. 7.72. Standpipe strains at positions 65/66, 67/68, 73/74, 75/76 - (Fig. 5.14) - Model 9/10.

FIG. 7.73. Standpipe strains at positions 69/70, 77/78 - (Fig. 5.14) - Model 9/10.

FIG. 7.74. Standpipe strains at positions 71/72, 79/80 - (Fig. 5.14) - Model 9/10.

S E R I E S 1 - 2 - 3:

Predicted tangential and radial stresses by the Rate of creep method, and the Effective modulus method.

FIG. 7.75. Series 1:
Experimental and predicted stress-time curves (radial and tangential) for solid specimen - Model 1/2.

FIG. 7.76. Series 2:
Experimental and predicted stress-time curves (radial and tangential) for solid specimen - Model 1/2.

FIG. 7.77. Series 3:
Experimental and predicted stress-time curves (radial and tangential) for solid specimen- Model 1/2.

FIG. 7.78. Series 1:
Tangential and radial stresses - R.C., method - position 1 - Composite specimen.

FIG. 7.79. Series 1:
Tangential and radial stresses - R.C., method - position 1 - Composite specimen.

FIG. 7.80. Series 1:
Tangential and radial stresses - R.C., method - position 3 - Composite specimen.

FIG. 7.81. Series 1:
Tangential and radial stresses - R.C., method - position 4 - Composite specimen.

FIG. 7.82. Series 1:
Tangential and radial stresses - R.C., method - position 5 - Composite specimen.

FIG. 7.83. Series 1:
Tangential and radial stresses - R.C., method - position 6 - Composite specimen.

FIG. 7.84. Series 2:
Tangential and radial stresses - R.C., method - position 1 - Composite specimen.

FIG. 7.85. Series 2:
Tangential and radial stresses - R.C., method - position 2 - Composite specimen.

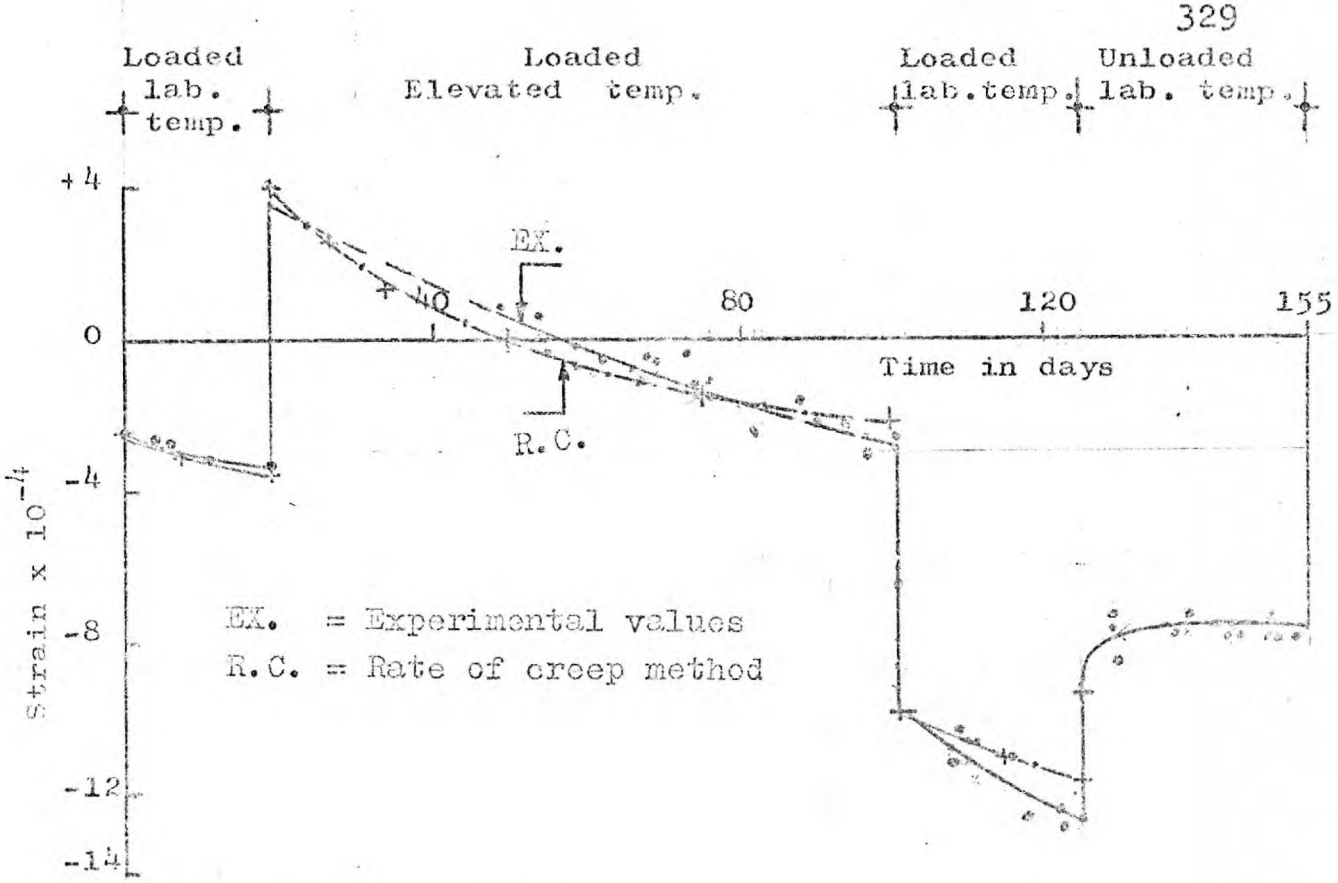

FIG.7.1. SERIES 1
TANGENTIAL GROSS STRAINS MODEL 1/2

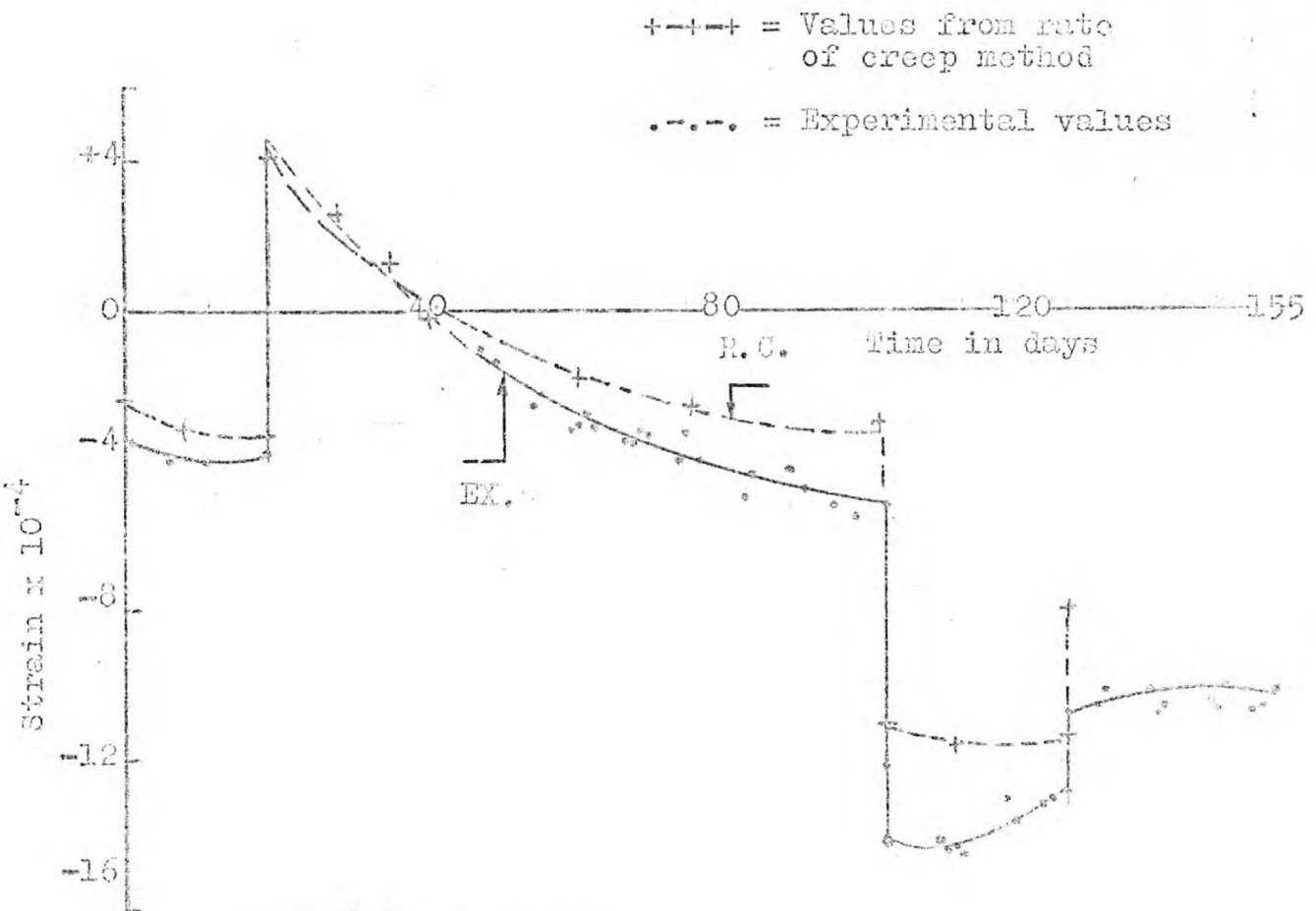

FIG.7.2. SERIES 1
RADIAL GROSS STRAINS MODEL 1/2

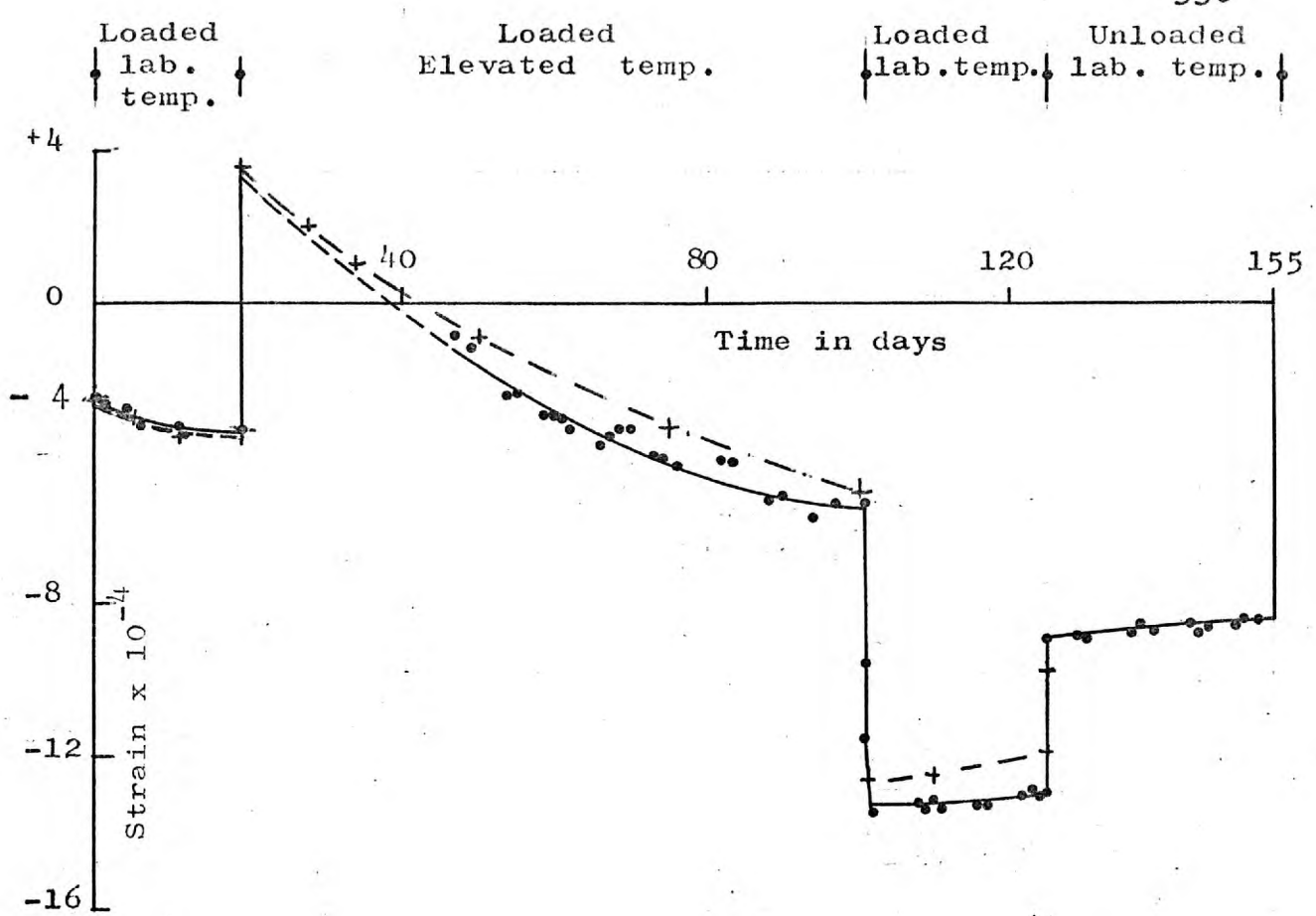

FIG. 7.3. SERIES 1
DIAMETER GROSS STRAINS MODEL 1/2

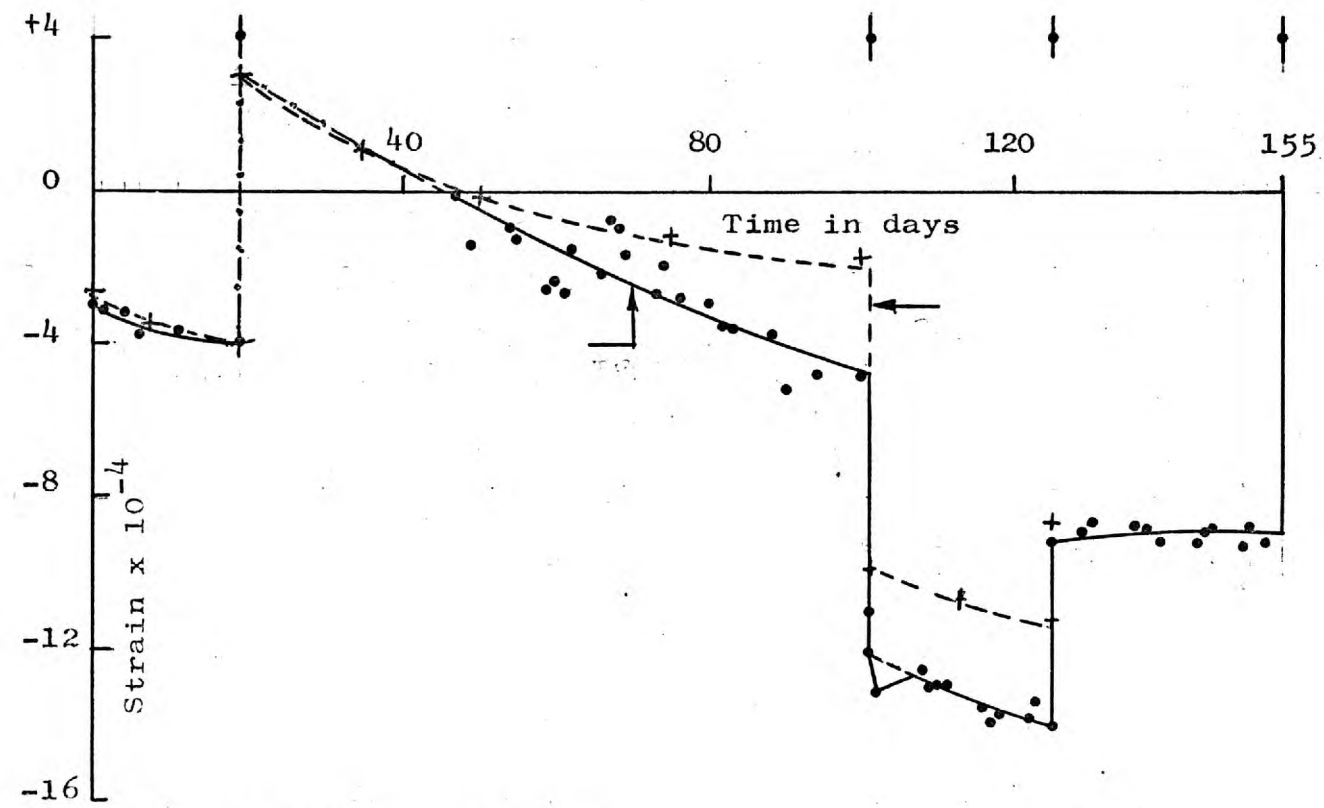

FIG. 7.4. SERIES 1
TANGENTIAL GROSS STRAINS MODEL 3/4

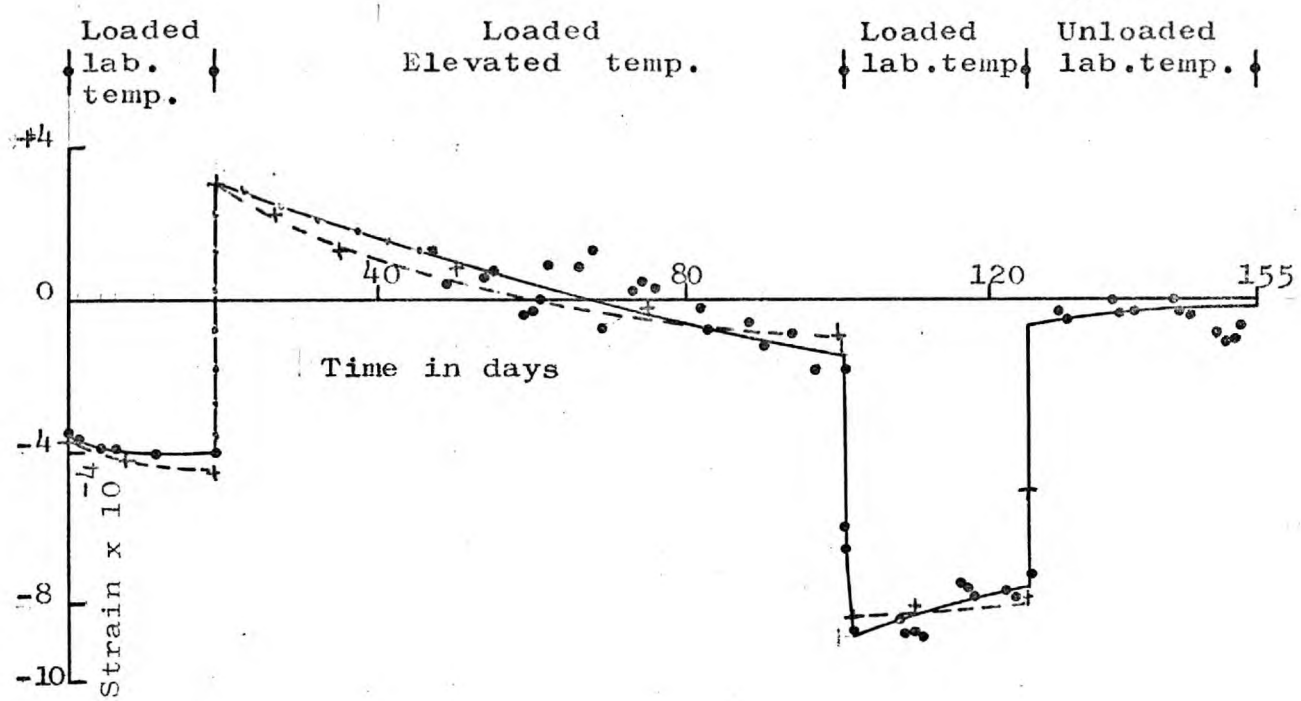

FIG. 7.5. SERIES 1
RADIAL GROSS STRAINS MODEL 3/4

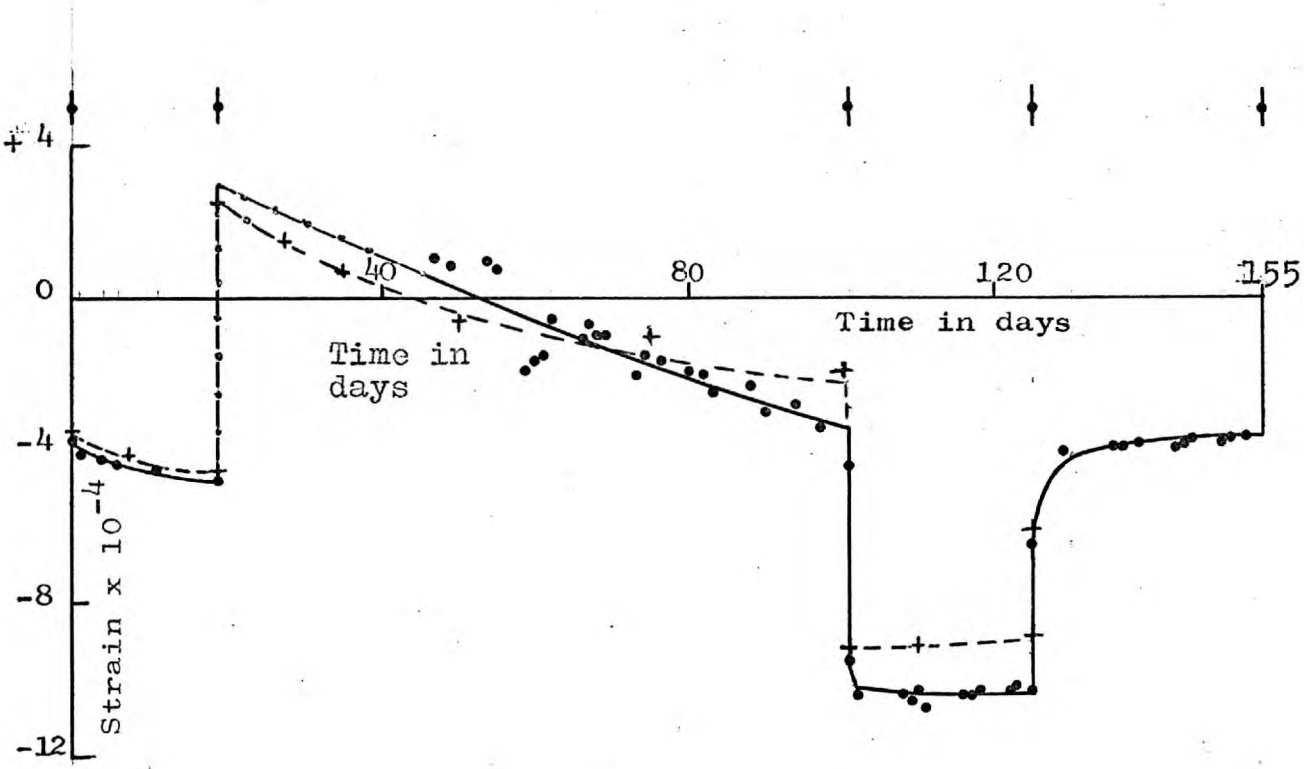

FIG. 7.6. SERIES 1
DIAMETER GROSS STRAINS MODEL 3/4

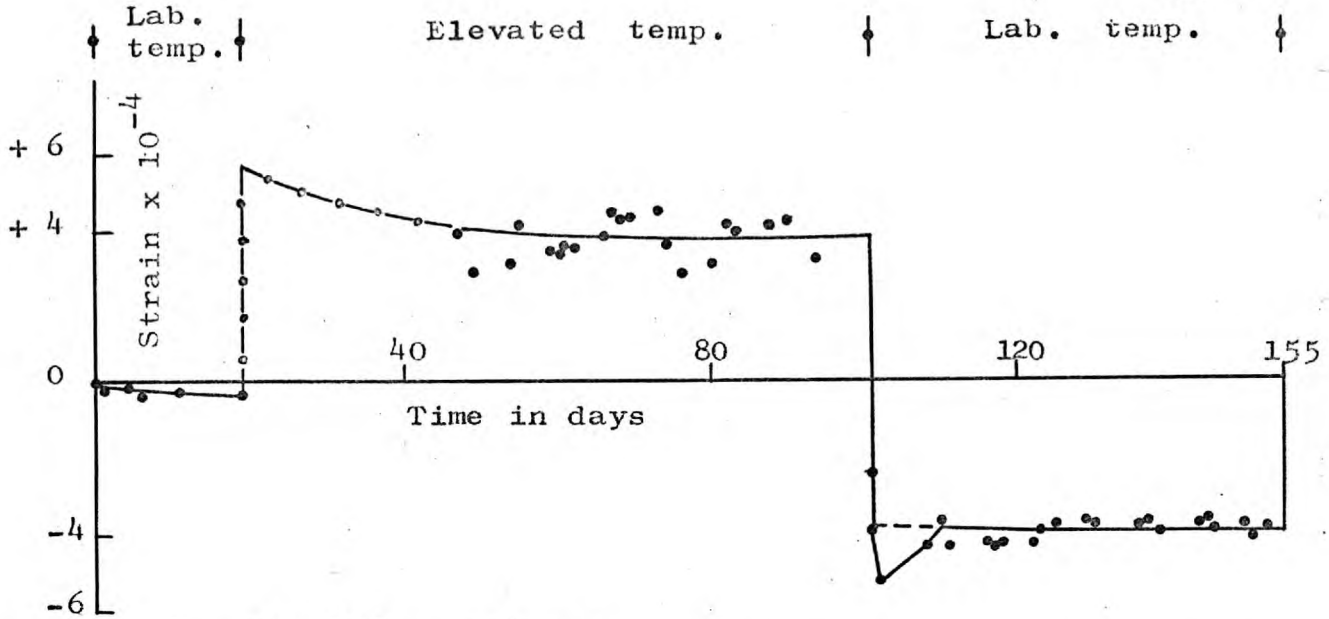

FIG.7.7. SERIES 1
TANGENTIAL SHRINKAGE AND THERMAL STRAINS
MODEL 5/6

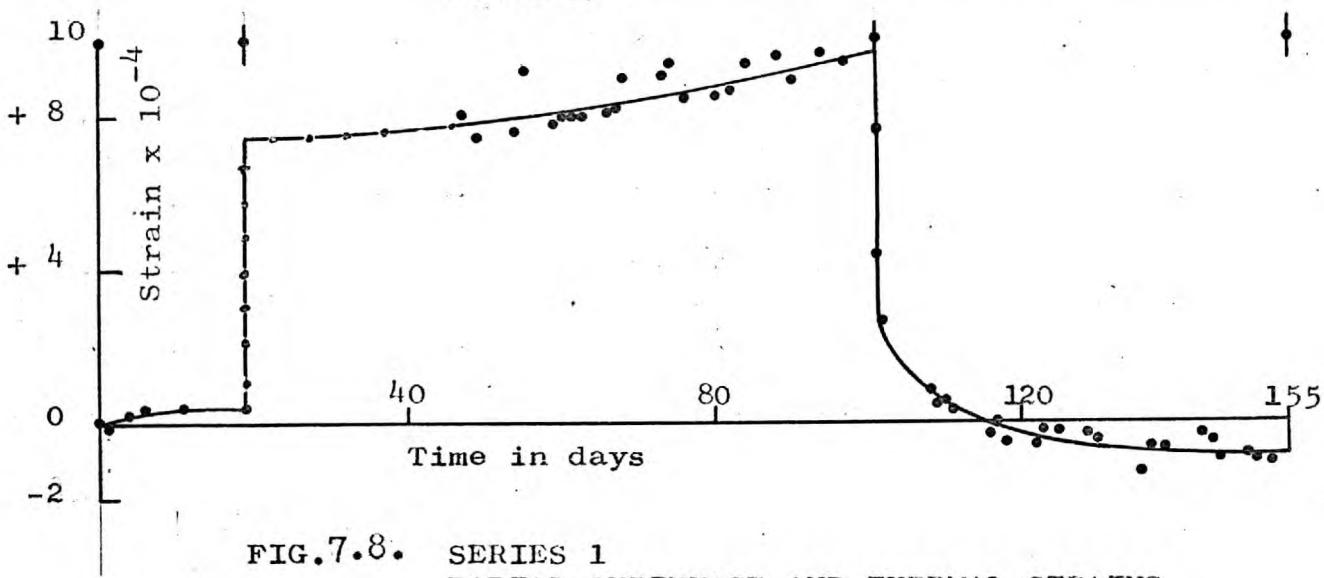

FIG.7.8. SERIES 1
RADIAL SHRINKAGE AND THERMAL STRAINS
MODEL 5/6

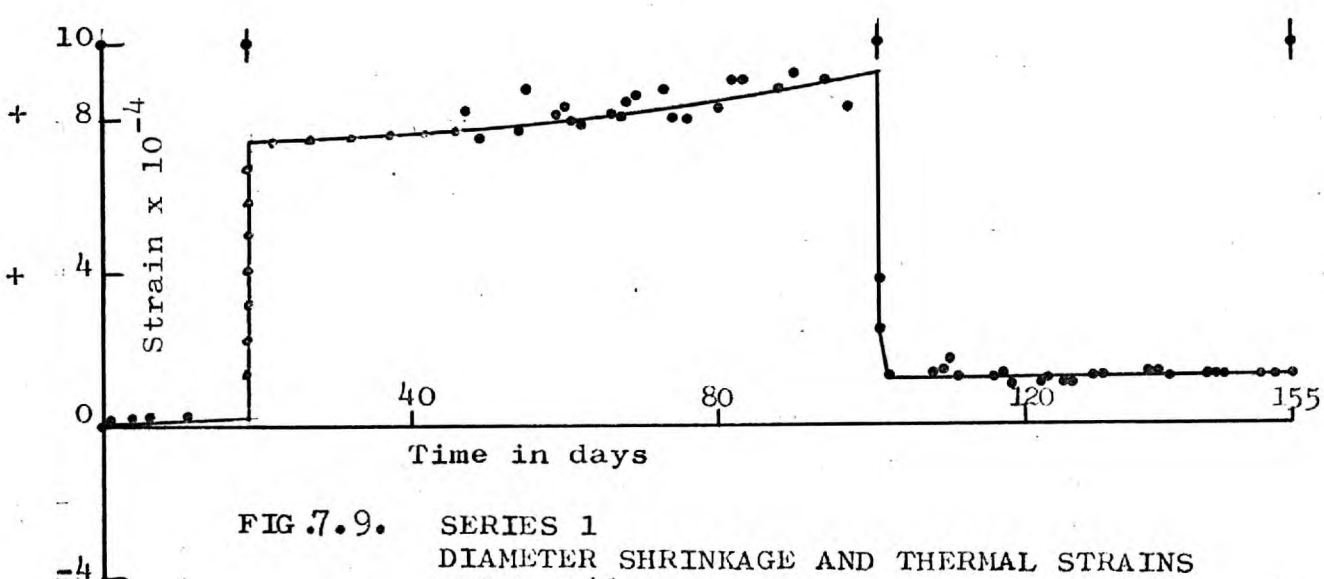

FIG.7.9. SERIES 1
DIAMETER SHRINKAGE AND THERMAL STRAINS
MODEL 5/6

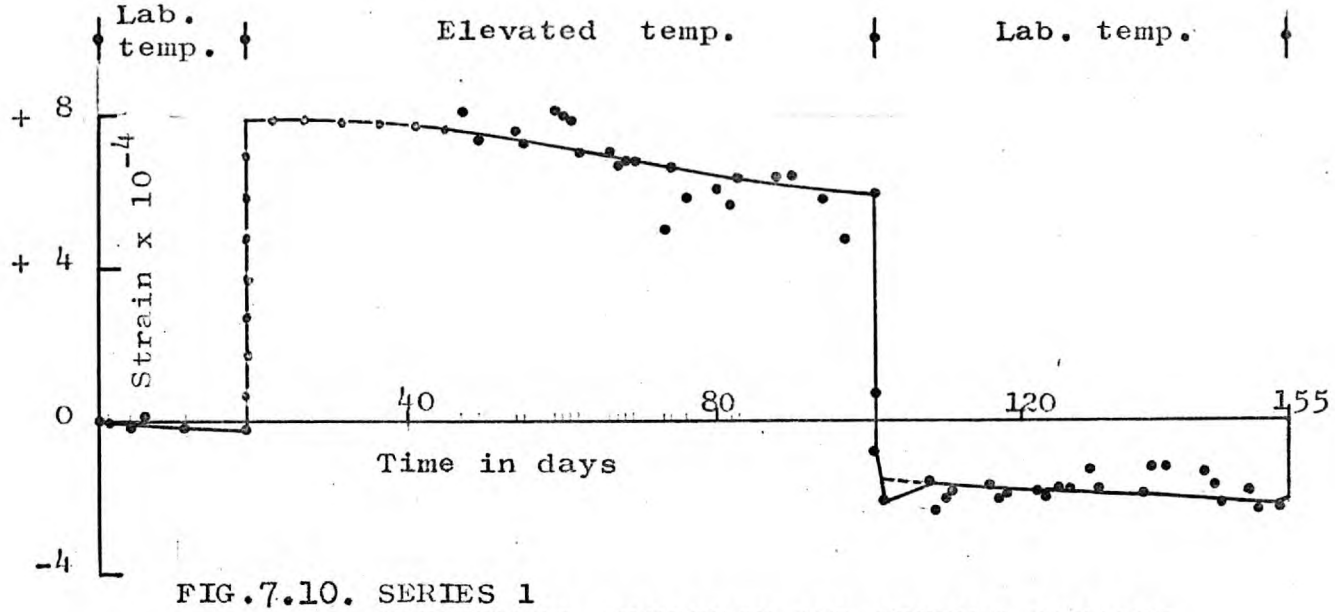

FIG.7.10. SERIES 1
TANGENTIAL SHRINKAGE AND THERMAL STRAINS
MODEL 7/8

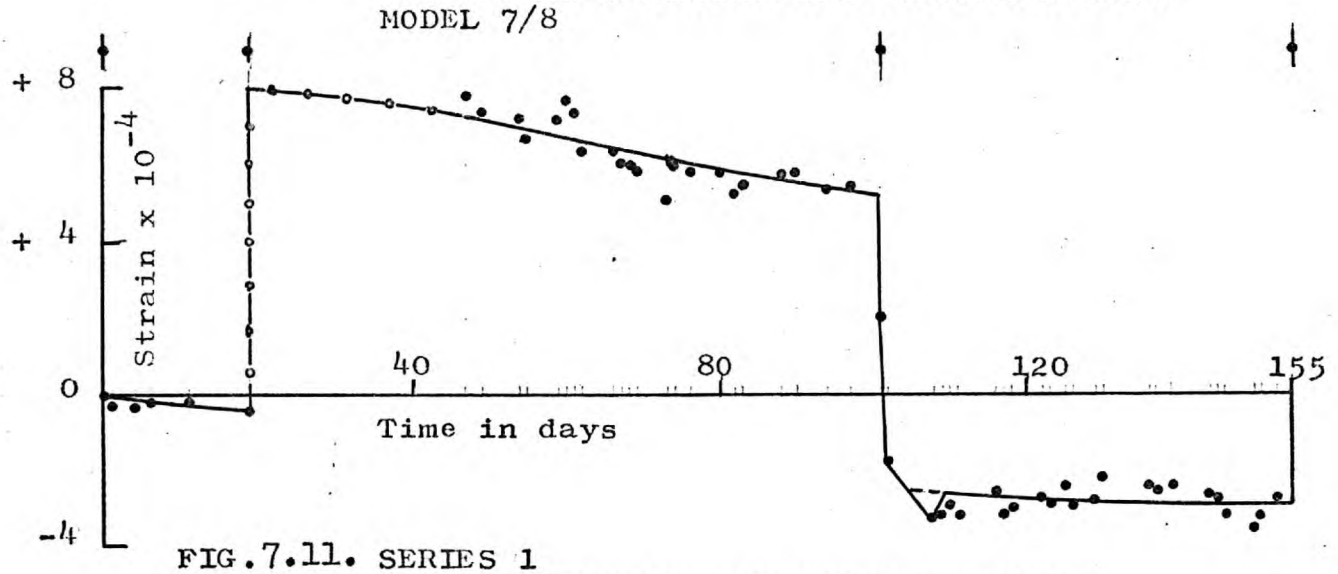

FIG.7.11. SERIES 1
RADIAL SHRINKAGE AND THERMAL STRAINS
MODEL 7/8

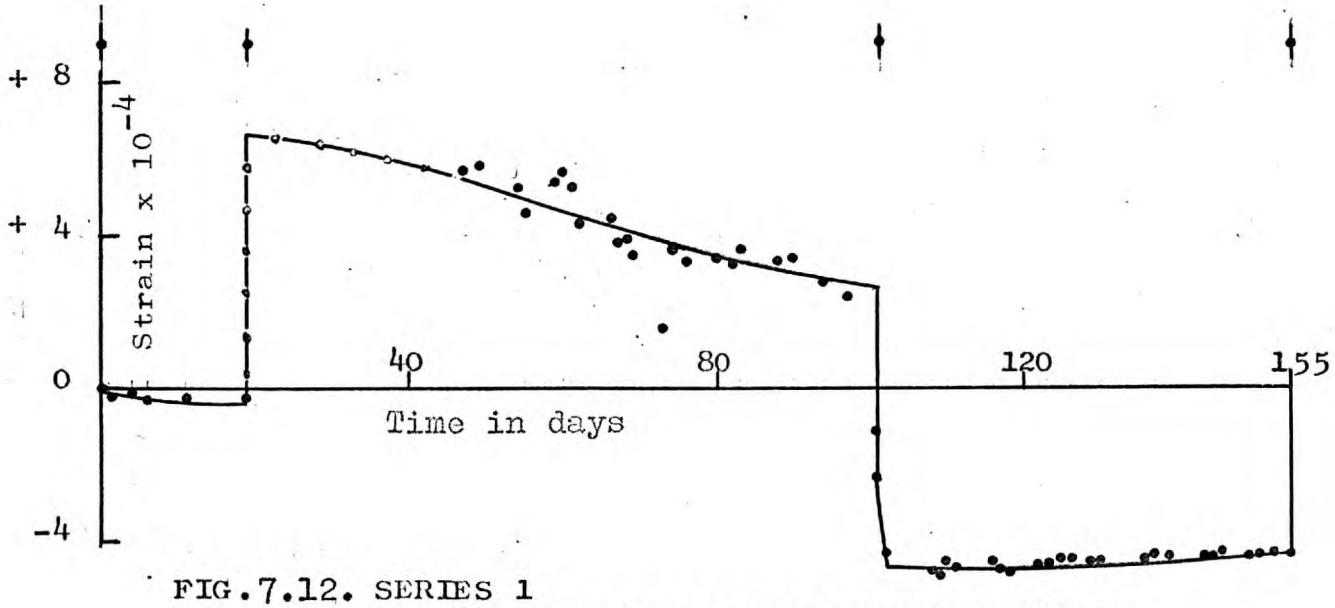

FIG.7.12. SERIES 1
DIAMETRAL SHRINKAGE AND THERMAL STRAINS
MODEL 7/8

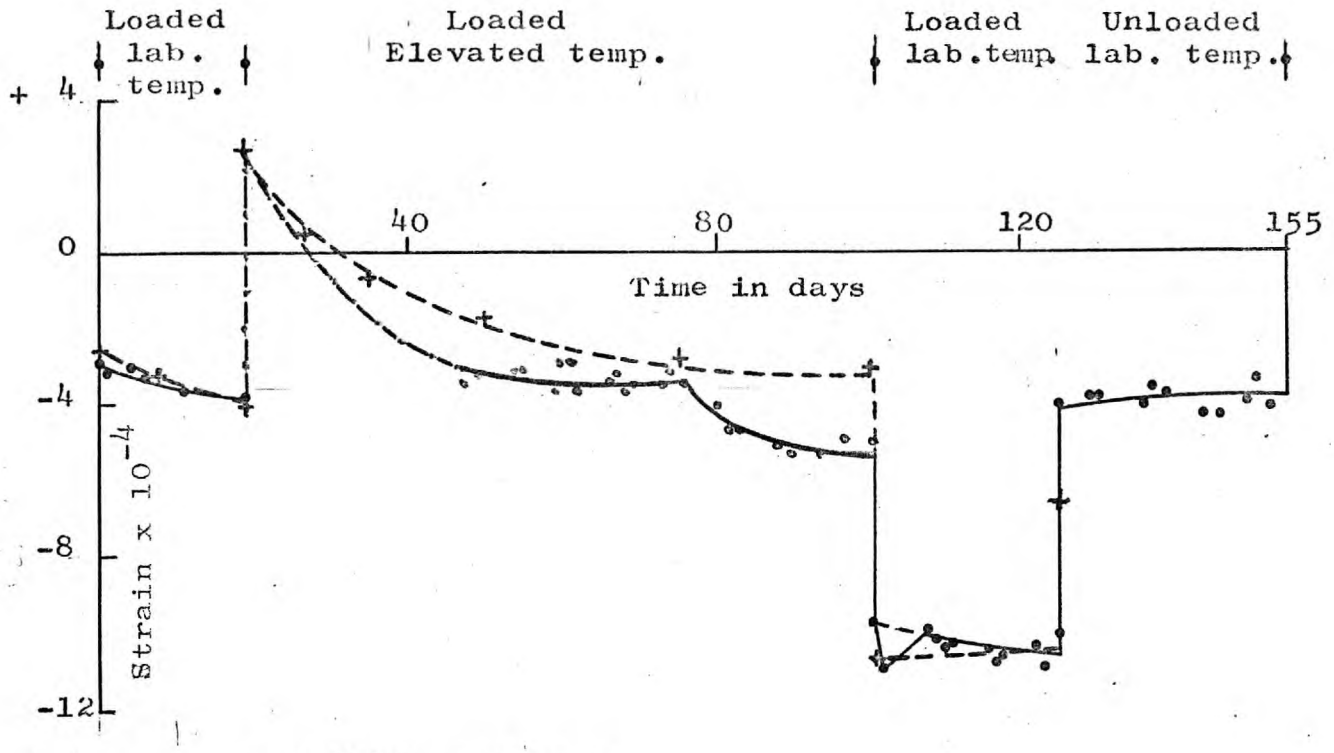

FIG.7.13. SERIES 1
TANGENTIAL GROSS STRAINS
PERFORATED ZONE MODEL 9/10

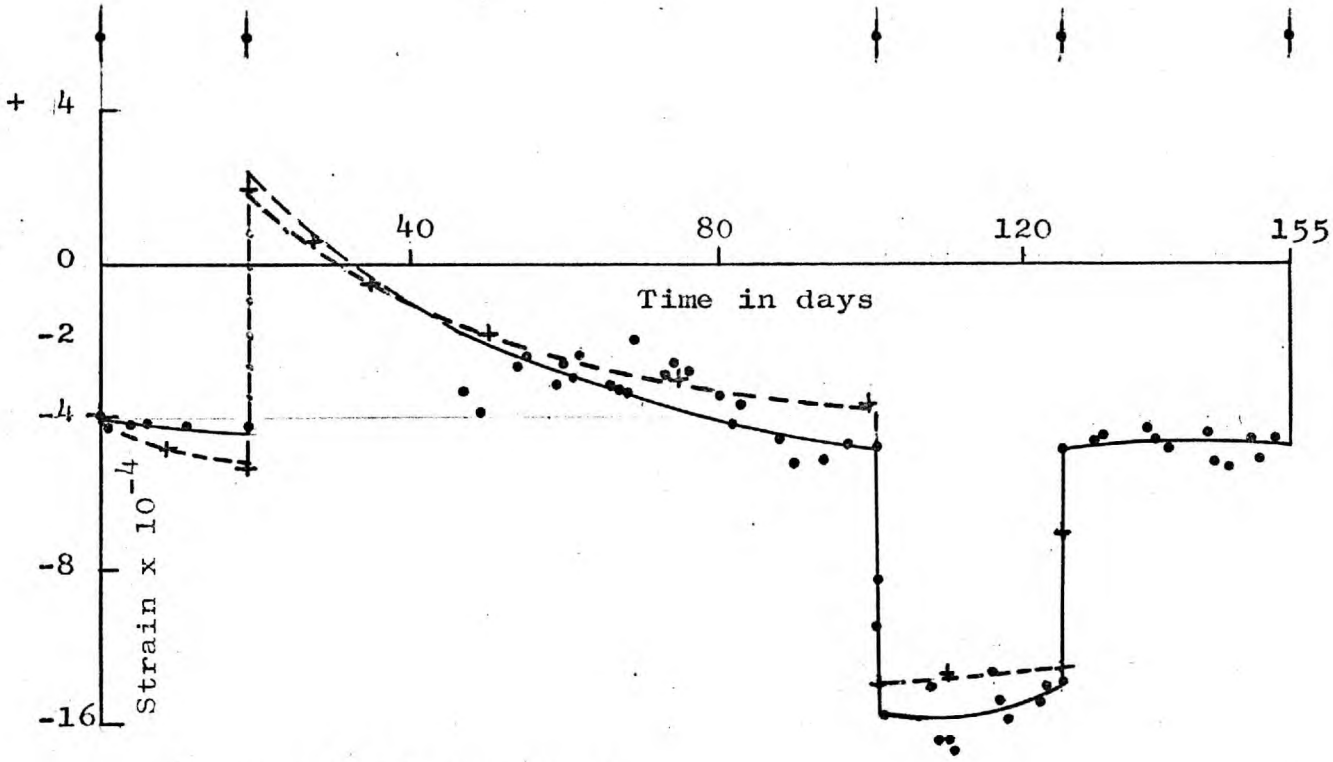

FIG.7.14. SERIES 1
RADIAL GROSS STRAINS
PERFORATED ZONE MODEL 9/10

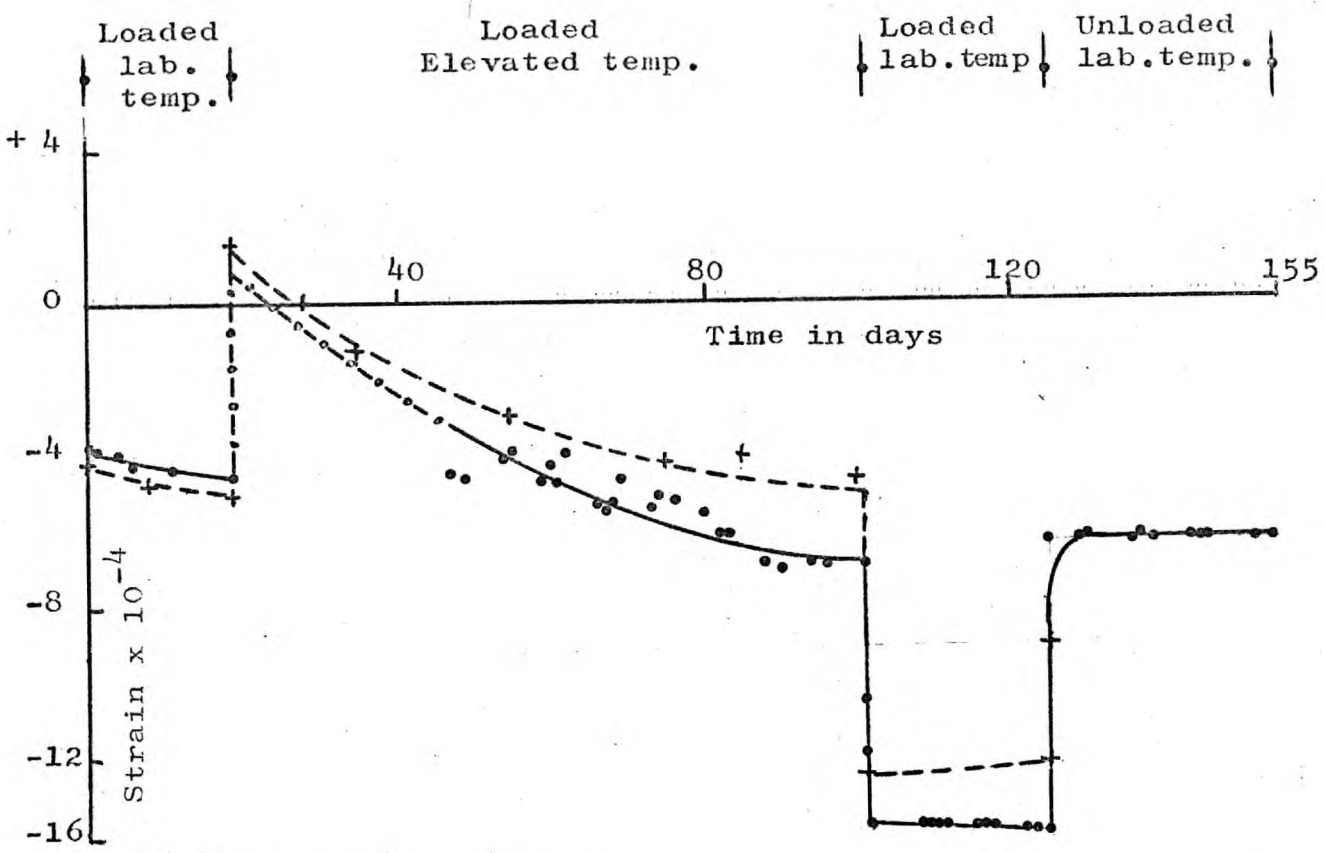

FIG.7.15. SERIES 1
DIAMETRAL GROSS STRAINS
PERFORATED ZONE MODEL 9/10

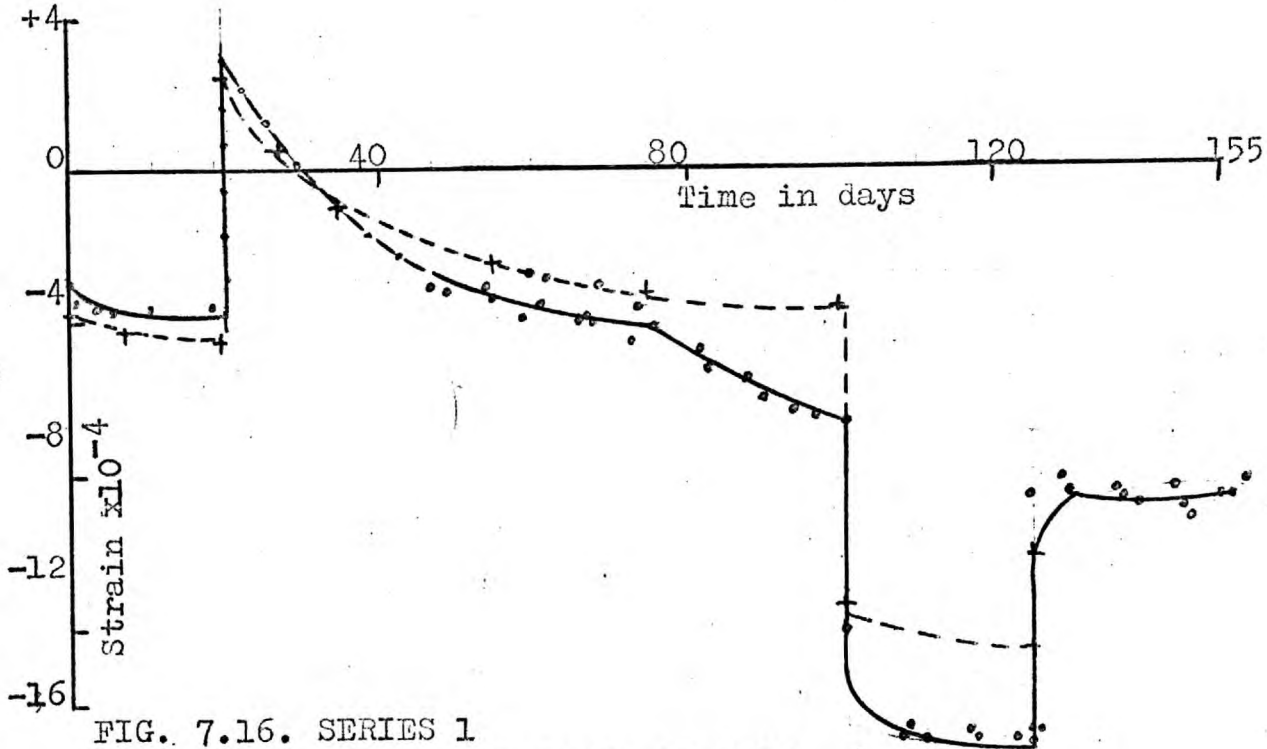

FIG. 7.16. SERIES 1
TANGENTIAL GROSS STRAINS
OUTER SATELITE IN ANNULUS
MODEL 9/10.

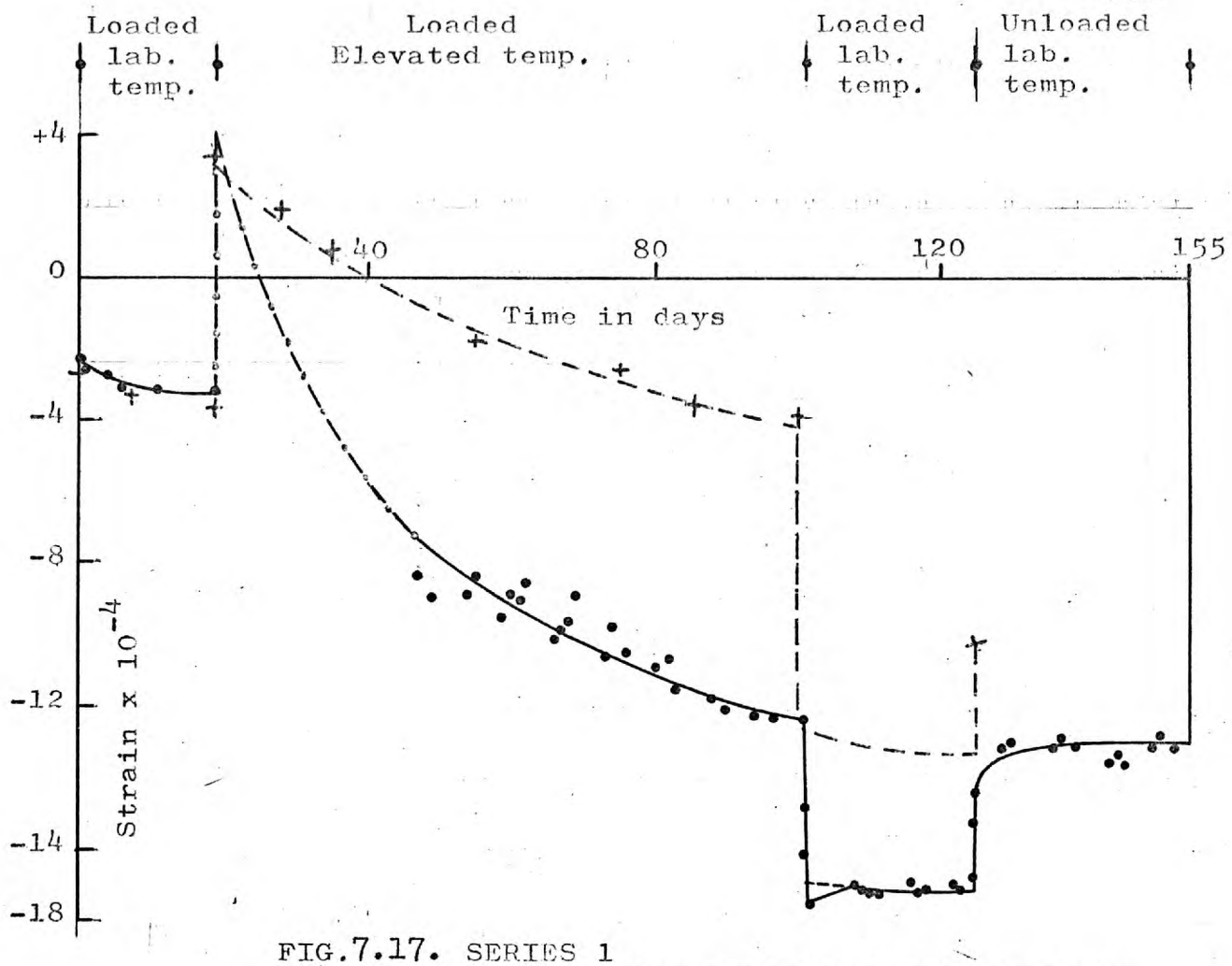

FIG.7.17. SERIES 1
RADIAL GROSS STRAINS OUTER SATELITE
IN ANNULUS MODEL 9/10

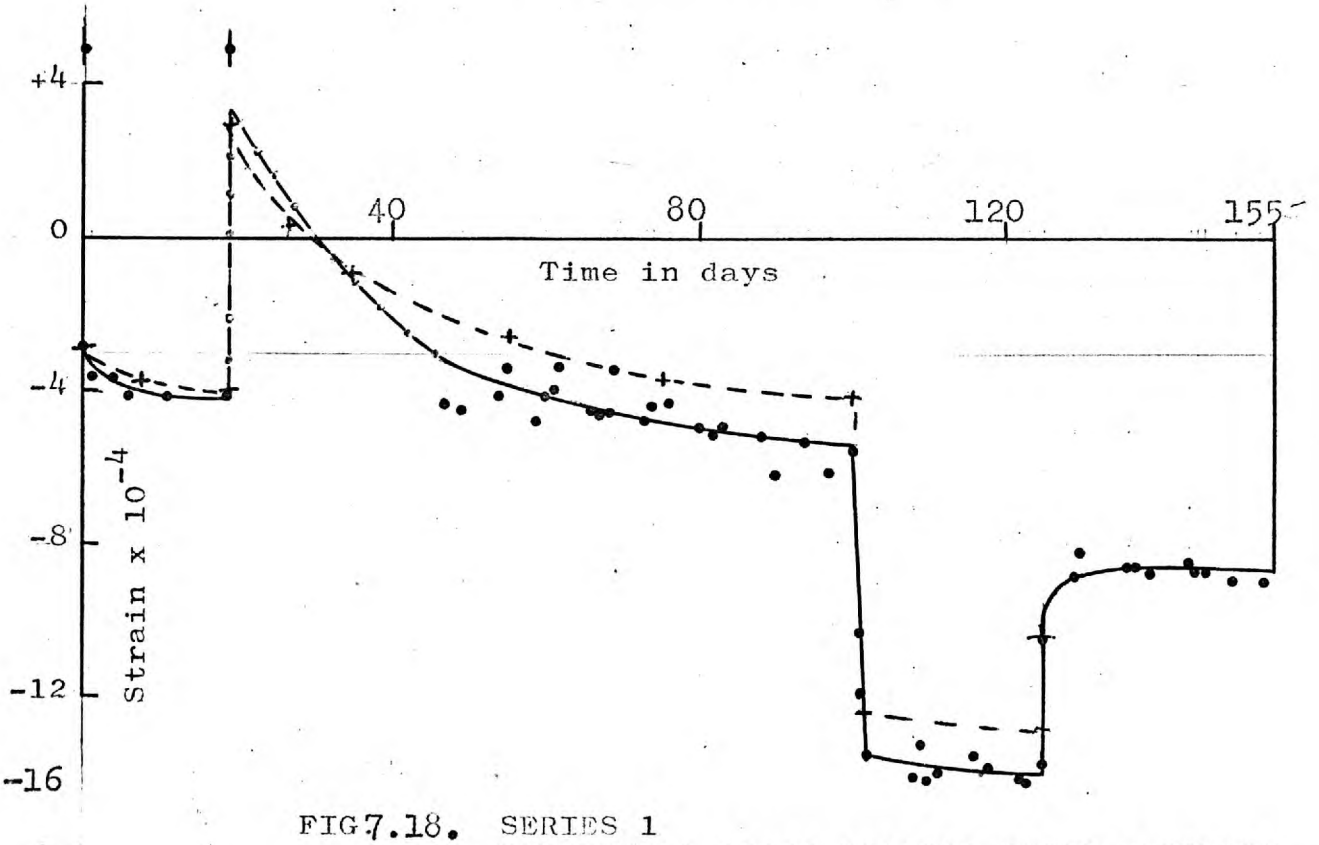

FIG7.18. SERIES 1
TANGENTIAL GROSS STRAINS INNER SATELITE
IN ANNULUS MODEL 9/10

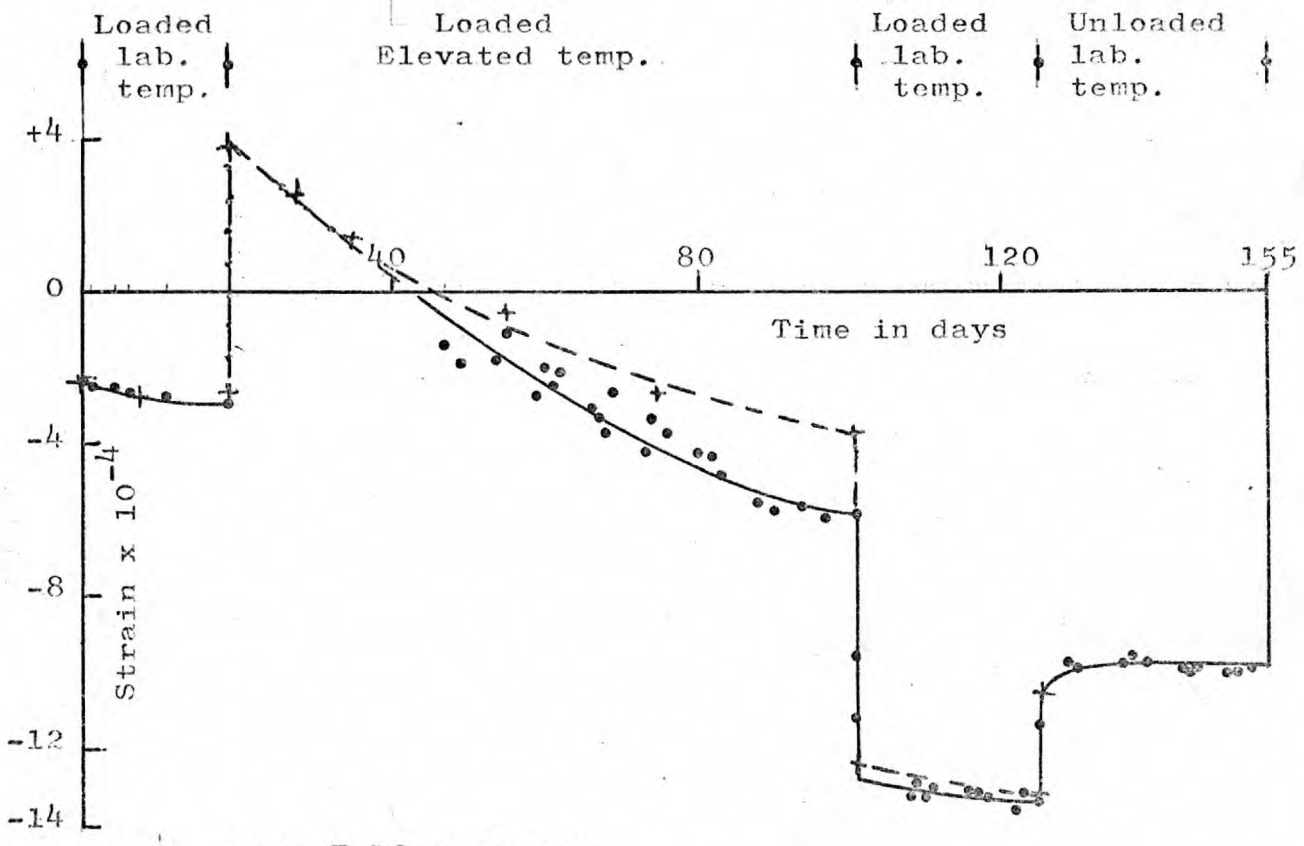

FIG. 7.19. SERIES 1
RADIAL GROSS STRAINS INNER SATELITE
IN ANNULUS MODEL 9/10

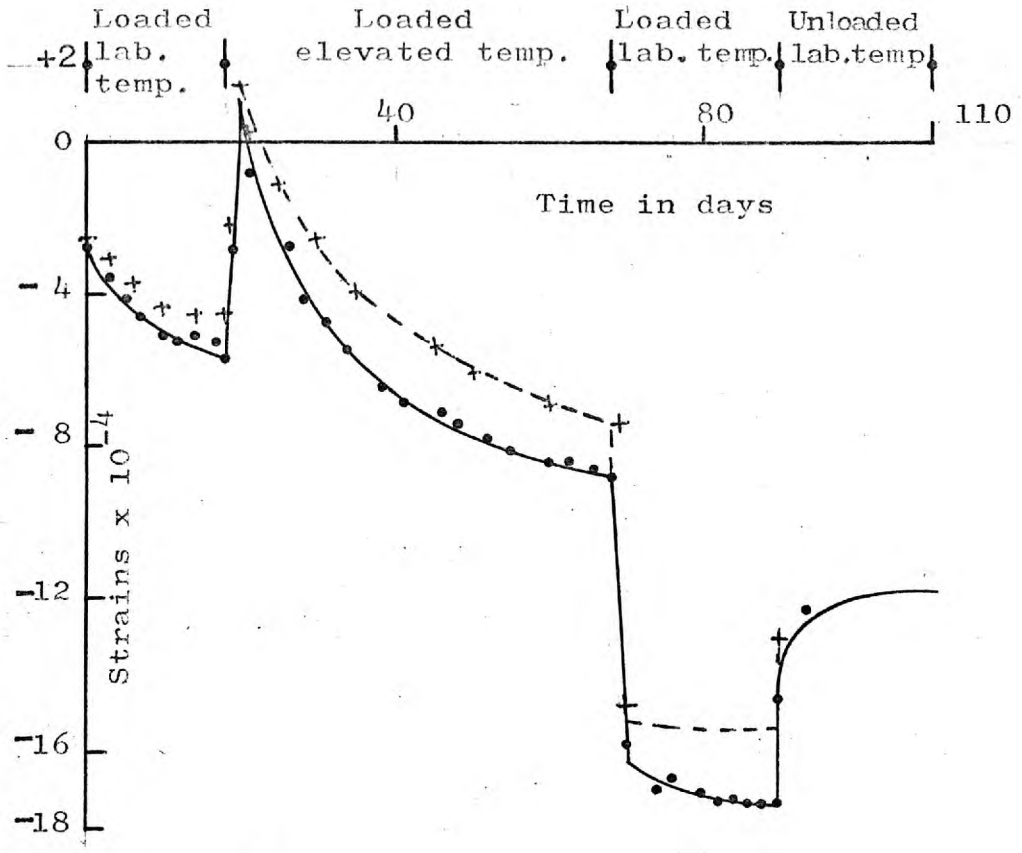

FIG. 7.20. SERIES 2
TANGENTIAL GROSS STRAINS MODEL 1/2

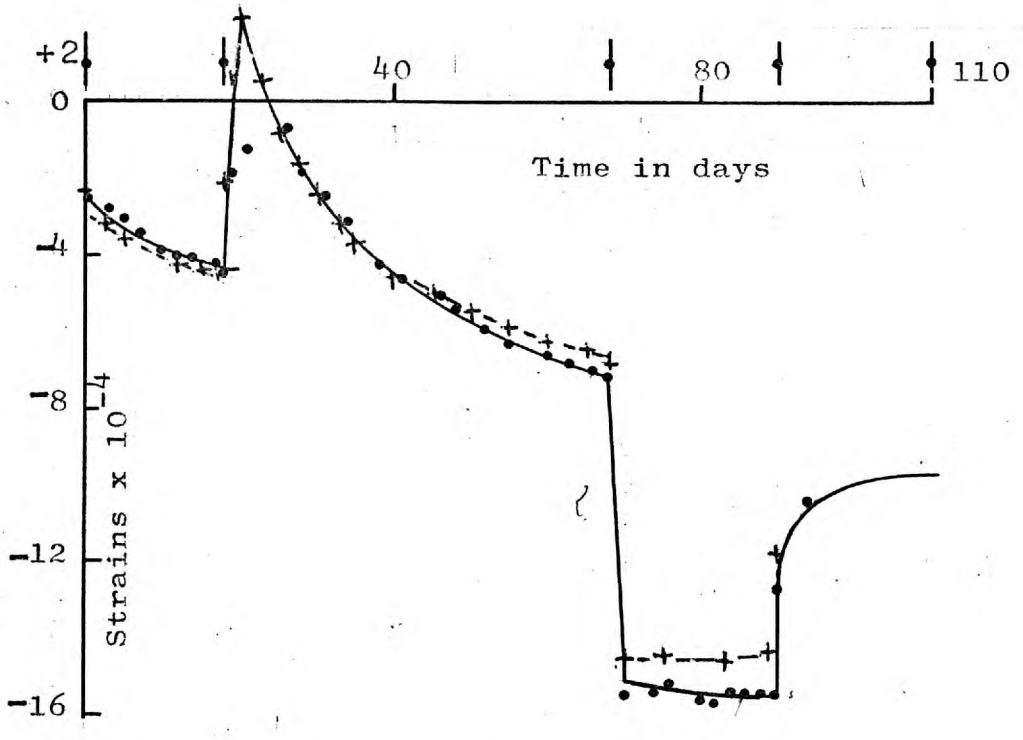

FIG. 7.21. SERIES 2
RADIAL GROSS STRAINS MODEL 1/2

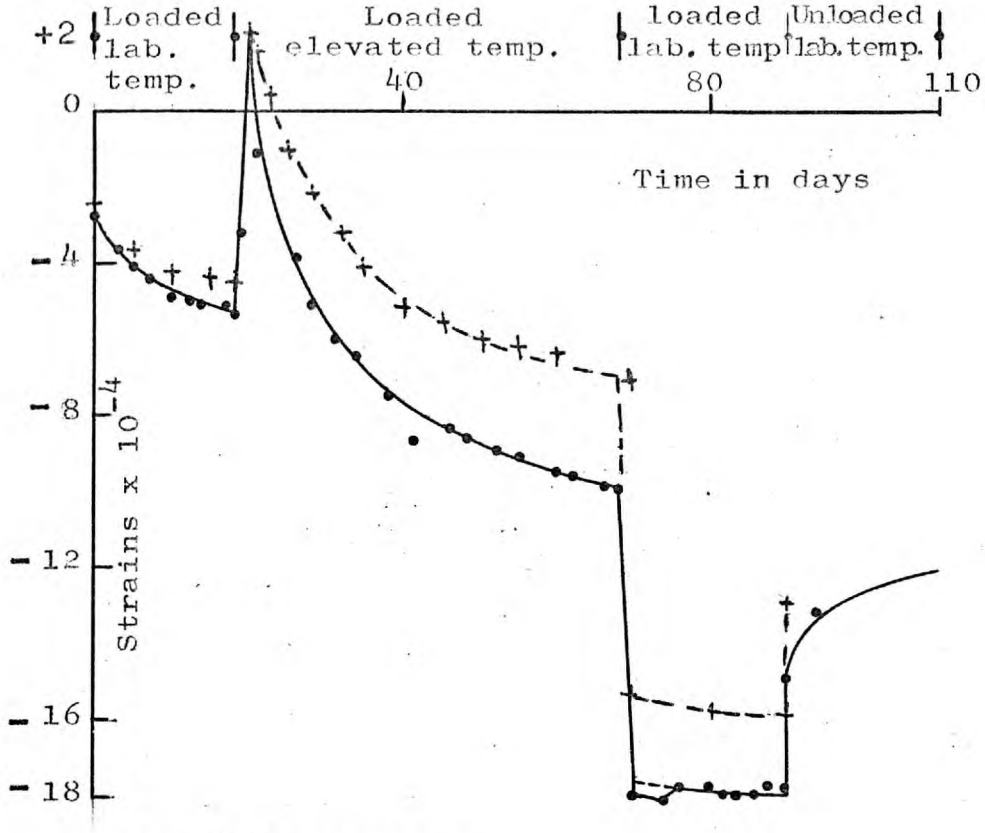

FIG. 7.22. SERIES 2
DIAMETER GROSS STRAINS MODEL 1/2

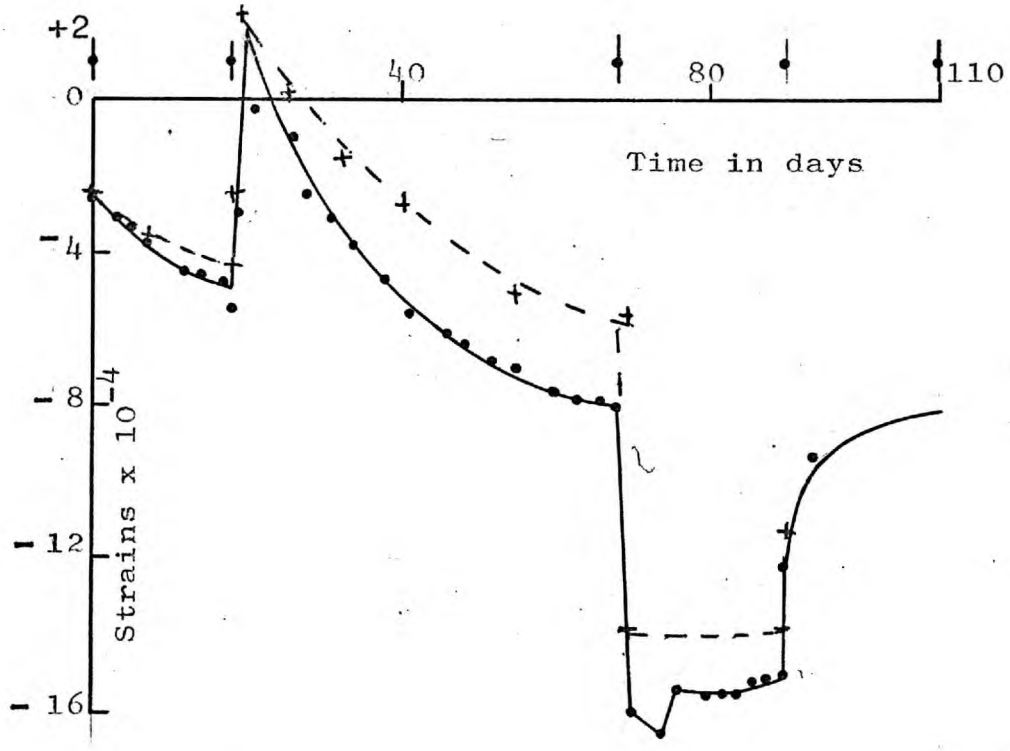

FIG. 7.23. SERIES 2
TANGENTIAL GROSS STRAINS MODEL 3/4

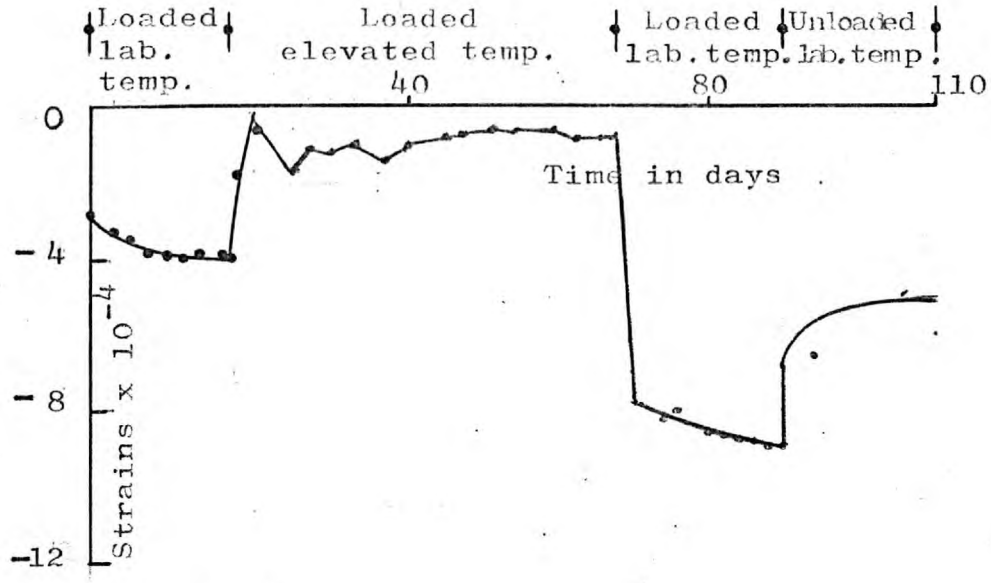

FIG.7.24. SERIES 2
RADIAL GROSS STRAINS MODEL 3/4

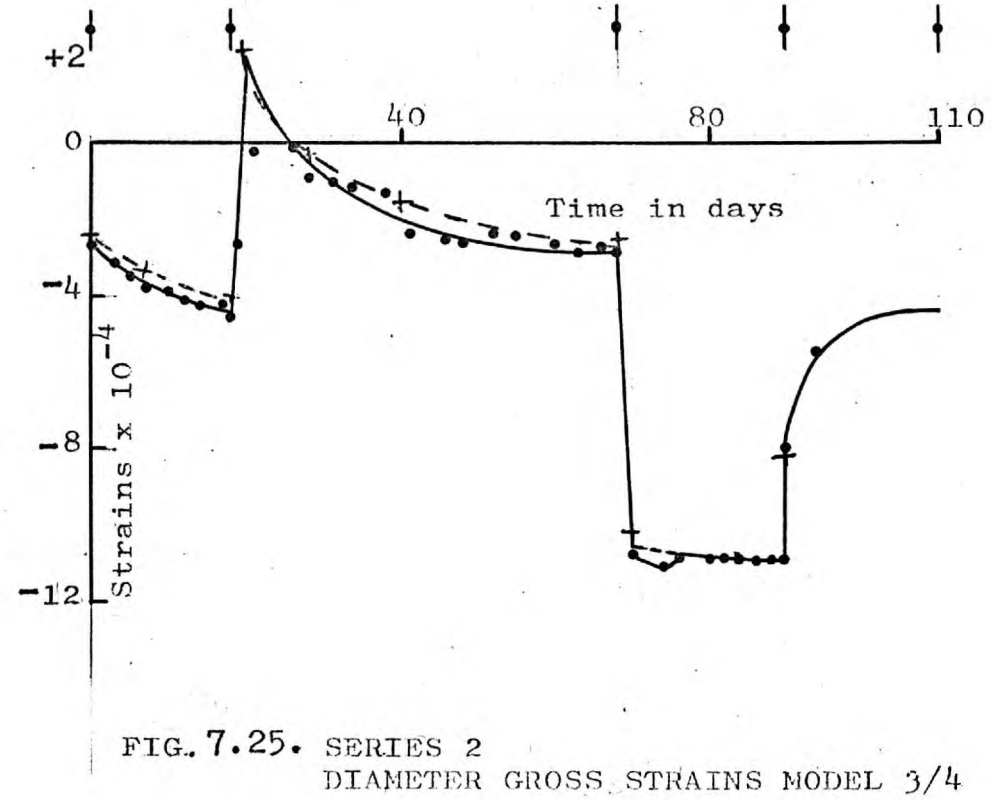

FIG. 7.25. SERIES 2
DIAMETER GROSS STRAINS MODEL 3/4

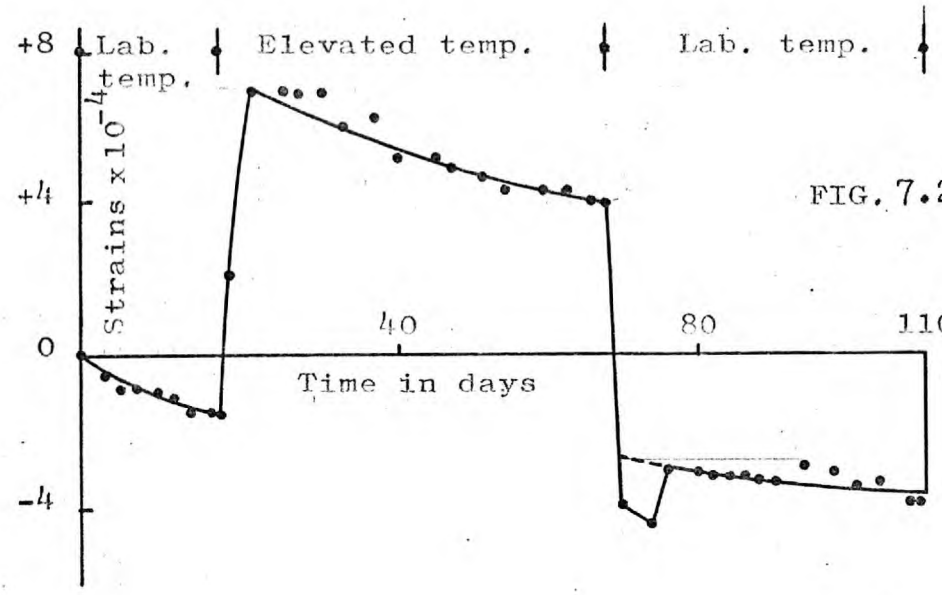

FIG. 7.26. SERIES 2 TANGENTIAL SHRINKAGE AND THERMAL STRAINS MODEL 5/6

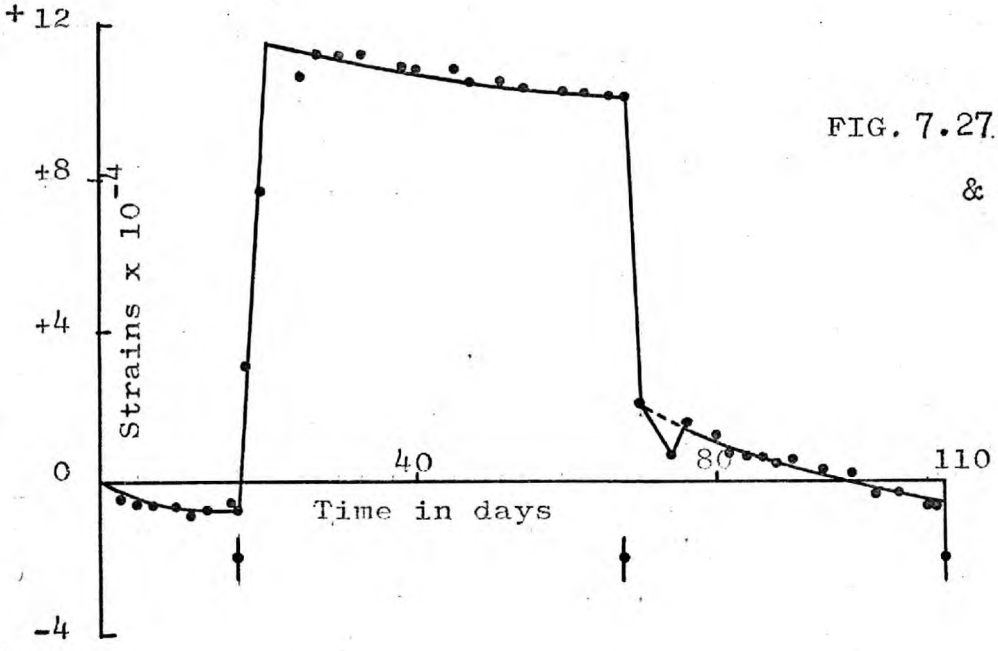

FIG. 7.27. SERIES 2 RADIAL SHRINKAGE & THERMAL STRAINS MODEL 5/6

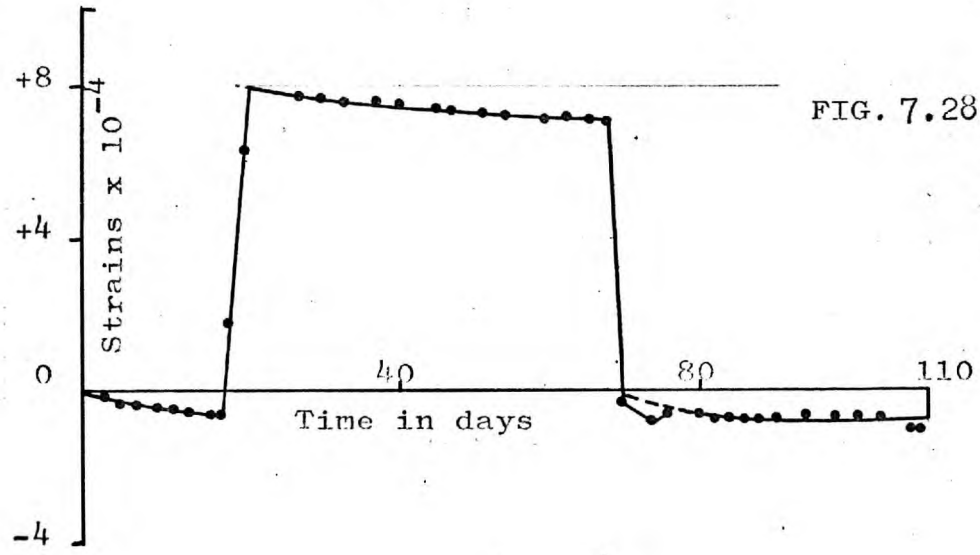

FIG. 7.28. SERIES 2 DIAMETER SHRINKAGE AND THERMAL STRAINS MODEL 5/6

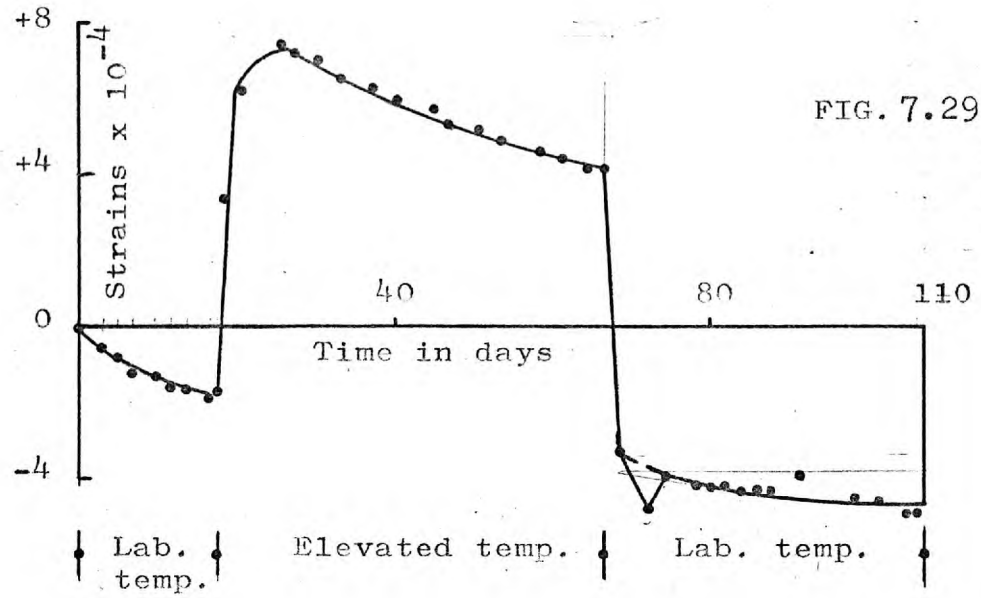

FIG. 7.29. SERIES 2 TANGENTIAL SHRINKAGE AND THERMAL STRAINS MODEL 7/8

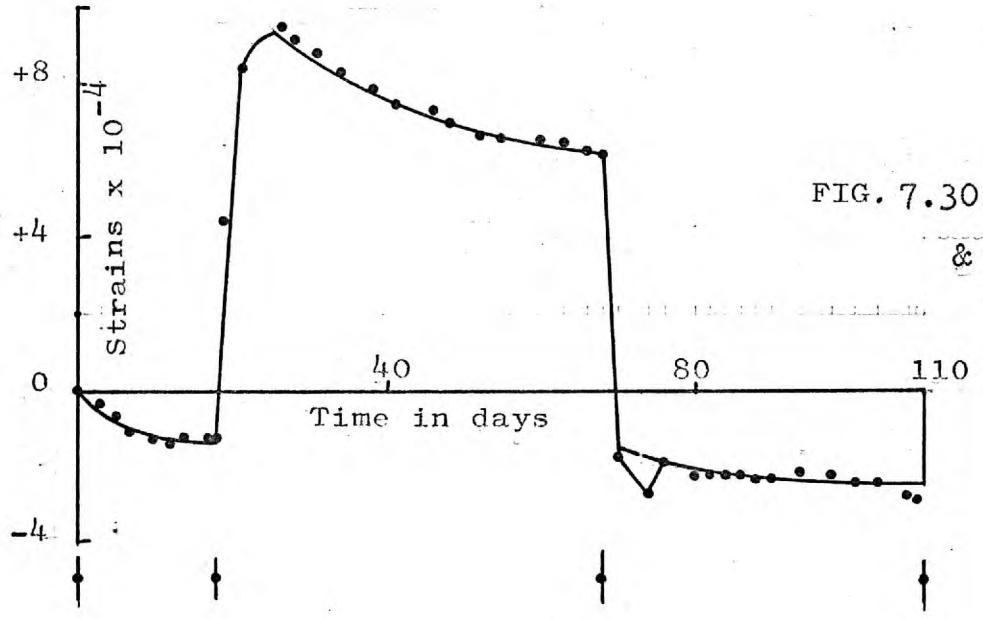

FIG. 7.30. SERIES 2 RADIAL SHRINKAGE & THERMAL STRAINS MODEL 7/8

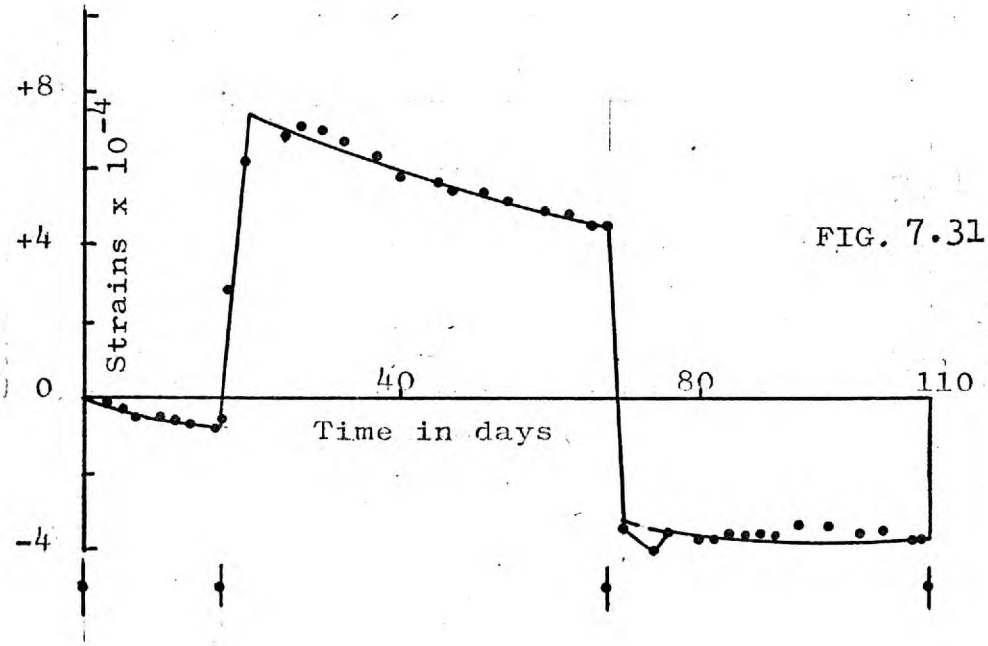

FIG. 7.31. SERIES 2 DIAMETER SHRINKAGE AND THERMAL STRAINS MODEL 7/8

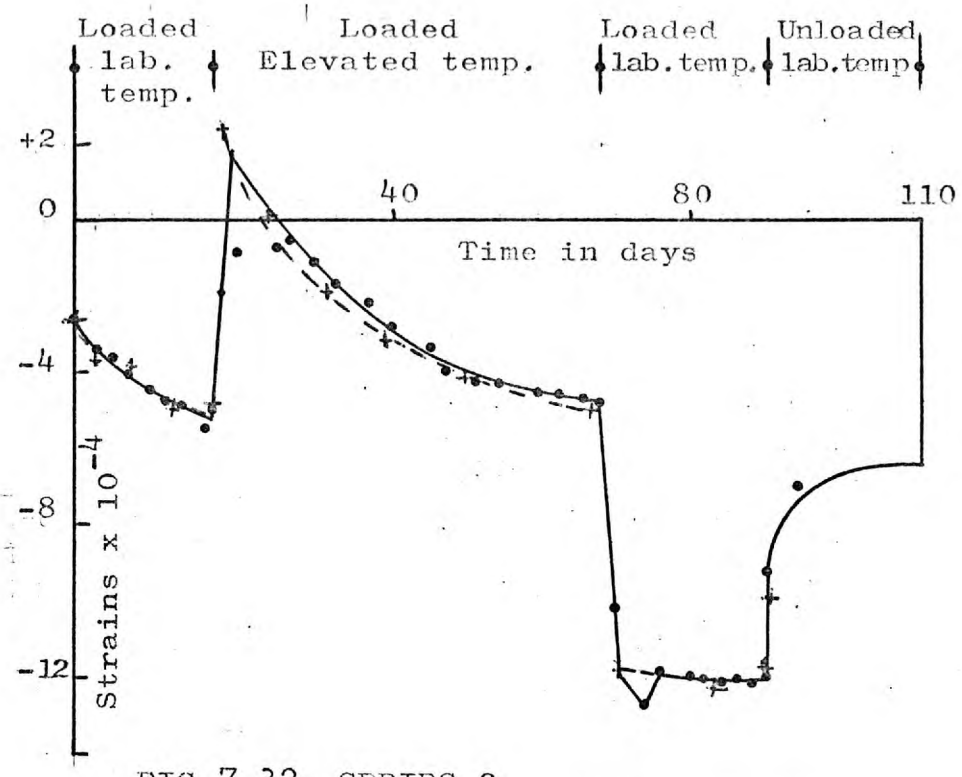

FIG.7.32. SERIES 2
TANGENTIAL GROSS STRAINS
MODEL 9/10 PERFORATED ZONE

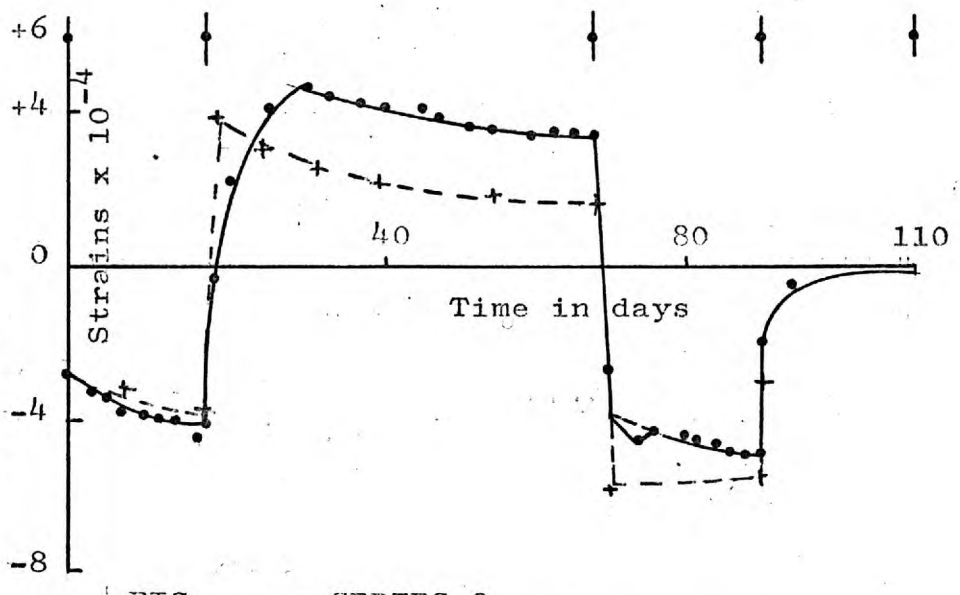

FIG.7.33. SERIES 2
RADIAL GROSS STRAINS
MODEL 9/10 PERFORATED ZONE

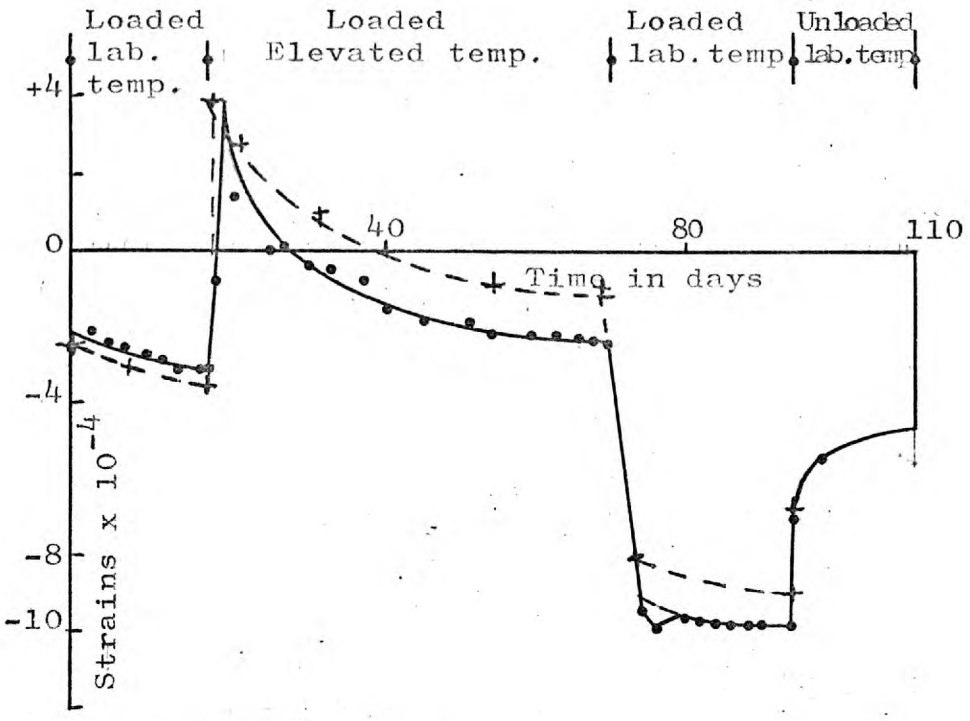

FIG.7.34. SERIES 2
DIAMETER GROSS STRAINS
MODEL 9/10 PERFORATED ZONE

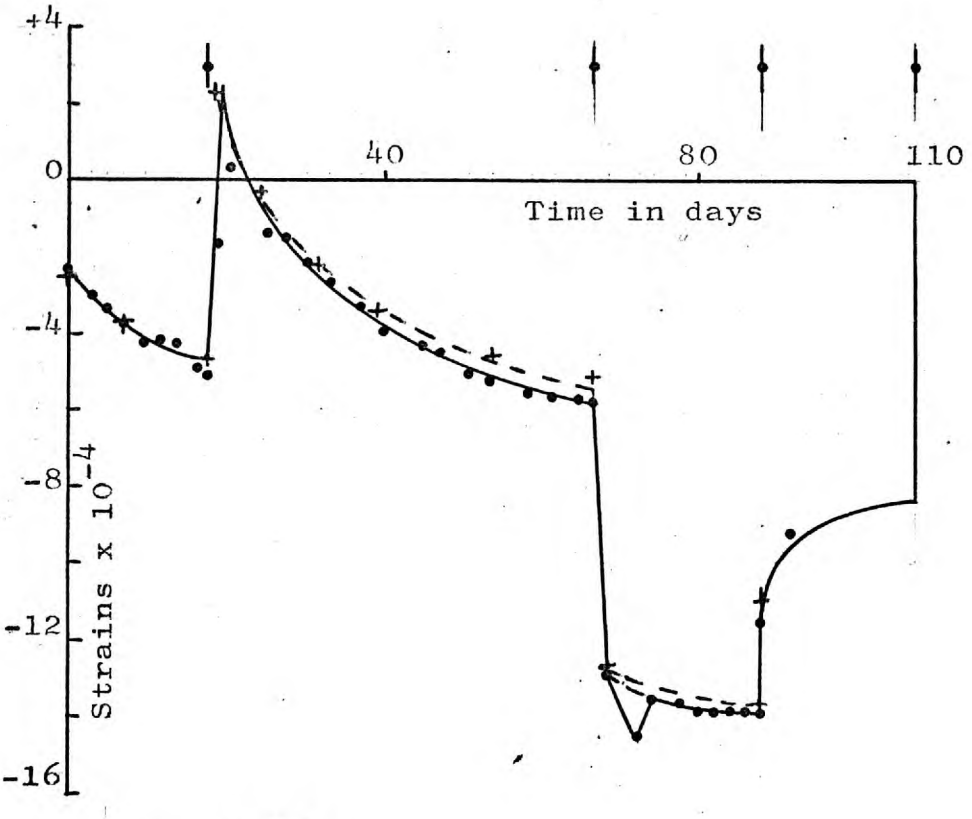

FIG. 7.35. SERIES 2
TANGENTIAL GROSS STRAINS
MODEL 9/10 OUTER SATELITE

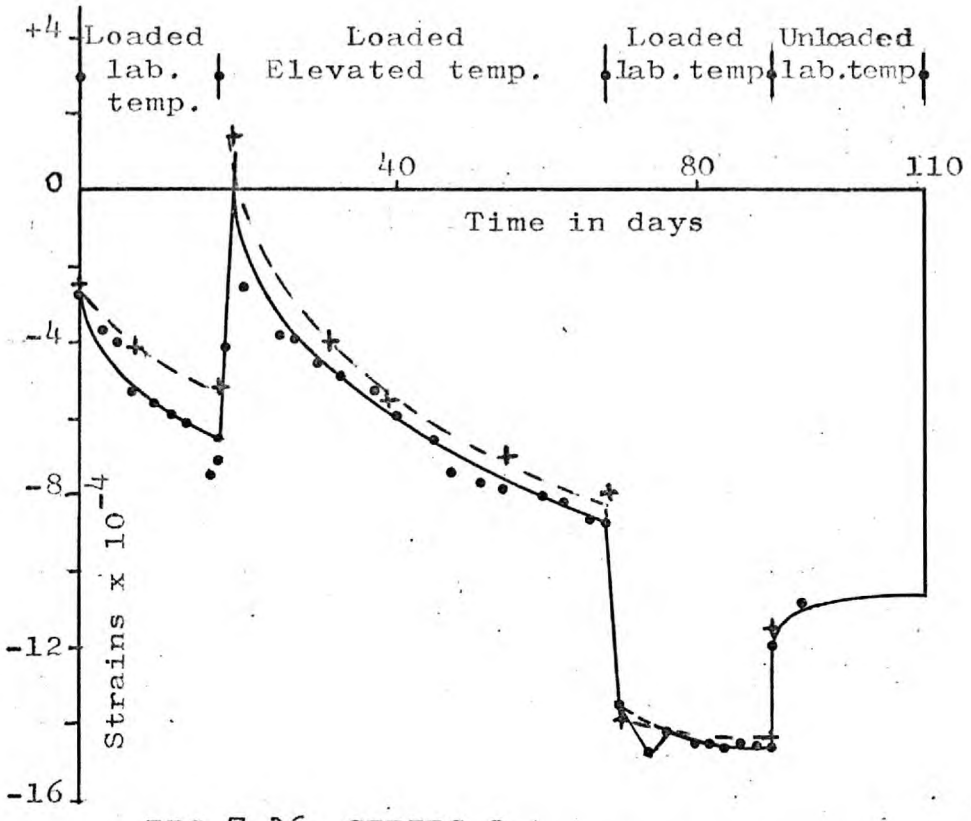

FIG.7.36. SERIES 2
RADIAL GROSS STRAINS OUTER SATELITE
IN ANNULUS MODEL 9/10

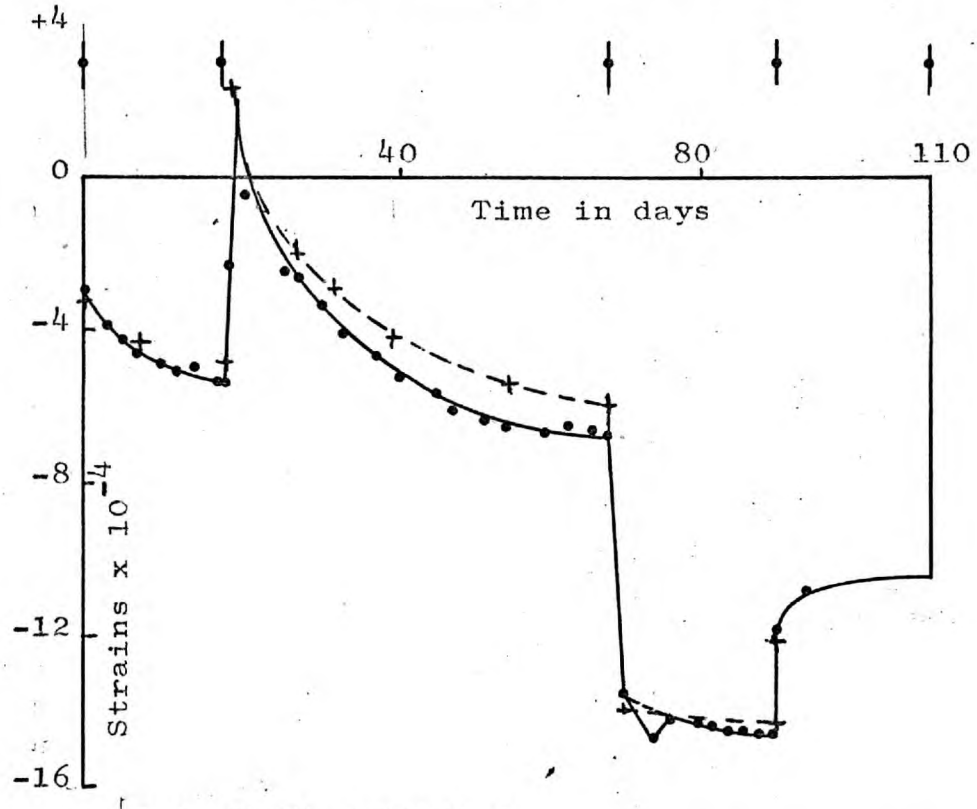

FIG. 7.37. SERIES 2
TANGENTIAL GROSS STRAINS INNER SATELITE
IN ANNULUS MODEL 9/10

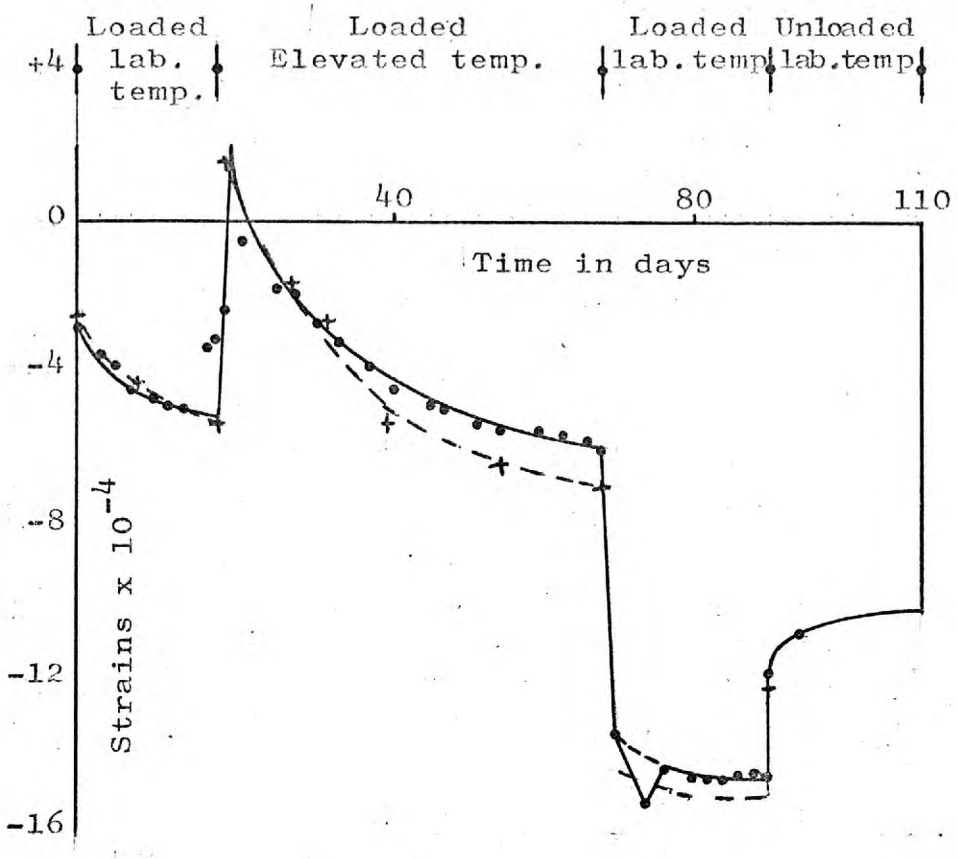

FIG.7.38. SERIES 2
RADIAL GROSS STRAINS INNER SATELITE
IN ANNULUS MODEL 9/10

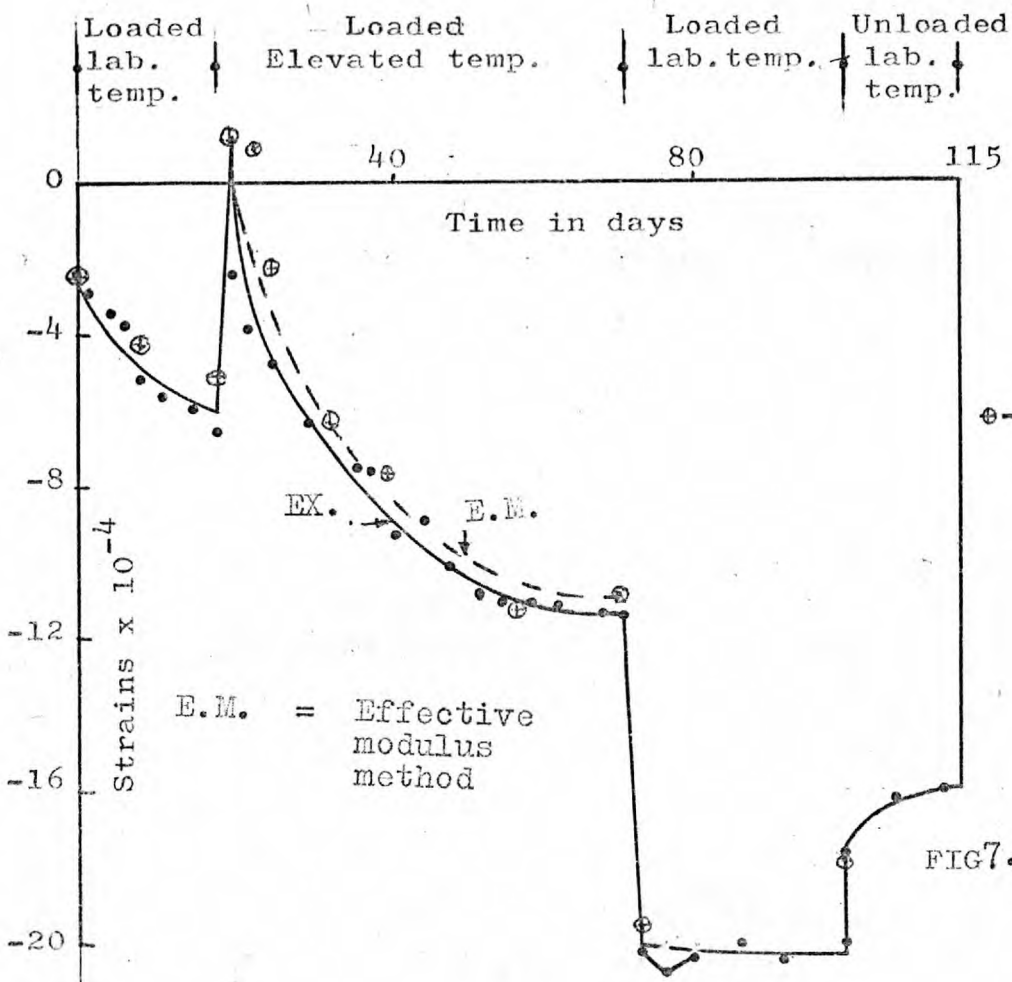

FIG7.39. SERIES 3 TANGENTIAL GROSS STRAINS MODEL 1/2

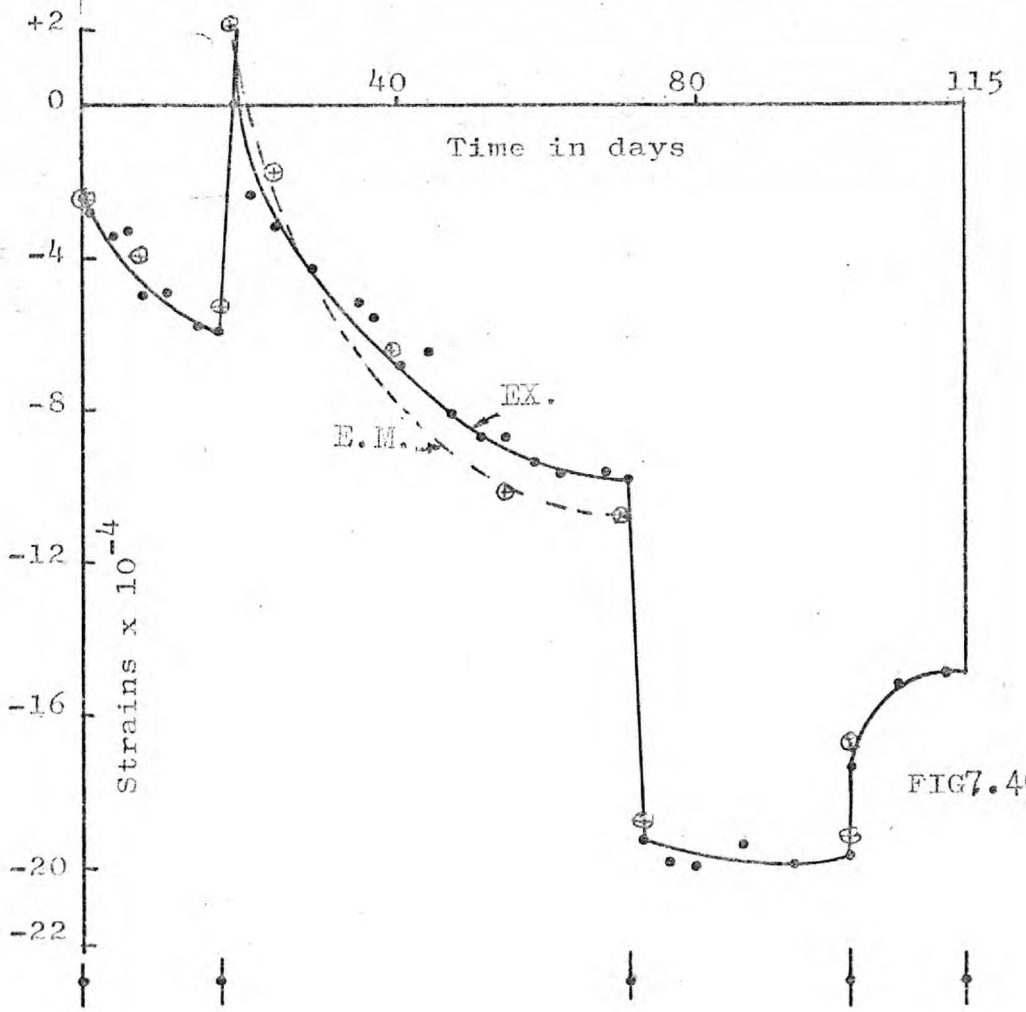

FIG7.40. SERIES 3 RADIAL GROSS STRAINS MODEL 1/2

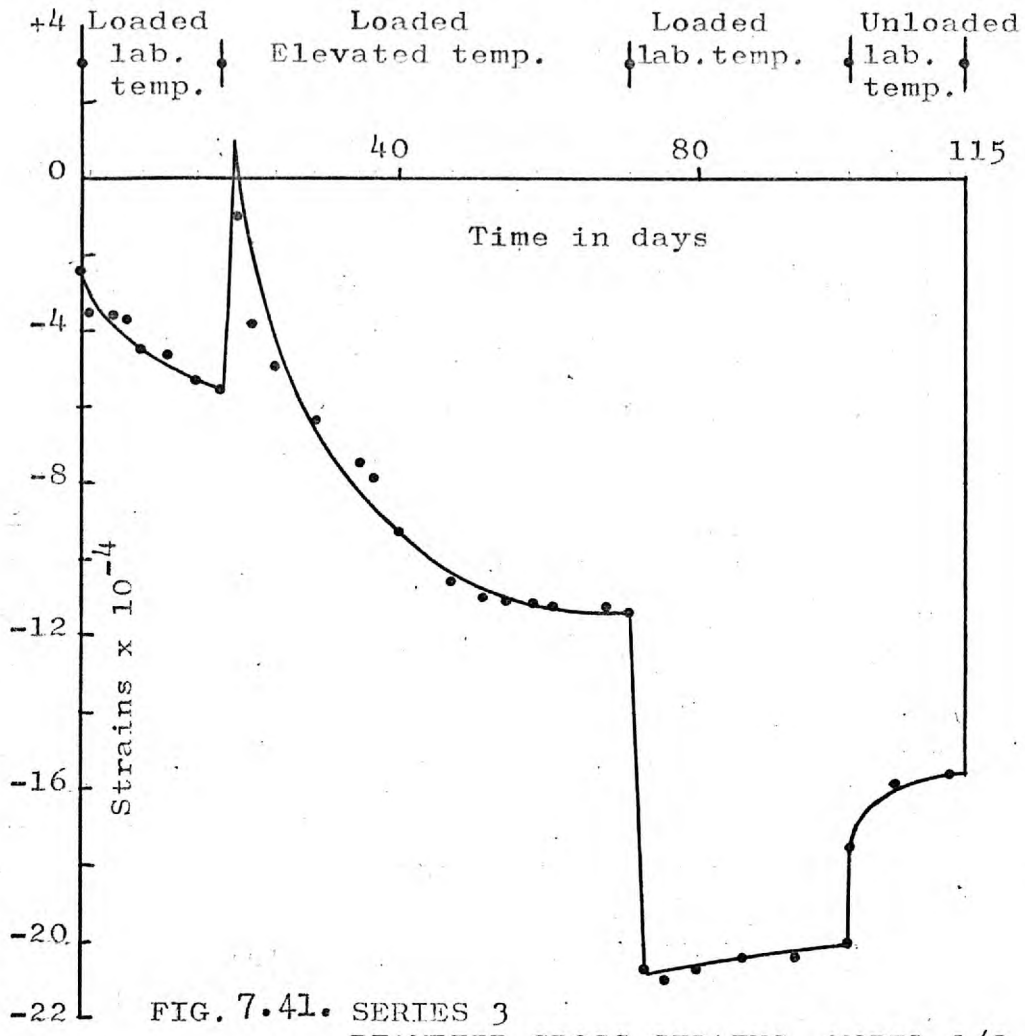

FIG. 7.41. SERIES 3
DIAMETER GROSS STRAINS MODEL 1/2

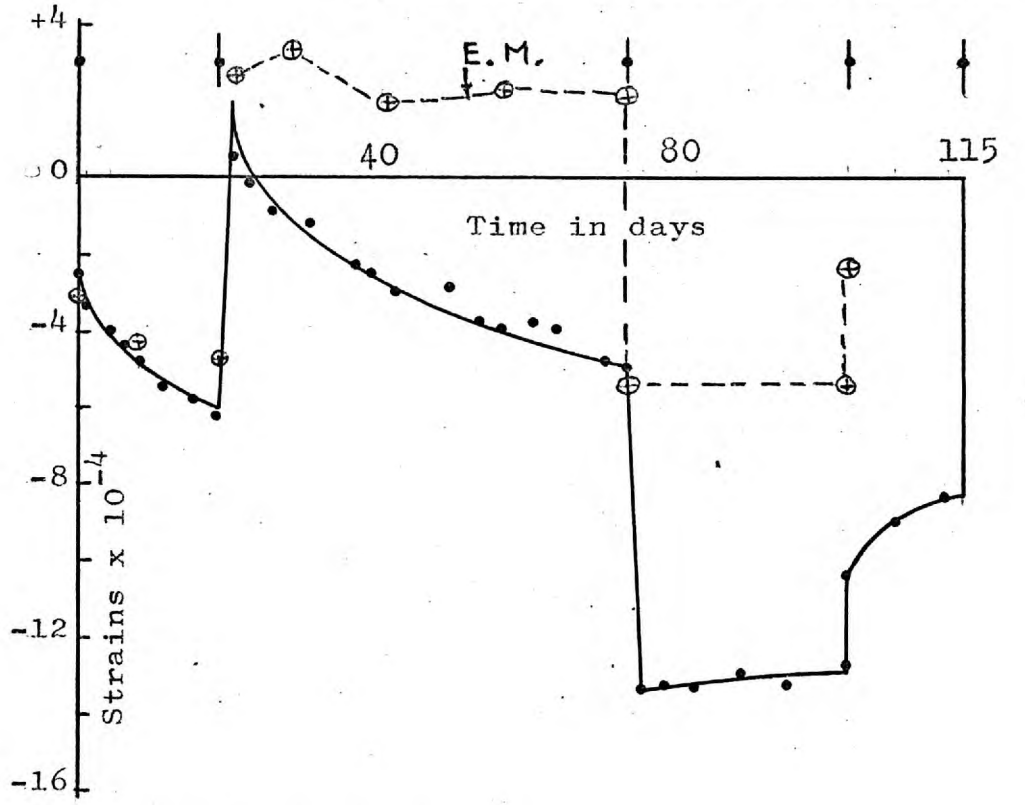

FIG. 7.42. SERIES 3
TANGENTIAL GROSS STRAINS MODEL 3/4

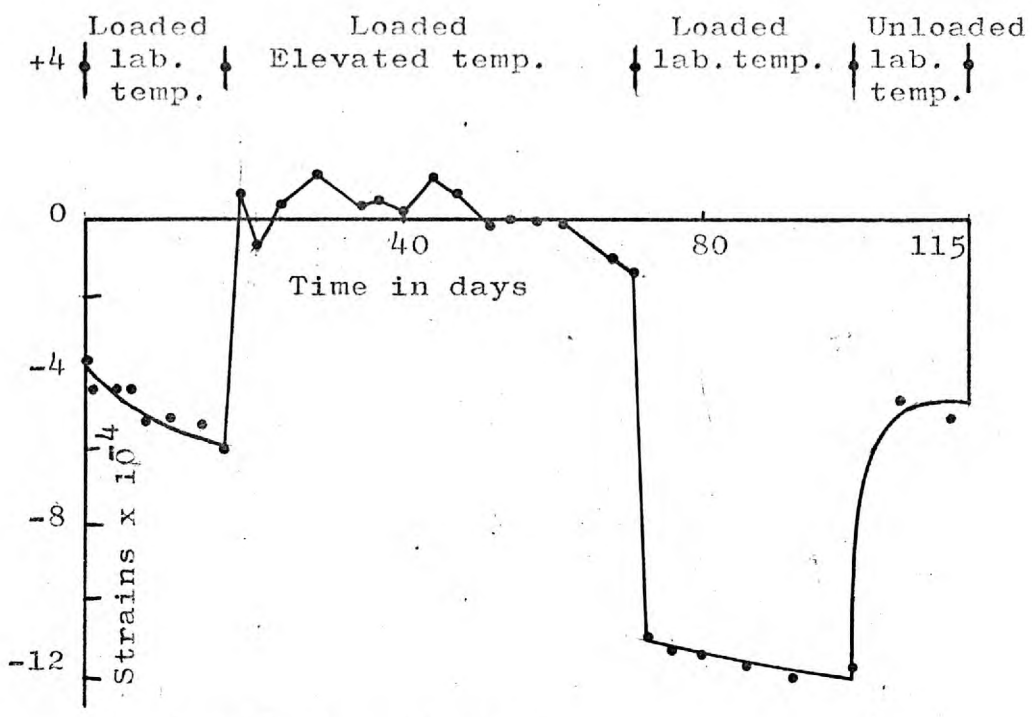

FIG. 7.43. SERIES 3
RADIAL GROSS STRAINS
MODEL 3/4

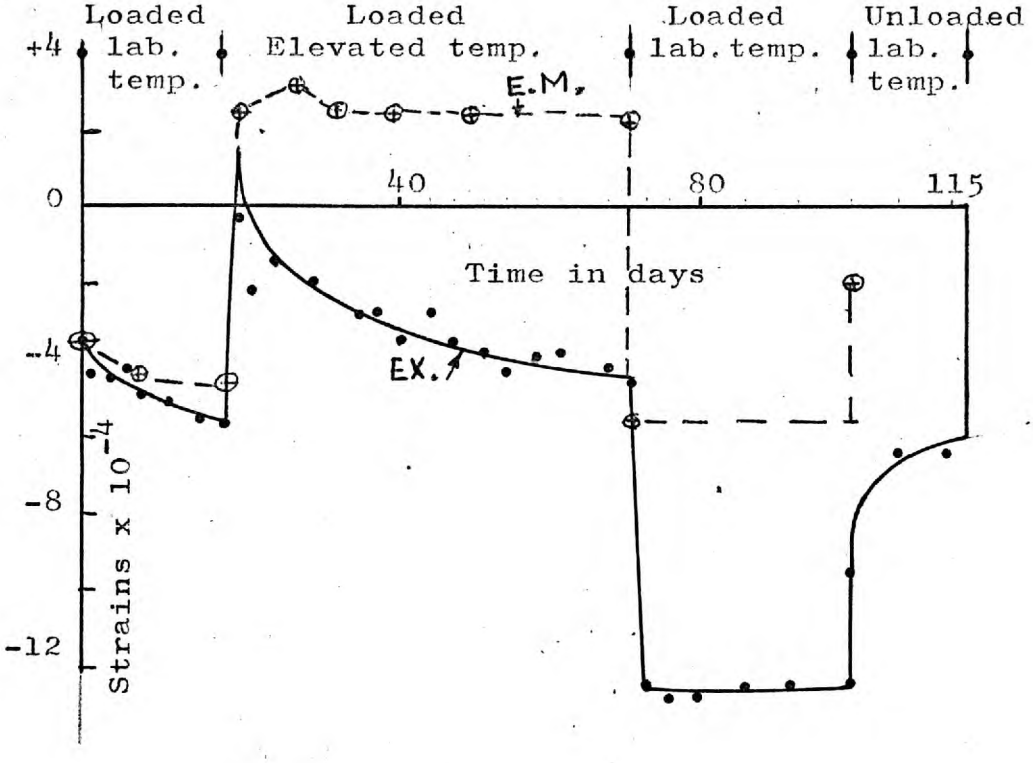

FIG. 7.44. SERIES 3
DIAMETER GROSS STRAINS
MODEL 3/4

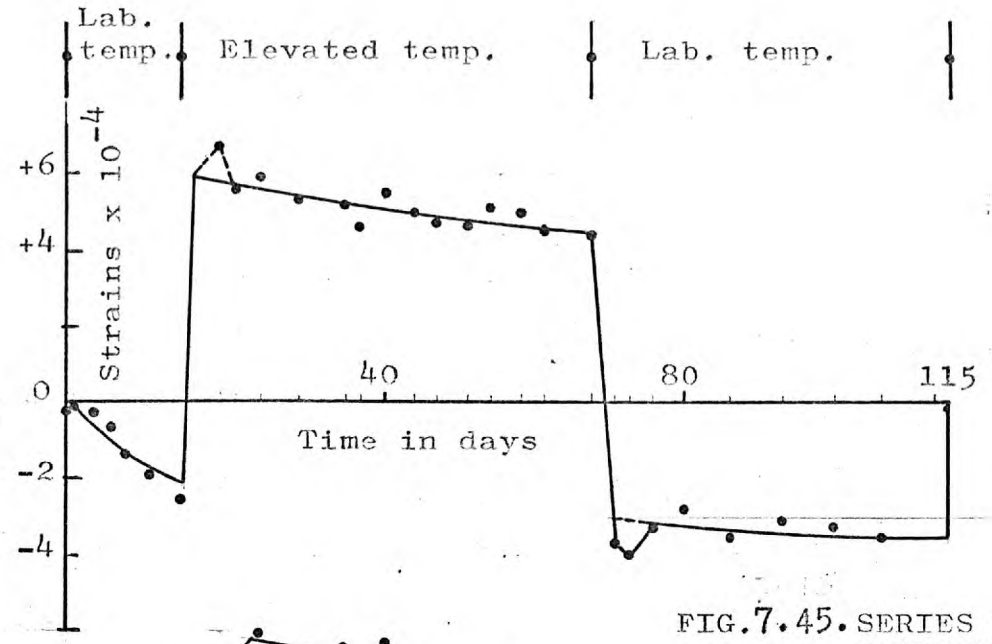

FIG.7.45. SERIES 3
TANGENTIAL SHRINKAGE
AND THERMAL STRAINS
MODEL 5/6

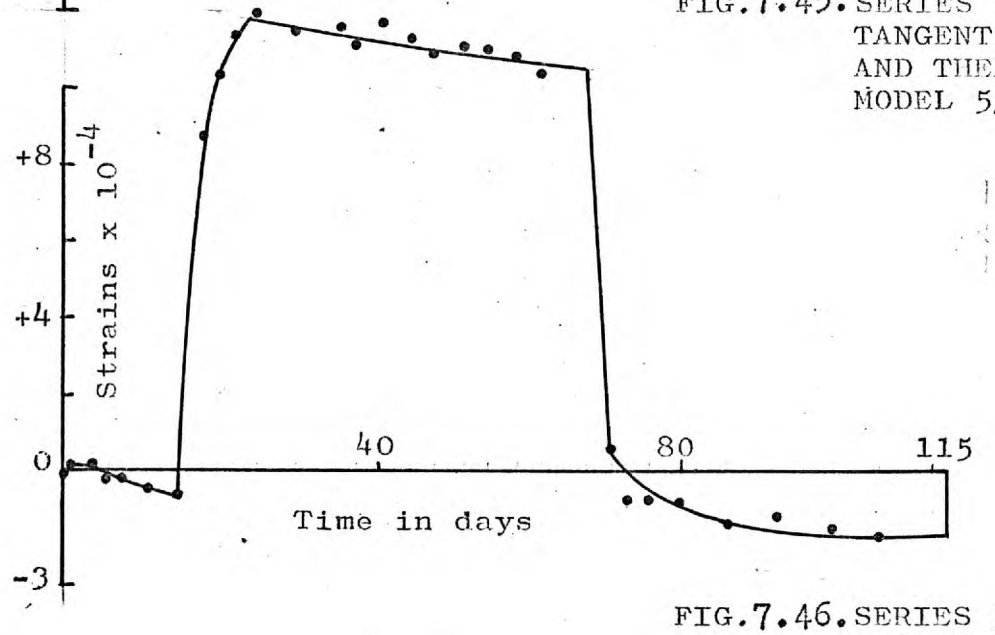

FIG.7.46. SERIES 3
RADIAL SHRINKAGE AND
THERMAL STRAINS
MODEL 5/6

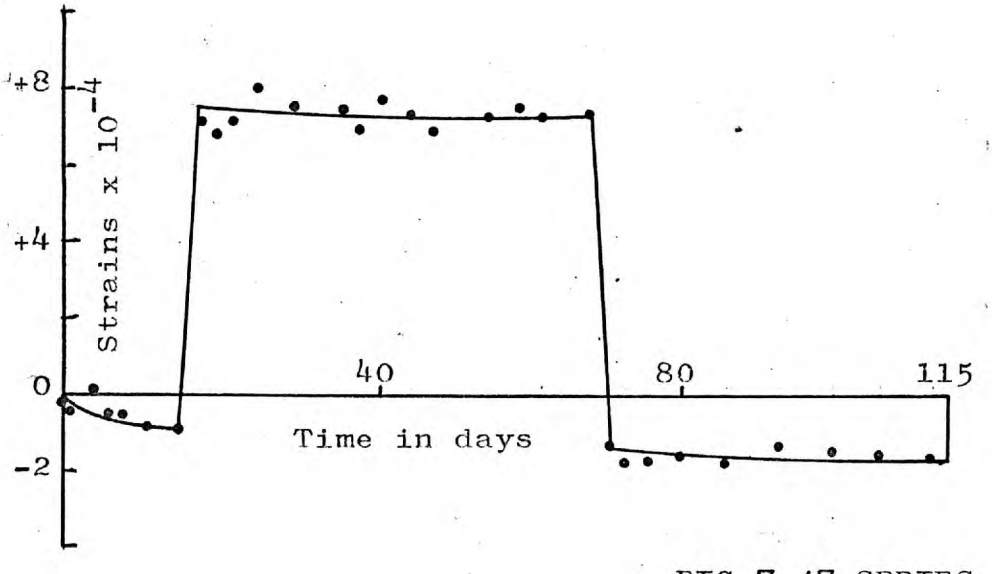

FIG.7.47. SERIES 3
DIAMETER SHRINKAGE
AND THERMAL STRAINS
MODEL 5/6

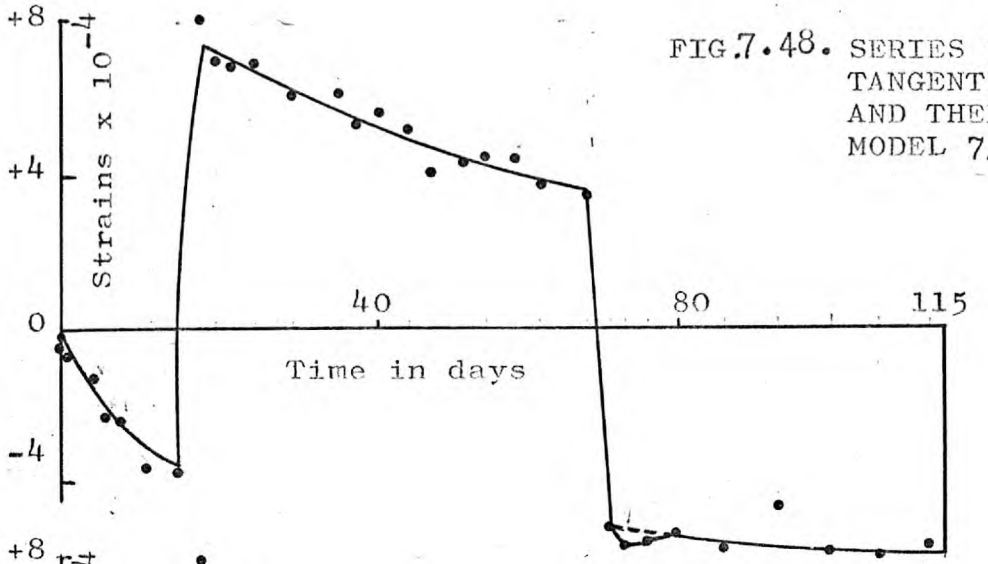

FIG.7.48. SERIES 3
TANGENTIAL SHRINKAGE
AND THERMAL STRAINS
MODEL 7/8

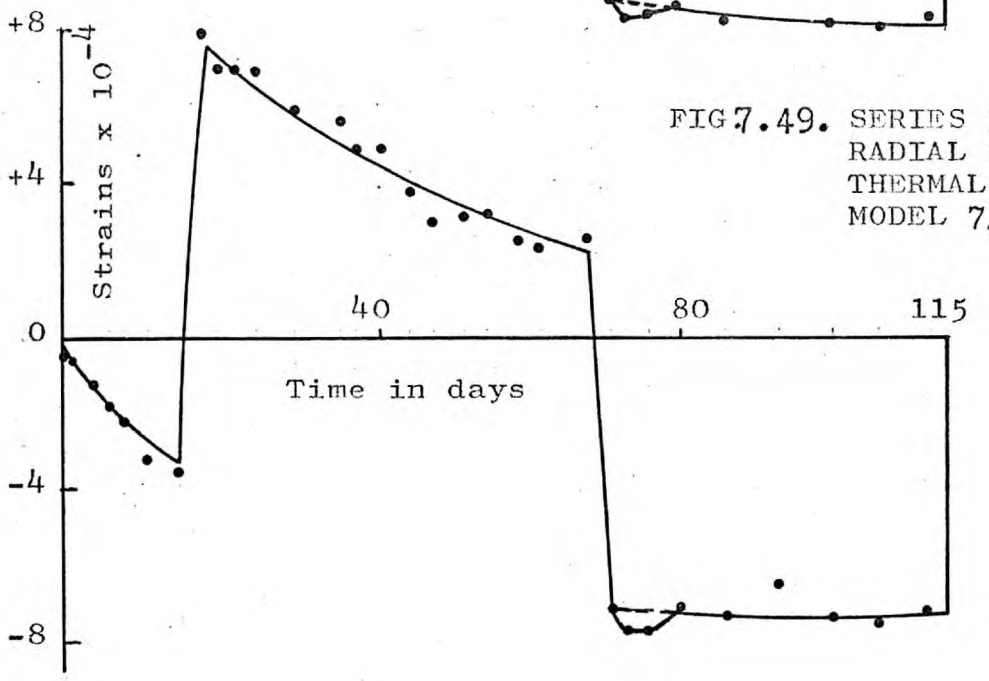

FIG.7.49. SERIES 3
RADIAL SHRINKAGE AND
THERMAL STRAINS
MODEL 7/8

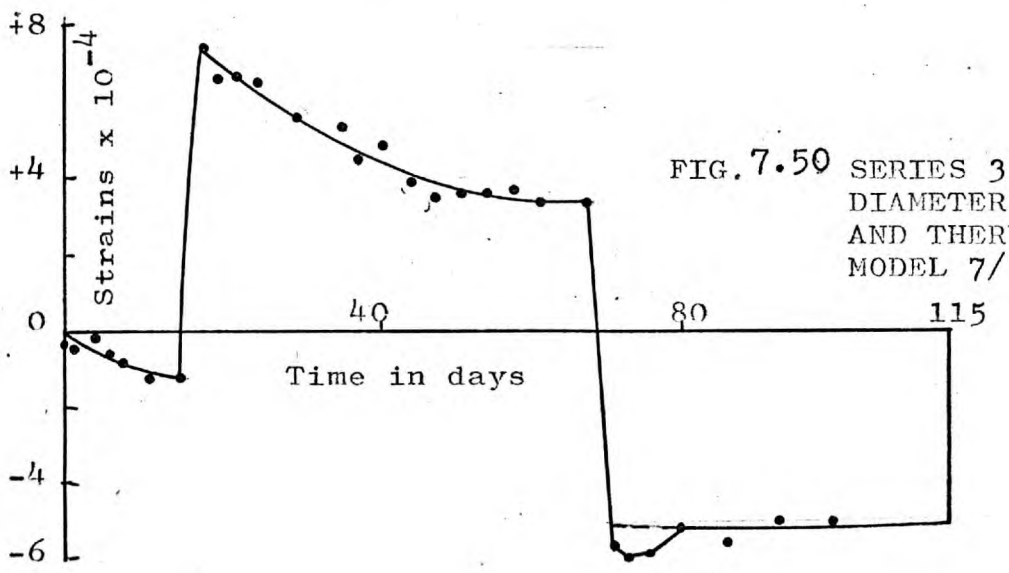

FIG.7.50 SERIES 3
DIAMETER SHRINKAGE
AND THERMAL STRAINS
MODEL 7/8

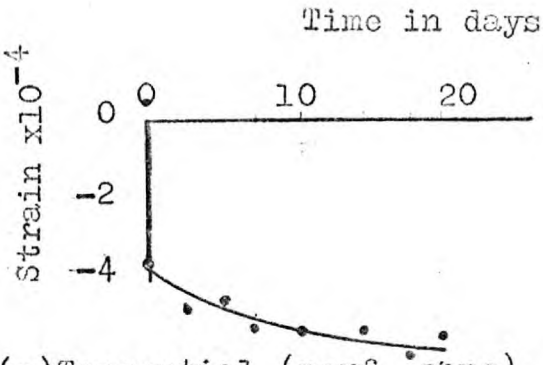

(a)Tangential (perf. zone).

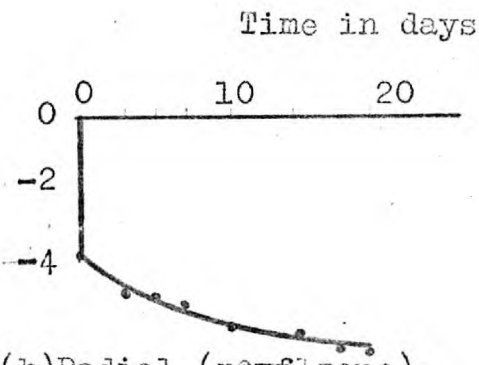

(b)Radial (perf.zone).

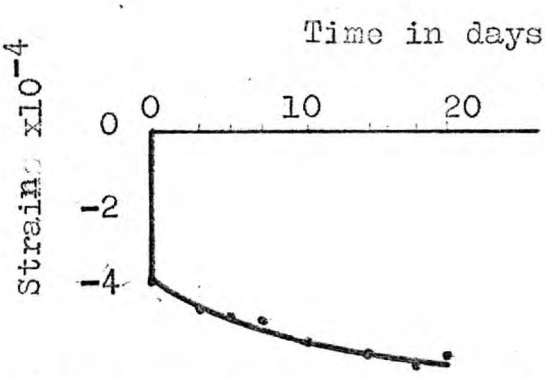

(c)Diametral (perf. zone).

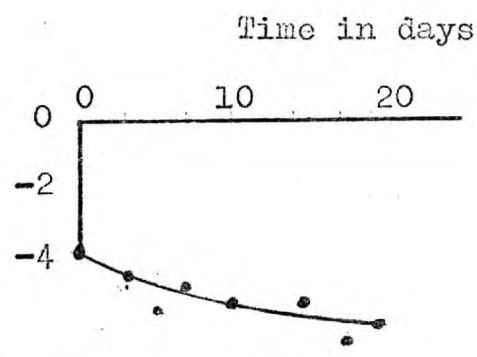

(d)Tangential (outer satelite in annulus).

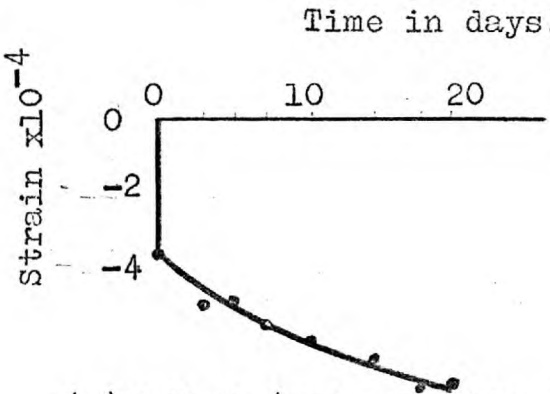

(e)Radial (out satelite in annulus).

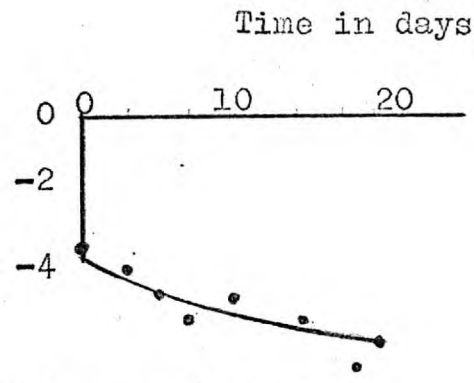

(f)Tangential (inner satelite in annulus).

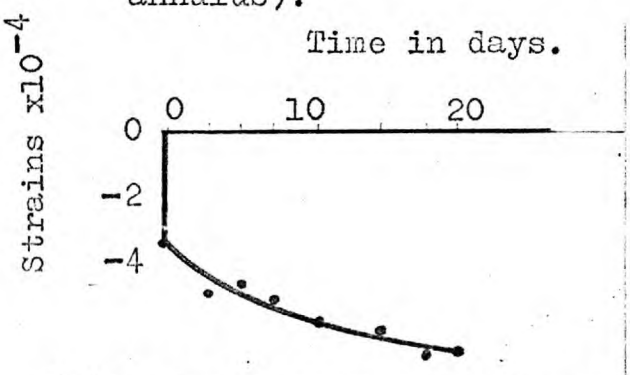

(g)Radial (inner satelite in annulus).

Fig.751 . Series 3.
Experimental gross strains
Composite Specimen(Model9/10)

On application of heat the pressure circuit failed, and the specimen cracked.

Test not completed.

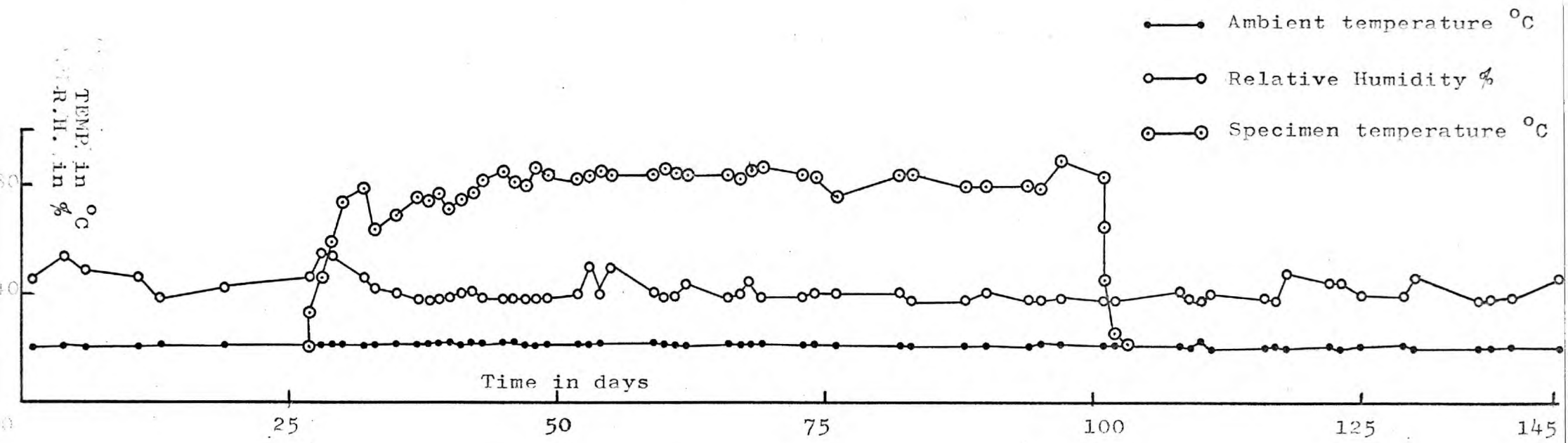

FIG. 7.52 SERIES 1
MODEL 1/2 TEMPERATURE AND RELATIVE HUMIDITY

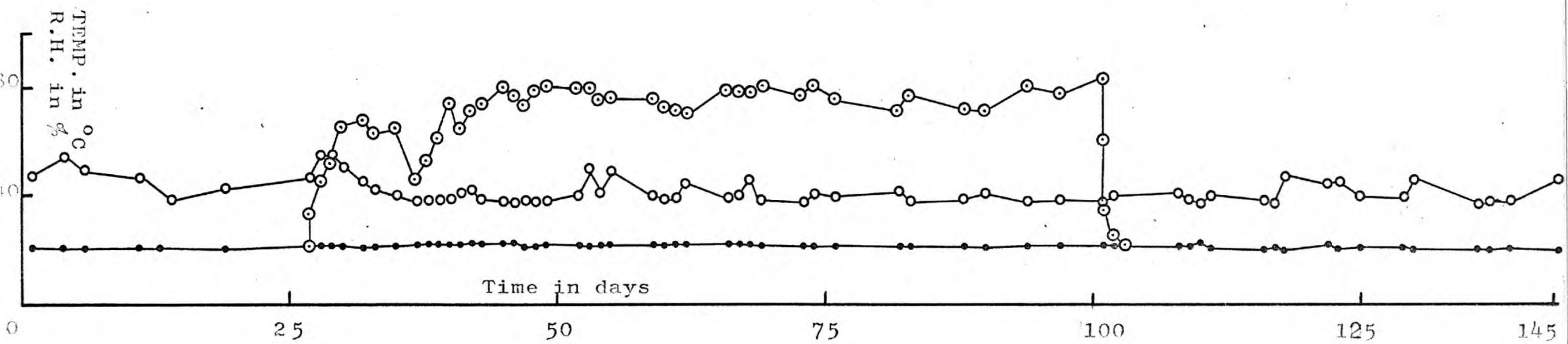

FIG. 7.53 SERIES 1
MODEL 3/4, TEMPERATURE AND RELATIVE HUMIDITY

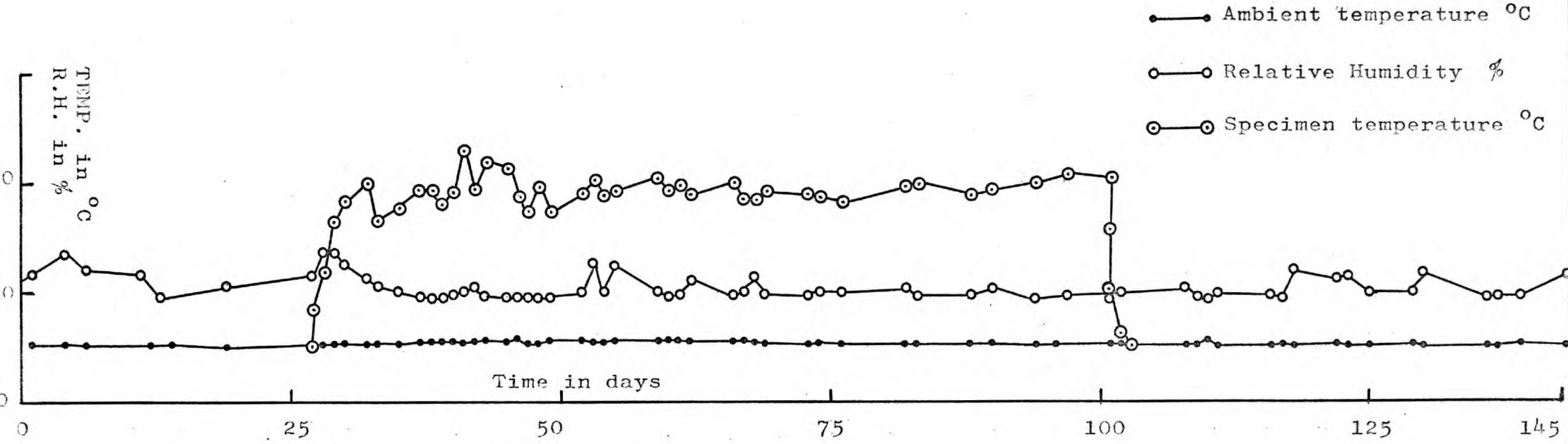

FIG. 7.54 SERIES 1
MODEL 5/6, TEMPERATURE AND RELATIVE HUMIDITY

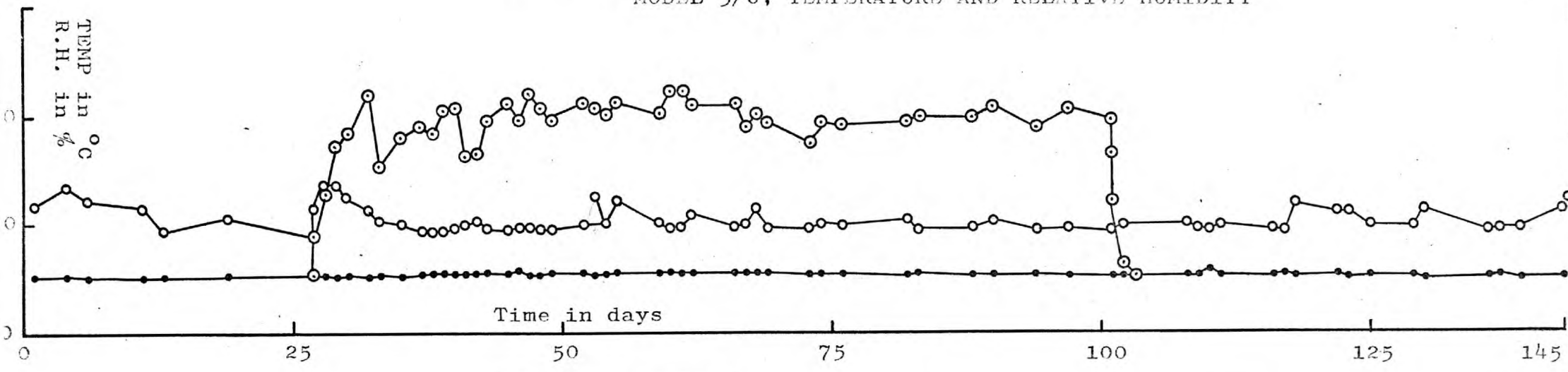

FIG. 7.55 SERIES 1
MODEL 7/8, TEMPERATURE AND RELATIVE HUMIDITY

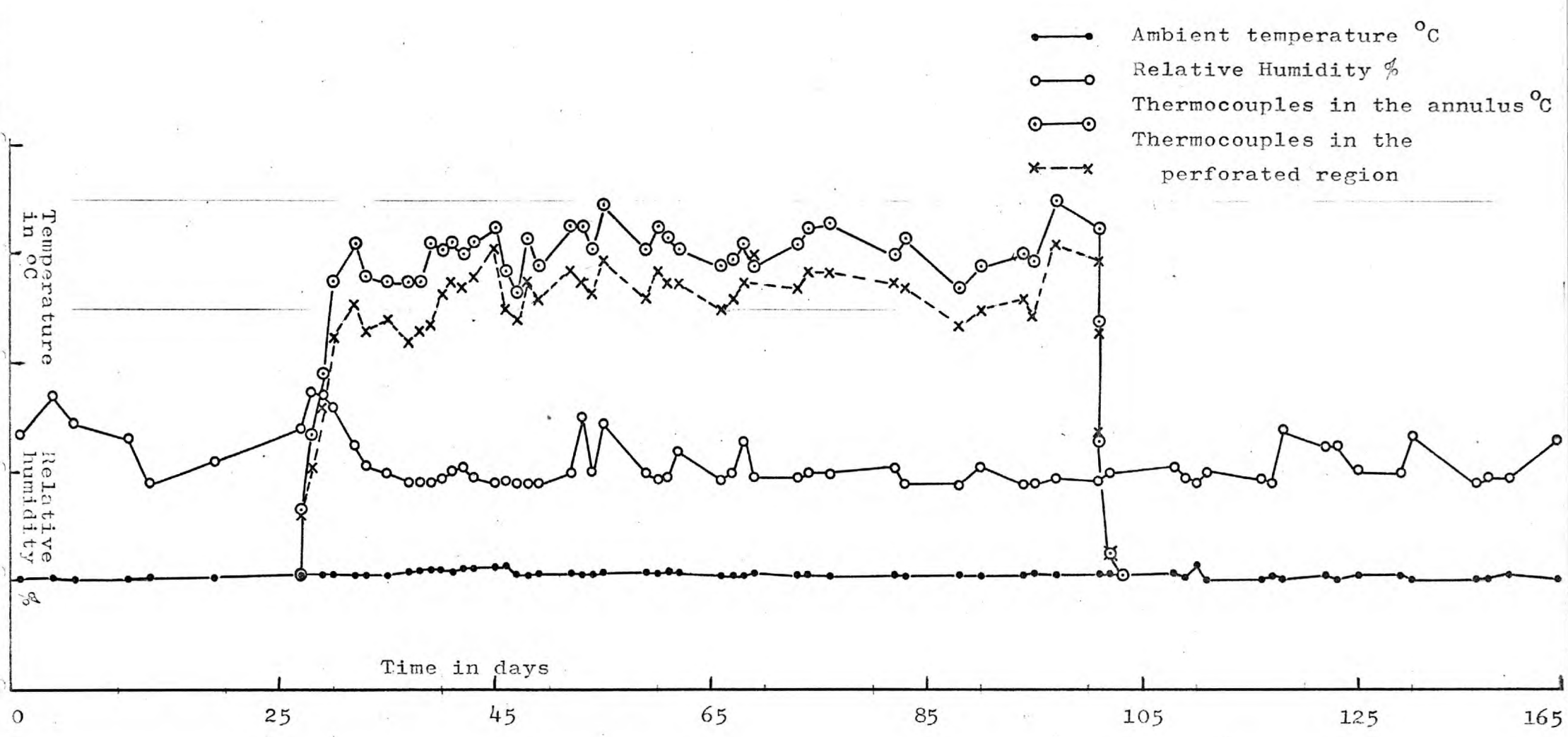

FIG. 7.56 SERIES 1
MODEL 9/10 COMPOSITE CREEP SPECIMEN

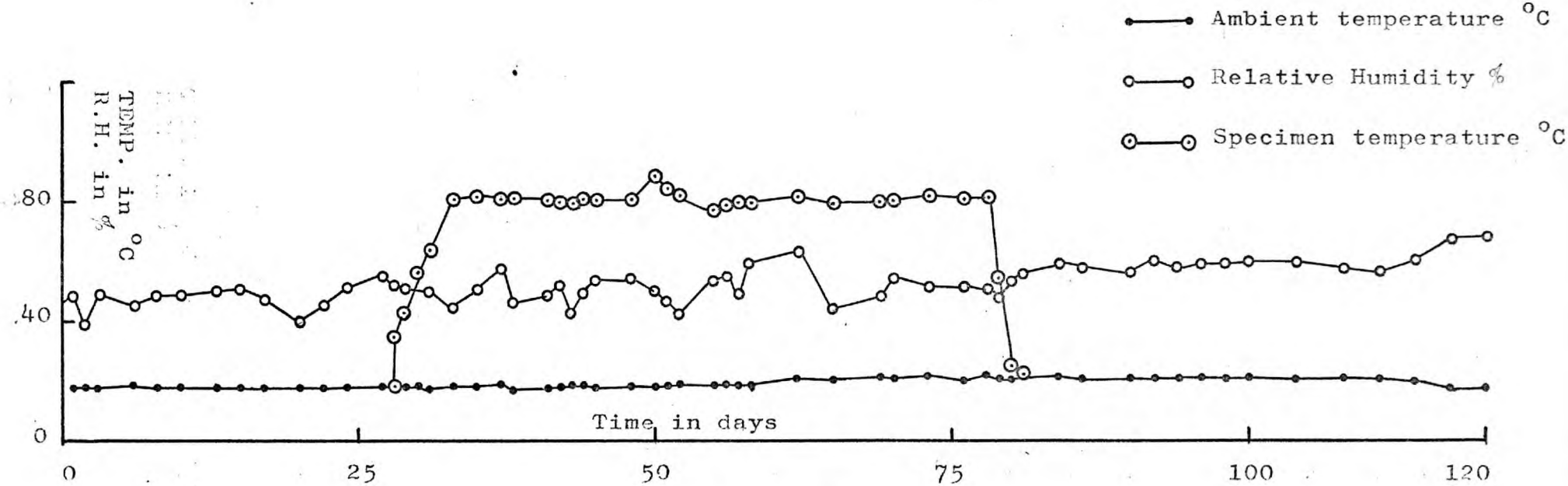

FIG. 7.57 SERIES 2
MODEL 1/2, TEMPERATURE AND RELATIVE HUMIDITY

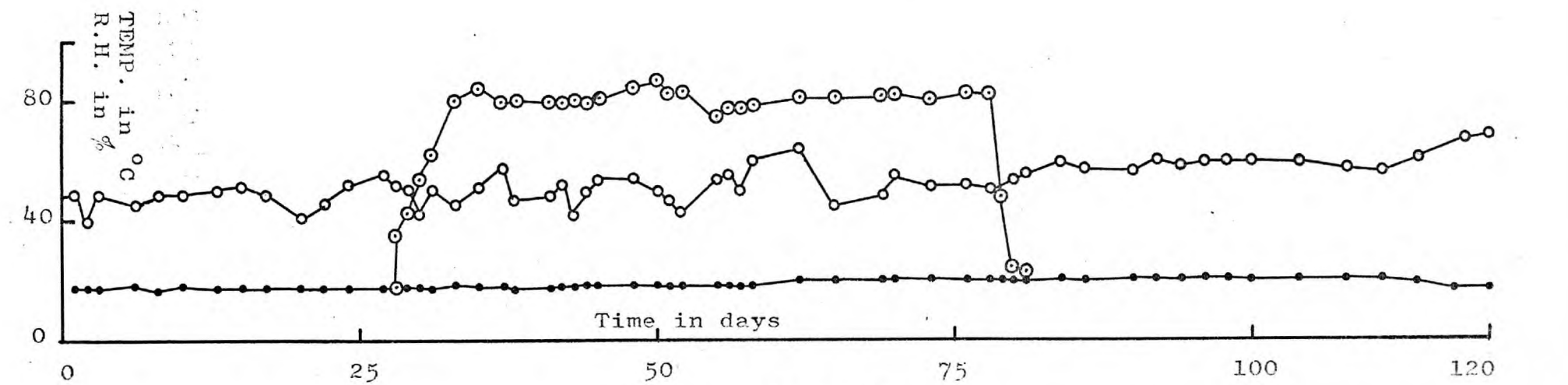

FIG. 7.58 SERIES 2
MODEL 3/4, TEMPERATURE AND RELATIVE HUMIDITY

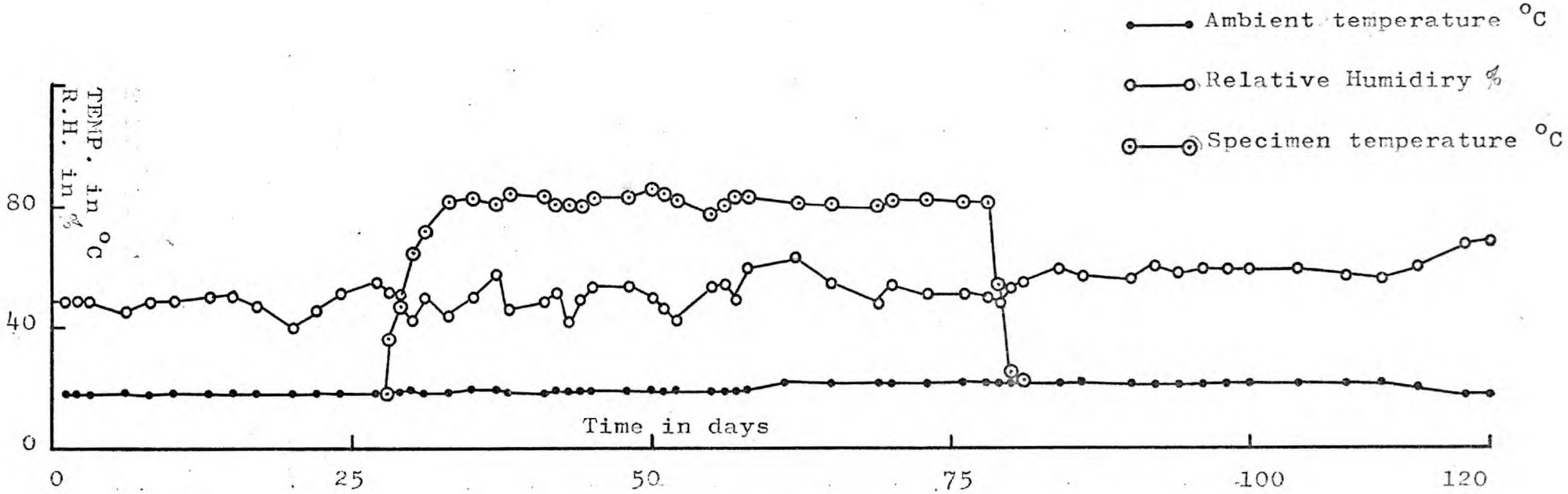

FIG. 7.59 SERIES 2
MODEL 5/6, TEMPERATURE AND RELATIVE HUMIDITY

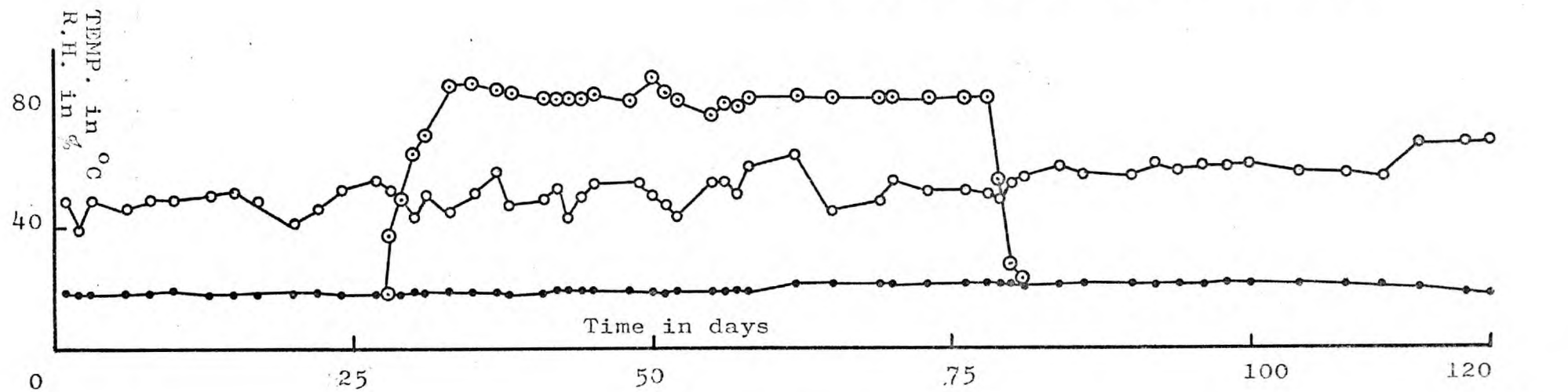

FIG. 7.60 SERIES 2
MODEL 7/8, TEMPERATURE AND RELATIVE HUMIDITY

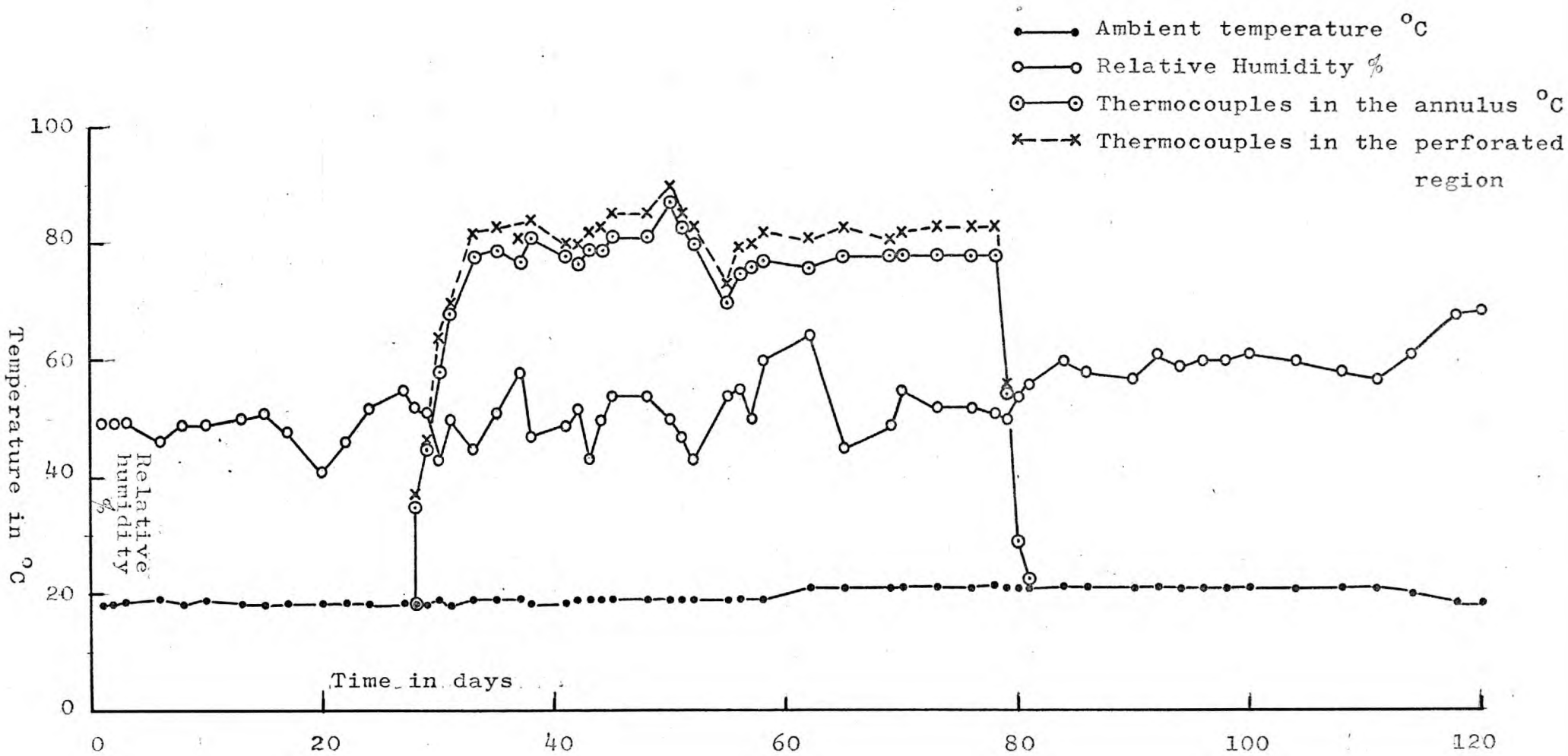

FIG. 7.61 SERIES 2
MODEL 9/10 COMPOSITE CREEP SPECIMEN

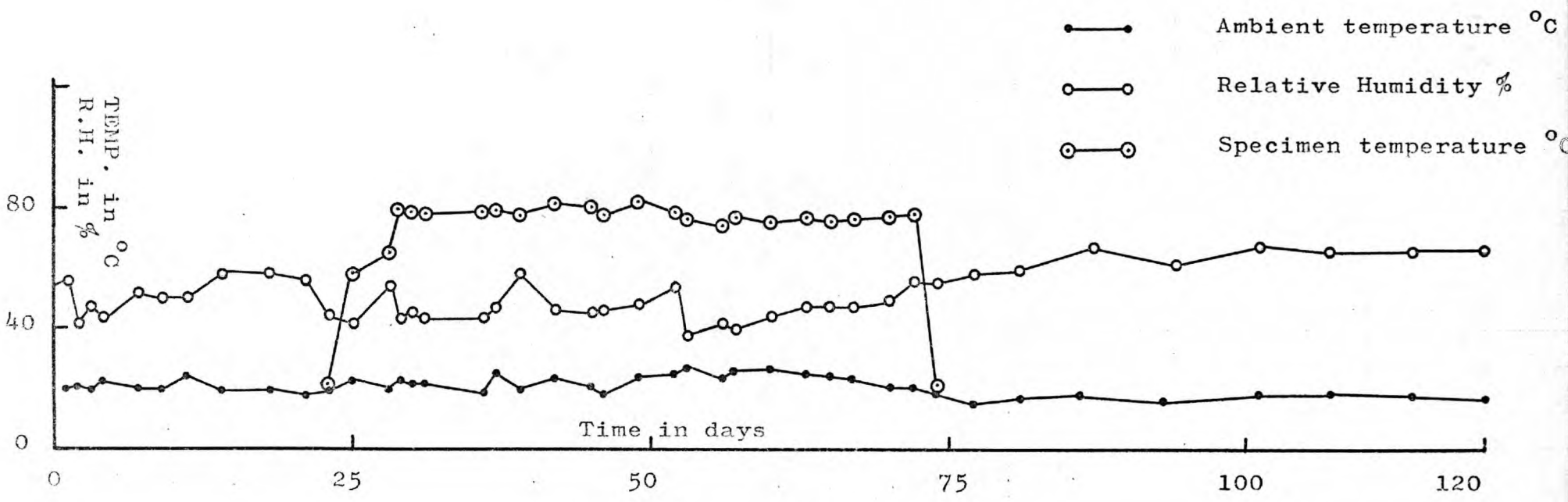

FIG. 7.62 SERIES 3
MODEL 1/2, TEMPERATURE AND RELATIVE HUMIDITY

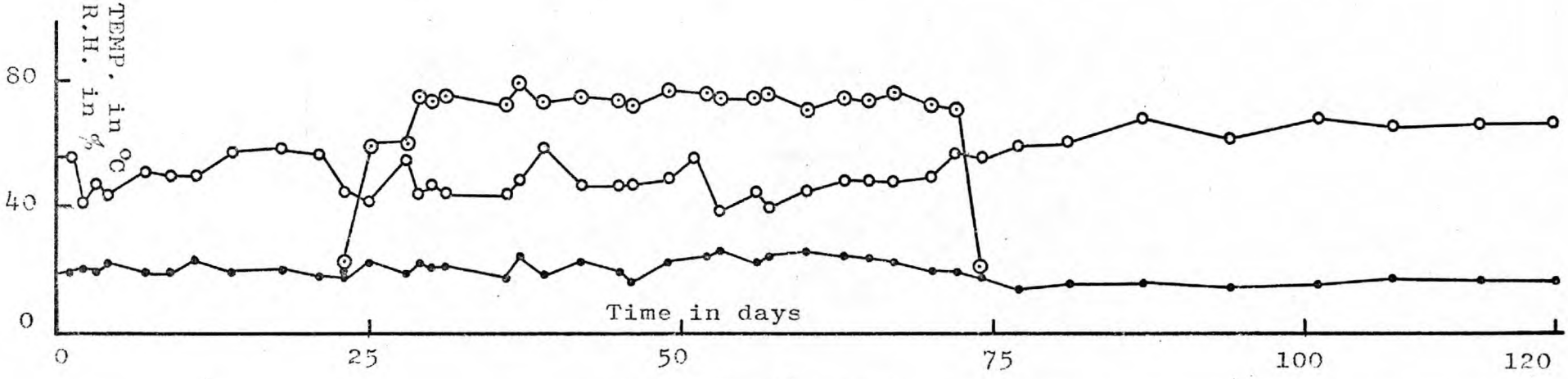

FIG. 7.63 SERIES 3
MODEL 3/4, TEMPERATURE AND RELATIVE HUMIDITY

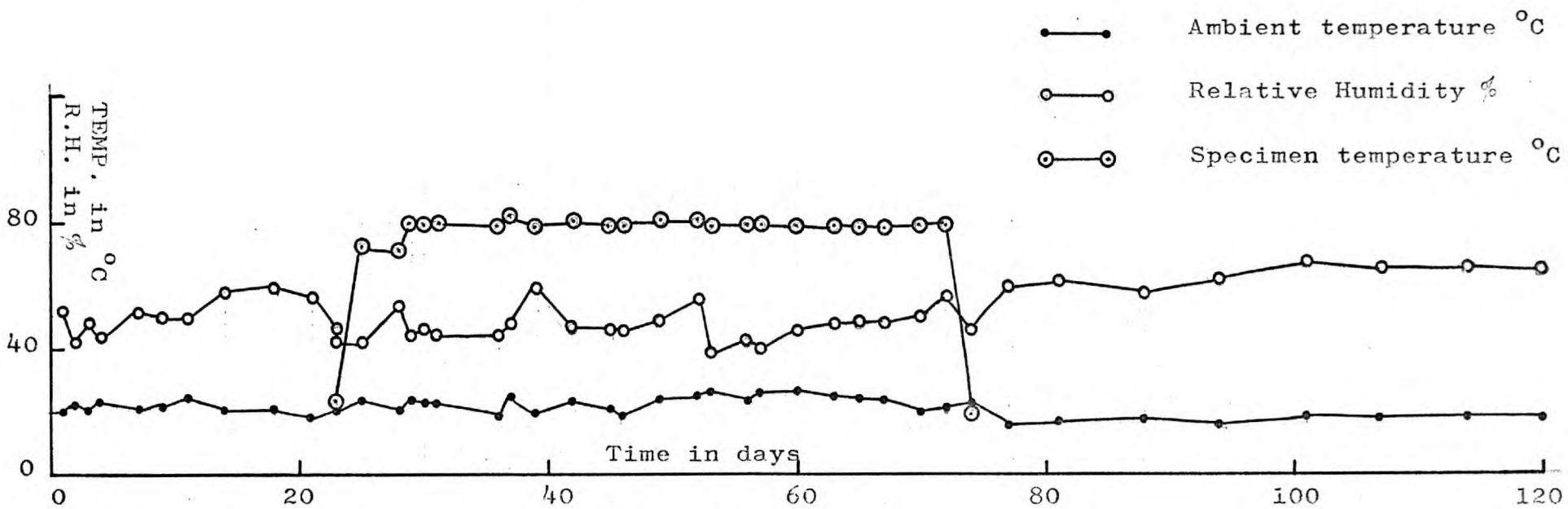

FIG. 764 SERIES 3
MODEL 5/6, TEMPERATURE AND RELATIVE HUMIDITY

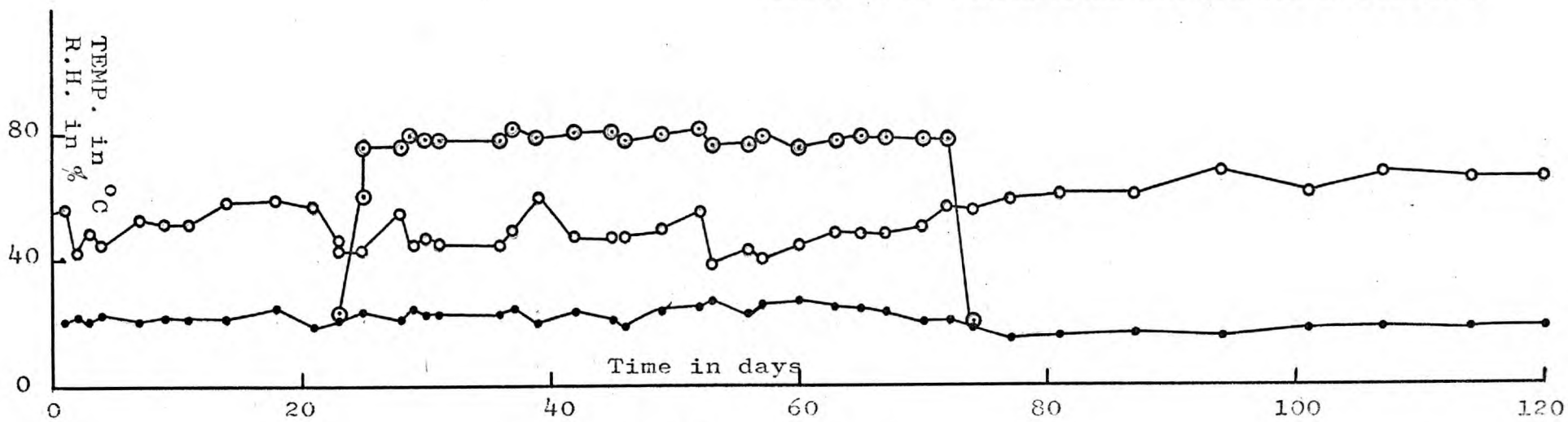

FIG. 765 SERIES 3
MODEL 7/8, TEMPERATURE AND RELATIVE HUMIDITY

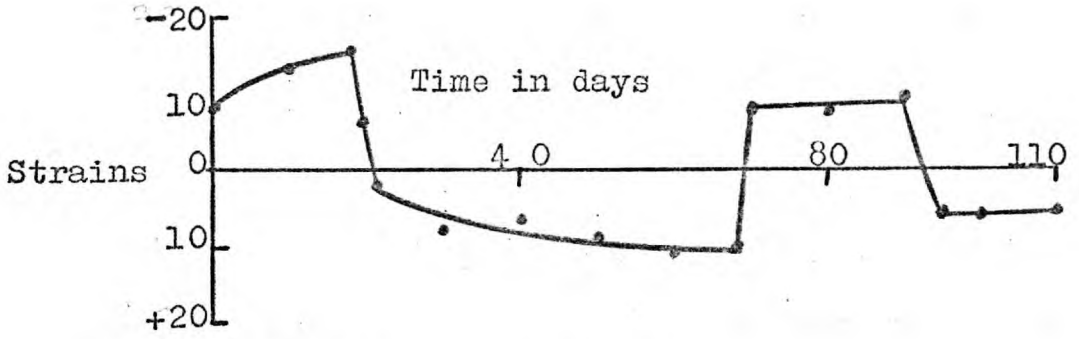

FIG. 7.66. Series 2:
Standpipe strains at positions
1/2, 3/4, 9/10, 11/12: (Fig.5.8).
Model 3/4:

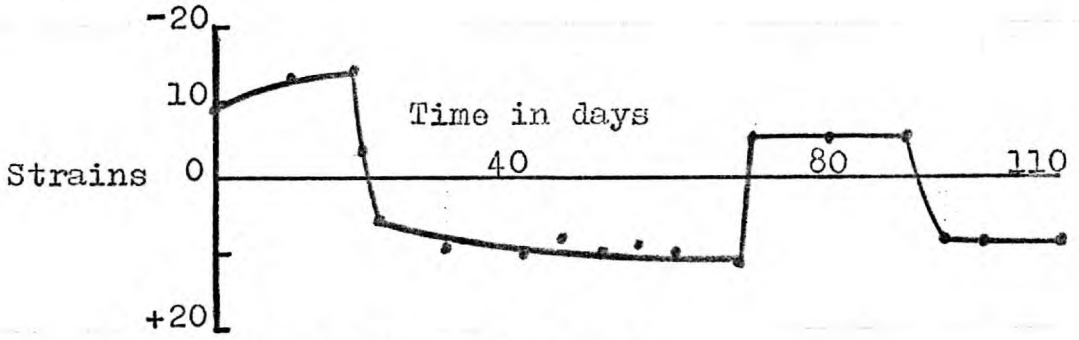

FIG. 7.67. Series 2:
Standpipe strains at positions
5/6, 13/14: (Fig.5.8).
Model 3/4:

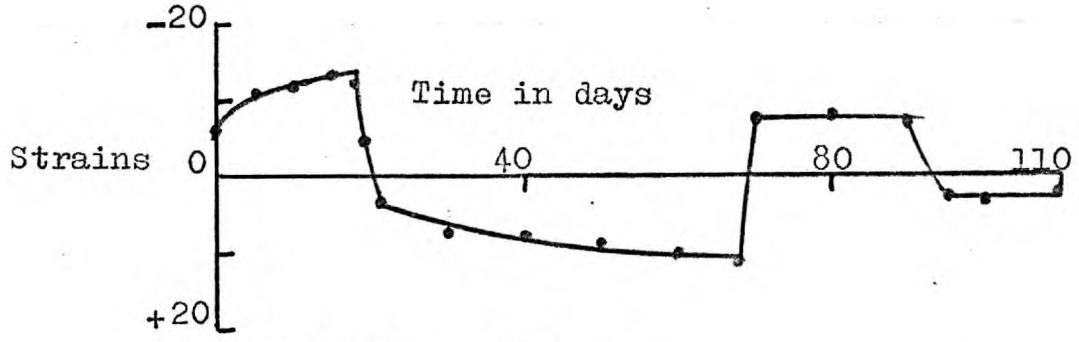

FIG. 7.68. Series 2:
Standpipe strains at positions
7/8, 15/16: (Fig.5.8.).
Model 3/4:

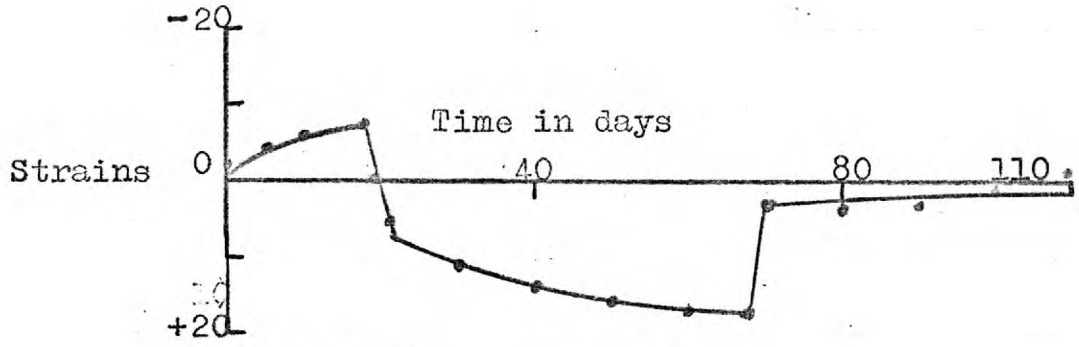

FIG. 7.69. Series 2:
Standpipe strains at positions
33/34, 35/36, 41/42, 43/44: (Fig. 5.10).
Model 5/6:

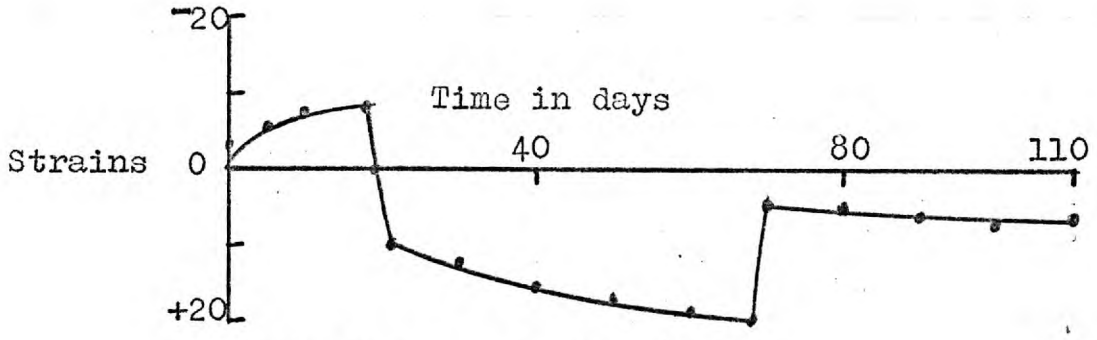

FIG. 7.70. Series 2:
Standpipe strains at positions
37/38, 45/46: (Fig. 5.10).
Model 5/6:

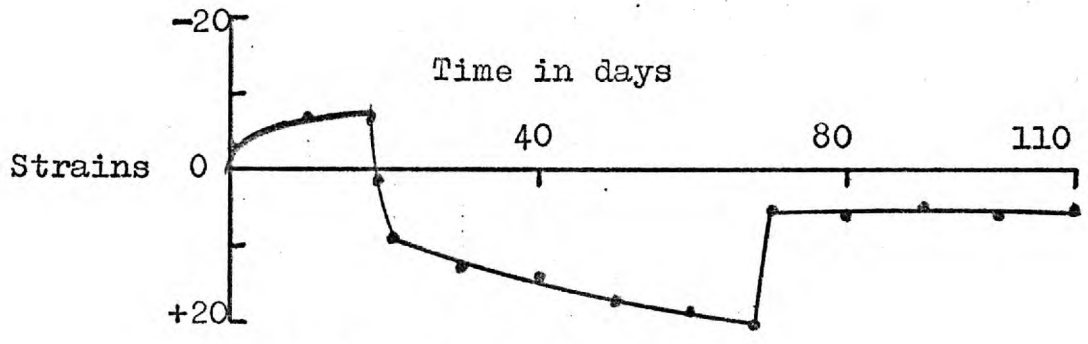

FIG. 7.71. Series 2:
Standpipe strains at positions
39/40, 47/48: (Fig. 5.10).
Model 5/6:

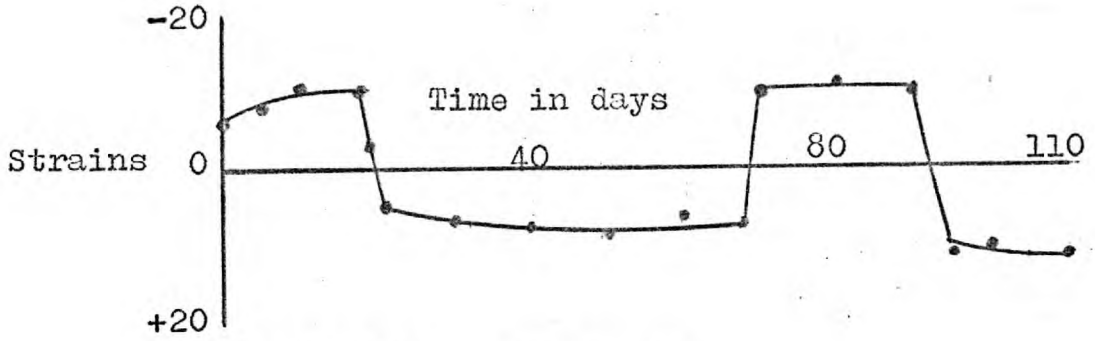

FIG. 7.72. Series 2:
Standpipe strains at positions
65/66, 67/68, 73/74, 75/76:(Fig.5.14).
Model 9/10:

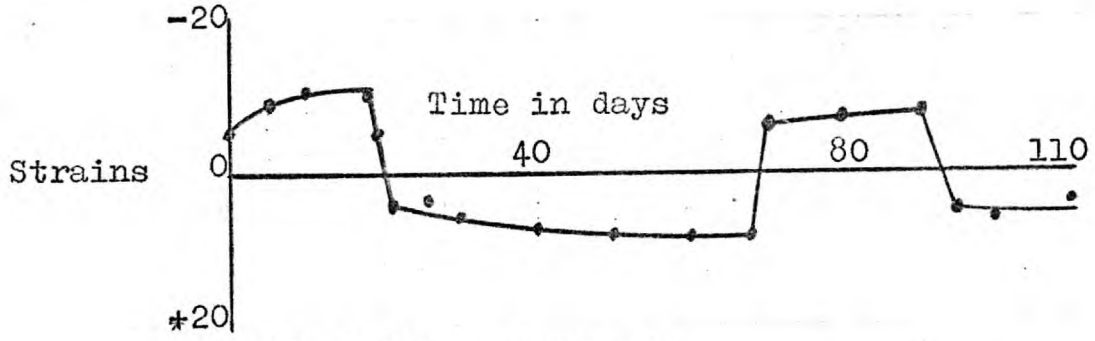

FIG. 7.73. Series 2:
Standpipe strains at positions
69/70, 77/78: (Fig. 5.14).
Model 9/10:

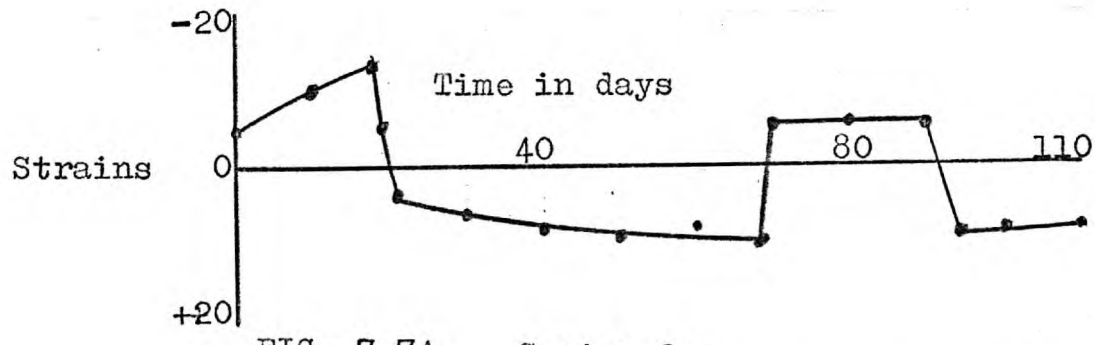

FIG. 7.74. Series 2:
Standpipe strains at positions
71/72, 79/80: (Fig. 5.14).
Model 9/10:

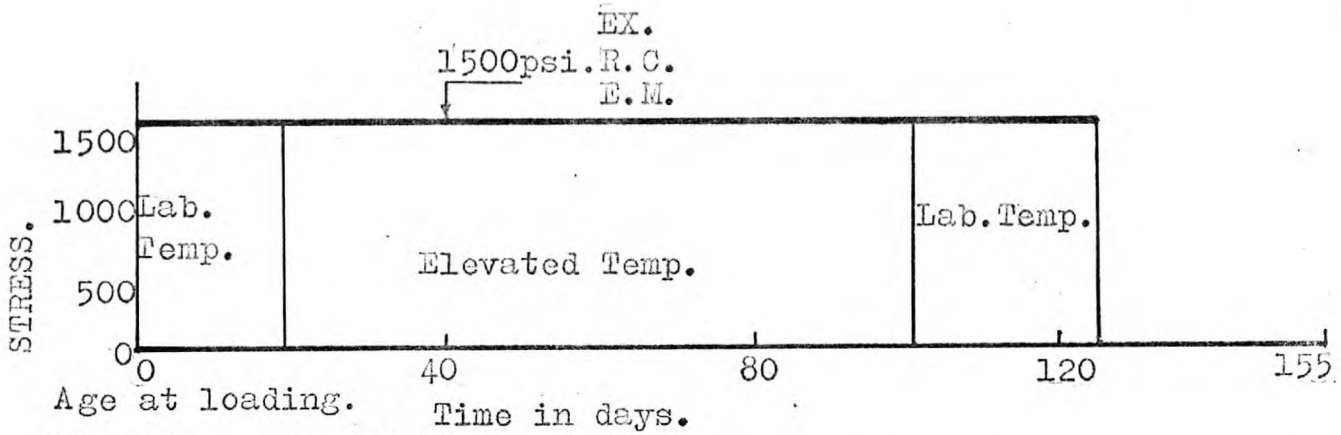

21 weeks. Fig.7.75. Series 1:
Experimental and predicted stress-time curves (radial and tangential) for solid specimen (Model 1/2).

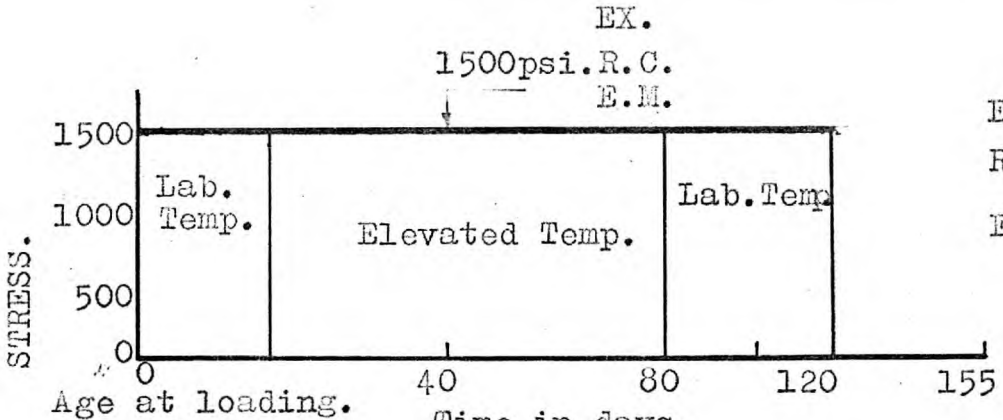

EX.= Experimental.
R.C.=Rate of creep method.
E.M.=Effective modulus method.

7 weeks. Fig.7.76. Series 2:
Experimental and predicted stress-time curves (radial and tangential) for solid specimen (Model 1/2).

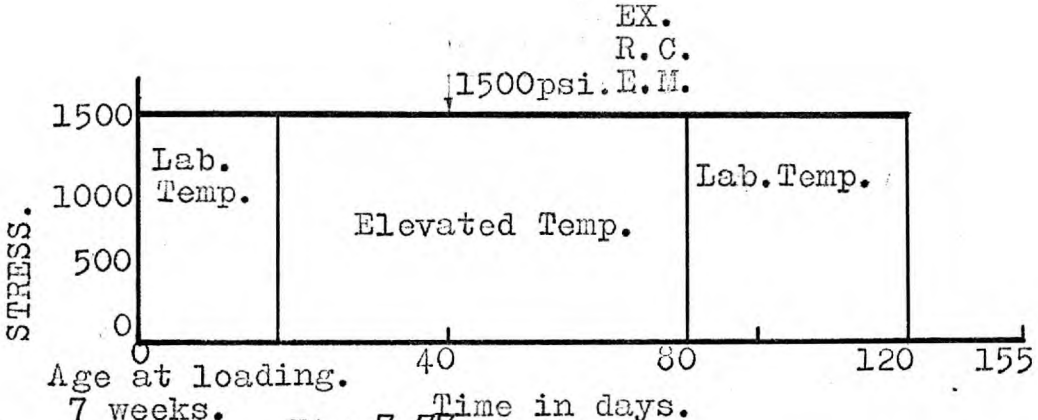

7 weeks. Fig.7.77. Series 3:
Experimental and predicted stress-time curves (radial and tangential) for solid specimen (model 1/2).

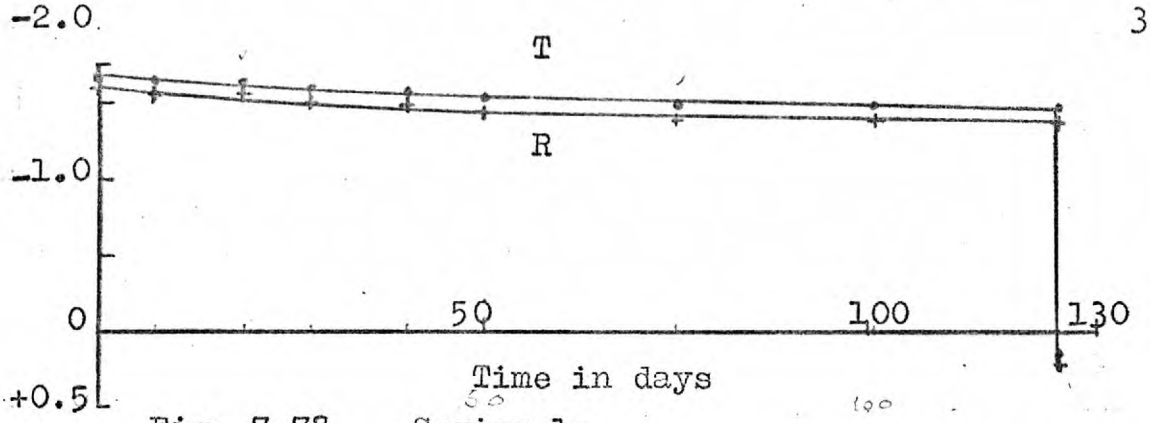

Fig. 7.78. Series 1:
Tangential and radial stresses - R.C.,method.
Position 1 - Composite Specimen:

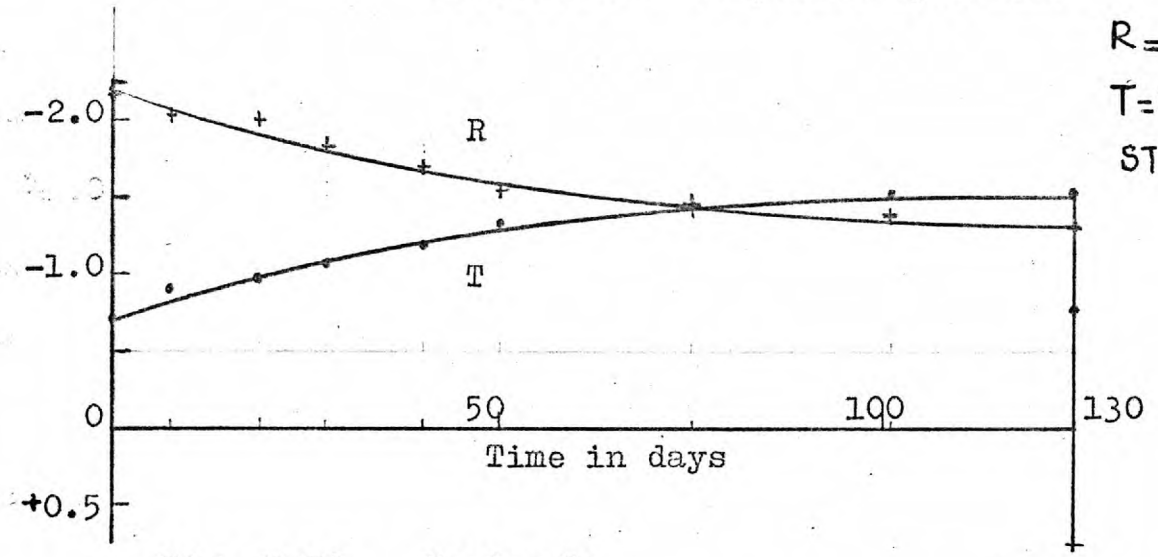

Fig. 7.79. Series 1:
Tangential and radial stresses - R.C.,method.
Position 2 - Composite Specimen:

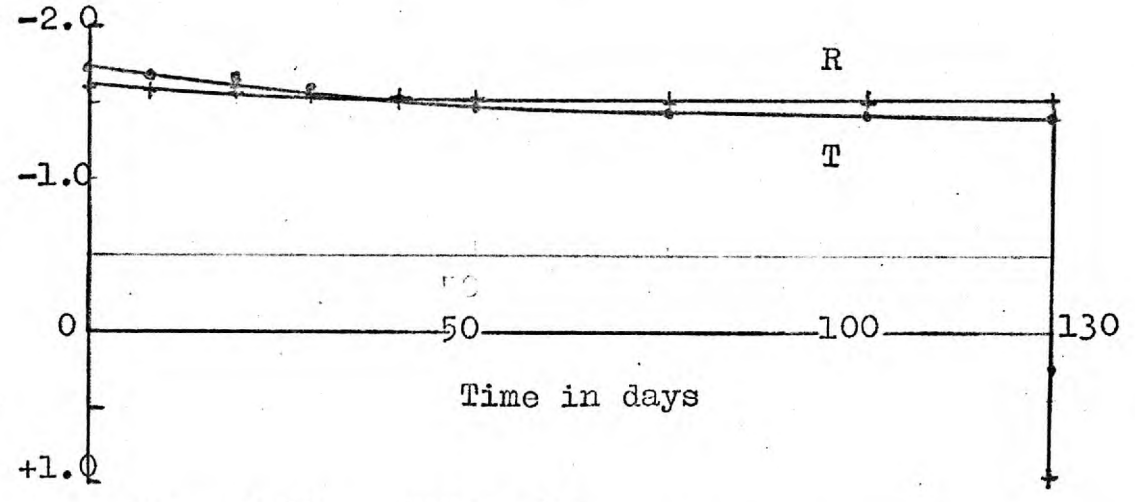

Fig. 7.80. Series 1:
Tangential and radial stresses - R.C.,method.
Position 3 - Composite Specimen:

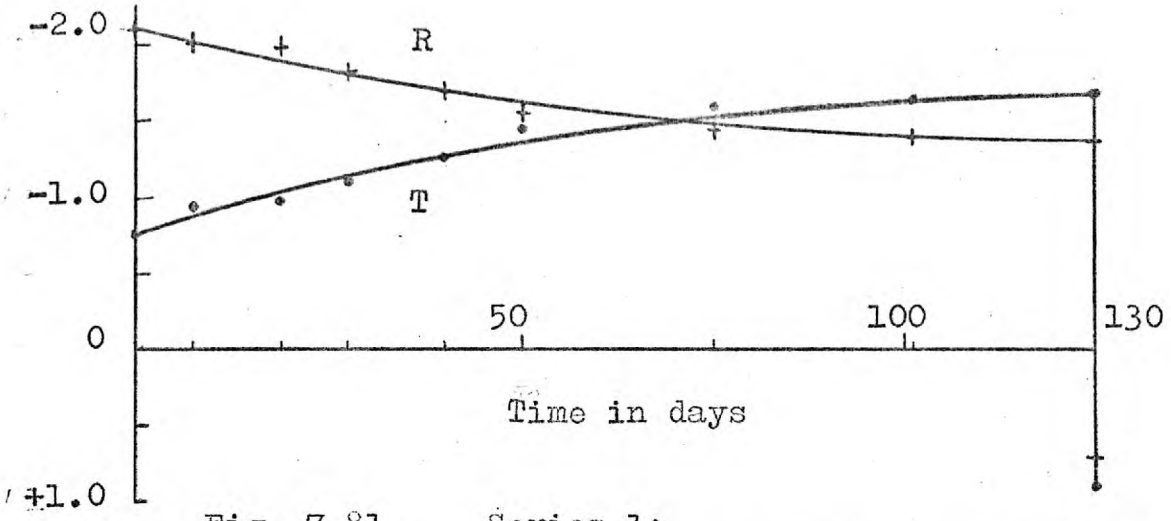

Fig. 7.81. Series 1:
Tangential and radial stresses - R.C.,method.
Position 4 - Composite Specimen:

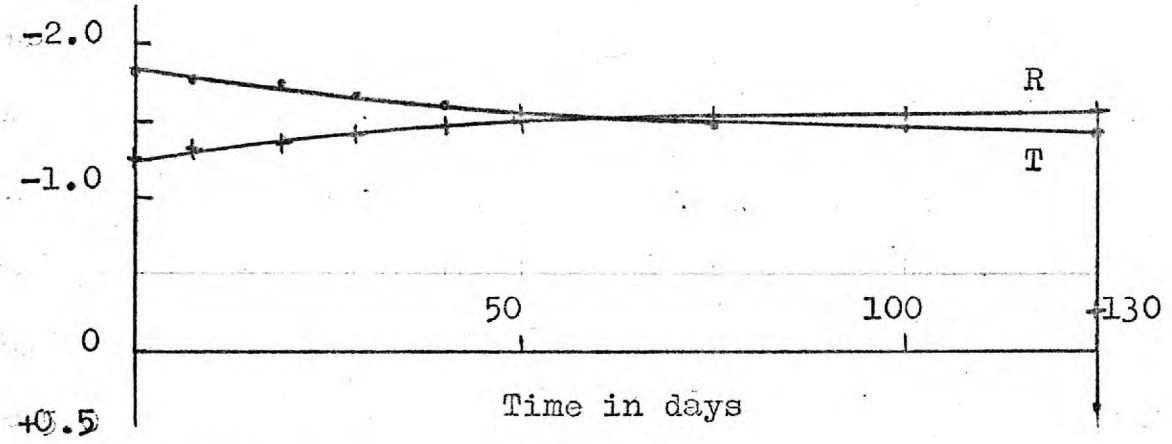

Fig. 7.82. Series 1:
Tangential and radial stresses - R.C.,method.
Position 5 - Composite Specimen:

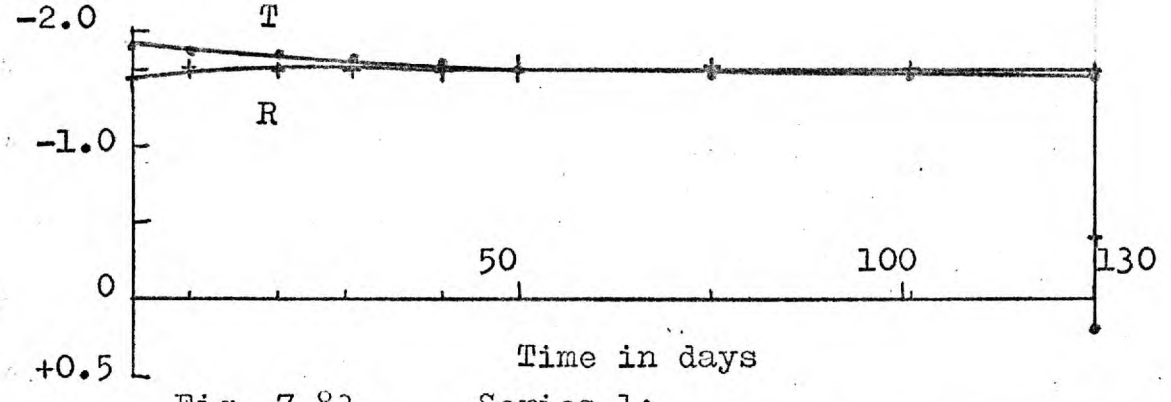

Fig. 7.83. Series 1:
Tangential and radial stresses - R.C.,method.
Position 6 - Composite Specimen:

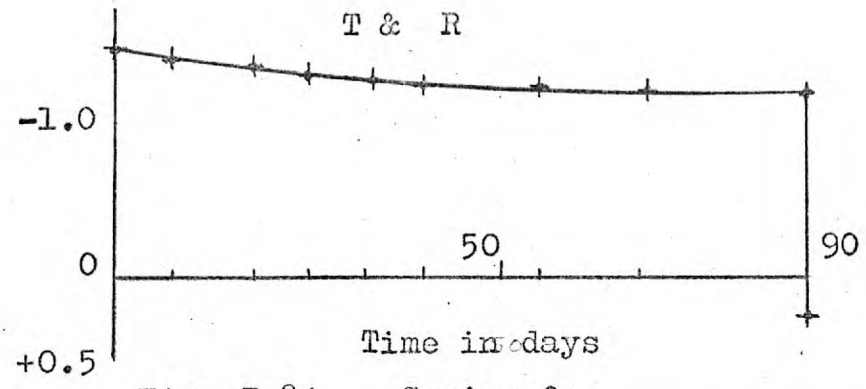

Fig. 7.84. Series 2:
Tangential and radial stresses - R.C., method.
Position 1 - Composite Specimen:

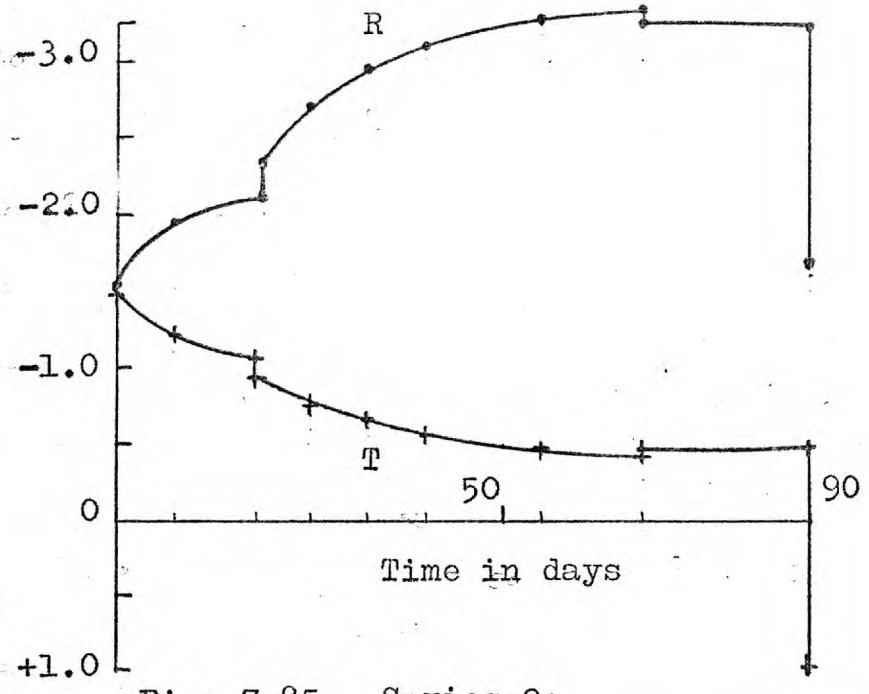

Fig. 7.85. Series 2:
Tangential and radial stresses - R.C., method.
Position 2 - Composite Specimen:

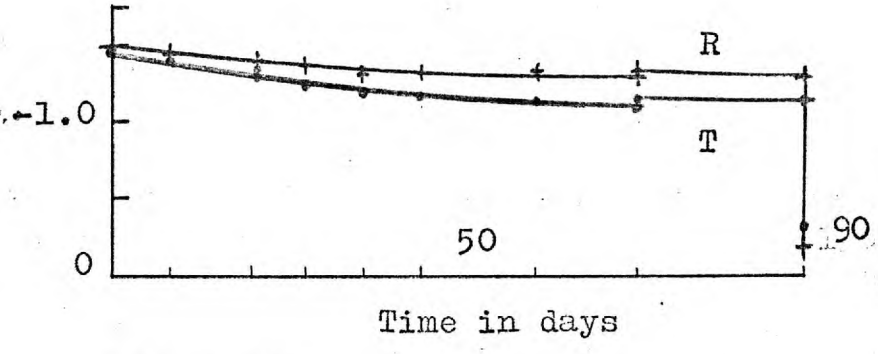

Fig. 7.86. Series 2:
Tangential and radial stresses - R.C., method.
Position 3 - Composite Specimen:

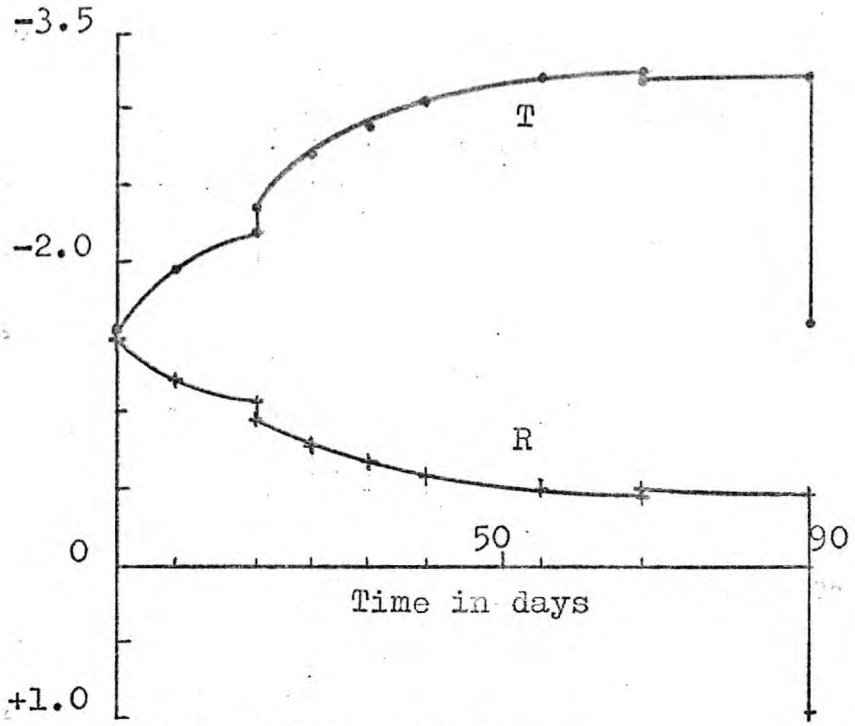

Fig. 7.87. Series 2:
Tangential and radial stresses - R.C.,method.
Position 4 - Composite Specimen:

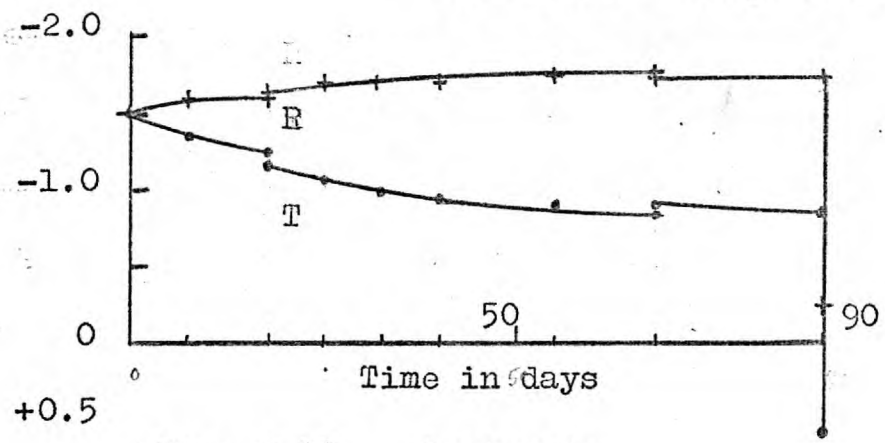

Fig. 7.88. Series 2:

Tangential and radial stresses - R.C., method. Position 5 - Composite Specimen:

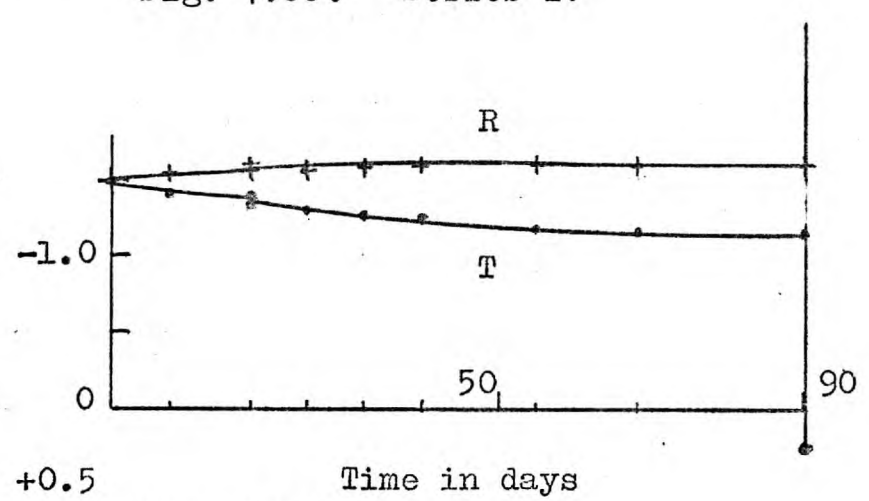

Fig. 7.89. Series 2:

Tangential and radial stresses - R.C., method. Position 6 - Composite Specimen:

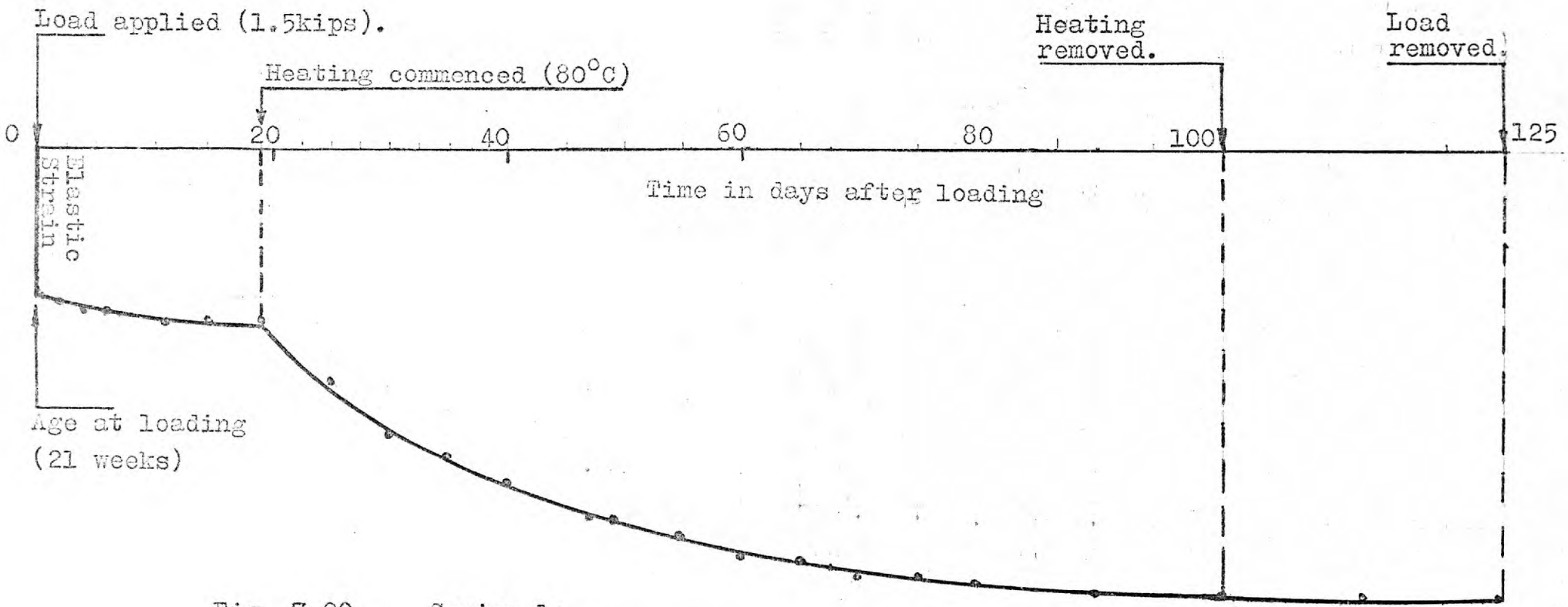

Fig. 7.90. Series 1:
Specific creep curve.

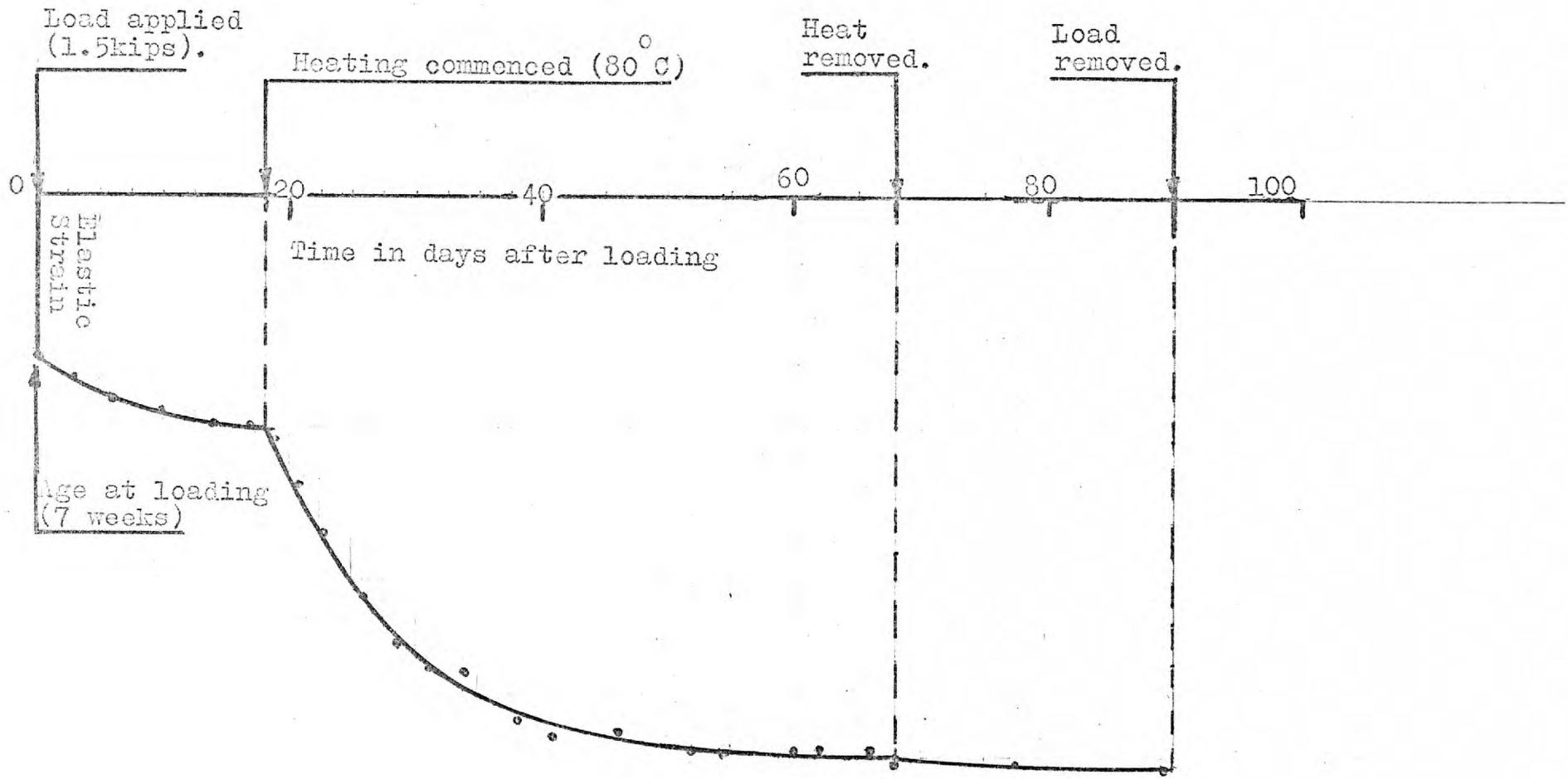

Fig. 7.91. Series 2:
Specific creep curve.

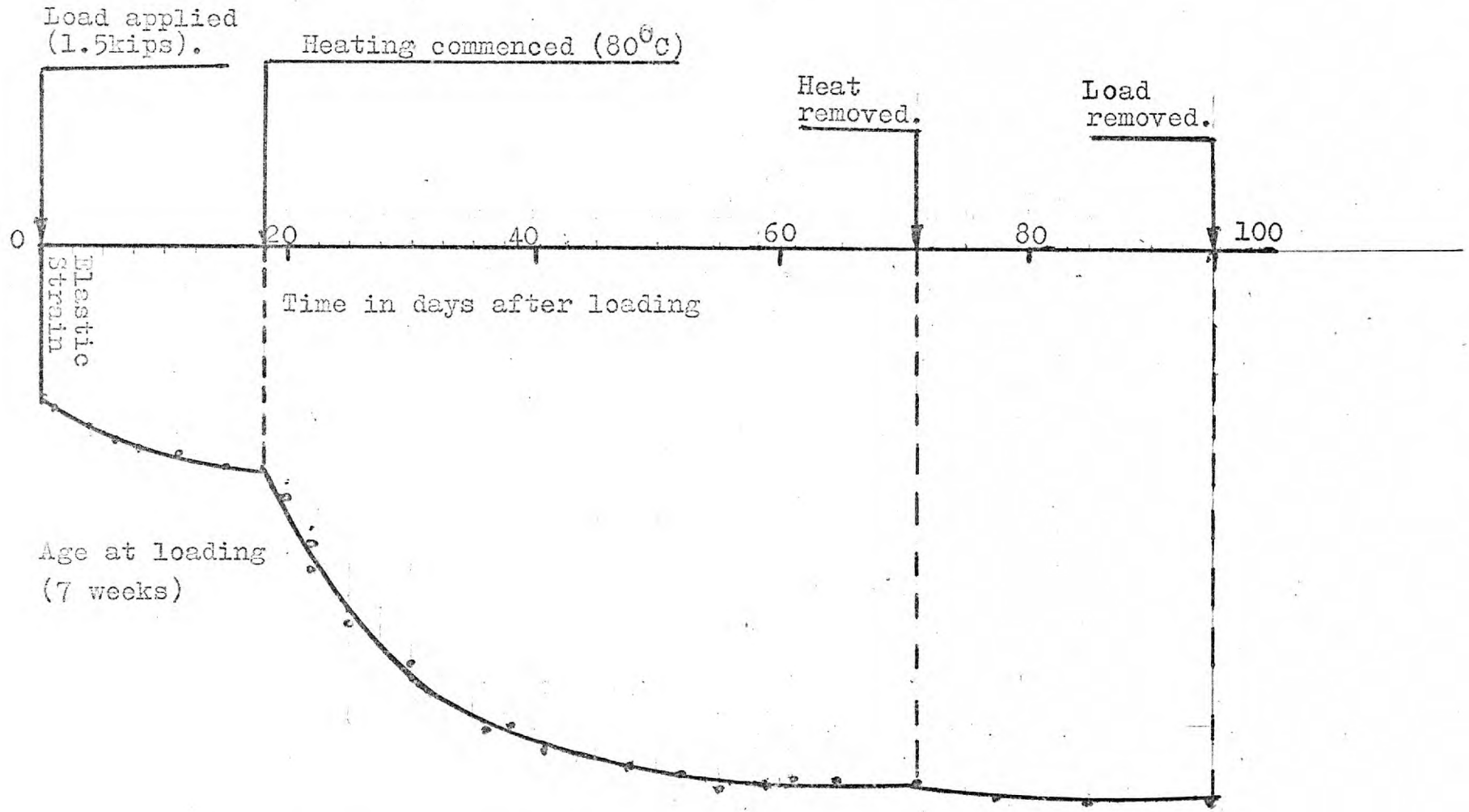

Fig. 7.92. Series 3:
Specific creep curve.

7.2. Methods and procedures adopted in presenting the experimental results.

The separate effects of the applied radial compression, creep, shrinkage and thermal expansion have been evaluated at different ages and temperatures.

A brief description of the various methods and the general procedures adopted to obtain these strains is given in Chapter I, and a more detailed one in Chapter V.

The principal procedures are as follows:-

In each series the shrinkage and thermal strains were provided from one unloaded solid specimen (Model 7/8), and from one unloaded perforated specimen (Model 5/6).

In addition, the combined elastic, creep, shrinkage and thermal strains were provided from one loaded solid specimen (Model 1/2), and from one loaded perforated specimen (Model 3/4). The loaded composite specimen also provided elastic, creep, shrinkage and thermal strains for the combined solid and perforated zones.

Accordingly, it was possible to identify separately each of the effects of elastic loading, thermal expansion, creep and shrinkage, by deducting the appropriately calculated or individually observed strains from the total strain readings at any stage of the test programme.

The loading and heating programme was phased at such intervals of time as to allow significant amounts of strains from whatever cause, to develop. This was in order to be able to plot meaningful curves of adequate length, based on readings of sufficient frequency to establish clear trends.

In the course of all phases of testing, measurements were taken:

a) across four diameters of two symmetrical standpipes on both sides in all perforated specimens by means of a modified Mercer bore gauge.

b) Of four radial and four tangential strains on both sides of the specimens over 2" gauge lengths and 11.438" gauge lengths (3 standpipe pitches) by appropriate Demec gauges.

The eight 2" gauge length readings taken on each face of all specimens were in the ligaments, or in positions in the solid specimens, corresponding to the ligaments.

In addition, on each face of the composite specimen, groups of four 2" gauge lengths were measured to ascertain the strains in the outer perforated region.

The graphs shown were drawn by averaging the readings on both faces of the specimens.

This operation would reduce any possible human errors, or errors due to instrument inaccuracies, as well as any other effects, such as those due to temperature differences, or uneven load distribution.

7. 3. Interpretation of experimental results.

The following are with reference to all specimens of the three test series in general.

7. 3. 1. Ambient temperature.

All tests started at ambient temperatures, and one set of readings was taken on all specimens.

One set of readings consisted of the following:-

a) Strain readings of 2" gauge lengths and 11.438" gauge lengths.
b) Standpipe diameter readings.
c) Recordings of ambient temperature and relative humidity.

This first set of readings formed the datum readings to which all subsequent readings were related.

The radial compression was then applied to the loaded specimens, and a second set of strain readings was taken.

The differences between the datum readings and the readings of the second set, gave the elastic strains of the loaded specimens.

Strains continued to be measured on the loaded and shrinkage specimens, to the end of the experiment.

The results obtained reflect the generally expected pattern of strain for the geometry and loading of the experiments.

7. 3. 2. Elevated temperatures.

In each specimen of the test series the temperatures were measured at three different positions as stated in Chapter V.

It was found that the temperature distribution over the area was almost uniformly distributed, except in the perforated zone of the composite specimen, where the temperature recorded was higher than the temperatures of the annulus.

The temperature across the thickness of the specimens was kept uniform, and possible deviations were considered to be very small and therefore, neglected.

Figures 7.52, to 7.65 , show the temperature distribution for all specimens.

It is seen that after two to five days of heating, (depending on the series) the temperature distribution stabilized. The small fluctuations exhibited could be incorporated in the analyses, and therefore,

their effects eliminated.

These fluctuations would have occurred due to possible variation of the input wattage of the electrical power, or variations of the laboratory temperatures.

However, these fluctuations could not have any appreciable effects on the specific thermal creep data curves, as these curves were drawn from direct readings on the specimens.

1. Commencement of heating:

The Demec gauge readings increased very rapidly on heating and reached a maximum value in about 2 to 5 days of heating, corresponding with the transient periods.

Thereafter, the decline in the readings was so rapid even though the temperatures on some specimens were still rising. This phenomenon may be attributed to rapid shrinkage and creep strains taking place in the concrete.

The decrease in the readings continued as expected at a decreasing rate, and after about five weeks of sustained heating, the readings became stabilized. This indicated that creep and shrinkage continued to occur at a decreasing rate.

Fluctuations in strain readings had been observed during heating in the earlier periods. It was observed that the fluctuations corresponded to fluctuations in the temperatures.

Despite the small fluctuations in the strain readings, the general trend appeared to be clear, (strain readings decreasing at a constant rate).

2. Removal of heat:

After eight weeks of sustained heating, the heating was switched off.

The strain readings decreased sharply as the temperatures reached those of the laboratory.

This occurred two days after the heating was switched off. During the next three weeks, the readings in most specimens continued to decrease at a very slow rate. In some specimens, a reversal of readings was observed, indicating that moisture absorption caused swelling which masked the creep strains .

During the heating period, time-dependent changes in the strains occurred.

Each "sudden" temperature change produced time-dependent changes in the strains which reduced the magnitude of the sharp strain changes brought on initially by the temperature variation.
Such time-dependent changes took place in decreasing rates.

3. Expected creep and shrinkage behaviour at ambient temperatures:

At ambient temperatures creep and shrinkage strains increased at a decreasing rate.

4. Expected creep and shrinkage behaviour at elevated temperatures:

At elevated temperatures the creep and shrinkage strains occurring in the specimens are governed by the temperatures in addition to the applied stresses.

5. Observed rapid initial increases, and subsequent decreases:

On heating due to positive imposed thermal strains, the strains would increase. However, creep and shrinkage occurring at a rapid rate, would slow down the initial increases in the strains.

6. After cooling:

The behaviour of some specimens after cooling indicates that creep in the concrete did not cease in this period, but the effect of moisture movements (swelling) over-rided the creep effects.

7. Moisture movements:

Moisture movements in the specimens caused swelling strains. When the moisture-state reaches equilibrium conditions, strain changes due to these effects, would have ceased. Such changes would fit into the observed pattern.

8. Reversed moisture movements on heat reduction:

Possible moisture movements which had become established after the first heating, could have

occurred again due to heat removal, but in a direction opposite to the earlier movements.
If this was the case, such movements would have caused strain changes.

9. Removal of the external load at the end of test:

When the external loads were removed from the specimens, there was an increase in the strains. This value differed only a small amount from the decrease which was obtained at the start of the test when the loads had been applied.

It would appear from such a result, that the specimens retained essentially the same elastic response.

It was possible, however, that the somewhat smaller value obtained on unloading was due to changes of the elastic properties of the material as a result of the heating, cooling, loading and unloading operations, as well as aging effects.

7. 3. 3. Comparison of test results between the series.

1. Series 1 and 3:

These two series of tests were virtually identical. The only difference between the series being in the test programme. This is shown in figures 1.9 and 1.11 .

For the first series the age of concrete at loading was 21 weeks, and for the third series 7 weeks.

Although the intension was to start the test a week after the specimens were taken out of curring, it was not possible to keep to this time in the case of the first series, for the following reasons:

Difficulties were encountered in obtaining the Demec gauge and standpipe diameter strain readings.

Various techniques were tried before a satisfactory result could be obtained.

It was possible, however, to keep closely to the test programme in the second series, and in order to have direct comparison of the test results between the two series, it was decided to cas and test new specimens.

Comparing the test results obtained from series 1 and 3, figures 7.1 to 7.19 , and figures 7.39 to 7.51 respectively, it can be seen that the strains generally follow the expected pattern, the only difference being in the values of the observed strains. This is mainly due to the difference in the age (at loading) of concrete.

As expected, the values obtained from the first series , where the age of concrete at loading was 21 weeks, are smaller to the corresponding values obtained from series 3, where the age of concrete at loading was 7 weeks.

However, initially the strains might be different, but towards the end of the heating period, they should have reached the same values, since thermal creep effects are predominant.

In the first series difficulties were also encountered in stabilizing the temperature at commencement of heating period. This was achieved 18 days after heating was switched on.

There are no records of strain changes during this period in the Demec gauge, or in the standpipes, and in order to obtain the graphs for this period, the results had to be extrapolated, and the free thermal expansion for 80°C, had to be assumed.

Figures 7.1 to 7.19 show the extrapolated values in dotted line.

The same extrapolation applied when the specific creep curve was drawn for the series.

2. Series 2:

This series differed from series 1 and 3 only in the standpipe thickness ($\frac{1}{4}$" thick), the test programme being almost identical to the test programme of the third series. Fig. 1.10 and 1.11,. The results reflect the generally expected pattern of strain for the geometry and loading of the experiment.

7. 4. Discussion of test results.

In studying the strain patterns obtained from plotting the experimental results, the following were disclosed:-

A reduction in the tangential and radial strains of the loaded specimens took place during the

periods of sustained loading and heating, followed by creep recovery after the load was removed.

Similar reductions were also observed in the strains of the unloaded specimens.

As expected, the rate of change in the strain of all specimens was greater at elevated than at ambient temperatures.

A substantial part of this reduction is attributed to the creep and shrinkage properties of the concrete.

Other possible causes in strain reduction could be due to changes in the material properties of the concrete as a result of loading, heating and aging.

However, for the perforated and composite specimens, the governing factor in the strain changes seemed to be the standpipe thickness which contributes to the overall rigidity of the plate.

In the first and third series with 1/16" thick liners, the effects of the penetrations is clearly shown by comparing the graphs obtained from the solid and perforated specimens (Figs. 7.1, 7.2, 7.3, with Figs. 7.4, 7.5, and 7.6, series 1, and Figs. 7.39, 7.40, 7.41, with Figs. 7.42, 7.43, and 7 44, series 3).

Differences in strain values are also observed when comparing the graphs corresponding to the perforated region of the composite specimen with those in the annulus (Figs. 7.13 to 7.19, series 1).

Experimental values of the equivalent effective modulus of the perforated zone are shown in Table TA4.

In the second series with $\frac{1}{4}$" thick liners, the effective elastic modulus of the perforated zone was found to be almost identical to the modulus of elasticity of concrete. (Compare Tables TA6, and TA7, Appendix 1).

Therefore, the strain changes in the perforated specimen were virtually identical with the strain changes in the solid specimen. (Compare Figs. 7.20, 7.21, and 7.22, with Figs. 7.23, 7.24, and 7.25).

The strain changes in the annulus of the composite specimen were also found identical with those of the perforated region for the same reasons.

The small changes in the strains observed during the "after heating" period, indicated that either there was very little, or practically no creep of concrete during these periods, or, strain changes due to some of the causes stated earlier in this Chapter, cancelled those due to creep of concrete. (Figs. 7.6, 7.15, 7.17, 7.32, 7.39, and 7.44).

Apart from this, it was considered reasonable to assume that within the small period of 1 to 2 days, during which the temperatures dropped considerably, especially after a long period of sustained loading and heating, very little creep would have occurred and almost the entire change in the radial or tangential strains occurring after the removal of heat, would be represented as due to the thermal contraction of the gauge length.

A reversal in the strains from the expected pattern would have indicated swelling to have occurred due to moisture absorption. (Figs. 7.2, 7.5, 7.14, 7.41, and 7.42).

Instead of smooth curves which would have been expected for the conditions of constant radial pressure and uniform elevated temperature, there were small fluctuations in the observed strains for the three series of tests.

It is considered, that such fluctuations were due to one or more of the following causes:-

i) Fluctuations in the temperature, which might have occurred during the sustained period, might have affected the creep (and shrinkage) strains, in such a manner, that during periods of increasing temperatures, the creep rates might have increased, and during periods of decreasing temperatures, the creep rates might have decreased.

ii) Fluctuations in the ambient temperature and relative humidity. The latter would have affected largely the shrinkage strains.

iii) Small fluctuations in the applied radial prestressing due to mal-functioning of the pressure circuit.

In order to facilitate the comparison of predicted values with the test results, smooth curves were drawn for each gauge length.

Strain recovery:

At the end of the test, the specimens were unloaded and the strain recoveries were recorded. It was found, that such strain recoveries were similar to the immediate strains which had occurred when the specimens were initially loaded.

The strain recoveries indicated that the specimens retained essentially the same elastic response due to removal of stress.

The average strain recovery, however, was found a little great in some specimens, than the value which would have been obtained with the original value of Young's modulus. It is considered that there occurred a very small reduction in the value of Young's modulus due to heating and aging of the specimens.

Such reductions in the Young's modulus of concrete (though small), were identified in the tests, and are shown in Tables TA3, TA6, and TA8, of Appendix 1.

Similar reductions were also identified in the equivalent elastic modulus of the perforated zone. (Tables TA4, TA7, and TA9, Appendix 1).

Standpipe strains.

Standpipe diametral deformations were measured during the test programme for the three series, at positions shown in Figures, 5.8, 5.10 and 5.14.

The method used to measure these deformations is described in Chapter V, paragraph 5.3.6, and the difficulties experienced in obtaining the readings in the same Chapter, paragraph 5.5.1 - 3.

Although every possible consideration was given to improve the measuring technique, the Mercer bore gauge proved to be too insensitive for the purpose.

The diametral deformations obtained from Series 2, were plotted and are shown in Figures, 7.66 to 7.74.

From these graphs, it is readily seen that the generally expected pattern is followed.

Deviations, however, from the expected pattern were disclosed but not shown in the graphs, in some readings taken on the shrinkage specimens. These indicate that an increase in the diametral deformations took place in the early days of the test programme.

A possible explanation to this unusual phenomenon,is that the concrete adequacy to the standpipe shrunk away from the standpipe wall being originally compressed by the concrete in the setting period.

The pattern in the readings was so inconsistent, that no conclusions could be drawn from these observations.

Unloading stage - crack formation.

The object of this test was to investigate the behaviour of the concrete in the ligaments of the perforated zone, and in particular, the onset of cracking in this region.

For this purpose, electrical resistance strain gauges were installed on the ligaments of the loaded perforated and solid specimens, as described in Chapter V, and the load was gradually reduced, searching for the onset of cracking in the ligaments.

For each unloading stage the load was reduced in steps of 50 psi. The tests revealed that cracking did occur in the concrete within the ligaments and in the annulus at the commencement of the final step (50 psi).

This indicated the existance of residual stresses within the perforated zone, mainly due to creep recovery, creating tensile stresses in the concrete of the perforated zone, and tensile hoop stresses in the concrete ring, surrounding the perforated zone.

The proposed analysis developed in this thesis also indicates this behaviour.
The cracks are shown in Plates P31, P32, P33, and P34.

The strain changes during the unloading stage in both the perforated and composite specimens, were

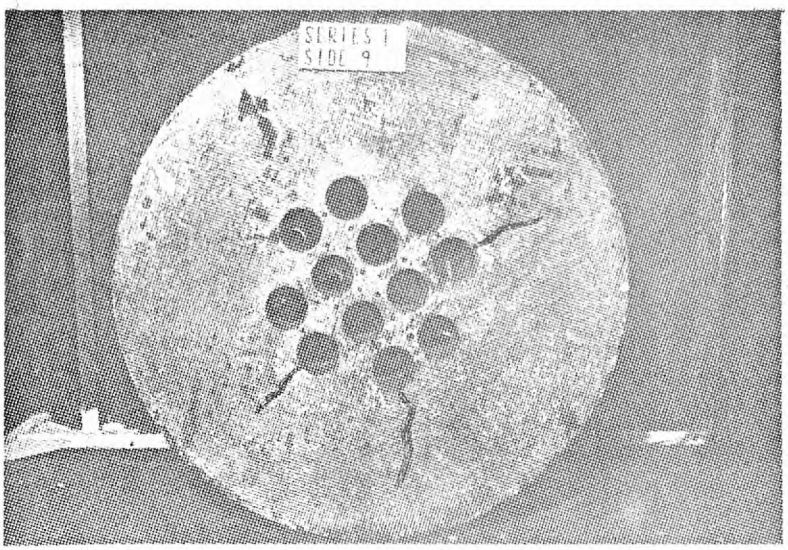

Plate P31.

Cracking pattern on side 9 (Model 9/10) Series 1, after unloading.

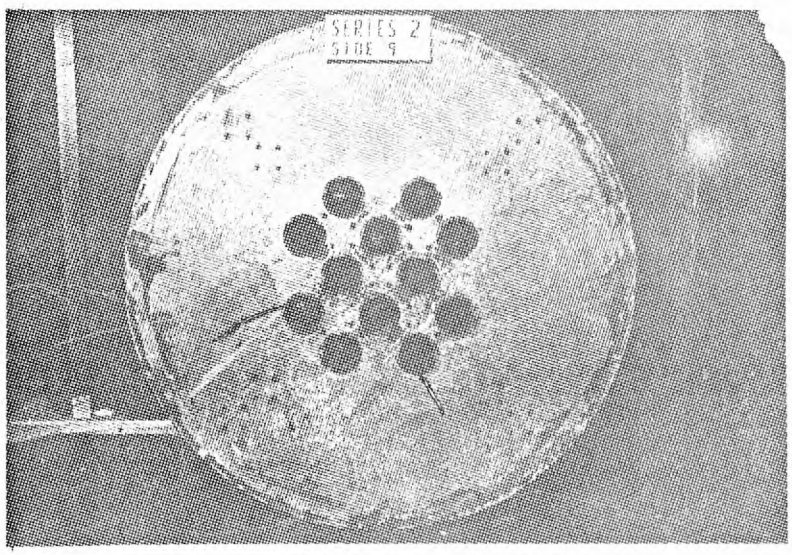

Plate P32.

Cracking pattern on side 9 (Model 9/10) Series 2, after unloading.

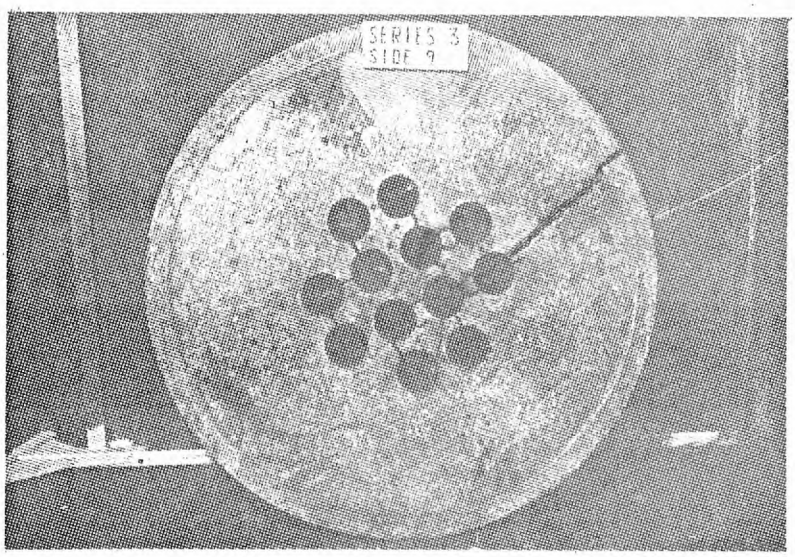

Plate P33.

Cracking pattern on side 9 (Model 9/10) Series 3, after unloading.

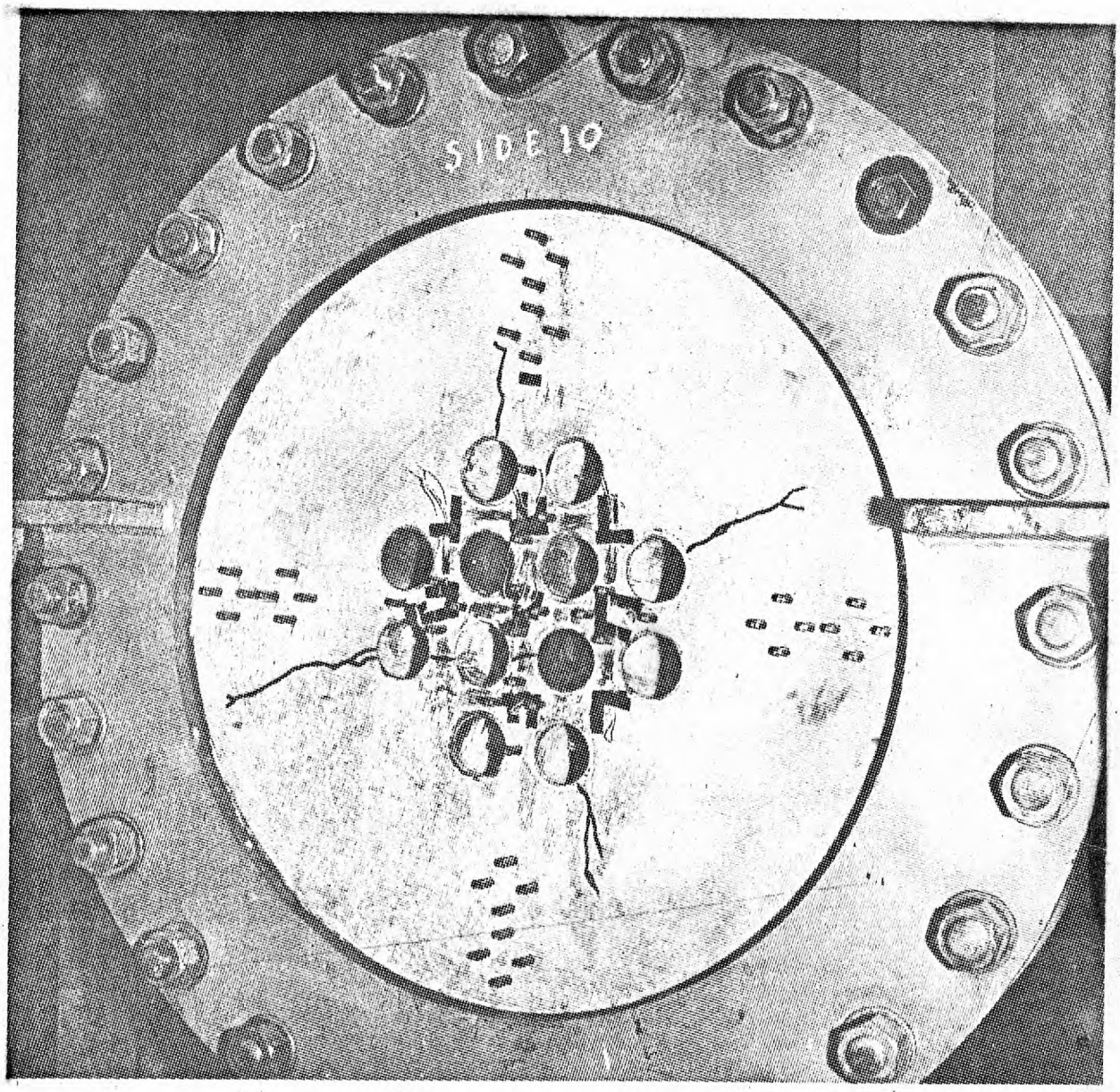

Plate P34.

Cracking pattern on side 10 (Model 9/10)
Series 2, after unloading.

checked by Demec gauges. However, it was not possible to identify any cracks which might have occurred in the ligaments of the perforated specimen, although the analysis predicted tensile stresses. This is perhaps, due to the adopted experimental method not being accurate enough.

Moreover, cracks were also observed in the ligaments of the perforated shrinkage specimen (Model 5/6), when the heating was removed, (Plate P30). These cracks were only surface cracks, and may be attributed to shrinkage effects.

Standpipe penetrations - Effects of standpipe thickness.

The steel liners seem to have a marked effect on the overall behaviour of the perforated and composite specimens.

An equivalent elastic modulus obtained from the tests indicates that the thickness of the liners is proportional to the equivalent modulus of the perforated zone, (Tables TA4, TA7 and TA9).

The effect of the standpipe thickness on the behaviour of the models may also be seen from a comparison of the observed and predicted results for Series 1 and 2.

7. 5. Predicted results.

7. 5. 1. General considerations.

The test results have been analysed by using the creep and shrinkage data obtained from the test specimens (Figs. 7.90, 7.91 and 7.92).

For the analysis, the loaded specimens were divided into a number of elements as shown in Figures 6.9, 6.10 and 6.11, and the test period into a number of time-intervals shown diagrammatically in Figure 6.16.

For each element, the elastic, thermal, creep and shrinkage strains were calculated using data from control and test specimens. The algebraic sum, thus yielding a net strain for each element at the end of the time-interval considered.

At this stage, the conditions of equilibirum and stress-strain compatibility were considered as described in Chapter VI, and the stress distribution for the commencement of the next time-interval was thus known.

In all the cases, the predictions showed the same variation in strain as did the experimental curve, (Figs. 7.1 to 7.51).

The predictions also showed variations in stresses due to thermal, creep and shrinkage. These variations can be seen in Figures 7.75 to 7.89.

The analysis was proceeded with, as outlined below.

A time-interval was considered for which the state of stress at the commencement of the interval was determined from a previous time-interval.

1) For each element the temperature during the interval was noted, and the free thermal expansion calculated. The temperatures were taken from the time-temperature graphs, shown in Figures 7.52 to 7.63.

2) Values of specific creep increments obtained from the experiment, and shown in Figures 7.90, 7.91 and 7.92, were written down for each element corresponding to the time-interval considered, and the temperature.

3) The creep strain for the time-interval was obtained by multiplying the specific creep from (2), by the stress prevailing at the start of the time-interval for each element, and the temperature function.

4) The total creep strain upto the end of the considered time-interval was then obtained for each element by summing-up the increments as in (3).

5) From the shrinkage strain - time curves, the shrinkage strain upto the end of the considered interval was deduced for each element. The assumption made here is that uniform shrinkage was assumed in all elements of the structure.

6) The thermal strain from (1), the creep strain from (4), and the shrinkage strain from (5), were added, and the net free total strain for each concrete element obtained.

For the steel elements, only thermal strain existed since creep and shrinkage in steel was neglected.

7) The ficticious forces due to these strains were calculated for each element at its nodes, and at the nodes of the structure. These forces were then added to the external load vector, and the general equation 6.6.6, was solved to give the displacements and hence, the stresses and strains for each element.

All these operations were performed using the technique described in Chapter VI.

In the analysis, the length of time-interval was governed by the rate of change of stress.

7. 5. 2. Assumptions and design - parameters for the analysis.

1) Plane sections.

Plane sections are assumed to remain plane before and after deformation.

2) Strain.

The total strain in the tested specimens is assumed to consist of four parts:-

Total strain = elastic + creep + shrinkage + thermal.

For the purposes of the analysis, each strain has been computed from the test data.

3) Creep recovery.

The delayed strain recovery exhibited by concrete on removal of the sustained load is not accounted for, in this analysis.

4) Modulus of elasticity of concrete.

The values of the Young's modulus of elasticity of concrete were obtained from control specimens and from strain readings, taken on the specimens as discussed in earlier paragraphs. These values are presented in Tables TA3, TA6, TA8.

The value of 5.0×10^6 psi., was adopted in the calculations as it was considered that such a value was representative of the concrete of all specimens.

Solutions obtained from varying E_c values, showed no significant effect on the stresses.

5) Creep data.

The specific creep increments were taken from the specific creep curves shown in Figures 7.90, 7.91 and 7.92, which were obtained from strain readings on specimen 1/2 for each series.

However, it has been recognised that the specific creep curves so obtained, might have contained errors due to the following reasons:-

i) The temperatures of the specimen (1/2) were not steady, but fluctuated during the test period. Such fluctuations have introduced varying rates of creep at different times.

ii) The value of the coefficient of thermal expansion used to evaluate the creep strains, might not have been representative of the entire gauge-length at a particular time considered.

iii) The shrinkage strain rates of the control specimen (7/8), might have been different from those of specimen 1/2.

iv) The temperature function $\phi(T)$ in the equation $c = \phi(T)c'$, might not have been T itself as has been assumed.

6) Shrinkage data.

The values of the shrinkage strain increments have also been taken from the appropriate shrinkage - strain - time graphs.

7) Thermal expansion.

The value of the coefficient of thermal expansion that was used, varied slightly for the analyses of the three series. At first, the value of $13.5 \times 10^{-6} {}^{o}C$, was adopted for all specimens. Later, values of $12.8 \times 10^{-6} {}^{o}C$, $13.0 \times 10^{-6} {}^{o}C$ and $13.5 \times 10^{-6} {}^{o}C$ were also used. The same values were assumed for steel.

7. 5. 3. Temperature states for analysis.

For the purposes of carrying out the various analyses, the initially increasing and subsequently, fluctuating temperature states of the loaded specimens were considered in three different ways:-

a) Stepped-input and a steady state of temperatures.

b) Transient states followed by a steady state of temperatures, and

c) Transient states followed by fluctuating temperature states.

a) Stepped-input and steady state of temperatures.

When temperatures are considered in this way, it is possible -

1) To examine the time-varying changes which occur due to the creep and shrinkage of concrete separately, and independent of fluctuating changes that may occur due to time-varying temperatures and independent of changes which could have occured due to relatively slow rate of build-up of temperatures.

2) To compare the two methods adopted for the analysis, namely, the Rate of creep, and the Effective modulus method, and examine their advantage and deficiencies under identical conditions.

b) Transient temperature states followed by a steady state of temperature.

When considering the temperatures in this manner, the effect of slow heating on the time-dependent changes can be studied, and the changes can be compared with the corresponding changes obtained under the stepped-input temperature states.

c) Transient states followed by a steady state , followed by fluctuating temperature states.

The temperatures are considered in this manner, in order to match the test conditions. The results as obtained, can then be compared. Deviations from the predicted values can be examined for possible causative factors, other than creep and shrinkage.

In this work state b) was adopted throughout this investigation.

7. 6. Comparison and discussion of predicted values with experimental results.

The proposed method of analysis was applied in conjunction with the Rate of creep approach to predict the radial, tangential and diametral strains in the loaded specimens, of the first and second series.

The Effective modulus approach was used to predict radial, tangential and diametral strains in the solid and perforated specimens of the third series.

Radial and tangential stresses were also predicted at selected points (Fig. 7.93) in the composite specimens of the first and second series by the Rate of creep approach, and in the solid specimens for the three series by the Effective modulus and the Rate of creep approach.

1) Predicted radial, tantengial and diametral strains by the Rate of creep approach:-

FIG. 7. 93. COMPOSITE SPECIMEN

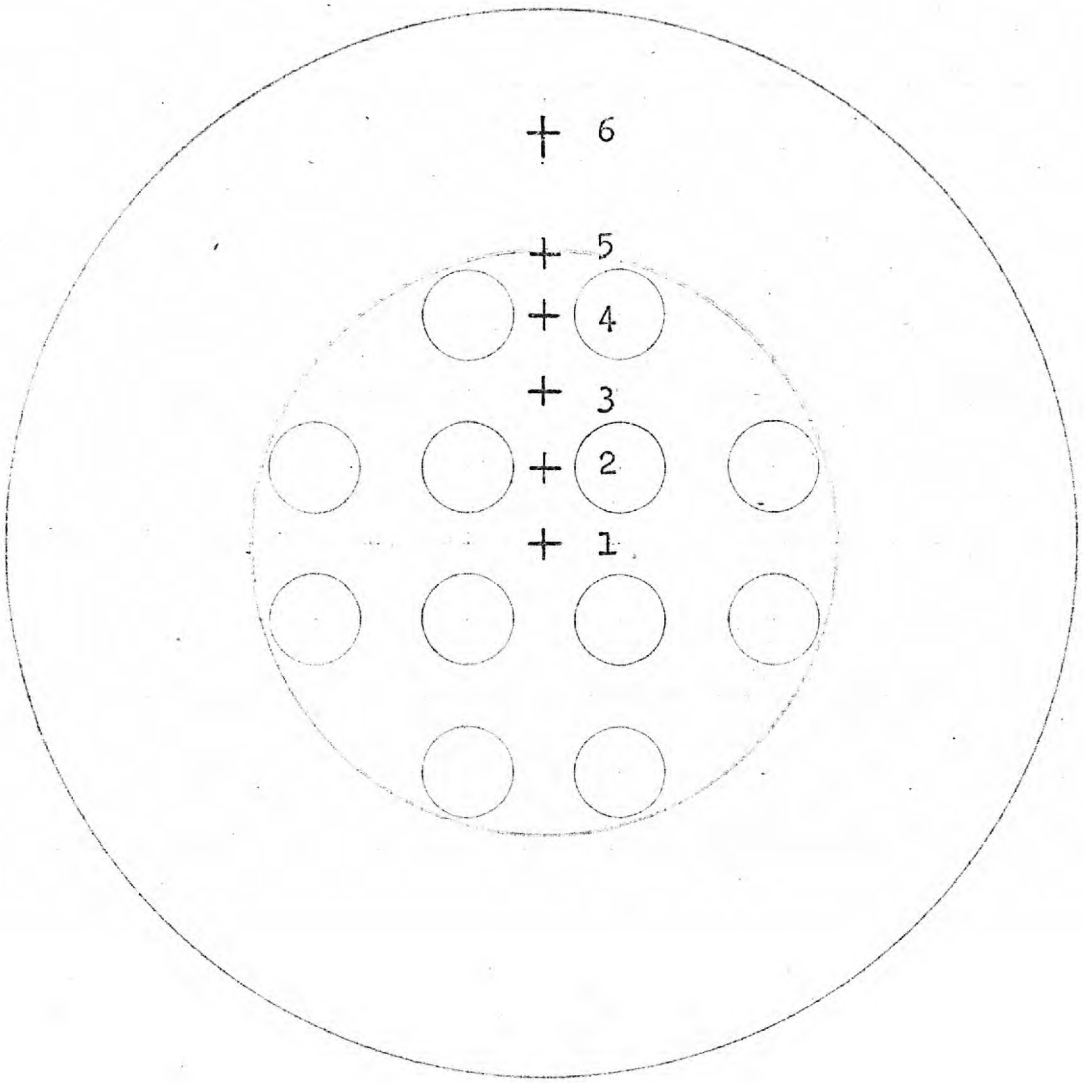

This figure indicates positions where the tangential and radial stresses were drawn as predicted by the Rate of Creep method.

These stresses are indicated in Figures 7.94,7.95.

Series 1:

Solid specimen - Figures 7.1, 7.2 and 7.3.
Perforated specimen - Figures 7.4, 7.5 and 7.6.
Composite specimen - Figures 7.13, to 7.19.

Series 2:

Solid specimen - Figures 7.20, 7.21 and 7.22.
Perforated specimen - Figures 7.23 and 7.25.
Composite specimen - Figures 7.32 to 7.38.

It can be seen from the graphs that this analysis predicts, in most of the cases, successfully the strains obtained from the experiments.

Discrepancies between the predicted and the experimental values may be accounted for by the following:-

Fluctuations in temperatures which might have occured during the heating period. Such fluctuations would have affected the strain readings. Actual conditions in the specimens to those assumed in the analysis. Assumptions in the material properties and the elastic constants.

Fluctuations in the applied radial prestressing. Small errors in strain measurements and finally, inherent inaccuracies of the proposed method.

2) Predicted radial, tangential and diametral strains, by the Effective modulus approach.

Series 3:

Solid specimen - Figures 7.39 and 7.40.

Perforated specimen - Figures 7.42 and 7.43.

It can be seen from the curves that the Effective modulus approach predicted fairly well the observed strains in the solid specimen, but the method failed to predict the strains in the perforated specimen.

3) Predicted radial and tangential stresses.

Series 1, 2 and 3:

Solid specimen - Figures 7.75, 7.76 and 7.77.

The predicted values obtained from the Rate of creep and the Effective modulus approach are shown in the above graphs. As expected, both methods predict identical results.

Series 1:

Composite specimen - Figures 7.78 to 7.83.

Series 2:

Composite specimen - Figures 7.84 to 7.89.

In these figures are shown the variations of the predicted radial and tangential stresses in the ligaments of the perforated zone, and in the annulus.

Six points were selected for this purpose and are shown in Fig. 7.93.
The Rate of creep approach was used to calculate these stresses.

From these observations, the following information was obtained:-

1) Reduction in the stresses.

From the stress-time graphs, it is seen that a reduction in the stress occurs in the perforated region and in the annulus, as a result of creep in the concrete.

This reduction takes place at a decreasing rate, and it is more rapid at elevated temperatures than at ambient.

As expected, stress concentrations are also disclosed in some stresses as a result of the standpipe penetrations.

2) Rigidity of the perforated zone - effect of standpipe thickness.

From the predicted stresses, it indicated that the rigidity of the perforated zone is governed by the thickness of the standpipes.

3) Equivalent elastic modulus of the perforated zone.

The analysis predicted successfully the Equivalent elastic modulus of the perforated zone.

This can be seen from the values of stress (at time t=0) in the graphs. The experimental values are given in Table TA4 and Table TA7.

4) Crack formation.

The appearance of cracks in the concrete within the ligaments and the annulus, during the unloading stage, is also predicted from the stresses.

For this purpose, an analysis was carried out on the composite specimens for the first and second series, where the radial compression was reduced in stages.

The stresses were checked at six chosen positions as shown in Fig. 7. 93, position 5, corresponding with the boundary of the perforated zone and the annulus.

The predicted hoop stresses in the final unloading stage were found to be 400 psi., for the first series, and 600 psi., for the second series, values which are well above the permissible tensile stress of concrete (Figures 7.82 and 7.88).

5) Stress in the standpipe steel.

The stresses in the steel of the standpipes are increased as a result of the compressive creep strains.

It is feared that the steel may easily exceed yielding unless the design is carefully conditioned to avoid this. Variations of the standpipe steel stresses are shown in Figs. 7.94, 7.95.

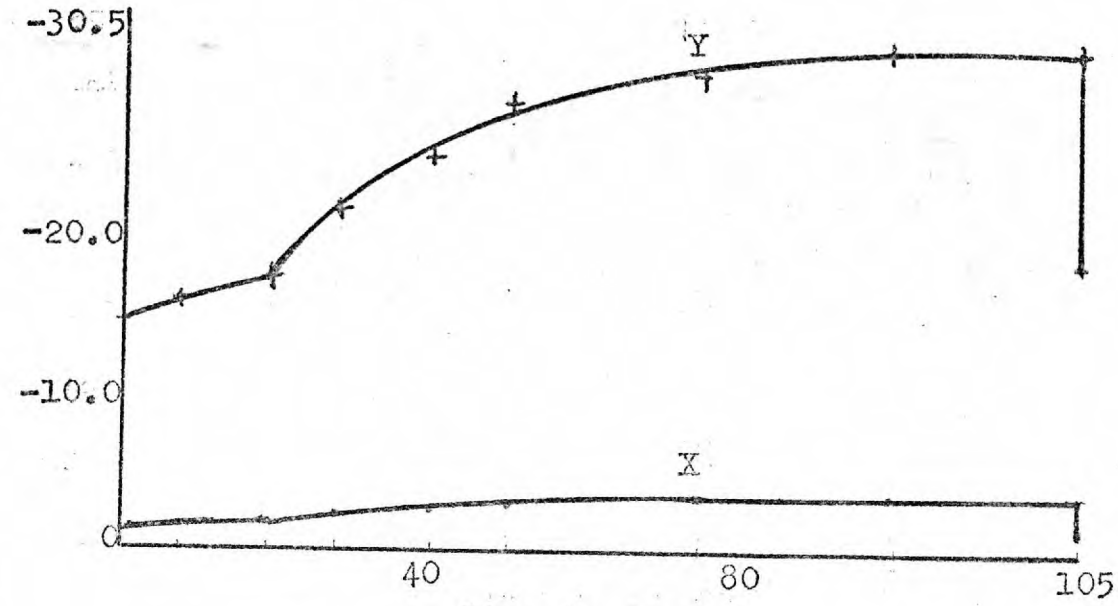

Time in days.

FIG. 7.94. Series 1: Stresses in X and Y at Position 1 - in the Standpipe.

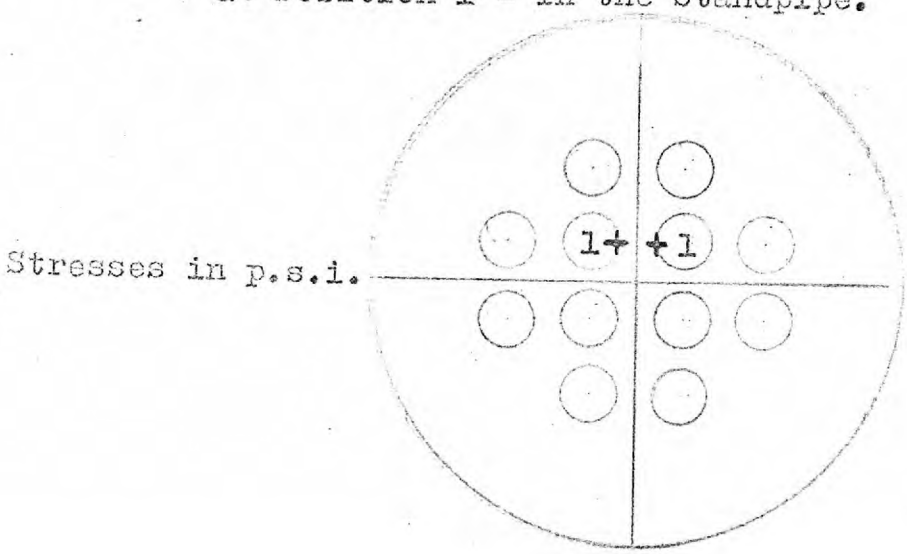

Positions where the steel stresses were checked.

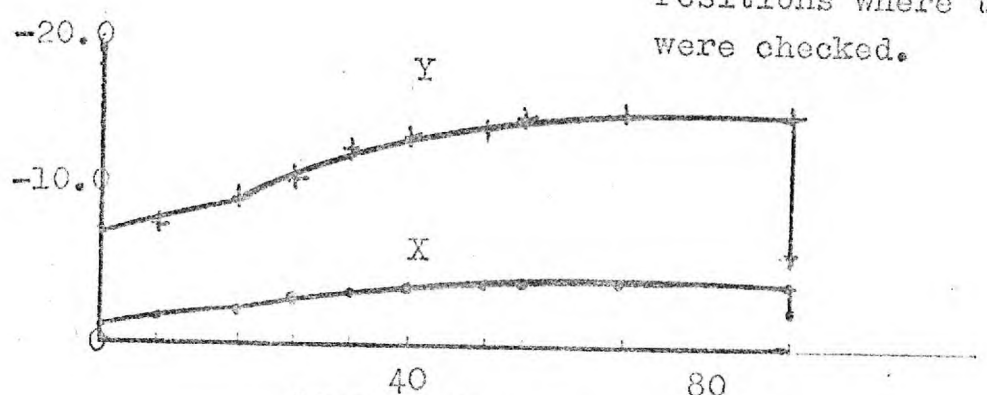

Time in days.

FIG. 7.95. Series 2: Stresses in X and Y at Position 1 - in the Standpipe.

6) Comments on the behaviour of full-scale vessel in the light of the observed model behaviour.

The observed model behaviour has indicated the following:-

1) Cracking will occur on unloading.

2) That there will be a certain amount of prestress loss resulting mainly from creep deformations and shrinkage.

3) Stress redistribution does occur in the concrete of the ligaments.

It is likely that similar behaviour will be exhibited in a full-scale vessel, even though a temperature gradient exists.

Two factors affect cracking in the end slabs:-

a) The relative stiffness of the perforated zones.

b) The degree to which creep recovery is able to put the annular unperforated zone into tension.

As far as a) is concerned, it is clear that by providing liners with adequatly thick walls, a satisfactory stiffness will be enssured for the inner perforated zone.

Gradual blow down and controlled cooling of the vessel can be considered to be necessary precautions in order to eliminate cracking under b).

Operating procedures could be modified to allow for more frequent stress cracking, and if necessary, restressing of the cables.

Moreover, internal gas pressure should not, most particularly in the early months of working, be reduced to zero.

Furthermore, if operating conditions permit a choice, blow down should not proceed to very low levels of pressure, even after several years of operation.

Addition of cold-worked reinforcement circumferentially arranged in the annular zone, would appear to be a necessary safety measure against cracking.

Redistribution of stress will occur in the actual vessel as a result of thermal creep, and stress concentrations are to be expected, because of the standpipe penetrations.

Better concrete with good creep properties (less creep), could be employed to reduce redistribution of stress, and with higher strengths to take into account stress concentrations.

Of course, if the proposed analysis is extended to include temperature gradients, transverse loading, and rim fixity, it is anticipated that it will provide more positive quantitative and qualitative information with reference to the above.

7) Loss of prestress.

The model tests have indicated that there exists a loss in prestress, particularly in the first series in the perforated region due to time-dependent effects.

To avoid this, the rigidity of the perforated zone must be carefully considered in the process of design.

Expedients which might be employed, in the light of the model results, to mitigate prestress losses, could include:-

1) Higher prestress levels might be considered.

2) Better concrete could be employed.

3) More frequent stress-checking as an operational procedure is required.

4) Restressing of the ungrouted ducts may be necessary.

5) Stiffening the geometry of the central zone appears to be essential.

These expedients might be looked upon as safety measures against the blowing-out of the central "wedge" of the end cap.

8) Application of the proposed method of analysis to actual design.

The applicability of the analytical method proposed in this thesis, to the geometry and loading conditions of the models investigated, has been established.

The method has successfully forecast the observed model behaviour.

Before a claim can be made that this approach is universally applicable to all geometries and loadings, it is felt that an intermediate experiment characterized by different conditions, must be undertaken.

These different conditions might include transverse loading, temperature gradients and rim fixity.

There is no reason to suppose, however, in view of the nature of the differences of these latter conditions from the conditions obtaining in the model, that the appropriateness of the proposed solution will be, in any way diminished.

This is because the changes in stress conditions due to these different loadings and boundary geometries, are likely to be in magnitude rather than in kind.

The additional stress-resultants could be superposed on the existing resultants, and the modification necessary to the analytical method proposed,

would be one of matrix reformulation and programme revision only.

9) Need for model testing in future full-scale analysis.

Once this intermediate testing has reaffirmed the validity of the method, it would appear feasible to apply it with confidence to full-scale structure analysis, without the need for further model testing in each case.

However, it is always likely to remain necessary to carry out the appropriate control tests to establish the elastic thermal creep and shrinkage characteristics of the materials under design.

C H A P T E R VIII

CONCLUSIONS AND SUGGESTIONS FOR FURTHER RESEARCH

8. 1. Conclusions.

The conclusions drawn from this investigation are limited to the loading and temperature conditions in the tests performed.

These conditions were:-

a) Uniform elevated temperature of 80°C.

b) Radial compression of 1500 psi.

1. Method of analysis.

A general method of analysis has been developed for forecasting the behaviour of the models investigated in these experiments under the chosen conditions of sustained loading and elevated temperature.

Two possible methods of apprach have been considered as a means of modifying this general analysis to take account of the effects of time-dependent phenomena. These are:-

a) The Rate of creep approach.

b) The Effective modulus approach.

2. The Rate of creep approach.

The general analysis when used in conjunction with the Rate of creep approach to incorporate time-dependent effects, predicted satisfactorily the observed experimental results.

As a consequence, the Rate of creep approach appears to be a reliable method for use on structures subjected to sustained load and temperature.

3. The Effective modulus approach.

The general analysis referred to in 1, when used in conjunction with the Effective modulus approach to incorporate time-dependent effects, predicted well the behaviour of the solid loaded specimen, but failed to predict satisfactorily, the behaviour of the perforated and composite loaded specimens.

The Effective modulus approach is, therefore, not to be recommended in conjunction with the proposed method of analysis in problems of this type.

4. Loss of prestress.

One of the main objectives of these experiments was to investigate whether a loss in prestress would occur in or around the perforated zone.

The behaviour of the models under loading and temperature, and more particularly, the confirming predictions of the analysis have indicated that such a loss in stress does, in fact, occur.

Precautions against such losses should be taken in future full-scale design.

5. Cracking.

At very low levels of load during the final unloading stage of the test programme, radial cracks appeared in the annular region of the composite specimen. Further cracks also appeared in the ligaments of this specimen at these low levels of load.

The tensile stresses giving rise to this cracking were accurately predicted by the proposed analysis.

6. Stress redistribution and stress concentrations.

It was also anticipated that due to creep and shrinkage, a redistribution of stress would occur in the perforated zone. This is confirmed by the analysis which also indicates stress concentration due to the liner penetrations.

7. It is considered that:-

a) The duration and character of the test programme

b) The geometry and number of the test specimens.

c) The instrumentation, and measuring techniques -

were all appropriate to the aims of the investigation

undertaken, and gave results lying within acceptable limits of experimental error.

8. 2. Suggestions for further research.

The experimental work performed in this investigation can be extended to include transverse loading, temperature gradients and peripheral moments.

Such conditions would be more representative of the perforated end cap for a reactor vessel.

It is, therefore, anticipated that any further information obtained from such tests would be very valuable for any future developments.

C H A P T E R IX

A P P E N D I C E S

1. Appendix 1:

2. Appendix 2:

3. Appendix 3:

A P P E N D I X 1

Control tests.

Crushing strength tests.

Tensile strength tests.

Young's modulus tests for concrete from control specimens.

a) At ambient temperatures.
b) At elevated temperatures.

Young's modulus of concrete from test specimens.

Equivalent elastic modulus of perforated zone.

Coefficient of linear thermal expansion of concrete.

A P P E N D I X 1

1. CONTROL TESTS:

1.1. Series 1.

The following control specimens were cast from the same mix as that used for the model specimens, and at the same time. Not all these controls were tested.

Batch 1. 4/4" x 4" x 4" cubes for concrete crushing tests.

2/4" x 4" x 12" prisms for Young's Modulus tests, one prism of which contained two thermocouples.

2/4" x 4" x 12" prisms for coefficient of liner expansion tests, each prism of which contained two thermocouples.

2/6" x 4" x 9" cylinders for the Brazilian tensile test.

Batch 2. As for Batch 1.

Batch 3. As for Batch 1, except for the cylinders.

These control specimens were cured under hessian kept constantly wet, until they were required for testing or for 28 days whichever was the shorter period.

1.2. CRUSHING STRENGTH TESTS:

One 4" x 4" x 4" cube from each batch, was crushed after fourteen days, and one from each batch thereafter was tested after twenty eight days, eight weeks and three months respectively.

The results and averages of the three tests at each age are given in Table (TA1).
The tests were carried out generally in accordance with B.S. 1881: 1952: Methods of Testing Concrete.

T A B L E TA1.

CONCRETE CRUSHING TESTS ON 4" CONTROL CUBES:

	AGE:	FAILURE LOAD:	CRUSHING STRENGTH:	AVERAGE CRUSHING STRENGTH:
Batch 1	14 days	39 tons	5470 psi.	
2	14 days	39 tons	5470 psi.	
3	14 days	37 tons	5180 psi.	5370 psi.
Batch 1	28 days	47.8 tons	6680 psi.	
2	28 days	47.75 tons	6680 psi.	
3	28 days	41.8 tons	5860 psi.	6410 psi.
Batch 1	8 weeks	54.0 tons	7560 psi.	
2	8 weeks	57.0 tons	7960 psi.	7760 psi.
Batch 2	3 months	65.0 tons	9100 psi.	
3	3 months	62.0 tons	8690 psi.	8895 psi.

....

1.3. THE BRAZILIAN TENSILE TESTS:

This indirect test of the tensile strength of concrete was applied to the cylindrical specimens generally in the manner of A.S.T.M. C496 - 62T.
The splitting tensile strength is given approximately by:-

$$\sigma = \frac{2p}{\pi d.l}$$

Where p = is the failure load in lbs.
d = is the diameter of the cylinder in ins.
l = is its length in ins.

The stress σ so obtained, is considered to be approximately 15% higher than the direct tensile strength.

The 6" x 9" cylinders were loaded in compression along a diameter, with the specimens on their sides, in contact at the top and bottom with $^1/8$" x 1" strips of hardboard.

The load was applied without impact and increased continuously at approximately 200 psi. minute, until the specimens split into two parts. There were no unusual failure planes or other abnormal features about the method of failure.

Two cylinders were crushed from Batch 1 after twenty eight days, and the remaining two from Batch 2 after three months. The results and averages of these tests at each age are given in Table TA2.

T A B L E TA2.

BRAZILIAN TENSILE TEST RESULTS ON 6" x 9" CYLINDERS:

	AGE:	FAILURE LOAD:	AVERAGE FAILURE LOAD:	SPLITTING TENSILE STRENGHT:	DIRECT TENSILE STRENGTH:
Batch 1	28 days	(15.7 tons)16.5 tons	16.1 tons	425lbsf/in^2	370lbsf/in^2
Batch 2	3months	(18.74tons)18.30tons	18.52tons	487lbsf/in^2	424lbsf/in^2

N.B.

Splitting Tensile Strength in psi.

$$\Omega \quad \frac{2p.}{\pi d.l.} = \sigma \text{ psi.}$$

Where p = failure load in lbs.
d = diameter in ins.
l = length in ins.

Direct Tensile Strength..

$$\Omega \quad \frac{\sigma \times 100}{115} \text{ psi.}$$

... ...

1.4. YOUNG'S MODULUS TESTS ON CONTROL SPECIMENS:

1) Room Temperature Tests.

These tests were carried out on Batch 1 and Batch 3 specimens, 4" x 4" x 12" long at ages of 11 weeks and 3 months respectively. The results for the Young's Modulus E so obtained, were supplemented by the elastic response data obtained by load-cycling the actual model specimens at various ages until the termination of the experimental programme.

Eight Demec gauge lengths were set out using Demec studs, fixed to opposite 12" x 4" faces of the concrete prisms, which were then loaded axially, lengthwise in an Amsler compression machine. The gauge length was positioned centrally in both directions on each of the two faces. The platen faces of the machine were bedded on to the ends of the specimens by means of 4" x 4" x $\frac{1}{2}$" steel plates and $\frac{1}{2}$" asbestos board.

The load was increased evenly and slowly in 2 ton increments to a maximum of 20 tons and then reduced at the same rate to zero. Four such cycles were applied to each specimen, Demec readings being taken on the two opposing faces, at each loading change, for averaging purposes.

For the calculation of E, early cycles were ignored. The fourth cycle gave a plot of stress and reading differences which was virtually linear.

To obtain the strain, the reading differences were multiplied by the gauge factor of the 8" Demec gauge, which was:-

$$k_1 = 1.00 \times 10^{-5}.$$

The room temperature tests gave a Young's Modulus for the control specimens of 4.97×10^6 lb/sq.in., and 4.94×10^6 lb/sq.in., for 11 weeks and 3 months respectively.

2) Tests at 80°C.

Similar tests were also carried out at 80°C on Batch 1 and Batch 3 specimens, 4" x 4" x 12" long, at an age of 15 weeks. The Batch 1 specimen was given five cycles and the Batch 3 specimen four cycles. The loading range was again 0 to 20 tons in 2 tons increments. The same 8" Demec gauge was used having a gauge factor of:-

$$k_2 = 1.005 \times 10^{-5}.$$

Into these control specimens, two thermocouples had been symmetrically introduced at the time of casting. These thermocouples were identical to those used in the main experiment and they were spot-welded at their junction. They were then coated with PS adhesive which was allowed to dry before the thermocouples were cast in the concrete.

Flexible load compensating cables were joined to the thermocouples by twisting together the two appropriate pairs of bared ends soldering, and then wrapping in insulation tape.

The lengths and resistances of the cable leads, and the dummy lead were identical, and the leads were connected to a switch-box in series with a scalamp galvanometer. The reading scale of the scalamp was calibrated against the boiling point of pure water.

The temperature of the specimens was raised by means of Isopad heating tapes which were wrapped continuously round the prisms leaving only the Demec points accessible.

The specification of the tapes was precisely as that described for the heating of the main specimens. The heat input was controlled by means of a variable transformer and the required temperature of 80°C was achieved after about three hours.
The adjustment on the transformer was sensitive enough to maintain this temperature during the test without the need for thermostats or other controls.

The thermocouples and heating circuits were in operation whilst the specimens were actually in the Amsler machine under test.

A diagrammatic representation of the thermocouple and heating circuit is shown in Fig. A1., and a view of the set up in Plate P A1.

The 80°C E tests gave a value for Young's Modulus for the Batch 1 specimen at 15 weeks of 4.80×10^{-6} lb/sq.in, and for the Batch 3 specimen at the same age of 5.0×10^{-6} lb/sq.in.

Young's modulus of concrete obtained from the test specimens.

The Young's modulus of concrete was determined from strain-changes which occurred when the solid specimen (Model 1/2), was load-cycled at three different stages of the test programme.

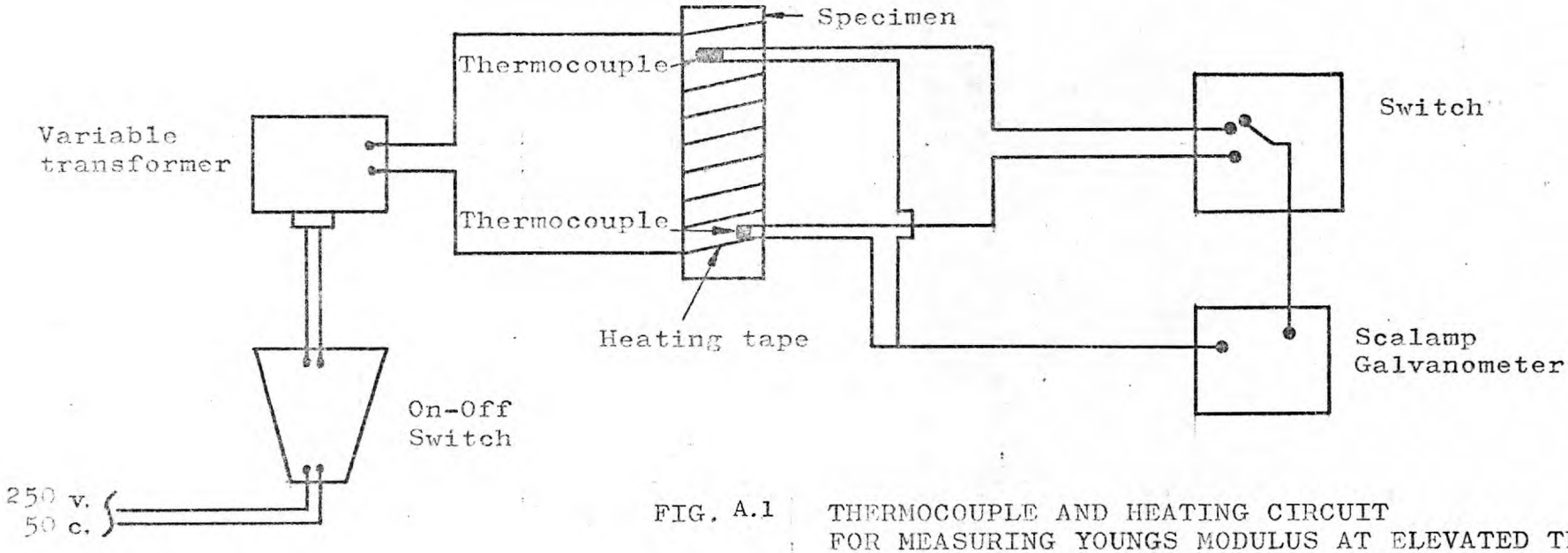

FIG. A.1 THERMOCOUPLE AND HEATING CIRCUIT FOR MEASURING YOUNGS MODULUS AT ELEVATED TEMPERATURES

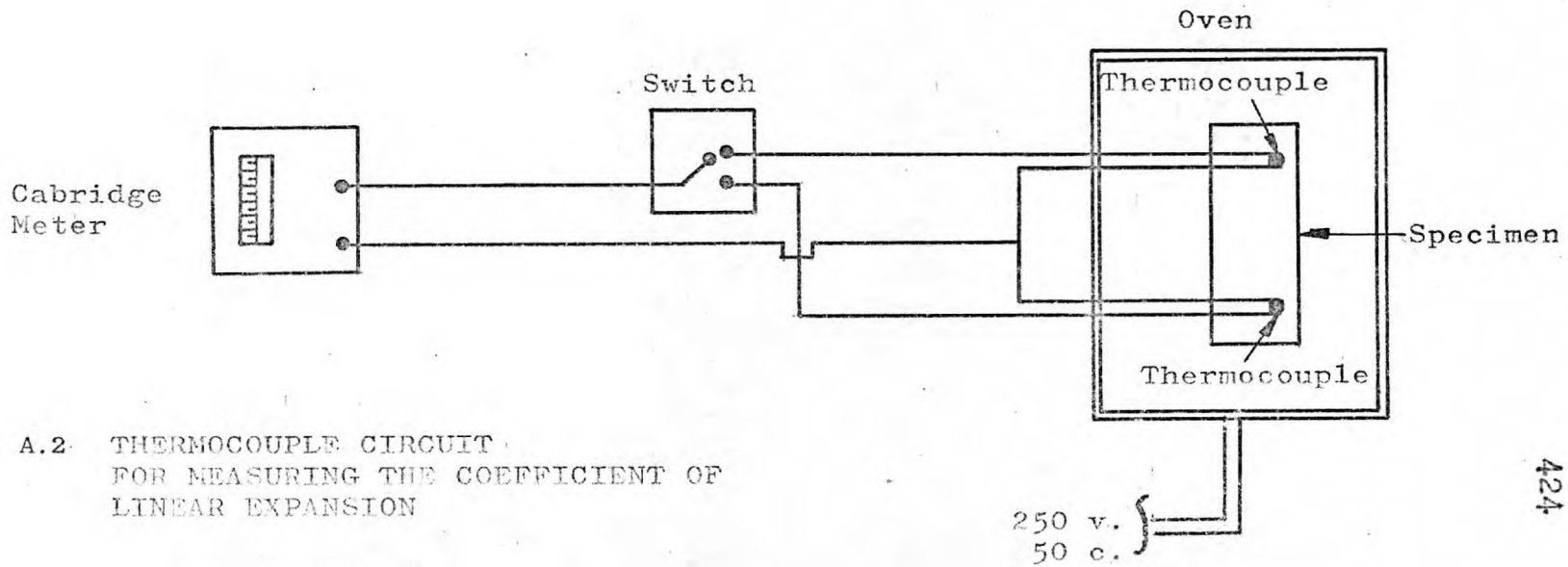

FIG. A.2 THERMOCOUPLE CIRCUIT FOR MEASURING THE COEFFICIENT OF LINEAR EXPANSION

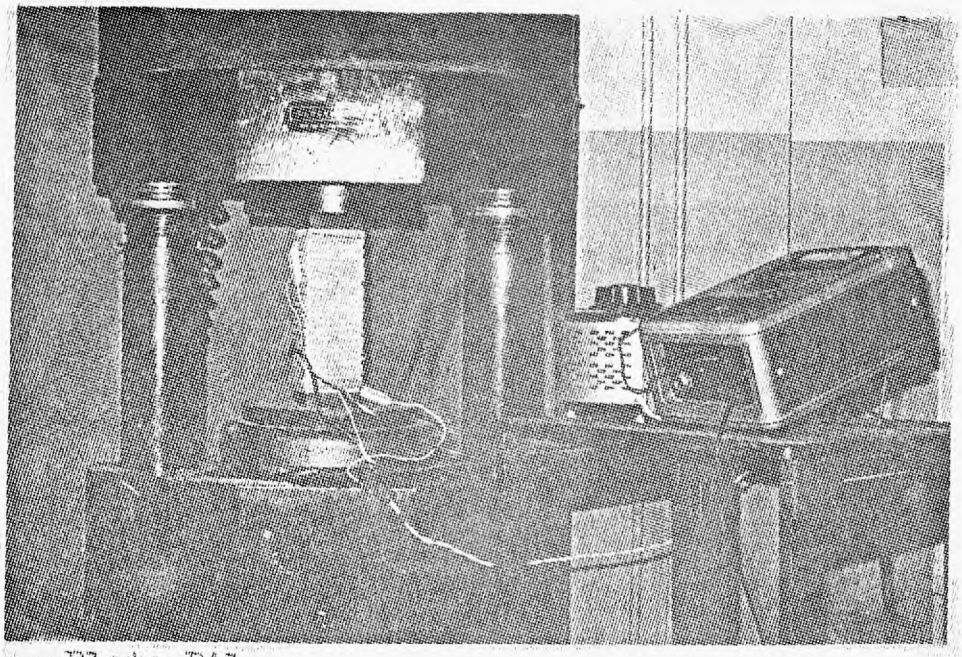

Plate PA1.

Control specimen and the test equipment for Young's modulus of concrete at elevated temperatures.

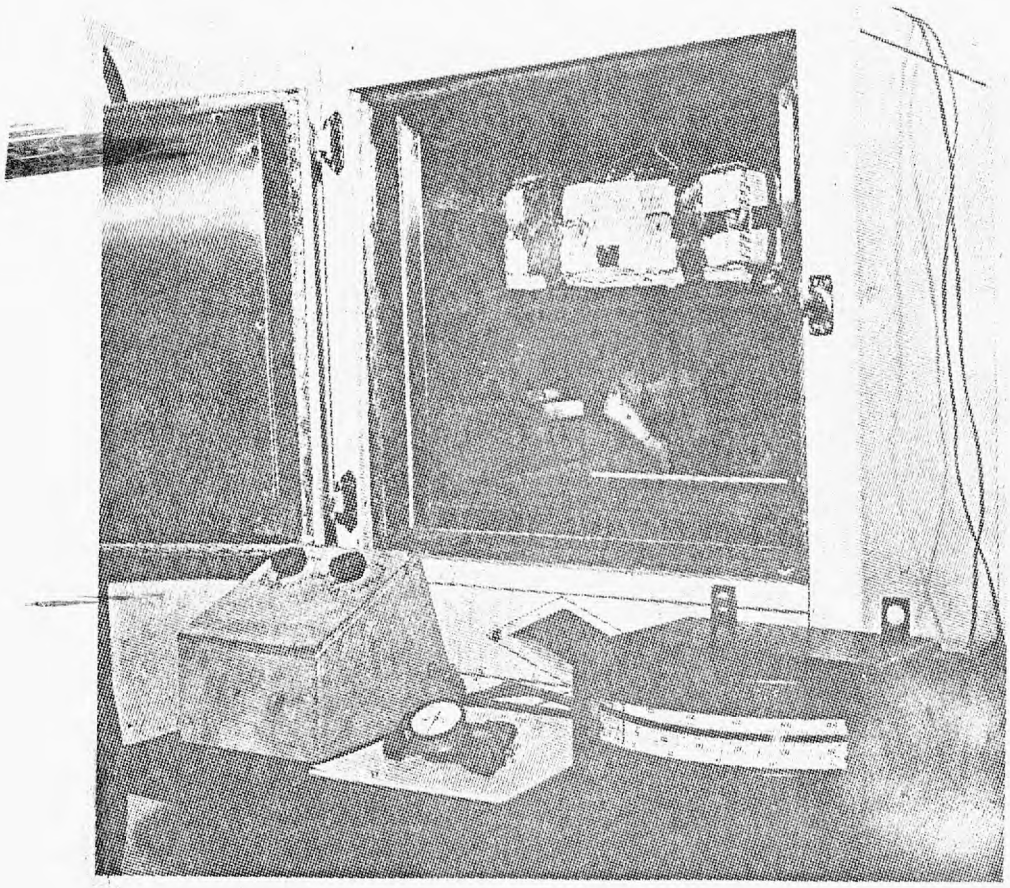

Plate PA2.

Oven and other test equipment for the coefficient of thermal expansion of concrete.

Stage 1: Commencement of test, at ambient temperature.
Stage 2: Before heat was switched off.
Stage 3: Before load was removed.

Procedure.

Three load-cycles were performed during which the strain readings from 2" gauge lengths, tangential and radial, and from 3-pitch gauge lengths (11.438") diametral, were recorded.

Graphs were plotted and a Secant modulus was obtained for the three gauge lenths. These values were averaged and the results are given in Table TA3.

Equivalent elastic modulus of perforated zone.

Similarly, the Effective elastic modulus of the perforated zone was determined from the perforated specimen, and for the same stages.

Procedure.

The same procedure was followed as for the determination of the Young's modulus of concrete. Strain changes were recorded from the 3-pitch gauge lengths only. The values obtained are given in Table TA4.

T A B L E TA3.

Series 1:

Stage:	Temperature:	Young's modulus of concrete:
1 Commencement of test:	Ambient:	4.95×10^6 psi 5.25 5.30
2 Before removal of heat:	80°C:	4.90 4.75 5.00
3 Before unloading:	Ambient:	4.87 4.75 4.90

The above results indicate that the variations in the values of the Secant modulus obtained from specimen (Model 1/2), and the control specimens, are not large.

It is also indicated that small reductions in the values of Secant modulus obtained from the control and test specimens, had taken place due to thermal and aging effects.

However, such reductions were small, and lay within the observed overall variation.

The mean value of 5.0×10^{-6} psi, was considered representative of the concrete of all the specimens and for the three series of test (some mix design was adopted for the three series).

T A B L E TA4.

Series 1:

Stage:	Temperature:	Equivalent Secant modulus of perforated zone:
1 Commencement of test:	Ambient:	3.06 $\times 10^6$ psi 3.16 2.84
2 Before removal of heat:	80°C:	3.00 2.85 2.95
3 Before unloading:	Ambient:	2.85 2.90 2.78

The above results clearly indicate a marked difference between the Young's modulus of concrete and the equivalent elastic modulus of perforated zone.

It is also indicated that small reductions in the values of Secant modulus had taken place due to thermal and aging effects.

1.5 COEFFICIENT OF LINEAR EXPANSION OF CONCRETE:

These tests were carried out on 4" x 4" x 12" prisms cast from Batch 1 at ages of 3 months and 30 weeks.

The prisms for these tests contained two equally-spaced thermocouples each, and they were lagged on the side faces with a 7/8" thick layer of cellular asbestos aluminium insulation panelling. Strain readings were taken on a 4" gauge length with a Demec gauge, having a gauge factor of:-

$$k_3 = 2.03 \times 10^{-5}.$$

The gauge points were on Demec studs affixed in pairs on opposite sides of the prism so that average readings could be calculated.

The prisms were mounted over 3/4" steel bars on the top of an oven with thermostatic control. The specimens were heated slowly from the laboratory ambient temperature of 20°C upto 80°C, over a period of two days, and then allowed to cool down again at a similar rate.

The thermocouple circuit is shown diagrammatically in Fig. A2. , and a view of the set up in Plate PA2 .

Strain measurements were taken at hourly intervals. The measurements each took less than a minute and since the specimens were insulated, the opening of the oven door for the purpose of taking readings had a negligible cooling effect. The whole heating and cooling cycle took 5 days approximately.

The shrinkage suffered by the specimen, could be calculated from the initial and final readings. The specimens used in these tests were taken out of curing after 28 days, and thus, the results presented are those of concrete prisms under drying conditions.

The linear coefficient of thermal expansion, according to Arthanari, varies little with the age of concrete at the start of such tests, but decreases at lower moisture contents as the specimen dries out.

The present tests were carried out at 3 months and 30 weeks, and it is probably that the dry condition of the specimens and particularly, of the latter specimen, approximated to both the moisture content of the main specimens, and to that of an operating reactor shield slab.

The tests gave an average value for the coefficient of linear thermal expansion for concrete, equal to:-

$$a = 13.78 \times 10^{-6}.$$

In addition, the values of the coefficient of thermal expansion were also obtained from thermal strains which occurred in the solid specimens (Models 1/2, 7/8), when heat was first applied and when it was removed.

The strain changes of 2" gauge longths,and 3-pitch gauge lenghts were recorded and an average value for the coefficient of thermal expansion was obtained.

T A B L E TA5.

Series 1: Coefficient of thermal expansion of concrete:

		13.50×10^{-6} per °C:
Commencement of heat:	1) Model 1/2:	12.85 "
	2) Model 7/8:	12.65 "
		13.00 "
Removal of heat:	1) Model 1/2:	13.70×10^{-6} per °C:
	2) Model 7/8:	14.00 "
		12.90 "
		13.50 "

Series 2 and 3:

There were no special control tests carried out for these series except for the standard crushing strength tests.

The Young's modulus of concrete, the Elastic effective modulus of the perforated zone, and the coefficient of linear thermal expansion were obtained in the manner described in Series 1.

The values so obtained are given in the following tables:-

T A B L E TA6.

Series 2:

Stage:	Temperature:	Young's modulus of concrete:
1 Commencement of test:	Ambeint:	4.80 5.10
2 Before removal of heat:	80°C:	4.78 4.95
3 Before unloading:	Ambient:	4.84 4.70

T A B L E TA7:

Series 2:

Stage:	Temperature:	Equivalent Secant modulus of perforated zone:
1 Commencement of test:	Ambient:	4.90
2 Before removal of heat:	80°C:	4.84
3 Before unloading:	Ambient:	4.75

T A B L E TA8.

Series 3:

Stage:	Temperature:	Young's modulus of concrete:
1 Commencement of test:	Ambient:	4.88
2 Before removal of heat:	80°C:	4.80

T A B L E TA9.

Series 3:

Stage:	Temperature:	Equivalent Secant modulus of perforated zone:
1 Commencement of test:	Ambient:	2.84
2 Before removal of heat:	80°C:	2.78

The coefficient of linear thermal expansion of concrete obtained from average strain readings on specimens (Models 1/2 and 7/8) was:-

Series 2: 13.2×10^{-6} per °C.
Series 3: 13.6×10^{-6} per °C.

A P P E N D I X 2

The Effective Modulus Method for the assessment of load distribution at the boundary of the perforated zone in the composite specimen.

A P P E N D I X 2.

1. The Effective Modulus Method for the assessment of load distribution at the boundary of the perforated zone in the composite specimen.

An analysis has been carried out based on the Effective Modulus Method, to calculate the load distribution around the perforated zone of the composite 36" diameter specimen (model 9/10), of the second series (III).

The results obtained from the analysis are presented in analytical and graphical form at seven different phases of the test programme. The data used in the analysis were obtained from curves drawn from experimental observations during the test programme Fig. A3 (b,c,d,f).

The equivalent elastic modulus, and the creep and shrinkage laws required for the perforated zone of the composite specimen were obtained from the $16\frac{3}{4}$" diameter perforated specimen (model 3/4), subsequently referred to as the "control" specimen.

It was, therefore, assumed that the perforated zone of the composite specimen would exhibit the same creep and shrinkage characteristics and have the same elastic constants as the perforated "control" specimen.

Such an assumption seems to be justified from the following considerations:-

(a) the geometrical data of the perforated zone, and the "control" specimen were identical.

(b) both specimens were subjected to the same elevated temperature.

(c) the "control" specimen and the perforated zone of the composite specimen were under the same state of stress at the start of the test. This was confirmed using thick-walled cylinder analogy.

Hence, it seemed reasonable to use the equivalent elastic modulus, and the creep and shrinkage data, obtained from the "control" specimen for the perforated zone of the composite specimen.

The equivalent elastic modulus for the perforated zone was assessed by subjecting the "control" specimen to a load-cycling.

Three load-cyclings were carried out for this purpose, corresponding to the three phases of the test programme:-

(1) specimens loaded at ambient temperature.

(2) specimens loaded at elevated temperature.

(3) specimens loaded after cooling.

The values obtained were appropriatly used in the analysis for the various times considered.

The stresses were checked at seven different phases of the test programme:-

a) at time T_1 on loading the specimen to obtain the elastic stress.

b) at time T_2 immediately before heating commenced, to obtain stresses due to creep strains at ambient temperature.

c) at time T_2 immediately after heat was applied to calculate the thermoelastic stresses due to restrained thermal expansion.

d) at time T_3 immediately before heat was removed to obtain the stresses and to forecast the effects of thermal creep on the structure.

e) at time T_3 immediately after heat was removed.

f) at time T_4 immediately before unloading.

g) finally, at T_4 immediately after unloading.

2. Formulation of the problem.

2.1. Notation and sign convention.

The notation and sign convention used throughout the analysis are shown in Figs. (A4), (A5).

Figure (A4), represents diagrammatically the total strains for a loaded specimen plotted against a time-basis, where the total strain includes the elastic, creep, shrinkage and thermal strains.

Figure (A5), represents diagrammatically the shrinkage and thermal strains for an unloaded shrinkage specimen.

2.2. Equations used in the analysis.

The following relations were used in the calculations.

The subscripts e, c, s and t refer to elastic, creep, shrinkage and temperature respectively, and the indeces refer to the time a solution is given.

Indeces for Young's modulus, E, of concrete, refer to the three phases of the test programme.

p_i = the load distribution

e = the strain

c = the specific creep

σ = applied stress.

a = coefficient of linear expression.

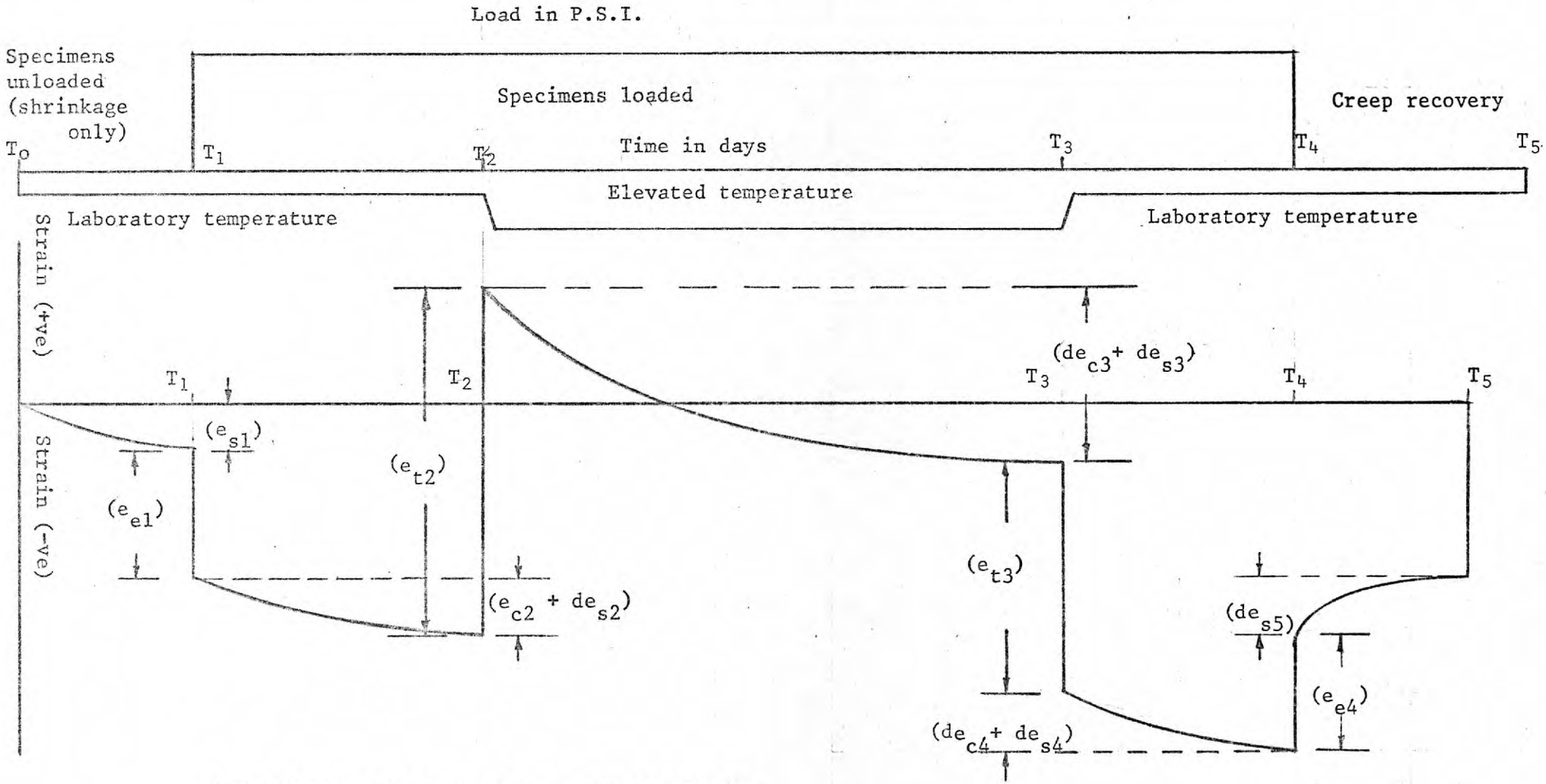

FIG. A4. Typical Strain-line curve for loaded specimens.

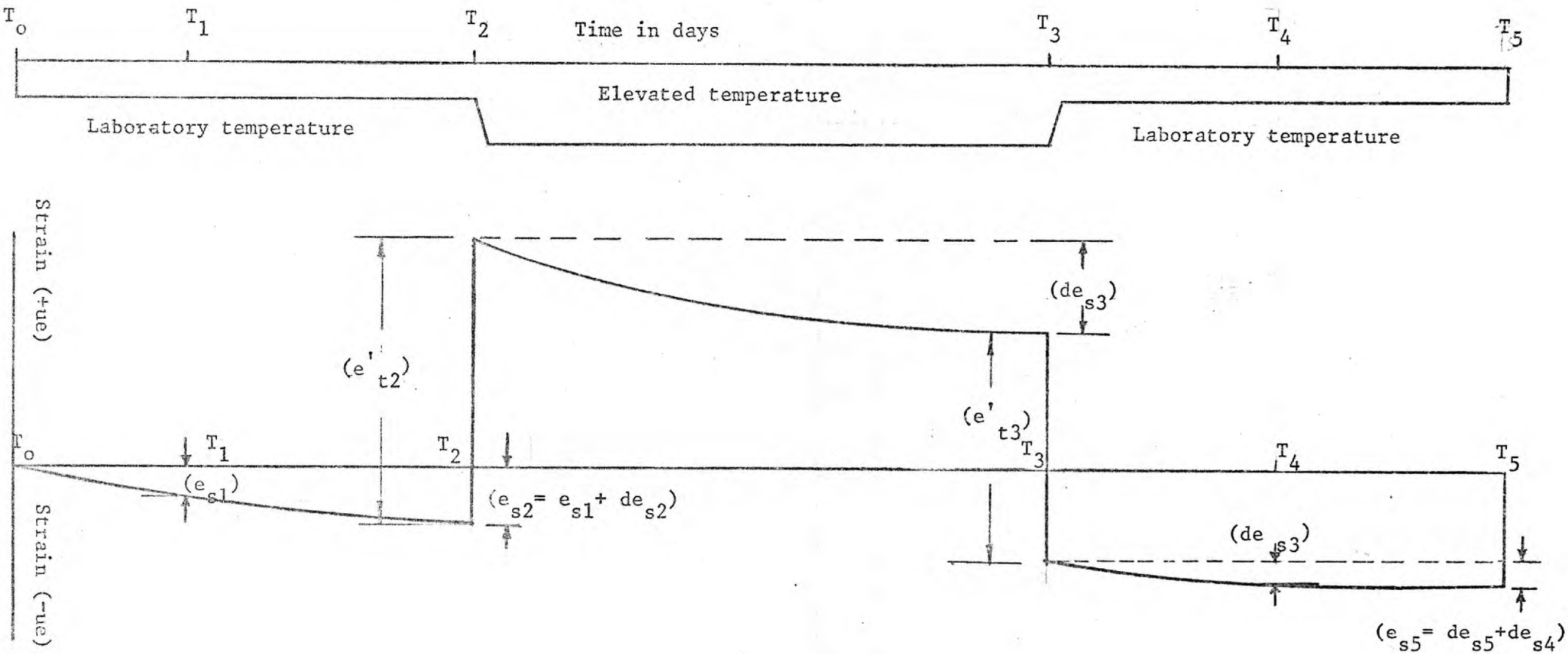

FIG.A5. Typical shrinkage time curve for unloaded specimens.

The effects of shrinkage have not been included in the calculations.

Equation 4.4. defining the Effective Modulus for concrete in terms of the specific creep is restated in the form:-

$$E' = \frac{1}{E^{-1} + c} \qquad 9.1.$$

a) At time T_1

Specimens at ambient temperature.

$$p_1 = \frac{e_{el}}{1/E_1} \qquad 9.2.$$

b) At time T_2

1) Before the application of heat.

$$p_2 = \frac{e_{el} + e_{c2}}{1/E_1 + c_2} \qquad 9.3.$$

$$c = \frac{e_c}{\sigma} \qquad \text{specific creep.}$$

2) Immediately after heat was applied.

Thermoelastic effects included.

$$p_2' = \frac{e_{el} + de_{t2} + e_{c2}}{1/E_2 + c_2} \qquad 9.4.$$

Thermoelastic effects excluded.

$$p'_{2*} = \frac{e_{el} + e_{c2}}{1/E_2 + c_2} \qquad 9.5.$$

c) At time T_3

1) Before heat was removed.

Thermoelastic effects included.

$$p_3 = \frac{e_{el} + de_{t2} + e_{c3}}{1/E_2 + c_3} \qquad 9.6.$$

Thermoelastic effects excluded.

$$p'_{3*} = \frac{e_{el} + e_{c3}}{1/E_2 + c_3} \qquad 9.7.$$

2) After heat was removed.

$$p'_3 = \frac{e_{el} + de_{t2} - de_{t3} + e_{c3}}{1/E_3 + c_3} \qquad 9.8.$$

d) At time T_4

1) Before load was removed.

$$p_4 = \frac{e_{el} + de_{t2} - de_{t3} + e_{c4}}{1/E_3 + c_4} \qquad 9.9.$$

Thermoelastic effects excluded.

$$p_{4*} = \frac{e_{e1} + e_{c4}}{1/E_3 + c_4} \qquad 9.10.$$

2) After load was removed.

$$p_4' = \frac{e_{e1} + de_{t2} - de_{t3} + e_{c4} - e_{c4}}{1/E_3 + c_4} \qquad 9.11.$$

3. Temperature data.

The temperature data used in this analysis are given here in tabular form:-

a) At time T_1

All specimens at $t = 22.5^{\circ}C$.

b) At time T_2

All specimens at $t = 22.5^{\circ}C$.

At time T_2'

Specimen:	Time: 8.30am:	12.30pm:	
1 / 2	64.5°C	66.4°C	
3 / 4	62.5°C	63.7°C	
5 / 6	71.5°C	72.9°C	
7 / 9	70.5°C	71.1°C	
9 /10	)73.7°C	76.2°C	Perforations.
	(66.1°C	66.7°C	Ring.

At time T_2''

	Time:		
Specimen:	8.45am:	1.30pm:	
1 / 2	82.1°C	82.2°C	
3 / 4	80.7°C	78.8°C	
5 / 6	77.1°C	75.7°C	
7 / 8	79.6°C	80.2°C	
9 /10	)83.1°C	81.7°C	Perforations.
	(74.2°C	71.9°C	Ring.

c) At time T_3

1 / 2	82.5°C	
3 / 4	83.0°C	
5 / 6	82.6°C	
7 / 8	83.1°C	
9 /10	)86.4°C	Perforations.
	(79.8°C	Ring.

At time T_3'

	9.30am:	1.15pm:	
1 / 2	26.3°C	25.5°C	
3 / 4	35.3°C	25.0°C	
5 / 6	26.6°C	25.5°C	
7 / 8	28.9°C	27.0°C	
9 /10	)32.7°C	30.1°C	Perforations.
	(31.3°C	29.2°C	Ring.

At time T_3''

All specimens at $t = 22.5°C$.

4. Evaluations of strains.

Control specimen.

At time T_1

$t_1 = 22.5^{\circ}C.$ $E_1 = 4.4 \times 10^6$

$e_{s1} = 0.65 \times 10^{-4}.$ $e_{e1} = 3.65 \times 10^{-4}.$

At time T_2

a) Cold. T_2.

$t_2 = 22.5^{\circ}C.$ $E_1 = 4.4 \times 10^6.$

$e_{s1} = 0.65 \times 10^{-4}.$

$e_{c2} + de_{s2} \cdot = 1.8 \times 10^{-4}.$

$e_{s2} = e_{s1} + de_{s2} = 1.2 \times 10^{-4}.$

$de_{s2} = 0.55 \times 10^{-4}.$ $e_{c2} = 1.25 \times 10^{-4}.$

$e_{s2} = 1.20 \times 10^{-4}.$

b) Hot. T_2'.

i) $dt_2' = 40.5^{\circ}C.$ $a = 12.8 \times 10^{-6}.$

$de_{t2}' = 5.2 \times 10^{-4}.$

ii) $dt_2' = 60.5^{\circ}C.$ $a = 12.8 \times 10^{-6}.$

$de_{t2}' = 7.72 \times 10^{-4}.$

c) Hot. T_2''.

$dt_2'' = 56.3^{\circ}C.$ $a = 12.8 \times 10^{-6}$.

$de_{t2} = 7.2 \times 10^{-4}$.

At time T_3

a) Hot. T_3.

$dt_3 = 60.5^{\circ}C.$ $a = 12.8 \times 10^{-6}$.

$e_{e1} = 3.65 \times 10^{-4}$.

$e_{s3} = e_{s2} + de_{s3}$.

$e_{c3} = e_{c2} + de_{c3}$.

$de_{c3} + de_{s3} = 3.25 \times 10^{-4}$.

$de_{s3} = 0.40 \times 10^{-4}$. $de_{c3} = 2.85 \times 10^{-4}$.

$e_{s3} = 1.60 \times 10^{-4}$. $e_{c3} = 4.10 \times 10^{-4}$.

b) Cold. T_3'.

$dt_3' = 7.8^{\circ}C.$ $a = 12.8 \times 10^{-6}$.

$de_{t3} = 0.95 \times 10^{-4}$.

c) Completely cold. T_3''.

$dt_3'' = 60.5^{\circ}C.$ $a = 12.8 \times 10^{-6}$.

$de_{t3}'' = 7.7 \times 10^{-4}$.

$de_{t3}'' = 7.8 \times 10^{-4}$. value obtained from graph.

d) At time T_4

1) Before unloading.

$E_3 = 4.3 \times 10^{-4}$. $e_{e4} = 3.5 \times 10^{-4}$.

$t_4 = 22.5^{\circ}C$.

$e_{s4} = e_{s3} + de_{s4}$.

$e_{c4} = e_{c3} + de_{c4}$.

$de_{s4} = 0.25 \times 10^{-4}$.

$de_{c4} = 0.3 \times 10^{-4}$. $de_{c4} = 3.8 \times 10^{-4}$.

$e_{c4} = 3.8 \times 10^{-4}$. $e_{s4} = 1.85 \times 10^{-4}$.

Composite specimen.

At time T_1

$t_1 = 22.5^{\circ}C$. $E_1 = 4.4 \times 10^{-4}$.

$e_{s1} = 0.4 \times 10^{-4}$. $e_{e1} = 3.45 \times 10^{-4}$.

At time T_2

a) Cold. T_2.

$t_2 = 22.5^{\circ}C.$ $e_{c1} = 3.45 \times 10^{-4}.$

$e_{s1} = 0.4 \times 10^{-4}.$ $e_{s2} = 1.0 \times 10^{-4}.$

$e_{s2} = e_{s1} + de_{s2}$

$e_{c2} = e_{c2}.$

$e_{c2} = de_{s2} = 1.55 \times 10^{-4}.$

$de_{s2} = 0.6 \times 10^{-4}.$ $e_{s2} = 0.95 \times 10^{-4}.$

b) Hot. T_2'.

$dt_2' = 51.2^{\circ}C.$ $a = 12.8 \times 10^{-6}.$

$de_{t2}' = 6.55 \times 10^{-4}.$

$de_{t2}' = 4.7 \times 10^{-4}.$ value obtained from graph.

Temperature of perforated zone $= 81.7^{\circ}C.$

Temperature of ring zone $= 71.9^{\circ}C.$

$dt' = 9.8^{\circ}C.$

Restrained thermal expansion $= adt'$.

$e_{t2}' = 1.25 \times 10^{-4}.$

At time T_3

a) Hot. T_3.

$dt_3 = 63.9^{\circ}C.$ $\quad a = 12.8 \times 10^{-6}.$

$e_{s3} = e_{s2} + de_{s3}$

$e_{s2} = 10 \times 10^{-4}.$ $\quad de_{s3} = 0.4 \times 10^{-4}.$

$e_{c3} = e_{c2} + de_{c3}.$

$de_{c3} + de_{s3} = 3.65 \times 10^{-4}.$

$e_{s3} = 1.4 \times 10^{-4}.$ $\quad de_{c3} = 3.25 \times 10^{-4}.$

$e_{c3} = e_{c2} + de_{c3} = 4.2 \times 10^{-4}.$

b) Cold. T_3'.

$dt_3' = 51.1^{\circ}C.$ $\quad de_{t3}' = 6.52 \times 10^{-4}.$

$de_{t3}' = 7.65 \times 10^{-4}.$ $\quad de_{t3}'' = 1.13 \times 10^{-4}.$

value obtained from graphs.

Temperatore of perforated zone = $86.8^{\circ}C.$

Temperature of ring zone = $79.8^{\circ}C.$

$dt_3' = 7.8^{\circ}C.$

$de_{t3}' = 0.9 \times 10^{-4}.$

At time T_4

a) Hot. T_4.

$t_4 = 22.5^{o}C.$ $\quad e_{s3} = 1.4x10^{-4}.$

$e_{s4} = e_{s3} + de_{s4}.$

$e_{c4} = e_{c3} + de_{c4}.$

$de_{s4} = 0.11x10^{-4}.$

$e_{s4} = 1.5x10^{-4}.$ $\quad de_{c4} + de_{s4} = 0.10x10^{-4}.$

$de_{c4} = 0.0.$ $\quad e_{c4} = 4.2x10^{-4}.$

Having evaluated the strains from the above relationships, the load distribution around the perforated zone of the composite specimen, was calculated from equations 9.1. to 9.11.

The stresses obtained for the load distributions areshown in Fig. A3. (g).

It is evident that the stresses around the perforated of the composite specimen decrease with time. This reduction in stress appears to be relatively small and should not have any serious effects on the integrity of structure.

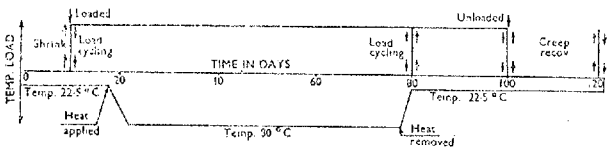

(a)

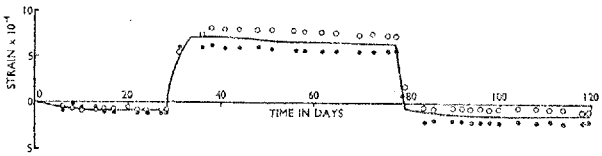

(b)

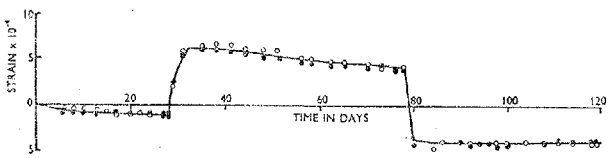

(c)

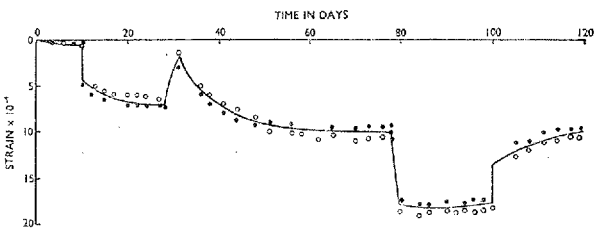

(d)

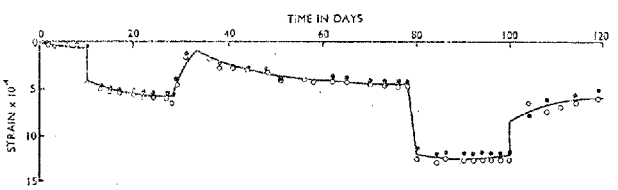

(e)

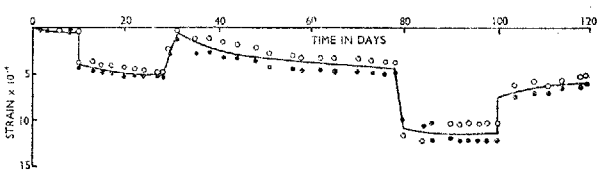

(f)

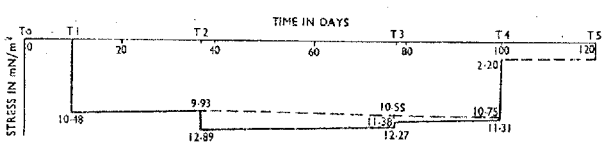

(g)

FIG. A3.

A P P E N D I X 3.

Computer output.

A typical output of the computer programme for the composite specimen (Model 9/10), of Series 2, is given here.

The computed displacements are given at ten nodal points, and the stress and strains at the centre of gravity of ten elements, for the time-intervals indicated.

At time = 0.0	Elastic solution.
At time = 6.0	Heat applied at end of interval.
At time = 9.0	End of transient period, (maximum temperature reached).
At time = 24.0	Heat removed at the end of interval.
At time = 27.0	End of cooling period.
At time = 30.0	Final unloading stage, (end of test programme).

R E S U L T S A T T I M E = 0.0 W E E K S

D I S P L A C E M E N T S

NODAL POINT NO.	DIS. IN-X (IN.)	DIS. IN-Y (IN.)
1	0.	0.
2	0.	-.22165849E-03
3	-.22162662E-03	0.
4	0.	-.70729795E-03
5	-.10212980E-03	-.46442296E-03
6	-.20758337E-03	-.20761155E-03
7	-.46436801E-03	-.10212954E-03
8	-.70722806E-03	0.
9	-.20713452E-03	-.72143341E-03
10	-.19797533E-03	-.73051048E-03

NORMAL AND SHEARING STRESSES AT C.G. OF ELEMENT

EMENT NO.	NORMAL STRESS IN-X (KIP/SQ IN)	NORMAL STRESS IN-Y (KIP/SQ IN)	SHEARING STRESS IN-XY (KIP/SQ IN)
1	-.15015683E+01	-.15017183E+01	0.
2	-.15452256E+01	-.14922393E+01	.29270891E-03
3	-.15037476E+01	-.14832957E+01	-.80298115E-02
4	-.15072876E+01	-.15074292E+01	-.39715127E-02
5	-.14832012E+01	-.15038936E+01	-.80072561E-02
6	-.14921404E+01	-.15452046E+01	.31425162E-03
7	-.15012012E+01	-.14835795E+01	.82692342E-02
8	-.34239742E+01	-.69659949E+01	-.39677445E+01
9	-.17710525E+01	-.78028805E+01	-.12361297E+01
10	-.17707224E+01	-.78017801E+01	.12367233E+01

ELEMENT STRAINS AT C.G. OF ELEMENT

	STRAINS IN X-AXIS	STRAINS IN Y-AXIS	STRAINS IN XY-AXIS
1	-.24625180E-03	-.24628721E-03	0.
2	-.25532451E-03	-.24281973E-03	.13815860E-06
3	-.24736087E-03	-.24252422E-03	-.37900711E-05
4	-.24719008E-03	-.24722344E-03	-.18745540E-05
5	-.24250008E-03	-.24733348E-03	-.37794249E-05
6	-.34200072E-03	-.25532336E-03	.14832676E-06
7	-.24643138E-03	-.24267266E-03	.39030785E-05
8	-.44652524E-04	-.19790609E-03	-.34387119E-03
9	.18993721E-04	-.24238540E-03	-.10713124E-03
10	.18993721E-04	-.24235211E-03	.10718268E-03

RESULTS AT TIME = 3.0 WEEKS

DISPLACEMENTS

NODAL POINT NO.	DIS. IN-X (IN.)	DIS. IN-Y (IN.)
1	0.	0.
2	0.	-.34795111E-03
3	-.34022572E-03	0.
4	0.	-.98038298E-03
5	-.20399031E-03	-.66437877E-03
6	-.35097999E-03	-.35064516E-03
7	-.66497462E-03	-.20384981E-03
8	-.98142701E-03	0.
9	-.34570094E-03	-.98099436E-03
10	-.33439767E-03	-.99261890E-03

NORMAL AND SHEARING STRESSES AT C.G. OF ELEMENT

ELEMENT NO.	NORMAL STRESS IN-X (KIP/SQ IN)	NORMAL STRESS IN-Y (KIP/SQ IN)	SHEARING STRESS IN-XY (KIP/SQ IN)
1	-.14372480E+01	-.14360522E+01	0.
2	-.19401038E+01	-.12142639E+01	-.10815614E-02
3	-.15250685E+01	-.10957933E+01	-.11417257E+00
4	-.16141630E+01	-.16165822E+01	-.12558686E+00
5	-.10968001E+01	-.15234238E+01	-.11438946E+00
6	-.12167769E+01	-.19387944E+01	-.78479566E-03
7	-.15036503E+01	-.10967706E+01	.11055019E+00
8	-.43837190E+01	-.86056536E+01	-.50309728E+01
9	-.23084816E+01	-.96247699E+01	-.16723539E+01
10	-.23002950E+01	-.95978479E+01	.16660571E+01

ELEMENT STRAINS AT C.G. OF ELEMENT

	STRAINS IN X-AXIS	STRAINS IN Y-AXIS	STRAINS IN XY-AXIS
1	-.38691747E-03	-.38661235E-03	0.
2	-.50997577E-03	-.31621594E-03	-.52931679E-06
3	-.42039284E-03	-.30839076E-03	-.60925425E-04
4	-.42021147E-03	-.41980566E-03	-.66487311E-04
5	-.30857520E-03	-.41999554E-03	-.61035856E-04
6	-.31660064E-03	-.50962452E-03	-.37064343E-06
7	-.41544023E-03	-.30750936E-03	.59051346E-04
8	-.50857430E-04	-.24301703E-03	-.43601764E-03
9	.19314978E-04	-.29774235E-03	-.14493734E-03
10	.19304978E-04	-.23692621E-03	.14439161E-03

RESULTS AT TIME = 6.0 WEEKS

DISPLACEMENTS

NODAL POINT NO.	DIS. IN-X (IN.)	DIS. IN-Y (IN.)
1	0.	0.
2	0.	-.43284657E-03
3	-.43333912E-03	0.
4	0.	-.11573772E-02
5	-.27519219E-03	-.79553886E-03
6	-.44835071E-03	-.44774465E-03
7	-.79659534E-03	-.27494405E-03
8	-.11692877E-02	0.
9	-.44150321E-03	-.11480182E-02
10	-.42724615E-03	-.11612189E-02

NORMAL AND SHEARING STRESSES AT C.G. OF ELEMENT

ELEMENT NO.	NORMAL STRESS IN-X (KIP/SQ IN)	NORMAL STRESS IN-Y (KIP/SQ IN)	SHEARING STRESS IN-XY (KIP/SQ IN)
1	-.13983730E+01	-.13964019E+01	0.
2	-.21843784E+01	-.10462976E+01	-.19843779E-02
3	-.15362164E+01	-.86323965E+00	-.17864225E+00
4	-.16822256E+01	-.16795835E+01	-.19702034E+00
5	-.86483188E+00	-.15334550E+01	-.17902321E+00
6	-.10507160E+01	-.21822175E+01	-.15280284E-02
7	-.15043192E+01	-.86444877E+00	.17275375E+00
8	-.49634458E+01	-.95937873E+01	-.56810913E+01
9	-.26403182E+01	-.10721743E+02	-.19451350E+01
10	-.26270544E+01	-.10677530E+02	.19340909E+01

ELEMENT STRAINS AT C.G. OF ELEMENT

	STRAINS IN X-AXIS	STRAINS IN Y-AXIS	STRAINS IN XY-AXIS
1	-.43143791E-03	-.48094063E-03	0.
2	-.63799047E-03	-.36226531E-03	-.10674289E-05
3	-.53803501E-03	-.34572024E-03	-.10240829E-03
4	-.53777108E-03	-.53703617E-03	-.11237870E-03
5	-.34621600E-03	-.33731631E-03	-.10261819E-03
6	-.36293431E-03	-.68736012E-03	-.80489264E-06
7	-.53014965E-03	-.34745439E-03	.99108216E-04
8	-.62723625E-04	-.27009446E-03	-.49236124E-03
9	.19296823E-04	-.33093825E-03	-.16657637E-03
10	.19296823E-04	-.32964714E-03	.16762121E-03

RESULTS AT TIME = 9.0 WEEKS

DISPLACEMENTS

NODAL POINT NO.	DIS. IN-X (IN.)	DIS. IN-Y (IN.)
1	0.	0.
2	0.	.20386580E-03
3	.20315045E-03	0.
4	0.	.10028698E-02
5	-.31371482E-04	.60265842E-03
6	.12536269E-03	.12727941E-03
7	.60113136E-03	-.30989771E-04
8	.10002351E-02	0.
9	.13563560E-03	.10716451E-02
10	.29465006E-03	.91397243E-03

NORMAL AND SHEARING STRESSES AT C.G. OF ELEMENT

ELEMENT NO.	NORMAL STRESS IN-X (KIP/SQ IN)	NORMAL STRESS IN-Y (KIP/SQ IN)	SHEARING STRESS IN-XY (KIP/SQ IN)
1	-.13734649E+01	-.13710848E+01	0.
2	-.23553686E+01	-.94639482E+00	-.27933206E-02
3	-.15372574E+01	-.71749509E+00	-.22099238E+00
4	-.17163965E+01	-.17130223E+01	-.23796302E+00
5	-.71927313E+00	-.15356935E+01	-.22152419E+00
6	-.94922835E+00	-.23529789E+01	-.23585143E-02
7	-.15034029E+01	-.71835599E+00	.21375040E+00
8	-.53701605E+01	-.10225637E+02	-.61185555E+01
9	-.28727640E+01	-.11420615E+02	-.21436824E+01
10	-.28545643E+01	-.11360283E+02	.21278606E+01

ELEMENT STRAINS AT C.G. OF ELEMENT

	STRAINS IN X-AXIS	STRAINS IN Y-AXIS	STRAINS IN XY-AXIS
1	.22572272E-03	.22651756E-03	0.
2	-.78428706E-04	.39950202E-03	-.17735012E-05
3	.14407454E-03	.42317171E-03	-.14994903E-03
4	.14464016E-03	.14575410E-03	-.16184582E-03
5	.42247626E-03	.14516206E-03	-.15029172E-03
6	.39854232E-03	-.77474427E-04	-.14022767E-05
7	.15480707E-03	.42003483E-03	.14510282E-03
8	.71975102E-03	.50934705E-03	-.53027481E-03
9	.31494735E-03	.44454347E-03	-.16578551E-03
10	.31494735E-03	.44637058E-03	.16441458E-03

RESULTS AT TIME = 12.0 WEEKS

DISPLACEMENTS

NODAL POINT NO.	DIS. IN-X (IN.)	DIS. IN-Y (IN.)
1	0.	0.
2	0.	-.22067075E-04
3	-.23420053E-04	0.
4	0.	.61197624E-03
5	-.25657856E-03	.29324175E-03
6	-.14330771E-03	-.14142099E-03
7	.29036505E-03	-.25574659E-03
8	.60702627E-03	0.
9	-.12766592E-03	.71700913E-03
10	.34373852E-04	.55695597E-03

NORMAL AND SHEARING STRESSES AT C.G. OF ELEMENT

ELEMENT NO.	NORMAL STRESS IN-X (KIP/SQ IN)	NORMAL STRESS IN-Y (KIP/SQ IN)	SHEARING STRESS IN-XY (KIP/SQ IN)
1	-.13240598E+01	-.13210910E+01	0.
2	-.27261563E+01	-.75220295E+00	-.49393341E-02
3	-.15374934E+01	-.43370660E+00	-.30741016E+00
4	-.17712439E+01	-.17664068E+01	-.31010764E+00
5	-.43559232E+00	-.15322663E+01	-.30829224E+00
6	-.75551170E+00	-.27222117E+01	-.42729584E-02
7	-.14991030E+01	-.43280922E+00	.29764343E+00
8	-.62160991E+01	-.11483172E+02	-.70316171E+01
9	-.33749702E+01	-.12806443E+02	-.25858517E+01
10	-.33430004E+01	-.12703877E+02	.25568822E+01

ELEMENT STRAINS AT C.G. OF ELEMENT

	STRAINS IN X-AXIS	STRAINS IN Y-AXIS	STRAINS IN XY-AXIS
1	-.26022281E-04	-.24518972E-04	0.
2	-.64144639E-03	.31702166E-03	-.42820736E-05
3	-.18348336E-03	.30130669E-03	-.29934987E-03
4	-.14172612E-03	-.17942238E-03	-.31060775E-03
5	.36057239E-03	-.16144188E-03	-.30013807E-03
6	.31522316E-03	-.63936647E-03	-.35951545E-05
7	-.16557944E-03	.35850709E-03	.28977829E-03
8	.70410175E-03	.47589661E-03	-.60940681E-03
9	.31207875E-03	.40336428E-03	-.22410715E-03
10	.31207875E-03	.40647545E-03	.22159646E-03

RESULTS AT TIME = 15.0 WEEKS

DISPLACEMENTS

NODAL POINT NO.	DIS. IN-X (IN.)	DIS. IN-Y (IN.)
1	0.	0.
2	0.	-.21688895E-03
3	-.21376133E-03	0.
4	0.	.29508989E-03
5	-.46156529E-03	.36310013E-04
6	-.37742090E-03	-.37465535E-03
7	.32314549E-04	-.46021503E-03
8	.28620820E-03	0.
9	-.35715972E-03	.43309181E-03
10	-.19310267E-03	.27153162E-03

NORMAL AND SHEARING STRESSES AT C.G. OF ELEMENT

ELEMENT NO.	NORMAL STRESS IN-X (KIP/SQ IN)	NORMAL STRESS IN-Y (KIP/SQ IN)	SHEARING STRESS IN-XY (KIP/SQ IN)
1	-.12950786E+01	-.12919325E+01	0.
2	-.29629657E+01	-.64082111E+00	-.65485243E-02
3	-.15330877E+01	-.26787535E+00	-.36995251E+00
4	-.17930819E+01	-.17924751E+01	-.34865956E+00
5	-.26953849E+00	-.15269697E+01	-.34101395E+00
6	-.64421584E+00	-.29565499E+01	-.58285290E-02
7	-.14953762E+01	-.26529106E+00	.34872583E+00
8	-.67454443E+01	-.12235691E+02	-.75967376E+01
9	-.36928282E+01	-.13633141E+02	-.28721801E+01
10	-.36520213E+01	-.13499785E+02	.28332376E+01

ELEMENT STRAINS AT C.G. OF ELEMENT

	STRAINS IN X-AXIS	STRAINS IN Y-AXIS	STRAINS IN XY-AXIS
1	-.24306814E-03	-.24098772E-03	0.
2	-.11537632E-02	.25598942E-03	-.69761484E-05
3	-.46847872E-03	.31920566E-03	-.43897055E-03
4	-.40517540E-03	-.46178986E-03	-.44290939E-03
5	.31755505E-03	-.46558826E-03	-.44017767E-03
6	.25348476E-03	-.11505376E-02	-.60222158E-05
7	-.44542712E-03	.31548133E-03	.42508806E-03
8	.69309210E-03	.45610307E-03	-.65838392E-03
9	.[illegible]73714E-03	.37899024E-03	-.24892228E-03
10	.[illegible]73714E-03	.38038536E-03	.24554726E-03

RESULTS AT TIME = 18.0 WEEKS

DISPLACEMENTS

NODAL POINT NO.	DIS. IN-X (IN.)	DIS. IN-Y (IN.)
1	0.	0.
2	0.	-.33384373E-03
3	-.33601174E-03	0.
4	0.	.96994124E-04
5	-.58136273E-03	-.12184437E-03
6	-.51670996E-03	-.51344727E-03
7	-.12548299E-03	-.57980555E-03
8	.88999044E-04	0.
9	-.40379264E-03	.25368749E-03
10	-.32948125E-03	.91064165E-04

NORMAL AND SHEARING STRESSES AT C.G. OF ELEMENT

ELEMENT NO.	NORMAL STRESS IN-X (KIP/SQ IN)	NORMAL STRESS IN-Y (KIP/SQ IN)	SHEARING STRESS IN-XY (KIP/SQ IN)
1	-.12733389E+01	-.12689270E+01	0.
2	-.31237669E+01	-.54836668E+00	-.74874566E-02
3	-.15340063E+01	-.13427432E+00	-.39475517E+00
4	-.18272454E+01	-.18210656E+01	-.34465124E+00
5	-.13603770E+00	-.15277530E+01	-.40091763E+00
6	-.56210032E+00	-.31218132E+01	-.57009446E-02
7	-.14945527E+01	-.13101959E+00	.38728864E+00
8	-.71211982E+01	-.12824771E+02	-.30129094E+01
9	-.39177394E+01	-.14283425E+02	-.30672721E+01
10	-.38723702E+01	-.14132247E+02	.39227620E+01

ELEMENT STRAINS AT C.G. OF ELEMENT

	STRAINS IN X-AXIS	STRAINS IN Y-AXIS	STRAINS IN XY-AXIS
1	-.37334634E-03	-.37003744E-03	0.
2	-.14534068E-02	.21541873E-03	-.85489101E-05
3	-.63541635E-03	.26926028E-03	-.51914848E-03
4	-.83372972E-03	-.62973207E-03	-.51917793E-03
5	.24736504E-03	-.63453104E-03	-.52058362E-03
6	.21250539E-03	-.14495130E-02	-.74416172E-05
7	-.61140168E-03	.28530237E-03	.50276701E-03
8	.58716777E-03	.44022301E-03	-.69545215E-03
9	.58374317E-03	.35955313E-03	-.26583024E-03
10	.58374317E-03	.36414838E-03	.26197270E-03

RESULTS AT TIME = 21.0 WEEKS

DISPLACEMENTS

NODAL POINT NO.	DIS. IN-X (IN.)	DIS. IN-Y (IN.)
1	0.	0.
2	0.	-.43131133E-03
3	-.43372270E-03	0.
4	0.	-.71166738E-04
5	-.67988845E-03	-.25516932E-03
6	-.63237765E-03	-.62871079E-03
7	-.26033865E-03	-.67811366E-03
8	-.80680767E-04	0.
9	-.60724358E-03	.10072726E-03
10	-.44972724E-03	-.62850507E-04

NORMAL AND SHEARING STRESSES AT C.G. OF ELEMENT

ELEMENT NO.	NORMAL STRESS IN-X (KIP/SQ IN)	NORMAL STRESS IN-Y (KIP/SQ IN)	SHEARING STRESS IN-XY (KIP/SQ IN)
1	-.12512925E+01	-.12475996E+01	0.
2	-.3277[illegible]193E+01	-.46180112E+00	-.32698075E-02
3	-.15357103E+01	-.10009704E-01	-.43619507E+00
4	-.18563272E+01	-.18493135E+01	-.41918970E+00
5	-.11953272E-01	-.15295726E+01	-.43744651E+00
6	-.46570413E+00	-.32701526E+01	-.74158080E-02
7	-.14241938E+01	-.63007524E-02	.42256647E+00
8	-.74753363E+01	-.13368367E+02	-.33910100E+01
9	-.41197117E+01	-.14854245E+02	-.32406204E+01
10	-.4069[illegible]866E+01	-.14716161E+02	.31915365E+01

ELEMENT STRAINS AT C.G. OF ELEMENT

	STRAINS IN X-AXIS	STRAINS IN Y-AXIS	STRAINS IN XY-AXIS
1	-.43141412E-03	-.47923402E-03	0.
2	-.16997211E-02	.18007230E-03	-.98257114E-05
3	-.77913305E-03	.26263702E-03	-.56447474E-03
4	-.77367026E-03	-.76917525E-03	-.58169658E-03
5	.26053771E-03	-.77476575E-03	-.56609151E-03
6	.17682097E-03	-.16952842E-02	-.85922668E-05
7	-.75004269E-03	.25847195E-03	.56604460E-03
8	.56098911E-03	.42564613E-03	-.12722067E-03
9	.[illegible]1001973E-03	.34155561E-03	-.26045374E-03
10	.[illegible]3018973E-03	.34659349E-03	.27059943E-03

RESULTS AT TIME = 24.0 WEEKS

DISPLACEMENTS

NODAL POINT NO.	DIS. IN-X (IN.)	DIS. IN-Y (IN.)
1	0.	0.
2	0.	-.47043021E-03
3	-.47293900E-03	0.
4	0.	-.14229603E-03
5	-.71773047E-03	-.31047493E-03
6	-.67037219E-03	-.67455287E-03
7	-.31535567E-03	-.71587686E-03
8	-.15157503E-03	0.
9	-.65229436E-03	.35291547E-04
10	-.43519131E-03	-.12875605E-03

NORMAL AND SHEARING STRESSES AT C.G. OF ELEMENT

ELEMENT NO.	NORMAL STRESS IN-X (KIP/SQ IN)	NORMAL STRESS IN-Y (KIP/SQ IN)	SHEARING STRESS IN-XY (KIP/SQ IN)
1	-.12493864E+01	-.12365163E+01	0.
2	-.33503643E+01	-.41609523E+00	-.36026980E-02
3	-.15309663E+01	.54834400E-01	-.45471382E+00
4	-.18724278E+01	-.18654316E+01	-.43512910E+00
5	.52769136E-01	-.15314263E+01	-.45600920E+00
6	-.42023236E+00	-.33429872E+01	-.77089595E-02
7	-.14344942E+01	.58637693E-01	.44046849E+00
8	-.76433851E+01	-.13648199E+02	-.35806599E+01
9	-.42139669E+01	-.15194179E+02	-.33241735E+01
10	-.41672372E+01	-.15021746E+02	.32732141E+01

ELEMENT STRAINS AT C.G. OF ELEMENT

	STRAINS IN X-AXIS	STRAINS IN Y-AXIS	STRAINS IN XY-AXIS
1	-.52548778E-03	-.52270023E-03	0.
2	-.17943262E-02	.16406709E-03	-.10279526E-04
3	-.83429539E-03	.25001331E-03	-.60887739E-03
4	-.82223579E-03	-.82460366E-03	-.60570144E-03
5	.24782786E-03	-.83044615E-03	-.61055972E-03
6	.16088198E-03	-.17896922E-02	-.89966374E-05
7	-.80441503E-03	.24572373E-03	.58966655E-03
8	.57833562E-03	.41804390E-03	-.74365719E-03
9	.50748956E-03	.33221705E-03	-.26809504E-03
10	.50748956E-03	.33744749E-03	.28367855E-03

RESULTS AT TIME = 27.0 WEEKS

DISPLACEMENTS

NODAL POINT NO.	DIS. IN-X (IN.)	DIS. IN-Y (IN.)
1	0.	0.
2	0.	-.11996770E-02
3	-.12021572E-02	0.
4	0.	-.24986928E-02
5	-.13403177E-02	-.18533073E-02
6	-.13573229E-02	-.13535227E-02
7	-.13586294E-02	-.10384637E-02
8	-.25078738E-02	0.
9	-.13316758E-02	-.23711045E-02
10	-.13132689E-02	-.23865388E-02

NORMAL AND SHEARING STRESSES AT C.G. OF ELEMENT

ELEMENT NO.	NORMAL STRESS IN-X (KIP/SQ IN)	NORMAL STRESS IN-Y (KIP/SQ IN)	SHEARING STRESS IN-XY (KIP/SQ IN)
1	-.12505189E+01	-.12468802E+01	0.
2	-.32916996E+01	-.46051536E+00	-.44435364E-02
3	-.15350137E+01	-.55443142E-02	-.43827295E+00
4	-.13530283E+01	-.16471006E+01	-.41817570E+00
5	-.84059683E-02	-.15276475E+01	-.43953510E+00
6	-.46441748E+00	-.32840841E+01	-.75969194E-02
7	-.14935916E+01	-.25271525E-02	.42464118E+00
8	-.75033411E+01	-.13391476E+02	-.84179115E+01
9	-.41384962E+01	-.14908411E+02	-.32602641E+01
10	-.40876481E+01	-.14738917E+02	.32099969E+01

ELEMENT STRAINS AT C.G. OF ELEMENT

	STRAINS IN X-AXIS	STRAINS IN Y-AXIS	STRAINS IN XY-AXIS
1	-.13357302E-02	-.13329745E-02	0.
2	-.36007943E-02	-.64950790E-03	-.10305914E-04
3	-.16432198E-02	-.56424901E-03	-.60648292E-03
4	-.16374090E-02	-.16327430E-02	-.60145336E-03
5	-.56440068E-03	-.16386927E-02	-.60816466E-03
6	-.65245828E-03	-.25961593E-02	-.90347202E-05
7	-.16145357E-02	-.56838940E-03	.58739359E-03
8	-.14310661E-03	-.39834911E-03	-.72955233E-03
9	-.15865769E-04	-.44256205E-03	-.26255622E-03
10	-.15865769E-04	-.47742074E-03	.27819973E-03

RESULTS AT TIME = 30.0 WEEKS

DISPLACEMENTS

NODAL POINT NO.	DIS. IN-X (IN.)	DIS. IN-Y (IN.)
1	0.	0.
2	0.	-.97502981E-03
3	-.97753468E-03	0.
4	0.	-.17745707E-02
5	-.94062515E-03	-.13790397E-02
6	-.11475650E-02	-.11437102E-02
7	-.13144854E-02	-.93874954E-03
8	-.17838059E-02	0.
9	-.11226110E-02	-.16320072E-02
10	-.11137366E-02	-.16380562E-02

NORMAL AND SHEARING STRESSES AT C.G. OF ELEMENT

ELEMENT NO.	NORMAL STRESS IN-X (KIP/SQ IN)	NORMAL STRESS IN-Y (KIP/SQ IN)	SHEARING STRESS IN-XY (KIP/SQ IN)
1	.24253788E+00	.24611416E+00	0.
2	-.16993620E+01	.99396551E+00	-.86430046E-02
3	-.27363205E-01	.14249709E+01	-.41564350E+00
4	-.33011022E+00	-.32347110E+00	-.39687769E+00
5	.14232083E+01	-.20084553E-01	-.41790084E+00
6	.99022831E+00	-.16916699E+01	-.79601115E-02
7	.81611687E-02	.14295304E+01	.40329569E+00
8	-.39561235E+01	-.62110451E+01	-.43170269E+01
9	-.23023947E+01	-.68664647E+01	-.19739668E+01
10	-.22523854E+01	-.66997671E+01	.19234108E+01

ELEMENT STRAINS AT C.G. OF ELEMENT

	STRAINS IN X-AXIS	STRAINS IN Y-AXIS	STRAINS IN XY-AXIS
1	-.10851496E-02	-.10833665E-02	0.
2	-.23515629E-02	-.39977047E-03	-.10598515E-04
3	-.13935215E-02	-.31469089E-03	-.60651404E-03
4	-.13876573E-02	-.13829695E-02	-.60114070E-03
5	-.31655100E-03	-.13869389E-02	-.60822328E-03
6	-.40313563E-03	-.23468738E-02	-.93377295E-05
7	-.13646395E-02	-.31854243E-03	.58724094E-03
8	-.75740931E-04	-.19447350E-03	-.37414233E-03
9	-.35[illegible]510E-04	-.23235321E-03	-.17107712E-03
10	-.32098510E-04	-.22779672E-03	.16669560E-03

LIST OF REFERENCES

Abbreviations

I.C.E.	Institution of Civil Engineers
C.C.E.	Concrete and Constructional Engineering
A.S.C.E.	American Society of Civil Engineers
P.C.A.	Portland Cement Association
A.C.I.	American Concrete Institution
J.A.C.I.	Journal of the American Concrete Institute
A.S.T.M.	American Society of Testing Materials
U.S.B.R.	United States Bureau of Reclamation
R.I.L.E.M.	Reunion Internationale des Laboratoties d'Essais et de Recherches sur les Mäteriax et les Constructions
J.R.N.B.S.	Journal of Research of the National Bureau of Standards
M.C.R.	Magazine of Concrete Research

1. NEVILLE, A.M. "Theories of creep in concrete." Proc. A.C.I., V. 52, (1955), 47-60.

2. TROXELL, G.E., RAPHAEL, J.M., AND DAVIS, R.E. "Long-term creep and shrinkage tests of plain and reinforced concrete." A.S.T.M., 1958, pp. 91.

3. DAVIS, R.E., DAVIS, H.E., and BROWN, F.H. "Plastic flow and volume changes of concrete." Proc. A.S.T.M., Vol. 38, Part II, 1938, pp. 410-417.

4. NEVILLE, A.M. "Tests on the influence of the properties of cement on the creep of mortars." R.I.L.E.M., Collognium, Munich, 1948.

5. CARLSON, R.W. "Drying shrinkage of concrete as affected by many factors." Proc. A.S.T.M., V. 38, Part II, 1938, pp. 419-437.

6. DAVIS, R.E., CARLSON, R.W., TROXELL, G.E., and KELLEY, J.W. "Cement investigation for Hover Dam." A.C.I., Proc. V. 29, 1933, pp. 275-284.

7. NEVILLE, A.M. "Role of cement in the creep of mortars." A.C.I., Proc. V. 54, 1958-9, p. 963.

8. SHANK, F.R. "The flow of concrete at high overload." A.C.I., Proc. V. 45, 1949, pp. 493-500.

9. DAVIS, R.E., DAVIS, H.E., and HAMILTON, J.S. "Plastic flow of concrete under sustained stress." A.S.T.M., Proc. V. 34, Part II, 1934, pp. 354-386.

10. NEVILLE, A.M. "Properties of concrete." Sir Isaac Pitman and Sons, Ltd., London, 1963.

11. ILLSTON, J.M. "The creep of concrete under uniaxial tension." M.C.R., Vol. 17, No. 51, June, 1965, pp. 77-84.

12. HANSEN, T.C., and MATTOCK, A.H. "Influence of size and shape of member on the shrinkage and creep of concrete." P.C.A., Research and Development Laboratories, Development Dept., Bulletin, D. 103.

13. ROSS, A.D. "Experiments on creep of concrete under two-dimensional stresses." M.C.R., Vol. 6, No. 16, June, 1954, pp. 3-10.

14. DAVIS, R. E., DAVIS, H. E., and BROWN, F.H. "Plastic flow and volume changes of concrete." Proc. A.S.T.M., Vol. 37, Part II, 1937, pp. 317-330.

15. ISHAI, O. "Elastic and inelastic behaviour of hardened mortar in torsion." Symposium on creep of concrete, Detroit, A.C.I., March, 1964, Publication SP-9, 65-94.

16. DAVIS, R.E., and DAVIS, H.E. "Flow of concrete under sustained compressive stress." A.S.T.M., Proc. V. 30, Part II, 1930, p. 707.

17. ROSS, A.D. "Creep of concrete under variable stress." A.C.I., Proc. V. 54, 1958, pp. 739-758.

18. WHITNEY, C.S. "Plain and reinforced concrete arches." A.C.I., Proc. V. 28, 1932, pp. 479-519.

19. A.S.T.M., Report on the significance of tests and properties of concrete and concrete aggregates." A.S.T.M., Committee, C. 9, A.S.T.M., Philadelphia, 1935, 1943, 1955, (A.S.T.M., Special Tech. Publication).

20. EVANS, R.H. "Some new facts concerning creep in concrete." V. 37, No. 12, 1942, pp. 429-432.

21. DAVIS, R.E. "A summary of the results of investigations having to do with volumetric changes in cement, mortars and concretes, due to causes other than stress." A.C.I., Proc. V. 26, 1930, pp. 407-443.

22. WEIL, G. "Influence of dimensions and stress on the shrinkage and creep of concrete." R.I.L.E.M., Bulletin, No. 3, July, 1959, pp. 4-14.

23. ROSS, A.D. "Shape, size and shrinkage." C.C.E., Vol. 39, No. 8, August, 1944, pp. 193-199.

24. L'HERMITE, R., and MAMILLAN, M. "Further results of shrinkage and creep tests." International conference on the structure of concrete, London, 1965, Paper H. 2.

25. NEVILLE, A.M. "Creep as a function of cement paste content." M.C.R., Vol. 16, No. 46, March, 1964, pp. 21-30.

26. NEVILLE, A.M. "The relation between creep of concrete and the stress-strength ratio." Applied Scientific Research, Vol. 9, A., 1960, pp. 285-292.

27. HANSEN, T.C. "Creep and stress relaxation of concrete. A theoretical and experimental investigation." Swedish Cement and Concrete Research Institute at the Royal Institute of Technology, Stockholm, Proc. No. 31, 1960.

28. GLUCKLICH, J., and ISHAI, O. "The effect of temperature on the deformation of hardened cement paste. R.I.L.E.M., Symposium on concrete and reinforced concrete in hot countries. Haifa, July, 1960, Vol. 1.

29. ROSS, A.D. "Creep and shrinkage in plain, reinforced and prestressed concrete. A general method of calculation." J. I.C.E., Vol. 21, November, 1943, pp. 38-58.

30. ALI, I., and KESLER, C.E. "Mechanism of creep in concrete." Symposium on creep of concrete, Paper No. 2, A.C.I., Special Publication SP-9, 1964.

31. WASHA, G.W., and FLUCK, P.G. "Effect of compressive reinforcement on the plastic flow of reinforced concrete beam." J.A.C.I., Vol. 49, 1952, pp. 89-109.

32. MURASHEV, V.I. "Some characteristics of the theory of design of heat-resistant, plain and reinforced concrete structures." Investigation of heat-resistant concrete and reinforced concrete, State Press for Literature on Building and Architecture, Moscow, 1954, pp. 9-29.

33. KURENKOV, A.F. "Thermal stresses in reinforced concrete shafts." Reference as 32, pp. 167-202.

34. KELLY, J.W. "Some time-temperature effects in mass concrete." J.A.C.I., Vol. 34, 1938, pp. 573-586.

35. LEE, C.R. "Creep and shrinkage in restrained concrete." Fourth Congress on Large Dams, 1951, Vol. 3, Question 15, R. 46.

36. THEUER, A.U. "Effect of temperature on the stress-deformation of concrete." J.R.N.B.S., V. 18, February, 1937, pp.195-204.

37. ENGLAND, G.L., and ROSS. A.D. "Reinforced concrete under thermal gradients." M.C.R., Vol. 14, No. 40, March, 1962, pp. 5-12.

38. NASSER, K.W., and NEVILLE, A.M. "Creep of concrete at elevated temperatures." J. A.C.I., December, 1965, Proc. V. 62, pp. 1567-1579.

39. ARTHANARI, S., and YU, C.W. "Creep of concrete under uniaxial and biaxial stresses at elevated temperatures." M.C.R., Vol. 19, No. 60, September, 1967.

40. HANNANT, D.J. "Thermal stresses in reinforced concrete." Ph.D. Thesis, University of Nottingham, May, 1961.

41. HANNANT, D.J. "Strain behaviour of concrete upto 95°C under compressive stresses." Group C, Paper 17, Proceedings of the Conference on Prestressed Concrete Pressure Vessels, I.C.E., 1968.

42. BROWNE, R.D. "Properties of concrete in reactor vessels." Proceedings of the Conference on Prestressed Concrete Pressure Vessels, Group C, Paper 13, March, 1967, I.C.E., 1968.

43. SAEMANN, J.C., WARREN, C., and WASHA, G.W. "Effect of curing on the properties affecting shrinkage cracking of concrete block." J.A.C.I., Vol. 51, 1955, pp. 833-852.

44. PICKETT, G. "The effect of change in moisture-content on the creep of concrete under a sustained load." Proc. A.C.I., V. 38, pp. 333-1942.

45. GLUCKLICH, J. "Long-term compressive strength of concrete." Proceedings of the Conference on Prestressed Concrete Pressure Vessels, Group C, Paper No. 18, I.C.E., 1968.

46. ROLL, F. "Long-term creep recovery of highly stressed concrete cylinders." Symlosium on Creep of Concrete, A.C.I., Special Publication, SP.-9,1964.

47. FULTON, F.S. "Concrete Technology." A South African Handbook, The Portland Cement Institute, Johannesburg, 1964.

48. MIRONOV, S.A., and BUZHEVICH, G.A. "Experience in concreting in regions with dry and torrid climate in the U.S.S.R." R.I.L.E.M., Symposium on Concrete and Reinforced Concrete in Hot Countries, Haifa, July, 1960, Part I.

49. MALHOTRA, H.L. "The effect of temperature on the compressive strength of concrete." M.C.R., Vol.8, No. 22, 1956, pp. 85-94.

50. SAEMANN, J.C., and WASHA, G.W. "Variation of mortar and concrete properties with temperature." Proc., A.C.I., Vol. 54, November, 1957, pp. 385-395.

51. HANNAH, I.W. "Thermal stress in concrete." Nuclear Engineering, Vol. 6, February, 1961, pp.60-74.

52. KORDINA, K. "Experiments on the influence of the mineralogical character of aggregates on the creep of concrete." R.I.L.E.M., Bulletin No. 6, March, 1960, pp. 7-22.

53. DAVIS, R. E., and TROXELL, G.E. "Variation of mortar and concrete properties with temperature." Proc. A.C.I., Vol. 54, November, 1957, pp. 385-395.

54. DUKE, C.M., and DAVIS, H.E. "Some properties of concrete under sustained combined stress." A.S.T.M., Proc. Vol. 44, 1944, pp. 888-896.

55. L'HERMITE, R. "Volume changes of concrete." Proceedings of the Fourth International Symposium on the Chemistry of Cement, Washington, 1960. Monograph No. 43, National Bureau of Standards, 1962, Vol. 2, pp. 659-694.

56. U.S.B.R. "A 10-year study of creep properties of concrete." Report SP-38, Denver, Colo., 1953.

57. PHILLEO, R. "Some physical properties of concrete at high temperatures." Proc. A.C.I., Vol. 54, 1957, pp. 857-864.

58. SERAFIM, J.L., and GUERRIRO, M.Q. "Influence of temperature on the creep of mass concrete." R.I.L.E.M., Bulletin, No. 6, March, 1960, pp.23-32.

59. ENGLAND, G.L. "A study of the time-dependent strains in concrete maintained at elevated temperatures and their effects in reinforced concrete." Ph.D. Thesis,University of London, 1961.

60. ARTHANARI,S. "Influence of temperature and biaxial stresses on creep in concrete." Ph.D. Thesis, University of London, 1966.

61. KOVENKOV, A.F. "Thermal stresses in reinforced concrete shafts." Investigation of heat-resistant concrete. State Press for Literature on Building and Architecture, Moscow, 1955, pp. 167-202.

62. ROSS, A.D. and BRAY, J.W. "The prediction of temperatures in mass concrete by numerical computation." M.C.R., Vol. 1, No. 1, January, 1949, pp. 9-12.

63. DAVEY, N., and FOX, E.N. "Temperature Rise in Hydrating Concrete." Building Research Technical Paper No. 15, D.S.I.R., (London), H.M.S.O., 1933.

64. BREWER, H.W. "General relation of heat flow factors to the unit weight of concrete." J. P.C.A, Research and Development Laboratories, Vol. 9, No.1, January, 1967, pp. 48-60.

65. KLEIN, A., PIRTZ, D., and ADAMS, R.F. "Thermal properties of mass concrete during adiabatic curing." A.C.I., Symposium on Mass Concrete, Special Publication, SP-6, 1963.

66. LEONHARDT, F. "Prestressed concrete - design and construction." Wilhelm Ernst and Sohn, Berling, 2nd Ed., 1964 (English translation).

67. ROSS, A.D. "The loss of prestress in concrete." Civil Engineering and Public Works Review, Vol. 45, No. 527, May, 1950, pp. 3070309.

68. ROSS, A.D. "Concrete creep data." The Structural Engineer, Vol. 15, No. 8, August, 1937, pp.314-326.

69. ENGLAND, G.L. "Steady-state" stresses in concrete structures subjected to sustained temperature and loads. Part I." Nuclear Engineering and Design 3, 1966, pp. 54-65.

70. DAVIS, H.S. "Thermal consideration in the design of concrete shields." Proceedings, A.S.C.E., Vol. 84, No. ST5, September, 1958, Part I, pp.1755.

71. ROSS, A.D., ENGLAND, G.L., and SUAN, R.H. "Prestressed concrete beams under sustained temperature cross fall." M.C.R., Vol. 17, No. 52, September, 1965, pp. 117-126.

72. McHENRY, D. "A new aspect of creep in concrete and its applications to design." Proc., of A.S.T.M., Vol. 43, 1943.

73. ENGLAND, G.L., and ILLSTON, J.M. "Methods of computing stress in concrete from a history of measured strain." Civil Engineering and Public Works Review, April, 1965, pp. 513-517.

74. ENGLAND, G.L. "Numerical creep analyses applied to concrete structures." Proc., A.C.I., Vol. 64, J., June, 1967, pp. 301-311.

75. ZIENKIEWICZ, O.C. "Analysis of visco-elastic behaviour of concrete structures with particular reference to thermal stress." Proc., A.C.I., Vol. 58, pp. 383-394.

76. CHRISHNAMOORTHY, S. "Thermal creep behaviour of concrete portal frames. Ph. D., Thesis, London University, June, 1969.

77. TIMOSHENKO, S. "Stresses in a plate with a circular hole." 1907, Bull. Polyt. Inst., Kiev.

78. KIRSCH, G. "Theories der elastizitatsbedurfnisse der festigkeitslchle." 1898 Z. Ver. Dtsch. Ing., Vol. 42, p. 113.

79. JEFFREY, G.B. "Plane stress and strain in bipolar co-ordinates." 1920, Phil. Trans., Vol. A221, p. 265.

80. HOWLAND, R.C.J. "On the stresses in the neighbourhood of a circular hole in a strip under tension." 1930, Phil. Trans. Vol. A229, p. 49.

81. KNIGHT, R.C. "On the stresses in a perforated strip." 1934, Quart. F. Math., Vol. 5, p. 255.

82. HOWLAND, R.C. "Stresses in a plate containing an infinite row of holes." 1935, Proc. Roy. Soc., Vol. A148, p. 471.

83. ATSUMI, A. "On stresses in strip under tension and containing two equal circular holes placed longitudinally." 1956, A.S.M.E., P. 56-APM-12, presented at National Applied Mechanics Conference, Urbana, Ill., U.S.A., June, 14-16.

84. HORVAY, G. "Plane stress problems of perforated plates." 1952, F. Appl. Mech., Vol. 19, p. 355.

85. DUNCAN, J.P. "Structural efficiency of tube-plates for heat exchangers." 1955, Proc. Inst., Mech., Eng., London, Vol. 169, p. 789.

86. BAILEY, R. and HICKS R. "Behaviour of perforated plates under plane stress." J., Mech., Eng., Science, Vol. 2, p. 2, 1960.

87. HARROP, J. and ABDUL-WAHAB, H.M.S. "An experimental study of the rigidity of perforated plates. Nuclear Engineering and Design 4, 1966, p. 480-489.

88. ABDUL-WAHAB, H.M.S. "The rigidity of perforated plates with reinforced holes." Nuclear Engineering and Design 5, 1967, p. 134-141.

89. SLOT, T. "Note on stresses and displacements in square plates and cylinders with pressurised central circular holes." Nuclear Engineering and Design 5, 1967, p. 142-1949.

90. KINKEAD, A.N. "Round holes in reactor vessels." p. 6896, I.C.E., Abstract - "The Dragon Project Report, 353."

91. BAILEY, R.W. and FIDLER, R. "Stress analysis of plates and shells containing patterns of reinforced holes." Nuclear Engineering and Design 3, 1966, p. 41-53.

92. SHEFFIELD, C. Report No. W/AT 854/1962. The English Electric Company Limited, Atomic Power Division, Whetstone, U.K.

93. HRENNIKOFF, A. "Solution of problems of elasticity by the framework method." J., Applied Mechanics, December, 1941.

94. McHENRY, D. "A lattice analogy for the sulution of stress problems." J., Inst., Civil Engineers, December, 1943, p. 59-82.

95. McCORMICK, C.W. "Plane stress analysis." J., Structural Division, A.S.C.E., Vol. 89, No. ST4, August, 1963.

96. TURNER, M.J. CLOUGH, R.W., MARTIN, H.C., and TOPP, L.J. "Stiffness and deflection analyses of complex structures." J., Aeronautical Sciences, Vol. 23, No. 9, September, 1956, p. 805.

97. LANGEFORS, B. SAAB TN. 3. "Structural analysis of swept-back wings by matrix transformation." SAAB TN. 38. "Algebraic methods for the numerical analysis of built-up systems.

98. ARGYRIS, J.H. "Aircraft engineering, October, 1954 - May, 1959. "Energy theorems and structural analysis."

99. ZIENKIEWICZ. O.C. "The finite element method in structural continuum mechanics. McGraw-Hill, London, 1967.

100. CLOUGH, R.W. "The finite element method in plane stress analysis." Proc. ASCE, 2nd Conference On Electronic Computation, Pittsburgh, Pa., September, 1960.

101. WILSON, E.L. "Finite element analysis of two-dimensional structures." A thesis, Structural and Materials Research Report No. 63-2, Department of Civil Engineering, University of California, Berkeley, June, 1963.

102. LANSING, W., JENSEN, W. R., and FALBY, W. "Matrix analysis methods for inelastic structures." Report No. ADR. 02-11-65.4, Grumman Aircraft Engineering Corp., Bethpage, N.Y., November, 1965.

103. KING, I.P. "On the finite element analysis of two-dimensional stress problems, with time-dependent properties." A thesis, Division of Structural Engineering and Structural Mechanics, University of California, Berkeley, 1965.

104. BRESLER, B., and BERTERO. V. "Influence of load history on cracking in reinforced concrete." Report to California Division of Highways, Department of Civil Engineering, Division of Structural Engineering and Structural Mechanics, University of California, Berkely, August, 1966.

105. NGO, D. "A study of cracked reinforced concrete beams by the finite element method." Graduate Student Research Report No. 216, Division of Structural Engineering and Structural Mechanics, University of California, Berkeley, 1965.

106. NGO, D., and SCORDELIS, A.C. "Finite element analysis of reinforced concrete beams." J., ACI., Vol. 64, No. 3, March, 1967.

107. MELESH, R.J. "Structural analysis of solids." J., Structural Division, A.S.C.E., Vol. 89, No. ST4, August, 1963.

108. GALLAGHER, R.H., PADLOG, J., and BIJLAARD, P.P. "Stress analysis of heated complex shapes." J., American Rocket Society, Vol. 32, No. 5, May, 1962.

109. RASHID, Y.R. "Solution of elastostatic boundary value problems by the finite element method. A thesis, Division of Structural Engineering and Structural Mechanics, University of California, Berkeley, 1965.

110. MALLETT, R.H., "Mathematical models for structural discrete elements," unpublished lecture notes, Cornell University, Fall, 1966.

111. STEFANOU, G.D., YU, C.W., and GILL, S. "An experimental investigation into the behaviour of perforated end slabs for concrete pressure vessels under temperature and external load." International conference on "Model techniques for Prestressed Concrete Pressure Vessels." The British Nuclear Energy Society, London, July, 1969.

112. GILL, S. "Structures for nuclear power." C.R. Books, Ltd., London, 1964.

113. TAYLOR, R.S. "The wylfa vessels." International Conference on Prestressed Concrete Pressure Vessels.' I.C.E., B.N.E.S., & J.B.C.S.A., London, March, 1967.

114. WARNER, P.C. "The Dungeness B Vessels." International Conference on Prestressed Concrete Pressure Vessels." I.C.E., B.N.E.S., & J.B.C.S.A, London, March, 1967.

115. ZIENKIEWICZ, O.C. et al. "Stress analysis by the finite element method - thermal effects." International conference on Prestressed Concrete Pressure Vessels. I.C.E., B.N.E.S., & J.B.C.S.A., London, March, 1967.

116. TURNER, M.J., MARTIN, H.C., and WEIKEL, R.C. "Further development and application of the stiffness method." AGARD, Structures and Materials Panel, Paris, France, July, 1962.

117. CLOUGH, R.W. "The finite element method in structural mechanics. Ch. 7. Stress analysis, ed. O.C. Zienkiewicz and G.S. Holister. Wiley, New York, 1965.